THE ORIGIN OF RNA ON BIOGENIC WORLDS

THE ORIGIN OF RNA ON BIOGENIC WORLDS

By BEN K. D. PEARCE, M. SC.

A Thesis Submitted to the School of Graduate Studies in Partial Fulfillment of the
Requirements for the Degree Doctor of Philosophy

McMaster University

McMaster University DOCTOR OF PHILOSOPHY (2021) Hamilton, Ontario (Physics & Astronomy - Astrobiology)
TITLE: The Origin of RNA on Biogenic Worlds
AUTHOR: Ben K. D. Pearce, M.Sc. (McMaster University), B.Sc. (×2) (University of British Columbia, University of Calgary)
SUPERVISOR: Professor Ralph E. Pudritz
NUMBER OF PAGES: ix, 348

Abstract

Given the role of HCN as a reactant in RNA building block production (e.g. nucleobases, ribose, and 2-aminooxazole), we propose that an atmosphere rich in hydrogen cyanide (HCN) is a distinguishing feature of what we term *biogenic worlds.* These are worlds that can produce key biomolecules for the emergence of life *in situ* rather than requiring they be delivered, e.g., by meteorites. To attack the question of whether early Earth was biogenic, we develop a series of new capabilities including the calculation of missing/unknown HCN reaction rate coefficients, the simulation of HCN chemistry in planetary atmospheres, and the coupling of atmospheric HCN chemistry and rain-out to the production and evolution of RNA building blocks in warm little ponds (WLPs). We make a major leap in understanding the origin of RNA on a biogenic early Earth by building a comprehensive model that couples terrestrial geochemistry, radiative transfer, atmospheric photochemistry, lightning chemistry, and aqueous pond chemistry.

We begin by developing an accurate and feasible method to calculate missing reaction rate coefficients related to HCN chemistry in planetary atmospheres. We use density functional theory simulations to solve the transition states for various reactions, and use the simulated energies and partition functions to calculate the corresponding rate coefficients using the principles of statistical mechanics. We initially explore and calculate rate coefficients for a total of 110 reactions present in reducing atmospheres dominated by N_2, CH_4, and H_2, including 48 reactions that were previously unknown in the literature. Our rate coefficients are most commonly within a factor of two of experimental values, and generally always within an order of magnitude of these values. This accuracy is consistent with the typical uncertainties assigned in large-scale kinetic data evaluations.

Next, we develop a consistent reduced atmospheric hybrid chemical network (CRAHCN) containing experimental values when available (32%) and our calculated rate coefficients otherwise (68%). To validate our chemistry, we couple CRAHCN to a 1D disequilibrium chemical kinetic model (ChemKM) to compute HCN production in the reducing atmosphere of Saturn's moon Titan. Our calculated atmospheric HCN profile agrees very well with the measurements performed by instruments aboard the Cassini spacecraft, suggesting our chemical network is accurate for modeling HCN production in reducing environments. We also perform sensitivity analyses on this chemistry and find HCN production and destruction on Titan can be understood in terms of only 19 dominant reactions. The process begins with UV photodissociation of N_2 and CH_4 in the upper atmosphere, and galactic cosmic ray dissociation of these species in the lower atmosphere. The dissociation radicals then proceed to react along four main channels to produce HCN. It is of particular excitement that one of these channels was newly discovered in this work.

Moving forward to modeling early Earth, we expand upon CRAHCN by exploring and calculating rate coefficients related to HCN and H_2CO chemistry in atmospheres with oxidizing conditions. We calculate the rate coefficients for 126 new reactions, including 45 reactions that were first discovered in this work. We find the accuracy of our method continues to produce most commonly factor of two agreement with respect to experimental values. Next, we develop the oxygen extension to CRAHCN (CRAHCN-O), containing a total of 259 reactions for computing HCN and H_2CO production in atmospheres dominated by N_2, CO_2, H_2, CH_4, and H_2O. Again, experimental rate coefficients are used when available (43%), and our calculated values are used otherwise (57%).

We then build a comprehensive model with a unique coupling of early Earth geochemistry, radiative transfer, atmospheric UV and lightning chemistry, and aqueous chemistry in WLPs. We calculate self-consistent pressure-temperature profiles using a 1D radiative transfer code called petitRADTRANS, and couple these to CRAHCN-O and ChemKM to simulate HCN and H_2CO production on early Earth. We model two epochs, at 4.4 and 4.0 billion years ago (bya), which differ in atmospheric composition, luminosity, UV intensity, radical production from lightning, and impact bombardment rate. The respective reducing and oxidizing atmospheric compositions of the 4.4 and 4.0 bya epochs are mainly driven by the balance of H_2 impact degassing and CO_2 outgassing from volcanoes. We then couple the rain-out of HCN with a comprehensive WLP model to compute the *in situ* production of RNA building blocks for each epoch. HCN pond concentrations are multiplied by experimental yields to calculate biomolecule production, and there are various biomolecule sinks present including UV photodissociation, hydrolysis and seepage.

At 4.4 bya, we find that HCN rain-out leads to peak adenine production of 2.8μM (378 ppb) for maximum lightning conditions. These concentrations are comparable to the peak adenine concentrations delivered by carbon-rich meteorites (10.6μM);

however, the concentrations from *in situ* production persist for $>$ 100 million years in contrast to $\sim$days for meteoritic concentrations. Guanine, cytosine, uracil and thymine concentrations from *in situ* production at this time peak in the 0.19–3.2μM range, and ribose and 2-aminooxazole peak in the nM range. We note that cytosine and thymine are not present in meteorites, suggesting this biogenic pathway may be one of the only plausible origins of these RNA and DNA building blocks. We find that the high mixing ratio of HCN near the surface of our 4.4 bya model is mainly driven by lightning chemistry rather than UV chemistry. Our results show that HCN production at the surface is linearly dependent on lightning flash density. This result supports a lightning-based Miller-Urey scenario for the origin of RNA building blocks. At 4.0 bya, HCN production and rain-out is 2–3 orders of magnitude less abundant than it is at 4.4 bya, leading to negligible concentrations of RNA building blocks in WLPs during this late oxidizing phase. Similar to HCN production in Titan's atmosphere, HCN production in early Earth's atmosphere is strongly correlated with CH_4 content. Reducing (H_2-dominant) conditions sustain CH_4 levels at a roughly constant ppm-level over 100 million years, which is favourable for HCN production. In oxidizing conditions, CH_4 is readily oxidized into CO_2, leading to less HCN. These results suggest that early Earth was biogenic at 4.4 bya, and remained so for at least $\sim$100 million years, but was over by 4.0 bya due to oxidation of the atmosphere.

This thesis provides a firm theoretical foundation for an origin of RNA in WLPs on a biogenic early Earth within about 200 million years after the Moon-forming impact and the cooling of the magma ocean.

Acknowledgments

I'll start by thanking my supervisor, who has put years of work into training and mentoring me, and who has made an incredible impact on me during my graduate studies. Ralph, I am so grateful that you chose me to work with you as an undergraduate research assistant back in 2014. This opened up my world to astrobiology in a big way and I feel incredibly lucky to now be part of a field that gives me a deep sense of belonging and purpose. You have taught me so much about science, academia, and being a member of the scientific community. About the shiny fun parts that bring us joy, excitement, and celebration, and the not so shiny parts that I've learned how to hold, not take personally, and later laugh about. You've been a critical eye in our research, always pushing for deeper understanding. I'm extremely proud of every paper we've written together, and I look forward to many more.

Next, I want to thank Karan Molaverdikhani. Karan, you've contributed a great deal of work to this thesis and I am extremely grateful to call you my collaborator and friend. You are an absolute pleasure to work with, even through my calculation errors and re-simulation requests, you've been patient and supportive without fail. I hope we continue to collaborate and maintain our friendship for many years to come.

Thomas Henning, thank you for being a great collaborator, mentor and member of my PhD committee. You've always been encouraging and supportive, and you've opened up many possibilities for me as a scientist. My time spent at MPIA has been a cornerstone to my early career. You have done so much to support me, and and contributed a great deal to the fascinating science we've faced in our origins of life research.

Greg Slater, thanks for being on my PhD committee, and for providing early opportunities for me to get involved in Canadian astrobiology. I value your candor and admire your balanced attitude. You are certainly someone who I look up to.

Paul Ayers, thank you for teaching me quantum chemistry and for being a huge source of chemical intuition and expertise for me as I navigated a new field. I would not have had the confidence to develop these methods without knowing you were available to question and solicit advice when things weren't working. Your down-to-earth attitude is a comfort to a stressed graduate student. I intend to emulate this if I find myself running a research group in the future.

To my astrobiology grad student crew, Sian, Nick, and Andrew: navigating this field with you and all the research and outreach we've done together has given me a deep sense of belonging. Your equal passions for this field and our comradeship has made this degree an incredible experience. Friends and colleagues for life.

To the grad students senior to me who gave me guidance as I navigated this PhD, Ian, Matt, Gwen, Ashley, Corey, Alex, Ryan, Sam, and Ben, thank you for your insight, kindness, encouragement and friendship.

To the students in Ralph's research group during my time as a PhD, Matt, Alix, Kaitlin, Rachel, Jess, Joshua, Akash, Julie, Bo, Gillian, Lisa, and Sanne, it's been a pleasure to work with you, share research, and discuss science and other interesting things going on in the world every week.

To all the other grad students and friends who I brewed beer with, bouldered and climbed with, and who were an important social outlet for me during my PhD: Ian, Ashley, Jacqueline, Kevin, Vanessa, Annica, Sean, James, James, Carmen, Thanassis, Ryan, Matt, Aaron, and Joey. Thanks for all the wonderful memories.

Lastly, I have to thank the person who supported me mentally and emotionally the most during my PhD. Laura, you were there for me every day, thick and thin, through what might be one of the most difficult journeys I'll face in my life. It will be impossible to think back on my PhD without remembering the support I got at home from you and the dogs (Boo, Buddy, and Charlie). You were my partner and friend, and although we've gone our separate ways now, I truly appreciate all you've done for me.

Contents

List of Figures

List of Tables

List of Abbreviations and Symbols

μM	micromolar
ωB/d	ωB97XD/aug-cc-pVDZ
‰	parts-per-thousand
^{26}Al	Aluminum-26
AMP	Adenosine monophosphate
ATP	Adenosine triphosphate
aug-cc-pVDZ	Augmented correlation-consistent polarized valence double-ζ
B-O	Born-Oppenheimer
BH/d	BHandHLYP/aug-cc-pVDZ
BH/t	BHandHLYP/aug-cc-pVTZ
BHandHLYP	Becke–Half-and-Half–Lee–Yang–Parr
bya	Billion years ago
CC/t	CCSD/aug-cc-pVTZ
CCSD	Coupled Cluster Singles and Doubles
CH_4	Methane
ChemKM	Chemical Kinetic Model
CIRS	Composite Infrared Spectrometer

CMP	Cytidine monophosphate
CO	Carbon monoxide
CO_2	Carbon dioxide
CRAHCN	Consistent Reduced Atmospheric Hybrid Chemical Network
CRAHCN-O	Consistent Reduced Atmospheric Hybrid Chemical Network Oxygen Extension
CVT	Canonical Variational Transition State Theory
DFT	Density Functional Theory
DNA	Deoxyribonucleic acid
FUV	Far ultraviolet
Ga	Giga years ago
GMP	Guanosine monophosphate
GT	Generalized Transition State
H_2	Hydrogen
H_2CO	Formaldehyde
H_2O	Water
HCN	Hydrogen cyanide
HF	Hartree–Fock
IDP	Interplanetary dust particle
INMS	Ion and Neutral Mass Spectrometer
K_0	Surface eddy diffusion coefficient
K_z	Eddy diffusion coefficient
LV	Late Veneer

ME	Master equation
MEP	Minimum energy path
$\mathbf{N}_2$	Nitrogen
$\mathbf{NH}_3$	Ammonia
nM	nanomolar
nt	nucleotide
$\mathbf{P}_{surf}$	Surface pressure
ppb	parts-per-billion
ppm	parts-per-million
ppq	parts-per-quadrillion
pptr	parts-per-trillion
RNA	Ribonucleic acid
RRKM	Rice–Ramsperger–Kassel–Marcus
SI	Supporting Information
TOA	Top of Atmosphere
TST	Transition State Theory
UMP	Uridine monophosphate
UV	Ultraviolet
UVC	Ultraviolet C
UVIS	Ultraviolet Imaging Spectrograph
VIMS	Visible and Infrared Mapping Spectrometer
WFC3	Wide Field Camera 3
WLP	Warm little pond
XUV	Solar soft x-ray

Declaration of Academic Achievement

I, Ben K. D. Pearce, declare that this thesis ‘The Origin of RNA on Biogenic Worlds’ and the work presented in it are my own. Where the thesis is based on work done by myself jointly with others, I have made clear exactly what was done by others and what I have contributed myself. The details of such contributions are outlined below.

The majority of the model development and analysis, and the writing and editing in this thesis was done by Ben K. D. Pearce. Quantum chemistry (Chapters 2–4) and warm little pond model simulations (Chapter 5) were performed by Ben K. D. Pearce. Disequilibrium atmospheric model simulations (Chapters 3 and 5) were performed by Dr. Karan Molaverdikhani. Pressure-temperature profile simulations (Chapter 5) were performed by Kaitlin Cerrillo and Ben K. D. Pearce.

My supervisor, Prof. Ralph Pudritz, contributed a great deal to all aspects of this thesis, including ideas development, model design and analysis, and writing/editing.

Introduction and Conclusion Chapters 1 and 6 were written by Ben K. D. Pearce and edited by Prof. Pudritz.

Prof. Paul Ayers provided valuable insight and assisted with emergent issues during the quantum chemistry methods development for Chapters 2–4. He also contributed to the editing of Chapter 2. Ben K. D. Pearce developed and performed all quantum chemistry simulations and developed the chemical networks used for the atmospheric models in Chapters 3 and 5.

The atmospheric models in Chapters 3 and 5 were designed and developed by Ben K. D. Pearce, Dr. Karan Molaverdikhani, Prof. Ralph Pudritz and Prof. Thomas Henning. Dr. Molaverdikhani performed all disequilibrium atmospheric simulations on the cluster at the Max Planck Institute for Astronomy using the ChemKM code. He also developed new ChemKM functionality for these projects, including self-consistent rain-out and GCR chemistry. Atmospheric models were analyzed by Ben K. D. Pearce, Prof. Pudritz, Dr. Molaverdikhani, and Prof. Henning.

Input parameters for our Titan model in Chapter 3 largely followed the 2012 model performed by Prof. Hébrard. Prof. Hébrard shared some of this input data for direct use in our models, including photochemistry, top-of-atmosphere radiation, and GCR chemistry. He also contributed to the editing of Chapter 3.

Kaitlin Cerrillo and Ben K. D. Pearce developed the iterative pressure-temperature profile calculations using the petitRADTRANS code, for input into our early Earth models in Chapter 5. petitRADTRANS simulations were largely carried out by Kaitlin Cerrillo.

Artist Steve Janzen designed Figure 1 in Chapter 5 based on a rough drawing developed by Ben K. D. Pearce and Prof. Pudritz.

I dedicate this thesis to my teachers and mentors.
I couldn't have done it without you.

Chapter 1

Introduction

> ”*The origin of life is an inalienable part of the general process of the development of the universe and, in particular, the development of the earth.*
>
> — **Alexander Oparin**

One of the deepest questions humans can ponder is: where did we come from? This question is so ingrained in who we are as humans, that scientists, philosophers and theists alike have studied it for millennia. Perhaps the first scientific thinking on this topic was from Thales of Miletus (c. 624–545 BC), ancient Greek philosopher. He postulated that water was the origin of all things; the substance from which everything emerges [1]. This idea is a fundamental principle in origins of life research today.

Fast-forwarding to the 20th century, the discoveries of DNA, RNA, and proteins have led us what is known as the “Central Dogma” of life [2]. We now know life’s key components. Information about an organism is stored in polymers (i.e. DNA/RNA). Polymers are chained molecules with repeating subunits. DNA and RNA have four different subunits, or bases, which allow for unique sequences when chained together. The blueprints for the functionality of an organism are stored in the base sequences of its DNA. To express a certain functionality (e.g. cell repair), RNA transcribes the respective blueprint and delivers it to the ribosome. The ribosome then uses the blueprint to build the corresponding protein out of amino acids. Proteins carry out nearly all the functionality in life as we know it.

Charles Darwin didn't know the details of how DNA, RNA and proteins operated in living organisms, but his letter to J. D. Hooker in 1871 is still remarkably relevant for origins of life research today [3]. Darwin envisaged "some warm little pond with all sorts of ammonia & phosphoric salts,–light, heat, electricity &c present, that a protein compound was chemically formed, ready to undergo still more complex changes, at the present day such matter wd be instantly devoured, or absorbed, which would not have been the case before living creatures were formed [4]."

Building off of Darwin were Alexander Oparin and John Haldane, who independently introduced the idea of the primordial soup in the 1920's [5, 6]. This was the idea that biomolecules were produced by the combination of UV light and simple molecules (e.g. methane, ammonia) in the early atmosphere, and that these biomolecules "must have accumulated until the primitive oceans reached the consistency of hot dilute soup" [7].

Up until this point, origins of life as a field of inquiry was largely theoretical. There were some experiments in the late 1800's and early 1900's that demonstrated organic synthesis in aqueous solution [8, 9], and using electric discharges [10]; however, they were not performed in the context of trying to understand the origin of life [11].

This all changed in the early 1950's when Stanley Miller and Harold Urey produced the first experimental results testing the primordial soup hypothesis. Miller built an apparatus to simulate lightning chemistry in a early reducing atmosphere composed of H_2, CH_4, NH_3 and H_2O, and condensed the products into a aqueous reservoir to simulate biomolecule synthesis in the early ocean [12]. Miller identified five amino acids in the original experiment, and dozens of others have been identified in similar experiments since then [13–16] . These experiments have also been performed with more neutral/oxidizing compositions (N_2/CO_2); however, amino acid yields are generally orders of magnitude lower [13, 14]. This experiment was transformational for the origins of life field, as it was the first demonstration of a clear route to biomolecule production in simulated primitive Earth conditions [17]. Since then, nucleobases, the building blocks of RNA, have also been identified in Miller-Urey experiments [18, 19].

Origins of life research connected with the field of meteoritics when nucleobases were detected in the Orgeil meteorite in 1964 [20] and amino acids were detected in the Murray and Murchison meteorites in 1966, and 1969, respectively [21, 22]. These discoveries suggested an alternate origin of biomolecules to Miller-Urey synthesis, an origin that resided in meteorite parent bodies in the protoplanetary disk.

By the late 1980's, even more potential sources of biomolecules were being explored, including interplanetary dust particles (IDPs) [23] and impact shocks [24]. Chyba and Sagan [25] were the first to do a comprehensive analysis of the various potential sources of biomolecules to early Earth, and estimated that IDPs and atmospheric production via UV irradiation were dominant sources in terms of mass influx rates.

What wasn't considered in the benchmark study by Chyba & Sagan was the location biomolecules would need to be delivered in order for subsequent reaction and RNA polymerization to occur. For example, the ocean is too large of a water reservoir to easily concentrate biomolecules. On the other hand, warm little ponds (WLPs) periodically evaporate which is a natural way to concentrate a biomolecule solution. Furthermore, an environment that cycles between wet and dry conditions provides both the dehydrated conditions necessary for polymerization, and the hydrated conditions necessary for diffusive mixing [26–29].

In my MSc thesis [30], we explored the plausibility of a meteoritic and IDP origin of nucleobases to WLPs by building a comprehensive sources and sinks numerical model of these environments [31]. Our WLP model included meteorites and IDPs as nucleobase sources, and UV photodissociation, hydrolysis and seepage as nucleobase sinks. In the face of these destructive sinks, only meteorites were were found to be a viable source of nucleobases, as they delivered μg of nucleobases in a single deposit, which survived for up to a few years. IDPs, on the other hand, rained down into WLPs too slowly for their $\sim$pg abundances to accumulate.

A critical issue that was not addressed in this work was whether meteoritic delivery was necessary for the emergence of life on Earth. We know from Miller-Urey experiments that particular atmospheric conditions can lead to biomolecule production in surface reservoirs. This brings us to a new concept we introduce in this thesis: *biogenic worlds*. These are worlds that do not require external delivery of key biomolecules for the origin of life.

The word biogenic has been used in the literature to mean, "present in life," e.g. the biogenic elements (CHNOPS) [32], as well as "generated by life," e.g., biogenic emissions [33]. Here we use the term biogenic to mean capable of generating biomolecules for life.

The question of whether early Earth was biogenic serves as guiding motivation for my PhD thesis. Key to answering this question is understanding and modeling the atmospheric chemistry that occurred on the early planet.

It is now understood that a key precursor for the production of biomolecules in

Miller-Urey experiments is hydrogen cyanide (HCN) [17, 18, 34]. HCN is water soluble, and has a great tendency to transform and polymerize, making it an exceptional precursor to complex biomolecules [35]. HCN is produced in atmospheres from reactive radicals (e.g. N atoms, CH_3) that come from the dissociation of stable species such as N_2 and CH_4 [36]. When HCN dissolves in rain droplets and enters WLPs, it can react in the presence of UV light to produce formaldehyde (H_2CO), as well as multiple key RNA building blocks, such as nucleobases [37, 38], ribose [9, 39, 40], and 2-aminooxazole (the key intermediate in the Powner-Sutherland approach to RNA building block production) [39, 41, 42]. H_2CO, which is an intermediate for the production of ribose, 2-aminooxazole, and the pyrimidine nucleobases (cytosine, uracil, thymine), can also enter ponds via atmospheric rain-out [43].

Modeling disequilibrium HCN chemistry requires a thorough network of reactions characterizing the production and destruction of this molecule in the gas phase. Reaction frequencies are characterized by their rate coefficient, and can vary as a function of temperature and/or pressure. Unfortunately many of these reactions remain uncharacterized by experiments and theory, and a complete picture of HCN production in planetary atmospheres is not fully understood.

In this thesis, in the effort to better understand HCN chemistry and its relation to biogenicity, we first develop an accurate and feasible method to calculate reaction rate coefficients using quantum chemistry and use it to explore and calculate previously unknown reactions related to HCN chemistry (Chapters 2–4). We validate this chemistry by modeling the atmosphere of Saturn's moon Titan: a world rich in HCN with accurate measurements performed by the Cassini spacecraft (Chapter 3). We also explore and calculate previously unknown H_2CO chemistry, with the aim to uncover the origin of this species in WLPs (Chapter 4). Finally, we model HCN (and H_2CO) production on early Earth and couple it (via atmospheric rain-out) to our WLP models to compute the *in situ* production of the building blocks of RNA (Chapter 5).

The introduction to this thesis will proceed as follows. In Section 1.1, we give an overview of the present state of the origins of life field including the main hypotheses and the justification for our chosen path of inquiry. Then, in Section 1.2, we introduce the physical and chemical processes that occur in planetary atmospheres that leads to HCN production. Lastly, we finish the introduction in Section 1.3 with an outline of the thesis chapters.

1.1 Origins of Life Hypotheses

The most recent astrophysical, geophysical, and biological evidence suggests that life emerged on Earth sometime between 4.5 and 3.7 billion years ago (bya) (see Figure 1.1) [44]. This interval is constrained by two boundaries: the habitability boundary at 4.5 bya, and the biosignature boundary at 3.7 bya. After the Moon-forming impact (4.52 bya at the earliest), the Earth had a global magma ocean that took 0.02–100 Myr to solidify, depending on cooling efficiency [45–47]. Once the temperature dropped to below the boiling point of water, a stable hydrosphere formed, and the Earth could support life. However, it isn't until 3.7 bya that we have compelling evidence that life had already existed on the surface, in the form of stromatolite fossils and light carbon isotopes in rocks of sedimentary origin [48–50]. Unfortunately, the fossil record doesn't extend earlier than 3.7 bya (as far as we know). Biosignatures earlier than 3.7 bya are mainly ^{13}C depletion signatures of zircons, which are not entirely convincing given the multiple abiotic mechanisms of producing the same signatures at zircon-formation temperatures (644–801°C) [44].

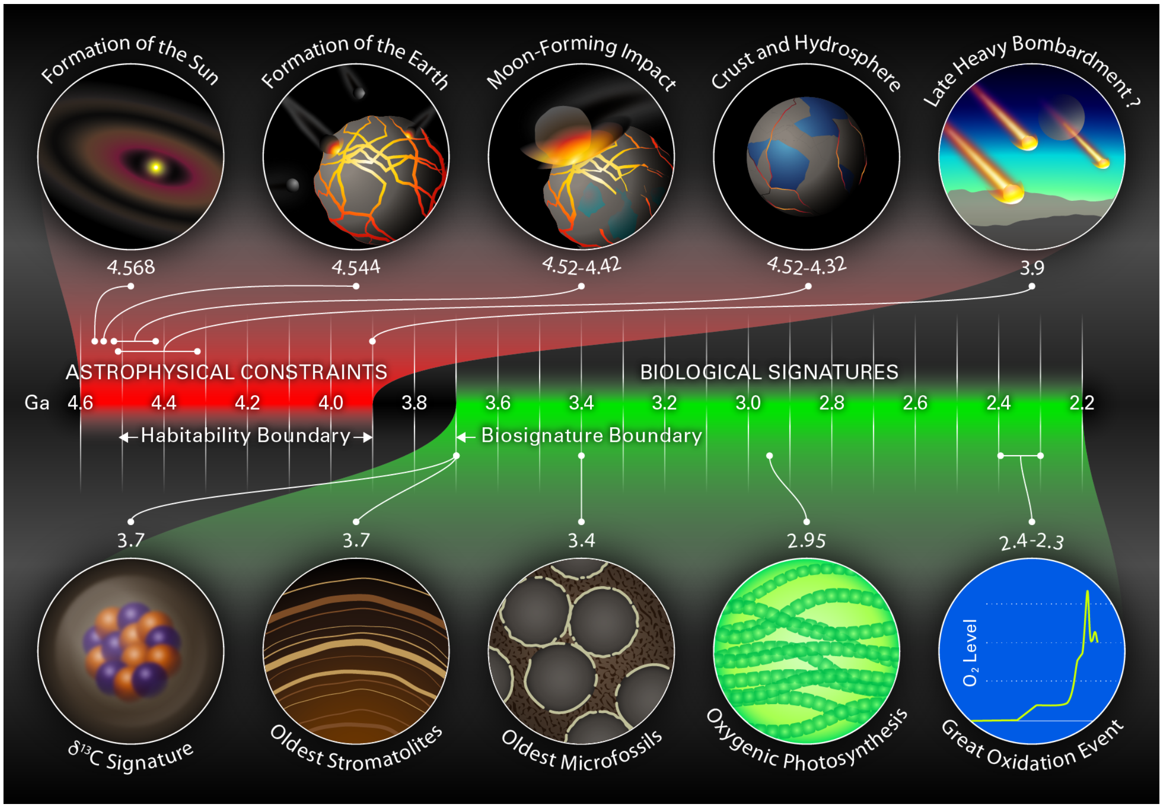

Figure 1.1: Overview of the time interval for the origin of life on Earth. The time interval is constrained by the habitability boundary at 4.5–3.9 billion years ago (bya) and the biosignature boundary at 3.7 bya. Source: [44].

1.1.1 Warm Little Ponds vs. Hydrothermal Vents

The question of where life emerged on early Earth is a consistent source of debate in the field. Scientific research is most active for two competing hypotheses: freshwater ponds at the surface, and saline hydrothermal vents at the ocean floor (See Figure 1.2 for images of these environments). These environments are substantially different across many parameters including: salinity, pH, source of organics, wet-dry cycle availability, UV exposure, redox gradients, concentration, minerals, pressure, and temperature. Furthermore, the principles for life's emergence differ between these hypotheses.

WLPs are natural environments in which information polymers can form, and as such, are the preferred setting for the "information first" hypothesis. In other words, researchers focus on finding an abiotic route to producing information polymers such as ribonucleic acid (RNA) and finding an evolutionary route from an RNA world to the DNA/RNA/protein world of life today [51, 52]. Because ponds evaporate, there

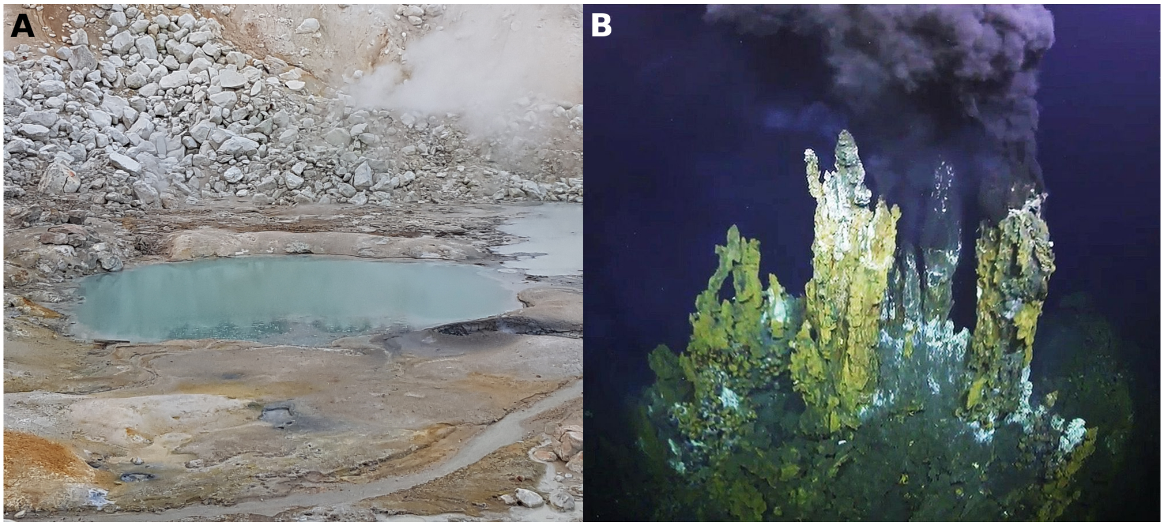

Figure 1.2: **A)** An image of a "warm little pond" from the Bumpass Hell trail in Lassen Volcanic National Park. (credit: Ben K. D. Pearce). **B)** Hydrothermal vent chimneys at Site BBC in the Lau Basin (credit: Schmidt Ocean Institute).

is a natural concentrating mechanism for biomolecules arriving from meteorites and biomolecule precursors raining out of the atmosphere (such as HCN). The cycling between wet and dry conditions also provides the thermodynamic energy and the dehydrating conditions necessary for forming covalent bonds between information building blocks such as nucleotides [27, 51, 53].

The origin of life in hydrothermal vents is a "metabolism first" hypothesis. Hydrothermal vents at the ocean floor have no access to meteoritic or atmospheric sources of biomolecules and precursors, given the ocean would dilute such sources immediately upon entering. Therefore, in order to have biomolecules form in these environments, a prebiotic metabolism ("Krebs cycle") must emerge that makes use of the concentrated CO_2 and H_2 present at the vent opening [54–57]. The strength of this hypothesis is that the geochemistry present in hydrothermal vents is similar to biochemistry. For example, there are naturally pre-existing proton and pH gradients in hydrothermal vents, similar to the proton and pH gradients across the mitochondrial membrane that powers cells [54, 56, 58].

Because the principles of each hypothesis differ so greatly, scientists generally contribute research to one hypothesis or the other, although clearly both information and metabolism must ultimately be linked in a complete picture. We research the WLP hypothesis mainly because of the great deal of experimental testing this hypothesis has undergone with large success, and the fact that there are fewer and smaller hurdles associated with it that are still to overcome. For example, experiments have demonstrated the polymerization of long (> 300 nt) strands of RNA by subjecting ribonucleotides (i.e. RNA monomers) to wet-dry cycles similar to WLP environments [26–29]. Other experiments have shown the catalytic replication and polymerization properties of folded RNA molecules (i.e. ribozymes) that are 65–187 bases long [59–62]. This suggests a fairly conceivable pathway from RNA building blocks to self-replicating RNA polymers in WLP environments. The main components of this process that still need to be demonstrated are producing ribonucleotides in a single step (i.e. "one-pot synthesis") at high yield, and the complete self-replication of a ribozyme. Both of these components have been partially demonstrated, suggesting these hurdles are capable of being overcome.

For example, ribonucleosides (adenosine, cytidine, uridine) have been produced in 0.7–2.7% yields from ribonucleotide building blocks (nucleobases, ribose, phosphoric acid) in microdroplets [63, 64], and a complete ribonucleotide (adenosine monophosphate: AMP) has been produced in low yield (0.08%) from the same starting molecules in bulk solution [65]. Powner et al. [42] synthesized the pyrimidine ribonucleotides (cytidine monophosphate: CMP, uridine monophosphate: UMP) using a different strategy that didn't involve nucleobases or ribose as starting materials. Their process was 3–4 steps and involved reacting glycolaldehyde, cyanamide, glyceraldehyde, and cyanoacetylene to produce CMP at 32–46% yield, and exposing CMP to UV irradiation to obtain UMP. The key product of the first step in this process is 2-aminooxazole (an amino group ($-NH_2$) attached to an oxazole ring), which has also been produced by radiating solutions of HCN [39]. Most recently, Becker et al. [66] have synthesized the pyrimidine nucleosides and nucleotides by exposing cyanoacetylene, hydroxylamine, urea, metal ions, ribose and phosphate-containing minerals to wet-dry cycles akin to WLPs (yields not reported). Finally, the DNA nucleosides have also been recently synthesized by reacting nucleobases with acetaldehyde and sugar-forming precursors (glyceraldehyde, formaldehyde) [67].

With respect to self-replicating ribozymes, a pair of cross-replicating ribozymes were discovered that catalyze each other's synthesis [60]. Specifically, these ribozymes could combine two strands of RNA in the environment to produce their complimentary ribozyme. Their complimentary ribozyme could then combine two strands of RNA in the environment to reproduce the original ribozyme. Another ribozyme was discovered that can synthesize its own ancestor [59]. These ribozymes aren't quite self-replicating, but they do demonstrate genetic systems in the complete absence of proteins or other biological materials.

Hydrothermal vents have much larger hurdles to overcome with regard to synthesizing information polymers. The largest issue here is that the metabolisms imagined to have emerged in these environments are still at a theoretical stage and have not been experimentally tested [55–57, 68, 69]. Dave Deamer often uses the words of Karl Popper [70] when critiquing the hydrothermal vent scenario, that a hypothesis must be capable of being falsified [71].

Because there has been no experimental demonstration of emergent metabolism in hydrothermal conditions, there has been little success at demonstrating a route to information polymers in these environments. Information molecules do not polymerize in aqueous solution unless their monomers are chemically activated, and even this is difficult in solutions simulating the salinity, pH, and elemental composition of hydrothermal vents. The general logic is that the phosphodiester bond that links two RNA monomers together requires a condensation reaction where a molecule of water is removed, and this reaction is thermodynamically uphill in conditions with high water activity [51]. One way to activate nucleotide monomers is through metabolic pathways to synthesize ATP [51]. Another is to introduce an imidazole ester "leaving group" to the nucleotide [72]. Experiments simulating RNA polymerization from unactivated nucleotides in hydrothermal vent environments have only succeeded at synthesizing polymers up to 3 units in length [73, 74]. Burcar et al. [74] also tried to polymerize RNA using imidazole-actived nucleotides in hydrothermal-simulated conditions, and were only able to synthsize up to tetramers (4 nt). These lengths fall short of the 65–187 nt ribozymes used in the lab to demonstrate catalytic replicative activity [59–62].

1.1.2 The RNA World

The WLP hypothesis for the origin of life is most commonly based on the so-called RNA world [75–80]. First proposed by Alex Rich and popularized by Walter Gilbert in the 1980's, the RNA world is a hypothetical evolutionary stage of life between non-living biomolecules and the DNA/RNA/protein world that operates in all living organisms today. During this stage, RNA acted as both the information and the enzymatic activity needed for life; roles that have now been usurped by DNA and proteins, respectively.

The main reasons why the RNA world is so widely accepted are:

1. Long (>300 monomer) chains of RNA form when exposing ribonucleotides to wet-dry cycles representative of WLP environments, suggestive of a prebiotic route to the RNA world. There is no analogous prebiotic route to DNA or peptides (i.e. amino acid polymers).
2. RNA is capable of acting as information polymer, when unfolded, and enzyme for copying (ribozyme), when folded (see Figure 1.3). DNA is a more stable information polymer than RNA, and proteins are much more sophisticated enzymes than ribozymes, suggesting a logical evolutionary path from an RNA world to the DNA/RNA/protein world of today.
3. Evolution tends to maintain ancestral traits. This may be why RNA still plays a large role in life today (e.g. ribosomal RNA, messenger RNA, transfer RNA). Certain RNA viruses are also thought to be vestiges of an prebiotic world [81].

There has been some discussion about the possibility of a simultaneous origin of RNA and DNA [83, 84]. The main motivation behind this additional hypothesis is that RNA is too “sticky” and doesn’t easily separate after a complementary strand is copied onto a template. A strand composed of part RNA, part DNA on the other hand, may get around this problem [83].

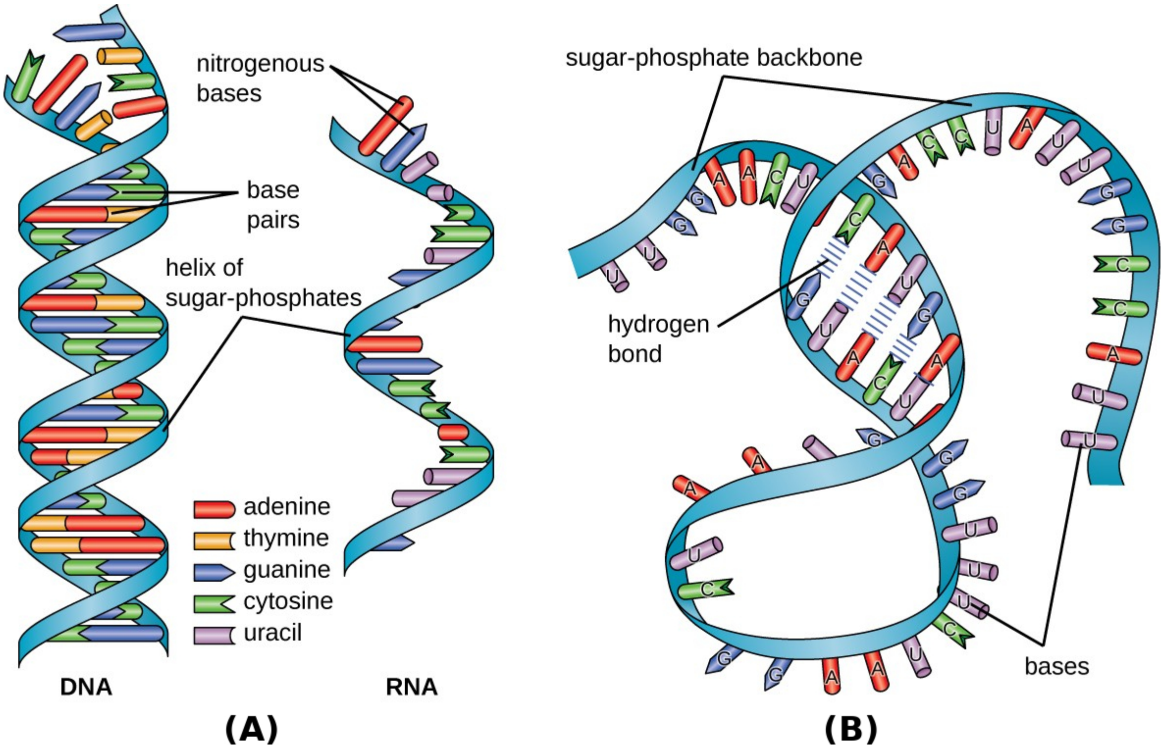

Figure 1.3: **(A)** DNA and RNA as unfolded information templates for copying. **(B)** RNA in a folded (catalytic) state. RNA is made up of ribonucleotide building blocks, which are further subdivided into the nucleobase base-pairing component and the ribose-phosphate backbone. When RNA is folded, it can exhibit catalytic behavior such as synthesizing other RNA molecules from an unfolded template. Sources: [82].

1.1.3 Sources of RNA building blocks

Before RNA could polymerize and form ribozymes in WLPs, the building blocks of RNA would need to become present in these environments. The question of how RNA building blocks got there is the guiding motivation for this thesis work.

Chyba & Sagan [25] were the first to try to narrow down the origin of biomolecules on early Earth's surface by compiling estimates of organic carbon influx rates from various sources including lightning, UV radiation, coronal discharges, atmospheric shocks, meteorites, and interplanetary dust particles (IDPs).

They divided these sources into three categories:

1. Extraterrestrial sources (meteorites, interplanetary dust, comets),

2. Production driven by impact shocks, or

3. Production driven by other energy sources (lightning, UV radiation)

It is also useful to use this categorization when thinking about the potential origins of RNA building blocks. However, it is important to specify that category three produces HCN in atmospheres, and the actual RNA building blocks themselves are formed when this HCN enters WLPs [17, 36, 85].

Here we describe each of these sources as they pertain to the origin of RNA building blocks in more detail.

1.1.3.1 Extraterrestrial sources

In Figure 1.4, we display the two major extraterrestrial sources of the building blocks of RNA: carbon-rich meteorites, and interplanetary dust particles (IDPs).

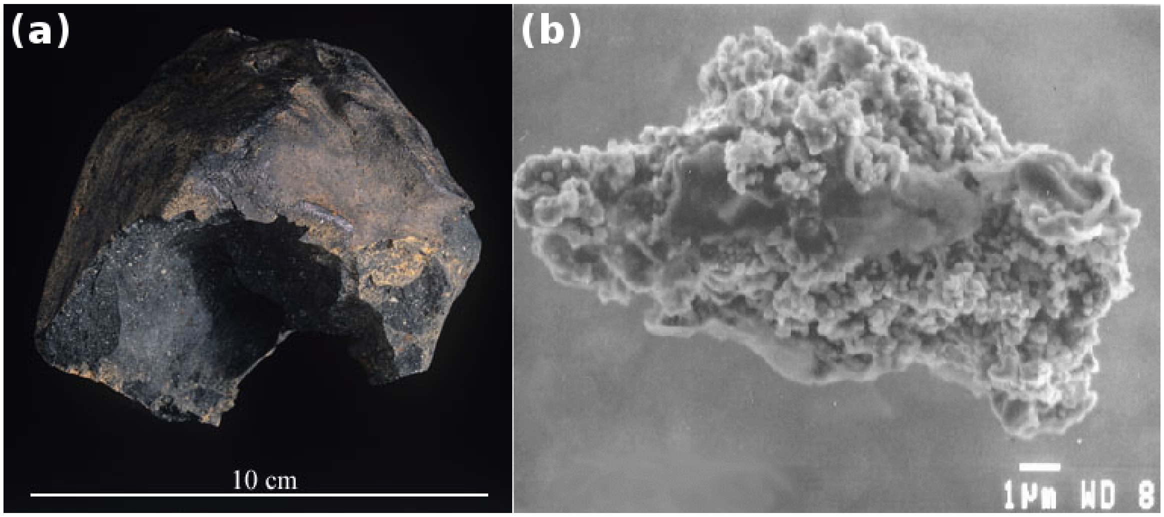

Figure 1.4: **(a)** The Murchison meteorite, a carbon-rich meteorite containing various biomolecules including 3 of the 4 nucleobases in RNA. It fell to the surface in 1969 near Murchison, Victoria, Australia. **(b)** An interplanetary dust particle under microscope. These particles are collected in Earth's atmosphere, usually by airplane. Sources: [86, 87].

Carbon-rich meteorites collected on Earth's surface have been analyzed for organics, and have been found to carry a vast inventory of different biomolecules, including nucleobases [88, 89], amino acids [90, 91], sugars [92, 93], and fatty acids [94, 95]. The isotopic and chiral compositions of these biomolecules suggests that they are indigenous to the meteorites, and are low in contaminant [89, 91, 95].

In my undergraduate thesis [96], we performed thermodynamic simulations of nucleobase synthesis in meteorite parent bodies and compared the distributions of these biomolecules for various reactions with those in meteorite samples. From these analyses, we determined that nucleobases are mainly produced via two pathways: 1) Fischer-Tropsch synthesis, a gas-state reaction involving CO, H_2, NH_3 and a mineral catalyst, and 2) aqueous HCN-based reactions [97].

There have been no biomolecule analyses of IDPs; however, time-of-flight secondary ion mass spectrometry has been performed on IDP samples to measure elemental abundances, and some IDPs have elemental ratios similar to carbon-rich meteorites [98]. Furthermore, laboratory experiments have produced all five nucleobases on the surfaces of icy interplanetary dust analogous containing pyrimidine or purine through exposure to UV radiation [99, 100]. Ribose has also been synthesized by irradiating icy grains containing methanol, water and ammonia [101].

In Pearce et al. [31], we developed a comprehensive numerical model to determine the fate of nucleobases in WLPs from meteorite and IDP sources. When nucleobases enter the pond, they are faced with various destructive sinks including hydrolysis, UV photodissociation, and seepage (through pores in the base of the pond). The pond also has seasonal wet-dry cycles driven by the balance of precipitation, evaporation and seepage. The model is summarized visually in Figure 1.5.

From these models, we found that carbon-rich meteorites were a plausible source of ppm–ppb-level concentrations to WLPs on early Earth for up to a few years, but that IDPs delivered negligible concentrations. A finite supply of nucleobases, such as what would be delivered during a meteorite deposition, would need to react and polymerize quickly (within a few years) in order to survive in WLPs.

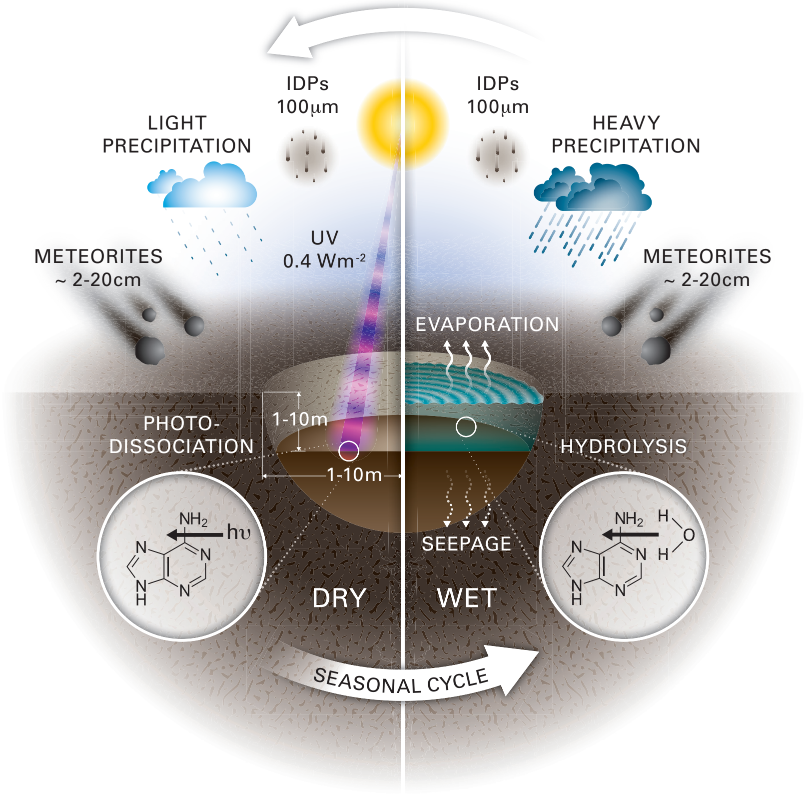

Figure 1.5: Summary of our sources and sinks numerical warm little pond model. Nucleobase sources are meteorites and IDPs, and sinks are hydrolysis and seepage in the wet phase, and UV photodissociation in the dry phase. For water, precipitation is the only source, and evaporation and seepage are sinks. Source: [31].

1.1.3.2 Production driven by impact shocks

Very large planetesimals such as an asteroids or a comets cannot be slowed to terminal velocity by the atmosphere, resulting in hypervelocity impacts [25, 102]. These impacts result in high-energy density shocks that vapourize the impactor and are favourable for gas-state organic synthesis [103–106].

Ferus et al. [105, 106] produced all five nucleobases as well as ribose in experiments simulating the conditions of a hypervelocity asteroid descent and impact. In particular, they mimicked the plasma conditions from these high-energy events by irradiating formamide and formaldehyde ice samples with a high-power laser.

The big question with impact shock synthesis of RNA building blocks, is whether the building blocks will survive in the environment while the post-impact area cools. These building blocks would need to remain localized to eventually concentrate in

WLPs. Like meteorites, this RNA building block source is also finite, as a subsequent hypervelocity impact in a WLP environment would destroy the pond and reset the process.

1.1.3.3 Production driven by other energy sources

This last category is the process by which a biogenic planet would produce the biomolecules for life, and is the focus of this thesis. To summarize the steps: UV radiation-driven chemistry in the upper atmosphere, and lightning-driven chemistry in the lower atmosphere produces HCN [85, 107]. This HCN, being water soluble, dissolves in rain droplets and lands in WLPs [107]. UV-based aqueous chemistry then proceeds in WLPs to produce the building blocks of RNA, including nucleobases, ribose, and 2-aminooxazole [9, 37–40, 42].

Unlike meteorites and production by impact shocks, these sources provide a steady supply of precursor HCN to WLPs as long as the atmospheric composition is favourable for HCN production via these energy sources. In the following section, we outline the physical and chemical processes related to atmsopheric HCN production in detail.

1.2 HCN Production in Atmospheres

HCN is a fairly common atmospheric species whenever methane is present. For example, the richest HCN atmosphere in the Solar System—belonging to Saturn's moon Titan—has a CH_4 composition of ∼5.7% [108]. With such a large supply of methane, Titan produces ∼0.1–10 ppm HCN in the lower atmosphere (<600 km) and ∼0.01–0.5% HCN in the upper atmosphere (>700 km)—as measured by instruments aboard the Cassini spacescraft [109–112].

The New Horizons spacecraft performed UV solar occultation measurements as it flew by Pluto in 2015, and this data suggested its atmosphere was roughly 0.25% CH_4 [113]. A couple years later, ∼40 ppm HCN was observed in Pluto's atmosphere with the Atacama Large Millimeter/submillimeter Array (ALMA) [114]. Baines et al. [115] used a combination of observations performed by the International Ultraviolet Explorer spacecraft and ground-based spectrometers to determine Neptune's CH_4 content at ∼3%, and Karkoschka & Tomasko [116] used the spectrometer aboard the Hubble spacecraft to determine Uranus has ∼2% CH_4. Observations by the James

Clerk Maxwell Telescope detect HCN on these worlds with abundances of ∼1 ppb, and <0.1 ppb, respectively [117].

Methane has also potentially been detected on Mars. The Tunable Laser Spectrometer aboard the Curiosity rover measured background CH_4 abundances of ∼0.4 ppb [118]; however, these measurements have recently come into question [119] given that the ExoMars Trace Gas Orbiter did not detect any atmospheric methane [120]. The only HCN measured on Mars is from samples of mudstone and aeolian deposits taken from the surface, at 2-40 nmol [121]. It remains unclear whether atmospheric methane and HCN are present in detectable levels on Mars.

In terms of exoplanets, HCN has been tentatively detected in the atmospheres of 55 Cancri e [122] and WASP-63b [123] using the WFC3 camera aboard the Hubble telescope. However, the absorption signals corresponding to CH_4 are undetermined or hidden below the HCN absorption on these worlds.

Models of HCN production in hypothetical exoplanet atmospheres have shown that HCN is most readily produced in atmospheres rich in CH_4, but that CH_4 isn't a requirement for HCN production. For instance, an atmosphere rich in C_2H_2 can also lead to rich HCN production, and a CO atmosphere can even produce modest > ppm amounts of HCN [124]. In general, these models suggest free availability of N_2 and a C/O ratio ≥ 1 are the key requirements for efficient HCN production.

Atmospheric models of HCN production in early Earth's atmosphere have also noted the dependence of CH_4 abundance on HCN production [107, 125]. The reason for this dependence is that atmospheric HCN is mainly produced from reactions involving methane and nitrogen radicals [36, 126]. These radicals form when an energy source breaks apart stable CH_4 and N_2, leaving behind reactive species such as CH_3, $^3CH_2$, $^1CH_2$, CH, H, ^4N and ^2N.[1] Examples of input energy are: UV radiation, lightning, galactic cosmic rays (GCRs), the solar wind, impacts, and heat. For atmospheric temperatures $\gtrsim$ 1000 K, the chemistry of HCN can be approximated using thermodynamic equilibrium models [127, 128]; however, for cooler atmospheres such as early Earth and Titan, a chemical kinetics approach is required to model the non-equilibrium processes involved in producing HCN [107, 124–126, 129–133].

---

[1] The superscript in front of the molecular or atomic species refers to the spin state. For example, ^4N, or quartet nitrogen, is the ground state for nitrogen atoms. This is the state where the $2p_x$, $2p_y$, and $2p_z$ orbital electrons are all unpaired and aligned (all ↑ or all ↓). Doublet nitrogen, ^2N, is a higher-energy excited state, where one of the 2p electrons is anti-aligned and paired with another 2p electron.

1D atmospheric chemical kinetics models compute the change in abundance (i.e. molar mixing ratio) of each molecule in a chemical network as a function of location (atmospheric layer) and time. The chemical network is a collection of reaction rate coefficients which describe the frequency at which each reaction occurs as a function of temperature and pressure. Because chemical kinetics models are time-dependent, they can be coupled with other time-dependent atmospheric processes including: photochemistry, GCRs, turbulent mixing, diffusive mixing, lightning chemistry, outgassing, rain-out and hydrodynamic escape from the upper atmosphere. Presently, atmospheric chemical kinetics models are limited to being run with a static pressure-temperature profile under the assumption that it does not change drastically over the course of the simulation. This is a topic for future work that will be discussed in more detail in Chapter 6.

In the perfect scenario, all the rate coefficients in a chemical network would come from experimental measurements performed over a range of temperatures and pressures. However, such experiments are time consuming and are not yet complete for the breadth of reactions, temperatures, and pressures occurring in planetary atmospheres. An alternate source of rate coefficients is to calculate theoretical values using quantum computational chemistry methods (e.g. [134–136]). Quantum chemistry simulations of small molecular systems (e.g. 2–12 atoms) only take hours to complete on a computer cluster, and one can explore a large range of potential reactions simultaneously. This approach often leads to discovery of new reactions that were previously unknown in the literature. In this thesis, we develop such quantum chemistry methods, and uncover 93 reactions relevant to HCN and H_2CO chemistry in terrestrial planetary atmospheres that were previously missing from the literature. We validated our methods on hundreds of reactions that have experimental measurements, and found our calculations are most often within a factor of 2 of experimental values and generally always within an order of magnitude of these values. This accuracy is consistent with the typical uncertainties assigned in large scale experimental rate coefficient evaluations (e.g. Baulch et al. [137]).

1.2.1 Calculating Atmospheric Rate Coefficients using Computational Quantum Chemistry

A large portion of this PhD thesis involves computing reaction rate coefficients for HCN and formaldehyde (H_2CO) chemistry in planetary atmospheres (Chapters 2–4). In this section, I will give a brief overview of computational quantum chemistry, and the methods we use to calculate rate coefficients for atmospheric chemical kinetics modeling.

The basis of computational quantum chemistry methods is to solve the Schödinger Equation (Equation 1.1) for a system of particles that interact by Coulomb attraction and repulsion forces. Because the nuclei are much heavier than electrons, they move much slower and appear stationary to the electrons. For this reason it is convenient to separate the motion of the nuclei and the electrons [138]. This is known as the Born-Oppenheimer (B-O) approximation and is fundamental to computational quantum chemistry.

$$\hat{H}\Psi = E\Psi \tag{1.1}$$

$\hat{H}$ represents the molecular Hamiltonian, Ψ represents the wavefunction and E represents the energy. The molecular Hamiltonian can be broken into five components.

$$\hat{H} = -\frac{1}{2}\sum_{i=1}^{N}\nabla_i^2 - \frac{1}{2}\sum_{A=1}^{M}\frac{1}{M_A}\nabla_A^2 - \sum_{i=1}^{N}\sum_{A=1}^{M}\frac{Z_A}{r_{iA}} + \sum_{i=1}^{N}\sum_{j>i}^{N}\frac{1}{r_{ij}} + \sum_{A=1}^{M}\sum_{B>A}^{M}\frac{Z_A Z_B}{r_{AB}} \tag{1.2}$$

The first term represents the electronic kinetic energy, the second term represents the nuclear kinetic energy, the third term represents the electron-electron repulsion, the fourth term represents the nuclear-electron attraction, and the last term represents the nuclear-nuclear repulsion. M, Z, and r represent mass, atomic number, and separation, respectively. Electron indicies are from i or j to N and nucleus indicies are from A or B to M. Atomic units are used in this form of the equation for simplification (e.g. $\hbar = 1$). In practice, using the B-O approximation means the second term is gone, i.e., the nuclear motion is effectively zero, and the last term, the nuclear-nuclear repulsion, is a constant.

For our purposes, we focus on a particular method which provides an approximate solution to the Schödinger Equation known as density functional theory (DFT), developed by Pierre Hohenberg, Walter Kohn, and Lu Jeu Sham in 1964–1965 [139, 140]. DFT is widely used in the field of physics. An analysis of citation data showed DFT was the most active field in physics during 1980–2010, claiming 8 of the top 10 most cited physics papers [141]. The underlying principle of DFT is that each of the electronic terms in the Schödinger Equation above is a functional (i.e. a function of another function) of the electron density. The electron density ($\rho(\vec{r})$) is the probability of finding any of the N electrons in the volume element $\vec{r}$. The process of a DFT algorithm is to use an initial guess for $\rho(\vec{r})$ to solve for the potential energy terms and the wavefunction. From these parameters, a new density is calculated from the quantum mechanical expectation value (Equation 1.3), and the process is repeated until convergence [142].

$$\rho(\vec{r}) = \sum_{i=1}^{N} f_i |\Psi(\vec{r})|^2 \tag{1.3}$$

f_i is the occupation number for orbital i.

Using $\rho(\vec{r})$ to obtain an approximate solution to the Schödinger Equation greatly speeds up numerical computations, as electron density is only a function of x, y and z, whereas methods that deal with the many-body electronic wavefunction have to keep track of 3N variables—where N is the number of electrons in the system. DFT is ideal for our purposes, as it combines high computational efficiency with very good physical accuracy [143, 144], allowing us to explore and calculate rate coefficients for a dozen or so reactions a day.

Calculating rate coefficients using DFT is based on a technique known as transition state theory (TST). The main concept of TST is that the frequency of a reaction is characterized by the size of the energy barrier in transitioning from reactants to products. In practice, this involves finding the highest energy point along a minimum energy path (MEP) between the reactant and product geometries. A handy way to visualize the principles of TST is to use a potential energy surface (see Figure 1.6). The x and y coordinates represent the distances and/or angles that describe the structure for the reaction, and the z coordinate represents the potential energy. In order for a reactant structure to leave its minimum energy well, it must overcome an energy barrier corresponding to a transition state structure. On the other side of the transition state, is another minimum energy well representing the product structure. Knowledge of the transition state for a reaction provides us with the statistical mechanical data necessary for calculating the rate coefficient.

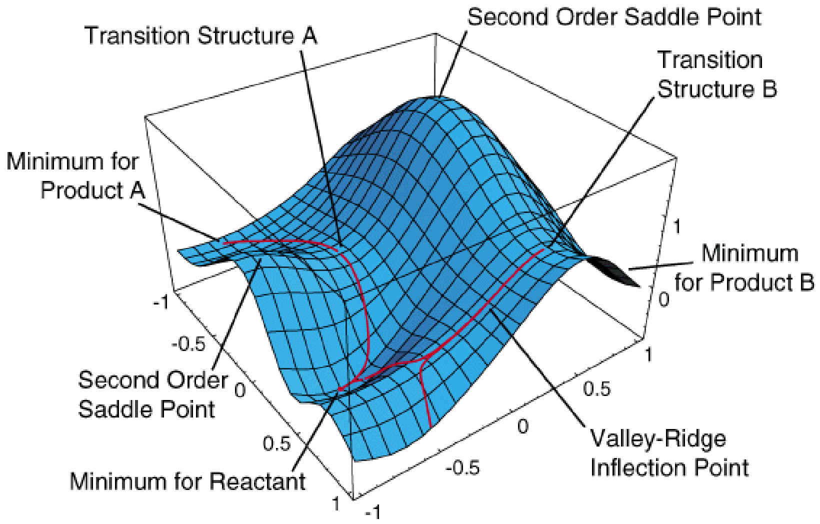

Figure 1.6: A visualization of the potential energy surface for a reaction. The reactant structure is at a minimum, and must overcome a transition barrier to change to another low energy structure by traveling along a minimum energy path (red lines). Source: [145].

In Figure 1.7, we show the change in structure for the reaction $CH_4 + CN \longrightarrow CH_3 + HCN$ as it travels along the MEP through its transition state. Finding the transition state for this reaction involves freezing the bond distance between "H2" and "C1" at different intervals, and then using DFT to optimize each geometry to the lowest energy structure to obtain points along the MEP. We use the maximum Gibbs free energy criterion (instead of maximum total energy) as this method offers a compromise of energetic and entropic effects, and can be used for reactions without energy barriers (i.e. only entropic barriers) [146, 147]. In Figure 1.8, we can see the transition state for $CH_4 + CN \longrightarrow CH_3 + HCN$ corresponds to a C-H distance of 1.86Å.

With the data from the DFT simulations of the transition state at a chosen temperature, we can plug the energies and partition functions into the statistical mechanical rate coefficient equation, originally developed by Henry Eyring, Meredith Gwynne Evans, and Michael Polanyi in 1935 [149, 150]

$$k_{GT}(T,s) = \sigma \frac{k_B T}{h} \frac{Q^{\ddagger}(T,s)}{\prod_{i=1}^{N} Q_i^{n_i}(T)} e^{-E_0(s)/RT}, \tag{1.4}$$

where σ is the reaction path multiplicity, k_B is the Boltzmann constant (1.38×10^{-23}

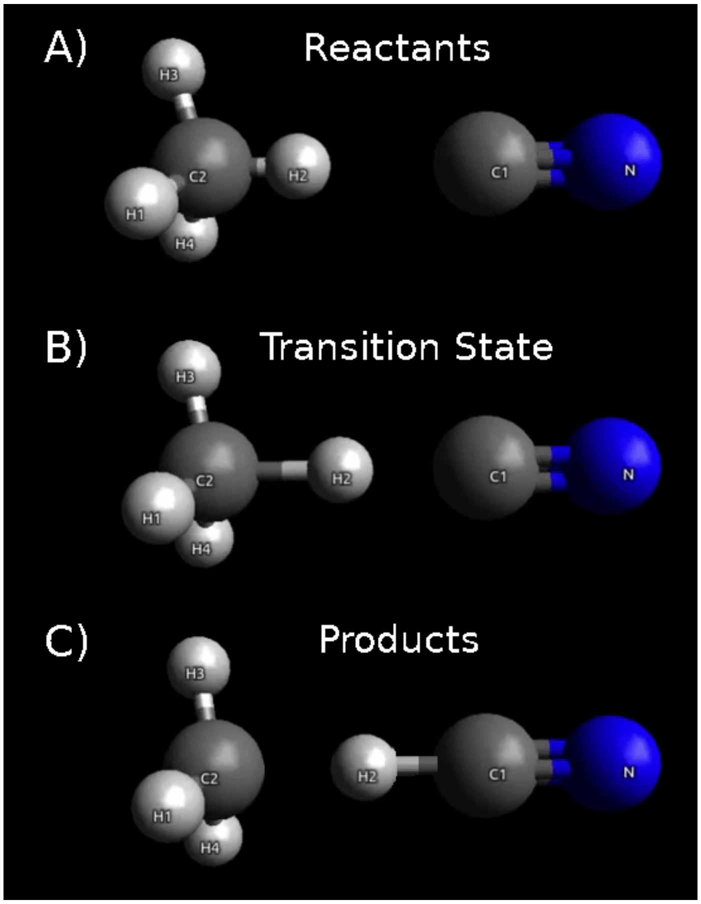

Figure 1.7: A visualization of the minimum energy path between reactants (CH_4 + CN) and products (CH_3 + HCN), through the transition state. Made using Avogadro open-source chemistry visualization tool [148].

J K^{-1}), T is temperature (K), h is the Planck constant (6.63×10^{-34} J·s), $Q^{\ddagger}$ is the partition function of the transition state per unit volume (cm^{-3}), Q_i is the partition function of reactant species i per unit volume, n_i is the stoichiometric coefficient of species i, N is the number of reactant species, E_0 is the difference in zero-point energies between the transition state and the reactants (kJ mol^{-1}) (0 for barrierless reactions), and R is the gas constant (8.314×10^{-3} kJ K^{-1} mol^{-1}).

The frequency at which a reaction occurs is dependent on the probability of the system being in the transition state versus the probability of the system being in the reactant state. These probabilities are characterized by the partition functions. Because classical partition functions involve integrating over the Boltzmann factor ($e^{-E/RT}$), an additional exponential factor appears naturally in the equation due to

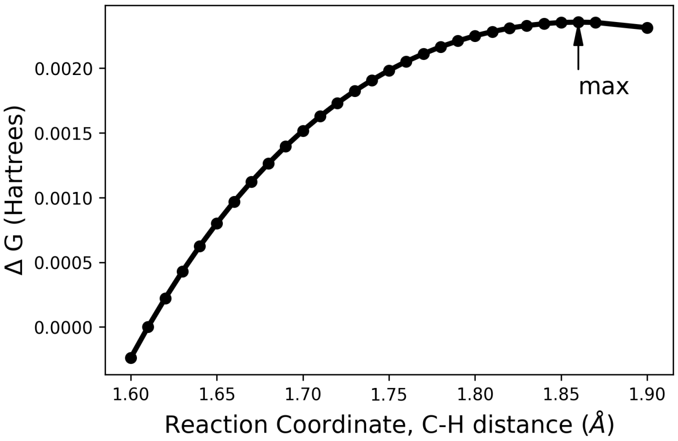

Figure 1.8: Gibbs free energies along the minimum energy path for the reaction $\mathrm{CH4} + \mathrm{CN} \longrightarrow \mathrm{CH3} + \mathrm{HCN}$.

the difference in zeros of energy between the transition state and reactant states.

Additional simulations are performed for reactions with pressure dependence. An example pressure-dependent reaction would be $\mathrm{CN} + \mathrm{H} + \mathrm{M} \longrightarrow \mathrm{HCN} + \mathrm{M}$, where M is a atmospheric species that collisionally stabilizes HCN. In the absense of a third body, the product would vibrationally decay back into the reactants. We perform collisional Monte Carlo simulations employing Rice–Ramsperger–Kassel–Marcus/master equation (RRKM/ME) theory [151] in order to determine the relation between pressure and the probability of reaction products becoming collisionally stabilized.

We refer the reader to Chapters 2, 3, and 4 for complete details of the theoretical and computational quantum methods used to calculate rate coefficients.

1.2.2 Physical processes in atmospheres

A key connection between physics and chemistry in planetary atmospheres is radiative transfer. Radiation interacts with molecules in the atmosphere via absorption and scattering, and breaks down molecular species via photodissociation processes.

In order to compute photochemistry, 1D atmospheric chemical kinetics models keep track of radiation emitted by and passing through the atmospheric layers. Radiative transfer is set up via the two-stream equations for upward and downward flux [152]

$$\frac{d}{d\tau_\nu} I_+ = -I_+ + \pi B(\nu, T(\tau_\nu)) \tag{1.5}$$

$$\frac{d}{d\tau_\nu} I_{-} = I_{-} - \pi B(\nu, T(\tau_\nu)) \tag{1.6}$$

where, for a layer of optical thickness τ_ν at frequency ν, the first terms on the right hand side represent absorption of incoming radiation I by the atmospheric layer, and second term, $B(\nu, T(\tau_\nu))$ is the Planck function to represent emission by the atmospheric layer in local thermodynamic equilibrium (LTE).

The absorption of radiation is controlled by the opacity κ, which is related to τ via [152]

$$\frac{d(\tau_\nu cos\theta)}{dp} = -\frac{1}{\kappa} g, \tag{1.7}$$

where θ is the angle of propagation relative to the vertical, p is pressure and g is gravitational acceleration.

Typical assumptions for 1D radiative transfer codes are that the atmosphere is plane-parallel (i.e. no curvature), that the layers are in LTE, that the average intensity is described by the Eddington approximation (i.e. near-isotropic radiation), that the atmosphere is at steady state in terms of atmospheric pressure (i.e. chemistry only affects mixing ratios), and that the atmosphere is “grey” (i.e. the opacity across all wavelengths is calculated as the Rosseland mean opacity) [152].

Our models also include Rayleigh scattering, which is radiation emitted by an atmospheric particle oscillating as a dipole. Essentially, incident radiation has an electric field and can cause opposite charges on a molecule to migrate to opposite ends. This induced dipole moment oscillates at the same frequency as that of the incident wave [152]. Rayleigh scattering is an elastic process; therefore, the energy created due to scattering is lost by the incoming beam. The cross-section for Rayleigh scattering is

$$\chi_{sca} = \frac{8\pi}{3} \frac{2\pi}{\lambda}^4 \alpha_p^2, \tag{1.8}$$

where λ is the wavelength of light, and α_p is the polarizability constant of the scattering molecule. Rayleigh scattering dominates at the blue and violet end of the visible spectrum, which is the cause of our blue skies. The Rayleigh scattering cross-section is included in the optical depth, and terms are added to the two-stream equations to account for the scattering source.

The main reason to include radiative transfer in chemical kinetics models is to calculate photochemistry, i.e. the dissociation of molecules into their fragments. In the code, this is handled by the wavelength-dependent absorption cross-sections, and the branching coefficients for each decay pathway. Absorption cross-sections are typically measured in the laboratory and cover the extreme ultra-violet (EUV) and UVC range i.e. ∼1–280nm [153]. Radiation at these wavelengths attenuates as it propagates towards the surface from the top of the atmosphere; therefore, for typical terrestrial atmospheres that are optically thick at these wavelengths ($P_{surf} = 1$ bar), photochemistry is predominantly an upper atmospheric process.

Photodissociation can be generally broken down into non-ionization and ionization processes. When the energy of the absorbed photon is below the ionizing energy for a molecular species, an electronic transition occurs from the ground state to an excited state. This transition is "instantaneous" with respect to nuclear motion, therefore the molecule does not change shape during excitation. In terms of Figure 1.6, this can be visualized as maintaining the position on a potential energy surface, but changing the landscape below it. The position of the molecule on the new excited-state landscape is not always going to be near a stable minimum. In some cases, it will find itself on the steep slope leading to one of the dissociation minima for that species [154].

Alternately, if the absorbed photon is high enough energy to ionize the molecule, the ionized species can undergo dissociative recombination. This is the main mechanism for N_2 dissociation at wavelengths below ∼ 80 nm [36, 155]. The two step process is as follows

$$N_2 + h\nu \longrightarrow {N_2}^+ + e^- \tag{1.9}$$

$$ {N_2}^+ + e^- \longrightarrow {}^4N + {}^2N \tag{1.10}$$

where the ^{4} and ^{2} superscripts represent the ground (quartet) and excited (doublet) spin states for the nitrogen atom.

The other sources of energy that dissociate molecular species in the atmosphere like galactic cosmic rays (GCRs) and lightning are not dependent on radiative transfer. GCRs are small ions like protons that precipitate down and collide with molecules in the upper atmosphere to produce a secondary shower of electrons. This secondary shower propogates to the lower (denser) region of the atmosphere and excites and ionizes molecules, which leads to dissociation in a similar way to photochemistry [156, 157]. GCRs are particularly important for modeling chemistry in the atmosphere of Titan, as the area surrounding Saturn is particularly enriched in GCRs due to the presence of the planet's powerful magnetic field. Instead of doing radiative transfer on a secondary field ("GCR radiation"), we model GCR-based dissociation by inputting fixed molecular destruction rates from models (e.g. [156, 157]) in the area where collisions with the secondary electron shower occur (e.g. similar to [133]).

Finally, lighting produces a great deal of thermal energy along the ion channel (T $\simeq$ 30000 K) [158], making collisions between atmospheric gases frequent. These collisions excite or ionize molecules in a similar way as GCR collisions, which leads to dissociation [159] and other high temperature chemistry such as NO production [160]. Because the chemical equilibrium timescale above 10000 K is short (μs) compared to the eddy diffusion timescale ($\sim$10μs) and the cooling time of the lightning channel ($\sim$100 ms), we can calculate the products of lightning chemistry using a thermodynamic approach [161, 162]. These products are then input into the bottom layer of our atmospheres at a rate that corresponds with the model lightning flash density (e.g. 0.3–28.9 flashes km^{-2} yr^{-1} on Earth today [163])

There are two main processes by which molecules move between atmospheric layers: molecular diffusion and eddy diffusion. Molecular diffusion is movement due to the thermal motions of gases, whereas eddy diffusion is movement due to turbulence in the atmosphere (e.g. convection). On top of these sources of movement, there can also be influxes and outfluxes at boundaries due to things like outgassing, rain-out and escape.

In 1D atmospheric chemical kinetics models, the movements of molecules and the chemistry are coupled in what is known as the continuity-transport equation [164]

$$\frac{dn}{dt} = P - nL + D_E\frac{dn}{dz} + D_M\frac{dn}{dz} - D_M n\left(\frac{1}{H_0} - \frac{1}{H} - \frac{\alpha_T}{T}\frac{dT}{dz}\right) + R \tag{1.11}$$

where n is the number density of a certain species (cm^{-3}), P is the production rate of the species (cm^{-3} s^{-1}), L is the loss rate of the species (s^{-1}), D_E is the eddy diffusion coefficient, D_M is the molecular diffusion coefficient, H_0 is the mean scale height, H is the molecular scale height, T is the temperature (K), α_T is the thermal diffusion factor and R describes the influx/outflux for the molecule if it's at a boundary (cm^{-3} s^{-1}). The second last term represents the advective (bulk motion) component of molecular transport.

In Figure 1.9, we display a range of eddy diffusion profiles (D_E) and the methane molecular diffusion profile (D_M) used in atmospheric chemical kinetics models of Titan's atmosphere. Note how in the lower atmosphere, molecular diffusion is negligible in comparison to turbulent mixing. In the uppermost atmosphere, molecular diffusion takes over as the dominant mode of molecular movement. This is because molecular diffusion is inversely proportional to density, whereas turbulence is most prominent in the high-pressure convective regions of atmospheres.

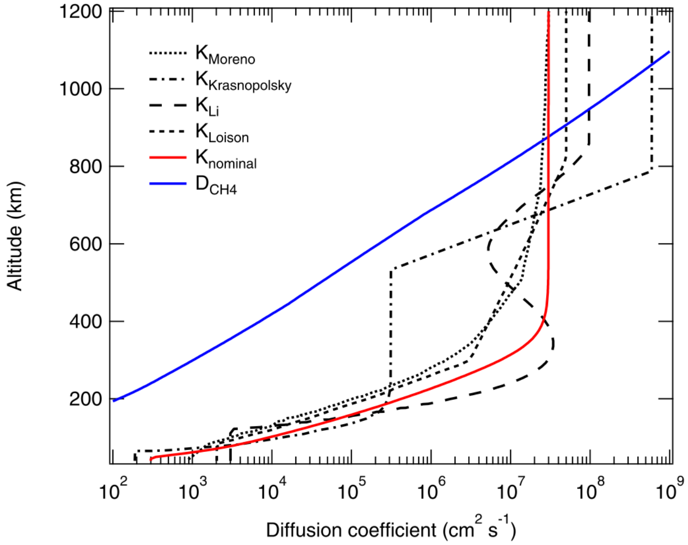

Figure 1.9: Various eddy diffusion profiles employed by atmospheric chemical kinetic models of Titan's atmosphere, as well as the methane molecular diffusion profile for comparison. Source: [130].

The R term in the continuity-transport equation can describe inflows and outflows at the surface or top-of-atmosphere (TOA). Hydrodynamic escape is a common outflow for models of atmospheres containing hydrogen gas (e.g. Zahnle et al. [129, 165]). This process occurs when the upper atmosphere absorbs solar soft X-ray (XUV) and far ultraviolet (FUV) radiation, warms up, and expands, pushing gas upward. As the gas rises, it accelerates smoothly through the speed of sound until it reaches to escape velocity [166].

The hydrodynamic escape of hydrogen can be modeled as diffusion-limited or energy-limited, depending on the amount of XUV and FUV radiation incident on the TOA. In the high XUV and FUV regime, molecules at the top of the atmosphere are cleared out efficiently upon absorption, and the bottleneck for the escape of hydrogen to space becomes the upwards diffusion of gases through the upper atmosphere. In the low XUV and FUV regime, the bottleneck is the amount of radiation incident on the top of the atmosphere. Zahnle et al. [165] developed a model that blends the energy-limited escape with the diffusion-limited escape as a function of XUV/FUV flux. They fit their model to the following equation, which we use in our early Earth models.

$$\left(\frac{dN_{H_2}}{dt}\right)_{esc} = -\frac{AS}{\sqrt{1+B^2S^2}}\frac{N_{H_2}}{\Sigma_j N_j}(cm^{-2}s^{-1}) \tag{1.12}$$

where A = 2×10^{12} cm^{-2} s^{-1}, $B^2 = 0.006$, S is the XUV and FUV irradiation relative to modern Sun, N_{H_2} is the number of H_2 molecules, and N_j is the number of molecules of species j. The maximum hydrogen escape rate (i.e. $\frac{N_{H_2}}{\Sigma_j N_j} = 1$) for early Earth XUV and FUV fluxes is $\sim10^{13}$ cm^{-2} s^{-1}. We use H_2 impact degassing rates that are below the maximum H_2 escape rate in order to maintain the validity of the static pressure assumption of our atmospheric models.

Near the bottom of the atmosphere, where rain clouds form, water-soluble species dissolve in rain droplets and fall to the surface. The velocity at which species rain-out of the atmosphere is roughly dependent on their solubility [107, 167]. For example, the Henry's law constant for HCN is ∼12 M atm^{-1}, which is approximately 2 orders of magnitude lower than the Henry's law constant for H_2CO of ∼3400 M atm^{-1} [168, 169]. Similarly, HCN rain-out is typically paramaterized with a deposition velocty of 7×10^{-4} cm/s, which is approximately 2 orders of magnitude lower than the deposition velocity for H_2CO (0.1 cm/s) [107, 164]. In the case of a planet with a large liquid reservoir such as an ocean, the flux of evaporation at the surface dominates over rain-out. This is because H_2O from the troposphere is efficiently removed by tubulent mixing and photochemistry, preventing H_2O levels from reaching the saturation vapour pressure. We include ocean-atmosphere coupling in our early Earth models (Chapter 5) by providing a contant influx of H_2O at the surface. In our Titan models, we include H_2O influx at the TOA to represent water delivered by micrometeorites, as this is the dominant source of water on Titan [133].

We also include surface influxes in our early Earth models representing the main sources of the key atmospheric species during the Hadean eon (∼4.5–3.9 bya), i.e. H_2, CO_2, and CH_4.

The main source of H_2 on early Earth is impact degassing [129]. When iron-rich asteroids impact the surface and vapourize, iron is oxidized by water in the reaction

$Fe + H_2O \longrightarrow FeO + H_2$. Fits to the lunar cratering record suggest that the impact bombardment rate declined linearly from 4.5 to 3.9 bya. This suggests that impact degassing was a rich source of H_2 early after the planet became habitable, and became less abundant over time.

Analyses of the oxidation state of ∼4.35 bya zircons suggests that the early mantle was already oxidized by this time. In this case, the main outgassed species from volcanoes through most of the Hadean was CO_2 rather than H_2 and CH_4 [170]. More recent works analyzing younger (∼3.5–3.8 bya) metamorphosed mid-oceanic ridge basalts and komatiitic and picritic systems suggest a slightly less oxidized mantle around this time with a slightly lower proportion of CO_2 to H_2 and CH_4 outgassed from volcanoes during the Hadean eon as compared to today [171, 172].

Finally, the main source of CH_4 depends on the size of impactors during the sustained declining bombardment of the Hadean eon. If there was one or more impactors with a size of the Vesta asteroid or greater (525–2300 km in diameter), then post impact temperatures would be high enough to rapidly produce CH_4 [129]. This scenario is often paired with the Late Veneer Hypothesis (LVH), which suggests that ∼1% of the Earth's mass was delivered after the magma ocean cooled and solidified. The evidence for the LV, is the enrichment of the elemental composition (e.g. Os, Ir, Ru, Rh, Pt, Pd) of the primitive surface from what would be expected after differentiation [173–175].

One issue with having a single Vesta-sized impactor for the LV rather than multiple smaller impactors, is that such large impactors are improbable during the Hadean. The largest lunar projectile was ∼200 km in size—as seen in the cratering record—so it is expected that few objects greater than 300 km would have impacted the early planet [176]. It is also unclear how habitability would evolve in a Vesta-sized LV scenario, and whether WLPs could exist during a high-pressure, methane-rich post-impact phase. Greenhouse effects due to collision-induced absorption [177] and increased atmospheric methane [178] could create global temperatures that are too hot for WLPs. In such a scenario, the methane content may be diluted by the time the atmosphere cools to pond-forming temperatures.

In the absence of such large impactors, the main source of CH_4 is generally thought to be from water-dependent processes in hydrothermal systems. First, serpentinization of Fe- and Mg-rich ultramafic rocks (e.g. olivine) in mid-ocean ridges and forearc systems produces H_2. Then, H_2 reduces the CO_2 in these environments via mineralcatalyzed Fischer-Tropsch synthesis to produce CH_4 [179, 180]. The abiotic reduction of CO_2 is considered to be slow at low temperatures (< 300 °C) given the kinetic barriers to methane production [181]. Field studies of hydrothermal systems suggest abiotic CH_4 is generated in these environments; however, experiments of Fischer-Tropsch synthesis from olivine typically find very low yields [182]. Therefore, the source and abundance of abiotic methane production in hydrothermal systems is still somewhat uncertain.

Considering the dependence of reducing gases such as H_2 and CH_4 on biomolecule production in Miller-Urey experiments [12, 14], the hypothesis in this thesis is that early Earth's best chance for biogenicity was near the beginning of the Hadean eon. At this stage, reducing conditions were driven by a high H_2 impact degassing rate that is in equilibrium with hydrodynamic escape from the TOA. As the bombardment rate declined into the late Hadean, molecules such as N_2, and CO_2 would begin to dominate, shifting the atmosphere to more oxidizing conditions. The main goal of this thesis is to model atmospheric HCN production during these different epochs and to couple HCN rain-out to biomolecule production in WLPs to understand if and when early Earth was biogenic.

1.3 Thesis Outline

The chapters in this thesis will proceed as follows.

In Chapter 2 (Pearce, B. K. D., Ayers, P. W., & Pudritz, R. E. 2019. "A Consistent Reduced Network for HCN Chemistry in Early Earth and Titan Atmospheres: Quantum Calculations of Reaction Rate Coefficients". *J Phys Chem A*, 123, 1861–1873), we develop the initial methods for calculating two-body reaction rate coefficients for atmospheric reactions using quantum chemistry. We do an initial quantum methods comparison analysis on a well-studied reaction using 6 different commonly used quantum methods in order to find the most accurate method for further calculations. We then use the most accurate method from this analysis to calculate a consistent reduced network of 42 reactions for HCN chemistry in early Earth and Titan atmospheres. We validate our method by comparing our calculated rate coefficients with experimental values when available (∼64% of reactions). Fifteen reactions previously unknown in the literature are discovered in this chapter.

Then, in Chapter 3 (Pearce, B. K. D., Molaverdikhani, K., Pudritz, R. E., Henning, Th. & Hébrard, E. 2020. "HCN production in Titan's Atmosphere: Coupling quantum chemistry and disequilibrium atmospheric modeling". *Astrophys J*, 901, 110), we improve the accuracy of our methods for calculating two-body reaction rate coefficients by a factor of ∼2, and develop the methods for calculating three-body reaction rate coefficients as a function of pressure. First, we use these methods to recalculate the original reactions from Chapter 2. Then, in order to leave no stone unturned, we explore the entire field of possible reactions for a list of primary species in N_2-, CH_4-, and H_2-dominated atmospheres. In this effort, we calculate 36 new two-body reactions and 32 new three-body reactions related to HCN chemistry in Titan's atmosphere. Thirty-three of these new reactions were previously unknown in the literature. Next, we develop a consistent reduced atmospheric hybrid chemical network (CRAHCN) containing experimental values when available and our calculated rate coefficients otherwise. We then couple this network with an atmospheric chemical kinetics model to simulate HCN chemistry in Titan's atmosphere. We compare our simulated profile with observations taken by instruments aboard the Cassini spacecraft and find excellent agreement. We also perform sensitivity analyses in order to discover the 19 dominant reactions responsible for HCN production and destruction in Titan's atmosphere and build a complete picture of HCN chemistry in this environment. Finally, we perform a comprehensive quantum methods comparison on 11 of the 19 dominant reactions that have experimental values. We compare the accuracy of 3 commonly used quantum methods and find our initial selection is most commonly the most accurate.

Next, in Chapter 4 (Pearce, B. K. D., Ayers, P. W., & Pudritz, R. E. 2020. "CRAHCN-O: A Consistent Reduced Atmospheric Hybrid Chemical Network Oxygen Extension for Hydrogen Cyanide and Formaldehyde Chemistry in CO_2-, N_2-, H_2O-, CH_4-, and H_2-Dominated Atmospheres". *J Phys Chem A*, 124, 8594–8606), we expand on CRAHCN to include oxygen chemistry so that it is applicable to early Earth's atmosphere containing CO_2, H_2O, and H_2CO. We take a similar approach to Chapter 3, and explore the entire field of reactions for a list of primary species. In this effort, we calculate the rate coefficients for 95 new one- and two-body reactions, as well as 31 new three-body reactions related to HCN and H_2CO chemistry in early Earth's atmosphere. We continue to validate our methods by comparing with experimental values when available. Fourty-five of the new reactions calculated in this work were previously undiscovered in the literature. We identify 6 reactions from this list that are likely to dominate HCN and H_2CO production and destruction in planetary atmospheres containing oxygen species. Finally, we develop the oxygen extension to our consistent reduced atmospheric hybrid chemical network (CRAHCN-O), using experimental values when available, and our theoretical values otherwise. This network can be used to simulate HCN and H_2CO chemistry in atmospheres dominated by any of CO_2, N_2, H_2O, CH_4, and H_2.

All of this work leads to Chapter 5 (Pearce, B. K. D., Molaverdikhani, K., Pudritz, R. E., Henning, Th. & Cerrillo, K. E. 2021. "En route to RNA life: From atmospheric HCN to biomolecule production in warm little ponds", *Nature Astronomy*, submitted), where we couple terrestrial geochemistry, radiative transfer, atmospheric photochemistry, lightning chemistry and aqueous pond chemistry to determine if and when early Earth was biogenic. First, we employ two specially developed atmosphere codes and the CRAHCN-O network to develop a self-consistent chemical kinetics model for the production and rain-out of HCN in early Earth's atmosphere. Then, we couple the rain-out of HCN at two different epochs (4.4 and 4.0 Ga) to our comprehensive numerical model of warm little ponds developed during my M.Sc. to compute the *in situ* production of the building blocks of RNA. These epochs differ in composition (reducing versus oxidizing conditions), luminosity, UV intensity, lightning production of HCN and radicals, and impact bombardment rate. We then compare the nucleobase concentrations from *in situ* production with those from meteoritic delivery in order to determine whether early Earth was biogenic. We also calculate the concentrations of other key building blocks of RNA, including the other four nucleobases (guanine, uracil, cytosine, thymine), ribose, and 2-aminooxazole (an intermediate in the Powner-Sutherland synthesis of nucleotides) [42]. Our models suggest that early Earth was biogenic during the early reducing phase of the Hadean eon at 4.4 Ga, and that this phase lasted for at least 100 million years.

Finally, in Chapter 6, we summarize the main conclusions of this thesis and describe our aims for future work.

Chapter 2

A Consistent Reduced Network for HCN Chemistry in Early Earth and Titan Atmospheres: Quantum Calculations of Reaction Rate Coefficients

> ” *Science and everyday life cannot and should not be separated.*
>
> — **Rosalind Franklin**

Ben K. D. Pearce, Paul W. Ayers, & Ralph E. Pudritz

N.B. This chapter was published in The Journal of Physical Chemistry A (DOI: 10.1021/acs.jpca.8b11323) on February 5th*, 2019.*

Abstract

HCN is a key ingredient for synthesizing biomolecules such as nucleobases and amino acids. We calculate 42 reaction rate coefficients directly involved with or in competition with the production of HCN in the early Earth or Titan atmospheres. These reactions are driven by methane and nitrogen radicals produced via UV photodissociation or lightning. For every reaction in this network, we calculate rate coefficients at 298 K using canonical variational transition state theory (CVT) paired with computational quantum chemistry simulations at the BHandHLYP/aug-cc-pVDZ level of theory. We also calculate the temperature dependence of the rate coefficients for the reactions that have barriers from 50–400 K. We present 15 new reaction rate coefficients with no previous known value. 93% of our calculated coefficients are within an order of magnitude of the nearest experimental or recommended values. Above 320 K, the rate coefficient for the new reaction $H_2CN \longrightarrow HCN + H$ dominates. Contrary to experiments, we find the HCN reaction pathway, $N + CH_3 \longrightarrow HCN + H_2$, to be inefficient, and suggest the experimental rate coefficient actually corresponds to an indirect pathway, through the H_2CN intermediate. We present CVT using energies computed with density functional theory as a feasible and accurate method for calculating a large network of rate coefficients of small-molecule reactions.

2.1 Introduction

HCN is a precursor to the building blocks of life. For example, HCN reacts to produce nucleobases, the building blocks of RNA/DNA, as well as amino acids, the building blocks of proteins, in aqueous environments [38, 85, 89, 91, 183]. For adenine synthesis, HCN first condenses in water to form oligomers, which then forms adenine upon hydrolysis [184]. HCN may have formed in the atmosphere of the prebiotic Earth through the reaction of photochemically driven and/or lightning-induced methane and nitrogen radicals [17, 36]. HCN is similarly produced in Titan's present-day atmosphere [126].

Given the significance HCN as a precursor to biomolecules, it is of interest to discern how much was produced in the early Earth atmosphere in order to understand whether it potentially played a role in the emergence of life in warm little ponds [52]. Titan provides a good test environment for atmospheric HCN production, given that one can compare abundances from chemical simulations to the measured HCN profile from the Cassini mission [110, 111].

Chemical networks including a variety of species and reactions have been employed to simulate the atmospheric HCN composition of early Earth [107, 125] and Titan [126, 133, 185–187]. The reaction rate coefficients in these networks are generally a combination of a) theoretical, b) experimental, and c) suggested values typically estimated using thermodynamics, similar reactions and/or experimental results at much higher temperatures. Each of these sources has errors associated with it, and there are often a range of experimental and theoretical values to choose from for a single reaction. As a result, atmospheric HCN compositions can vary by orders of magnitude from one simulation to the next. Therefore, it is perhaps unsurprising that, as of yet, no simulation has matched the HCN profile of Titan completely.

There are also several reactions without past experimental, theoretical, or suggested values that are missing in these networks that may play important roles in HCN formation (e.g. $^1CH_2 + ^2N \longrightarrow H_2CN$ and $H_2CN \longrightarrow HCN + H$).

The focus of this work is to create a theoretical reduced HCN chemical network, where all the rate coefficients are consistently calculated with the same theoretical and computational method. Using this strategy, all reactions can be theoretically validated before being employed in a chemical network, and key reaction pathways with previously unknown rate coefficients can be included. Furthermore, by constructing a model chemistry [188, 189] the errors for consistently calculated rate coefficients are expected to be similar, thus employing such a network has a chance to improve accuracy.

The limitation of calculating a consistent theoretical network is that one cannot feasibly include a large number of molecular species. For every additional species, there is a potential additional reaction with all the existing species in the network. Therefore in this work, we focus only on the small set of reactions involved in the production of HCN from methane and nitrogen dissociation radicals, as well as the direct competing reactions. This totals 42 reactions between 11 species. We are the first to calculate a completely consistent theoretical reaction network of this size for atmospheric chemistry simulations.

In the Background section of this paper, we motivate and describe the reactions in our chemical network. Then in the Methods section, we detail the theoretical and computational methods used to calculate the reaction rate coefficients in our network. In the Results section, we present the results of our calculations, including their conformance to experimental values, and the effects of spin configuration on these values. The reader who is just interested in the calculated rate coefficients can skip ahead to Tables 3.7 and 2.4, where we present the calculated reaction rate coefficients at 298 K, and the Arrhenius coefficients for temperature dependences, respectively.

Finally, in the Conclusions section we summarize the main results of the paper.

The supporting information (SI) contains a wealth of technical data and calculation details including: 1) a summary of the experimentally measured and previously theoretically calculated rate coefficients in this network, 2) an example rate coefficient calculation using the CVT method and a computational methods comparison, 3) a breakdown of the calculations of specific reactions, and 4) reaction path symmetry number calculations.

2.2 Background

The abiotic production of biomolecules such as nucleobases and amino acids requires a reactive source of nitrogen, typically HCN or NH_3 [17, 18, 89, 104, 190]. HCN can be produced in early Earth and Titan atmospheres through reactions involving N_2 and CH_4 dissociation products. Such dissociation products are produced when N_2 and CH_4 interact with UV photons [36], cosmic rays [191], or lightning [192]. N_2 and CH_4 photodissociation can be broken down into the following pathways

$$\mathrm{N_2} + h\nu \longrightarrow \mathrm{N_2}^{+} + \mathrm{e}^{-} \tag{2.1}$$

$$\mathrm{N_2}^{+} + \mathrm{e}^{-} \longrightarrow {}^{4}\mathrm{N} + {}^{2}\mathrm{N} \tag{2.2}$$

$$\mathrm{CH_4} + h\nu \longrightarrow \mathrm{CH_3} + \mathrm{H} \qquad \Phi_{118.2} = 0.26, \Phi_{121.6} = 0.42, \tag{2.3}$$

$$\mathrm{CH_4} + h\nu \longrightarrow {}^{1}\mathrm{CH_2} + \mathrm{H_2} \qquad \Phi_{118.2} = 0.17, \Phi_{121.6} = 0.48, \tag{2.4}$$

$$\mathrm{CH_4} + h\nu \longrightarrow {}^{3}\mathrm{CH_2} + 2\,\mathrm{H} \qquad \Phi_{118.2} = 0.48, \Phi_{121.6} = 0.03, \tag{2.5}$$

$$\mathrm{CH4} + h\nu \longrightarrow \mathrm{CH} + \mathrm{H2} + \mathrm{H} \qquad \Phi_{118.2} = 0.09, \Phi_{121.6} = 0.07, \quad (2.6)$$

where the leading superscripts signify the singlet, doublet, and quartet spin states, $h\nu$ signifies an ultraviolet photon and $\Phi_{118.2}$ and $\Phi_{118.2}$ signify the branching ratios measured from lab experiments at 118.2 and 121.6 nm, respectively [36, 193, 194].

Multiple possible pathways to produce HCN from the above radicals (at or near 298 K) have been reported from experiments or suggested in the literature. Note that molecular spin states are not included in this list and that each of these reactions represents 1–5 reaction spin configurations; each with a unique reaction rate coefficient.

$$^{\dagger}\mathrm{CH3} + \mathrm{N} \longrightarrow \mathrm{H2CN} + \mathrm{H} \quad (2.7)$$

$$^{\dagger}\mathrm{CH2} + \mathrm{N} \longrightarrow \mathrm{H2CN} \quad (2.8)$$

$$^{\dagger}\mathrm{H2CN} \longleftrightarrow \mathrm{HCN} + \mathrm{H} \quad (2.9)$$

$$\mathrm{H2CN} + \mathrm{H} \longrightarrow \mathrm{HCN} + \mathrm{H2} \quad (2.10)$$

$$\mathrm{H2CN} + \mathrm{N} \longrightarrow \mathrm{HCN} + \mathrm{NH} \quad (2.11)$$

$$2\,\mathrm{H2CN} \longrightarrow \mathrm{HCN} + \mathrm{H2CNH} \quad (2.12)$$

Three experimentally reported or suggested reaction pathways have not been included in this list as our theoretical work shows they more likely proceed through two steps involving combinations of the above equations. These reactions are $\mathrm{CH3} + \mathrm{N} \longrightarrow \mathrm{HCN} + \mathrm{H2}$ [195], $\mathrm{CH3} + \mathrm{N} \longrightarrow \mathrm{HCN} + 2\,\mathrm{H}$ [195], and $\mathrm{CH2} + \mathrm{N} \longrightarrow \mathrm{HCN} + \mathrm{H}$ [36] (see theoretical case studies in SI for complete analysis).

There are also multiple competing reaction pathways to the above reactions at or near 298 K. In this network, we only include competing pathways involving the radicals produced from N_2 and CH_4 dissociation in the atmosphere. One exception is that we also include the reactions of ^{3}NH with H and N as recombination pathways to H_2 and N_2. See Table 4.1 for list of primary molecular species.

$$\mathrm{CH4} + \mathrm{H} \longleftrightarrow \mathrm{CH3} + \mathrm{H2} \quad (2.13)$$

[†] Reactions without experimental or suggested values for at least one spin configuration in this network.

Table 2.1: List of primary molecular species involved in this study and their spin states.

Species	Spin state	Ground/Excited state
HCN	singlet	ground
H_2CN	doublet	ground
N_2	singlet	ground
^2N	doublet	excited
^4N	quartet	ground
CH_4	singlet	ground
CH_3	doublet	ground
$^1CH_2$	singlet	excited
$^3CH_2$	triplet	ground
CH	doublet	ground
H_2	singlet	ground
H	doublet	ground
^3NH	triplet	ground

$$\mathrm{CH4 + N \longrightarrow H2CNH + H} \tag{2.14}$$

$$\mathrm{CH3 + H \longrightarrow CH4} \tag{2.15}$$

$$\mathrm{2\,CH3 \longrightarrow C2H6} \tag{2.16}$$

$$\mathrm{CH2 + H \longrightarrow CH3} \tag{2.17}$$

$$\mathrm{CH2 + H2 \longrightarrow CH4} \tag{2.18}$$

$$^{\dagger}\mathrm{CH2 + H2 \longleftrightarrow CH3 + H} \tag{2.19}$$

$$\mathrm{2\,CH2 \longrightarrow C2H4} \tag{2.20}$$

$$\mathrm{CH2 + CH3 \longrightarrow C2H4 + H} \tag{2.21}$$

$$\mathrm{CH2 + CH4 \longrightarrow C2H6} \tag{2.22}$$

$$^{\dagger}\mathrm{CH2 + CH4 \longleftrightarrow 2\,CH3} \tag{2.23}$$

$$^{\dagger}\mathrm{CH + H \longrightarrow CH2} \tag{2.24}$$

$$\mathrm{CH + H2 \longrightarrow CH3} \tag{2.25}$$

$$^{\dagger}\mathrm{CH + N \longrightarrow CN + H} \tag{2.26}$$

$$2\,CH \longrightarrow C_2H_2 \tag{2.27}$$

$$CH + CH_4 \longrightarrow C_2H_4 + H \tag{2.28}$$

$$NH + H \longleftrightarrow H_2 + N \tag{2.29}$$

$$^{\dagger}NH + N \longrightarrow N_2 + H \tag{2.30}$$

Four experimentally reported [196–205] two-step reaction pathways have been reduced to their first steps in this list. These reactions are

$$CH + H_2 \longleftrightarrow CH_3\cdot \longleftrightarrow {}^{3,1}CH_2 + H,$$
$$^{1}CH_2 + H_2 \longrightarrow CH_4\cdot \longrightarrow CH_3 + H,$$
$$^{1}CH_2 + CH_4 \longrightarrow C_2H_6\cdot \longrightarrow 2\,CH_3.$$

Our theoretical work shows the first steps are the rate-limiting steps, and the intermediates are reactants with other available reaction pathways in our chemical network (see theoretical case studies in SI for complete details).

One other experimentally reported [206] reaction has not been included in this list. This reaction is

$$CH_4 + {}^{2}N \longrightarrow {}^{1}H_3CNH\cdot \longrightarrow CH_3 + {}^{3}NH.$$

Experiments suggest that $^{1}H_3CNH$ decays into CH_3 + ^{3}NH with a branching ratio of 0.3 ± 0.1, and that the majority of $^{1}H_3CNH$ decays into $^{1}H_2CNH$ + H ($\Phi = 0.8 \pm 0.2$). Our theoretical work also suggests $^{1}H_3CNH$ preferentially decays into $^{1}H_2CNH$ + H, however we alternatively find the decay into CH_3 + ^{3}NH to be very inefficient ($k \sim 10^{-29}$ cm^3 s^{-1}); therefore we do not consider this decay pathway in this network.

The focus of this work is to calculate the rate coefficients for an atmospheric HCN reaction network which can be applied to both Titan and early Earth atmospheres. For each reaction, a detailed analysis of spin state configurations and an series of computational quantum chemistry simulations are performed at temperatures between 50–400 K.

In Table 2.2 we summarize the molecules and spin states involved in this reaction network. We define reactions with rate coefficients greater than 10^{-21} s^{-1} for unimolecular reactions or greater than 10^{-21} cm^{3}s^{-1} for bimolecular reactions as "fast," and exclude the “slow” reactions with smaller rate coefficients from this network.

Table 2.2: Detailed list of reactions considered in this study, including the accessible potential energy surfaces, and spin-state configurations. The focus of this network is reactions involved in the production of HCN from nitrogen and methane dissociation radicals. Direct competing reactions are also included. We define a fast reaction rate coefficient to be $>10^{-21}$ $\mathrm{s^{-1}}$ for unimolecular reactions and $>10^{-21}$ $\mathrm{cm^3s^{-1}}$ for bimolecular reactions.

Reaction equation	PES	Spin Configuration	Fast $k_f(298)$?	Fast $k_r(298)$?
$\mathrm{H_2CN \longleftrightarrow HCN + H}$	doublet	$\mathrm{H_2CN \longleftrightarrow HCN + H}$	Y	Y
$\mathrm{H_2CN + H \longleftrightarrow HCN + H_2}$	singlet	$\mathrm{H_2CN + H \longleftrightarrow HCN + H_2}$	Y	N
$\mathrm{H_2CN + N \longleftrightarrow HCN + NH}$	singlet	$\mathrm{H_2CN} + {}^{2}\mathrm{N} \longleftrightarrow \mathrm{HCN} + {}^{1}\mathrm{NH}$	N	N
	triplet	$\mathrm{H_2CN} + {}^{4}\mathrm{N} \longleftrightarrow \mathrm{HCN} + {}^{3}\mathrm{NH}$	Y	N
		$\mathrm{H_2CN} + {}^{2}\mathrm{N} \longleftrightarrow \mathrm{HCN} + {}^{3}\mathrm{NH}$	N	N
$\mathrm{2\,H_2CN \longleftrightarrow HCN + H_2CNH}$	singlet	$\mathrm{2\,H_2CN \longleftrightarrow HCN + H_2CNH}$	Y	N
$\mathrm{CH_4 + H \longleftrightarrow CH_3 + H_2}$	doublet	$\mathrm{CH_4 + H \longleftrightarrow CH_3 + H_2}$	Y	Y
$\mathrm{CH_4 + N \longleftrightarrow H_3CNH\cdot \longleftrightarrow H_2CNH + H}$	doublet	$\mathrm{CH_4} + {}^{2}\mathrm{N} \longleftrightarrow \mathrm{H_3CNH\cdot \longleftrightarrow H_2CNH + H}$	Y	N
$\mathrm{CH_4 + N \longleftrightarrow H_3CNH\cdot \longleftrightarrow CH_3 + NH}$	doublet	$\mathrm{CH_4} + {}^{2}\mathrm{N} \longleftrightarrow \mathrm{H_3CNH\cdot \longleftrightarrow CH_3} + {}^{3}\mathrm{NH}$	N	N
$\mathrm{CH_3 + H \longleftrightarrow CH_4}$	singlet	$\mathrm{CH_3 + H \longleftrightarrow CH_4}$	Y	N
$\mathrm{CH_3 + N \longleftrightarrow H_3CN\cdot \longleftrightarrow HCN + H_2}$	singlet	$\mathrm{CH_3} + {}^{2}\mathrm{N} \longleftrightarrow {}^{1}\mathrm{H_3CN\cdot \longleftrightarrow HCN + H_2}$	N	N
$\mathrm{CH_3 + N \longleftrightarrow H_3CN\cdot \longleftrightarrow H_2CN + H}$	singlet	$\mathrm{CH_3} + {}^{2}\mathrm{N} \longleftrightarrow {}^{1}\mathrm{H_3CN\cdot \longleftrightarrow H_2CN + H}$	Y	N
	triplet	$\mathrm{CH_3} + {}^{4}\mathrm{N} \longleftrightarrow {}^{3}\mathrm{H_3CN\cdot \longleftrightarrow H_2CN + H}$	Y	N
		$\mathrm{CH_3} + {}^{2}\mathrm{N} \longleftrightarrow {}^{3}\mathrm{H_3CN\cdot \longleftrightarrow H_2CN + H}$	Y	N
$\mathrm{2\,CH_3 \longleftrightarrow C_2H_6}$	singlet	$\mathrm{2\,CH_3 \longleftrightarrow C_2H_6}$	Y	N
$\mathrm{CH_2 + H \longleftrightarrow CH_3}$	doublet	${}^{3}\mathrm{CH_2 + H \longleftrightarrow CH_3}$	Y	N
		${}^{1}\mathrm{CH_2 + H \longleftrightarrow CH_3}$	Y	N
$\mathrm{CH_2 + H_2 \longleftrightarrow CH_4}$	singlet	${}^{1}\mathrm{CH_2 + H_2 \longleftrightarrow CH_4}$	Y	N
$\mathrm{CH_2 + H_2 \longleftrightarrow CH_3 + H}$	triplet	${}^{3}\mathrm{CH_2 + H_2 \longleftrightarrow CH_3 + H}$	Y	Y
$\mathrm{CH_2 + N \longleftrightarrow H_2CN}$	doublet	${}^{3}\mathrm{CH_2} + {}^{4}\mathrm{N} \longleftrightarrow {}^{2}\mathrm{H_2CN}$	Y	N
		${}^{3}\mathrm{CH_2} + {}^{2}\mathrm{N} \longleftrightarrow {}^{2}\mathrm{H_2CN}$	Y	N
		${}^{1}\mathrm{CH_2} + {}^{2}\mathrm{N} \longleftrightarrow {}^{2}\mathrm{H_2CN}$	Y	N
	quartet	${}^{1}\mathrm{CH_2} + {}^{4}\mathrm{N} \longleftrightarrow {}^{4}\mathrm{H_2CN}$	Y	N
		${}^{3}\mathrm{CH_2} + {}^{2}\mathrm{N} \longleftrightarrow {}^{4}\mathrm{H_2CN}$	Y	N
$\mathrm{2\,CH_2 \longleftrightarrow C_2H_4}$	singlet	${}^{3}\mathrm{CH_2} + {}^{3}\mathrm{CH_2} \longleftrightarrow {}^{1}\mathrm{C_2H_4}$	Y	N
		${}^{1}\mathrm{CH_2} + {}^{1}\mathrm{CH_2} \longleftrightarrow {}^{1}\mathrm{C_2H_4}$	Y	N
	triplet	${}^{3}\mathrm{CH_2} + {}^{1}\mathrm{CH_2} \longleftrightarrow {}^{3}\mathrm{C_2H_4}$	Y	N
$\mathrm{CH_2 + CH_3 \longleftrightarrow C_2H_5\cdot \longleftrightarrow C_2H_4 + H}$	doublet	${}^{3}\mathrm{CH_2 + CH_3 \longleftrightarrow C_2H_5\cdot \longleftrightarrow} {}^{1}\mathrm{C_2H_4 + H}$	Y	N
		${}^{1}\mathrm{CH_2 + CH_3 \longleftrightarrow C_2H_5\cdot \longleftrightarrow} {}^{1}\mathrm{C_2H_4 + H}$	Y	N
	quartet	${}^{3}\mathrm{CH_2 + CH_3} \longleftrightarrow {}^{4}\mathrm{C_2H_5\cdot} \longleftrightarrow {}^{3}\mathrm{C_2H_4 + H}$	N	N/A
$\mathrm{CH_2 + CH_4 \longleftrightarrow C_2H_6}$	singlet	${}^{1}\mathrm{CH_2 + CH_4 \longleftrightarrow C_2H_6}$	Y	N
$\mathrm{CH_2 + CH_4 \longleftrightarrow 2\,CH_3}$	triplet	${}^{3}\mathrm{CH_2 + CH_4 \longleftrightarrow 2\,CH_3}$	Y	Y
$\mathrm{CH + H \longleftrightarrow CH_2}$	singlet	$\mathrm{CH + H} \longleftrightarrow {}^{1}\mathrm{CH_2}$	Y	N
	triplet	$\mathrm{CH + H} \longleftrightarrow {}^{3}\mathrm{CH_2}$	Y	N
$\mathrm{CH + H_2 \longleftrightarrow CH_3}$	doublet	$\mathrm{CH + H_2 \longleftrightarrow CH_3}$	Y	N
$\mathrm{CH + N \longleftrightarrow HCN \longleftrightarrow CN + H}$	triplet	$\mathrm{CH} + {}^{4}\mathrm{N} \longleftrightarrow {}^{3}\mathrm{HCN \longleftrightarrow CN + H}$	Y	N
		$\mathrm{CH} + {}^{2}\mathrm{N} \longleftrightarrow {}^{3}\mathrm{HCN \longleftrightarrow CN + H}$	Y	N
$\mathrm{2\,CH \longleftrightarrow C_2H_2}$	singlet	$\mathrm{CH + CH \longleftrightarrow C_2H_2}$	Y	N
$\mathrm{CH + CH_4 \longleftrightarrow C_2H_5\cdot \longleftrightarrow C_2H_4 + H}$	doublet	$\mathrm{CH + CH_4 \longleftrightarrow C_2H_5\cdot \longleftrightarrow C_2H_4 + H}$	Y	N
$\mathrm{NH + H \longleftrightarrow H_2 + N}$	doublet	${}^{1}\mathrm{NH + H \longleftrightarrow H_2} + {}^{2}\mathrm{N}$	N/A	N
		${}^{3}\mathrm{NH + H \longleftrightarrow NH_2\cdot \longleftrightarrow H_2} + {}^{2}\mathrm{N}$	N	Y
	quartet	${}^{3}\mathrm{NH + H \longleftrightarrow H_2} + {}^{4}\mathrm{N}$	Y	N
$\mathrm{NH + N \longleftrightarrow N_2H\cdot \longleftrightarrow N_2 + H}$	doublet	${}^{3}\mathrm{NH} + {}^{4}\mathrm{N} \longleftrightarrow \mathrm{N_2H\cdot \longleftrightarrow N_2 + H}$	Y	N
		${}^{1}\mathrm{NH} + {}^{2}\mathrm{N} \longleftrightarrow \mathrm{N_2H\cdot \longleftrightarrow N_2 + H}$	N/A	N
		${}^{3}\mathrm{NH} + {}^{2}\mathrm{N} \longleftrightarrow \mathrm{N_2H\cdot \longleftrightarrow N_2 + H}$	Y	N

Reactions are N/A if they require species that are not efficiently produced in this network.

2.3 Methods

2.3.1 Variational Transition State Theory

Reactions can be visualized in one dimension using potential energy diagrams (see Figure 2.1). A reaction proceeds along a coordinate (e.g. the distance between two atoms), from the reactant geometry, to the product geometry. In some cases, the minimum energy path (MEP) from reactants to products requires proceeding through a geometry of higher potential energy than the reactant and product geometries. This increase in potential energy along a reaction coordinate is known as the energy barrier. The peak of the energy barrier describes the conventional transition state.

In reality, reactions have more than one dimension (e.g. bond distances, angles between bonds, dihedral angles), thus the energy barrier is more appropriately described as a saddle point, and the MEP is the path of steepest descent from saddle point to the reactant and product minima. The rate of a reaction can be described as how frequently molecules travel the entire MEP, and is quantified by the reaction rate coefficient, k.

We calculate gas phase chemical reaction rate coefficients using canonical variational transition state theory (CVT). The basis for this method is to vary the reaction coordinate (e.g. the carbon-hydrogen bond distance) along the MEP in order to find the minimum rate constant. Unlike conventional transition state theory, CVT allows us to calculate reaction rate coefficients for both barrierless and non-barrierless reactions, while minimizing the error due to trajectories that recross the transition state rather than descend into products [207]. This can be visualized as finding a location past the saddle point of the MEP, that recrossing reactants tend not to reach (see Figure 2.1). This location is determined as the location where the generalized transition state (GT) rate coefficient is at its smallest value, therefore providing best dynamical bottleneck [207].

The CVT reaction rate coefficient is expressed as [134, 146, 208]

$$k_{CVT}(T,s) = \min_{s} \left\{ k_{GT}(T,s) \right\}. \tag{2.31}$$

Neglecting the tunneling effect, the generalized transition state theory (GT) reaction rate coefficient can be approximated via the Eyring Equation [134, 146, 149, 208–213]. The Eyring equation uses a statistical mechanics approach to calculate the rate coefficient by dividing the density of forward-crossing states per unit time by the density of reactant states.

$$k_{GT}(T,s) = \sigma \frac{k_B T}{h} \frac{Q^{\ddagger}(T,s)}{\prod_{i=1}^{N} Q_i^{n_i}(T)} e^{-E_0(s)/RT} \tag{2.32}$$

where σ is the reaction path symmetry number or reaction path multiplicity (i.e. the number of equivalent reaction paths from reactants to products), k_B is the Boltzmann constant (1.38×10^{-23} J K^{-1}), T is temperature (K), h is the Planck constant (6.63×10^{-34} J·s), $Q^{\ddagger}$ is the partition function of the transition state per unit volume (cm^{-3}), with its zero of energy at the saddle point, Q_i is the partition function of species i per unit volume, with its zero of energy at the equilibrium position of species i (i.e. as if it is infinitely separated from any other reactant), n_i is the stoichiometric coefficient of species i, N is the number of reactant species, E_0 is the energy barrier (the difference in zero-point energies between the generalized transition state and the reactants) (kJ mol^{-1}), and R is the gas constant (8.314×10^{-3} kJ K^{-1} mol^{-1}).

Because classical partition functions involve integrating over the Boltzmann factor ($e^{-E/RT}$), an additional exponential factor appears naturally in the Eyring equation due to the difference in zeros of energy between the transition state and reactant states.

To find the location along the MEP where the GT rate coefficient is at its smallest value, we use the maximum Gibbs free energy criterion, which gives a compromise of energetic and entropic effects [146, 147]. To obtain a similar accuracy for all calculations, we use a reaction coordinate precision of 0.01 Å. Looking at the quasithermodynamic representation of transition-state theory, we see that the maximum value for $\Delta G_{GT}(T,s)$ corresponds to a minimum value for $k_{GT}(T,s)$

$$k_{GT}(T,s) = \frac{k_B T}{h} K^0 e^{-\Delta G_{GT}(T,s)/RT}, \tag{2.33}$$

where K^0 is the reaction quotient under standard state conditions (i.e. 1 for unimolecular reactions, and 1 cm^3 for bimolecular reactions), and $\Delta G_{GT}(T,s)$ is the difference in the Gibbs free energy between transition state and reactants (kJ mol^{-1}).

The conventional transition state, energy barrier, and variational transition state are illustrated with a potential energy diagram in Figure 2.1.

The zero-point energies and partition functions for the reactants and transition states are calculated using the Gaussian 09 software package [214]. A brief summary

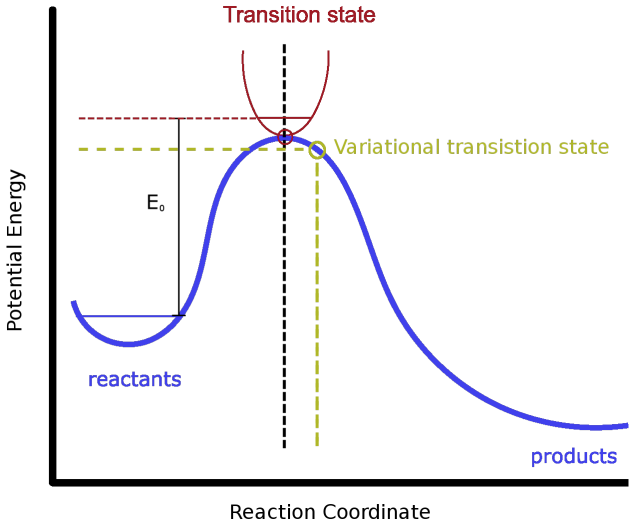

Figure 2.1: A schematic representation of a reaction: proceeding from the reactants, over the potential energy barrier, E_0, through the transition state (red circle), and onto the products. The variational transition state (gold circle) is a location beyond the conventional transition state, where reactants that recross the barrier tend not to reach. The variational transition state is located where the reaction rate coefficient is at a minimum, thus providing the best dynamical bottleneck.

of the theory behind these calculations is detailed below. We refer the reader to Ochterski[215] for further details.

The partition functions per unit volume are expanded into their 4 components

$$Q = \frac{q_t}{V} q_e q_v q_r. \tag{2.34}$$

where q_t is the translational component, V is the volume (cm^{-3}), q_e is the electronic component, q_v is the vibrational component, q_r is the rotational component not including the rotational symmetry number (this is included in the reaction path multiplicity).

From classical statistical mechanics, the translational partition function per unit volume is [215]

$$\frac{q_t}{V} = \left(\frac{2\pi m k_B T}{h^2}\right)^{3/2}, \tag{2.35}$$

where m is the mass of the species (kg).

The electronic partition function is estimated as the degeneracy of the first energy level, *i.e.* the spin multiplicity [215]

$$q_e = 2S + 1, \tag{2.36}$$

where S is the total spin due to unpaired electrons. For example, a hydrogen atom has 1 unpaired electron of spin $1/2$, and thus its $q_e = 2(1/2) + 1 = 2$.

Gaussian calculates the vibrational partition function as a quantum harmonic oscillator. We note that for the zero-point energies of molecules, Gaussian places the zero of energy at the bottom of the internuclear potential. Thus, with this same location for the zero of energy, the vibrational partition function equates to

$$q_v = \prod_{n=1}^{N} \frac{e^{-\Theta_n/2T}}{1 - e^{-\Theta_n/T}}, \tag{2.37}$$

where N is the number of vibrational modes, Θ_n is the vibrational temperature of the nth mode ($\Theta_n = \frac{\hbar\omega_n}{k_B}$), and T is temperature.

By default, Gaussian calculates the rotational partition function as a rigid rotor. For linear molecules excluding rotational symmetry,

$$q_r = \left(\frac{T}{\Theta_r}\right), \tag{2.38}$$

and for polyatomic molecules excluding rotational symmetry,

$$q_r = \pi^{1/2}\left(\frac{T^{3/2}}{(\Theta_{r,x}\Theta_{r,y}\Theta_{r,z})^{3/2}}\right), \tag{2.39}$$

where Θ_r is the rotational temperature ($\Theta_r = \frac{h^2}{8\pi^2 I k_B}$, and I is the moment of inertia (in the case of a polyatomic molecule, I_x, I_y, and I_z are the principal moments of inertia).

Gaussian displays an output for the rotational symmetry number (σ_r) of each molecule, however for all the reactants, transition states and products in our study, Gaussian displayed $\sigma_r = 1$. For this reason we calculate the rotational symmetry in Equation 4.12 manually [212] (the calculated symmetry numbers are listed in Table S10 in SI).

2.3.2 Quantum Computational Simulations

We perform quantum computational simulations with the Gaussian software package [214] using the Becke-Half-and-Half-Lee-Yang-Parr (BHandHLYP) density functional [216, 217]. We chose BHandHLYP for two reasons. Firstly, it is a relatively inexpensive method that can be used for an extended transition state study such as this. Secondly, in a computational methods comparison of the well-studied reaction $CH_4 + H \longrightarrow CH_3 + H_2$, BHandHLYP provided the most accurate rate coefficient compared to calculations using HF, CCSD, B3LYP, and M06-2x (see computational methods comparison in SI for more details). CAM-B3LYP also provided an accurate rate coefficient for this reaction, however the value from BHandHLYP offers a better compromise between experimental and suggested values.

Hartree-Fock (HF) methods tend to overestimate the energy barrier, whereas Density Functional Theory (DFT) methods (e.g. B3LYP) tend to underestimate the energy barrier. BHandHLYP is a hybrid functional that improves performance by using 50% HF and 50% DFT for the exchange energy calculation. All simulations are performed with the augmented correlation consistent polarized valence double zeta (aug-cc-pVDZ) basis set in order to achieve reasonable computation times.

Typically, when there is only one reaction spin configuration for a given PES, we do not specify the local spins in Gaussian when calculating the MEP. However in some cases not specifying the local spin, regardless of the number of possible spin configurations, leads to convergence issues. In these cases we specify the local spins to allow the calculation to converge. When there is more than one reaction spin configuration for a given PES, e.g., $CH_3 + {}^4N \longrightarrow {}^3H_3CN\cdot \longrightarrow H_2CN + H$ and $CH_3 + {}^2N \longrightarrow {}^3H_3CN\cdot \longrightarrow H_2CN + H$ on the triplet surface, we specify the local spins of the reactants in Gaussian to find the MEP's for each individual spin configuration.

2.3.3 Temperature Dependence of Rate Coefficients

Temperatures in the early Earth and Titan atmospheres fit comfortably within the range of 50–400 K [107, 108, 218]. The CVT rate coefficient equation for reactions with barriers includes a temperature-dependent exponential term (see Equation 4.12). This exponential temperature dependence typically leads to reaction rate coefficients which vary by multiple orders of magnitude over 50–400 K. The exponential term is omitted for barrierless reactions, and thus the temperature dependence for barrierless reaction rate coefficients is much smaller. Typically rate coefficients for barrierless reactions have either no temperature dependence, or a weak temperature dependence, varying by less than a factor of a two or three from 50–400 K [208, 219–222].

Temperature dependence for rate coefficients can be expressed using the Arrhenius equation [223],

$$k(T) = \alpha \left(\frac{T}{300}\right)^{\beta} e^{-\gamma/T}, \tag{2.40}$$

where α, β, and γ are fitting parameters, which we will refer to as the Arrhenius coefficients. Units for $k(T)$ are s^{-1} for unimolecular reactions and cm^3s^{-1} for bimolecular reactions.

We calculate the rate coefficients for the reactions with barriers at 50, 100, 200, 298, and 400 K and fit the results to the expression above to obtain the Arrhenius coefficients. For the sake of feasibility, we assume the rate coefficient for barrierless reactions is constant within this temperature range, as is typical [137].

2.4 Results

For detailed results, see theoretical case studies for 35 of the reactions in SI.

In Table 3.7, we display the reaction rate coefficients calculated using the CVT method described above at 298 K, and the comparative ranges of experimental values.

2.4.1 Conformance to Experiments

Of the 42 total reactions in this network, ∼54% have been studied experimentally at or near 298 K (see the "k(298) experimental" column in Table 3.7 for experimental values). Another ∼10% have been estimated based on the rate coefficients of similar bond additions and decompositions, and/or thermodynamics. 36% of the reactions have no experimental rate coefficients (those with no "k(298) experimental" value in Table 3.7), and in most cases, we are the first to calculate them theoretically.

Table 2.3: Reaction rate coefficients for the atmospheric reaction network calculated in this study. All reactions are involved in HCN production in the early Earth atmosphere or are key competing reactions. Calculations are performed at the BHandHLYP/aug-cc-pVDZ level of theory. Slow reactions ($k < 10^{-21}$), either forward or reverse, are not included in this network. In the column labeled "barrier?" we specify whether the rate-limiting step (or the only step) of the reaction has an energy barrier. The error factor is the multiplicative or divisional factor from the nearest experimental or suggested value; the error factor is 1 if the calculated value is within the range of experimental or suggested values. 36% of these reactions have no experimental or suggested rate coefficients. First-order rate coefficients have units s^{-1}. Second-order rate coefficients have units $cm^3 s^{-1}$.

Reaction equation	Forward or Reverse?	Barrier?	k(298) calculated	k(298) experimental	Error factor
$H_2CN \longleftrightarrow HCN + H$	F	Y	1.6×10^{-11}		
	R	Y	2.7×10^{-14}		
$H_2CN + H \longrightarrow HCN + H_2$	F	N	1.8×10^{-11}	8.3×10^{-11}	5
$H_2CN + {}^4N \longleftrightarrow HCN + {}^3NH$	F	Y	9.4×10^{-13}	4.4×10^{-11}	47
$2\,H_2CN \longleftrightarrow HCN + H_2CNH$	F	N	[a] 3.7×10^{-14}	$3.3\text{–}8.3\times10^{-12}$	89
$CH_4 + H \longleftrightarrow CH_3 + H_2$	F	Y	8.1×10^{-18}	$8.2\times10^{-19}\text{–}3.5\times10^{-17}$	1
	R	Y	3.2×10^{-21}	$9.6\times10^{-21}\text{–}1.3\times10^{-20}$	3
$CH_4 + {}^2N \longleftrightarrow H_3CNH \longleftrightarrow {}^1H_2CNH + H$	F	Y	[b] 4.7×10^{-11}	$2.4\text{–}4.5\times10^{-12}$	10
$CH_3 + H \longleftrightarrow CH_4$	F	N	7.9×10^{-11}	$1.5\text{–}4.7\times10^{-10}$	2
$CH_3 + {}^4N \longleftrightarrow {}^3H_3CN\cdot \longleftrightarrow H_2CN + H$	F	N	3.3×10^{-11}	$5.0\text{–}7.7\times10^{-11}$	1.5
$CH_3 + {}^2N \longleftrightarrow {}^3H_3CN\cdot \longleftrightarrow H_2CN + H$	F	N	1.0×10^{-10}		
$CH_3 + {}^2N \longleftrightarrow {}^1H_3CN\cdot \longleftrightarrow H_2CN + H$	F	N	3.1×10^{-11}		
$2\,CH_3 \longleftrightarrow C_2H_6$	F	N	7.3×10^{-13}	$3.5\text{–}6.5\times10^{-11}$	48
${}^1CH_2 + H \longleftrightarrow CH_3$	F	N	8.4×10^{-11}	5.0×10^{-11}	2
${}^1CH_2 + H_2 \longleftrightarrow CH_4$	F	N	1.0×10^{-11}	[c] $7.0\times10^{-12}\text{–}1.3\times10^{-10}$	1
${}^1CH_2 + {}^4N \longleftrightarrow {}^4H_2CN$	F	N	1.1×10^{-10}		
${}^1CH_2 + {}^2N \longleftrightarrow {}^2H_2CN$	F	N	1.5×10^{-10}		
${}^1CH_2 + {}^1CH_2 \longleftrightarrow C_2H_4$	F	N	9.9×10^{-12}	5.0×10^{-11}	5
${}^1CH_2 + {}^3CH_2 \longleftrightarrow C_2H_4$	F	N	[d] 3.5×10^{-11}	3.0×10^{-11}	1
${}^1CH_2 + CH_3 \longleftrightarrow C_2H_5\cdot \longleftrightarrow C_2H_4 + H$	F	N	2.3×10^{-11}	3.0×10^{-11}	1
${}^1CH_2 + CH_4 \longleftrightarrow C_2H_6$	F	N	6.1×10^{-13}	[e] $1.9\times10^{-12}\text{–}7.3\times10^{-11}$	3
${}^3CH_2 + H \longleftrightarrow CH_3$	F	N	5.6×10^{-10}	[f] $8.3\times10^{-11}\text{–}2.7\times10^{-10}$	2
${}^3CH_2 + H_2 \longleftrightarrow CH_3 + H$	F	Y	2.5×10^{-16}	$<5.0\times10^{-14}\text{–}5.0\times10^{-15}$	[g]
	R	Y	1.4×10^{-20}		
${}^3CH_2 + {}^4N \longleftrightarrow {}^2H_2CN$	F	N	1.3×10^{-10}		
${}^3CH_2 + {}^2N \longleftrightarrow {}^2H_2CN$	F	N	2.7×10^{-10}		
${}^3CH_2 + {}^2N \longleftrightarrow {}^4H_2CN$	F	N	4.3×10^{-10}		
${}^3CH_2 + {}^3CH_2 \longleftrightarrow C_2H_4$	F	N	4.2×10^{-11}	5.3×10^{-11}	1
${}^3CH_2 + CH_3 \longleftrightarrow C_2H_5\cdot \longleftrightarrow C_2H_4 + H$	F	N	8.8×10^{-12}	$5.0\times10^{-11}\text{–}2.1\times10^{-10}$	6
${}^3CH_2 + CH_4 \longleftrightarrow 2\,CH_3$	F	Y	1.4×10^{-16}	$<5.0\times10^{-14}\text{–}3.0\times10^{-19}$	[g]
	R	N	5.5×10^{-11}		
$CH + H \longleftrightarrow {}^1CH_2$	F	N	1.5×10^{-10}		
$CH + H \longleftrightarrow {}^3CH_2$	F	N	5.3×10^{-10}		
$CH + H_2 \longleftrightarrow CH_3$	F	N	7.9×10^{-11}	$1.0\times10^{-12}\text{–}1.6\times10^{-10}$	1
$CH + {}^4N \longleftrightarrow {}^3HCN \longleftrightarrow CN + H$	F	N	1.1×10^{-10}	$2.1\times10^{-11}\text{–}1.6\times10^{-10}$	1
$CH + {}^2N \longleftrightarrow {}^3HCN \longleftrightarrow CN + H$	F	N	2.7×10^{-10}		
$2\,CH \longleftrightarrow C_2H_2$	F	N	1.3×10^{-11}	$1.7\text{–}2.0\times10^{-10}$	13
$CH + CH_4 \longleftrightarrow C_2H_5\cdot \longleftrightarrow C_2H_4 + H$	F	N	3.8×10^{-13}	$2.0\times10^{-12}\text{–}3.0\times10^{-10}$	5
${}^3NH + H \longleftrightarrow H_2 + {}^4N$	F	Y	1.4×10^{-11}	3.2×10^{-12}	4
${}^3NH + H \longleftrightarrow NH_2\cdot \longleftrightarrow H_2 + {}^2N$	R	Y	5.1×10^{-11}	$1.7\text{–}5.0\times10^{-12}$	10
${}^3NH + {}^4N \longleftrightarrow N_2H\cdot \longleftrightarrow N_2 + H$	F	N	4.0×10^{-11}	$2.5\text{–}2.6\times10^{-11}$	1.5
${}^3NH + {}^2N \longleftrightarrow N_2H\cdot \longleftrightarrow N_2 + H$	F	N	5.5×10^{-11}		

[a] Simulations did not converge beyond a H-N bond distance of 1.95Å. The calculated rate coefficient is a lower bound.

[b] Simulations did not converge beyond a H-N bond distance of 2.82Å. The calculated rate coefficient is a lower bound.

[c] Experimental values are from the two-step reaction ${}^1CH_2 + H_2 \longrightarrow CH_4\cdot \longrightarrow CH_3 + H$. Our theoretical work suggests the first step is the rate-limiting step, thus these values can be attributed to ${}^1CH_2 + H_2 \longrightarrow CH_4$.

[d] Simulations did not converge beyond a C-C bond distance of 3.52Å. The calculated rate coefficient is a lower bound.

[e] Experimental values are from the two-step reaction ${}^1CH_2 + CH_4 \longrightarrow C_2H_6\cdot \longrightarrow 2\,CH_3$. Our theoretical work suggests the first step is the rate-limiting step, thus these values can be attributed to ${}^1CH_2 + CH_4 \longrightarrow C_2H_6$.

[f] Experimental values are from the two-step reaction $^3CH_2 + H \longrightarrow CH_3 \cdot \longrightarrow CH + H_2$. Our theoretical work suggests the first step is the rate-limiting step, thus these values can be attributed to $^3CH_2 + H \longrightarrow CH_3$.
[g] The theoretical value agrees with the experimental upper bounds.

It is often assumed that experiments provide the closest values to the true reaction rate coefficients. However for a single reaction, separate experiments can measure coefficients that differ by over 2 orders of magnitude (e.g. for $CH + CH_4 \longrightarrow C_2H_4 + H$, $k = 2.0\times10^{-12}$ to 3.0×10^{-10} cm^{3}s^{-1}). This variation can be due to differing experimental methods, instrumentation, and analytical techniques. Furthermore, the reactions reported in experiments may not correspond to direct pathways. Instead there may be intermediates embedded in multiple reaction steps that correspond to the overall measured reaction rate coefficient. Theoretical analysis and mechanistic modeling can be used to sort out the most likely steps in a multiple-step reaction in order to avoid the inclusion of redundant reaction pathways in chemical networks.

In this work, we calculate the reaction rate coefficients for the reactions involved in HCN production from atmospheric nitrogen and methane radicals, as well as the most direct competing reactions. This network includes 15 reactions that have no experimental or suggested value in the literature, and six of these are directly involved in atmospheric HCN synthesis. All our calculations are performed at the same level of theory, i.e. BHandHLYP/aug-cc-pVDZ, therefore we expect the error in the rate coefficients to be similar for all reactions.

The largest discrepancy between experiments and theory is for the reaction of $CH_3 + N \longrightarrow$ products. Stief et al.[224] measured the rate coefficient of $CH_3 + N \longrightarrow$ products to be 8.6×10^{-11} cm^{3}s^{-1}, and Marston et al.[195] reported the experimental branching ratios to be

$$CH_3 + N \longrightarrow H_2CN + H \qquad \Phi \sim 0.9,$$

and

$$CH_3 + N \longrightarrow HCN + H_2 \qquad \Phi \sim 0.1.$$

However, we find only the first of these reactions has an efficient rate coefficient (k =

3.3×10^{-11} cm^{3}s^{-1}), and that the second reaction is very inefficient (k $\sim 10^{-28}$ cm^{3}s^{-1}). This result agrees with past theoretical work, which suggests the measurement of the second reaction likely corresponds to a series of reactions passing through the H_2CN intermediate [225]. For more details of our analysis, see theoretical case study 4 in SI.

Our theoretical reaction rate coefficients are within an order of magnitude of the closest experimental or suggested value from the literature 93% of the time. The theoretical reaction rate coefficients for $H_2CN + {}^4N \longrightarrow HCN + {}^3NH$, $2\,CH_3 \longrightarrow C_2H_6$, and $2\,H_2CN \longrightarrow HCN + H_2CNH$, on the other hand, differ by factors of 47, 48, and 89 from the closest experimental values, respectively. In the case of $2\,H_2CN \longrightarrow HCN + H_2CNH$, we are unable to converge the calculations beyond a H-N bond distance of 1.95 Å, and in this case, the rate coefficients increase towards the experimental values with increasing H-N bond distance. Therefore we expect the major source of discrepancy between theory and experiment for this reaction is due to computational convergence. With regards to the other two reactions, we find the discrepancies to be due to our chosen computational method. Calculations at the CCSD/aug-cc-pVDZ level of theory bring the rate coefficient for $2\,CH_3 \longrightarrow C_2H_6$ to within its experimental range. CCSD calculations, however, do not universally increase accuracy. The rate coefficient for $H_2CN + {}^4N \longrightarrow HCN + {}^3NH$ when calculated using CCSD/aug-cc-pVDZ is over 3 orders of magnitude smaller than the experimental value. On the other hand, this reaction rate coefficient comes to within ~80% of the experimental value when using CAM-B3LYP/aug-cc-pVDZ. Because CAM-B3LYP has less short-range HF exchange than BHandHLYP[226], this method is expected to predict a smaller barrier height than BHandHLYP. Thus in this case, where BHandHLYP overestimates the barrier height (underestimates the rate coefficient) with respect to the experimental value, CAM-B3LYP brings the calculated rate coefficient closer to the experimental value. Of future interest would be to test the accuracy of all the rate coefficients in our network when calculated with CAM-B3LYP/aug-cc-pVDZ.

2.4.2 Temperature Dependencies

In Table 2.4, we display the Arrhenius coefficients for the reactions in this network for temperatures between 50 and 400 K. We also display the temperature-dependent rate coefficients for the 10 reactions that have barriers in Figure 2.2.

Table 2.4: Arrhenius coefficients for the 42 reactions in this network. Rate coefficients are calculated for the reactions with barriers at 50, 100, 200, 298, and 400 K, and are fit to the Arhennius expression $k(T) = \alpha \left(\frac{T}{300}\right)^{\beta} e^{-\gamma/T}$. Barrierless reaction rate coefficients typically do not vary by more than a factor of 1–3 for temperatures between 50 and 400 K [208, 219–222], therefore for feasibility of calculations we set the β and γ for these reactions to zero. For the majority of reactions, fits to the Arrhenius expression are continuous in the temperature range from 50–400 K; however, for two reactions there are discontinuities and thus these reactions have two sets of Arrhenius coefficients.

Reaction equation	Forward or Reverse?	Temperature range (K)	α	β	γ
$H_2CN \longleftrightarrow HCN + H$	F	50–400	7.9×10^{13}	0	16952
	R	50–400	6.5×10^{-11}	0.7	2318
$H_2CN + H \longrightarrow HCN + H_2$	F	50–400	1.8×10^{-11}	0	0
$H_2CN + {}^4N \longleftrightarrow HCN + {}^3NH$	F	50–279	7.8×10^{-12}	1.63	938
	F	279–400	1.2×10^{-11}	0	758
$2\,H_2CN \longleftrightarrow HCN + H_2CNH$	F	50–400	3.7×10^{-14}	0	0
$CH_4 + H \longleftrightarrow CH_3 + H_2$	F	50–400	5.5×10^{-11}	0.6	4689
	R	50–400	1.5×10^{-11}	-0.32	6632
$CH_4 + {}^2N \longleftrightarrow H_3CNH \longleftrightarrow {}^1H_2CNH + H$	F	50–400	4.7×10^{-10}	0	700
$CH_3 + H \longleftrightarrow CH_4$	F	50–400	7.9×10^{-11}	0	0
$CH_3 + {}^4N \longleftrightarrow {}^3H_3CN\cdot \longleftrightarrow H_2CN + H$	F	50–400	3.3×10^{-11}	0	0
$CH_3 + {}^2N \longleftrightarrow {}^3H_3CN\cdot \longleftrightarrow H_2CN + H$	F	50–400	1.0×10^{-10}	0	0
$CH_3 + {}^2N \longleftrightarrow {}^1H_3CN\cdot \longleftrightarrow H_2CN + H$	F	50–400	3.1×10^{-11}	0	0
$2\,CH_3 \longleftrightarrow C_2H_6$	F	50–400	7.3×10^{-13}	0	0
${}^1CH_2 + H \longleftrightarrow CH_3$	F	50–400	8.4×10^{-11}	0	0
${}^1CH_2 + H_2 \longleftrightarrow CH_4$	F	50–400	1.0×10^{-11}	0	0
${}^1CH_2 + {}^4N \longleftrightarrow {}^4H_2CN$	F	50–400	1.1×10^{-10}	0	0
${}^1CH_2 + {}^2N \longleftrightarrow {}^2H_2CN$	F	50–400	1.5×10^{-10}	0	0
${}^1CH_2 + {}^1CH_2 \longleftrightarrow C_2H_4$	F	50–400	9.9×10^{-12}	0	0
${}^1CH_2 + {}^3CH_2 \longleftrightarrow C_2H_4$	F	50–400	3.5×10^{-11}	0	0
${}^1CH_2 + CH_3 \longleftrightarrow C_2H_5\cdot \longleftrightarrow C_2H_4 + H$	F	50–400	2.3×10^{-11}	0	0
${}^1CH_2 + CH_4 \longleftrightarrow C_2H_6$	F	50–400	6.1×10^{-13}	0	0
${}^3CH_2 + H \longleftrightarrow CH_3$	F	50–400	5.6×10^{-10}	0	0
${}^3CH_2 + H_2 \longleftrightarrow CH_3 + H$	F	50–400	5.4×10^{-11}	0	3661
	R	50–400	4.2×10^{-11}	0.82	6504
${}^3CH_2 + {}^4N \longleftrightarrow {}^2H_2CN$	F	50–400	1.3×10^{-10}	0	0
${}^3CH_2 + {}^2N \longleftrightarrow {}^2H_2CN$	F	50–400	2.7×10^{-10}	0	0
${}^3CH_2 + {}^2N \longleftrightarrow {}^4H_2CN$	F	50–400	4.3×10^{-10}	0	0
${}^3CH_2 + {}^3CH_2 \longleftrightarrow C_2H_4$	F	50–400	4.2×10^{-11}	0	0
${}^3CH_2 + CH_3 \longleftrightarrow C_2H_5\cdot \longleftrightarrow C_2H_4 + H$	F	50–400	8.8×10^{-12}	0	0
${}^3CH_2 + CH_4 \longleftrightarrow 2\,CH_3$	F	50–400	5.5×10^{-11}	1.63	3840
	R	50–400	5.5×10^{-11}	0	0
$CH + H \longleftrightarrow {}^1CH_2$	F	50–400	1.5×10^{-10}	0	0
$CH + H \longleftrightarrow {}^3CH_2$	F	50–400	5.3×10^{-10}	0	0
$CH + H_2 \longleftrightarrow CH_3$	F	50–400	7.9×10^{-11}	0	0
$CH + {}^4N \longleftrightarrow {}^3HCN \longleftrightarrow CN + H$	F	50–400	1.1×10^{-10}	0	0
$CH + {}^2N \longleftrightarrow {}^3HCN \longleftrightarrow CN + H$	F	50–400	2.7×10^{-10}	0	0
$2\,CH \longleftrightarrow C_2H_2$	F	50–400	1.3×10^{-11}	0	0
$CH + CH_4 \longleftrightarrow C_2H_5\cdot \longleftrightarrow C_2H_4 + H$	F	50–400	3.8×10^{-13}	0	0
${}^3NH + H \longleftrightarrow H_2 + {}^4N$	F	50–400	1.4×10^{-11}	0	0
${}^3NH + H \longleftrightarrow NH_2\cdot \longleftrightarrow H_2 + {}^2N$	R	50–304	1.1×10^{-9}	0.83	909
	R	304–400	1.5×10^{-9}	0	1128
${}^3NH + {}^4N \longleftrightarrow N_2H\cdot \longleftrightarrow N_2 + H$	F	50–400	4.0×10^{-11}	0	0
${}^3NH + {}^2N \longleftrightarrow N_2H\cdot \longleftrightarrow N_2 + H$	F	50–400	5.5×10^{-11}	0	0

The majority of the reactions with barriers fit to one Arrhenius expression for the 50–400 K temperature range, however there were two special cases that had discontinuous fits. Both $H_2CN + {}^4N \longrightarrow HCN + {}^3NH$ and $H_2 + {}^2N \longrightarrow NH_2\cdot \longrightarrow {}^3NH + H$

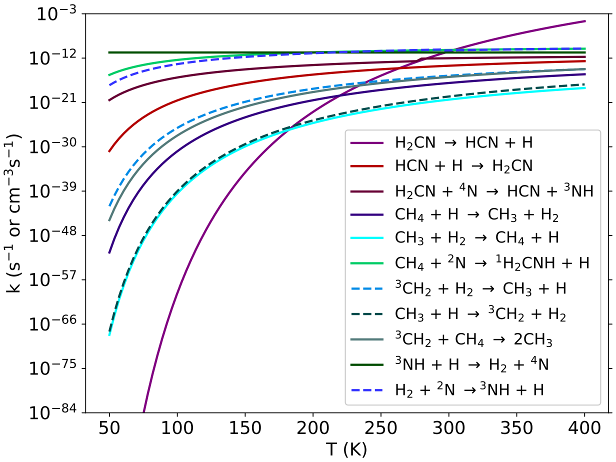

Figure 2.2: Temperature dependence of the 11 reactions in our network that have barriers. Rate coefficients are calculated at 50, 100, 200, 298, and 400 K, and are fit to the Arhennius expression $k(T) = \alpha \left(\frac{T}{300}\right)^{\beta} e^{-\gamma/T}$. Two of the fits have discontinuities: $H_2CN + {}^4N \longrightarrow HCN + {}^3NH$ at 279 K, and $H_2 + {}^2N \longrightarrow {}^3NH + H$ at 304 K. First-order rate coefficients have units s^{-1}. Second-order rate coefficients have units cm^3s^{-1}.

have two Gibbs maxima along their MEP's. As temperature increases, the shorter of the Gibbs humps increases in height until it reaches the same height as the other hump at some characteristic temperature. Beyond this temperature, the previously shorter Gibbs hump surpasses the other hump in height, becoming the new location of the variational transition state. Such a drastic change in the location of the variational transition state before and after the characteristic temperature creates a discontinuity in the temperature dependent rate coefficient, that is better fit to two separate sets of Arrhenius coefficients.

The rate coefficients of four of the reactions with barriers do not decrease rapidly with decreasing temperatures, and remain "fast" ($k > 10^{-21}$ cm^3s^{-1}) in the entire 50–400 K temperature range:

$$CH_4 + {}^2N \longrightarrow H_3CNH \longrightarrow {}^1H_2CNH + H,$$

$$^3NH + H \longrightarrow H_2 + {}^4N,$$

$$H_2 + {}^2N \longrightarrow NH_2\cdot \longrightarrow {}^3NH + H,$$

$$H_2CN + {}^4N \longrightarrow HCN + {}^3NH.$$

The rate coefficients of the other seven reactions with barriers drop off more rapidly for colder temperatures, and become "slow" in the ∼100–300 K range. One reaction's rate coefficient has a particularly interesting temperature dependence. $H_2CN \longrightarrow HCN + H$ has a rate coefficient as high as 3.1×10^{-5} s^{-1} at 400 K, and as low as 4.5×10^{-134} s^{-1} at 50 K. Above 320 K, $H_2CN \longrightarrow HCN + H$ has the highest rate coefficient in this network.

2.4.3 Effects of Spin Configuration on Rate Coefficients

Both ground state (e.g. ^4N, $^3CH_2$) and excited state (e.g. ^2N, $^1CH_2$) species are produced during the UV photodissociation of N_2 and CH_4. Because our network includes both ground state and excited state species, there is often more than one possible spin configuration for a given reaction. For example, the reaction

$$CH_3 + N \longrightarrow H_2CN + H$$

has three spin configurations. If the nitrogen is in the ground state, the reaction passes through the excited state ^3H_3CN intermediate before decaying into H_2CN + H directly, or after passing though the ^3H_2CNH intermediate. If the nitrogen is in the excited state, the reaction can either pass through the excited state ^3H_3CN intermediate, or the ground state ^1H_3CN intermediate, before decaying into H_2CN + H directly, or after passing through the ^3H_2CNH or ^1H_2CNH intermediates. In other words, on the triplet PES there are two possible reactions: $CH_3 + {}^4N \longrightarrow {}^3H_3CN \longrightarrow H_2CN + H$ and $CH_3 + {}^2N \longrightarrow {}^3H_3CN \longrightarrow H_2CN + H$, and on the singlet PES there is one reaction: $CH_3 + {}^2N \longrightarrow {}^1H_3CN \longrightarrow H_2CN + H$. The first steps of these reactions are the rate-limiting steps, and these steps are barrierless. All reactions have the same products, a ground state H_2CN molecule and H atom. However, the rate coefficient for $CH_3 + {}^2N \longrightarrow {}^3H_3CN \longrightarrow H_2CN + H$ is larger than the other two reactions by a factor of 3 (see Table 3.7 for calculated values).

Rate coefficients for different reaction spin configurations can also vary by several orders of magnitude, especially if a reaction barrier exists. The reaction $H_2CN + N \longrightarrow HCN + NH$ has three spin configurations that produce ground state HCN. On the singlet surface, there is $H_2CN + {}^2N \longrightarrow HCN + {}^1NH$, and on the triplet surface, there is $H_2CN + {}^4N \longrightarrow HCN + {}^3NH$ and $H_2CN + {}^2N \longrightarrow HCN + {}^3NH$. All these reactions have an energy barrier, but only the spin configuration involving the ^4N atom is efficient. We calculate the rate coefficient for $H_2CN + {}^4N \longrightarrow HCN + {}^3NH$ to be 9.4×10^{-13} cm^{3}s^{-1}, which is 16 and 18 orders of magnitude larger than our calculated rate coefficients for $H_2CN + {}^2N \longrightarrow HCN + {}^3NH$ and $H_2CN + {}^2N \longrightarrow HCN + {}^1NH$, respectively.

Different spin configurations for two reactants can also lead to different products. For example, when $^1CH_2$ and CH_4 react on the singlet surface, they come together to form C_2H_6. When the hydrogen from CH_4 bonds with the carbon of $^1CH_2$, the resultant CH_3 molecules each have an unpaired electron of opposite spin, allowing these molecules to rapidly bond to form C_2H_6. However, when $^3CH_2$ and CH_4 react on the triplet surface, they react directly to form two CH_3 molecules, each with an unpaired electron of the same spin. The rate coefficient of $^1CH_2 + CH_4 \longrightarrow C_2H_6$ is also 5 orders of magnitude larger than $^3CH_2 + CH_4 \longrightarrow 2\,CH_3$. This is largely due to the fact that $^1CH_2 + CH_4 \longrightarrow C_2H_6$ is barrierless, whereas $^3CH_2 + CH_4 \longrightarrow 2\,CH_3$ has an energy barrier.

2.5 Conclusions

In this work, we use canonical variational transition state theory (CVT) to calculate 42 rate coefficients that are directly involved with or are in competition with HCN production in early Earth or Titan atmospheres. Approximately 36% of these reactions have no previously reported experimental or suggested value. To make such a large network of calculations feasible, we make use of computational quantum chemistry simulations at an accurate yet inexpensive level of theory: BHandHLYP/aug-cc-pVDZ. Moreover, we only calculate the temperature dependence of the rate coefficients for the reactions that have barriers. By using one level of theory for all reaction rate coefficient calculations, we expect the computational errors to be similar.

In this network, we focus on HCN production from methane and nitrogen radicals, which are produced in the atmosphere via UV photodissociation or lightning. Dissociation of CH_4 and N_2 produces both excited and ground state species, therefore we calculate the rate coefficients for multiple spin configurations involving these species. The reactions in our network have 1–5 spin configurations.

We list our five most important results below.

- We provide consistently calculated rate coefficients for 15 reactions that have no previously suggested values. In this sense, we fill a substantial gap in the data.

These previously unknown rate coefficients include those of several key reactions in the pathway to produce atmospheric HCN (e.g. $CH_2 + N \longrightarrow H_2CN$ and $H_2CN \longrightarrow HCN + H$ [36]).

- Of the reactions in our network with past experimental or suggested values, 93% are within an order of magnitude of these values. The remaining 7% differ by less than 2 orders of magnitude from experimental values. These discrepancies are either due to convergence issues or our chosen computation method. When convergence isn't an issue, re-running rate coefficient calculations at the similarly expensive CAM-B3LYP/aug-cc-pVDZ level of theory or the more expensive CCSD/aug-cc-pVDZ level of theory decreases the discrepancy between theory and experimental values.

- We find the reaction of $CH_3 + N \longrightarrow HCN + H_2$ on the singlet surface to be inefficient, with a rate coefficient near 10^{-28} cm^3s^{-1} (confirming the results of Cimas and Largo[225]). This is in contrast to experimental results which suggest a rate coefficient to have a value near 10^{-11} cm^3s^{-1} [195]. The experimental result may be due to the measurement of multi-step reaction, e.g., $CH_3 + N \longrightarrow H_2CN + H$ and $H_2CN + H \longrightarrow HCN + H_2$. However, we cannot exclude the possibility of a spin-forbidden process accounting for this experimental value.

- The effects of reaction spin configuration on the rate coefficient can be both subtle and substantial. For a given reaction, differences in rate coefficients between spin configurations can range from factors of order unity, up to 18 orders of magnitude. If there is a barrier involved with one or more of the reaction spin configurations, the difference between their reaction rate coefficients tends to be much greater than if all the reaction spin configurations are barrierless.

- Seven reaction rate coefficients in our network decrease rapidly with decreasing temperature, and become "slow" ($k < 10^{-21}$) at temperatures below ∼100–300 K. One reaction, $H_2CN \longrightarrow HCN + H$, increases rapidly for increasing temperatures; above 320 K, this reaction has the highest rate coefficient in the network.

Overall, we find CVT and computational quantum chemistry simulations at the BHandHLYP/aug-cc-pVDZ level of theory to be a feasible and accurate method for calculating a large set of small-molecule, multiple-spin configuration reaction rate coefficients for a range of terrestrial atmospheric temperatures. We also note that although calculations at the CCSD/aug-cc-pVDZ level of theory often lead to improvements in the rate coefficients' conformance to experimental values, computational cost and convergence issues made calculating all the rate coefficients at this level of theory impossible. Based on a limited number of calculations, we also find CAM-B3LYP to be an accurate alternative functional for performing CVT rate coefficient calculations and recommend it for a wider study.

2.6 Acknowledgments

We thank the two anonymous referees, whose reports led to the improvement of this work. We gratefully acknowledge Anand Patel (McMaster) and Farnaz Heidar-Zadeh (Univ. of Luxembourg) whose previous work and comments helped in the development of this research. B.K.D.P. is supported by an NSERC Postgraduate Scholarship-Doctoral (PGS-D). P.W.A is supported by NSERC, the Canada Research Chairs, and Canarie. R.E.P. is supported by an NSERC Discovery Grant. We are grateful to Compute Canada for the computer time allocated for this research.

2.7 Supporting Information

2.7.1 Experimental Data

Experiments and reviews have measured and suggested reaction rate coefficients for several of the reactions in this network at or near ∼298 K. These values are listed in Table 4.7.

All available experimental or recommended reaction rate coefficients for the reactions in this study. For brevity, only the 13 most recent experimental rate coefficients are listed for $CH_3 + CH_3 \longrightarrow C_2H_6$, for a complete listing, we refer the reader to the NIST Chemical Kinetics Database[227]. First-order rate coefficients have units s^{-1}. Second-order rate coefficients have units cm^3s^{-1}.

k(298K)	Technique	Temp. (K)	Pressure (Torr)	Reference(s)
$H_2CN + H \longrightarrow HCN + H_2$				
8.3×10^{-11}	Z	independent		Tomeczek and Gradoń[228]
$H_2CN + {}^4N \longrightarrow HCN + {}^3NH$				
4.4×10^{-11}	M	298	1	Nesbitt et al.[229]
$2\,H_2CN \longrightarrow HCN + H_2CNH$				
$3.3–8.3\times10^{-12}$	M	300	120–480	Horne and Norrish[230]

$CH_4 + H \longrightarrow CH_3 + H_2$				
3.5×10^{-17}	M	298		Lawrence and Firestone[231]
1.7×10^{-17}	M	298	0.55	Jones and Ma[232]
8.2×10^{-19}	S	300		Baulch et al.[137]
$CH_4 + {}^2N \longrightarrow H_2CNH + H$				
${}^a4.5\times10^{-12}$	M	298	700	Takayanagi et al.[233], Umemoto et al.[206]
${}^a3.7\times10^{-12}$	M	300	6	Fell et al.[234], Umemoto et al.[206]
${}^a2.7\times10^{-12}$	M	295	20	Umemoto et al.[235], Umemoto et al.[206]
${}^a2.4\times10^{-12}$	M	300	3–5	Black et al.[236], Umemoto et al.[206]
${}^a3.2\times10^{-12}$	S	298		Herron[237], Umemoto et al.[206]
$CH_4 + {}^2N \longrightarrow CH_3 + {}^3NH$				
${}^b1.7\times10^{-12}$	M	298	700	Takayanagi et al.[233], Umemoto et al. [206]
${}^b1.4\times10^{-12}$	M	300	6	Fell et al.[234], Umemoto et al.[206]
${}^b1.0\times10^{-12}$	M	295	20	Umemoto et al.[235], Umemoto et al.[206]
${}^b9.0\times10^{-13}$	M	300	3–5	Black et al.[236], Umemoto et al.[206]
${}^b1.2\times10^{-12}$	S	298		Herron[237], Umemoto et al.[206]
$CH_3 + H \longrightarrow CH_4$				
4.7×10^{-10}	M	300	high-pressure limit	Brouard et al.[238]
3.3×10^{-10}	M	308	high-pressure limit	Cheng and Yeh[239]
2.5×10^{-10}	M	308	300	Cheng et al.[240]
2.0×10^{-10}	M	296	735–755	Sworski et al.[241]
1.5×10^{-10}	M	300	high-pressure limit	Patrick et al.[242]
3.4×10^{-10}	F	298	high-pressure limit	Michael et al.[243]
3.5×10^{-10}	S	independent	high-pressure limit	Cobos and Troe[244]
3.5×10^{-10}	S	independent	high-pressure limit	Baulch et al.[137]
2.0×10^{-10}	S	298	high-pressure limit	Tsang[245]
$CH_3 + H_2 \longrightarrow CH_4 + H$				
${}^c1.3\times10^{-20}$	M	300		Kobrinsky and Pacey[246]
1.2×10^{-20}	S	300		Tsang and Hampson[247]
9.6×10^{-21}	S	300		Baulch et al.[137]
$CH_3 + {}^4N \longrightarrow HCN + H_2$				
8.6×10^{-12}	M	298	0.3–1.6	Marston et al.[195], Stief et al.[224]
$CH_3 + {}^4N \longrightarrow H_2CN + H$				
7.7×10^{-11}	M	298	0.3–1.6	Marston et al.[195], Stief et al.[224]
5.0×10^{-11}	S	independent		Miller and Bowman[248]
$2\,CH_3 \longrightarrow C_2H_6$				
6.5×10^{-11}	M	300	high-pressure limit	Walter et al.[249]
6.5×10^{-11}	M	298	high-pressure limit	Macpherson et al.[250]
6.0×10^{-11}	M	298	high-pressure limit	Du et al.[251]
6.0×10^{-11}	M	298	high-pressure limit	Slagle et al.[252]
${}^d5.9\times10^{-11}$	M	292	758	Sangwan et al.[253]
5.8×10^{-11}	M	298	750	Pagsberg et al.[254]
5.5×10^{-11}	M	298	high-pressure limit	Hippler et al.[255]
5.2×10^{-11}	M	298	100	Fahr et al.[256]
4.6×10^{-11}	M	300	1	Wang et al.[257]
4.0×10^{-11}	M	302	81–571	Arthur[258]
3.5×10^{-11}	M	308	86	Anastasi and Arthur[259]
6.0×10^{-11}	S	independent	high-pressure limit	Baulch et al.[137]
4.4×10^{-11}	S	298	high-pressure limit	Tsang[245]
${}^1CH_2 + H \longrightarrow CH + H_2$				
5.0×10^{-11}	S			Tsang and Hampson[247]
${}^1CH_2 + H_2 \longrightarrow CH_4\cdot \longrightarrow CH_3 + H$				
1.3×10^{-10}	M	295	6	Langford et al.[204]
1.1×10^{-10}	M	298	10^{-4}–10	Ashfold et al.[205]
7.0×10^{-12}	M	298	10	Braun et al.[203]
1.2×10^{-10}	S			Tsang and Hampson[247]
1.2×10^{-10}	S	independent		Baulch et al.[137]
${}^1CH_2 + {}^1CH_2 \longrightarrow C_2H_2 + 2\,H$				

5.0×10^{-11}	S			Tsang and Hampson[247]
$^1CH_2 + {}^3CH_2 \longrightarrow C_2H_2 + H_2$				
3.0×10^{-11}	S			Tsang and Hampson[247]
$^1CH_2 + CH_3 \longrightarrow C_2H_4 + H$				
3.0×10^{-11}	S			Tsang and Hampson[247]
$^1CH_2 + CH_4 \longrightarrow 2\,CH_3$				
7.3×10^{-11}	M	298	10^{-4}–10	Ashfold et al.[205]
7.0×10^{-11}	M	295	6	Langford et al.[204]
1.9×10^{-12}	M	298	5–20	Braun et al.[203]
7.1×10^{-11}	S			Tsang and Hampson[247]
$^3CH_2 + H \longrightarrow CH_3\cdot \longrightarrow CH + H_2$				
2.7×10^{-10}	M	285	2	Boullart and Peeters[197]
2.7×10^{-10}	M	298	2	Böhland and Temps[200]
$^e2.6\times10^{-10}$	M	300	2	Devriendt et al.[196]
1.8×10^{-10}	M	298	1–2	Böhland et al.[198]
$^c1.4\times10^{-10}$	M	300	100	Zabarnick et al.[199]
8.3×10^{-11}	M	298	2	Grebe and Homann[201]
2.0×10^{-10}	S	300		Baulch et al.[137]
2.7×10^{-10}	S	298		Tsang and Hampson[247]
$^3CH_2 + H_2 \longrightarrow CH_3 + H$				
$<5.0\times10^{-14}$	M	298	10	Braun et al.[203]
$<6.9\times10^{-15}$	M	295	8	Darwin and Moore[260]
$<5.0\times10^{-15}$	M		10	Pilling and Robertson[261]
$^3CH_2 + {}^3CH_2 \longrightarrow C_2H_2 + 2\,H$				
5.3×10^{-11}	M	298	20–700	Braun et al.[203]
5.3×10^{-11}	S	300		Baulch et al.[137]
$^3CH_2 + CH_3 \longrightarrow C_2H_5\cdot \longrightarrow C_2H_4 + H$				
2.1×10^{-10}	M	300	1	Wang and Fockenberg[257]
1.1×10^{-10}	M	298	1	Deters et al.[262]
1.0×10^{-10}	M	308	50–700	Laufer and Bass[263]
5.0×10^{-11}	M		200	Pilling and Robertson[264]
7.0×10^{-11}	S	independent		Baulch et al.[137]
7.0×10^{-11}	S	298		Tsang and Hampson[247]
$^3CH_2 + CH_4 \longrightarrow 2\,CH_3$				
$<5.0\times10^{-14}$	M	298	10	Braun et al.[203]
$^f3.1\times10^{-19}$	M	298	2–3	Böhland et al.[265]
$<3.0\times10^{-19}$	S	298		Tsang and Hampson[247]
$CH + H_2 \longrightarrow CH_3$				
1.6×10^{-10}	M	294	high-pressure limit	Brownsword et al.[266]
5.1×10^{-11}	M	300	750	Fulle and Hippler[267]
4.5×10^{-11}	M	298	591	Becker et al.[202]
4.5×10^{-11}	M	279	600	Berman and Lin[268]
3.0×10^{-11}	M	294	750	McIlroy and Tully[269]
2.3×10^{-11}	M	298	100	Butler et al.[270]
1.7×10^{-11}	M			Bosnali and Perner[271]
1.0×10^{-12}	M	298	1–9	Braun et al.[272]
$CH + H_2 \longrightarrow CH_3\cdot \longrightarrow {}^3CH_2 + H$				
$^c9.1\times10^{-13}$	M	300	100	Zabarnick et al.[199]
1.2×10^{-12}	M	294	400	Brownsword et al.[266]
4.5×10^{-11}	M	298	591	Becker et al.[202]
$CH + {}^4N \longrightarrow {}^3HCN \longrightarrow CN + H$				
1.6×10^{-10}	M	298	4	Brownsword et al.[273]
$1.2–1.4\times10^{-10}$	M	296	5	Daranlot et al.[222]
2.1×10^{-11}	M	298	5–15	Messing et al.[274]
$2\,CH \longrightarrow C_2H_2$				
2.0×10^{-10}	M	298	1–330	Braun et al.[272]
1.7×10^{-10}	M	298	1–500	Braun et al.[275]
$CH + CH_4 \longrightarrow C_2H_4 + H$				
3.0×10^{-10}	M	298	30–100	Butler et al.[270]
1.0×10^{-10}	M	298	100	Butler et al.[276]
9.8×10^{-11}	M	298	100	Berman and Lin[277]
9.1×10^{-11}	M	298	50–300	Blitz et al.[278]
8.9×10^{-11}	M	295	9–12	Canosa et al.[279]
6.7×10^{-11}	M	298	100	Thiesemann et al.[280]
3.3×10^{-11}	M			Bosnali and Perner[271]
2.5×10^{-12}	M	298	100	Braun et al.[272]
2.0×10^{-12}	M	298	1-500	Braun et al.[275]
9.8×10^{-11}	S	298		Baulch et al.[137]
$^3NH + H \longrightarrow H_2 + {}^4N$				
3.2×10^{-12}	M	298	2–8	Adam et al.[281]

$^3NH + ^4N \longrightarrow N_2 + H$				
2.5×10^{-11}	M	298	11–15	Hack et al.[282]
2.6×10^{-11}	S	300		Konnov and De Ruyck[283]
$^2N + H_2 \longrightarrow NH_2\cdot \longrightarrow ^3NH + H$				
5.0×10^{-12}	M	300	3–5	Black et al.[236]
3.5×10^{-12}	M	300	6	Fell et al.[234]
2.7×10^{-12}	M	300	2–5	Black et al.[284]
2.4×10^{-12}	M	300	753	Suzuki et al.[285]
2.3×10^{-12}	M	295	30	Umemoto et al.[286]
2.3×10^{-12}	M	300	1–3	Piper et al.[287]
2.1×10^{-12}	M	300	26	Husain et al.[288]
1.8×10^{-12}	M	298	1	Whitefield et al.[289]
1.7×10^{-12}	M	300	50	Husain et al.[290]
2.2×10^{-12}	S	200–300		Herron[237]

[a] Experimental value of $CH_4 + ^2N \longrightarrow$ products, multiplied by a branching ratio of 0.8[206].

[b] Experimental value of $CH_4 + ^2N \longrightarrow$ products, multiplied by a branching ratio of 0.3[206].

[c] Experiments performed at 372 K and extrapolated to 300 K.

[d] Value taken as average of two identical experiments.

[e] Experiments performed at $\geq$ 400 K and extrapolated to 300 K.

[f] Experiments performed at $\geq$ 413 K and extrapolated to 300 K.

Z: Zero activation energy value. Calculated by numerical modeling using the chemical compositions of the flames of CH_4 + air.

M: Monitoring decay of reactants and/or production of products.

S: Suggested value based on experiments and/or evaluations at a range of temperatures.

F: Fitting of simulated concentration profiles to absolute concentration profiles from experiments reported by Barker et al.[291].

2.7.2 Previous Theoretical Data

Previous theoretical studies have been performed on the reactions in this network. In Table 2.6, we list the theoretical rate coefficients and the methods that were employed to calculate them.

Previous theoretical rate coefficients for the reactions in this study. For sources that performed multiple rate coefficient calculations with different theoretical and/or computational methods, we list the range of their results here. First-order rate coefficients have units s^{-1}. Second-order rate coefficients have units cm^3s^{-1}.

k(298K)	Theory	Computational Method	Reference(s)
$CH_4 + H \longrightarrow CH_3 + H_2$			
4.1×10^{-21}–2.2×10^{-18}	TST, quantum dynamics	CCSD(T)/cc-pVTZ[a]	Kerkeni and Clary[292]
8.4×10^{-19}–2.1×10^{-18}	CVT + SCT[b]	BH&HLYP/6-311G(d,p), PMP4/6-311+G(2df,2pd)[c]	Truong and Duncan[293]
1.6×10^{-18}	CVT + SCT	PMP4/cc-pVTZ[d]	Maity et al.[134]
1.3×10^{-18}	CVT + SCT[e]	QCISD/6-311G(d,p)	Truong[136]
9.8×10^{-19}	CVT + μOMT		Espinosa-García and Corchado[294], Jordan and Gilbert[295]
6.5×10^{-19}	CVT + μOMT		Espinosa-García and Corchado[294], Joseph et al.[296]
3.0×10^{-21}–6.0×10^{-19}	TST, quantum dynamics	CCSD(T)/cc-pVTZ[a]	Kerkeni and Clary[297]
3.8×10^{-19}	BEBO		Clark and Dove[298]
8.7×10^{-21}–2.4×10^{-19}	TST, CVT, CVT + SCT		Pu and Truhlar[299]
1.8×10^{-21}–1.6×10^{-19}	TST	G2(MP2)[f], BAC-MP4[g]	Berry et al.[300]
8.1×10^{-20}	TST + tunneling	UMP2/6-31G-(d,p)	Bryukov et al.[301]
4.6×10^{-20}	TST + WTC	PMP4SDTQ/6-311G**[h]	Gonzalez et al.[302]
$CH_3 + H_2 \longrightarrow CH_4 + H$			
1.2×10^{-19}	CVT + μOMT		Espinosa-García and Corchado[294], Joseph et al.[296]
1.1×10^{-19}	CVT + SCT	PMP4/cc-pVTZ[d]	Maity et al.[134]
1.5–8.2×10^{-20}	CVT + SCT[b]	BH&HLYP/6-311G(d,p), PMP4/6-311+G(2df,2pd)[c]	Truong and Duncan[293]
8.0×10^{-20}	CVT + μOMT		Espinosa-García and Corchado[294], Jordan and Gilbert[295]

5.2×10^{-20}	CVT + SCT[e]	QCISD/6-311G(d,p)	Truong[136]
1.7×10^{-20}	TST + tunneling	UMP2/6-31G-(d,p)	Bryukov et al.[301]
$CH_3 + {}^4N \longrightarrow H_3CN\cdot \longrightarrow H_2CN + H$			
1.9×10^{-10}	CVT + RRKM	CCSD(T)/CBS	Alves et al.[303]
9.1×10^{-12}	μVT + RRKM	CCSD(T)/cc-pVTZ[i]	Cimas and Largo[225]
$CH_4 + {}^2N \longrightarrow$ products			
8.5×10^{-14}	CVT	CASSCF(5,5)/6-311G**	Takayanagi et al.[233]
$CH_3 + H \longrightarrow CH_4$			
6.7×10^{-10}	CVT	MP4/6-31G**	Hase and Duchovic[304]
[j]4.7×10^{-10}	CVT + RRKM		Pilling[305]
[j]$4.3–4.7\times10^{-10}$	μVT + RRKM, CVT + RRKM		Forst[306]
[j]3.3×10^{-10}	SACM/CT	CASPT2/cc-pVDZ[k]	Troe and Ushakov[307]
[j]3.2×10^{-10}	VRC-TST	CASPT2/cc-pVDZ[k]	Harding et al.[308]
$2.0–2.7\times10^{-10}$	CVT	MP4/6-31G**, MRD-CI/6-31G**	Hase et al.[220]
2.1×10^{-10}	CVT	MCSCF-CI/DZP[l]	Takahashi et al.[309]
$2\,CH_3 \longrightarrow C_2H_6$			
$1.8\times10^{-10}–4.6\times10^{-9}$	CVT	CASPT2/ANO-L[m]	Li et al.[208]
[j]$6.9–8.4\times10^{-11}$	LTS	MC	Wardlaw and Marcus[310]
8.3×10^{-11}	CVT	MRD-CI/DZ	Darvesh et al.[311]
[j]7.2×10^{-11}	FTST	MC	Pesa et al.[312]
[j]$5.8–6.7\times10^{-11}$	μVT + RRKM		Forst[306]
[j]6.3×10^{-11}	CVT CVT + RRKM	CAS+1+2/cc-pVDZ	Klippenstein and Harding[313]
5.8×10^{-11}	VRC-TST	CASPT2/cc-pVDZ[k]	Klippenstein et al.[314]
[j]5.8×10^{-11}	RRKM + FTST		Wagner and Wardlaw[315]
[j]5.6×10^{-11}	CVT	MRCI+Q/aug-cc-pVTZ	Wang et al.[316]
2.0×10^{-11}	CVT	B3LYP/6-31G**	Lorant et al.[317]
${}^3CH_2 + H_2 \longrightarrow CH_3 + H$			
1.5×10^{-18}	TST	G2M(RCC2)[n]	Lu et al.[318]
${}^3CH_2 + {}^4N \longrightarrow H_2CN\cdot \longrightarrow HCN + H$			
7.9×10^{-11}	quantum dynamics	MP4SDTQ/6-311++G(3df,3pd)[o]	Herbst et al.[319]
${}^3CH_2 + {}^3CH_2 \longrightarrow C_2H_2 + 2\,H$			
1.5×10^{-10}	VRC-TST	CASPT2/aug-cc-pVTZ[p]	Jasper et al.[221]
${}^3CH_2 + CH_3 \longrightarrow C_2H_4 + H$			
2.2×10^{-10}	VRC-TST	CASPT2/aug-cc-pVTZ[p]	Jasper et al.[221]
$CH + H_2 \longrightarrow CH_3$			
[j]7.8×10^{-11}	RRKM		McIlroy and Tully[269]
$CH + H_2 \longrightarrow CH_3\cdot \longrightarrow {}^3CH_2 + H$			
3.3×10^{-11}	QCT	MRCI/aug-cc-pVTZ	Mayneris et al.[320]
$CH + N \longrightarrow {}^3HCN\cdot \longrightarrow CN + H$			
1.2×10^{-10}	quantum dynamics	MRCI+Q/AVTZ	Daranlot et al.[222]
${}^3NH + {}^4N \longrightarrow N_2 + H$			
1.9×10^{-11}	QCT	MRCI/aug-cc-pVQZ	Caridade et al.[321]
${}^3NH + H \longrightarrow H_2 + {}^4N$			
1.5×10^{-12}	CT	MRCI/aug-cc-pVQZ	Adam et al.[281]
$1.3–5.2\times10^{-12}$	CVT	MP-SAC4/6-311G**	Xu et al.[322]
$2.0–5.5\times10^{-13}$	QCT, CVT	MCQDPT2/6-311++G**[q]	Pascual et al.[323]
${}^2N + H_2 \longrightarrow NH_2\cdot \longrightarrow {}^3NH + H$			
$2.5–3.3\times10^{-12}$	quantum dynamics, QCT	FOCI/TZP	Takayanagi et al.[324]
$2.7–2.9\times10^{-12}$	QCT	FOCI/TZP	Kobayashi et al.[325]
$1.8–2.7\times10^{-12}$	QCT, CVT		Suzuki et al.[285]
8.9×10^{-13}	QCT	MRCI/aug-pVTZ	Pederson et al.[326]

---

[a] Single point energies are based on optimized geometries calculated at the MP2/cc-pVTZ level.

[b] Energy barrier scaled by a factor of 1.174.

[c] Single point energies are based on optimized geometries calculated at the BHandHLYP/6-311G(d,p) level.

[d] Single point energies are based on optimized geometries calculated at the BHandHLYP/cc-pVDZ level.

[e] Energy barrier scaled by a factor of 0.86.

[f] Single point energies are based on optimized geometries calculated at the MP2/6-31G(d) level.

[g] Single point energies are based on optimized geometries calculated at the HF/6-31G(d) level.

[h] Single point energies are based on optimized geometries calculated at the UMP2/6-31G** level.

[i] Single point energies are based on optimized geometries calculated at the B3LYP/cc-pVTZ level.

[j] Values calculated in the high-pressure limit (p $\rightarrow \infty$).

[k] Single point energies are based on optimized geometries calculated at the B3LYP/6-31G* level,

and corrections are applied at the CAS+1+2+QC/aug-cc-pVTZ level.

[l] CI calculations are based on optimized geometries calculated at the UHF/DZP level.

[m] Single point energies are based on optimized geometries calculated at the CASSCF/ANO-L level.

[n] Single point energies are based on optimized geometries calculated at the B3LYP/6-311++G(3df, 2p) level.

[o] Single point energies are based on optimized geometries calculated at the MP2/6-31G(d,p) level.

[p] Single point energies are based on optimized geometries calculated at the B3LYP/6-311++G(d,p) level.

[q] Single point energies are based on optimized geometries calculated at the FORS-MCSCF(7,6)/6-311++G** level.

TST: Transition state theory.
CVT: Canonical variational transition state theory.
SCT: Small curvature tunneling approximation
μOMT: Microcanonical optimized multidimensional tunneling.
BEBO: bond-energy-bond-order method.
WTC: Wigner tunneling correction.
RRKM: Rice-Ramsperger-Kassel-Marcus theory.
μVT: Microcanonical variational transition state theory.
SACM/CT: Statistical adiabatic channel model/classical trajectories approach.
VRC-TST: Variable reaction coordinate transition state theory.
LTS: Loose transition state model.
MC: Monte Carlo simulations.
FTST: Flexible transition state theory.
QCT: Quasi-classical trajectory method
CT: Classical trajectory method

2.7.3 Example Calculation and Computational Methods Comparison

The $CH_4 + H \longrightarrow CH_3 + H_2$ abstraction reaction has been thoroughly studied both experimentally and theoretically [134, 136, 137, 231, 232, 293–300, 302]. A pair of experiments at 298 K place its rate coefficient between 1.7–3.5$\times10^{-17}$ cm^{3}s^{-1} [231, 232]. However, based on a range of experiments and evaluations over a wider temperature range (300–2000 K), it has been suggested the rate coefficient is closer to 8.2$\times10^{-19}$ cm^{3}s^{-1} [137]. Previous theoretical studies have calculated its rate coefficient to be between 1.8$\times10^{-21}$ and 2.2$\times10^{-18}$ cm^{3}s^{-1} (see Table 2.6).

The geometry of this reaction progresses as follows: A single H atom approaches a CH_4 molecule directly in line with one of its H atoms and its central C atom. The H-C bond in methane then stretches until its H atom bonds with the adjacent H atom. The two newly formed molecules, H_2 and CH_3 then separate. The geometry of the transition state is depicted in Figure 2.4.

In Figure 2.4, we show $\Delta G_{GT}(298.15K, s)$ with the reaction coordinate representing the C-H bond distance. At the BHandHLYP/aug-cc-pVDZ level of theory, the maximum ΔG occurs at a C-H distance of 1.44Å, which is slightly farther along the reaction coordinate than the conventional transition state (1.409Å).

We calculate the rate coefficient for this reaction using 6 different computational methods, and display them in Table 2.7.

Rate coefficient calculations using BHandHLYP and CAM-B3LYP methods are

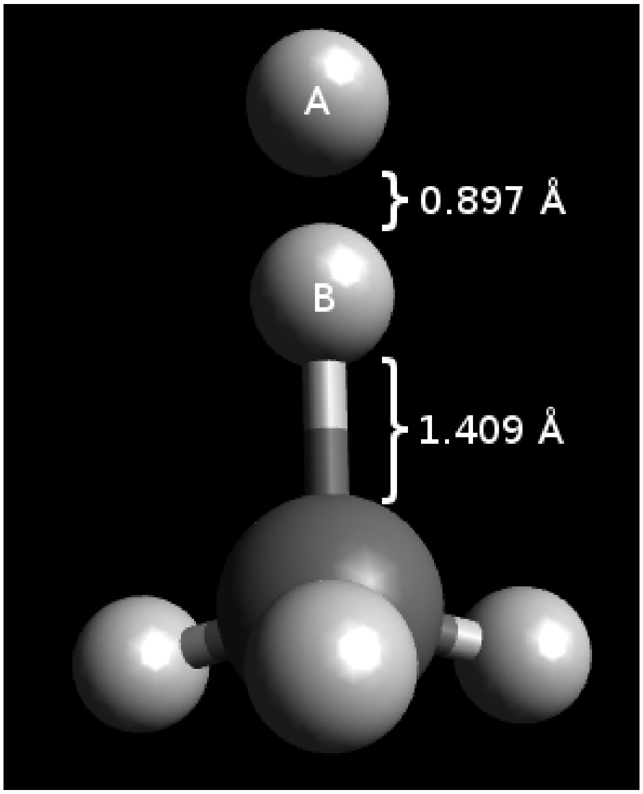

Figure 2.3: Geometry of the conventional transition state for $CH_4 + H \longrightarrow CH_3 + H_2$ at the BHandHLYP/aug-cc-pVDZ level of theory. In the reactant state, hydrogen B is 1.09Å from the central carbon. In the product state hydrogen B is 0.754 Å from hydrogen A.

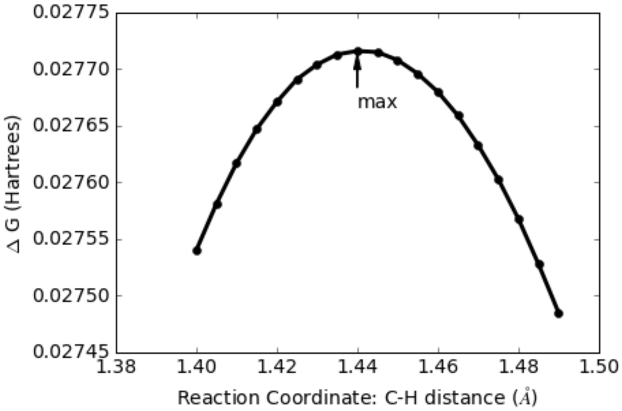

Figure 2.4: Gibbs free energy difference as a function of the reaction coordinate (C-H bond distance) for $CH_4 + H \longrightarrow CH_3 + H_2$ at the BHandHLYP/aug-cc-pVDZ level of theory. The maximum ΔG occurs at 1.44Å. ΔG is calculated as the Gibbs free energy at the reaction coordinate minus the Gibbs free energy of the reactants placed 100Å apart.

Table 2.7: Calculated rate coefficients for $CH_4 + H \longrightarrow CH_3 + H_2$ using 6 different computational methods with the aug-cc-pVDZ basis set. Experimental and suggested values range from 8.2×10^{-19} to 3.5×10^{-17} cm^3s^{-1} [137, 231, 232]. The error factor is the multiplicative or divisional factor from the nearest experimental or suggested value; the error factor is 1 if the calculated value is within the range of experimental or suggested values. Rate coefficients have units cm^3s^{-1}.

Computational Method	k(298)	Error factor
HF	3.5×10^{-25}	2×10^{6}
M06-2x	5.7×10^{-20}	14
CCSD	9.9×10^{-20}	8
BHandHLYP	8.1×10^{-18}	1
CAM-B3LYP	3.1×10^{-17}	1
B3LYP	3.9×10^{-16}	11

within the experimental and suggested range. Calculations using HF grossly overestimate the energy barrier, and provide a rate coefficient several orders of magnitude lower than the experimental and suggested range. M06-2x and CCSD methods also provide values lower than the experimental and suggested range, however only by approximately an order of magnitude. Calculations using B3LYP under-estimate the energy barrier, leading to a value approximately an order of magnitude higher than the experimental and suggested range.

The calculated rate coefficient using the BHandHLYP functional sits in the middle of the range of experimental and suggested values, whereas he rate coefficient calculated using CAM-B3LYP sits within ∼10% of the experimental value at the high end of the range. The BHandLYP result may provide the best compromise between the experimental and suggested rate coefficients for this reaction.

Finally, CCSD provides a fairly accurate rate coefficient within a factor of 8 of the suggested value.

2.7.4 Theoretical Case Studies

2.7.4.1 Case Study 1: $H_2CN + H \longrightarrow HCN + H_2$

Tomeczek and Gradoń[228] used published chemical compositions of the flames of CH_4 and O_2 + N_2 at 2500 to 1850 K to suggest a temperature-independent rate coefficient for $H_2CN + H \longrightarrow HCN + H_2$. They suggest the value 8.3×10^{-11} cm^3s^{-1} for this reaction. However, they note that this does not include the effects of an energy barrier. Another way to state this is, they suggest a value for the entropic component of this reaction, but not the energetic component.

We find no previous theoretical reaction rate coefficients for $H_2CN + H \longrightarrow HCN + H_2$.

This reaction occurs on the singlet and triplet PES's. There is no energy barrier for this reaction on the singlet PES. Conversely on the triplet PES, where excited ^3HCN is produced, the effects of the energy barrier are significant.

On the singlet surface, we calculate the reaction rate coefficient at the BHandHLYP/aug-cc-pVDZ level of theory to be 1.8×10^{-11} cm^3s^{-1}. This is less than a factor of 5 larger than the experimental value for the barrierless reaction.

On the triplet surface, the reaction rate coefficient is too small to consider in this study ($k < 10^{-21}$ cm^3s^{-1}).

2.7.4.2 Case Study 2: $2\,H_2CN \longrightarrow HCN + H_2CNH$

Horne and Norrish[230] calculated the experimental reaction rate coefficient for $2\,H_2CN \longrightarrow HCN + H_2CNH$ at 300 K by monitoring the decay of H_2CN. The assumption they made was that $2\,H_2CN \longrightarrow HCN + CH_2NH$ is the dominant decay pathway of H_2CN. The value they obtained was in the range of 3.3–8.3×10^{-12} cm^3s^{-1}.

No theoretical reaction rate coefficients for $2\,H_2CN \longrightarrow HCN + H_2CNH$ have been previously published.

We find a direct reaction pathway on the singlet PES that has no energy barrier. However, the simulations did not converge beyond a N-H bond distance of 1.95 Å and the Gibbs maximum was not found. However, choosing the reaction coordinate at a N-H bond distance of 1.95 Å for the calculation provides us with a lower bound estimate of the rate coefficient, which we calculate to be 3.7×10^{-14} cm^3s^{-1}. This value is a factor of 89 smaller than the closest experimental value. The discrepancy between the theoretical and experimental values is expected to be due to these convergence issues.

A higher energy reaction pathway involving two ground state H_2CN molecules exists on the triplet surface, however, this reaction produces excited ^3HCN and is likely much less efficient than the singlet case.

2.7.4.3 Case Study 3: $CH_4 + N \longrightarrow$ products

Several experiments have measured the rate coefficient of $CH_4 + {}^2N \longrightarrow$ products by monitoring the decay of ${}^2N$ in the presence of CH_4 at 295–300 K [233–236]. The measured values range from 3.0–5.4×10^{-12} cm^3s^{-1}. Herron[237] reviewed these experiments and recommended a value of k(298) = 4.0×10^{-12} cm^3s^{-1}. Umemoto et al.[206] measured the product yields of H and ${}^3NH$ in similar experiments to suggest branching ratios for $CH_4 + {}^2N \longrightarrow H_2CNH + H$ and $CH_4 + {}^2N \longrightarrow CH_3 + {}^3NH$ to be 0.8±0.2 and 0.3±0.1, respectively. Multiplying with these branching ratios, the experimental rate coefficients for $CH_4 + {}^2N \longrightarrow H_2CNH + H$ range from 2.4–4.5×10^{-12} cm^3s^{-1} and the experimental rate coefficients for $CH_4 + {}^2N \longrightarrow CH_3 + {}^3NH$ range from 0.9–1.7×10^{-12} cm^3s^{-1}.

Takayanagi et al.[233] used CVT at the CASSCF(5,5)/6-311G** level of theory to calculate the rate coefficient of $CH_4 + N \longrightarrow$ products to be 8.5×10^{-14} cm^3s^{-1}. They note that their disagreement between experimental and theoretical values is due to the CASSCF calculations estimating too large a barrier. Ouk et al.[327] used TST + WTC at the MRCI+P+Q/aug-cc-pVTZ level of theory to calculate the rate coefficient, and obtained a value closer to the experimental values at 6.8×10^{-12} cm^3s^{-1}. They confirm the results from experiment that suggests a small barrier exists, although no barrier is found using the CCSD(T) and B3LYP levels of theory [328]. The experimental barrier has a height of 6.3 kJ mol^{-1} [233].

In this case study, we analyze the two main branches for the reaction $CH_4 + {}^2N \longrightarrow$ products. The mechanistic model for these reactions is shown in Figure 2.5.

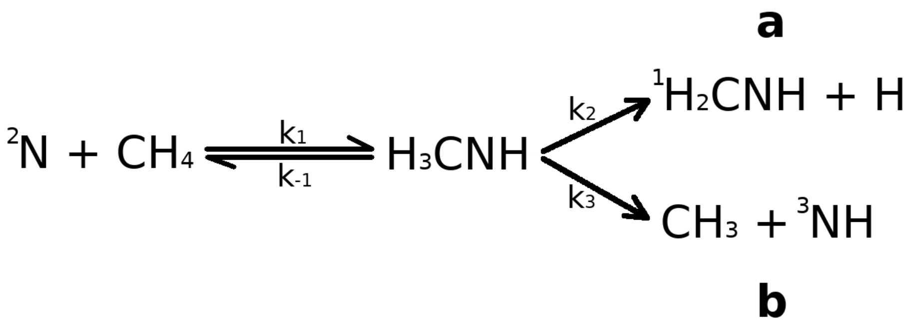

Figure 2.5: Mechanistic models for the production of (**a**) ${}^1H_2CNH$ + H and (**b**) CH_3 + ${}^3NH$ from ${}^2N$ + CH_4 on the doublet potential energy surface.

Similar to Balucani et al.[328], we find no barrier for the $CH_4 + {}^2N \longrightarrow H_3CNH$

reaction step. We also run into convergence problems when stretching the C-N bond distance farther than 2.82 Å. Therefore, we are unable to find a Gibbs maximum, and instead choose the reaction coordinate at 2.82 Å for our CVT calculation of k. Past theoretical works found the transition state to be at a C-N bond distance of 2.26–2.45 Å [327–329].

We find the barrierless reaction rate coefficient of $CH_4 + {}^2N \longrightarrow H_3CNH$ at the BHandHLYP/aug-cc-pVDZ level of theory to be 6.0×10^{-10} cm^3s^{-1}, a value two orders of magnitude greater than the closest experimental value. Given that there is likely a small barrier of ~6.3 kJ mol^{-1} for this reaction, we insert this experimental barrier into the calculation for k, and obtain a value of 4.7×10^{-11} cm^3s^{-1}. This is only a factor of 9 larger than the nearest experimental value.

There are several decay pathways for the H_3CNH molecule (e.g. [328]). Nevertheless, we calculate the upper bound for the rate coefficients of $CH_4 + {}^2N \longrightarrow H_2CNH + H$ and $CH_4 + {}^2N \longrightarrow CH_3 + {}^3NH$ by assuming H_3CNH only decays through these two dominant pathways.

The steady-state solution of the kinetic rate equations for the above mechanistic models lead to the overall rate constants for a) $CH_4 + {}^2N \longrightarrow {}^1H_2CNH + H$ and b) $CH_4 + {}^2N \longrightarrow CH_3 + {}^3NH$ on the doublet PES.

$$k_a = \frac{k_1 k_2}{k_{-1} + k_2 + k_3} \tag{2.41}$$

$$k_b = \frac{k_1 k_3}{k_{-1} + k_2 + k_3} \tag{2.42}$$

The values of the reaction rate constants at the BHandHLYP/aug-cc-pVDZ level of theory are listed in Table 2.8.

We calculate the overall rate constant for $CH_4 + {}^2N \longrightarrow H_3CNH\cdot \longrightarrow {}^1H_2CNH + H$ to be the same as the rate constant for $CH_4 + {}^2N \longrightarrow H_3CNH$. This means the first step is the rate-limiting step. We calculate the value for k_a to be 4.7×10^{-11} cm^3s^{-1}, which is approximately a factor of 10 smaller than the experimental values. We find the overall rate coefficient for $CH_4 + {}^2N \longrightarrow H_3CNH\cdot \longrightarrow CH_3 + {}^3NH$ to be inefficient ($k_b = 5.8\times10^{-29}$ cm^3s^{-1}). This is several orders of magnitude smaller than the rate coefficients suggested by the experimental branching ratios [206]. However, some theoretical branching ratios for $CH_4 + {}^2N \longrightarrow H_3CNH\cdot \longrightarrow CH_3 + {}^3NH$ are as low as 0.01 [327], and in every case, $CH_4 + {}^2N \longrightarrow H_3CNH\cdot \longrightarrow {}^1H_2CNH + H$

Table 2.8: Calculated overall rate coefficients for $CH_4 + {}^2N \longrightarrow {}^1H_2CNH + H$ and $CH_4 + {}^2N \longrightarrow CH_3 + {}^3NH$, as well as the intermediate forward and reverse rate coefficients which were used in the calculations. In all simulations, the BHandHLYP method was used with the aug-cc-pVDZ basis set. When using a branching ratio of 0.8 for $CH_4 + {}^2N \longrightarrow {}^1H_2CNH + H$ [206], experiments from 295–300 K provide k_a values between 2.4 and 4.5×10^{-12} cm^{3}s^{-1}. Similarly when using a branching ratio of 0.3 for $CH_4 + {}^2N \longrightarrow CH_3 + {}^3NH$, the same experiments provide k_b values between 0.9–1.7×10^{-12} cm^{3}s^{-1}. First-order rate coefficients have units s^{-1}. Second-order rate coefficients have units cm^{3}s^{-1}.

Rate coefficient	k(298)
k_a	4.7×10^{-11}
k_b	5.8×10^{-29}
k_1	$^a4.7\times10^{-11}$
k_{-1}	3.0×10^{-66}
k_2	4.9×10^{-13}
k_3	6.0×10^{-31}

^{a} Simulations did not converge beyond a C-N bond distance of 2.82Å; therefore the rate coefficient is a lower bound.

is the dominant product. Considering all this, we do not include the inefficient $CH_4 + {}^2N \longrightarrow H_3CNH\cdot \longrightarrow CH_3 + {}^3NH$ reaction in our network.

2.7.4.4 Case Study 4: $CH_3 + N \longrightarrow$ products

Stief et al.[224] experimentally calculated the overall reaction rate constant for $CH_3 + N \longrightarrow$ products at 298 K to be 8.6×10^{-11} cm^{3}s^{-1} by monitoring the decay of reactants CH_3 and N in a volume. Marston et al.[195] suggest the three possible branches for the reaction of $CH_3 + N \longrightarrow$ products are:

$$CH_3 + N \longrightarrow H_2CN + H,$$

$$CH_3 + N \longrightarrow HCN + H_2,$$

and

$$CH_3 + N \longrightarrow HCN + 2\,H.$$

Marston et al.[195] monitored the production of H_2, and H in experiments reacting CH_3 and N, and calculated the above reaction branching ratios to be approximately 0.9, 0.1, and 0 respectively. This suggests a preference for the $CH_3 + N \longrightarrow H_2CN + H$ pathway by approximately an order of magnitude over the $CH_3 + N \longrightarrow HCN + H_2$ pathway. It must be noted that in performing this calculation, Marston et al.[195] assumed that H_2 and H were solely generated through the above pathways. They caution the reader that it is also possible that these products formed through the H_2CN intermediate.

Miller and Bowman[248] suggested the rate coefficient of $CH_3 + N \longrightarrow H_2CN + H$ to be 5.0×10^{-11} cm^{3}s^{-1} based on thermodynamic calculations.

There are two main PES's that the CH_3 + N reaction evolves on: the triplet and the singlet surfaces. The quintet surface is also possible, however this reaction is much higher in energy and therefore much less likely to occur [225]. Both the ground state nitrogen atom (i.e. ^4N) and the excited nitrogen atom (i.e. ^2N) can react with CH_3 on the triplet PES. Only the excited state nitrogen atom can react with CH_3 on the singlet PES.

A computational study of the $CH_3 + N \longrightarrow$ products reaction shows a preference for the $CH_3 + {}^4N \longrightarrow H_2CN + H$ pathway [225]. This study finds the $CH_3 + {}^2N \longrightarrow HCN + H_2$ channel to be negligible. Cimas and Largo[225] suggest that the HCN measured in experiments by Marston et al.[195] formed through the H_2CN intermediate, via reaction equations 2.9–2.11. Chiba and Yoshida[330] alternatively suggest that HCN + H_2 may form through the triplet-singlet spin-forbidden process.

Alves et al.[303] and Cimas and Largo[225] analyzed $CH_3 + N \longrightarrow$ products theoretically using quantum computational simulations at the CCSD(T)/CBS and CCSD(T)/cc-pVTZ levels of theory, and calculated its reaction rate coefficients to be 1.93×10^{-10} cm^{3}s^{-1} and 9.1×10^{-12} cm^{3}s^{-1}, respectively.

In this case study, we analyze the three suggested main branches for $CH_3 + N \longrightarrow$ products using CVT (see the methods section for full details). Computational studies show that $CH_3 + {}^4N \longrightarrow$ products reactions first proceed through a barrierless reaction to H_3CN on the triplet surface [225, 303]. We confirm this barrierless reaction

($CH3 + {}^4N \longrightarrow {}^3H3CN$) and calculate its rate coefficients at the BHandHLYP/aug-cc-pVDZ level of theory to be 3.3×10^{-11} cm^{3}s^{-1}. This result is less than a factor of 3 smaller than the experimental result (8.6×10^{-11} cm^{3}s^{-1} [224]). Our calculated rate coefficient is also within a factor of 3 of the calculated value by Cimas and Largo[225] at the CCSD(T)/cc-pVTZ level of theory (9.1×10^{-12} cm^{3}s^{-1}).

We do not find a direct reaction pathway on the singlet or triplet surface to $CH3 + N \longrightarrow HCN + 2\,H$.

We display the mechanistic models for forming H_2CN + H, and HCN + H_2 from CH_3 + N in Figure 2.6. These mechanistic models are similar to that used in Alves et al.[303]. Note we do not analyze spin-forbidden processes in these models.

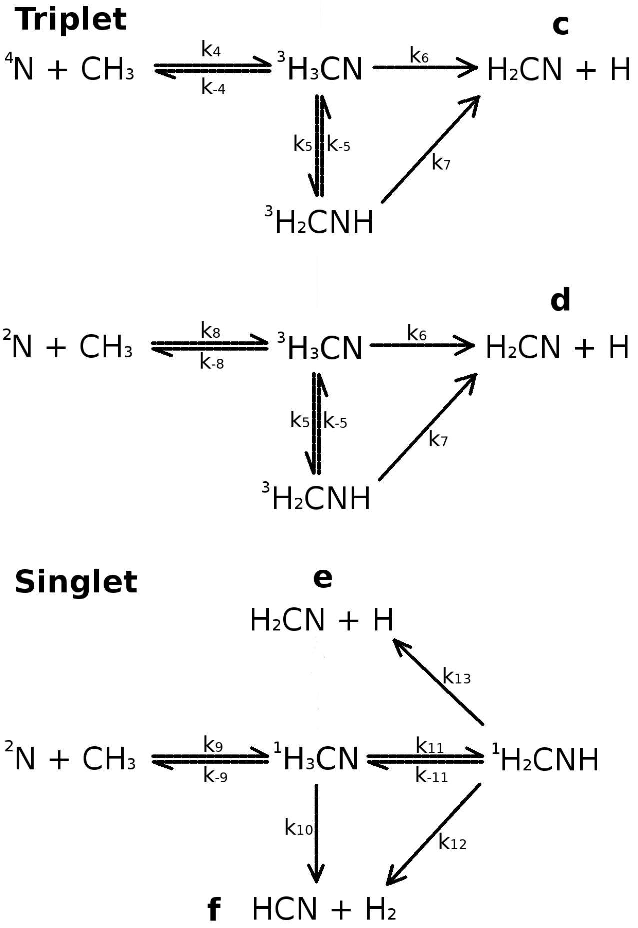

Figure 2.6: Mechanistic models for the production of H_2CN + H on the triplet surface from reactants (**c**) ${}^4N + CH_3$ and (**d**) ${}^2N + CH_3$, and production of (**e**) H_2CN + H and (**f**) HCN + H_2 on the singlet surface, from $CH_3 + {}^2N$.

H_2CN + H can form directly from ${}^3H_3CN$, or after isomerization from the intermediate ^3H_2CNH. Similarly, HCN + H_2 can form directly from ^1H_3CN, or from the intermediate ^1H_2CNH. On the singlet surface, we find H_2CN + H forms from the intermediate ^1H_2CNH, however we do not find a pathway from ^1H_3CN. We find a smooth decrease in Gibbs free energy along the MEP for the reaction $^1H_3CN \longrightarrow {}^1H_2CNH$, suggesting this reaction has neither an energy barrier nor an entropic barrier. We estimate the rate coefficient for this reaction by choosing the reactant geometry as the transition state. We find the overall rate coefficients for $CH_3 + N \longrightarrow H_2CN + H$ and $CH_3 + N \longrightarrow H_2CN + H$ to be insensitive to this intermediate rate coefficient by varying the latter's value by over 10 orders of magnitude in both directions. The optimization of ^1H_3CN does not converge, therefore we use a reactant geometry close to ^1H_3CN that has vibrational modes for HCN + H_2 and ^1H_2CNH. In any case, we find the values of k_c and k_d are independent of the ^1H_3CN geometry.

The steady-state solution of the kinetic rate equations for the above mechanistic models give us the overall rate constants for c) $CH_3 + {}^4N \longrightarrow H_2CN + H$ and d) $CH_3 + {}^2N \longrightarrow H_2CN + H$ on the triplet surface, and e) $CH_3 + {}^2N \longrightarrow H_2CN + H$ and f) $CH_3 + {}^2N \longrightarrow HCN + H_2$ on the singlet surface.

$$k_c = \frac{k_4}{A}\left(k_6 + \frac{k_5 k_7}{k_{-5} + k_7}\right). \tag{2.43}$$

$$k_d = \frac{k_8}{B}\left(k_6 + \frac{k_5 k_7}{k_{-5} + k_7}\right). \tag{2.44}$$

$$k_e = \frac{k_9}{C}\left(\frac{k_{11} k_{13}}{k_{-11} + k_{12} + k_{13}}\right). \tag{2.45}$$

$$k_f = \frac{k_9}{C}\left(k_{10} + \frac{k_{11} k_{12}}{k_{-11} + k_{12} + k_{13}}\right). \tag{2.46}$$

$$A = k_{-4} + k_5 + k_6 - \frac{k_{-5} k_5}{k_{-5} + k_7}. \tag{2.47}$$

$$B = k_{-8} + k_5 + k_6 - \frac{k_{-5} k_5}{k_{-5} + k_7}. \tag{2.48}$$

$$C = k_{-9} + k_{10} + k_{11} - \frac{k_{-11} k_{11}}{k_{-11} + k_{12} + k_{13}}. \tag{2.49}$$

The values of the reaction rate constants using the BHandHLYP method and aug-cc-pVDZ basis set are listed in Table 3.8.

The rate coefficients of k_c, k_d, and k_e are equivalent to those of k_4, k_8, and k_9, respectively. Thus the rate-limiting steps for these reactions are the first steps, i.e. $CH_3 + N \longrightarrow H_3CN$.

On the triplet surface, or theoretical value of k_c at the BHandHLYP/aug-cc-pVDZ level of theory is a factor of 1.5–2.5 smaller than the values calculated in experiments and suggested by thermodynamics [195, 224, 248].

On the singlet surface, there is a strong preference to produce H_2CN + H over HCN. The rate coefficient of $CH_3 + {}^2N \longrightarrow HCN + H_2$ is less than 10^{-21} cm^3s^{-1}, therefore we do not include this reaction in our network.

Table 2.9: Calculated overall rate coefficients for $CH_3 + {}^4N \longrightarrow H_2CN + H$ and $CH_3 + {}^2N \longrightarrow H_2CN + H$ on the triplet surface, and $CH_3 + {}^2N \longrightarrow H_2CN + H$ and $CH_3 + {}^2N \longrightarrow HCN + H_2$ on the singlet surface, as well as the intermediate forward and reverse rate coefficients which were used in the calculations. In all simulations, the BHandHLYP method was used with the aug-cc-pVDZ basis set. To reduce computational time, forward and reverse rate coefficients for k_5, k_7, and k_{12} were calculated with the transition state at the classical location (the saddle point) instead of the variational location. We find the overall rate coefficients k_c, k_d and k_e to be insensitive to changes in these intermediate coefficients of over 10 orders of magnitude. k_f is also insensitive to increases in k_{12} by over 10 orders of magnitude, however, decreasing k_{12} directly decreases k_f. Because we do not consider reactions with rate coefficients lower than 10^{-21} cm^{3}s^{-1}, we make no attempt to increase the accuracy of k_f. Experiments at 298 K provide a k_c value of 7.7×10^{-11} and a k_d value of 8.6×10^{-12} cm^{3}s^{-1} [195, 224]. First-order rate coefficients have units s^{-1}. Second-order rate coefficients have units cm^{3}s^{-1}.

Rate coefficient	k(298)
k_c	3.3×10^{-11}
k_d	1.0×10^{-10}
k_e	3.1×10^{-11}
k_f	2.3×10^{-28}
k_4	3.3×10^{-11}
k_{-4}	1.3×10^{-32}
k_5	1.1×10^{-19}
k_{-5}	8.2×10^{-11}
k_6	3.0×10^{-12}
k_7	5.6×10^{-7}
k_8	1.0×10^{-10}
k_{-8}	3.0×10^{-51}
k_9	3.1×10^{-11}
k_{-9}	6.3×10^{-41}
k_{10}	1.5×10^{-14}
[a]k_{11}	1.9×10^{13}
k_{-11}	3.9×10^{-57}
k_{12}	2.0×10^{-56}
k_{13}	2.9×10^{-39}

[a] No energy or entropic barrier. Transition state chosen at reactant geometry (^1H_3CN).

2.7.4.5 Case Study 5: $CH_2 + H \longleftrightarrow CH_3\cdot \longleftrightarrow CH + H_2$

There are three spin configurations for this reaction. $^3CH_2 + H \longrightarrow CH_3\cdot \longrightarrow CH + H_2$ and $^1CH_2 + H \longrightarrow CH_3\cdot \longrightarrow CH + H_2$ occur on the doublet PES, and $^3CH_2 + H \longrightarrow {}^4CH + H_2$ occurs on the quartet PES.

Several experiments have calculated the reaction rate coefficient for $^3CH_2 + H \longrightarrow CH + H_2$ at 285–300 K [196–201]. Although methodology differs between experiments, they generally involve monitoring the decay of $^3CH_2$. The experimental values are as low as 8.3×10^{-11} cm^{3}s^{-1} and as high as 2.7×10^{-10} cm^{3}s^{-1}. Two studies have reviewed a variety of experiments at a range of temperatures and suggested values of 2.7×10^{-10} cm^{3}s^{-1} [247] and 2.0×10^{-10} cm^{3}s^{-1} [137].

Although no experiments have been performed for the reaction of $^1CH_2 + H \longrightarrow CH + H_2$, Tsang and Hampson[247] suggest the value should be near 5.0×10^{-11} cm^{3}s^{-1} based on thermodynamics.

To date there have been no published theoretical reaction rate coefficients for any spin configuration of this reaction.

On the quartet PES, we find the reaction proceeds directly $^3CH_2 + H \longrightarrow {}^4CH + H_2$. We calculate the rate coefficient for this reaction at the BHandHLYP/aug-cc-pVDZ level of theory to be $\sim 10^{-25}$ cm^{3}s^{-1}, which is too inefficient to consider in this network.

The doublet PES reactions proceed through the CH_3 intermediate. The mechanistic model for these reactions is shown in Figure 2.7.

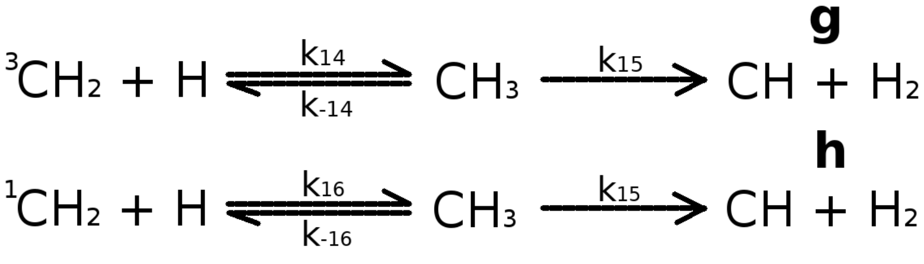

Figure 2.7: Mechanistic models for the production of CH + H_2 from $^3CH_2$ + H and $^1CH_2$ + H.

Although there are many reaction pathways for the CH_3 molecule, we calculate the upper bound for the rate constants of $^3CH_2 + H \longrightarrow CH_3\cdot \longrightarrow CH + H_2$ and $^1CH_2 + H \longrightarrow CH_3\cdot \longrightarrow CH + H_2$ by assuming all CH_3 reacts to form CH + H_2.

Table 2.10: Calculated overall rate coefficient for $^3CH_2 + H \longrightarrow CH + H_2$, and $^1CH_2 + H \longrightarrow CH + H_2$, as well as the intermediate forward and reverse rate coefficients which were used in the calculations. In all simulations, the BHandHLYP method was used with the aug-cc-pVDZ basis set. Experiments at 298 K provide k_g values between 8.3×10^{-11} and 2.7×10^{-10} cm^{3}s^{-1} [196–201]. A value of 5.0×10^{-11} ^{3}s^{-1} is suggested for k_h [247]. First-order rate coefficients have units s^{-1}. Second-order rate coefficients have units cm^{3}s^{-1}.

Rate coefficient	k(298)
k_g	4.3×10^{-10}
k_h	8.4×10^{-11}
k_{14}	5.6×10^{-10}
k_{-14}	3.7×10^{-58}
k_{15}	1.2×10^{-57}
k_{16}	8.4×10^{-11}
k_{-16}	9.5×10^{-68}

The steady-state solutions of the kinetic rate equations for these mechanistic models give us the overall rate constants for $^3CH_2 + H \longrightarrow CH + H_2$ and $^1CH_2 + H \longrightarrow CH + H_2$.

$$k_g = \frac{k_{15}k_{14}}{k_{-14} + k_{15}} \tag{2.50}$$

$$k_h = \frac{k_{15}k_{16}}{k_{-16} + k_{15}} \tag{2.51}$$

The values of the reaction rate constants using the BHandHLYP method and aug-cc-pVDZ basis set are listed in Table 2.10.

The theoretical value of k_h is equal to the value of k_{16}. Thus the first step is the rate-limiting step. The theoretical value of k_g is nearly the same as the value of k_{14}, however because the reverse rate coefficient (k_{-14}) is comparable to the rate coefficient of the second step (k_{15}), the value of k_g is slightly smaller than that of k_{11}. We calculate k_g to be 4.3×10^{-10} cm^{3}s^{-1}, which is within the range of experimental values for $^3CH_2 + H \longrightarrow CH + H_2$. We calculate k_h to be 8.4×10^{-11} cm^{3}s^{-1}, which is less than a factor of 2 larger than the suggested value by Tsang and Hampson[247]. Our calculations show $CH_3 \longrightarrow CH + H_2$ is inefficient ($k_{15} = \sim10^{-57}$ s^{-1}), therefore we do not consider the second step of this reaction in our study.

The same mechanistic approach can be used for the reverse reaction $CH + H_2 \longrightarrow CH_3\cdot \longrightarrow {}^3CH_2 + H$. This reaction could produce ${}^1CH_2$ + H as well, however k_{-14} is ~10 orders of magnitude larger than k_{-16}, suggesting the dominant pathway would be to produce ${}^3CH_2$ + H.

Several experiments have calculated the rate coefficient of $CH + H_2 \longrightarrow$ products by monitoring the decay of CH in the presence of H_2 [199, 202, 266–268, 270–272]. Becker et al.[202] find that 300 K is the threshold temperature, below which the CH_3 product is mainly formed, and above which the ${}^3CH_2$ + H products are mainly formed. Zabarnick et al.[199] also suggest CH_3 is the main product below temperatures of 300 K, and recommend a temperature of $>$ 400 K for the formation of CH_2 + H.

Rate coefficients for the reaction of $CH + H_2 \longrightarrow CH_3$ range from 1.0×10^{-12} to 1.6×10^{-10} cm^3s^{-1}.

Mayneris et al.[320] used the quasiclassical trajectory method to calculate the theoretical rate coefficient of $CH + H_2 \longrightarrow CH_3\cdot \longrightarrow {}^3CH_2 + H$. They calculated a value of 3.5×10^{-11} cm^3s^{-1}.

We find the first step of the reverse reaction to be the rate-limiting step, i.e. $CH + H_2 \longrightarrow CH_3$. We calculate the rate coefficient of the reverse reaction to be 7.9×10^{-11} cm^3s^{-1}. This is within the range of experimental values.

We find the second step of the reverse reaction ($CH_3 \longrightarrow CH_2 + H$) to be too inefficient to consider in this network (i.e. k $<10^{-21}$ s^{-1}).

2.7.4.6 Case Study 6: $CH_2 + H_2 \longrightarrow CH_3 + H$

This reaction occurs on the singlet and triplet surfaces, as ${}^1CH_2 + H_2 \longrightarrow CH_4\cdot \longrightarrow CH_3 + H$ and ${}^3CH_2 + H_2 \longrightarrow CH_3 + H$, respectively.

Experiments have measured the rate of ${}^1CH_2$ decay or CH_3 production to calculate the rate coefficient of ${}^1CH_2 + H_2 \longrightarrow CH_4\cdot \longrightarrow CH_3 + H$ at 295–298 K [203–205]. These values range from 7.0×10^{-12} to 1.3×10^{-10} cm^3s^{-1}. Studies reviewing these experiments suggest a rate coefficient of 1.2×10^{-10} cm^3s^{-1}[137, 247].

We find no theoretical rate coefficients for the ${}^1CH_2 + H_2 \longrightarrow CH_4\cdot \longrightarrow CH_3 + H$ reaction.

We find the first step to be the rate-limiting step in the reaction ${}^1CH_2 + H_2 \longrightarrow CH_4\cdot \longrightarrow CH_3 + H$. We calculate the rate coefficient to be 1.0×10^{-11} cm^3s^{-1}, which is within the range of experimental values. Because CH_4 is a stable product in our reaction network, we only include the first step of this reaction in our network. The second step, $CH_4 \longrightarrow CH_3 + H$, is very inefficient ($k \sim 10^{-60}$ s^{-1}) and we do not include it in our network.

Although no experiments have directly measured the rate coefficient of $^3CH_2 + H_2 \longrightarrow CH_3 + H$, a few models have place an upper bound on its value by considering the affect of various gases on the $^3CH_2$ molecule. These upper bounds range from 5.0×10^{-15} to 5.0×10^{-14} cm^3s^{-1}.

Lu et al.[318] calculated the theoretical rate coefficient of $^3CH_2 + H_2 \longrightarrow CH_3 + H$ using transition state theory. They employed the G2M(RCC2) computational method with B3LYP optimized geometries and obtained a value of $1.5\times10^{-18}cm^3s^{-1}$.

We calculate the rate coefficient of $^3CH_2 + H_2 \longrightarrow CH_3 + H$ to be 2.5×10^{-16} cm^3s^{-1}. This value agrees with the upper bounds for the rate coefficient from experiments.

We find the reverse rate coefficient, $CH_3 + H \longrightarrow {}^3CH_2 + H_2$ to have a value of 1.4×10^{-20} cm^3s^{-1}. We include this reverse reaction in our network as its rate coefficient is within the threshold of what we define to be a fast reaction (i.e. $k > 10^{-21}$ cm^3s^{-1}).

2.7.4.7 Case Study 7: $CH_2 + N \longrightarrow HCN + H$

Catling and Kasting[36] suggest $CH_2 + N \longrightarrow HCN + H$ is one of the main pathways forming HCN in the early atmosphere. They note however that the rate constant for this reaction has not yet been studied experimentally.

Herbst et al.[319] performed quantum dynamics simulations to calculate the rate coefficient of $^3CH_2 + {}^4N \longrightarrow H_2CN\cdot \longrightarrow HCN + H$. They calculated a value of 7.9×10^{-11} cm^3s^{-1}.

We find no direct reaction pathway for $CH_2 + N \longrightarrow HCN + H$ on the doublet, quartet, or sextet PES's. We do however find two-step reactions $CH_2 + N \longrightarrow H_2CN$ and $H_2CN \longrightarrow HCN + H$ on the doublet and quartet surfaces.

We list the calculated reaction rate coefficients on the doublet and quartet energy surfaces in Table 2.11.

All spin configurations of $CH_2 + N \longrightarrow H_2CN$ are barrierless and have efficient reaction rate coefficients. $H_2CN \longrightarrow HCN + H$, however, is only efficient on the doublet surface. We distinguish between the quartet and doublet H_2CN molecules in our network, as the deexcitation of ^4H_2CN to ^2H_2CN is spin-forbidden, and we can't assume ^4H_2CN will efficiently decay into its ground state in an atmosphere.

Table 2.11: Calculated rate coefficients for $CH_2 + N \longrightarrow H_2CN$, and $H_2CN \longrightarrow HCN + H$ on the doublet and quartet potential energy surfaces. In all simulations, the BHandHLYP method was used with the aug-cc-pVDZ basis set. First-order rate coefficients have units s^{-1}. Second-order rate coefficients have units cm^3s^{-1}.

Reaction	k(298) doublet	k(298) quartet
$^1CH_2 + {}^2N \longrightarrow H_2CN$	1.5×10^{-10}	
$^1CH_2 + {}^4N \longrightarrow H_2CN$		1.1×10^{-10}
$^3CH_2 + {}^4N \longrightarrow H_2CN$	1.3×10^{-10}	
$^3CH_2 + {}^2N \longrightarrow H_2CN$	2.7×10^{-10}	4.3×10^{-10}
$H_2CN \longrightarrow HCN + H$	1.6×10^{-11}	4.6×10^{-24}

Our calculated rate coefficient for $^3CH_2 + {}^4N \longrightarrow H_2CN$ is approximately a factor of 1.5 greater than the previous theoretical value [319].

We include all five $CH_2 + N \longrightarrow H_2CN$ reaction spin configurations as well as the efficient doublet $H_2CN \longrightarrow HCN + H$ reaction in our network.

2.7.4.8 Case Study 8: $2\,CH_2 \longrightarrow C_2H_4\cdot \longrightarrow$ products

There are three spin configurations for this reaction on a total of two PES's. On the singlet surface, there is $^3CH_2 + {}^3CH_2 \longrightarrow {}^1C_2H_4\cdot \longrightarrow C_2H_3\cdot + H\cdot \longrightarrow C_2H_2 + 2\,H$ and $^1CH_2 + {}^1CH_2 \longrightarrow {}^1C_2H_4\cdot \longrightarrow$ products, and on the triplet PES there is $^3CH_2 + {}^1CH_2 \longrightarrow {}^3C_2H_4\cdot \longrightarrow$ products.

Braun et al.[203] monitored the decay of $^3CH_2$ and the production of C_2H_2 in experiments to measure the rate coefficient of $^3CH_2 + {}^3CH_2 \longrightarrow C_2H_2 +$ product at 298 K. This measurement was 5.3×10^{-11} cm^3s^{-1}. Braun et al.[203] assumed that molecular hydrogen was produced along with C_2H_2 in this reaction, however Becerra et al.[331] modeled the reaction network starting from the decomposition of ketene and found that $^3CH_2 + {}^3CH_2 \longrightarrow C_2H_2 + 2\,H$ was more likely. Becerra et al.[331] found that $^3CH_2 + H \longrightarrow CH + H_2$ can account for the molecular hydrogen observed in reactions of this kind.

Braun et al.[203] suggest that the reaction of $^3CH_2$ with $^3CH_2$ passes through the C_2H_4 intermediate.

Jasper et al.[221] calculate the theoretical rate coefficient for $^3CH_2 + {}^3CH_2 \longrightarrow$

$C_2H_4\cdot \longrightarrow C_2H_2 + 2\,H$ using variable reaction coordinate transition state theory. Their value is 1.5 $\times 10^{-10}$ cm^3s^{-1}.

There is no experimental data for $^1CH_2 + {}^1CH_2 \longrightarrow C_2H_4\cdot \longrightarrow$ products, however it is expected to proceed rapidly, and yield the same products as $^3CH_2 + {}^3CH_2 \longrightarrow C_2H_4\cdot \longrightarrow C_2H_2 + 2\,H$ [247]. Tsang and Hampson[247] recommend a value of 5.0×10^{-11} cm^3s^{-1} for this reactions.

Similarly, there is no experimental data for $^3CH_2 + {}^1CH_2 \longrightarrow {}^3C_2H_4\cdot \longrightarrow$ products, however it is also expected to be rapid. Conversely, it is suggested that the preferred products for this reaction are $^3CH_2 + {}^1CH_2 \longrightarrow {}^3C_2H_4\cdot \longrightarrow {}^3C_2H_2 + H_2$. Tsang and Hampson[247] suggest a value of 3.0×10^{-11} cm^3s^{-1} for this reaction.

To our knowledge there have been no theoretical reaction rate coefficients for $^1CH_2 + {}^1CH_2 \longrightarrow C_2H_2 + 2\,H$, or $^1CH_2 + {}^3CH_2 \longrightarrow {}^3C_2H_2 + H_2$ published to date.

Because in some of the other reactions in our network, C_2H_4 is a stable product, i.e. $CH + CH_4 \longrightarrow C_2H_5\cdot \longrightarrow C_2H_4 + H$, $CH_2 + CH_3 \longrightarrow C_2H_5\cdot \longrightarrow C_2H_4 + H$, we only include the first steps of these reactions in our network (i.e. $2\,CH_2 \longrightarrow C_2H_4$). We find the first steps of reactions $^3CH_2 + {}^3CH_2 \longrightarrow C_2H_4\cdot \longrightarrow C_2H_2 + 2\,H$ and $^1CH_2 + {}^1CH_2 \longrightarrow C_2H_4\cdot \longrightarrow C_2H_2 + 2\,H$ to be the rate-limiting steps, and assume the same for $^1CH_2 + {}^3CH_2 \longrightarrow {}^3C_2H_4 \longrightarrow$ products.

We list the calculated reaction rate coefficients on the singlet and triplet energy surfaces in Table 2.12.

Our calculated k(298) value for $^3CH_2 + {}^3CH_2 \longrightarrow C_2H_4$ is within 30% of the experimental value for $^3CH_2 + {}^3CH_2 \longrightarrow C_2H_2 + 2\,H$. The k(298) value for $^1CH_2 + {}^1CH_2 \longrightarrow C_2H_4$ is a factor of 5 smaller than the suggested value. Simulations did not converge for $^1CH_2 + {}^3CH_2 \longrightarrow {}^3C_2H_4$ beyond a C-C reaction coordinate of 3.52 Å, however using this location for the variational transition state leads to a calculated rate coefficient that is within 20% of the suggested value.

Table 2.12: Calculated rate coefficients for $2\,CH_2 \longrightarrow C_2H_4$ on the singlet and triplet potential energy surfaces. These rate coefficients are compared with the experimental rate coefficient of the multi-step reaction $^3CH_2 + {}^3CH_2 \longrightarrow C_2H_4\cdot \longrightarrow C_2H_2 + 2\,H$ as well as the suggested rate coefficients for $^1CH_2 + {}^1CH_2 \longrightarrow C_2H_4\cdot \longrightarrow C_2H_2 + 2\,H$, and $^1CH_2 + {}^3CH_2 \longrightarrow {}^3C_2H_4\cdot \longrightarrow$ products in the literature. We find the first steps of the reactions of $^{3,1}CH_2 + {}^{3,1}CH_2 \longrightarrow C_2H_4\cdot \longrightarrow C_2H_2 + 2\,H$ to be the rate-limiting steps and assume the same for $^1CH_2 + {}^3CH_2 \longrightarrow {}^3C_2H_4\cdot \longrightarrow$ products. In all simulations, the BHandHLYP method was used with the aug-cc-pVDZ basis set. Rate coefficients have units cm^3s^{-1}.

	$^3CH_2$ + $^3CH_2$	$^1CH_2$ + $^1CH_2$	$^1CH_2$ + $^3CH_2$
$k_{calc}(298)$	4.2×10^{-11}	9.9×10^{-12}	$^a3.5\times10^{-11}$
$k_{lit}(298)$	5.3×10^{-11}	5.0×10^{-11}	3.0×10^{-11}

[a] Simulations did not converge beyond a C-C bond distance of 3.52Å. Therefore the calculated rate coefficient is a lower bound.

2.7.4.9 Case Study 9: $CH_2 + CH_3 \longrightarrow C_2H_5\cdot \longrightarrow C_2H_4 + H$

This is a two step reaction, passing through the C_2H_5 intermediate [247, 263, 264]. On the doublet surface, both $^3CH_2$ and $^1CH_2$ can react with CH_3 to produce the C_2H_5 intermediate. On the quartet surface, $^3CH_2$ reacts with CH_3 to produce excited $^4C_2H_5$. However this reaction is higher in energy than the doublet reactions, and has a very slow rate coefficient ($\sim10^{-57}$ cm^3s^{-1}).

Pilling and Robertson[264] and Laufer and Bass[263] experimentally measured the production of various products (e.g. C_2H_2, C_2H_4, C_2H_6) to model the reaction network spanned by reactions between $^3CH_2$ and CH_3. Their models led to reaction rate coefficients of 5.0×10^{-11} and 1.0×10^{-10} cm^3s^{-1}, respectively. Wang and Fockenberg[257] performed similar experiments but used the $^3CH_2$ decay profile for their calculation, and obtained a rate of 2.1×10^{-10} cm^3s^{-1} at 300 K. Deters et al.[262] measured the decay of both $^3CH_2$ and CH_3 in a similar experiment to obtain a rate coefficient of 1.1×10^{-10} cm^3s^{-1} at 298 K. Baulch et al.[137] and Tsang and Hampson[247] reviewed various experiments and suggest a value of 7.0×10^{-11} cm^3s^{-1} for the $^3CH_2 + CH_3 \longrightarrow C_2H_5\cdot \longrightarrow C_2H_4 + H$ rate coefficient.

Conversely, there is no experimental data for $^1CH_2 + CH_3 \longrightarrow C_2H_5\cdot \longrightarrow C_2H_4 + H$, however the reaction is thought to proceed rapidly and suggested to have a rate coefficient near 3.0×10^{-11} cm^3s^{-1} [247].

There have been no published theoretical reaction rate coefficients for $CH_2 + CH_3 \longrightarrow C_2H_4 + H$.

We find the first steps of these reactions, $^3CH_2 + CH_3 \longrightarrow C_2H_5$ and $^1CH_2 + CH_3 \longrightarrow C_2H_5$, do not have barriers. The second step however ($C_2H_5 \longrightarrow C_2H_4 + H$), has a barrier. The mechanistic model for the reaction, involving the triplet and singlet CH_2 molecule, is shown in Figure 2.8.

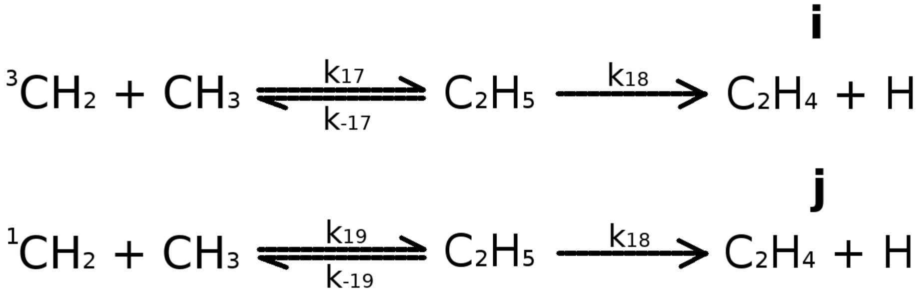

Figure 2.8: Mechanistic model for the production of C_2H_4 + H from **i)** $^3CH_2 + CH_3$ and **j)** $^1CH_2 + CH_3$ on the doublet surface.

We calculate the upper bounds for the rate constants by assuming all C_2H_5 reacts to form C_2H_4 + H.

The steady-state solutions of the kinetic rate equations for this mechanistic model gives us the overall rate constant for $CH_2 + CH_3 \longrightarrow C_2H_4 + H$.

$$k_i = \frac{k_{18}k_{17}}{k_{-17} + k_{18}} \tag{2.52}$$

$$k_j = \frac{k_{18}k_{19}}{k_{-19} + k_{18}} \tag{2.53}$$

We list the calculated reaction rate coefficients for this mechanistic model in Table 2.13.

The theoretical values of k_i and k_j are equal to the values of k_{17} and k_{19}, respectively. Thus the first steps of these reactions are the rate-limiting steps. At the BHandHLYP/aug-cc-pVDZ level of theory, we calculate k_i to be 8.8×10^{-12} cm^{3}s^{-1}. This value is approximately a factor of 6 slower than the slowest experimental value. Similarly, we calculate k_j to be 2.3×10^{-11} cm^{3}s^{-1}, which is within order unity of the suggested value.

Table 2.13: Calculated overall rate coefficient for $^3CH_2 + CH_3 \longrightarrow C_2H_4 + H$ and $^1CH_2 + CH_3 \longrightarrow C_2H_4 + H$, as well as the intermediate forward and reverse rate coefficients which were used in the calculation. In all simulations, the BHandHLYP method was used with the aug-cc-pVDZ basis set. Experiments at 298 K provide a k_i value in the range of 5.0×10^{-11} to 2.1×10^{-10} cm^3s^{-1} [257, 263, 264]. k_j is suggested to have a rate coefficient near 3.0×10^{-11} cm^3s^{-1} [247]. First-order rate coefficients have units s^{-1}. Second-order rate coefficients have units cm^3s^{-1}.

Rate coefficient	k(298)
k_i	8.8×10^{-12}
k_j	2.3×10^{-11}
k_{17}	8.8×10^{-12}
k_{-17}	1.4×10^{-48}
k_{18}	4.0×10^{-15}
k_{19}	2.3×10^{-11}
k_{-19}	3.0×10^{-57}

2.7.4.10 Case Study 10: $CH_2 + CH_4 \longrightarrow 2\,CH_3$

This reaction occurs on the singlet PES as $^1CH_2 + CH_4 \longrightarrow C_2H_6\cdot \longrightarrow 2\,CH_3$. and on the triplet PES as $^3CH_2 + CH_4 \longrightarrow 2\,CH_3$.

Experimentalists have measured the rate coefficient of $^1CH_2 + CH_4 \longrightarrow C_2H_6\cdot \longrightarrow 2\,CH_3$ at 295–298 K by measuring the decay of $^1CH_2$ or the production of CH_3. These values range from 1.9×10^{-12} to 7.3×10^{-11} cm^3s^{-1} [203–205]. Tsang and Hampson[247] reviewed these experiments and suggested a value of 7.1×10^{-11} cm^3s^{-1}. We find no published theoretical rate coefficients for this reaction.

We find the reaction on the singlet PES proceeds through the C_2H_6 intermediate and that the first step of this reaction is the rate-limiting step. We calculate its rate coefficient to be 6.1×10^{-13} cm^3s^{-1}, which is a factor of 3 smaller than the closest experimental value. Because C_2H_6 is a stable product in other reactions in our network (e.g. $2\,CH_3 \longrightarrow C_2H_6$), we only consider the first step of this reaction in our network. The second step of this reaction $C_2H_6 \longrightarrow 2\,CH_3$ is too slow to consider in this network ($k \sim 10^{-55}$ s^{-1}).

Böhland et al.[265] performed experiments on the reaction of $^3CH_2$ with n-hexane at T = 413–707 K to estimate the rate coefficient for $^3CH_2 + CH_4 \longrightarrow 2\,CH_3$ at 298 K. They calculated a value of 3.1×10^{-19} cm^3s^{-1}. Braun et al.[203] placed an upper bound on the rate coefficient by considering the affect of various gases on the $^3CH_2$ molecule. They estimate a value of <3.1×10^{-14} cm^{3}s^{-1}. Tsang and Hampson[247] suggest an upper bound of 3.0×10^{-19} cm^{3}s^{-1} based on the results of a photolysis study of the CH_2CO-CH_4 system. We find no theoretical rate coefficients for the $^3CH_2 + CH_4 \longrightarrow 2\,CH_3$ reaction.

We calculate $^3CH_2 + CH_4 \longrightarrow 2\,CH_3$ to have a rate coefficient of 1.4×10^{-16} cm^{3}s^{-1}. This value agrees with the upper bound from Braun et al.[203], and is a couple orders of magnitude higher than the experimental value from Böhland et al.[265].

2.7.4.11 Case Study 11: $CH + N \longrightarrow HCN \longrightarrow CN + H$

There are two spin configurations for this reaction on the triplet surface, which pass through the excited ^3HCN intermediate: $CH + {}^4N \longrightarrow {}^3HCN \longrightarrow CN + H$ and $CH + {}^2N \longrightarrow {}^3HCN \longrightarrow CN + H$. There is also potentially a reaction of CH + ^2N on the singlet surface to produce ground state HCN, however we were unable to obtain a convergent solution for such a reaction. Moreover, there is no experimental or past theoretical work for a singlet surface reaction of CH + ^2N to suggest it occurs efficiently. For these reasons, we only consider the two spin configurations on the triplet surface in this network.

A few experiments have measured the rate coefficient of $CH + {}^4N \longrightarrow CN + H$ at 296–298 K by monitoring the decay of CH and/or the production of CN [222, 273, 274]. The experimental values of the rate coefficient range from 2.1×10^{-11} to 1.6×10^{-10} cm^{3}s^{-1}.

Daranlot et al.[222] performed quantum dynamics calculations to obtain a theoretical rate coefficient for $CH + {}^4N \longrightarrow {}^3HCN \longrightarrow CN + H$. They calculate a value of k(298) = 1.2×10^{-10} cm^{3}s^{-1}.

We find no experimental or theoretical rate coefficients for $CH + {}^2N \longrightarrow {}^3HCN \longrightarrow CN + H$.

Our theoretical calculations show both $CH + {}^4N$ and $CH + {}^2N$ react without a barrier to form the ^3HCN intermediate. We find the first step for both of these reactions to be the rate-limiting steps. The second step of this reaction, i.e., the decay of ^3HCN into CN + H, is extremely efficient (k = 3.6×10^9 s^{-1}).

We calculate the rate coefficient for $CH + {}^4N \longrightarrow {}^3HCN \longrightarrow CN + H$ to be 1.1×10^{-10} cm^{3}s^{-1}. This value is within the range of experimental values, and agrees well with the previous calculated theoretical value [222].

We calculate the rate coefficient for $CH + {}^2N \longrightarrow {}^3HCN \longrightarrow CN + H$ to be 2.7×10^{-10} cm^3s^{-1}.

2.7.4.12 Case Study 12: $CH + CH_4 \longrightarrow C_2H_5\cdot \longrightarrow C_2H_4 + H$

This reaction occurs on the doublet surface. Several experiments have calculated the rate coefficient for this reaction at 295–298 K by monitoring the production of C_2H_4 or the decay of CH [270–272, 275–280]. The experimental rate coefficient ranges from 2.0×10^{-12} to 3.0×10^{-10} cm^3s^{-1}.

A pair of theoretical studies have been performed on this reaction, however theoretical rate coefficients were not calculated [332, 333].

At the BHandHLYP/aug-cc-pVDZ level of theory, we find this reaction to have a small barrier (E_0 = 11.5 kJ mol^{-1}). This is smaller than the barrier predicted by Yu et al.[332] (E_0 = 57.3 kJ mol^{-1}), who used the Moller-Plesset perturbation theory (MP) method with geometries optimized using the Hartree-Fock method. However, Wang et al.[333] calculated the reaction to be barrierless (-1.3 kJ mol^{-1}) using the MP method with MP optimized geometries. Experiments suggests the reaction is barrierless, with an activation energy of -1.7 kJ mol^{-1} [277]. At the B3LYP/aug-cc-pVDZ level of theory, we find this reaction to be barrierless, with an activation energy of -18.2 kJ mol^{-1}. Because experiment predicts this reaction to be barrierless [277, 278, 280], and the existence of the theoretical barrier is dependent on the computational method, we artificially remove the barrier from our calculation of the rate coefficient at the BHandHLYP/aug-cc-pVDZ level of theory.

We find the first step of this reaction $CH + CH_4 \longrightarrow C_2H_5$ to be the rate-limiting step, with a barrierless rate coefficient of 3.8×10^{-13} cm^3s^{-1}. This is a factor of 5 slower than the nearest experimental value. We calculate the rate coefficient of second step of this reaction $C_2H_5 \longrightarrow C_2H_4 + H$ to be 1.8×10^{-11} s^{-1}, suggesting the C_2H_5 intermediate is fairly unstable. Thus we include this two-step reaction in our network as a single step $CH + CH_4 \longrightarrow C_2H_4 + H$.

2.7.4.13 Case Study 13: $NH + H \longleftrightarrow N + H_2$

This reaction has two spin configurations on the doublet PES, ${}^1NH + H \longrightarrow {}^2N + H_2$ and ${}^3NH + H \longrightarrow {}^2N + H_2$, and one spin configuration on the quartet PES, ${}^3NH + H \longrightarrow {}^4N + H_2$.

Adam et al.[281] calculated the experimental rate coefficient of $^3\mathrm{NH} + \mathrm{H} \longrightarrow {}^4\mathrm{N} + \mathrm{H_2}$ at 298 K by monitoring the decay of ^{3}NH. They found the rate coefficient to have a value of 3.2×10^{-12} cm^{3}s^{-1}.

Adam et al.[281] also used the classical trajectory method to calculate the theoretical rate coefficient for $^3\mathrm{NH} + \mathrm{H} \longrightarrow {}^4\mathrm{N} + \mathrm{H_2}$ at the MRCI/aug-cc-pVQZ level of theory. They found this reaction proceeds directly, rather than through the NH_3 intermediate. They calculated the rate coefficient to be 1.5×10^{-12} cm^{3}s^{-1}. Other theoretical works calculated the rate coefficient with CVT and QCT to range from 2.0×10^{-13} to 5.2×10^{-12} cm^{3}s^{-1} [322, 323].

We find no published experimental or theoretical rate coefficients for the two spin configurations on the doublet PES.

On the quartet surface, we calculate the $^3\mathrm{NH} + \mathrm{H} \longrightarrow \mathrm{H_2} + {}^4\mathrm{N}$ configuration to be 1.4×10^{-11} cm^{3}s^{-1}. This is a factor of 4 greater than the experimental value reported by Adam et al.[281].

On the doublet surface, we do not calculate the $^1\mathrm{NH}+\mathrm{H} \longrightarrow \mathrm{H_2}+{}^2\mathrm{N}$ configuration as ^{1}NH is not efficiently produced in this reaction network.

We find the $^3\mathrm{NH} + \mathrm{H} \longrightarrow \mathrm{H_2} + {}^2\mathrm{N}$ configuration to proceed through the NH_2 intermediate. This is consistent with theoretical studies of the reverse reaction [325, 326]. We find the total forward rate coefficient to be too slow to consider in this study ($\sim10^{-80}$ cm^{3}s^{-1}).

Regarding the reverse reaction, various experiments have been performed on the deactivation of ^{2}N by H_2 at 295–300 K [234, 236, 284–290]. The rate coefficients have been measured by monitoring the decay of ^{2}N and range from 1.7–5.0×10^{-12} cm^{3}s^{-1}. Donovan and Husain[334] indicate that $^2\mathrm{N}$ + H_2 should readily undergo chemical reaction into ^{3}NH + H via a direct path on the doublet PES. However, theoretical works suggest this reaction will proceed through the NH_2 intermediate [325, 326]. Herron[237] reviewed the deactivation experiments and suggested a rate coefficient of 2.2×10^{-12} cm^{3}s^{-1} for $^2\mathrm{N} + \mathrm{H_2} \longrightarrow {}^3\mathrm{NH} + \mathrm{H}$.

Theoretical rate coefficient calculations of the reaction $^2\mathrm{N} + \mathrm{H_2} \longrightarrow {}^3\mathrm{NH} + \mathrm{H}$ have been performed using QCT [324–326], quantum dynamics [324], and CVT [325] with the CASSCF and MRCI computational methods. Kobayashi et al.[325] and Pederson et al.[326] suggest this reaction proceeds through the NH_2 intermediate. Pederson et al.[326] find the H_2 molecule approaches the N atom perpendicularly, and that there is no collinear reaction path. The calculated theoretical rate coefficients range from

8.9×10^{-13}–3.3×10^{-12} cm^{3}s^{-1}.

Experimental and theoretical studies both suggest $^2N + H_2 \longrightarrow {}^3NH + H$ has a small energy barrier. The experimental value is 7.3 kJ mol$^-$1 [285].

We find no published experimental or theoretical rate coefficients for the two other reverse reaction spin configurations ($^2N + H_2 \longrightarrow {}^1NH + H$ and $^4N + H_2 \longrightarrow {}^3NH + H$).

At the BHandHLYP/aug-cc-pVDZ level of theory, we find the first step of the reverse reaction, $H_2 + {}^2N \longrightarrow NH_2$, to be barrierless. This step is also the rate-limiting step. Similarly to Pederson et al.[326], we find the H_2 molecule approaches the N atom perpendicularly. The second step, $NH_2 \longrightarrow 3\,NH + H$, proceeds through a barrier. We calculate the overall barrierless rate coefficient to be 9.7×10^{-10} cm^{3}s^{-1}. This value is over 2 orders of magnitude larger than the experimental values. This disagreement with experiment is due to the lack of a barrier calculated when using the BHandHLYP method. For this reason, we introduce the experimental barrier of 7.3 kJ mol^{-1} [285] to our calculation to obtain an overall rate coefficient of 5.1 $\times10^{-10}$ cm^{3}s^{-1}. This value is only 1 order of magnitude larger than the experimental value.

We expect the remaining discrepancy to be a result of our chosen computational method, as our reaction geometry is the same as other theoretical works [325, 326].

We find the other two reverse rate coefficients ($^2N + H_2 \longrightarrow {}^1NH + H$ and $^4N + H_2 \longrightarrow {}^3NH + H$) to be too inefficient to consider in this study (k < 10^{-21} cm^{3}s^{-1}).

2.7.4.14 Case Study 14: $NH + N \longrightarrow N_2H\cdot \longrightarrow N_2 + H$

This reaction occurs on the doublet PES. There are three possible spin configurations: $^3NH + {}^4N \longrightarrow N_2H\cdot \longrightarrow N_2 + H$, $^3NH + {}^2N \longrightarrow N_2H\cdot \longrightarrow N_2 + H$, and $^1NH + {}^2N \longrightarrow N_2H\cdot \longrightarrow N_2 + H$. Because ^{1}NH is not produced efficiently by any reaction in this study, we only analyze the two spin configurations involving ^{3}NH.

Hack et al.[282] experimentally measured the rate coefficient of $^3NH + N \longrightarrow$ products at 298 K by monitoring the decay profile of ^{3}NH. They measured the value to be 2.5×10^{-11} cm^{3}s^{-1}.

Konnov and De Ruyck[283] used the experimental value from Hack et al.[282], as well as a suggested T$^{0.5}$ dependence to estimate a value of 2.6×10^{-11} cm^{3}s^{-1}.

Caridade et al.[321] calculated the theoretical rate coefficient of $^3NH + {}^4N \longrightarrow N_2H\cdot \longrightarrow N_2 + H$ to be 1.9×10^{-11} cm^{3}s^{-1} using quasi-classical trajectory theory at the MRCI/aug-cc-pVQZ level of theory.

We find no published experimental or theoretical rate coefficients for $^3\mathrm{NH} + {}^2\mathrm{N} \longrightarrow \mathrm{N_2H}\cdot \longrightarrow \mathrm{N_2} + \mathrm{H}$.

Consistent with a previous theoretical study, we find the $^3\mathrm{NH}$ + $^2\mathrm{N}$ reaction proceeds through the $\mathrm{N_2H}$ intermediate. We find the rate-limiting step to be $^3\mathrm{NH} + {}^4\mathrm{N} \longrightarrow \mathrm{N_2H}$, with a rate coefficient of 4.0×10^{-11} cm^{3}s^{-1}. This value is only a factor of 1.5 larger than the experimental value, and a factor of 2 larger than the theoretical value.

Table 2.14: Reaction path symmetry numbers for each reaction (σ), as well as the rotational symmetry numbers of the reactants (σ_i) and transition states ($\sigma^\dagger$) used in the calculation. All steps in multi-step reactions are included. Spins are labeled only if reaction spin configurations have different reaction path symmetry numbers. $\sigma = \frac{\prod_{i=1}^{N} \sigma_i}{\sigma^\dagger}$.

Reaction Equation	σ_1	σ_2	$\sigma^\dagger$	σ
$H_2CN \longrightarrow HCN + H$	2		1	2
$HCN + H \longrightarrow H_2CN$	1	1	1	1
$H_2CN + H \longrightarrow HCN + H_2$	2	1	1	2
$H_2CN + N \longrightarrow HCN + NH$	2	1	1	2
$2\,H_2CN \longrightarrow HCN + H_2CNH$	2	2	1	4
$CH_4 + H \longrightarrow CH_3 + H_2$	12	1	3	4
$CH_4 + N \longrightarrow H_3CNH$	12	1	1	12
$H_3CNH \longrightarrow H_2CNH + H$	1	1	1	1
$CH_3 + H \longrightarrow CH_4$	6	1	3	2
$CH_3 + H_2 \longrightarrow CH_4 + H$	6	2	3	4
$CH_3 + N \longrightarrow H_3CN$	6	1	3	2
$H_3CN \longrightarrow H_2CN + H$	3		1	3
$H_3CN \longrightarrow H_2CNH$	3		1	3
$H_2CNH \longrightarrow H_2CN + H$	1		1	1
$2\,CH_3 \longrightarrow C_2H_6$	6	6	6	6
$2\,CH_3 \longrightarrow CH_2 + CH_4$	6	6	1	36
$CH_2 + H \longrightarrow CH_3$	2	1	1	2
$CH_2 + H_2 \longrightarrow CH_4$	2	2	1	4
$CH_2 + H_2 \longrightarrow CH_3 + H$	2	2	2	2
$CH_2 + N \longrightarrow H_2CN$	2	1	1	2
${}^1CH_2 + {}^1CH_2 \longrightarrow C_2H_4$	2	2	1	4
${}^1CH_2 + {}^3CH_2 \longrightarrow C_2H_4$	2	2	1	4
${}^3CH_2 + {}^3CH_2 \longrightarrow C_2H_4$	2	2	2	2
$CH_2 + CH_3 \longrightarrow C_2H_5$	2	6	1	12
$C_2H_5 \longrightarrow C_2H_4 + H$	1		1	1
$CH_2 + CH_4 \longrightarrow C_2H_6$	2	12	1	24
$CH_2 + CH_4 \longrightarrow 2\,CH_3$	2	12	1	24
$CH + H_2 \longrightarrow CH_3$	1	2	1	2
$CH + N \longrightarrow HCN$	1	1	1	1
$HCN \longrightarrow CN + H$	1		1	1
$2\,CH \longrightarrow C_2H_2$	1	1	1	1
$CH + CH_4 \longrightarrow C_2H_5$	1	12	1	12
$NH + H \longrightarrow H_2 + N$	1	1	1	1
$N + H_2 \longrightarrow NH_2$	1	2	2	1
$NH_2 \longrightarrow NH + H$	2		1	2
$NH + N \longrightarrow N_2H$	1	1	1	1
$N_2H \longrightarrow N_2 + H$	1		1	1

2.7.5 Reaction Path Symmetry Numbers

The reaction path symmetry number, or reaction path multiplicity, can be calculated with the following equation.

$$\sigma = \frac{\prod_{i=1}^{N} \sigma_i}{\sigma^\dagger} \tag{2.54}$$

where σ is the reaction path symmetry number, σ_i is the rotational symmetry number of reactant i, and $\sigma^\dagger$ is the rotational symmetry number of the transition state.

In Table 2.14 we list the reaction path symmetry numbers for all the reactions in our network, as well as the rotational symmetry numbers of the reactants and products used in the calculation.

Chapter 3

HCN production in Titan's Atmosphere: Coupling quantum chemistry and disequilibrium atmospheric modeling

> ” *I'm gonna have to science the shit out of this...*
>
> — **Mark Watney, *The Martian***

Ben K. D. Pearce, Karan Molaverdikhani, Ralph E. Pudritz, Thomas Henning, & Eric Hébrard

N.B. This chapter was published in The Astrophysical Journal (DOI: 10.3847/1538-4357/abae5c) on September 28th, 2020.

Abstract

Hydrogen cyanide (HCN) is a critical reactive source of nitrogen for building key biomolecules relevant for the origin of life. Still, many HCN reactions remain uncharacterized by experiments and theory, and the complete picture of HCN production in planetary atmospheres is not fully understood. To improve this situation, we develop a novel technique making use of computational quantum chemistry, experimental data,

and atmospheric numerical simulations. First, we use quantum chemistry simulations to explore the entire field of possible reactions for a list of primary species in N_2-, CH_4-, and H_2-dominated atmospheres. In this process, we discover 33 new reactions with no previously known rate coefficients. From here, we develop a consistent reduced atmospheric hybrid chemical network (CRAHCN) containing experimental values when available, and our calculated rate coefficients otherwise. Next, we couple CRAHCN to a 1D chemical kinetic model (ChemKM) to compute the HCN abundance as a function of atmospheric depth on Titan. Our simulated atmospheric HCN profile agrees very well with the Cassini observations. CRAHCN contains 104 reactions however nearly all of the simulated atmospheric HCN profile can be obtained using a scaled down network of only 19 dominant reactions. From here, we form a complete picture of HCN chemistry in Titan's atmosphere, from the dissociation of the main atmospheric species, down to the direct production of HCN along 4 major channels. One of these channels was first discovered and characterized in Pearce et al. [335] and this work.

3.1 Introduction

Hydrogen cyanide (HCN) is a fundamental molecule in the origins of life. Both nucleobases, the building blocks of DNA/RNA, and amino acids, the building blocks of proteins form in HCN reactions [34, 183]. Consequently, a terrestrial atmosphere rich in HCN may be a distinct feature of what we term a *biogenic planet*, i.e. a planet capable of producing key biomolecules without requiring exogenous sources (e.g. meteorites).

In atmospheres, HCN generally forms out of the reactive radicals left over from methane (CH_4) and nitrogen (N_2) dissociation [36, 108, 335]. These radicals are ^4N, ^2N, CH_3, $^3CH_2$, $^1CH_2$, CH, H_2 and H, where the leading superscripts signify the singlet, doublet, triplet, and quartet spin states [193, 194]. There are various energy sources capable of dissociating CH_4 and N_2 in an atmosphere, including ultraviolet (UV) light, galactic cosmic rays (GCRs), and lightning.

The most HCN-rich atmosphere in the Solar System belongs to Saturn's moon Titan. From 2004–2009, 4 instruments aboard the Cassini spacecraft measured the HCN molar mixing ratios[1] in Titan's atmosphere to be ∼0.1–10ppm (parts-per-million)

---

[1] Molar mixing ratios are the molar abundances of species divided by that of the entire atmospheric composition.

in the lower atmosphere (<600 km), and ∼0.1–5‰ (parts-per-thousand) in the upper atmosphere (> 700 km) [109–112]. Titan has a surface temperature of ∼94 K, and an atmospheric composition of approximately 1.5 bars of N_2 (∼94.2%), CH_4 (∼5.7%) and H_2 (∼0.1%) with relatively low abundances of oxygen species (CO: 40–50 ppm, CO_2: 10–20 ppb, H_2O: 0.5–8 ppb) [108, 336]. UV light and GCRs are responsible for dissociating N_2 and CH_4 to produce radical species in Titan's upper and lower atmospheres, respectively [130, 156, 157]. Numerical simulations of N_2-rich exoplanet atmospheres suggest Titan's high atmospheric HCN composition is caused by its high atmospheric C/O ratio ($\gg 1$) [124].

HCN has also been detected in the atmospheres of Pluto and Neptune with concentrations of ∼40 ppm and ∼1 ppb (parts-per-billion), respectively [114, 117]. Observations have also been used to put an upper bound of 0.1 ppb on the HCN concentration in Uranus's atmosphere [117]. Finally, HCN has been tentatively detected in the exoplanet atmospheres of 55 Cancri e [122] and WASP-63b [123], and may have been present in the early Earth atmosphere prior to the origin of life [36].

Given the abundance of HCN in Titan's atmosphere, and the availability of the Cassini data, Titan is the perfect testbed for validating theoretical chemical networks for HCN production in atmospheres. In the past, large-scale networks containing 800–3000+ reactions have been paired with 1D chemical kinetic codes to calculate the HCN profile as well as other chemical profiles in Titan's atmosphere [126, 130–133, 186, 187, 337]. Past simulations provide a reasonable agreement with the Cassini atmospheric HCN measurements, and agree on the importance of $H_2CN + H \longrightarrow HCN + H_2$ as a pathway for HCN production, and HCN photolysis ($HCN + h\nu \longrightarrow CN + H$) as a destruction process [126, 130, 131, 133]. Rate coefficients in these networks are typically gathered from a variety of sources with differing accuracies (e.g. experiments, theoretical simulations, similar reactions, thermodynamics). Quantum chemistry methods are also occasionally used to introduce new reaction rate coefficients (e.g. Hébrard et al. [133], Loison et al. [126]; Vuitton et al. [130]).

Up until this point, there have been gaps in the HCN chemical data, preventing simulations from obtaining a complete picture of HCN production and destruction in Titan's atmosphere. There is a particular absence of rate coefficient data for reactions involving excited species such as doublet nitrogen atoms (^2N) and singlet methylene ($^1CH_2$): two species that are directly produced from ultraviolet (UV) and galactic cosmic ray (GCR) dissociation in Titan's upper and lower atmosphere, respectively

[130].

We take the next step in simulating HCN chemistry in Titan's atmosphere, by finding, calculating, and including all the missing reactions relevant to the production and destruction of HCN in this environment and any direct competing reactions. Furthermore, given the complexity and computational cost of analyzing large-scale networks, we take a different approach from past Titan simulations by building and implementing a reduced network. What we have discovered, is that HCN chemistry can really be understood with a highly reduced set of chemical reactions, and that this approach is invaluable to obtaining physical insights from the results. A reduced network approach has been taken in the past for modeling warm to hot hydrogen-dominated atmospheres, and has similarly been found to conserve most of the information and insight into the dominant production and destruction pathways of observable species [338]. Moreover, shifting the focus to the development of smaller chemical networks that are less computationally demanding would make them implementable in 3D atmosphere models (e.g., Lebonnois et al. [339]), which are the only ones that are able to reproduce seasonal effects.

To summarize our method, we develop a "bottom up" theoretical approach to analyze the main formation and destruction channels of HCN in Titan's atmosphere. We start by using computational quantum chemistry simulations to scan all possible reactions between a small set of primary species. The primary species are the main reactive constituents of Titan's atmosphere (CH_4, N_2, H_2, HCN), their dissociation products, and a few key intermediates (see Table 4.1 for list of primary species). We then use canonical variational transition state theory [207, 335] and Rice–Ramsperger–Kassel–Marcus/master equation (RRKM/ME) theory [151] to calculate the rate coefficients for all these reactions. Many of these reactions are discovered here for the first time. We validate these calculations by comparing with experimental values in the 32% of cases that are available.

From this, we combine our calculated rate coefficients with available experimental values to obtain a consistent and complete chemical network for the reduced set of primary species. We call this network CRAHCN (Consistent Reduced Atmospheric Hybrid Chemical Network). We then couple CRAHCN with a 1D chemical kinetic model (ChemKM) [340] in order to simulate the production and destruction of HCN in Titan's atmosphere.

This approach is beneficial in that it allows us to a) accept or reject previously reported reactions, b) discover previously unknown and potentially very important reactions, and c) develop a very fast, accurate, and consistent code to compute HCN chemistry in atmospheres.

We began this effort in Pearce et al. [335], where we developed a feasible and accurate method to calculate a small network of 41 unique reaction rate coefficients that are directly involved with or in competition with the production of HCN in atmospheres. We focused mainly on validating the method using reactions previously studied by theory or experiment; However 15 of the calculated rate coefficients in that work had no previously known values.

In this work, we expand the network to include CN as a primary reacting species. We also explore more deeply into the unknown territory of HCN chemistry by simulating *all* the possible efficient interactions between the primary molecular species in the network. In this expansion, we also include three-body reactions, where an atmospheric molecule collisionally deexcites a vibrationally excited intermediate. Next, we modify some of the reactions from Pearce et al. [335] due to new knowledge about vibrationally excited and unstable intermediates (see theoretical case studies in Appendix materials). Finally, we include two experimental spin-forbidden collisionally induced intersystem crossing reactions [285, 341] whose rate coefficients cannot be calculated using our theoretical method. We direct the reader to the Appendix Tables for the CRAHCN rate coefficient data.

In this process, we discover 33 brand new reactions, the majority of which are based on H_2CN, CN, CH, and electronically excited molecules (^2N and $^1CH_2$). Ultimately, we finish with a consistent reduced network containing 104 reactions, which is complete for the 14 primary species in this work. In the end, we discover that only 19 reactions are at the heart of HCN production and destruction in Titan's atmosphere.

This paper proceeds as follows: in Section 4.2 we describe the theoretical and computational quantum chemistry methods used to calculate the reaction rate coefficients in CRAHCN, and we outline the model parameters for our atmospheric numerical simulations of Titan. Then, in Section 3.3 we describe the results of the rate coefficient calculations, and their conformance to any experimentally measured values. We also perform a methods comparison to compare the accuracies of our chosen computational quantum chemistry method and two other widely used methods. Next, in Section 3.4 we analyze the results of our four numerical models of Titan's atmosphere: our fiducial model, a model with only 19 dominant reactions, a model with no GCRs, and a model with a different input for eddy diffusion. We then compare our results to the three most recent Titan models in the literature [126, 130, 131]. In this section, we also describe the two sensitivity analyses which allow us to identify the dominant pathways to HCN production and destruction on Titan. Sensitivity analyses involve running simulations where reactions from the network are excluded I) one at a time, and II) multiple at a time. Then, in Section 3.5 we present a step-by-step guide to the production of HCN in Titan's atmosphere, and we discuss how CRAHCN can be used for other atmospheric models. Finally, we summarize our main conclusions in Section 4.5.

The Appendix materials contains a) three tables comparing calculated rate coefficients at 298 K with experimental values, b) two tables containing the CRAHCN reaction rate coefficients, expressed as their Lindemann and Arrhenius parameters for temperatures from 50–400 K, c) any experimental data for the reactions calculated in this work, d) a breakdown of the calculations for some of the non-standard reactions in CRAHCN, and e) the raw computational quantum chemistry data used for rate coefficient calculations.

Table 3.1: List of primary molecular species in this network and their spin states.

Species	Spin state	Ground/Excited state
HCN	singlet	ground
H_2CN	doublet	ground
N_2	singlet	ground
CN	doublet	ground
^2N	doublet	excited
^4N	quartet	ground
CH_4	singlet	ground
CH_3	doublet	ground
$^1CH_2$	singlet	excited
$^3CH_2$	triplet	ground
CH	doublet	ground
H_2	singlet	ground
H	doublet	ground
NH	triplet	ground

3.2 Methods

Our atmospheric model can be roughly divided into two components, a) the chemical network, which is the collection of reactions and their experimental or calculated rate coefficients, and b) the chemical kinetic code, which handles radiative transfer, molecular and eddy diffusion, molecular influx and escape, photodissociation, and GCR dissociation.

3.2.1 Rate Coefficient Calculations

There are 104 reactions in our reduced network, representing all efficient reactions between the 14 primary species in our network (see Table 4.1). Our strategy for building up the network is as follows.

Firstly, if experimental data is available, we use it in this network. This accounts for 42 of the 104 reactions.

Second, we use a standard, fast, and accurate computational quantum chemistry method combined with standard theoretical methods to compute all possible rate coefficients and compare our results with any experimental values. This computational method is the Becke-Half-and-Half-Lee-Yang-Parr[2] (BHandHLYP) density functional and the augmented correlation-consistent polarized valence double-ζ (aug-cc-pVDZ) basis set[3] [216, 217, 342–344]. We call this method BH/d for short. We show that there is a good agreement between experimental and calculated rate coefficients when using this computational method, with the majority of calculations (64%) landing within a factor of 2 of experimental values and all values landing within about an order of magnitude of experimental values.

Typical uncertainties for rate coefficients—assigned in large-scale experimental data evaluations—range from a factor of 2 to an order of magnitude [137, 247]. As examples in our network, Baulch et al. [137] assign factor of 2–3 uncertainties to the rate coefficients of $H + H + M \longrightarrow H_2 + M$ and $CH_3 + H + M \longrightarrow CH_4 + M$, and

---

[2] Hartree-Fock (HF) methods tend to over-estimate energy barriers, and density functional theory (DFT) methods tend to under-estimate energy barriers. BHandHLYP offers a reasonable solution by using 50% Hartree-Fock and 50% density functional theory for the exchange energy calculation.

[3] The basis set is the defined space for the problem, in our case it represents the atomic orbitals. The aug-cc-pVDZ basis set includes all atomic orbitals within the electron shell that is 1 above the atom's valence shell.

order of magnitude uncertainties to the rate coefficients of $CH_4 + CH \longrightarrow$ products and $CN + {}^4N \longrightarrow N_2 + C$.

Third, we compare the accuracy of our BH/d calculations with A) a second DFT method, and B) an *ab inito* method. The DFT method we use for comparison is the fairly recently developed asymptotically corrected ωB97XD functional [345]. We again use the aug-cc-pVDZ basis set, and call this method ωB/d for short. The *ab inito* method is coupled-cluster singles and doubles [4] (CCSD) with the aug-cc-pVTZ basis set [348]. For convenience, we designate this as CC/t. We will show below that ωB/d and CC/t do not necessarily improve the accuracy of our calculations in terms of agreement with experimental rate coefficients. In 8 out of 12 cases, BH/d gives the best, or equal to the best agreement with experiment in comparison with the other two methods. The other two methods give the best, or equal to the best agreement in 7 out of 12 and 6 out of 12 cases, respectively. We summarize these results in detail in Section 3.3.1. For recent detailed reviews of DFT and coupled-cluster theory, we refer the reader to Mardirossian & Head-Gordon[349], and (2017), and Bartlett & Musial [350], respectively.

We have also compared the accuracy of a variety of different methods on a benchmark reaction (BHandHLYP, CCSD, HF, M06-2x, CAM-B3LYP and B3LYP) in past work, and found the BH/d computational method provided the best accuracy [335]. We note that the CAM-B3LYP/aug-cc-pVDZ method provided comparable accuracy to BH/d, and would be an interesting method to explore for future network calculations.

Finally, we compare the difference in accuracy for our benchmark method when increasing the size of the basis set from double-ζ to triple-ζ. We will show that there is no measurable improvement in accuracy for the 12 cases chosen in this work when increasing the basis set size by this level.

The theoretical methods we use to calculate rate coefficients are variational transition state theory (CVT) [146, 207, 335] and Rice–Ramsperger–Kassel–Marcus/master equation (RRKM/ME) theory [151]. These theoretical methods are described below.

---

[4] The major benefit of coupled-cluster theory over DFT tends to come into play for systems with strong electron correlation effects. Coupled-cluster methods are able to describe the quantum many-body effects of the electronic wave function at a computational cost is significantly more expensive than DFT. Coupled-cluster methods are size-extensive, and thus provide a correct scaling for the correlation energy with respect to the number of electrons [144, 346, 347].

3.2.1.1 One- and Two-Body Reactions

One- and two-body reaction rate coefficients are calculated using CVT. This method involves varying the reaction coordinate (e.g. a bond distance) along a minimum energy path in order to find the minimum rate coefficient. This is expressed as: [146]

$$k_{CVT}(T, s) = \min_{s} \left\{ k_{GT}(T, s) \right\}. \tag{3.1}$$

where $k_{GT}(T, s)$ is the generalized transition state theory rate coefficient, T is the temperature, and s is the reaction coordinate (e.g. bond distance).

Neglecting effects due to tunneling, the generalized transition state theory (GT) reaction rate coefficient is given by: [146, 149]

$$k_{GT}(T, s) = \sigma \frac{k_B T}{h} \frac{Q^{\ddagger}(T, s)}{\prod_{i=1}^{N} Q_i^{n_i}(T)} e^{-E_0(s)/RT}. \tag{3.2}$$

where σ is the reaction path multiplicity, k_B is the Boltzmann constant (1.38×10^{-23} J K^{-1}), T is temperature (K), h is the Planck constant (6.63×10^{-34} J·s), $Q^{\ddagger}$ is the partition function of the transition state per unit volume (cm^{-3}), with its zero of energy at the saddle point, Q_i is the partition function of species i per unit volume, with its zero of energy at the equilibrium position of species i, n_i is the stoichiometric coefficient of species i, N is the number of reactant species, E_0 is the difference in zero-point energies between the generalized transition state and the reactants (kJ mol^{-1}) (0 for barrierless reactions), and R is the gas constant (8.314×10^{-3} kJ K^{-1} mol^{-1}).

To find the location along the minimum energy path where the GT rate coefficient is smallest, we use the maximum Gibbs free energy criterion, which offers a compromise of energetic and entropic effects [146, 147].

The partition functions per unit volume have four components,

$$Q = \frac{q_t}{V} q_e q_v q_r. \tag{3.3}$$

where V is the volume (cm^{-3}) and the t, e, v, and r subscripts stand for translational, electronic, vibrational, and rotational, respectively.

The zero-point energies, Gibbs free energies, and partition functions are calculated for each reaction along its minimum energy path using the Gaussian 09 software package [214].

This accurate yet inexpensive method was developed in Pearce et al. [335] and typically provides rate coefficients within an order of magnitude of their published experimental values. In this work, in order to improve accuracy by a factor of 2 on average, we modify the location of the zero of energy for the vibrational partition function in Equation 4.12. Now, instead of being at the bottom of the internuclear potential energy well, we place it at the first vibrational level, i.e., the zero-point level. This gives the vibrational partition function the form:

$$q_v = \prod_{n=1}^{N} \frac{1}{1 - e^{-\Theta_n/T}}, \tag{3.4}$$

where N is the number of vibrational modes, Θ_n is the vibrational temperature of the nth mode ($\Theta_n = \frac{\hbar\omega_n}{k_B}$), and T is temperature.

Barrierless reaction rate coefficients do not typically vary by more than a factor of a few for temperatures between 50 and 400 K [208, 219–222], thus temperature dependences are only calculated for the reactions with barriers. This is done by calculating the rate coefficients at 50, 100, 200, 298.15, and 400 K and then fitting the results to the modified Arrhenius expression

$$k(T) = \alpha \left(\frac{T}{300}\right)^{\beta} e^{-\gamma/T}, \tag{3.5}$$

where $k(T)$ is the temperature-dependent second-order rate coefficient (cm^{3}s^{-1}), α, β, and γ are fit parameters, and T is temperature (in K).

3.2.1.2 Three-Body Reactions

When two reactants combine to form a single product, a third body is generally required to take away some of the excess vibrational energy from the reaction product, otherwise it will dissociate [351]. The mechanism of these three-body reactions is expressed as

$$\mathrm{A} + \mathrm{B} \longrightarrow \mathrm{C}_{(\nu)} \tag{3.6}$$

$$C_{(\nu)} \xrightarrow{+M} C. \tag{3.7}$$

In other words, reactants A and B combine to form a vibrationally excited product C$_{(\nu)}$. This product is then collisionally deexcited by species M.

The pressure-dependent rate law for this reaction is

$$\frac{d[C]}{dt} = k([M])[A][B]. \tag{3.8}$$

where $k([M])$ is the pressure-dependent second-order rate coefficient ($\mathrm{cm^3s^{-1}}$).

In the high atmospheric pressure regime, the collision rate approaches 100%, and since it cannot exceed this value, the reaction rate becomes pressure independent. Conversely, in the low atmospheric pressure regime, empirical data show that the reaction rate is linear with pressure. For this reason, the pressure dependent rate coefficient is expressed as a function of the Lindemann parameters, i.e., the high-pressure limit (k_∞ [$\mathrm{cm^3s^{-1}}$]) and low-pressure limit (k_0 [$\mathrm{cm^6s^{-1}}$]) rate coefficients [352].

$$k([M]) = \frac{k_0[M]/k_\infty}{1 + k_0[M]/k_\infty} k_\infty \tag{3.9}$$

It can be shown by taking the pressure limits of this equation that in the high-pressure limit, $k = k_\infty$, and in the low-pressure limit, $k = k_0[M]$.

We calculate the high-pressure limit rate coefficients in the same way as we calculate two-body rate coefficients, using CVT, however in this case we make use of the ktools code of the Mulitwell Program Suite [353–355]. This method employed in ktools is equivalent to our method of calculating two body rate coefficients; However, we choose to use ktools as it is convenient to building the input files required for calculating low-pressure limit rate coefficients. We find deviations of $< 5\%$ between our manual CVT calculations and those performed by ktools.

To calculate the low-pressure limit rate coefficients, we make use of the Multiwell Master Equation (ME) code, which employs RRKM theory. The ME describes the interaction between collisional energy transfer (with the atmospheric "bath" gas) and chemical reaction [356]. In the case of our three-body reactions, the ME contains the probabilities that our vibrationally excited product will collisionally stabilize for a given atmospheric pressure and temperature. The Multiwell ME code employs Monte Carlo sampling of the ME to build a statistical average of the possible outcomes of the reaction.

The low-pressure limit rate coefficients are then calculated using the output from these stochastic trials: [135, 354]

$$k_0([M]) = \frac{k_\infty f_{prod}}{[M]} \tag{3.10}$$

where k_∞ is the high-pressure limit rate coefficient, f_{prod} is the fractional yield of the collisionally deexcited product calculated by the Multiwell ME code, and [M] is the simulated concentration (cm^{-3}), which is low enough for k_0 to converge.

We used N_2 as a bath gas, as it is the primary constituent of Titan's atmosphere. The energy transfer was treated with a standard exponential-down model with $< \Delta E >_{down} = 0.8$ T K^{-1} cm^{-1} [357, 358]. The Lennard-Jones parameters[5] for N_2 and all the products were taken from the literature [359–361] and can be found in Table 4.8.

In the diffuse, upper regions of atmospheres, vibrationally excited species produced from the combination of two reactants will typically dissociate back into the original reactants. In these cases, the three-body reactions completely describe the chemistry occurring in both diffuse and dense regions of the atmosphere. However in some cases, the favourable vibrational decay products are not the original reactants (e.g. $CN + {}^4N \longrightarrow CN_{2(\nu)} \cdot \longrightarrow N_2 + C$). In these cases, we also include the two-body reactions to these favourable decay pathways.

We would expect these two-body reactions to be less efficient in the lower, denser regions of atmospheres where the vibrationally excited intermediates can be collisionally deexcited. Regardless, we allow these reaction rate coefficients to be independent of pressure. Since radicals are typically not very abundant in the denser regions of the atmosphere, this treatment should not produce significant error.

We verify the most efficient decay pathway of vibrationally excited molecules from previous experimental studies. For more details, we refer the reader to the theoretical case studies in the Appendix materials.

3.2.2 Atmospheric Model Parameters

Atmospheric numerical simulations are performed using a 1D chemical kinetic model (ChemKM). Radiative transfer in this code is calculated using the plane-parallel two-stream approximation. Photo-absorption and Rayleigh scattering are also included. ChemKM has been benchmarked with several other chemical kinetic codes[6] including

---

[5] The Lennard-Jones potential is used by the ME to model the collision between a molecule and the bath gas.

[6] https://www.issibern.ch/teams/1dchemkinetics/

Agúndez model [362, 363], ARGO [364], ATMO [365–367], Kasting model [368, 369], KINETICS [370–372], Venot model [127, 373], and VULCAN [374]. Models agree within the numerical precision, when using the same input and setup. For complete details on this atmospheric code, we refer the reader to Molaverdikhani et al. [340, 375].

The setup parameters for our fiducial Titan atmospheric model mostly match those in Hébrard et al. [133]. This includes the atmospheric temperature, pressure, and initial molar mixing ratios of N_2, CH_4, H_2, and CO, the eddy diffusion profile, the influx of H_2O from micrometeorites (5×10^6 cm^{-2}s^{-1}), and 21 of the photochemical reactions and cross-sections. We use the solar mean for the top-of-atmosphere radiation (with solar zenith angle of 50°) [376]. We also initially included the Jean's thermal escape of H and H_2, but found it did not significantly affect our results.

Eddy diffusion describes the turbulent mixing of molecules in an atmosphere. Its form in Hébrard et al. [133], which was originally developed by Hörst et al. [377], is

$$K(z) = \frac{K_o(p_o/p)^\gamma K_\infty}{K_o(p_o/p)^\gamma + K_\infty}, \tag{3.11}$$

where K_o is the surface eddy coefficient (400 cm^{2}s^{-1}), K_∞ is the top-of-atmosphere eddy coefficient (3×10^7 cm^{2}s^{-1}), p is the pressure (Pa), $p_o = 1.77\times10^3$ Pa and $\gamma = 2$.

In Figure 3.1, we plot our fiducial eddy diffusion profile along with the profiles of the three most recent Titan models in the literature [126, 130, 131].

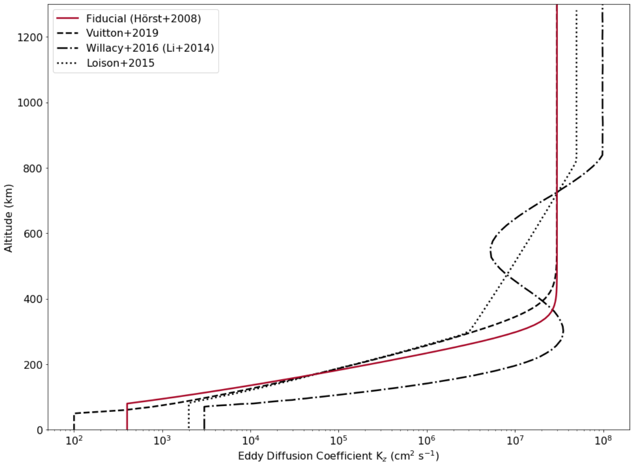

Figure 3.1: Eddy Diffusion profile used in our fiducial model compared with the profiles used in the three most recent Titan models in the literature [126, 130, 131].

Our grid is 100 uniform layers from 0 to 1300 km.

To handle the galactic cosmic ray (GCR) dissociation of N_2 and CH_4, we use the most recent GCR models by Gronoff et al. [156, 157]. However, we only include the GCR reactions which produce neutral species, as our network does not contain ions. These reactions are,

$$\begin{gathered} N_2 + GCR \longrightarrow {}^2N + {}^4N, \\ N_2 + GCR \longrightarrow {}^4N + {}^4N, \\ CH_4 + GCR \longrightarrow CH_3 + H, \\ CH_4 + GCR \longrightarrow {}^3CH_2 + H_2. \end{gathered}$$

We do not include condensation in our models, as we are primarily interested in the gas phase chemistry leading to the production of HCN. In addition, CRAHCN does not include the heavy hydrocarbons which produce the majority of hazes, therefore we do not include haze production/destruction.

3.3 Results - Rate Coefficients

In Pearce et al. [335], we calculated 42 reaction rate coefficients involved with or in competition with the production of HCN in early Earth and Titan atmospheres. In this work, we improve on the original network by including pressure dependence on addition reactions, by modifying the vibrational partition function to improve the accuracy of our calculations (by factor of ∼2 on average), and by removing the $2\,H_2CN \longrightarrow HCN + H_2CNH$ abstraction reaction, which our recalculations show has a large barrier. We also expand the original network to 104 reactions, which is the result of exploring the entire field of possible reactions for the list of primary species in Table 4.1.

In Table 3.6, we display the 34 pressure-independent rate coefficients from Pearce et al. [335], recalculated with a modified vibrational partition function described in Section 4.2. The only pressure-independent reaction not carried over from Pearce et al. [335] is $2\,H_2CN \longrightarrow HCN + H_2CNH$. Our recalculations show that this abstraction reaction actually has a large barrier and is therefore too inefficient to consider (k(298 K) $\sim 10^{-41}$ cm^{3}s^{-1}).

20 of these 34 reactions have experimentally measured rate coefficients, and all our calculations land within an order of magnitude of these experimental values. The majority (70%) land within a factor of 2 of the experimental values. This level of accuracy is consistent with the uncertainties assigned in large-scale experimental data evaluations [137, 247].

We note however that in two cases, our chosen computational method (BH/d) predicted barriers for reactions that did not have barriers. Moreover, in two other cases, this method predicted barrierless reactions for reactions with small experimental barriers. These are limitations of our chosen method, and in these few cases, we artificially remove the barriers from these calculations, or introduce experimental barriers to these calculations, respectively.

As a result of exploring the entire field of possible reactions for the primary species in this work, we calculate the rate coefficients of 36 new two-body reactions, and 32 new three-body reactions (68 total). 33 of these new reactions have no previously known rate coefficient.

In Table 3.7, we display the 36 new two-body reactions, along with our calculated rate coefficients at 298 K and any experimentally measured values. Seven of these reactions have experimental values, and the majority (71%) of our calculated rate coefficients are within a factor of 4 of these values. All our calculated values are within one order of magnitude of experimental values. However, in two cases our chosen computational method predicted no barrier for reactions that have small experimental barriers. As before, we artificially introduce the experimental barriers to these calculations.

In Table 3.8, we display the 32 calculated low pressure (k_0) and high pressure (k_∞) limit rate coefficients at 298 K for the three-body reactions in this work, as well as any experimentally measured values. 16 of the high pressure limit rate coefficients have experimental values, and the majority of cases (69%) are within a factor of 4 of these experimental values. Again, all calculations are within about an order of magnitude of experimental values.

Our calculated third-order, low pressure limit rate coefficients are within a factor of 2 of experimental values 67% of the time, and nearly within an order of magnitude in all cases. Only in the case of $\mathrm{CN} + {}^4\mathrm{N} + \mathrm{M} \longrightarrow \mathrm{CN}_2 + \mathrm{M}$ is our calculated rate coefficient slightly less accurate, differing from the one experimentally measured value [378] by a factor of 36. This reaction is not well studied, therefore it is possible that we are not as far off from the exact value as this discrepancy implies. Calculations at the CC/t level of theory only bring this third-order rate coefficient to within a factor of 28 of the experimental value. This reaction turns out not to be important in the story of HCN in Titan's atmosphere.

In Tables 4.5 and 4.6, we display the 104 pressure- and temperature-dependent rate coefficients for the fiducial chemical network used in this study. Experimentally measured rate coefficients are used when available, which is the case for 42 reactions. Sometimes experimental values are only available for one of either the high-pressure or low-pressure limit rate coefficient, in which case we use a combination of experimental and calculated values. Our calculated values are used in the majority of the network (68%).

3.3.1 Methods Comparison on Dominant Reactions

In a past computational methods comparison, our calculated rate coefficient for $CH_4 + H \longrightarrow CH_3 + H_2$ at the CCSD/aug-cc-pVDZ level of theory was a factor of 8 smaller than the experimental values [335]. Conversely, our calculated the rate coefficient at the BH/d level of theory was within the experimental range. This, along with speed, were major motivating factors for choosing BH/d for our large-scale theoretical chemical reaction rate study.

In our sensitivity analysis in Section 3.4.6, we find 19 reactions dominate the production and destruction of HCN in Titan's atmosphere. 11 of these 19 reactions have experimental rate coefficients. In the case of $CH_3 + H + M \longrightarrow CH_4 + M$, both the high- and low-pressure rate coefficients are experimentally measured.

In Table 3.2, we compare the accuracy of the BH/d, ωB/d, and CC/t for calculating the rate coefficients of these 11 dominant reactions. Based on general agreement to the experimental values, and a correct diagnosis of the reaction barrier, each method is found to have variable accuracy. In the following paragraphs, we move down through the reactions in Table 3.2, commenting on some of the most important results for selected reactions.

The results of this methods comparison shows a similar level of consistency in accuracy across all three methods. For the 12 coefficients, BH/d was the most accurate or tied for the most accurate method 8 times, ωB/d was the most accurate or tied for the most accurate method 7 times, and CC/t was the most accurate or tied for the most accurate method 6 times. When comparing only the DFT methods, BH/d

Table 3.2: A comparison of the accuracy of three methods for calculating rate coefficeints for the dominant reactions in this study. The methods are BHandHLYP/aug-cc-pVDZ (BH/d), ωB97XD/aug-cc-pVDZ (ωB/d), and CCSD/aug-cc-pVTZ (CC/t). Only 11 of the 19 dominant reactions have experimentally measured values and can be calculated using our theoretical methods. The error factor is the multiplicative or divisional factor from the nearest experimental or suggested value. For three-body reactions, the displayed rate coefficients are either the high-pressure limit (k_∞) or low-pressure limit (k_0). The aug-cc-pVDZ basis set is used for all calculations. Second-order rate coefficients have units cm^{3}s^{-1}. Third-order rate coefficients have units cm^{6}s^{-1}.

Reaction equation	k(298) experiment	k(298) BH/d	Error	k(298) ωB/d	Error	k(298) CC/t	Error	Winner(s)
$H_2CN + {}^4N \longrightarrow HCN + NH$	4.4×10^{-11}	[a]4.7×10^{-12}	9	3.4×10^{-12}	13	[a]5.1×10^{-12}	9	ωB
$CN + {}^4N \longrightarrow CN_2\cdot \longrightarrow N_2 + C$	$1.0–3.0\times10^{-10}$	4.3×10^{-11}	2	4.2×10^{-11}	2	2.6×10^{-11}	4	BH, ωB
$CN + CH_4 \longrightarrow HCN + CH_3$	$5.6–11\times10^{-13}$	[b]7.7×10^{-13}	1	[b]1.3×10^{-12}	1	4.5×10^{-13}	1	CC
$NH + {}^4N \longrightarrow N_2H\cdot \longrightarrow N_2 + H$	$2.5–2.6\times10^{-11}$	5.5×10^{-11}	2	5.6×10^{-11}	2	2.7×10^{-11}	1	CC
${}^4N + CH_3 \longrightarrow {}^3H_3CN\cdot \longrightarrow H_2CN + H$	$5.0–7.7\times10^{-11}$	6.2×10^{-11}	1	8.7×10^{-11}	1	[c]1.2×10^{-11}	4	BH, ωB
${}^2N + CH_4 \longrightarrow H_3CNH\cdot \longrightarrow {}^1H_2CNH\cdot + H\cdot \longrightarrow H_2CN + H_2$	$2.4–4.5\times10^{-12}$	[de]1.7×10^{-11}	4	[df]7.9×10^{-12}	2	[d]2.9×10^{-11}	6	tie
$CH_4 + {}^1CH_2 \longrightarrow C_2H_{6(\nu)}\cdot \longrightarrow CH_3 + CH_3$	$0.2–7.3\times10^{-11}$	2.1×10^{-11}	1	5.5×10^{-11}	1	1.3×10^{-11}	1	tie
$CH_4 + CH \longrightarrow CH_4{-}CH\cdot \longrightarrow C_2H_5\cdot \longrightarrow C_2H_4 + H$	$0.02–3\times10^{-10}$	[g]1.8×10^{-10}	1	9.2×10^{-12}	1	[g]1.0×10^{-9}	3	ωB
${}^3CH_2 + H \longrightarrow CH_{3(\nu)}\cdot \longrightarrow CH + H_2$	$0.8–2.7\times10^{-10}$	3.7×10^{-10}	1	7.8×10^{-10}	3	2.6×10^{-10}	1	BH, CC
$CH_3 + H \longrightarrow CH_4$ (k_∞)	$1.5–4.7\times10^{-10}$	1.4×10^{-10}	1	5.4×10^{-11}	3	[h]2.6×10^{-10}	1	BH
$CH_3 + H + M \longrightarrow CH_4 + M$ (k_0)	$0.2–5.5\times10^{-28}$	2.6×10^{-28}	1	3.3×10^{-28}	1	[h]1.0×10^{-27}	2	BH, ωB
$H + H + M \longrightarrow H_2 + M$ (k_0)	$4–250\times10^{-33}$	1.7×10^{-33}	2	4.4×10^{-34}	12	1.8×10^{-33}	2	BH, CC

[a] We remove the barrier from this calculation as experiments predict this reaction to be barrierless or nearly barrierless [229]. See Appendix materials for more details.

[b] We introduce an experimental barrier of 8.3 kJ mol^{-1} [379] to this calculation as no barrier is found at this level of theory.

[c] We remove the barrier from this calculation as experiments and theory predict this reaction to be barrierless [195, 248].

[d] We introduce an experimental barrier of 6.3 kJ mol^{-1} [233] to this calculation as no barrier is found at this level of theory.

[e] Simulations had sporadic convergence beyond a C-N bond distance of 2.76Å. The rate coefficient is calculated with the variational transition state at this location, which has the highest ΔG.

[f] Simulations had sporadic convergence beyond a C-N bond distance of 2.60Å. The rate coefficient is calculated with the variational transition state at this location, which has the highest ΔG.

[g] We remove the barrier from the rate limiting step of this calculation, i.e. $CH_4{-}CH\cdot \longrightarrow C_2H_5\cdot$ as experiments predict this reaction to be barrierless [277, 278, 280].

[h] We remove the barrier from this calculation as experiments and theory predict this reaction to be barrierless [238].

was more accurate than ωB/d 3 times, less accurate 2 times, and similarly accurate 7 times.

In some cases, one or more methods would miss a barrier, or find one when one should not be present. In these cases, a method that correctly diagnosed the barrier was considered more accurate than one that incorrectly diagnosed the barrier, regardless of the calculated error factor. Also, all methods that incorrectly diagnosed the barrier were considered equally accurate. CC/t incorrectly diagnosed barriers five times, BH/d incorrectly diagnosed barriers four times, and ωB/d incorrectly diagnosed barriers twice.

In the case of $H_2CN + {}^4N \longrightarrow HCN + NH$, the BH/d, ωB/d, and CC/t methods compute barriers of heights $E_0 \sim 15$, 2, and 23 kJ mol^{-1}, respectively. The one experimental measurement suggests little or no barrier is present [229] (see Appendix materials for more details). ωB/d computes the smallest barrier; However the rate coefficient calculated using this method is a factor of 13 smaller than the experimental value, removing the barrier brings the calculated rate coefficient to within a factor of 6 of experiment. Given these discrepancies, and the lack of theoretical studies on this reaction, we recommend both a thorough theoretical follow-up study and additional experimental measurements.

Both the BH/d and CC/t methods find the $CH_4{-}CH\cdot \longrightarrow C_2H_5\cdot$ step of the $CH_4 + CH \longrightarrow C_2H_4 + H$ reaction to have a barrier with a height above the reactants. This differs from our ωB/d calculation, the results of experiment, and other theoretical studies, which suggest this reaction is barrierless [277, 333, 380] (see Appendix materials for further details).

All three methods find no barrier for the ${}^2N + CH_4 \longrightarrow H_3CNH\cdot$ reaction step. This step is expected to have a small barrier of $E_0 = 6.3$ kJ mol^{-1} [233]. Similarly, Balucani et al. [328] did not find a barrier for this reaction using the CCSD(T)/aug-cc-pVTZ level of theory.

CC/t misdiagnoses the barrier for the three-body reaction $CH_3 + H + M \longrightarrow CH_4 + M$. This reaction is barrierless [238], however CC/t calculations estimate a barrier of $E_0 \sim 62$ kJ mol^{-1}. Similarly, CC/t misdiagnoses the barrier for ${}^4N + CH_3 \longrightarrow {}^3H_3CN\cdot$, which is also barrierless [195, 248]. The barrier height for this reaction at the CC/t level of theory is 17 kJ mol^{-1}. BH/d and ωB/d correctly calculate no barriers for these two reactions. Conversely, BH/d and ωB/d do not calculate barriers for $CN + CH_4 \longrightarrow HCN + CH_3$, which is expected to have a barrier of $E_0 = 8.3$ kJ mol^{-1} [379]. Our CC/t calculations find a barrier for this reaction of 6.7 kJ mol^{-1}.

Lastly, the BH/d and CC/t methods compute rate coefficients for $H + H + M \longrightarrow H_2 + M$ that are factors of 2 from the nearest experimental value, whereas the ωB97XD method computes a rate coefficient for this reaction that is a factor of 12 smaller than the nearest experimental value.

Overall, BH/d seems to be a reasonable choice for moving forward with a large scale atmospheric study such as ours, with typical deviations from experiment of a factor of ≤ 2. ωB/d would also have been a reasonable choice moving forward, as this method correctly diagnoses barriers more frequently than BH/d and CC/t for this sample size, while maintaining accuracy nearly within an order of magnitude of experimental values. CC/t was the stand alone most accurate method in a two cases, but it was the least accurate method in six cases. Given this, and the much higher computational cost, we do not recommend CC/t for performing rate coefficient calculations for large scale atmospheric studies such as ours. For more comprehensive reaction investigations, we recommend using multiple methods, including CCSD, ωB97XD, and BHandHLYP, to verify the presence or absence of reaction barriers.

3.3.2 Basis Set Comparison on Dominant Reactions

In Table 3.3, we compare the accuracy of the aug-cc-pVDZ and aug-cc-pVTZ basis sets, paired with the BHandHLYP method, on the dominant reactions in this study that have experimental rate coefficients. The intent is to see, for our chosen method, if increasing the basis set size from double-ζ to triple-ζ leads to an improvement in accuracy with respect to agreement with experimental values.

What we find, is that rate coefficients calculated at the double-ζ level are generally very close to the values calculated at the triple-ζ level. Typical differences are less than 15%. In two out of twelve cases, the rate coefficients at the double-ζ level differ from the triple-ζ values by a factor of $\sim$2. However, in none of these twelve cases is the rate coefficient triple-ζ level more accurate than the rate coefficient at the double-ζ level with respect to experimental agreement. For this reason, and considering the added computational cost, we do not upgrade to the triple-ζ level for our large scale atmospheric study.

Table 3.3: A comparison of the accuracy of BHandHLYP/aug-cc-pVDZ, and BHandHLYP/aug-cc-pVTZ for calculating rate coefficeints for the difficult dominant reactions in this study. For three-body reactions, the displayed rate coefficients are either the high-pressure limit (k_∞) or low-pressure limit (k_0). Second-order rate coefficients have units cm^3s^{-1}. Third-order rate coefficients have units cm^6s^{-1}.

Reaction equation	k(298 K) experiment	k(298 K) BH/d	Error	k(298 K) BH/t	Error	% Difference
$H_2CN + {}^4N \longrightarrow HCN + NH$	4.4×10^{-11}	[a]4.7×10^{-12}	9	[a]4.8×10^{-12}	9	2
$CN + {}^4N \longrightarrow CN_2\cdot \longrightarrow N_2 + C$	$1.0–3.0\times10^{-10}$	4.3×10^{-11}	2	4.1×10^{-11}	2	5
$CN + CH_4 \longrightarrow HCN + CH_3$	$5.6–11\times10^{-13}$	[b]7.7×10^{-13}	1	[b]5.6×10^{-13}	1	27
$NH + {}^4N \longrightarrow N_2H\cdot \longrightarrow N_2 + H$	$2.5–2.6\times10^{-11}$	5.5×10^{-11}	2	5.2×10^{-11}	2	5
${}^4N + CH_3 \longrightarrow {}^3H_3CN\cdot \longrightarrow H_2CN + H$	$5.0–7.7\times10^{-11}$	6.2×10^{-11}	1	6.2×10^{-11}	1	0
${}^2N + CH_4 \longrightarrow H_3CNH\cdot \longrightarrow {}^1H_2CNH\cdot + H\cdot \longrightarrow H_2CN + H_2$	$2.4–4.5\times10^{-12}$	[cd]1.7×10^{-11}	4	[ce]3.3×10^{-11}	7	94
$CH_4 + {}^1CH_2 \longrightarrow C_2H_{6(\nu)}\cdot \longrightarrow CH_3 + CH_3$	$0.2–7.3\times10^{-11}$	2.1×10^{-11}	1	2.4×10^{-11}	1	14
$CH_4 + CH \longrightarrow CH_4{-}CH\cdot \longrightarrow C_2H_5\cdot \longrightarrow C_2H_4 + H$	$0.02–3\times10^{-10}$	[f]1.8×10^{-10}	1	[f]4.1×10^{-10}	1	128
${}^3CH_2 + H \longrightarrow CH_{3(\nu)}\cdot \longrightarrow CH + H_2$	$0.8–2.7\times10^{-10}$	3.7×10^{-10}	1	3.7×10^{-10}	1	0
$CH_3 + H \longrightarrow CH_4$ (k_∞)	$1.5–4.7\times10^{-10}$	1.4×10^{-10}	1	1.4×10^{-10}	1	0
$CH_3 + H + M \longrightarrow CH_4 + M$ (k_0)	$0.2–5.5\times10^{-28}$	2.6×10^{-28}	1	2.7×10^{-28}	1	4
$H + H + M \longrightarrow H_2 + M$ (k_0)	$4–250\times10^{-33}$	1.7×10^{-33}	2	1.6×10^{-33}	2	6

[a] We remove the barrier from this calculation as experiments predict this reaction to be barrierless or nearly barrierless.

[b] We introduce an experimental barrier of 8.3 kJ mol^{-1} [379] to this calculation as no barrier is found at this level of theory.

[c] We introduce an experimental barrier of 6.3 kJ mol^{-1} [233] to this calculation as no barrier is found at this level of theory.

[d] Simulations had sporadic convergence beyond a C-N bond distance of 2.76Å. The rate coefficient is calculated with the variational transition state at this location, which has the highest ΔG.

[e] Simulations had sporadic convergence beyond a C-N bond distance of 2.73Å. The rate coefficient is calculated with the variational transition state at this location, which has the highest ΔG.

[f] We remove the barrier from the rate limiting step of this calculation, i.e. $CH_4{-}CH\cdot \longrightarrow C_2H_5\cdot$ as experiments predict this reaction to be barrierless [277, 278, 280].

3.4 Results - HCN in Titan's Atmosphere

In Figure 3.2A, we display our 4 modeled atmospheric HCN profiles for Titan, as well as the HCN observations made in Titan's atmosphere by the Cassini spacecraft. Each model is discussed in detail in the subsections below. In Figure 3.2B, we compare our fiducial HCN profile to those of the three most recent Titan models in the literature [126, 130, 131].

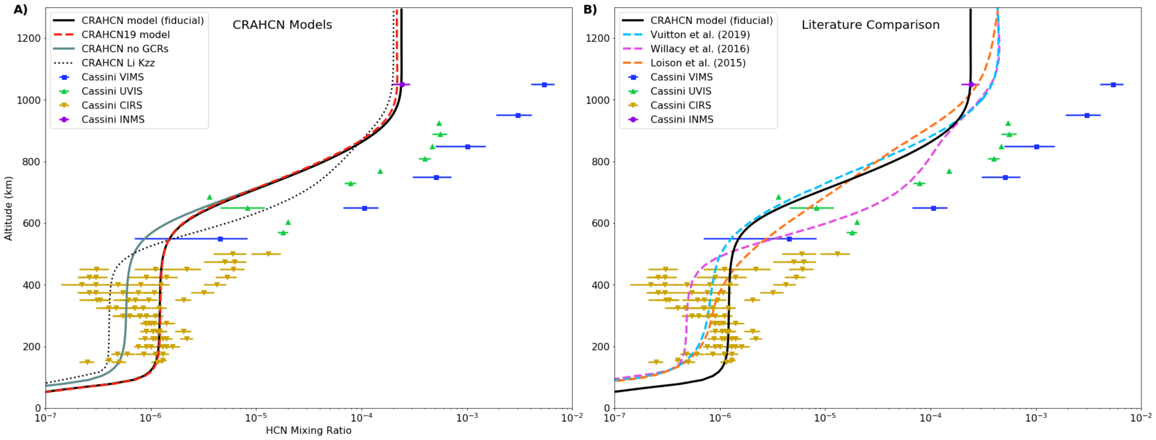

Figure 3.2: Numerical simulations of the HCN molar mixing ratio in Titan's atmosphere compared with observations taken by Cassini. **A)** CRAHCN model: our fiducial model, which uses the CRAHCN network (Tables 4.5 and 4.6) and fiducial model parameters. CRAHCN19 model: fiducial model parameters, and a chemical network containing only the dominant 19 reactions. CRAHCN no GCRs: fiducial model parameters and the CRAHCN chemical network, but all GCR reactions are turned off. CRAHCN Li Kzz: same as the CRAHCN no GCRs model, except we use the eddy diffusion profile from Li et al. [132] instead of the fiducial one from Hörst et al. [377]. The data points represent observations taken by the Cassini spacecraft. The spread in the Cassini CIRS data is due to measurements taken at various latitudes [110]. **B)** CRAHCN Model comparison with the three most recent Titan atmospheric chemistry models in the literature [126, 130, 131]. For the literature model parameters, see Table 3.4.

3.4.1 CRAHCN model (fiducial)

For our fiducial model, we use the CRAHCN network and the fiducial model parameters as described in Section 3.2.2. In Figure 3.2A, we see that the HCN profile from our fiducial model agrees very well with the HCN observations in Titan's lower atmosphere, landing right in the middle of the Cassini CIRS measurements. Our fiducial profile also nails the single Cassini INMS data point at 1050 km, which is the only *in situ* HCN measurement of Titan's atmosphere. The trade-off in agreeing so well with the INMS measurement, is that we do not agree as well with the VIMS limb measurements, or the UVIS stellar occultation measurements. This, as can be seen in Figure 3.2B, is standard for current state-of-the-art Titan models.

3.4.2 CRAHCN19 model

Our sensitivity analyses of the CRAHCN network (discussed in Section 3.4.6 below) revealed that 19 reactions are predominantly involved in the production and destruction of HCN in Titan's atmosphere. For the CRAHCN19 model, we use the fiducial model parameters, and a network containing only the 19 dominant reactions out of the 104 total reactions in CRAHCN. In Figure 3.2A, we see the HCN profile from the CRAHCN19 model almost perfectly aligns with the profile from the CRAHCN model. Maximum deviations between these model curves in the upper atmosphere are ∼10%. The total HCN produced in the CRAHCN19 model is only 6% more than the HCN produced in the fiducial model. This is mainly due to slight deviations in the lower atmosphere between models. This result suggests that the CRAHCN19 network contains nearly all that is necessary to simulate the production of HCN in Titan-like atmospheres.

3.4.3 CRAHCN no GCRs model

The aim of the CRAHCN no GCRs model is to examine the sensitivity of HCN production in the lower atmosphere to GCR flux. Thus, this model is similar to our fiducial model, except that all GCR reactions are removed. In Figure 3.2A, we see the HCN profile from the CRAHCN no GCRs model overlaps with the fiducial model in the upper atmosphere, where no GCR reactions occur. The HCN profile in the mid-lower atmosphere is only reduced by a factor of ∼2 compared to the fiducial model. Overall, the CRAHCN no GCRs model produces about one-third as much HCN in Titan's atmosphere as the fiducial model. This result suggests that GCRs are not critical for the production of HCN in Titan's atmosphere, however they boost total HCN production by about a factor of ∼3.

3.4.4 CRAHCN Li Kzz model

To investigate the effects of eddy diffusivity in the distribution of atmospheric HCN, we present a model in which we modify the eddy diffusion profile to match that of Li et al. [132] (see Figure 3.1). This profile differs from the Hörst et al. [377] profile used in all other models in that the profile inverts at 350 km, creating a low eddy diffusion zone near 550 km. This is also the profile used in the Willacy et al. [131]

Titan model. In Figure 3.2A, we see that using this eddy diffusion profile reduces the HCN abundance in the lower atmosphere by a factor of ∼3, and increases the HCN abundance in the mid atmosphere by a factor of ∼4 with respect to our fiducial model. Overall, the HCN profile from this model does not agree with the Cassini CIRS data as well as our fiducial model, as the former misses the range of CIRS measurements from 200–300 km by about a factor of 3.

3.4.5 Comparison to Other Recent Titan Models

In Figure 3.2B, we plot HCN profiles from the three most recent Titan models [126, 130, 131] to compare with our fiducial HCN profile. It is important to emphasize that the three models from the literature focused on reproducing the observed profiles of many chemical species, only one of which was HCN. The differences in parameters and chemistry between these models is summarized in Table 3.4 and Figure 3.1.

Table 3.4: Summary of the major differences in model parameters and chemistry between our fiducial model and the three most recent Titan models in the literature [126, 130, 131]. There are multiple Titan models in Vuitton et al. [130] and Willacy et al. [131]: we choose the models that best agree with the Cassini HCN measurements.

Model	Reaction Network	Photolytic processes	Eddy diffusion	GCR processes
Fiducial (this work)	104	21	Figure 3.1	N_2 and CH_4
Vuitton et al. [130] (K_o=100)	> 3000 reactions	116	”	N_2 and CH_4
Willacy et al. [131] (Model A/B)	not listed	not listed	”	none
Loison et al. [126]	969	171	”	N_2 only

Differences between all four model curves are within a factor of ∼3 in the lower atmosphere, a factor of ∼8 in the mid atmosphere, and a factor of ∼2 in the upper atmosphere. Given the differences in eddy diffusion profiles, condensation/sedimentation, photochemistry, GCR chemistry, and reaction networks, a complete explanation on the variations between these curves is not possible, however, we note a few things below.

The HCN profile from Willacy et al. [131] varies the most from our fiducial model. However, comparing the HCN model profile from Willacy et al. [131] to our CRAHCN Li Kzz model in Figure 3.2A, we can see that the curves have a very similar form in the lower and mid atmosphere. Therefore, we suspect the major differences between our fiducial HCN profile and the HCN profile in Willacy et al. [131] to be due to differences in eddy diffusion.

The HCN model from Vuitton et al. [130] varies from our fiducial HCN model by $\lesssim$2. Vuitton et al. [130] parameterized eddy diffusion in the same way we do, however we use a slightly higher surface eddy coefficient (K_o = 400 cm^2s^{-1} versus 100 cm^2s^{-1}, see Figure 3.1). Vuitton et al. [130] analyzed how changes to their surface eddy coefficient affected their HCN profile, and found that shifting K_o = 100 cm^2s^{-1} to 1000 cm^2s^{-1} decreased their HCN content in the lower atmosphere. This suggests that the major differences between our fiducial HCN profile and the HCN profile in Vuitton et al. [130] are due to differences in chemical networks and photochemistry, rather than eddy diffusion.

Differences between our fiducial HCN profile and the HCN profile in Loison et al. [126] also vary by $\lesssim$2. However, due to lack of data, we cannot comment on a major source of the discrepancies.

Other differences between our model and those in the literature include treatments for condensation/sedimentation and haze formation. We do not include condensation/sedimentation in our fiducial model, as we are mainly interested in the gas phase chemistry leading to the production of HCN. In addition, CRAHCN does not include the heavy hydrocarbons that produce the majority of hazes. Willacy et al. [131] find that condensation/sedimentation only affects the HCN profile below ~100 km, which is below any Cassini measurement. Willacy et al. [131] also included the permanent removal of HCN via haze production in one of their models (Model C), which resulted in a reduction of HCN below ~500 km of approximately a factor of 4 compared to their models without hazes (Models A and B). Their haze model, however, does not agree with the Cassini CIRS HCN data as well as their models without haze production.

Overall, our fiducial HCN model is in general agreement with the most recent Titan models in the literature.

3.4.6 Sensitivity Analyses

Not every reaction in an atmospheric chemical network contributes significantly to the production and destruction of a given species. To discover which reactions in CRAHCN contributes to the fiducial HCN profile we perform two types of sensitivity analyses on our fiducial model.

3.4.6.1 Sensitivity Analysis I

The first sensitivity analysis involves running 104 additional numerical simulations of Titan's atmosphere. In each simulation, one of the 104 reactions in CRAHCN is removed, and the resultant HCN profile compared with the fiducial HCN profile. We also perform this sensitivity analysis on the CRAHCN/no GCRs model.

This first sensitivity analysis revealed 17 of the 19 dominant reactions. In Figure 3.3A we display the changes to the HCN profiles that occur when each of these 17 reactions are removed. The removal of all other reactions did not significantly effect the fiducial HCN profile.

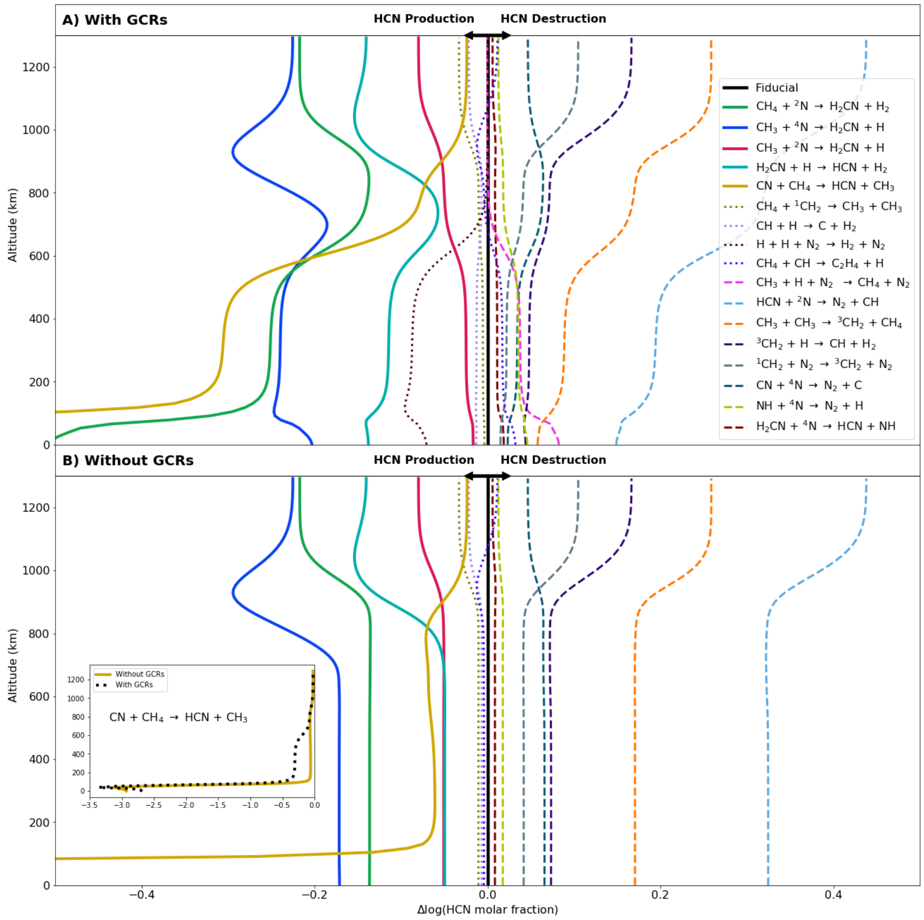

Figure 3.3: Sensitivity analysis I revealing 17 of the dominant 19 reactions in Titan's atmosphere. Each reaction curve shows the difference in HCN molar mixing ratio when excluding that reaction from **A)** the fiducial model, and **B)** the CRAHCN/no GCRs model. All of the other reactions in CRAHCN did not greatly affect the HCN profile upon their exclusion; for both models.

3.4.6.2 Sensitivity Analysis II

The second sensitivity analysis involves running a much larger number of simulations. Starting with all 104 reactions, as was done in sensitivity analysis I, each reaction is excluded in a simulation to see how it effects the HCN profile. The reaction whose removal affects the HCN profile the least is then removed, and the process is repeated with 103 reactions. The least important reaction is removed at each stage, until the exclusion of any of the remaining reactions leads to a $\gtrsim$10% deviation from the fiducial HCN profile.

The second sensitivity analysis revealed 2 additional dominant reactions, $CH_3 + CH \longrightarrow C_2H_2 + H + H$ and $^3CH_2 + CH \longrightarrow C_2H + H + H$, bringing the total to 19 dominant reactions. In Figure 3.4A we display the changes to the HCN profiles that occur when each of these 19 reactions are removed from a network containing only these 19 reactions (CRAHCN19).

3.4.6.3 19 Dominant Reactions

The 19 dominant reactions are listed in Table 3.5 below. Five reactions dominate the production of HCN, four are critical for increasing the feedstock of precursor molecules that react to produce HCN, one reaction dominates the destruction of HCN, seven reactions reduce the key precursor molecules that produce HCN, one reaction attenuates the precursor sinks by reducing H abundance, and one reaction acts as both a precursor source and sink.

The biggest impact to the fiducial HCN profile is the removal of $CN + CH_4 \longrightarrow HCN + CH_3$. This is the key reaction that recycles CN—primarily from HCN photodissociation—back into HCN. This reaction accounts for ∼36–46%[7] of the total HCN in Titan's atmosphere, and is dominant primarily because of Titan's high atmospheric CH_4 abundance.

The next most important channel is $^2N + CH_4 \longrightarrow H_2CN + H_2$, followed by $H_2CN + H \longrightarrow HCN + H_2$. Again, due primarily to the high atmospheric CH_4 concentrations, this multi-step reaction is responsible for ∼32–38% of the total HCN in Titan's atmosphere.

---

[7] Percent contributions for the four main HCN channels are calculated by dividing the difference in the total HCN abundance (integrated over all altitudes) when removing that reaction, by the summed up total differences in HCN abundances when removing each of the four main reactions. Calculations differ when using the fiducial and CRAHCN19 models, therefore we express the values as a range.

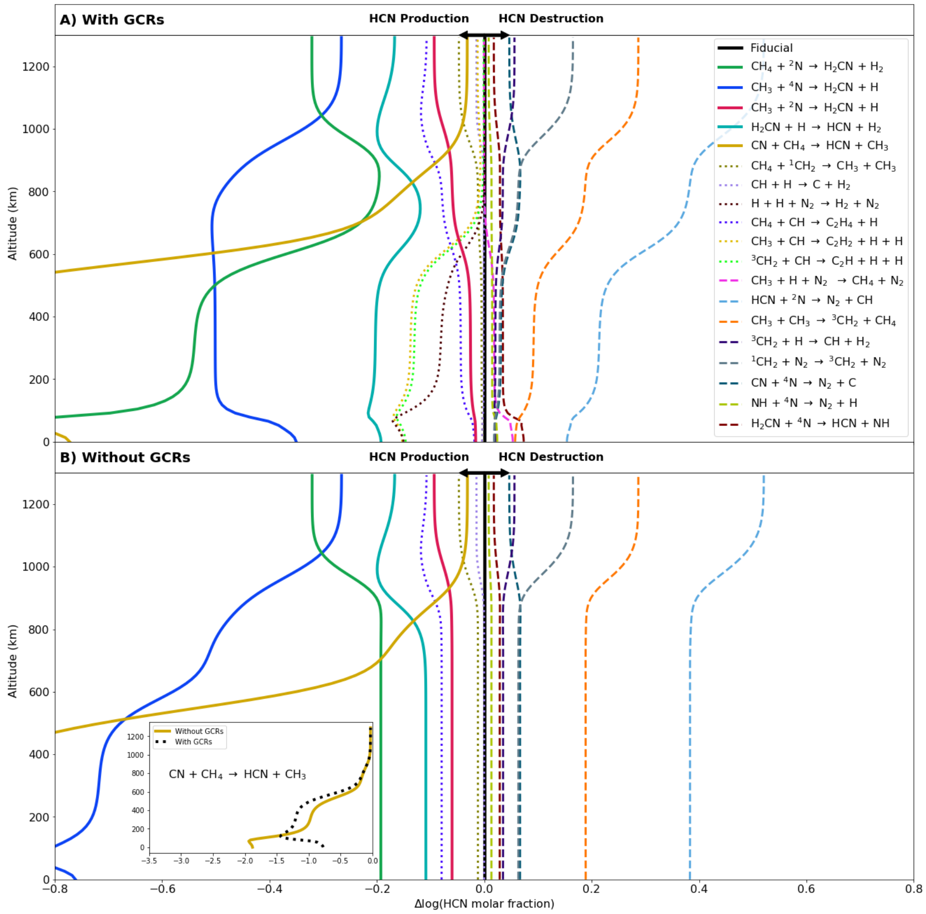

Figure 3.4: Sensitivity analysis II revealing all 19 dominant reactions in Titan's atmosphere. Each reaction curve shows the difference in HCN molar mixing ratio when excluding that reaction from **A)** the CRAHCN19 model, and **B)** the CRAHCN19/no GCRs model. All of the other reactions in CRAHCN did not greatly affect the HCN profile upon their exclusion; for both models.

The next leading reaction for HCN production is $^4\mathrm{N} + \mathrm{CH_3} \longrightarrow \mathrm{H_2CN} + \mathrm{H} \longrightarrow \mathrm{HCN} + \mathrm{H_2}$, which accounts for ∼20–25% of the total HCN in Titan's atmosphere.

Finally, the final dominant reaction for HCN production in Titan's atmosphere, is $^2\mathrm{N} + \mathrm{CH_3} \longrightarrow \mathrm{H_2CN} + \mathrm{H} \longrightarrow \mathrm{HCN} + \mathrm{H_2}$. This reaction was discovered by Pearce et al. [335], and had no known rate coefficient prior to that work. It accounts for ∼2% of the total HCN in Titan's atmosphere.

It is worth noting that the leading reaction, $\mathrm{CN} + \mathrm{CH_4} \longrightarrow \mathrm{HCN} + \mathrm{CH_3}$, only produces HCN if CN is present. CN primarily comes from the photodestruction of HCN, therefore this reaction is not responsible for starting HCN synthesis in Titan's

Table 3.5: The 19 reactions responsible for the production and destruction of HCN in Titan's atmosphere, labelled with their dominant role. For simplicity, reaction intermediates are not listed here. See Tables 4.5 and 4.6 for full details of reaction intermediates. Reactions are considered "well studied" if they have more than one experimental measurement or theoretical study at room temperature

Role	No.	Reaction equation	Well studied?
HCN sources	54.	$CN + CH_4 \longrightarrow HCN + CH_3$	Yes
	73.	$^2N + CH_4 \longrightarrow H_2CN + H_2$	Yes
	69.	$^4N + CH_3 \longrightarrow H_2CN + H$	Yes
	74.	$^2N + CH_3 \longrightarrow H_2CN + H$	No
	43.	$H_2CN + H \longrightarrow HCN + H_2$	No
Precursor sources	82.	$CH_4 + {}^1CH_2 \longrightarrow CH_3 + CH_3$	Yes
	89.	$CH_3 + CH \longrightarrow C_2H_2 + H + H$	No
	95.	$^3CH_2 + CH \longrightarrow C_2H + H + H$	No
	104.	$CH + H \longrightarrow C + H_2$	No
HCN sink	46.	$HCN + {}^2N \longrightarrow N_2 + CH$	No
Precursor sinks	81.	$CH_3 + CH_3 \longrightarrow {}^3CH_2 + CH_4$	No
	34.	$^1CH_2 + N_2 \longrightarrow {}^3CH_2 + N_2$	Yes
	52.	$CN + {}^4N \longrightarrow N_2 + C$	Yes
	96.	$^3CH_2 + H \longrightarrow CH + H_2$	Yes
	37.	$H_2CN + {}^4N \longrightarrow HCN + NH$	No
	22.	$CH_3 + H + N_2 \longrightarrow CH_4 + N_2$	Yes
	61.	$NH + {}^4N \longrightarrow N_2 + H$	Yes
Precursor sink attenuation	32.	$H + H + N_2 \longrightarrow H_2 + N_2$	Yes
Precursor source/sink	83.	$CH_4 + CH \longrightarrow C_2H_4 + H$	Yes

atmosphere, but rather, maintaining it. Given that we ignore this maintenance reaction, the other three leading channels produce approximately 59%, 37%, and 4% of the total *initial* HCN in Titan's atmosphere, respectively.

There are four reactions that play an important role in processing radical species to produce the precursors for HCN production reactions. The main one in the upper atmosphere is $CH_4 + {}^1CH_2 \longrightarrow CH_3 + CH_3$, which provides CH_3 for reactions 69 and 74. Although this reaction removes a CH_4 molecule, which is also a reactant for HCN production via reactions 54 and 73, the rate coefficients for these CH_4-based reactions are 2–5 orders of magnitude smaller than those for reactions 69 and 74, and thus producing more CH_3 leads to more efficient HCN production. The other upper atmospheric precursor source is $CH + H \longrightarrow C + H_2$ followed by the photolysis of H_2 to form two H atoms to be used by reaction 43.

The other two processing reactions, which were only revealed by the second sensitivity analysis, produce the H atoms necessary for $H_2CN + H \longrightarrow HCN + H_2$. These reactions dominate in the lower atmosphere, where UV light does not reach and thus H_2 photodissociation does not occur.

The dominant sink for HCN is $HCN + {}^2N \longrightarrow N_2 + CH$ and accounts for nearly 100% of total HCN removal. Although the photodissociation reaction $HCN + h\nu \longrightarrow CN + H$ destroys HCN efficiently, the removal of this reaction does not significantly affect the total HCN abundance in Titan's atmosphere. This is because CN efficiently reacts with CH_4 to recycle back into HCN.

Several reactions reduce HCN production by acting as sinks to important HCN precursors, i.e., CH_3, CN, CH_4, ${}^1CH_2$, ${}^3CH_2$, ${}^4N$, and H. One of these precursor sink reactions (no. 37) ironically produces HCN. However, since this reaction also produces NH, the dominant effect is the removal of ${}^4N$ from the atmosphere via $NH + {}^4N \longrightarrow N_2 + H$. One reaction, $CH_4 + CH \longrightarrow C_2H_4 + H$, seems to act as a precursor sink in the lower atmosphere, and a precursor source in the mid-upper atmosphere. However, this changes when switching from the fiducial to the CRAHCN19 models, and therefore the true role of this reaction is uncertain.

Finally, one reaction is key to attenuating the effect of a precursor sink in the lower atmosphere. $H + H + N_2 \longrightarrow H_2 + N_2$ reduces the H-atom abundance to attenuate the effects of $CH_3 + H + N_2 \longrightarrow CH_4 + N_2$.

3.4.7 The Case of No GCRs

In Figures 3.3B and 3.4B, we display the changes to the HCN profiles that occur when each the 19 dominant reactions are removed from the CRAHCN/no GCRs and CRAHCN19/no GCRs models, respectively. As a reminder, the 19 dominant reactions are the reactions which upon their removal, have the greatest effect the HCN profile.

Interestingly, only 15 reactions, upon their removal, affected the no GCR HCN profiles. The removal of $CH_3 + CH \longrightarrow C_2H_2 + H + H$, $^3CH_2 + CH \longrightarrow C_2H + H + H$, $CH_3 + H + N_2 \longrightarrow CH_4 + N_2$ and $H + H + N_2 \longrightarrow H_2 + N_2$ did not significantly effect the CRAHCN/no GCRs or CRAHCN19/noGCRs HCN profiles.

These four particular reactions require high abundances of CH_3, $^3CH_2$, and H produced by the GCR destruction of CH_4 in the lower atmosphere in order to become important for HCN production and destruction. It can be seen in Figures 3.3A and 3.4A that these four reactions have no affect on the HCN profiles in the upper atmosphere, where GCR reactions do not occur.

In the upper atmospheres, the HCN difference profiles in Figures 3.3B and 3.4B look nearly identical to the like-colored profiles in Figure 3.3A. Differences between any two like-colored curves are more drastic in the lower atmospheres, where GCR reactions occur. Removing GCR reactions changes the feedstock of methane and nitrogen radicals, and therefore adjusts the relative importance of each of the dominant reactions that use these radicals.

The dominant pathways to HCN formation in the CRAHCN/no GCRs models are the same as those in the fiducial model, however their percent contributions differ by up to 20% from the fiducial model values. $CN + CH_4 \longrightarrow HCN + CH_3$ in the no GCRs case contributes ∼42–52% to the total HCN in Titan's atmosphere. The other three channels, i.e. $^2N + CH_4 + H \longrightarrow H_2CN + H_2 + H \longrightarrow HCN + 2\,H_2$, $^4N + CH_3 \longrightarrow H_2CN + H \longrightarrow HCN + H_2$, and $^2N + CH_3 \longrightarrow H_2CN + H \longrightarrow HCN + H_2$, contribute ∼16–18%, ∼22–36%, and ∼6–8%, respectively.

Overall, these results suggest that GCR reactions do not significantly control which reactions dominate at producing and destroying HCN in Titan's atmosphere, but they do affect the relative amount that they contribute to the overall HCN abundance.

3.5 Discussion

3.5.1 How HCN is Produced in Titan's Atmosphere

Out of the 104 chemical reactions in CRAHCN, we find only 19 reactions significantly contribute to the production and destruction of HCN in Titan's atmosphere. Most of these reactions are direct sources and sinks for HCN and sources and sinks for the precursors to HCN (e.g. CH_3, ^4N). In the only other case, a reaction has the role of attenuating the effects of a precursor sink.

In Figure 3.5, we describe the step-by-step process of HCN production in Titan's atmosphere. First, UV radiation in the upper atmosphere, and GCRs in the lower atmosphere, break apart CH_4, N_2, and H_2 into reactive high-energy radical species. Second, these radicals get processed via chemical reactions to form HCN precursors (e.g. CH_3 and H). These processing reactions differ in the upper and lower atmosphere. For example, $CH_4 + {}^1CH_2 \longrightarrow CH_3 + CH_3$ is only a key processing reaction in the upper atmosphere where the reactant ${}^1CH_2$ is produced from the UV dissociation of CH_4. Conversely, $CH_3 + CH \longrightarrow C_2H_2 + H + H$ is only important in the lower atmosphere where a key alternate H-atom source (UV dissociation of H_2) does not occur.

Somewhat unintuitively, too much H in the lower atmosphere can lead to less HCN, as it is a reactant in the precursor sink reaction $CH_3 + H + N_2 \longrightarrow CH_4 + N_2$. For this reason, the precusor sink attenuation reaction $H + H + N_2 \longrightarrow H_2 + N_2$ is also important for increasing HCN production in the lower atmosphere.

Next, HCN production occurs through 3 main channels, with the total *initial* percent contributions labeled in parentheses

Channel A:

$$ {}^2N + CH_4 + H \longrightarrow H_2CN + H_2 + H \longrightarrow HCN + 2\,H_2 \quad (59\%), $$

Channel B:

$$ {}^4N + CH_3 \longrightarrow H_2CN + H \longrightarrow HCN + H_2 \quad (37\%), $$

Channel C:

$$ {}^2N + CH_3 \longrightarrow H_2CN + H \longrightarrow HCN + H_2 \quad (4\%). $$

In the upper atmosphere, where partial pressures are low, UV radiation is the main dissociating agent; it generates reactants for Channels A–C. Channel B dominates the HCN production in this region, due to its comparatively high rate coefficient. Here, UV radiation is also responsible for breaking apart HCN into CN + H. Eddy diffusion

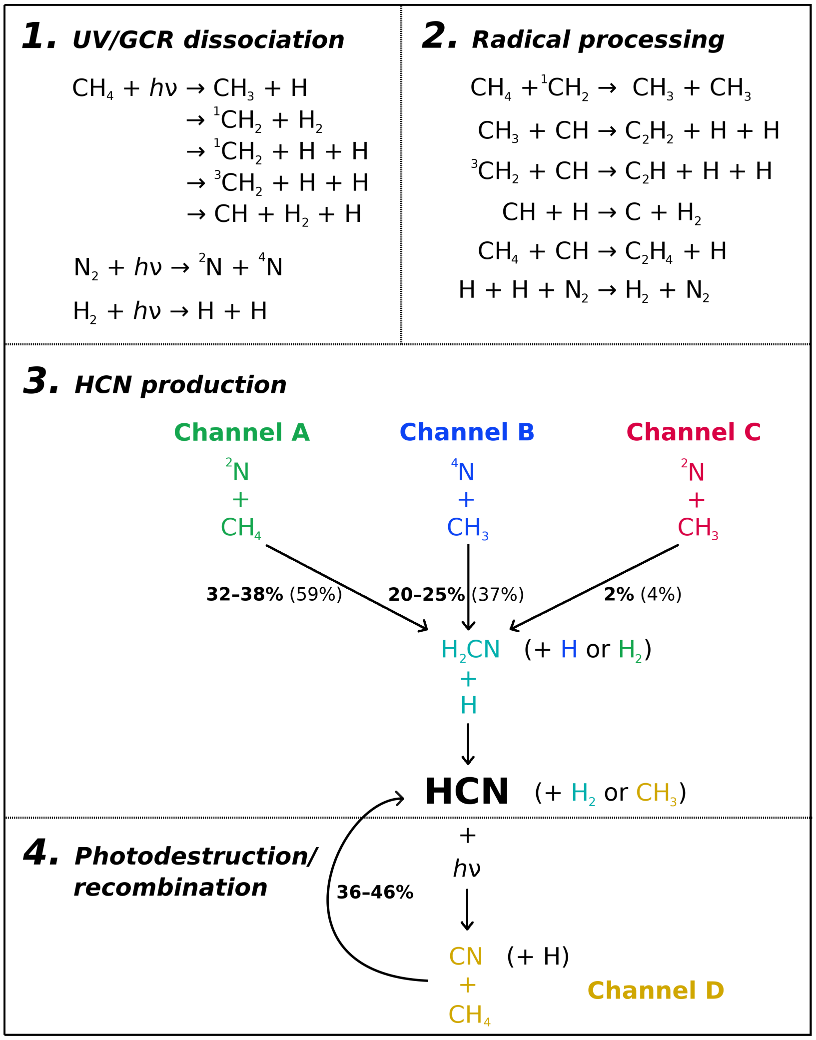

Figure 3.5: Summary of how HCN is produced in Titan's atmosphere. Stage 1: Destruction of methane, nitrogen and hydrogen by ultraviolet light in the upper atmosphere and galactic cosmic rays (GCRs) in the lower atmosphere. Stage 2: Increasing the abundance of HCN precursors and attenuating the effects of HCN precursor sinks. Stage 3: Production of HCN from methane and nitrogen fragments. Stage 4: HCN photodestruction to produce CN, and recycling of CN back into HCN via reaction with CH4. Bold percentages include all HCN reaction routes, including CN recombination after photodestruction. Percentages in parentheses represent *initial* HCN production and do not include CN recombination.

mixes species including CN from the upper atmosphere into the lower atmosphere, where Channels A and D mainly take over HCN production. In the lower atmosphere, high partial pressures screen out UV radiation and increase the probability for GCR collisions, therefore GCRs become the main dissociating agent here. In this region, concentrations of CH_4 are high enough that the relative reaction rate of Channel A surpasses that of Channel B. These high concentrations of CH_4 also drastically increase the reaction rate of Channel D, which recycles CN back into HCN. This recycling process is the overall dominant channel to HCN, accounting for 36–46% of the total HCN in Titan's atmosphere. Channel C remains the fourth most important HCN source in both areas of the atmosphere, as although the rate coefficient of ^2N reacting with CH_3 is higher than that of ^2N reacting with CH_4, there is a much higher concentration of CH_4 compared with CH_3 in all areas of the atmosphere.

3.5.2 Using CRAHCN

Due to the exceptional alignment of the HCN profiles from the CRAHCN19 and CRAHCN models, we suggest the CRAHCN19 network provides a lean, accurate, fast, and intuitively clear code to calculate the HCN abundance in Titan-like atmospheres. Without data from higher pressure and temperature planetary atmospheres, we cannot be certain that these same 19 reactions would suffice for other planetary environments of Titan-like composition. For this reason, we advocate using the full (104 reaction) CRAHCN network to simulate the production of HCN in N_2-, CH_4-, and H_2-dominated atmospheres.

We emphasize that this is a reduced network to accurately model HCN chemistry, rather than an extended network to cover the chemistry of a large range of species. For this reason, CRAHCN should only be used to simulate the production HCN.

3.6 Conclusions

In this paper, we calculate the production of HCN in Titan's atmosphere using a novel quantum chemistry and atmospheric modeling strategy. This strategy has two components: 1) we use quantum chemistry simulations to scan the entire field of possible reactions for a list of primary species relevant to N_2-, CH_4-, and H_2-dominated atmospheres. We then calculate the rate coefficients for the uncovered reactions and construct a consistent reduced atmospheric hybrid chemical network (CRAHCN). This network contains experimental rate coefficients when available (32% of cases), but is predominantly composed of our calculated values using a consistent computational and theoretical method. 2) We pair CRAHCN with a chemical kinetic code called

ChemKM to model the atmosphere of Titan. HCN has been observed at a range of altitudes in Titan's atmosphere by the Cassini spacecraft, making it an excellent testbed for validating chemical networks for HCN production in atmospheres.

We list the major conclusions of this work in bullet form below.

- CRAHCN contains 104 reactions, 33 of which are newly discovered in this work.
- Our calculated rate coefficients are accurate to within about an order of magnitude of experimental values, which is consistent with the uncertainties assigned in large-scale experimental data evaluations.
- In comparison with other widely used computational quantum methods, BHandHLYP/aug-cc-pVDZ is found to provide a reasonable balance of speed and acceptable accuracy for our large scale atmospheric study. Increasing the basis set to aug-cc-pVTZ did not improve the accuracy of calculations with respect to agreement with experimental values.
- The HCN profile from our fiducial model of Titan's atmosphere agrees very well with the Cassini observations, and is well in line with the three most recent Titan models in the literature.
- Only 19 reactions are responsible for the production and destruction of HCN in Titan's atmosphere. These reactions are sources and sinks of HCN, sources and sinks of the precursors to HCN, and a presursor sink attenuation reaction.
- There are 4 main channels to HCN production:
  - $CN + CH_4 \longrightarrow HCN + CH_3$ (∼36–46%),
  - $^2N + CH_4 + H \longrightarrow H_2CN + H_2 + H \longrightarrow HCN + 2\,H_2$ (∼32–38%),
  - $^4N + CH_3 \longrightarrow H_2CN + H \longrightarrow HCN + H_2$ (∼20–25%),
  - $^2N + CH_3 \longrightarrow H_2CN + H \longrightarrow HCN + H_2$ (∼2%).
- The first and second reactions dominate in the lower atmosphere, whereas the second, third, and fourth reactions dominate in the upper atmosphere. In the upper atmosphere, where partial pressures are low, relatively high rate coefficients tend to dictate the dominant reactions. In the lower atmosphere, the high CH_4 partial pressure increases the reaction rates for the first two reactions, which is the reason for their dominance here.

- The fourth dominant source of HCN in Titan's atmosphere is a reaction first discovered in our recent work [335].
- $HCN + {}^2N \longrightarrow N_2 + CH$ is the main sink for HCN. Conversely, $HCN + h\nu \longrightarrow CN + H$ is not an effective HCN sink, because it produces a CN molecule that reacts with CH_4 to form back into HCN.
- GCRs triple the total production of HCN in Titan's atmosphere, however they do not affect which reactions dominate HCN production and destruction.

Our work suggests that chemical networks of hundreds or thousands of reactions are not necessary to accurately simulate the production of HCN in N_2-, CH_4-, and H_2-dominated atmospheres. Instead, using our novel strategy of exploring the entire field of possible reactions for a short list of primary atmospheric species has proven to be valuable at uncovering the dominant chemical pathways to producing HCN in Titan's atmosphere.

In upcoming work, we will use this strategy to expand CRAHCN to explore the production of HCN in the early Earth atmosphere, which, along with N_2, CH_4, and H_2, is expected to have contained oxygen-based primary species such as CO_2 and H_2O, as well as their dissociation fragments.

Acknowledgments

We thank the two anonymous referees, whose detailed reports led to improvements to this work. We gratefully acknowledge Profs. Paul Ayers (McMaster) and Sarah Hörst (Johns Hopkins University), whose advice and comments were valuable to this research. B.K.D.P. is supported by an NSERC Canada Graduate Scholarships-Doctoral (CGS-D). R.E.P. is supported by an NSERC Discovery Grant. T.H. acknowledges support from the European Research Council under the Horizon 2020 Framework Program via the ERC Advanced Grant Origins 83 24 28. We are grateful to Compute Canada for the computer time allocated for this research. This research is part of a collaboration between the Origins Institute and the Heidelberg Initiative for the Origins of Life.

3.7 Appendix Materials

3.7.1 Rate Coefficient Calculations

In Table 3.6, we display the recalculated two-body reaction rate coefficients from Pearce et al. [335], with the modified vibrational partition function described in Section 4.2.

Table 3.6: Re-calculated two-body reaction rate coefficients at 298 K from Pearce et al. [335] with new vibrational partition function model. For these calculations, the vibrational partition functions are adjusted so that the zero of energy is at the first vibrational level, i.e., the zero-point level. Calculations are performed at the BHandHLYP/aug-cc-pVDZ level of theory. The presence or absence of an energy barrier in the rate-limiting step of the reaction is specified. The error factor is the multiplicative or divisional factor from the nearest experimental or suggested value.

Reaction equation	Forw./Rev.	Barrier?	k(298) calculated	k(298) experimental	Error factor
$\mathrm{H_2CN + {}^4N \longrightarrow HCN + NH}$	F	Y	$^a4.7\times10^{-12}$	4.4×10^{-11}	9
$\mathrm{H_2CN + H \longrightarrow HCN + H_2}$	F	Y	2.2×10^{-11}	8.3×10^{-11}	4
$\mathrm{H_2CN \longrightarrow HCN + H}$	F	Y	2.2×10^{-15}		
$\mathrm{NH + {}^4N \longrightarrow N_2H\cdot \longrightarrow N_2 + H}$	F	N	5.5×10^{-11}	$2.5–2.6\times10^{-11}$	2
$\mathrm{NH + {}^2N \longrightarrow N_2H\cdot \longrightarrow N_2 + H}$	F	N	8.8×10^{-11}		
$\mathrm{NH + H \longrightarrow H_2 + {}^4N}$	F	Y	7.1×10^{-12}	3.2×10^{-12}	2
$\mathrm{{}^4N + CH_3 \longrightarrow {}^3H_3CN\cdot \longrightarrow H_2CN + H}$	F	N	6.2×10^{-11}	$5–7.7\times10^{-11}$	1
$\mathrm{{}^4N + {}^3CH_2 \longrightarrow H_2CN_{(\nu)}\cdot \longrightarrow HCN + H}$	F	N	1.0×10^{-10}		
$\mathrm{{}^4N + {}^1CH_2 \longrightarrow {}^4H_2CN \longrightarrow {}^3HCN\cdot + H\cdot \longrightarrow CN + H + H}$	F	N	1.9×10^{-10}		
$\mathrm{{}^4N + CH \longrightarrow {}^3HCN\cdot \longrightarrow CN + H}$	F	N	1.5×10^{-10}	$0.2–1.6\times10^{-10}$	1
$\mathrm{{}^2N + CH_4 \longrightarrow H_3CNH\cdot \longrightarrow {}^1H_2CNH\cdot + H\cdot \longrightarrow H_2CN + H_2}$	F	N	$^b1.7\times10^{-11}$	$2.4–4.5\times10^{-12}$	4
$\mathrm{{}^2N + CH_3 \longrightarrow {}^{3,1}H_3CN\cdot \longrightarrow {}^{3,1}H_2CNH\cdot\ H_2CN + H}$	F	N	2.3×10^{-10}		
$\mathrm{{}^2N + {}^3CH_2 \longrightarrow H_2CN_{(\nu)}\cdot \longrightarrow HCN + H}$	F	N	2.1×10^{-10}		
$\mathrm{{}^2N + {}^3CH_2 \longrightarrow {}^4H_2CN\cdot \longrightarrow {}^3HCN\cdot + H\cdot \longrightarrow CN + H + H}$	F	N	3.5×10^{-10}		
$\mathrm{{}^2N + {}^1CH_2 \longrightarrow H_2CN_{(\nu)}\cdot \longrightarrow HCN + H}$	F	N	2.4×10^{-10}		
$\mathrm{{}^2N + CH \longrightarrow {}^3HCN\cdot \longrightarrow CN + H}$	F	N	3.5×10^{-10}		
$\mathrm{{}^2N + H_2 \longrightarrow NH_{2(\nu)}\cdot \longrightarrow NH + H}$	F	N	$^c3.3\times10^{-11}$	$1.7–5.0\times10^{-12}$	7
$\mathrm{CH_4 + {}^3CH_2 \longrightarrow CH_3 + CH_3}$	F	Y	5.7×10^{-18}	$<3\text{-}500000\times10^{-19}$	1
$\mathrm{CH_4 + {}^3CH_2 \longleftarrow CH_3 + CH_3}$	R	N	5.3×10^{-11}		
$\mathrm{CH_4 + {}^1CH_2 \longrightarrow C_2H_{6(\nu)}\cdot \longrightarrow CH_3 + CH_3}$	F	N	2.1×10^{-11}	$0.2–7.3\times10^{-11}$	1
$\mathrm{CH_4 + CH \longrightarrow CH_4{-}CH\cdot \longrightarrow C_2H_5\cdot \longrightarrow C_2H_4 + H}$	F	N	$^d1.8\times10^{-10}$	$0.02–3\times10^{-10}$	1
$\mathrm{CH_4 + H \longrightarrow CH_3 + H_2}$	F	Y	8.9×10^{-19}	$8.2–350\times10^{-19}$	1
$\mathrm{CH_4 + H \longleftarrow CH_3 + H_2}$	R	Y	3.3×10^{-20}	$9.6–13\times10^{-21}$	3
$\mathrm{CH_3 + {}^3CH_2 \longrightarrow C_2H_5\cdot \longrightarrow C_2H_4 + H}$	F	N	5.9×10^{-11}	$5–21\times10^{-11}$	1
$\mathrm{CH_3 + {}^1CH_2 \longrightarrow C_2H_5\cdot \longrightarrow C_2H_4 + H}$	F	N	1.3×10^{-10}	3.0×10^{-11}	2
$\mathrm{CH_3 + H \longrightarrow {}^3CH_2 + H_2}$	F	Y	8.1×10^{-21}		
$\mathrm{CH_3 + H \longleftarrow {}^3CH_2 + H_2}$	R	Y	5.9×10^{-16}	$<5–50\times10^{-15}$	1
$\mathrm{{}^3CH_2 + {}^3CH_2 \longrightarrow C_2H_{4(\nu)}\cdot \longrightarrow C_2H_2 + H_2}$	F	N	3.6×10^{-11}	5.3×10^{-11}	1
$\mathrm{{}^3CH_2 + {}^1CH_2 \longrightarrow {}^3C_2H_4\cdot \longrightarrow C_2H_3\cdot + H \longrightarrow C_2H_2 + H + H}$	F	N	2.1×10^{-10}	3.0×10^{-11}	7
$\mathrm{{}^1CH_2 + {}^1CH_2 \longrightarrow C_2H_{4(\nu)}\cdot \longrightarrow C_2H_2 + H_2}$	F	N	7.1×10^{-11}	5.0×10^{-11}	1
$\mathrm{{}^1CH_2 + H_2 \longrightarrow CH_{4(\nu)}\cdot \longrightarrow CH_3 + H}$	F	N	1.0×10^{-10}	$0.07–1.3\times10^{-10}$	1
$\mathrm{CH + CH \longrightarrow {}^3C_2H_2\cdot \longrightarrow C_2H + H}$	F	N	1.4×10^{-10}		
$\mathrm{CH + H_2 \longrightarrow CH_{3(\nu)}\cdot \longrightarrow {}^3CH_2 + H}$	F	N	5.4×10^{-11}	$0.1–16\times10^{-11}$	1
$\mathrm{CH + H \longrightarrow {}^3CH_{2(\nu)}\cdot \longrightarrow C + H_2}$	F	N	6.9×10^{-10}		

[a] We remove the barrier from this calculation as experiments predict this reaction to be barrierless or nearly barrierless [229]. See case study 1 for more details.

[b] The existence of a barrier for this reaction is dependent on computational method. We introduce an experimental barrier of 6.3 kJ $\mathrm{mol^{-1}}$

[233] to this calculation as at the BHandHLYP/aug-cc-pVDZ level of theory, we find this reaction to be barrierless. Simulations had sporadic convergence beyond a C-N bond distance of 2.76Å. The rate coefficient is calculated with the variational transition state at this location, which has the highest ΔG.

[c] The existence of a barrier for this reaction is dependent on computational method. We introduce an experimental barrier of 7.3 kJ mol^{-1} [285] to this calculation as at the BHandHLYP/aug-cc-pVDZ level of theory, we find this reaction to be barrierless.

[d] We remove the barrier from the rate limiting step of this calculation, i.e. $CH_4{-}CH\cdot \longrightarrow C_2H_5\cdot$ as experiments predict this reaction to be barrierless [277, 278, 280].

In Table 3.7, we list the new two-body reaction rate coefficients calculated in this work at 298 K, along with any experimental values.

Table 3.7: New two-body reaction rate coefficients calculated in this work at 298 K. Calculations are performed at the BHandHLYP/aug-cc-pVDZ level of theory. Reactions with rate coefficients slower than k = 10^{-21} cm^{3}s^{-1} are not included in this network. The presence or absence of an energy barrier in the rate-limiting step of the reaction is specified. The error factor is the multiplicative or divisional factor from the nearest experimental or suggested value.

Reaction equation	Forw./Rev.	Barrier?	k(298) calculated	k(298) experimental	Error factor
$H_2CN + NH \longrightarrow HCN + NH_2$	F	Y	1.4×10^{-13}		
$H_2CN + {}^4N \longrightarrow {}^3H_2CNN\cdot \longrightarrow N_2 + {}^3CH_2$	F	N	4.3×10^{-12}		
$H_2CN + {}^2N \longrightarrow {}^3H_2CNN\cdot \longrightarrow N_2 + {}^3CH_2$	F	N	3.2×10^{-11}		
$H_2CN + {}^2N \longrightarrow {}^1H_2CNN\cdot \longrightarrow N_2 + {}^1CH_2$	F	N	6.4×10^{-12}		
$H_2CN + CH \longrightarrow {}^1H_2CNCH\cdot \longrightarrow H_2CNC_a\cdot + H\cdot \longrightarrow H_2CNC_b\cdot + H\cdot \longrightarrow CH_2CN + H$	F	Y	1.4×10^{-11}		
$H_2CN + CH \longrightarrow {}^3H_2CNCH\cdot \longrightarrow HCN + {}^3CH_2$	F	N	2.2×10^{-11}		
$H_2CN + CH \longrightarrow {}^1H_2CNCH\cdot \longrightarrow HCN + {}^1CH_2$	F	Y	3.3×10^{-11}		
$HCN + CN \longrightarrow HNCCN\cdot \longrightarrow NCCN + H$	F	N	3.7×10^{-12}	0.2–4.1×10^{-13}	9
$HCN + {}^2N \longrightarrow N_2 + CH$	F	N	6.8×10^{-11}		
$HCN + {}^1CH_2 \longrightarrow CH_2HCN\cdot \longrightarrow CH_2NC_a\cdot + H\cdot \longrightarrow CH_2NC_b\cdot + H\cdot \longrightarrow CH_2CN + H$	F	N	3.7×10^{-13}		
$HCN + H \longrightarrow HCNH\cdot \longrightarrow HNC + H$	F	Y	2.7×10^{-20}		
$HCN + H \longleftarrow HCNH\cdot \longleftarrow HNC + H$	R	Y	1.0×10^{-11}		
$CN + NH \longrightarrow HCN + {}^4N$	F	Y	1.9×10^{-14}		
$CN + NH \longrightarrow HNNC\cdot \longrightarrow CHN_{2a}\cdot \longrightarrow CHN_{2b}\cdot \longrightarrow CH + N_2$	F	Y	1.9×10^{-12}		
$CN + {}^4N \longrightarrow CN_{2(\nu)}\cdot \longrightarrow N_2 + C$	F	N	4.3×10^{-11}	1.0–3.0×10^{-10}	2
$CN + {}^2N \longrightarrow CN_{2(\nu)}\cdot \longrightarrow N_2 + C$	F	N	1.6×10^{-10}		
$CN + CH_4 \longrightarrow HCN + CH_3$	F	Y	[a]7.7×10^{-13}	5.6–11×10^{-13}	1
$CN + CH_3 \longrightarrow HCN + {}^3CH_2$	F	N	6.7×10^{-12}		
$CN + CH \longrightarrow HCN + C$	F	N	1.4×10^{-11}		
$CN + CH \longrightarrow HNC + C$	F	N	[b]5.4×10^{-13}		
$CN + H_2 \longrightarrow HCN + H$	F	Y	[c]1.3×10^{-15}	1.2–4.9×10^{-14}	9
$NH + NH \longrightarrow N_2H_2\cdot \longrightarrow N_2H\cdot + H\cdot \longrightarrow N_2 + H + H$	F	N	4.1×10^{-12}	3.5×10^{-12}	1
$NH + NH \longrightarrow NH_2 + {}^4N$	F	Y	6.8×10^{-18}		
$NH + CH_3 \longrightarrow H_3CNH\cdot \longrightarrow {}^1H_2CNH\cdot + H\cdot \longrightarrow H_2CN + H_2$	F	N	2.0×10^{-11}		
$NH + {}^3CH_2 \longrightarrow {}^1H_2CNH\cdot \longrightarrow H_2CN + H$	F	N	1.9×10^{-11}		
$NH + {}^1CH_2 \longrightarrow {}^3H_2CNH\cdot \longrightarrow H_2CN + H$	F	N	4.6×10^{-11}		
$NH + CH \longrightarrow HNCH\cdot \longrightarrow HCN + H$	F	N	[d]4.5×10^{-11}		
$NH + CH \longrightarrow HNCH\cdot \longrightarrow HNC + H$	F	Y	[d]3.9×10^{-15}		
$CH_3 + CH \longrightarrow {}^1CH_3CH\cdot \longrightarrow C_2H_3\cdot + H\cdot \longrightarrow C_2H_4$	F	N	5.5×10^{-11}		
$CH_3 + CH \longrightarrow {}^3CH_3CH\cdot \longrightarrow C_2H_3\cdot + H\cdot \longrightarrow C_2H_2 + H + H$	F	N	2.4×10^{-10}		
${}^3CH_2 + CH \longrightarrow C_2H_3\cdot \longrightarrow C_2H_2 + H$	F	N	6.3×10^{-11}		
${}^3CH_2 + CH \longrightarrow {}^4C_2H_3\cdot \longrightarrow {}^3C_2H_2\cdot + H\cdot \longrightarrow C_2H + H + H$	F	N	1.1×10^{-10}		
${}^3CH_2 + H \longrightarrow CH_{3(\nu)}\cdot \longrightarrow CH + H_2$	F	N	3.7×10^{-10}	0.8–2.7×10^{-10}	1
${}^1CH_2 + CH \longrightarrow C_2H_3\cdot \longrightarrow C_2H_2 + H$	F	N	1.6×10^{-10}		

$^1CH_2 + H \longrightarrow CH_{3(v)}\cdot \longrightarrow CH + H_2$	F	N	1.8×10^{-10}	5.0×10^{-11}	4
$^1CH_2 + H \longrightarrow CH_{3(v)}\cdot \longrightarrow {}^3CH_2 + H$	F	N	4.6×10^{-11}		

[a] The existence of a barrier for this reaction is dependent on computational method. We introduce an experimental barrier of 8.3 kJ mol^{-1} [379] to this calculation as at the BHandHLYP/aug-cc-pVDZ level of theory, we find this reaction to be barrierless.

[b] Simulations had sporadic convergence beyond a H-N bond distance of 1.45Å. The rate coefficient is calculated with the variational transition state at this location, which has the highest ΔG.

[c] The existence of a barrier for this reaction is dependent on computational method. We introduce an experimental barrier of 13.4 kJ mol^{-1} [381] to this calculation as at the BHandHLYP/aug-cc-pVDZ level of theory, we find this reaction to be barrierless.

[d] Simulations did not converge beyond a N-C bond distance of 3.33Å. The rate coefficient is calculated with the variational transition state at this location, which has the highest ΔG.

In Table 3.8, we display the reduced Lindemann parameters for the three-body reactions calculated in this work, along with any experimental values.

Table 3.8: Lindemann coefficients for the three-body reactions calculated in this work at 298 K. Calculations are performed at the BHandHLYP/aug-cc-pVDZ level of theory, and are valid within the 50–400 K temperature range. k_∞ is the second-order rate coefficient in the high pressure limit with units cm^{3}s^{-1}. k_0 is the third-order rate coefficient in the low pressure limit with units cm^{6}s^{-1}. These values fit into the pressure-dependent rate coefficient equation $k = \frac{k_0[M]/k_\infty}{1+k_0[M]/k_\infty}k_\infty$. Reactions with rate coefficients slower than $k_\infty = 10^{-13}$ cm^{3}s^{-1} are not included in this network. The error factor is the multiplicative or divisional factor from the nearest experimental or suggested value.

Reaction equation	$k_\infty(298)$ calc.	$k_\infty(298)$ exp.	$Error_\infty$	$k_0(298)$ calc.	$k_0(298)$ exp.	$Error_0$
$HCN + CH + M \longrightarrow HCNCH_a\cdot + M\cdot \longrightarrow HCNCH_b\cdot + M\cdot \longrightarrow CH_2NC\cdot + M\cdot \longrightarrow CH_2CN + M$	7.1×10^{-11}	2.7×10^{-10}	4	3.3×10^{-29}		
$CN + CN + M \longrightarrow NCCN + M$	1.6×10^{-12}	$1.0–9.4\times10^{-12}$	1	5.3×10^{-29}	$4.7–4900\times10^{-32}$	1
$CN + CN + M \longrightarrow CNCN + M$	6.3×10^{-12}			2.2×10^{-30}		
$CN + NH + M \longrightarrow HNCN + M$	2.3×10^{-11}			5.9×10^{-29}		
$CN + {}^4N + M \longrightarrow CN_2 + M$	4.3×10^{-11}	$1.0–3.0\times10^{-10}$	2	1.0×10^{-30}	2.8×10^{-32}	36
$CN + {}^2N + M \longrightarrow CN_2 + M$	1.6×10^{-10}			1.1×10^{-29}		
$CN + CH_3 + M \longrightarrow CH_3CN + M$	1.3×10^{-11}			3.8×10^{-26}		
$CN + {}^3CH_2 + M \longrightarrow CH_2CN + M$	2.9×10^{-11}			8.5×10^{-27}		
$CN + {}^1CH_2 + M \longrightarrow CH_2CN + M$	6.3×10^{-11}			3.5×10^{-26}		
$CN + CH + M \longrightarrow {}^3HCCN + M$	1.1×10^{-11}			6.5×10^{-28}		
$CN + CH + M \longrightarrow {}^1HCCN + M \longrightarrow {}^1HC_2N + M$	2.9×10^{-11}			1.2×10^{-28}		
$CN + H + M \longrightarrow HCN + M$	4.5×10^{-11}	1.7×10^{-10}	4	1.7×10^{-30}	$1.3–1.6\times10^{-30}$	1
${}^4N + {}^3CH_2 + M \longrightarrow H_2CN + M$	1.0×10^{-10}			1.2×10^{-28}		
${}^4N + {}^4N + M \longrightarrow N_2 + M$	1.4×10^{-11}			4.2×10^{-34}	$2.2–130\times10^{-33}$	5
${}^4N + H + M \longrightarrow NH + M$	4.3×10^{-10}			3.2×10^{-33}	$1.4–64\times10^{-33}$	1
${}^2N + {}^3CH_2 + M \longrightarrow H_2CN + M$	2.1×10^{-10}			6.2×10^{-28}		
${}^2N + {}^1CH_2 + M \longrightarrow H_2CN + M$	2.4×10^{-10}			1.5×10^{-27}		
${}^2N + {}^2N + M \longrightarrow N_2 + M$	5.7×10^{-11}			1.7×10^{-33}		
${}^2N + H + M \longrightarrow NH + M$	7.7×10^{-10}			7.0×10^{-32}		
$CH_4 + {}^1CH_2 + M \longrightarrow C_2H_6 + M$	2.1×10^{-11}	$0.2–7.3\times10^{-11}$	1	7.2×10^{-24}		
$CH_3 + CH_3 + M \longrightarrow C_2H_6 + M$	5.9×10^{-12}	$3.5–6.5\times10^{-11}$	6	1.7×10^{-26}	$1.7–3.3\times10^{-26}$	1
$CH_3 + H + M \longrightarrow CH_4 + M$	1.4×10^{-10}	$1.5–4.7\times10^{-10}$	1	2.6×10^{-28}	$1.5–55\times10^{-29}$	1
${}^3CH_2 + {}^3CH_2 + M \longrightarrow C_2H_4 + M$	3.5×10^{-11}	5.3×10^{-11}	2	2.6×10^{-26}		
${}^3CH_2 + H + M \longrightarrow CH_3 + M$	4.6×10^{-10}	$8.3–27\times10^{-11}$	2	4.8×10^{-29}		
${}^1CH_2 + {}^1CH_2 + M \longrightarrow C_2H_4 + M$	7.1×10^{-11}	5.0×10^{-11}	1	5.4×10^{-25}		
${}^1CH_2 + H_2 + M \longrightarrow CH_4 + M$	1.0×10^{-10}	$7–130\times10^{-12}$	1	1.4×10^{-27}		
${}^1CH_2 + H + M \longrightarrow CH_3 + M$	2.3×10^{-10}	5.0×10^{-11}	5	3.7×10^{-28}		
$CH + CH + M \longrightarrow C_2H_2 + M$	1.2×10^{-11}	$1.7–2.0\times10^{-10}$	14	3.5×10^{-28}		
$CH + H_2 + M \longrightarrow CH_3 + M$	2.7×10^{-10}	$6.3–2000\times10^{-13}$	1	7.8×10^{-29}	9.0×10^{-30}	9
$CH + H + M \longrightarrow {}^3CH_2 + M$	6.9×10^{-10}	$1.4–5.0\times10^{-11}$	14	2.0×10^{-28}		
$CH + H + M \longrightarrow {}^1CH_2 + M$	2.1×10^{-10}	1.4×10^{-11}	15	4.4×10^{-31}		
$H + H + M \longrightarrow H_2 + M$	1.9×10^{-10}			1.7×10^{-33}	$4.0–250\times10^{-33}$	2

3.7.2 CRAHCN

In Table 4.5, we display the Lindemann coefficients for the three-body reactions in CRAHCN, along with their sources. When available, rate coefficients in CRAHCN are experimental values; However, the majority of rate coefficients have not been experimentally measured, and thus we use the consistently calculated values from this work. These three-body reactions, along with the one- and two-body reactions in Table 4.6, make up CRAHCN.

Table 3.9: Lindemann coefficients for the three-body reactions in the consistent reduced atmospheric hybrid chemical network (CRAHCN), valid within the 50–400 K temperature range. Experimental values are used when available, and calculated rate coefficients from this work are used otherwise. k_∞ is the second-order rate coefficient in the high pressure limit with units cm^{3}s^{-1}. k_0 is the third-order rate coefficient in the low pressure limit with units cm^{6}s^{-1}. These values fit into the pressure-dependent rate coefficient equation $k = \frac{k_0[M]/k_\infty}{1+k_0[M]/k_\infty} k_\infty$.

No.	Reaction equation	$k_\infty(298)$	$k_0(298)$	Source(s)
*1.	$HCN + CH + M \longrightarrow HCNCH_a\cdot + M\cdot \longrightarrow HCNCH_b\cdot + M\cdot \longrightarrow CH_2NC\cdot + M\cdot \longrightarrow CH_2CN + M$	2.7×10^{-10}	3.3×10^{-29}	This work, Zabarnick et al. [382]
2.	$CN + CN + M \longrightarrow NCCN + M$	1.0×10^{-12}	4.7×10^{-32}	Basco et al. [383]
*3.	$CN + CN + M \longrightarrow CNCN + M$	6.3×10^{-12}	2.2×10^{-30}	This work
*4.	$CN + NH + M \longrightarrow HNCN + M$	2.3×10^{-11}	5.9×10^{-29}	This work
5.	$CN + {}^4N + M \longrightarrow CN_2 + M$	1.1×10^{-10}	2.8×10^{-32}	Atakan et al. [384], Whyte & Phillips[385] Provencher & McKenney [378]
*6.	$CN + {}^2N + M \longrightarrow CN_2 + M$	1.6×10^{-10}	1.1×10^{-29}	This work
*7.	$CN + CH_3 + M \longrightarrow CH_3CN + M$	1.3×10^{-11}	3.8×10^{-26}	This work
*8.	$CN + {}^3CH_2 + M \longrightarrow CH_2CN + M$	2.9×10^{-11}	8.5×10^{-27}	This work
*9.	$CN + {}^1CH_2 + M \longrightarrow CH_2CN + M$	6.3×10^{-11}	3.5×10^{-26}	This work
*10.	$CN + CH + M \longrightarrow {}^3HCCN + M$	1.1×10^{-11}	6.5×10^{-28}	This work
*11.	$CN + CH + M \longrightarrow {}^1HCCN + M \longrightarrow {}^1HC_2N + M$	2.9×10^{-11}	1.2×10^{-28}	This work
12.	$CN + H + M \longrightarrow HCN + M$	4.5×10^{-11}	1.7×10^{-30}	This work
*13.	${}^4N + {}^3CH_2 + M \longrightarrow H_2CN + M$	1.0×10^{-10}	1.2×10^{-28}	This work
14.	${}^4N + {}^4N + M \longrightarrow N_2 + M$	1.4×10^{-11}	1.9×10^{-32}	This work, Average of experimental
15.	${}^4N + H + M \longrightarrow NH + M$	4.3×10^{-10}	4.8×10^{-32}	This work, Brown [386]
*16.	${}^2N + {}^3CH_2 + M \longrightarrow H_2CN + M$	2.1×10^{-10}	6.2×10^{-28}	This work
*17.	${}^2N + {}^1CH_2 + M \longrightarrow H_2CN + M$	2.4×10^{-10}	1.5×10^{-27}	This work
*18.	${}^2N + {}^2N + M \longrightarrow N_2 + M$	5.7×10^{-11}	1.7×10^{-33}	This work
*19.	${}^2N + H + M \longrightarrow NH + M$	7.7×10^{-10}	7.0×10^{-32}	This work
*20.	$CH_4 + {}^1CH_2 + M \longrightarrow C_2H_6 + M$	7.1×10^{-11}	7.2×10^{-24}	Tsang & Hampson [247], This work
21.	$CH_3 + CH_3 + M \longrightarrow C_2H_6 + M$	6.0×10^{-11}	2.5×10^{-26}	Baulch et al. [137], Slagle et al. [387], MacPherson et al. [388]
22.	$CH_3 + H + M \longrightarrow CH_4 + M$	3.5×10^{-10}	1.4×10^{-28}	Baulch et al. [137]
*23.	${}^3CH_2 + {}^3CH_2 + M \longrightarrow C_2H_4 + M$	5.3×10^{-11}	2.6×10^{-26}	Baulch et al. [137], This work
24.	${}^3CH_2 + H + M \longrightarrow CH_3 + M$	2.0×10^{-10}	4.8×10^{-29}	Baulch et al. [137], This work
*25.	${}^1CH_2 + {}^1CH_2 + M \longrightarrow C_2H_4 + M$	7.1×10^{-11}	5.4×10^{-25}	This work
*26.	${}^1CH_2 + H_2 + M \longrightarrow CH_4 + M$	1.2×10^{-10}	1.4×10^{-27}	Baulch et al. [137], This work
*27.	${}^1CH_2 + H + M \longrightarrow CH_3 + M$	2.3×10^{-10}	3.7×10^{-28}	This work
*28.	$CH + CH + M \longrightarrow C_2H_2 + M$	1.9×10^{-10}	3.5×10^{-28}	Braun et al. [272, 275], This work
29.	$CH + H_2 + M \longrightarrow CH_3 + M$	9.6×10^{-11}	9.0×10^{-30}	Average of experimental values, Becker et al. [202]
*30.	$CH + H + M \longrightarrow {}^3CH_2 + M$	3.2×10^{-11}	2.0×10^{-28}	Average of experimental values, This work
*31.	$CH + H + M \longrightarrow {}^1CH_2 + M$	1.4×10^{-11}	4.4×10^{-31}	Becker et al. [389], This work
32.	$H + H + M \longrightarrow H_2 + M$	1.9×10^{-10}	7.4×10^{-33}	This work, Baulch et al. [137]

$*$ Reactions with no previously known rate coefficients.

In Table 4.6, we display the temperature-dependent Arrhenius parameters calculated for the one- and two-body reactions in CRAHCN.

Table 3.10: Arrhenius coefficients for the one- and two-body reactions in the consistent reduced atmospheric hybrid chemical network (CRAHCN). Experimental values are used when available, and calculated rate coefficients from this work are used otherwise. For the reactions with barriers from this work, rate coefficients are calculated at 50, 100, 200, 298, and 400 K, and are fit to the modified Arrhenius expression $k(T) = \alpha \left(\frac{T}{300}\right)^{\beta} e^{-\gamma/T}$. Barrierless reaction rate coefficients do not typically vary by more than a factor of 1–3 for temperatures between 50 and 400 K [208, 219–222]. Intermediate molecules are labelled with a bullet, and are included to describe the precise reaction pathway for multi-step reactions. First- and second-order reactions with rate coefficients slower than k = 10^{-21} cm^{3}s^{-1} are not included in this network. First-order rate coefficients have units s^{-1}. Second-order rate coefficients have units cm^{3}s^{-1}.

No.	Reaction equation	Forw./Rev.	α	β	γ	Source
33.	$N_2 + {}^2N \longrightarrow N_2 + {}^4N$	F	$5.4{\times}10^{-12}$	0	1620	Suzuki et al. [285]
34.	$N_2 + {}^1CH_2 \longrightarrow N_2 + {}^3CH_2$	F	$2.3{\times}10^{-12}$	-2.15	74	Douglas et al. [341]
35.	$H_2CN + NH \longrightarrow HCN + NH_2$	F	$4.3{\times}10^{-13}$	2.05	331	This work
36.	$H_2CN + {}^4N \longrightarrow {}^3H_2CNN\cdot \longrightarrow N_2 + {}^3CH_2$	F	$4.3{\times}10^{-12}$	0	0	This work
37.	$H_2CN + {}^4N \longrightarrow HCN + NH$	F	$1.0{\times}10^{-10}$	0	200	Nesbitt et al. [229]
*38.	$H_2CN + {}^2N \longrightarrow {}^3H_2CNN\cdot \longrightarrow N_2 + {}^3CH_2$	F	$3.2{\times}10^{-11}$	0	0	This work
*39.	$H_2CN + {}^2N \longrightarrow {}^1H_2CNN\cdot \longrightarrow N_2 + {}^1CH_2$	F	$6.4{\times}10^{-12}$	0	0	This work
*40.	$H_2CN + CH \longrightarrow {}^1H_2CNCH\cdot \longrightarrow H_2CNC_a\cdot + H\cdot \longrightarrow H_2CNC_b\cdot + H\cdot \longrightarrow CH_2CN + H$	F	$2.6{\times}10^{-11}$	-1.66	119	This work
*41.	$H_2CN + CH \longrightarrow {}^3H_2CNCH\cdot \longrightarrow HCN + {}^3CH_2$	F	$2.2{\times}10^{-11}$	0	0	This work
*42.	$H_2CN + CH \longrightarrow {}^1H_2CNCH\cdot \longrightarrow HCN + {}^1CH_2$	F	$6.4{\times}10^{-10}$	-2.04	904	This work
43.	$H_2CN + H \longrightarrow HCN + H_2$	F	$2.2{\times}10^{-11}$	0	0	This work
44.	$H_2CN \longrightarrow HCN + H$	F	$1.3{\times}10^{+13}$	1.74	19060	Pearce et al. [335] + This work
45.	$HCN + CN \longrightarrow HNCCN\cdot \longrightarrow NCCN + H$	F	$1.5{\times}10^{-13}$	0	0	Avg. of exper. vals
46.	$HCN + {}^2N \longrightarrow N_2 + CH$	F	$6.8{\times}10^{-11}$	0	0	This work
*47.	$HCN + {}^1CH_2 \longrightarrow CH_2HCN\cdot \longrightarrow CH_2NC_a\cdot + H\cdot \longrightarrow CH_2NC_b\cdot + H\cdot \longrightarrow CH_2CN + H$	F	$3.7{\times}10^{-13}$	0	0	This work
48.	$HCN + H \longrightarrow HCNH\cdot \longrightarrow HNC + H$	F	$9.0{\times}10^{-11}$	1.20	6249	This work
49.	$HCN + H \longleftarrow HCNH\cdot \longleftarrow HNC + H$	R	$8.9{\times}10^{-11}$	0.80	649	This work
50.	$CN + NH \longrightarrow HCN + {}^4N$	F	$1.1{\times}10^{-13}$	0.15	528	This work
51.	$CN + NH \longrightarrow HNNC\cdot \longrightarrow CHN_{2a}\cdot \longrightarrow CHN_{2b}\cdot \longrightarrow CH + N_2$	F	$4.6{\times}10^{-12}$	1.22	263	This work
52.	$CN + {}^4N \longrightarrow CN_{2(\nu)}\cdot \longrightarrow N_2 + C$	F	$1.1{\times}10^{-10}$	0	0	Avg. of exper. vals
*53.	$CN + {}^2N \longrightarrow CN_{2(\nu)}\cdot \longrightarrow N_2 + C$	F	$1.6{\times}10^{-10}$	0	0	This work
54.	$CN + CH_4 \longrightarrow HCN + CH_3$	F	$1.5{\times}10^{-11}$	0	940	Baulch et al. [137]
55.	$CN + CH_3 \longrightarrow HCN + {}^3CH_2$	F	$6.7{\times}10^{-12}$	0	0	This work
56.	$CN + CH \longrightarrow HCN + C$	F	$1.4{\times}10^{-11}$	0	0	This work
57.	$CN + CH \longrightarrow HNC + C$	F	$5.4{\times}10^{-13}$	0	0	This work
58.	$CN + H_2 \longrightarrow HCN + H$	F	$4.1{\times}10^{-12}$	1.55	1510	Tsang [390]
59.	$NH + NH \longrightarrow N_2H_2\cdot \longrightarrow N_2H\cdot + H\cdot \longrightarrow N_2 + H + H$	F	$3.5{\times}10^{-12}$	0	0	Nicholas et al. [391]
60.	$NH + NH \longrightarrow NH_2 + {}^4N$	F	$1.9{\times}10^{-12}$	0.47	3738	This work
61.	$NH + {}^4N \longrightarrow N_2H\cdot \longrightarrow N_2 + H$	F	$2.5{\times}10^{-11}$	0	0	Hack et al. [282]
62.	$NH + {}^2N \longrightarrow N_2H\cdot \longrightarrow N_2 + H$	F	$8.8{\times}10^{-11}$	0	0	Pearce et al. [335] + This work
63.	$NH + CH_3 \longrightarrow H_3CNH\cdot \longrightarrow {}^1H_2CNH\cdot + H\cdot \longrightarrow H_2CN + H_2$	F	$2.0{\times}10^{-11}$	0	0	This work
64.	$NH + {}^3CH_2 \longrightarrow {}^1H_2CNH\cdot \longrightarrow H_2CN + H$	F	$1.9{\times}10^{-11}$	0	0	This work
*65.	$NH + {}^1CH_2 \longrightarrow {}^3H_2CNH\cdot \longrightarrow H_2CN + H$	F	$4.6{\times}10^{-11}$	0	0	This work
66.	$NH + CH \longrightarrow HNCH\cdot \longrightarrow HCN + H$	F	$4.5{\times}10^{-11}$	0	0	This work

67.	$NH + CH \longrightarrow HNCH\cdot \longrightarrow HNC + H$	F	5.2×10^{-11}	1.04	2551	This work
68.	$NH + H \longrightarrow H_2 + {}^4N$	F	2.2×10^{-12}	1.55	103	Adam et al. [281]
69.	${}^4N + CH_3 \longrightarrow {}^3H_3CN\cdot \longrightarrow H_2CN + H$	F	7.7×10^{-11}	0	0	Marston et al. [195] + Stief et al. [224]
70.	${}^4N + {}^3CH_2 \longrightarrow H_2CN_{(\nu)}\cdot \longrightarrow HCN + H$	F	1.0×10^{-10}	0	0	Pearce et al. [335] + This work
71.	${}^4N + {}^1CH_2 \longrightarrow {}^4H_2CN \longrightarrow {}^3HCN\cdot + H\cdot \longrightarrow CN + H + H$	F	1.9×10^{-10}	0	0	Pearce et al. [335] + This work
72.	${}^4N + CH \longrightarrow {}^3HCN\cdot \longrightarrow CN + H$	F	1.1×10^{-10}	0	0	Avg. of exper. vals
73.	${}^2N + CH_4 \longrightarrow H_3CNH\cdot \longrightarrow {}^1H_2CNH\cdot + H\cdot \longrightarrow H_2CN + H_2$	F	4.8×10^{-11}	0	750	Herron [237]
74.	${}^2N + CH_3 \longrightarrow {}^{3,1}H_3CN\cdot \longrightarrow {}^{3,1}H_2CNH\cdot$ $H_2CN + H$	F	2.3×10^{-10}	0	0	Pearce et al. [335] + This work
75.	${}^2N + {}^3CH_2 \longrightarrow H_2CN_{(\nu)}\cdot \longrightarrow HCN + H$	F	2.1×10^{-10}	0	0	Pearce et al. [335] + This work
76.	${}^2N + {}^3CH_2 \longrightarrow {}^4H_2CN\cdot \longrightarrow {}^3HCN\cdot + H\cdot \longrightarrow CN + H + H$	F	3.5×10^{-10}	0	0	Pearce et al. [335] + This work
77.	${}^2N + {}^1CH_2 \longrightarrow H_2CN_{(\nu)}\cdot \longrightarrow HCN + H$	F	2.4×10^{-10}	0	0	Pearce et al. [335] + This work
78.	${}^2N + CH \longrightarrow {}^3HCN\cdot \longrightarrow CN + H$	F	3.5×10^{-10}	0	0	Pearce et al. [335] + This work
79.	${}^2N + H_2 \longrightarrow NH_{2(\nu)}\cdot \longrightarrow NH + H$	F	4.2×10^{-11}	0	880	Herron [237]
80.	$CH_4 + {}^3CH_2 \longrightarrow CH_3 + CH_3$	F	5.4×10^{-13}	7.45	3401	Pearce et al. [335] + This work
81.	$CH_4 + {}^3CH_2 \longleftarrow CH_3 + CH_3$	R	5.3×10^{-11}	0	0	Pearce et al. [335] + This work
82.	$CH_4 + {}^1CH_2 \longrightarrow C_2H_{6(\nu)}\cdot \longrightarrow CH_3 + CH_3$	F	7.1×10^{-11}	0	0	Tsang & Hampson [247]
83.	$CH_4 + CH \longrightarrow CH_4{-}CH\cdot \longrightarrow C_2H_5\cdot \longrightarrow C_2H_4 + H$	F	9.8×10^{-11}	0	0	Baulch et al. [137]
84.	$CH_4 + H \longrightarrow CH_3 + H_2$	F	5.9×10^{-13}	3.0	4045	Baulch et al. [137]
85.	$CH_4 + H \longleftarrow CH_3 + H_2$	R	7.0×10^{-14}	2.74	4740	Baulch et al. [137]
86.	$CH_3 + {}^3CH_2 \longrightarrow C_2H_5\cdot \longrightarrow C_2H_4 + H$	F	7.0×10^{-11}	0	0	Baulch et al. [137]
87.	$CH_3 + {}^1CH_2 \longrightarrow C_2H_5\cdot \longrightarrow C_2H_4 + H$	F	1.3×10^{-10}	0	0	Pearce et al. [335] + This work
88.	$CH_3 + CH \longrightarrow {}^1CH_3CH\cdot \longrightarrow C_2H_3\cdot + H\cdot \longrightarrow C_2H_4$	F	5.5×10^{-11}	0	0	This work
89.	$CH_3 + CH \longrightarrow {}^3CH_3CH\cdot \longrightarrow C_2H_3\cdot + H\cdot \longrightarrow C_2H_2 + H + H$	F	2.4×10^{-10}	0	0	This work
90.	$CH_3 + H \longrightarrow {}^3CH_2 + H_2$	F	2.6×10^{-11}	1.15	6529	Pearce et al. [335] + This work
91.	$CH_3 + H \longleftarrow {}^3CH_2 + H_2$	R	8.1×10^{-14}	9.04	1450	Pearce et al. [335] + This work
92.	${}^3CH_2 + {}^3CH_2 \longrightarrow C_2H_{4(\nu)}\cdot \longrightarrow C_2H_2 + H_2$	F	5.3×10^{-11}	0	0	Baulch et al. [137]
93.	${}^3CH_2 + {}^1CH_2 \longrightarrow {}^3C_2H_4\cdot \longrightarrow C_2H_3\cdot + H \longrightarrow C_2H_2 + H + H$	F	2.1×10^{-10}	0	0	Pearce et al. [335] + This work
94.	${}^3CH_2 + CH \longrightarrow C_2H_3\cdot \longrightarrow C_2H_2 + H$	F	6.3×10^{-11}	0	0	This work
*95.	${}^3CH_2 + CH \longrightarrow {}^4C_2H_3\cdot \longrightarrow {}^3C_2H_2\cdot + H\cdot \longrightarrow C_2H + H + H$	F	1.1×10^{-10}	0	0	This work
96.	${}^3CH_2 + H \longrightarrow CH_{3(\nu)}\cdot \longrightarrow CH + H_2$	F	2.0×10^{-10}	0	0	Baulch et al. [137]
97.	${}^1CH_2 + {}^1CH_2 \longrightarrow C_2H_{4(\nu)}\cdot \longrightarrow C_2H_2 + H_2$	F	7.1×10^{-11}	0	0	Pearce et al. [335] + This work
*98.	${}^1CH_2 + CH \longrightarrow C_2H_3\cdot \longrightarrow C_2H_2 + H$	F	1.6×10^{-10}	0	0	This work
99.	${}^1CH_2 + H_2 \longrightarrow CH_{4(\nu)}\cdot \longrightarrow CH_3 + H$	F	1.2×10^{-10}	0	0	Baulch et al. [137]
100.	${}^1CH_2 + H \longrightarrow CH_{3(\nu)}\cdot \longrightarrow CH + H_2$	F	1.8×10^{-10}	0	0	This work + González et al. [392]
*101.	${}^1CH_2 + H \longrightarrow CH_{3(\nu)}\cdot \longrightarrow {}^3CH_2 + H$	F	4.6×10^{-11}	0	0	This work + González et al. [392]
102.	$CH + CH \longrightarrow {}^3C_2H_2\cdot \longrightarrow C_2H + H$	F	1.4×10^{-10}	0	0	Pearce et al. [335] + This work
103.	$CH + H_2 \longrightarrow CH_{3(\nu)}\cdot \longrightarrow {}^3CH_2 + H$	F	3.1×10^{-10}	0	1650	Brownsword et al. [266]
104.	$CH + H \longrightarrow {}^3CH_{2(\nu)}\cdot \longrightarrow C + H_2$	F	6.9×10^{-10}	0	0	Pearce et al. [335] + This work

∗ Reactions with no previously known rate coefficients.

Vibrationally excited molecules are labeled with a $_{(\nu)}$ subscript.

3.7.3 Experimental Data

In Table 4.7, we list all experimental rate coefficients for the reactions calculated in this work.

Table 3.11: Available experimental or recommended reaction rate coefficients for the new reactions in this paper. For brevity, only the 10 most recent measurements are included; for a complete listing, we refer the reader to the NIST Chemical Kinetics Database [227]. First-order rate coefficients have units s^{-1}. Second-order rate coefficients have units cm^3s^{-1}. Third-order rate coefficients have units cm^6s^{-1}.

k(298K)	Technique	Temp. (K)	Pressure (Torr)	Reference(s)
$H_2CN + {}^4N \longrightarrow HCN + NH$				
$4.4{\times}10^{-11}$	M	298	1	Nesbitt et al. [229]
$H_2CN + H \longrightarrow HCN + H_2$				
$8.3{\times}10^{-11}$	Z	independent		Tomeczek & Gradon [228]
$HCN + CN \longrightarrow NCCN + H$				
$4.1{\times}10^{-13}$	M	298	20	Zabarnick & Lin [393]
$3.2{\times}10^{-14}$	M	298	100–600	Yang et al. [394]
$1.8{\times}10^{-14}$	M	300	5–25	Li et al. [395]
$3.2{\times}10^{-14}$	S	298		Tsang [390]
$HCN + CH \longrightarrow$ products				
$2.7{\times}10^{-10}$	M	298	100	Zabarnick et al. [382]
$CN + CN + M \longrightarrow NCCN + M$				
$4.7{\times}10^{-32}$	M	298	1–27	Basco et al. [383]
$3.3\text{–}4.9{\times}10^{-29}$	S	298		Tsang [390]
$CN + CN \longrightarrow NCCN$				
$1.0{\times}10^{-12}$	M	298	1–27	Basco et al. [383]
$9.4{\times}10^{-12}$	S	298		Tsang [390]
$CN + {}^4N \longrightarrow N_2 + C$				
$1.2{\times}10^{-10}$	M	298	7	Atakan et al. [384]
$1.0{\times}10^{-10}$	M	300	2	Whyte & Phillips [385]
$3.0{\times}10^{-10}$	S	298		Baulch et al. [137]
$CN + {}^4N + M \longrightarrow CN_2 + M$				
$2.8{\times}10^{-32}$	M	298	1–10	Provencher & McKenney [378]
$CN + CH_4 \longrightarrow HCN + CH_3$				
$1.1{\times}10^{-12}$	M	298		Anastasi & Hancock [396]
$1.1{\times}10^{-12}$	M	295	53	Lichtin & Lin [397]
$9.2{\times}10^{-13}$	M	298	4–38	Atakan & Wolfrum [398]
$7.8{\times}10^{-13}$	M	298	1–200	Balla & Pasternack [399]
$7.5{\times}10^{-13}$	M	297	20	Copeland et al. [400]
$7.4{\times}10^{-13}$	M	298		Sims et al. [401]
$7.4{\times}10^{-13}$	M	298		Herbert et al. [402]
$5.8{\times}10^{-13}$	M	298	47–490	Yang et al. [403]
$5.6{\times}10^{-13}$	M	294	5–30	Sayah et al. [404]
$6.4{\times}10^{-13}$	S	298		Baulch et al. [137]
$CN + H_2 \longrightarrow HCN + H$				
$4.9{\times}10^{-14}$	M	294	52	Lichtin & Lin [397]
$2.5\text{–}2.9{\times}10^{-14}$	M	298	50	Choi et al. [405]
$2.5\text{–}2.7{\times}10^{-14}$	M	294	3–6	He et al. [406]
$2.7{\times}10^{-14}$	M	298	50–500	Sun et al. [407]
$2.7{\times}10^{-14}$	M	298	50	Sims & Smith [408]
$2.2\text{–}2.6{\times}10^{-14}$	M	298	1–200	Balla & Pasternack [399]
$2.5{\times}10^{-14}$	M	295	10–30	De Juan et al. [409]
$1.4{\times}10^{-14}$	M	298	3–50	Atakan et al. [410]
$1.2{\times}10^{-14}$	M	298	4–21	Jacobs et al. [411]
$2.6{\times}10^{-14}$	S	298		Tsang [390]
$CN + H + M \longrightarrow HCN + M$				
$1.3\text{–}1.6{\times}10^{-30}$	S	298		Tsang [390]
$NH + NH \longrightarrow N_2H_2\cdot \longrightarrow$ products				
$3.5{\times}10^{-12}$	M	298	3–10	Nicholas et al. [391]
$NH + {}^4N \longrightarrow N_2 + H$				
$2.5{\times}10^{-11}$	M	298	11–15	Hack et al. [282]
$2.6{\times}10^{-11}$	S	300		Konnov & De Ruyck [283]

$\mathrm{NH + H \longrightarrow H_2 + {}^4N}$				
3.2×10^{-12}	M	298	2–8	Adam et al. [281]
$\mathrm{{}^4N + {}^4N + M \longrightarrow N_2 + M}$				
1.3×10^{-31}	M	298		Emel'kin & Marusin[412]
$1.1–3.2\times10^{-32}$	M	300		Brennen & Shane[413]
$1.1–2.3\times10^{-32}$	M	300		Emel'kin & Marusin [414]
2.3×10^{-32}	M	298	0.3–7	Evenson & Burch [415]
1.7×10^{-32}	M	298	0.5–1.3	Harteck et al. [416]
$7.4–9.7\times10^{-33}$	M	298	1–13	Clyne & Stedman [417]
$6.1–7.2\times10^{-33}$	M	298	2–10	Campbell & Thrush [418]
$3.8–5.3\times10^{-33}$	M	298	2–10	Campbell & Thrush [419]
3.3×10^{-33}	M	297	14	Lambert et al. [420]
2.2×10^{-33}	M	298	2–9	Kretschmer & Petersen[421]
$\mathrm{{}^4N + CH_3 \longrightarrow HCN + H_2}$				
8.6×10^{-12}	M	298	0.3–1.6	Marston et al. [195], Stief et al. [224]
$\mathrm{{}^4N + CH_3 \longrightarrow H_2CN + H}$				
7.7×10^{-11}	M	298	0.3–1.6	Marston et al. [195], Stief et al. [224]
5.0×10^{-11}	S	independent		Miller & Bowman [248]
$\mathrm{{}^4N + CH \longrightarrow {}^3HCN \longrightarrow CN + H}$				
1.6×10^{-10}	M	298	4	Brownsword et al. [273]
$1.2–1.4\times10^{-10}$	M	296	5	Daranlot et al. [222]
2.1×10^{-11}	M	298	5–15	Messing et al. [274]
$\mathrm{{}^4N + H + M \longrightarrow NH + M}$				
$3.1–6.4\times10^{-32}$	M	298		Brown [386]
$>1.3\times10^{-33}$	M	298	2.5–4.5	Mavroyannis & Winkler [422]
$\mathrm{{}^2N + CH_4 \longrightarrow H_2CNH + H}$				
$^a4.5\times10^{-12}$	M	298	700	Takayanagi et al. [233], Umemoto et al. [206]
$^a3.7\times10^{-12}$	M	300	6	Fell et al. [234], Umemoto et al. [206]
$^a2.7\times10^{-12}$	M	295	20	Umemoto et al. [235], Umemoto et al. [206]
$^a2.4\times10^{-12}$	M	300	3–5	Black et al. [236], Umemoto et al. [206]
$^a3.2\times10^{-12}$	S	298		Herron [237], Umemoto et al. [206]
$\mathrm{{}^2N + H_2 \longrightarrow NH_2\cdot \longrightarrow NH + H}$				
5.0×10^{-12}	M	300	3–5	Black et al. [236]
3.5×10^{-12}	M	300	6	Fell et al. [234]
2.7×10^{-12}	M	300	2–5	Black et al. [284]
2.4×10^{-12}	M	300	753	Suzuki et al. [285]
2.3×10^{-12}	M	295	30	Umemoto et al. [286]
2.3×10^{-12}	M	300	1–3	Piper et al. [287]
2.1×10^{-12}	M	300	26	Husain et al. [288]
1.8×10^{-12}	M	298	1	Whitefield & Hovis [289]
1.7×10^{-12}	M	300	50	Husain et al. [290]
2.2×10^{-12}	S	200–300		Herron [237]
$\mathrm{CH_4 + {}^3CH_2 \longrightarrow 2\,CH_3}$				
$<5.0\times10^{-14}$	M	298	10	Braun et al. [203]
$^f3.1\times10^{-19}$	M	298	2–3	Böhland et al. [265]
$<3.0\times10^{-19}$	S	298		Tsang & Hampson [247]
$\mathrm{CH_4 + {}^1CH_2 \longrightarrow 2\,CH_3}$				
7.3×10^{-11}	M	298	10^{-4}–10	Ashfold et al. [205]
7.0×10^{-11}	M	295	6	Langford et al. [204]
1.9×10^{-12}	M	298	5–20	Braun et al. [203]
7.1×10^{-11}	S			Tsang & Hampson [247]
$\mathrm{CH_4 + CH \longrightarrow C_2H_4 + H}$				
3.0×10^{-10}	M	298	30–100	Butler et al. [270]
1.0×10^{-10}	M	298	100	Butler et al. [276]
9.8×10^{-11}	M	298	100	Berman & Lin [277]
9.1×10^{-11}	M	298	50–300	Blitz et al. [278]
8.9×10^{-11}	M	295	9–12	Canosa et al. [279]
6.7×10^{-11}	M	298	100	Thiesemann et al. [280]
3.3×10^{-11}	M			Bosnali & Perner [271]
2.5×10^{-12}	M	298	100	Braun et al. [272]
2.0×10^{-12}	M	298	1-500	Braun et al. [275]
9.8×10^{-11}	S	298		Baulch et al. [137]
$\mathrm{CH_4 + H \longrightarrow CH_3 + H_2}$				

3.5×10^{-17}	M	298		Lawrence, Jr. & Firestone [231]
1.7×10^{-17}	M	298	0.55	Jones & Ma [232]
8.2×10^{-19}	S	300		Baulch et al. [137]
$CH_3 + CH_3 + M \longrightarrow C_2H_6 + M$				
3.3×10^{-26}	M	298	5–600	Slagle et al. [387]
1.7×10^{-26}	M	298	5–500	MacPherson et al. [388]
$2\,CH_3 \longrightarrow C_2H_6$				
6.5×10^{-11}	M	300	high-pressure limit	Walter et al. [249]
6.5×10^{-11}	M	298	high-pressure limit	Macpherson et al. [250]
6.0×10^{-11}	M	298	high-pressure limit	Du et al. [251]
6.0×10^{-11}	M	298	high-pressure limit	Slagle et al. [252]
$^{d}5.9\times10^{-11}$	M	292	758	Sangwan et al. [253]
5.8×10^{-11}	M	298	750	Pagsberg et al. [254]
5.5×10^{-11}	M	298	high-pressure limit	Hippler et al. [255]
5.2×10^{-11}	M	298	100	Fahr et al. [256]
4.6×10^{-11}	M	300	1	Wang & Fockenberg [257]
4.0×10^{-11}	M	302	81–571	Arthur [258]
3.5×10^{-11}	M	308	86	Anastasi & Arthur [259]
6.0×10^{-11}	S	independent	high-pressure limit	Baulch et al. [137]
4.4×10^{-11}	S	298	high-pressure limit	Tsang [245]
$CH_3 + {}^3CH_2 \longrightarrow C_2H_5\cdot \longrightarrow C_2H_4 + H$				
2.1×10^{-10}	M	300	1 l	Wang & Fockenberg [257]
1.1×10^{-10}	M	298	1	Deters et al. [262]
1.0×10^{-10}	M	308	50–700	Laufer & Bass [263]
5.0×10^{-11}	M		200	Pilling & Robertson [264]
7.0×10^{-11}	S	independent		Baulch et al. [137]
7.0×10^{-11}	S	298		Tsang & Hampson [247]
$CH_3 + {}^1CH_2 \longrightarrow C_2H_4 + H$				
3.0×10^{-11}	S			Tsang & Hampson [247]
$CH_3 + H_2 \longrightarrow CH_4 + H$				
$^{c}1.3\times10^{-20}$	M	300		Kobrinsky & Pacey [246]
1.2×10^{-20}	S	300		Tsang & Hampson [247]
9.6×10^{-21}	S	300		Baulch et al. [137]
$CH_3 + H + M \longrightarrow CH_4 + M$				
$1.5–55\times10^{-29}$	M	295	6–15	Pratt & Veltman [423]
2.6×10^{-29}	M	298	2–10	Pratt & Wood [424]
$6.2–30\times10^{-29}$	S	298		Baulch et al. [137]
$CH_3 + H \longrightarrow CH_4$				
4.7×10^{-10}	M	300	high-pressure limit	Brouard et al. [238]
3.3×10^{-10}	M	308	high-pressure limit	Cheng & Yeh [239]
2.5×10^{-10}	M	308	300	Cheng et al. [240]
2.0×10^{-10}	M	296	735–755	Sworski et al. [241]
1.5×10^{-10}	M	300	high-pressure limit	Patrick et al. [242]
3.4×10^{-10}	F	298	high-pressure limit	Michael et al. [243]
3.5×10^{-10}	S	independent	high-pressure limit	Cobos & Troe [244]
3.5×10^{-10}	S	independent	high-pressure limit	Baulch et al. [137]
2.0×10^{-10}	S	298	high-pressure limit	Tsang [245]
${}^3CH_2 + {}^3CH_2 \longrightarrow C_2H_2 + 2\,H$				
5.3×10^{-11}	M	298	20–700	Braun et al. [203]
5.3×10^{-11}	S	300		Baulch et al. [137]
${}^3CH_2 + {}^1CH_2 \longrightarrow C_2H_2 + H_2$				
3.0×10^{-11}	S			Tsang & Hampson [247]
${}^3CH_2 + H_2 \longrightarrow CH_3 + H$				
$<5.0\times10^{-14}$	M	298	10	Braun et al. [203]
$<6.9\times10^{-15}$	M	295	8	Darwin & Moore [260]
$<5.0\times10^{-15}$	M		10	Pilling & Robertson [261]
${}^3CH_2 + H \longrightarrow CH_3\cdot \longrightarrow CH + H_2$				
2.7×10^{-10}	M	285	2	Boullart & Peeters [197]
2.7×10^{-10}	M	298	2	Böhland & Temps [200]
$^{e}2.6\times10^{-10}$	M	300	2	Devriendt et al. [196]
1.8×10^{-10}	M	298	1–2	Böhland et al. [198]
$^{c}1.4\times10^{-10}$	M	300	100	Zabarnick et al. [199]
8.3×10^{-11}	M	298	2	Grebe & Homann [201]
2.0×10^{-10}	S	300		Baulch et al. [137]
2.7×10^{-10}	S	298		Tsang & Hampson [247]
${}^1CH_2 + {}^1CH_2 \longrightarrow C_2H_2 + 2\,H$				
5.0×10^{-11}	S			Tsang & Hampson [247]
${}^1CH_2 + H_2 \longrightarrow CH_4\cdot \longrightarrow CH_3 + H$				
1.3×10^{-10}	M	295	6	Langford et al. [204]
1.1×10^{-10}	M	298	10^{-4}–10	Ashfold et al. [205]

7.0×10^{-12}	M	298	10	Braun et al. [203]
1.2×10^{-10}	S			Tsang & Hampson [247]
1.2×10^{-10}	S	independent		Baulch et al. [137]
$^{1}CH_2 + H \longrightarrow CH + H_2$				
5.0×10^{-11}	S			Tsang & Hampson [247]
$2\,CH \longrightarrow C_2H_2$				
2.0×10^{-10}	M	298	1–330	Braun et al. [272]
1.7×10^{-10}	M	298	1–500	Braun et al. [275]
$CH + H_2 + M \longrightarrow CH_3 + M$				
9.0×10^{-30}	M	298	2–591	Becker et al. [202]
$CH + H_2 \longrightarrow CH_3$				
1.6×10^{-10}	M	294	high-pressure limit	Brownsword et al. [266]
5.1×10^{-11}	M	300	750	Fulle & Hippler [267]
4.5×10^{-11}	M	298	591	Becker et al. [202]
4.5×10^{-11}	M	279	600	Berman & Lin [268]
3.0×10^{-11}	M	294	750	McIlroy & Tully [269]
2.3×10^{-11}	M	298	100	Butler et al. [270]
1.7×10^{-11}	M			Bosnali & Perner [271]
1.0×10^{-12}	M	298	1–9	Butler et al. [272]
$CH + H_2 \longrightarrow CH_3\cdot \longrightarrow {}^{3}CH_2 + H$				
[c]9.1×10^{-13}	M	300	100	Zabarnick et al. [199]
1.2×10^{-12}	M	294	400	Brownsword et al. [266]
4.5×10^{-11}	M	298	591	Becker et al. [202]
$CH + H \longrightarrow C + H_2$				
5.0×10^{-11}	M	298		Grebe & Homann [425]
$CH + H \longrightarrow$ products				
1.4×10^{-11}	M	297	2	Becker et al. [389]
$H + H + M \longrightarrow H_2 + M$				
2.5×10^{-31}	M	303		Eberius et al. [426]
$7.0–20\times10^{-33}$	M	295	6	Walkauskas & Kaufman [427]
$5.9–10\times10^{-33}$	M	298	500-1500	Lynch et al. [428]
9.4×10^{-33}	M	298	50–250	Bennett & Blackmore[429]
$7.0–9.2\times10^{-33}$	M	298	2–15	Trainor et al. [430]
$5.6–6.7\times10^{-33}$	M	297	6–18	Mitchell & LeRoy [431]
$4.0–5.1\times10^{-33}$	M	298	1.5–4.5	Teng & Winkler [432]
$6.4–92\times10^{-33}$	S	298		Cohen & Westberg [433]
9.1×10^{-33}	S	298		Tsang & Hampson [247]
$6.0–8.8\times10^{-33}$	S	298		Baulch et al. [137]

M: Monitoring decay of reactants and/or production of products.

Z: Zero activation energy value. Calculated by numerical modeling using the chemical compositions of the flames of CH_4 + air.

S: Suggested value based on experiments and/or evaluations at a range of temperatures.

Table 3.12: Lennard-Jones force constants used in this study. Values are obtained from viscosity data when possible.

Molecule	σ (Å)	ϵ/k_b (K)	Source
NCCN	4.38	339	Welty et al. [360]
CNCN	[a]4.38	[a]339	Welty et al. [360]
CH_3CN	[b]4.418	[b]230	Welty et al. [360]
CH_2CN	[c]4.232	[c]205	Welty et al. [360]
$HCNCH_a$	[c]4.232	[c]205	Welty et al. [360]
HNCN	[d]3.996	[d]190	Welty et al. [360]
CN_2	[d]3.996	[d]190	Welty et al. [360]
$^{3}HCCN$	[e]4.221	[e]185	Welty et al. [360]
$^{1}HCCN$	[e]4.221	[e]185	Welty et al. [360]

H_2CN	[f]3.63	[f]569.1	Reid et al. [359]
HCN	3.63	569.1	Reid et al. [359]
N_2	3.681	91.5	Welty et al. [360]
NH	[g]2.75	[g]80	Wang et al. [361]
C_2H_6	4.418	230	Welty et al. [360]
C_2H_4	4.232	205	Welty et al. [360]
C_2H_2	4.221	185	Welty et al. [360]
CH_4	3.822	136.5	Welty et al. [360]
CH_3	3.8	144	Wang et al. [361]
$^3CH_2$	3.8	144	Wang et al. [361]
$^1CH_2$	3.8	144	Wang et al. [361]
H_2	2.968	33.3	Welty et al. [360]

[a] L-J parameters based on those for NCCN

[b] L-J parameters based on those for C_2H_6

[c] L-J parameters based on those for C_2H_4

[d] L-J parameters based on those for CO_2

[e] L-J parameters based on those for C_2H_2

[f] L-J parameters based on those for HCN

[g] L-J parameters based on those for OH and CH

3.7.4 Theoretical Case Studies

The following theoretical case studies provide additional details for some of the non-standard reactions in CRAHCN. For example, these reactions might have an excited intermediate, or may have a barrier that isn't detected by our chosen computational method.

3.7.4.1 Case Study 1: $H_2CN + {}^4N \longrightarrow HCN + NH$

One experiment has measured the rate coefficient for this reaction to have a value of $k(298\text{ K}) = 4.4{\times}10^{-11}\text{ cm}^3\text{s}^{-1}$ [229]. No isotope effect was observed, which is consistent with a barrierless reaction. Using three temperature data points (200K, 298K, 363K), the authors suggest Arrhenius parameters indicative of a very small barrier. However, with the small number of data points, and the data uncertainties, complete temperature independence of this reaction would also fit these data points [229].

Nesbitt et al. [229] suggest this reaction either proceeds through the $N-CH_2N$ complex, or via direct abstraction. We find the addition reaction forming the $N-CH_2N$ complex to have a large barrier at the BH/d level of theory (82 kJ mol^{-1}).

Furthermore, we find the addition reaction forming ^3H_2CNN to efficiently decay into the N_2 and $^3CH_2$ products. ^3H_2CNN isomerization barriers proceeding to HCN + NH decay are too large to consider this pathway.

At the BH/d and CC/t levels of theory, we find the direct abstraction reaction to have barriers of 15.4 and 23.0 kJ mol^{-1}, respectively. On the other hand, at the B3LYP/aug-cc-pVDZ and ωB/d levels of theory, we find the abstraction reaction to be barrierless and nearly barrierless (E_0 = 1.9 kJ mol^{-1}), respectively.

Including the barriers, the rate coefficients for $H_2CN + {}^4N \longrightarrow HCN + NH$ at the BH/d and CC/t levels of theory are 9.5×10^{-15} and 7.1×10^{-14} cm^{3}s^{-1}, respectively. These are several orders of magnitude lower than the experimentally measured value.

We find it likely that BH/d and CC/t calculate barriers when there should not be any. When removing the barriers from the calculation, the rate coefficients at the BH/d and CC/t levels of theory are 4.7×10^{-12} and 5.1×10^{-12} cm^{3}s^{-1}, respectively. This reduces the discrepancy between experiment and calculation to factors of 9.

The rate coefficients at the ωB/d and B3LYP/aug-cc-pVDZ levels of theory are 3.4 and 9.4×10^{-12} cm^{3}s^{-1}, which are factors of 13 and 5 smaller than the experimental value. Given all these discrepancies, we recommend further experimental and theoretical analyses be carried out for this reaction.

3.7.4.2 Case Study 2: $CN + N \longrightarrow CN_{2(\nu)}\cdot \longrightarrow N_2 + C$

Experimental measurements of this reaction near 298 K range from 1.0 to 1.2×10^{-10} cm^{3}s^{-1} [384, 385]. Baulch et al. [137] reviewed both high- and low-temperature measurements and recommended a value of $k = 3.0\times10^{-10}$ cm^{3}s^{-1}.

The mechanism of the reaction is not previously well understood, however authors have suggested this reaction may pass through the $CN_2\cdot$ intermediate [137, 384]. Our theoretical simulations suggest this is indeed the correct mechanism.

We calculate the rate coefficient of $CN + N \longrightarrow CN_2$ at 298 K using the BH/d level of theory to be 3.4×10^{-11} cm^{3}s^{-1}. We find the decay of $CN_{2(\nu=0)}$ into N_2 + C to be slow ($\sim10^{-41}$ s^{-1}). This suggests that this reaction likely proceeds through vibrationally excited CN_2, as is to be expected when two reactants combine to form a single product [351].

Our calculated rate coefficient for $CN + N \longrightarrow CN_{2(\nu)} \cdot \longrightarrow N_2 + C$ (4.3×10^{-11} cm^3s^{-1}) is only a factor of 2 smaller than the experimentally measured values.

3.7.4.3 Case Study 3: $CN + CH_4 \longrightarrow HCN + CH_3$

The experimental rate coefficient for this reaction at 298 K ranges from 5.6×10^{-13} to 1.1×10^{-12} cm^3s^{-1} [396–402, 404].

The experimental barrier for this reaction is about 8.3 kJ mol^{-1} [379]. This matches well with the MP4 theoretical barriers calculated by Yang et al. [403] which range from 7.5–8.8 kJ mol^{-1}. We calculate a barrier for this reaction at the CC/t level of theory to be 6.7 kJ mol^{-1}.

We do not calculate a barrier for this reaction at the BH/d or ωB/d levels of theory. We calculate a barrierless rate coefficients at 298 K at to be 2.2 and 3.7 $\times10^{-11}$ cm^3s^{-1}, respectively, which are over an order of magnitude greater than the nearest experimental value. This disagreement with experiment is due to the lack of barriers calculated at these levels of theory. For this reason, we introduce the experimental barrier of 8.3 kJ mol^{-1} [379] to our BH/d calculation. This produces a rate coefficient at 298 K of 7.7×10^{-13} cm^3s^{-1}, which is within the experimental range.

3.7.4.4 Case Study 4: $CN + H_2 \longrightarrow HCN + H$

Experiments measure the rate coefficient for this reaction to be between 1.2 and 4.9×10^{-14} cm^3s^{-1} [397, 399, 405–411].

Experiments generally agree on a barrier for this reaction of ~16.7 kJ mol^{-1} [434]. However, an *ab initio* theoretical study suggests a barrier of 13.4 kJ mol^{-1} provides a much better agreement between theory and experiment [381].

We calculate no barrier for this reaction at the BH/d level of theory. The barrierless rate coefficient we calculate at 298 K is 8.7×10^{-13} cm^3s^{-1}, which is a factor of 18 larger than the nearest experimental value. This discrepancy is due to the lack of barrier in our calculation when one should be present.

Similarly to ter Horst et al. [381], when including a barrier of ~16.7 kJ mol^{-1}, the calculated rate coefficient at 298 K is too low with respect to experimental values. Therefore, we include an experimental barrier of 13.4 kJ mol^{-1} in our calculation and obtain a rate coefficient of $k(298\text{ K}) = 3.9{\times}10^{-15}$ cm^{3}s^{-1}. This value is only a factor of 3 smaller than the nearest experimental value.

3.7.4.5 Case Study 5: $CH_4 + {}^1CH_2 \longrightarrow C_2H_6(\nu)\cdot \longrightarrow CH_3 + CH_3$

${}^1CH_2$ inserts into the C-H bond of CH_4 to produce the C_2H_6 intermediate, and subsequently dissociates into $CH_3 + CH_3$ [204, 205, 247].

We calculate the decay of C_2H_6 in the ground vibrational state into $CH_3 + CH_3$ to be slow ($< 10^{-37}$ s^{-1}), which suggests this reaction proceeds through an excited vibrational state.

In previous work we only included the reaction $CH_4 + {}^1CH_2 \longrightarrow C_2H_6$ in the network [335]; However this is only valid in high atmospheric pressures. We therefore include calculations of both the high pressure ($CH_4 + {}^1CH_2 + M \longrightarrow C_2H_6 + M$ and low pressure reactions ($CH_4 + {}^1CH_2 \longrightarrow C_2H_6(\nu)\cdot \longrightarrow CH_3 + CH_3$), with BH/d rate coefficients at 298 K of $7.2{\times}10^{-24}$ cm^{6}s^{-1} and $2.1{\times}10^{-11}$ cm^{3}s^{-1}, respectively.

3.7.4.6 Case Study 6: $CH_4 + CH \longrightarrow CH_4{-}CH\cdot \longrightarrow C_2H_5\cdot \longrightarrow C_2H_4 + H$

Experimentally measured rate coefficients for this reaction range from $k(298) = 0.02$–$3{\times}10^{-10}$ cm^{3}s^{-1} [270–272, 275–280]. Experiment suggests this reaction proceeds without a barrier [277].

Previous theoretical studies find this reaction proceeds through three steps, first forming a $CH_4{-}CH$ complex, then C_2H_5, and finally, decay into $C_2H_4 + H$ [333, 380]. At the CCSD(T)-F12/CBS//B3LYP/6-311G(d,p) + ZPE(B3LYP/6-311G(d,p)) level of theory, Ribeiro & Mebel [380] found the first step of this reaction to be barrierless, and the second step to have a barrier 2.3 kJ mol^{-1} lower than the reactants. At the UMP2/6-31G(d,p) and UMP4/6-311++(2d,p)//UMP2/6-31G(d,p) levels of theory, Wang et al. [333] found similar results, with a barrierless first step, and second step barriers 0.3 and 0.2 kJ mol^{-1} below the reactants, respectively.

At the BH/d level of theory, we also find the first step to be barrierless; However, we find the $CH_4{-}CH\cdot \longrightarrow C_2H_5\cdot$ step to have a barrier 11.5 kJ mol^{-1} above the reactants. This is similar to our result at the CC/t level of theory, where we find this step to have a barrier 7.7 kJ mol^{-1} above the reactants.

At the ωB/d and B3LYP/aug-cc-pvDZ levels of theory, we find the $CH_4{-}CH\cdot \longrightarrow C_2H_5\cdot$ step to be barrierless.

Because theory and experiment suggest the $CH_4{-}CH\cdot \longrightarrow C_2H_5\cdot$ step is not rate-limiting, we remove the barrier from this calculation. This adjustment leads to a BH/d calculated rate coefficient of $1.8{\times}10^{-10}$ cm^{3}s^{-1}, which is within the experimental range.

3.7.4.7 Case Study 7: $^3CH_2 + H \longleftrightarrow CH_{3(\nu)}\cdot \longleftrightarrow CH + H_2$

Reactions of $^3CH_2 + H$ and $CH + H_2$ are suggested to produce vibrationally excited $CH_{3(\nu)}$ [196]. This is what is to be expected when two reactants combine to form a single product [351]. In high atmospheric pressure, $CH_{3(\nu)}$ collisionally deexcites $CH_{3(\nu)} + M \longrightarrow CH_3 + M$ [196, 267]. In low atmospheric pressure, $CH_{3(\nu)}$ dissociates into $CH + H_2$ approximately 80% of the time, and $^3CH_2 + H$ approximately 20% of the time [392].

In previous work, we only included reactions $^3CH_2 + H \longrightarrow CH_3$ and $CH + H_2 \longrightarrow CH_3$ in the network [335]. These are only valid for high atmospheric pressures; Therefore, we modify the network to include the three-body reactions,

$$^3CH_2 + H + M \longrightarrow CH_3 + M,$$

$$CH + H_2 + M \longrightarrow CH_3 + M.$$

We calculate these rate coefficients at the BH/d level of theory to be $k = 4.8$ and $7.8{\times}10^{-29}$ cm^{6}s^{-1}, respectively.

We also include the two-body reactions,

$$^3CH_2 + H \longrightarrow CH_{3(\nu)}\cdot \longrightarrow CH + H_2,$$

$$CH + H_2 \longrightarrow CH_{3(\nu)}\cdot \longrightarrow {}^3CH_2 + H,$$

with adjusted calculated rate coefficients $k = 3.7{\times}10^{-10}$ and $5.4{\times}10^{-11}$ cm^{3}s^{-1}, respectively.

The rate coefficients for $^3CH_2 + H \longrightarrow CH_{3(\nu)}\cdot \longrightarrow CH + H_2$ and $CH + H_2 \longrightarrow CH_{3(\nu)}\cdot \longrightarrow {}^3CH_2 + H$ are reduced by 80% and 20% based on the $CH_{3(\nu)}$ dissociation probabilities calculated by González et al. (2011) [392].

The same treatment is applied to the reaction of excited state $^1CH_2$ with H. We calculate the reaction rate coefficient for $^1CH_2 + H + M \longrightarrow CH_3 + M$ to be 3.7×10^{-28} cm^6s^{-1}. We also adjust our previously calculated reaction rate coefficient for $^1CH_2 + H \longrightarrow CH_3$ [335] to dissociate along the channels $CH + H_2$ and $^3CH_2 + H$ with the same branching ratios as above. These new rate coefficients are 1.8×10^{-10} and 4.6×10^{-11} cm^3s^{-1}, respectively.

3.7.4.8 Case Study 8: $^1CH_2 + H_2 \longrightarrow CH_{4(\nu)}\cdot \longrightarrow CH_3 + H$

The reaction of $^1CH_2 + H_2$ proceeds through an excited methane molecule before most commonly decaying into $CH_3 + H$ [203, 204].

In previous work, we only included the reaction $^1CH_2 + H_2 \longrightarrow CH_4$ in the network [335]. This is only valid for high pressure environments; Therefore we now include the three-body reaction $^1CH_2 + H_2 + M \longrightarrow CH_4 + M$, and we apply our previously calculated rate coefficient to the two-body reaction $^1CH_2 + H_2 \longrightarrow CH_{4(\nu)}\cdot \longrightarrow CH_3 + H$, by assuming vibrational decay into $CH_3 + H$. These reactions have calculated rate coefficients k(298 K) = 1.4×10^{-27} cm^6s^{-1}, and 1.0×10^{-10} cm^3s^{-1}, at the BH/d level of theory, respectively.

3.7.4.9 Case Study 9: $CH + H \longrightarrow {}^3CH_{2(\nu)}\cdot \longrightarrow C + H_2$

The reaction of $CH + H$ proceeds through $^3CH_2$ before decaying into $C + H_2$ [435]. It is expected that the intermediate would be vibrationally exited [351].

In previous work, we only included $CH + H \longrightarrow {}^3CH_2$ in the network [335]; However, this is only valid in the high-pressure limit. We now include both the three-body reaction $CH + H + M \longrightarrow {}^3CH_2 + M$ and the low-pressure vibrational decay reaction $CH + H \longrightarrow {}^3CH_{2(\nu)}\cdot \longrightarrow C + H_2$ with calculated rate coefficients k(298) = 2.0×10^{-28} cm^6s^{-1}, and 6.9×10^{-10} cm^3s^{-1}, at the BH/d level of theory, respectively.

We also adjust our previously calculated reaction $CH + H \longrightarrow {}^1CH_2$ to be a three-body reaction with a low pressure rate coefficient of 4.4×10^{-31} cm^6s^{-1}. We assume that in low pressures the $^1CH_{2(\nu)}$ molecule vibrationally decays back into $CH + H$.

3.8 Quantum Chemistry Data

Quantum Chemistry Data has been moved to Appendix A at the end of this thesis.

Chapter 4

CRAHCN-O: A Consistent Reduced Atmospheric Hybrid Chemical Network Oxygen Extension for Hydrogen Cyanide and Formaldehyde Chemistry in CO_2-, N_2-, H_2O-, CH_4-, and H_2-Dominated Atmospheres

> *And what greater might do we possess as human beings than our capacity to question and to learn?*
>
> — **Ann Druyan**

Ben K. D. Pearce, Paul W. Ayers, & Ralph E. Pudritz

N.B. This chapter was published in The Journal of Physical Chemistry A (DOI: 10.1021/acs.jpca.0c06804) on September 22nd, 2020.

Abstract

Hydrogen cyanide (HCN) and formaldehyde (H_2CO) are key precursors to biomolecules such as nucleobases and amino acids in planetary atmospheres; However, many reactions which produce and destroy these species in atmospheres containing CO_2 and H_2O are still missing from the literature. We use a quantum chemistry approach to find these missing reactions and calculate their rate coefficients using canonical variational transition state theory and Rice–Ramsperger–Kassel–Marcus/master equation theory at the BHandHLYP/aug-cc-pVDZ level of theory. We calculate the rate coefficients for 126 total reactions, and validate our calculations by comparing with experimental data in the 39% of available cases. Our calculated rate coefficients are most frequently within a factor of 2 of experimental values, and generally always within an order of magnitude of these values. We discover 45 previously unknown reactions, and identify 6 from this list that are most likely to dominate H_2CO and HCN production and destruction in planetary atmospheres. We highlight $^1O + CH_3 \longrightarrow H_2CO + H$ as a new key source, and $H_2CO + {}^1O \longrightarrow HCO + OH$ as a new key sink, for H_2CO in upper planetary atmospheres. In this effort, we develop an oxygen extension to our consistent reduced atmospheric hybrid chemical network (CRAHCN-O), building off our previously developed network for HCN production in N_2-, CH_4- and H_2-dominated atmospheres (CRAHCN). This extension can be used to simulate both HCN and H_2CO production in atmospheres dominated by any of CO_2, N_2, H_2O, CH_4, and H_2.

4.1 Introduction

Hydrogen cyanide (HCN) and formaldehyde (H_2CO) are key precursors to various biomolecules required for the origin of life. The four nucleobases in RNA, i.e., adenine, guanine, cytosine and uracil, form in aqueous solutions containing one or both of these reactants [38, 106, 183]. Ribose, which pairs with phosphate to make up the backbone of RNA, forms from the oligomerization of H_2CO [9, 40]. Amino acids form via Strecker synthesis, which includes both HCN and an aldehyde (H_2CO for glycine) as reactants [8, 436].

Given their substantial role in producing biomolecules, HCN and H_2CO may be distinguishing atmospheric features of what we call *biogenic worlds*. These are worlds capable of producing key biomolecules rather than requiring they be delivered (e.g., by meteorites). It is presently unknown whether the early Earth was biogenic.

The redox state of the oldest minerals on the planet suggests the early Earth atmosphere was composed of "weakly reducing" gases, i.e., CO_2, N_2, and H_2O, with relatively smaller amounts of CH_4, CO, and H_2 [36, 170]. These atmospheric species are broken up into reactive radicals by UV radiation, lightning, and/or galactic cosmic rays (GCRs), which allows disequilibrium chemistry and the production of HCN and H_2CO to occur [36, 43]. The following pathways are possible from the dissociation of these "weakly reducing" species[193, 194, 437–439]:

$$\mathrm{CO_2} + h\nu \longrightarrow \mathrm{CO} + {}^3\mathrm{O} \tag{4.1}$$

$$\longrightarrow \mathrm{CO} + {}^1\mathrm{O} \tag{4.2}$$

$$\mathrm{N_2} + h\nu \longrightarrow {}^4\mathrm{N} + {}^2\mathrm{N} \tag{4.3}$$

$$\mathrm{CH_4} + h\nu \longrightarrow \mathrm{CH_3} + \mathrm{H} \tag{4.4}$$

$$\longrightarrow {}^3\mathrm{CH_2} + 2\,\mathrm{H} \tag{4.5}$$

$$\longrightarrow {}^1\mathrm{CH_2} + \mathrm{H_2} \tag{4.6}$$

$$\longrightarrow \mathrm{CH} + \mathrm{H_2} + \mathrm{H} \tag{4.7}$$

$$\mathrm{H_2O} + h\nu \longrightarrow \mathrm{OH} + \mathrm{H} \tag{4.8}$$

$$\mathrm{H_2} + h\nu \longrightarrow 2\,\mathrm{H} \tag{4.9}$$

where the superscripts, ^{1}, ^{2}, ^{3}, and ^{4} refer to the singlet, doublet, triplet and quartet electronic spin states.

One way to better understand the biogenicity of the early Earth, is to use chemical kinetic models to simulate the production of HCN and H_2CO in plausible early Earth atmospheres. Atmospheric simulations of these species for primitive Earth conditions have been performed in the past [43, 107, 125], which make use of collections of reaction rate coefficients typically gathered from various sources the literature (e.g. experiment, theoretical simulations, thermodynamics, similar reactions).

The literature, however, is still missing several reactions between the radicals produced in CO_2-, N_2-, H_2O-, CH_4-, and H_2-dominated atmospheres, and these reactions may be crucial to understanding HCN and H_2CO chemistry in early Earth and other terrestrial environments. The largest gap in rate coefficient data is for reactions involving electronically excited species, e.g. ^1O, ^2N, and $^1CH_2$, which are directly produced from the dissociation of CO_2, N_2, and CH_4, respectively.

In Pearce et al. [335, 440], we developed an accurate and feasible method making use of computational quantum chemistry coupled with canonical variational transition state theory (CVT) [207] and Rice–Ramsperger–Kassel–Marcus/master equation (RRKM/ME) theory [151] to calculate a large network of reaction rate coefficients for one-, two- and three-body reactions. We first used this method to explore the entire field of possible reactions for a list of primary species in N_2-, CH_4-, and H_2-dominated atmospheres, and uncovered 48 previously unknown reactions; many of which were based on excited species such as ^2N and $^1CH_2$. We then built an initial reduced network of 104 reactions based on this exploratory study, and used it to simulate HCN production in Titan's atmosphere [440]. This approach provided us with a more complete picture of HCN chemistry on Titan, as one of our newly discovered reactions was found to be one of the four dominant channels to HCN production on Titan [440].

In this work, we use the same theoretical approach to expand upon our initial network, by exploring and calculating all the potential reactions between three key oxygen species present on the early Earth (CO_2, H_2O, H_2CO), their dissociation radicals (CO, ^3O, ^1O, OH, and HCO), and all the non-oxygen primary species in our network (see Table 4.1 for the list of primary species). In this effort, we discover 45 brand new reactions, which are mainly based on HCO, H_2CN, ^1O, ^2N, $^1CH_2$, and CH. We calculate the rate coefficients for a total of 126 reactions, and validate our calculations by comparing with experimental data in the 39% of available cases.

Finally, we build the consistent reduced atmospheric hybrid chemical network oxygen extension (CRAHCN-O), composed of experimental rate coefficients when available, and our calculated values otherwise. CRAHCN-O is the amalgamation of the network developed in Pearce et al. [440], and the oxygen reactions explored in this work. This network can be used to accurately simulate HCN and H_2CO production in CO_2-, N_2-, H_2O-, CH_4-, and H_2-dominated atmospheres.

The paper is outlined as follows: In the Methods section, we detail the theoretical and computational approach we use to explore reactions and calculate their rate coefficients. In the Results section, we describe the results of our rate coefficient calculations, including their agreement with any available experiments. We also discuss the limitations of our theoretical approach. In the Discussion section, we highlight 6 new reactions from this work which are potentially key production and destruction pathways to H_2CO and HCN in planetary atmospheres. We also summarize CRAHCN-O and describe how it can be used for other atmospheric models. Finally, in the Conclusions section, we summarize the main conclusions from this work.

The Supporting Information (SI) contains two tables summarizing the new CRAHCN-O rate coefficient data (the non-oxygen reaction data can be found in Pearce et al. [440]), any experimental rate coefficient data for reactions calculated in this work, the Lennard-Jones parameters used for three-body reaction rate coefficient calculations, a breakdown of some of the non-standard reaction calculations, and the quantum chemistry data used in our calculations.

Table 4.1: List of primary molecular species involved in this study and their spin states. Reactions strictly between non-oxygen species (below center line) were explored in Pearce et al. [335, 440]. Reactions involving the oxygen species (above center line) are new to this study.

Species	Spin state	Ground/Excited state
CO_2	singlet	ground
H_2CO	singlet	ground
HCO	doublet	ground
CO	singlet	ground
H_2O	singlet	ground
OH	doublet	ground
^3O	triplet	ground
^1O	singlet	excited
H_2CN	doublet	ground
HCN	singlet	ground
CN	doublet	ground
N_2	singlet	ground
NH	triplet	ground
^2N	doublet	excited
^4N	quartet	ground
CH_4	singlet	ground
CH_3	doublet	ground
$^1CH_2$	singlet	excited
$^3CH_2$	triplet	ground
CH	doublet	ground
H_2	singlet	ground
H	doublet	ground

4.2 Methods

There are four phases to this work: First we explore all the potential reactions between eight oxygen species (CO_2, CO, ^3O, ^1O, H_2O, OH, H_2CO, and HCO) and the primary species in Table 4.1. These species are the the dominant sources of oxygen in the early Earth atmosphere (CO_2 and H_2O), a key biomolecule precursor (H_2CO) and their dissociation radicals. In this process, we characterize 81 known reactions and discover 45 previously unknown reactions. Second, we calculate the rate coefficients for every reaction that we find at 298 K, and validate the calculations by comparing to experimental data when available (in 39% of cases). Third, we calculate the temperature dependencies for the reactions that have no experimental measurements and have barriers (i.e. strong temperature dependencies from 50–400 K). Last, we gather the experimental and theoretical rate coefficients into the consistent reduced atmospheric hybrid chemical network oxygen extension (CRAHCN-O), which contains experimental values when available, and our calculated rate coefficients otherwise.

4.2.1 Computational Quantum Method and Basis Set

All exploration and rate coefficient calculations are performed with the Becke-Half-and-Half-Lee-Yang-Parr[1] (BHandHLYP) density functional and the augmented correlation-consistent polarized valence double-ζ (aug-cc-pVDZ) basis set [216, 217, 342–344].

We have four key reasons for choosing this level of theory to perform our calculations:

1) We have benchmarked BHandHLYP/aug-cc-pVDZ rate coefficient calculations by comparing with experimental values in the past, and this method most frequently provides the best accuracy with respect to agreement with experimental values in comparison with other widely used, computationally cost effective methods.

In Pearce et al. [440], we compared the accuracy of 3 methods for calculating 12 reaction rate coefficients. We found BHandHLYP/aug-cc-pVDZ rate coefficient calculations give the best, or equal to the best agreement with experiment in 8 out of 12 cases. This is compared to ωB97XD/aug-cc-pVDZ and CCSD/aug-cc-pVTZ, which gave the best, or equal to the best agreement with experiment in 7 out of 12 and 6 out of 12 cases, respectively [440]. In another method-comparison study on a single

---

[1] This hybrid functional uses 50% Hartree-Fock (HF) and 50% density functional theory (DFT) for the exchange energy calculation, offering a compromise between HF, which tends to overestimate energy barriers, and DFT, which tends to underestimate energy barriers.

reaction between BHandHLYP, CCSD, CAM-B3LYP, M06-2x, B3LYP and HF, all with the aug-cc-pVDZ basis set, we found that only BHandHLYP and CAM-B3LYP provide rate coefficients within the experimental range [335].

2) BHandHLYP/aug-cc-pVDZ calculations paired with CVT and RRKM/ME theory typically compute rate coefficients within a factor of two of experimental values, and all calculations generally fall within an order of magnitude of experimental values. This accuracy is consistent with typical uncertainties assigned in large-scale experimental data evaluations [137, 247].

For examples in our network, Baulch et al. [137] assign uncertainties of 2–3 to $HCO + HCO \longrightarrow H_2CO + CO$ and ${}^3O + CH \longrightarrow CO + H$ and order-of-magnitude uncertainties to $CO_2 + CH \longrightarrow$ products, $H_2O + CH \longrightarrow$ products, and $H_2CO + CH \longrightarrow$ products.

3) BHandHLYP/aug-cc-pVDZ calculations are computationally cost effective, and therefore feasible for a large scale exploratory study such as ours.

We have also shown in previous work for 12 rate coefficients, that increasing the basis set to the more computationally expensive aug-cc-pVTZ level does not increase the accuracy of our calculations with respect to agreement with experimental values [440].

4) Finally, using the BHandHLYP/aug-cc-pVDZ level of theory for all the calculations in this oxygen extension allows us to maintain consistency with the calculations in the original network (CRAHCN [440]).

4.2.2 Reaction Exploration

Using the Gaussian 09 software package [214], we perform a thorough search for reactions between eight oxygen species (CO_2, CO, ${}^3O$, ${}^1O$, H_2O, OH, H_2CO, and HCO) and the 22 primary species in this study (see Table 4.1). The procedure below is carried out for 8×22 = 176 pairs of species.

Using the Avogadro molecular visualization software [148, 441], we placed each species at a handful of different distances and orientations form its reaction partner. We use a bit of chemical intuition when determining the distance between the species, e.g., abstraction reactions in our network tend to occur at short separations (1–2 Å), whereas addition reactions tend to be longer range (2–6 Å).

We then copy the geometries into Gaussian input files, and use the 'opt=modredundant' option to freeze the bond distances between one atom of each species. We run the

Gaussian simulations with vibrational analyses to allow us to identify whether points along the MEP were found. A point along a MEP is identified by a single negative frequency that oscillates in the direction of the reaction. We run multiple simulations to look for possible abstraction, addition, and bond insertion reactions. For reactions that form a single product, we continue the exploration of that product by searching for efficient decay and/or isomerization pathways. In many cases, we find the product efficiently decays into other products, sometimes after one or more isomerizations.

For cases where our above approach fails to find a MEP, we have developed a Python program that can be used to perform a more thorough scan of the potential energy surface. This program takes two species geometries as input, selects, e.g., 10 random separations and orientations for those species, and runs those Gaussian simulations in parallel. This program is especially useful for MEPs that turn out to be not strictly intuitive (e.g. $\mathrm{OH} + {}^1\mathrm{CH}_2$).

Once we find a point along a MEP, we then characterize the reaction path by doing a coarse-grain scan backwards and forwards from the identified point in intervals of 0.1Å. We then plot the Gibbs free energies of these optimized points along the reaction path, and analyze the points using Avogadro to find the rough location(s) of the transition state(s). In several cases we find more than one transition state along a reaction path, with one or more stable structures between the reactants and the products.

4.2.3 Rate coefficient calculations

4.2.3.1 One- and Two-body Reactions

We calculate one- and two-body reaction rate coefficients using canonical variational transition state theory (CVT). This is a statistical mechanics approach which makes use of the canonical ensemble. This method can be used to calculate rate coefficients for reactions with and without energy barriers [207].

CVT can be explained as follows. There is a point that is far enough along the minimum energy reaction path (MEP), that the reactants that cross over this point are unlikely to cross back. This point is defined as the location where the generalized transition state (GT) rate coefficient is at its smallest value, therefore providing best dynamical bottleneck [207]. This is expressed as: [146]

$$k_{CVT}(T,s) = \min_{s} \left\{ k_{GT}(T,s) \right\}. \tag{4.10}$$

where $k_{GT}(T,s)$ is the generalized transition state theory rate coefficient, T is the temperature, and s is a point along the MEP (e.g. bond distance).

To find the location along the MEP where the rate coefficient is at a minimum, we use the maximum Gibbs free energy criterion [146, 147]. It can be seen from the quasi-thermodynamic equation of transition-state theory that the maximum value for $\Delta G_{GT}(T,s)$ corresponds to a minimum value for $k_{GT}(T,s)$.

$$k_{GT}(T,s) = \frac{k_B T}{h} K^0 e^{-\Delta G_{GT}(T,s)/RT}, \tag{4.11}$$

where K^0 is the reaction quotient under standard state conditions (i.e. 1 cm^3 for second-order reactions, 1 cm^6 for third-order reactions), and $\Delta G_{GT}(T,s)$ is the difference in the Gibbs free energy between transition state and reactants (kJ mol^{-1}).

This method offers a compromise of energetic and entropic effects, as ΔG contains both enthalpy and entropy [146, 147]. To obtain a similar accuracy for all calculations, we refine our coarse grain scans near the Gibbs maxima to a precision of 0.01 Å.

The generalized transition state theory rate coefficient, neglecting effects due to tunneling, can be calculated with the equation[146, 149]

$$k_{GT}(T,s) = \sigma \frac{k_B T}{h} \frac{Q^{\ddagger}(T,s)}{\prod_{i=1}^{N} Q_i^{n_i}(T)} e^{-E_0(s)/RT}. \tag{4.12}$$

where σ is the reaction path multiplicity, k_B is the Boltzmann constant (1.38×10^{-23} J K^{-1}), T is temperature (K), h is the Planck constant (6.63×10^{-34} J·s), $Q^{\ddagger}$ is the partition function of the transition state per unit volume (cm^{-3}), with its zero of energy at the saddle point, Q_i is the partition function of species i per unit volume, with its zero of energy at the equilibrium position of species i, n_i is the stoichiometric coefficient of species i, N is the number of reactant species, E_0 is the difference in zero-point energies between the generalized transition state and the reactants (kJ mol^{-1}) (0 for barrierless reactions), and R is the gas constant (8.314×10^{-3} kJ K^{-1} mol^{-1}).

The partition functions per unit volume have four components and are gathered from the Gaussian output files,

$$Q = \frac{q_t}{V} q_e q_v q_r . \tag{4.13}$$

where V is the volume (cm^{-3}) and the t, e, v, and r subscripts stand for translational, electronic, vibrational, and rotational, respectively.

In some cases, there are multiple steps (i.e. transition states) to a single reaction, and we must use mechanistic modeling in order to determine the steady-state solution of the overall rate equation. We place an example of a mechanistic model in Case Study 9 in the SI.

4.2.3.2 Three-body reactions

In the cases where two reactants form a single product, a colliding third body is required to remove excess vibrational energy from the product to prevent it from dissociating [351]. This is expressed as,

$$\mathrm{A} + \mathrm{B} \longrightarrow \mathrm{C}_{(\nu)} \tag{4.14}$$

$$C_{(\nu)} \xrightarrow{+M} C. \tag{4.15}$$

The rate coefficient for these three-body reactions is expressed as[352]:

$$k([M]) = \frac{k_0[M]/k_\infty}{1 + k_0[M]/k_\infty} k_\infty \tag{4.16}$$

where k_0 is the third-order low-pressure limit rate coefficient (cm^{6}s^{-1}), [M] is the number density of the colliding third body, and k_∞ is the second-order high-pressure limit rate coefficient (cm^{3}s^{-1}).

The high-pressure limit rate coefficients are equivalent to the two-body reaction rate coefficients (i.e., $\mathrm{A} + \mathrm{B} \longrightarrow \mathrm{C}$), and can be calculated using CVT as above. We make use of the ktools code of the Multiwell Program Suite for the high pressure limit rate coefficient calculations [353–355].

The low-pressure limit rate coefficients, on the other hand, require information about the collisional third body for their calculation. To calculate these values, we use the Multiwell Master Equation (ME) code, which employs RRKM theory. The ME contains the probabilities that the vibrationally excited product will be stabilized by a colliding third body [356]. Multiwell employs Monte Carlo sampling of the ME to build up a statistical average for the two outcomes of the reaction (i.e., destabilize back into reactants, or stabilize the product).

With the output from these stochastic trials, we calculate the low-pressure limit rate coefficient with the following equation [135, 354]:

$$k_0([M]) = \frac{k_\infty f_{prod}}{[M]} \tag{4.17}$$

where k_∞ is the high-pressure limit rate coefficient, f_{prod} is the fractional yield of the collisionally stabilized product, and [M] is the simulation number density (cm^{-3}), which we lower until k_0 converges.

We simulate three-body reactions using three different colliding bodies, corresponding to potential dominant species in the early Earth atmosphere (N_2, CO_2, and H_2). The energy transfer was treated with a standard exponential-down model with $< \Delta E >_{down} = 0.8$ T K^{-1} cm^{-1} [357, 358]. The Lennard-Jones parameters for the bath gases and all the products were taken from the literature [359–361] and can be found in Table S4.

In some cases, when two reactants come together to form a single product, the vibrationally excited product preferably decays along a different channel into something other than the original reactants (e.g. $^1\mathrm{O} + \mathrm{H_2} \longrightarrow \mathrm{H_2O_{(\nu)}} \cdot \longrightarrow \mathrm{OH} + \mathrm{H}$). In these cases, we also include the second-order reactions to these favourable decay pathways in our network. We verify the preferred decay pathways of vibrationally excited molecules by looking at previous experimental studies.

4.2.3.3 Temperature dependencies

For the one- and two-body reactions in this study with barriers, and no experimental measurements, we calculate temperature dependencies for the rate coefficients in the 50–400 K range. Barrierless reaction rate coefficients do not typically vary by more than a factor of ∼3 between 50 and 400 K [208, 219–222]. To obtain temperature dependencies, we calculate the rate coefficients at 50, 100, 200, 298.15, and 400 K and fit the results to the modified Arrhenius expression

$$k(T) = \alpha \left(\frac{T}{300}\right)^{\beta} e^{-\gamma/T}, \tag{4.18}$$

where $k(T)$ is the temperature-dependent second-order rate coefficient ($\mathrm{cm^3 s^{-1}}$), α, β, and γ are fit parameters, and T is temperature (in K).

4.3 Results

4.3.1 Comparison with Experiments

In Table 4.2 we display the three-body high- and low-pressure limit calculated rate coefficients at 298 K. Out of these 31 reactions, 12 have experimentally measured high-pressure limit rate coefficients. For the low-pressure limit rate coefficients, 9 of the 31 reactions have experimental measurements; However, the bath gases used in the low-pressure experiments often differ from the colliding third bodies in our calculations (i.e. N_2, CO_2, and H_2). When using several different bath gases, low-pressure limit rate coefficients tend to range by ~ an order of magnitude [137, 442–444].

Table 4.2: Lindemann coefficients for the three body reactions in this paper, calculated at 298 K, and valid within the 50–400 K temperature range. k_∞ and k_0 are the third-order rate coefficients in the high and low pressure limits, with units $\mathrm{cm^3 s^{-1}}$ and $\mathrm{cm^6 s^{-1}}$, respectively. These values are for usage in the pressure-dependent rate coefficient equation $k = \frac{k_0[M]/k_\infty}{1+k_0[M]/k_\infty} k_\infty$. Calculations are performed at the BHandHLYP/aug-cc-pVDZ level of theory. Low-pressure limit rate coefficients are calculated for three different bath gases (N_2, CO_2, and H_2). Reactions with rate coefficients slower than $k_\infty = 10^{-13}$ $\mathrm{cm^3 s^{-1}}$ are not included in this network. The error factor is the multiplicative or divisional factor from the nearest experimental or suggested value.

No.	Reaction equation	$k_\infty(298)$ calc.	$k_\infty(298)$ exp.	Error_∞	$k_0(298)$ calc.	$k_0(298)$ exp.	Error_0
*1.	$CO_2 + {}^1O + M \longrightarrow CO_3 + M$	3.8×10^{-11}	$0.1\text{–}23\times10^{-11}$	1	($M=N_2$) 3.0×10^{-29} (CO_2) 3.1×10^{-29} (H_2) 6.7×10^{-29}		
*2.	$HCO + {}^2N + M \longrightarrow$ $HCON\cdot + M\cdot \longrightarrow HCNO + M$	2.0×10^{-11}			(N_2) 5.0×10^{-30} (CO_2) 5.6×10^{-30} (H_2) 9.7×10^{-30}		
*3.	$HCO + CH_3 + M \longrightarrow$ $CH_3CHO + M$	5.7×10^{-12}	$6.3\text{–}44\times10^{-12}$	1	(N_2) 5.3×10^{-27} (CO_2) 6.4×10^{-27} (H_2) 1.2×10^{-27}		
4.	$HCO + H + M \longrightarrow H_2CO + M$	4.9×10^{-11}			(N_2) 7.4×10^{-30} (CO_2) 9.5×10^{-30} (H_2) 1.4×10^{-29}		
*5.	$CO + CN + M \longrightarrow NCCO + M$	6.0×10^{-12}			(N_2) 6.2×10^{-31} (CO_2) 6.8×10^{-31} (H_2) 1.3×10^{-30}		
6.	$CO + {}^1O + M \longrightarrow CO_2 + M$	2.8×10^{-11}	$0.3\text{–}7\times10^{-11}$	1	(N_2) 2.8×10^{-30} (CO_2) 3.0×10^{-30} (H_2) 5.9×10^{-30}	(CO_2) 2.8×10^{-29} " "	10 9 5
*7.	$CO + {}^1CH_2 + M \longrightarrow$ $CH_2CO + M$	1.3×10^{-11}			(N_2) 1.7×10^{-28} (CO_2) 1.9×10^{-28} (H_2) 3.3×10^{-28}		
8.	$CO + CH + M \longrightarrow HCCO + M$	4.6×10^{-11}	$0.5\text{–}17\times10^{-11}$	1	(N_2) 1.2×10^{-29} (CO_2) 1.3×10^{-29}	(Ar,He) $2.4\text{–}4.1\times10^{-30}$ "	3 3

					(H_2) 2.4×10^{-29}	"	6
9.	$CO + H + M \longrightarrow HCO + M$	2.7×10^{-12}			(N_2) 1.8×10^{-33}	(Ne,H_2) 0.5–3.3×10^{-34}	5
					(CO_2) 2.1×10^{-33}	(CO,H_2) 0.8–3.3×10^{-34}	6
					(H_2) 3.4×10^{-33}	(H_2) 0.8–3.3×10^{-34}	10
*10.	$OH + H_2CN + M \longrightarrow H_2CNOH + M$	6.9×10^{-12}	6.0×10^{-12}	1	(N_2) 6.5×10^{-30}		
					(CO_2) 7.4×10^{-30}		
					(H_2) 1.3×10^{-29}		
*11.	$OH + CN + M \longrightarrow HOCN + M$	1.0×10^{-12}			(N_2) 2.7×10^{-30}		
					(CO_2) 2.9×10^{-30}		
					(H_2) 5.1×10^{-30}		
12.	$OH + OH + M \longrightarrow H_2O_2 + M$	2.3×10^{-11}	1.5–6.5×10^{-11}	1	(N_2) 4.9×10^{-32}	(N_2) 5.1–330×10^{-32}	1
					(CO_2) 5.5×10^{-32}	(CO_2) 6.4–420×10^{-32}	1
					(H_2) 9.9×10^{-32}	(He,H_2O) 1.3–1800×10^{-32}	1
*13.	$OH + {}^3O + M \longrightarrow HO_2 + M$	7.4×10^{-11}			(N_2) 8.5×10^{-32}		
					(CO_2) 9.4×10^{-32}		
					(H_2) 1.8×10^{-31}		
*14.	$OH + {}^1O + M \longrightarrow HO_2 + M$	1.0×10^{-9}			(N_2) 4.1×10^{-30}		
					(CO_2) 4.5×10^{-30}		
					(H_2) 8.3×10^{-30}		
15.	$OH + NH + M \longrightarrow OH \cdots NH\cdot + M\cdot \longrightarrow trans{-}HNOH + M$	7.0×10^{-12}			(N_2) 8.5×10^{-31}		
					(CO_2) 9.2×10^{-31}		
					(H_2) 1.7×10^{-30}		
16.	$OH + CH_3 + M \longrightarrow OH \cdots CH_3\cdot + M\cdot \longrightarrow CH_3OH + M$	2.0×10^{-11}	9.3–17×10^{-11}	5	(N_2) 2.1×10^{-27}	(He,SF_6) 2.0–7.2×10^{-27}	1
					(CO_2) 2.3×10^{-27}	"	1
					(H_2) 3.8×10^{-27}	"	1
17.	$OH + H + M \longrightarrow H_2O + M$	2.4×10^{-10}			(N_2) 3.0×10^{-31}	(N_2) 4.8–6.8×10^{-31}	2
					(CO_2) 3.7×10^{-31}	(CO_2) 9.0×10^{-31}	2
					(H_2) 5.1×10^{-31}	(He,H_2O) 1.5–6.8×10^{-31}	1
*18.	${}^3O + CN + M \longrightarrow NCO + M$	7.1×10^{-12}	9.4–16×10^{-12}	1	(N_2) 1.3×10^{-30}		
					(CO_2) 1.5×10^{-30}		
					(H_2) 2.6×10^{-30}		
19.	${}^3O + {}^3O + M \longrightarrow O_2 + M$	1.8×10^{-11}			(N_2) 3.0×10^{-34}	(N_2) 3.1–10×10^{-33}	10
					(CO_2) 3.2×10^{-34}	(Ar, O_2) 3.9–100×10^{-34}	1
					(H_2) 6.1×10^{-34}	(Ar, N_2) 3.9–100×10^{-34}	1
20.	${}^3O + {}^4N + M \longrightarrow NO + M$	6.6×10^{-11}			(N_2) 1.6×10^{-33}	(N_2) 5–11×10^{-33}	3
					(CO_2) 1.8×10^{-33}	(CO_2) 1.8×10^{-32}	10
					(H_2) 3.3×10^{-33}	(He, N_2) 3.8–11×10^{-33}	1
*21.	${}^3O + {}^3CH_2 + M \longrightarrow H_2CO + M$	6.7×10^{-11}	1.9–20×10^{-11}	1	(N_2) 9.2×10^{-29}		
					(CO_2) 1.1×10^{-28}		
					(H_2) 1.7×10^{-28}		
*22.	${}^3O + CH + M \longrightarrow HCO + M$	1.1×10^{-10}	6.6–9.5×10^{-11}	1	(N_2) 5.2×10^{-30}		
					(CO_2) 6.2×10^{-30}		
					(H_2) 9.9×10^{-30}		
23.	${}^3O + H + M \longrightarrow OH + M$	3.5×10^{-10}			(N_2) 2.6×10^{-33}	(M) 1–8000×10^{-33}	1
					(CO_2) 2.9×10^{-33}	"	1
					(H_2) 4.6×10^{-33}	"	1
*24.	${}^1O + HCN + M \longrightarrow HCNO + M$	3.3×10^{-11}			(N_2) 4.0×10^{-29}		
					(CO_2) 4.6×10^{-29}		
					(H_2) 8.0×10^{-29}		
*25.	${}^1O + CN + M \longrightarrow NCO + M$	8.9×10^{-11}			(N_2) 1.9×10^{-29}		
					(CO_2) 2.1×10^{-29}		
					(H_2) 3.6×10^{-29}		

*26.	$^1O + ^1O + M \longrightarrow O_2 + M$	2.3×10^{-10}			(N_2) 8.8×10^{-33} (CO_2) 9.6×10^{-33} (H_2) 1.8×10^{-32}
*27.	$^1O + CH_4 + M \longrightarrow CH_3OH + M$	5.8×10^{-9}	$1.4\text{–}4.0\times10^{-10}$	15	(N_2) 3.6×10^{-23} (CO_2) 3.9×10^{-23} (H_2) 6.3×10^{-23}
*28.	$^1O + ^1CH_2 + M \longrightarrow H_2CO + M$	3.3×10^{-10}			(N_2) 6.6×10^{-27} (CO_2) 7.7×10^{-27} (H_2) 1.2×10^{-26}
*29.	$^1O + CH + M \longrightarrow HCO + M$	9.2×10^{-11}			(N_2) 4.9×10^{-29} (CO_2) 5.8×10^{-29} (H_2) 9.1×10^{-29}
*30.	$^1O + H_2 + M \longrightarrow H_2O + M$	7.1×10^{-10}	$1.1\text{–}3.0\times10^{-10}$	2	(N_2) 1.2×10^{-29} (CO_2) 1.4×10^{-29} (H_2) 2.0×10^{-29}
*31.	$^1O + H + M \longrightarrow OH + M$	1.1×10^{-9}			(N_2) 1.4×10^{-32} (CO_2) 1.5×10^{-32} (H_2) 2.3×10^{-32}

∗ Reactions with no previously known rate coefficients.

Our calculated high-pressure rate coefficients are within the range of experimental values in 9 out of 12 cases. The other three rate coefficients are factors of 2, 5, and 15 from the nearest experimental values. Typical uncertainties for rate coefficients–as assigned in large experimental data evaluations–range from factors of 2–10 [137, 247]; Therefore, this calculated accuracy is consistent with the levels of uncertainty typically found in the literature.

Each low-pressure limit rate coefficient was calculated for three bath gases (N_2, CO_2, and H_2) and compared to experiments performed with matching bath gases when possible, and any bath gases otherwise. Nine of the reactions had experimentally measured low-pressure limit rate coefficients for one or more bath gases. All of our calculated rate coefficients for these reactions landed within an order of magnitude of the experimental range for the matching bath gas when possible, or another bath gas otherwise. Most commonly (67% of the time), our rate coefficients were within a factor of 3 from the nearest experimental measurement. Larger deviations tended to occur for cases that only have a single experimental measurement for comparison.

In Table 4.3, we display the 95 one- and two-body reaction rate coefficients calculated at 298K with any experimental or suggested values. 47 of these reactions have experimental or suggested values, and our calculations are within approximately one order of magnitude of these values in all but one case. In 60% of cases our calculated rate coefficients are within a factor of 2 of experimental values, and in 83% of cases our calculated rate coefficients are within a factor of 6 of experimental values.

In one case, $OH + CH_4 \longrightarrow H_2O + CH_3$, our calculated rate coefficient has a slightly higher than an order of magnitude deviation from experiment (factor of 54). We attribute this error to the lack of a quantum tunneling correction in our calculations. Bravo-Pérez et al. [445] performed transition state theory calculations for this reaction at the BHandHLYP/6-311G(d,p) level of theory, and calculated a tunneling factor of 30.56 at 298 K using an Eckart model. If we applied this factor to our calculation, our rate coefficient would be within a factor of two of the experimental range.

Table 4.3: Calculated reaction rate coefficients at 298 K for the one- and two-body reactions in this paper. Calculations are performed at the BHandHLYP/aug-cc-pVDZ level of theory. Reactions with rate coefficients slower than $k = 10^{-21}$ are not included in this network. The precense or absence of an energy barrier in the rate-limiting step (or the only step) of the reaction is specified. The error factor is the multiplicative or divisional factor from the nearest experimental or suggested value; the error factor is 1 if the calculated value is within the range of experimental or suggested values. First-order rate coefficients have units s^{-1}. Second-order rate coefficients have units cm^3s^{-1}.

No.	Reaction equation	Forw./Rev.	Barrier?	k(298) calculated	k(298) experimental	Error factor
*32.	$NCCO \longrightarrow CO + CN$	F	Y	9.4×10^{-12}		
33.	$CO_2 + {}^1O \longrightarrow {}^1CO_3\cdot \longrightarrow {}^3CO_3\cdot \longrightarrow CO_2 + {}^3O$	F	N	3.8×10^{-11}	$0.1–23\times10^{-11}$	1
34.	$CO_2 + {}^2N \longrightarrow NCO_2\cdot \longrightarrow OCNO\cdot \longrightarrow CO + NO$	F	^{a}Y	3.2×10^{-14}	$1.8–6.8\times10^{-13}$	6
35.	$CO_2 + {}^1CH_2 \longrightarrow {}^1CH_2CO_2\cdot \longrightarrow H_2CO + CO$	F	N	8.0×10^{-13}		
36.	$CO_2 + CH \longrightarrow CHCO_2\cdot \longrightarrow HCOCO\cdot \longrightarrow HCO + CO$	F	^{b}N	3.1×10^{-12}	$1.8–2.1\times10^{-12}$	1
37.	$H_2O_2 \longrightarrow OH + OH$	F	Y	5.1×10^{-9}		
38.	$H_2CO + CN \longrightarrow HCN + HCO$	F	N	1.7×10^{-11}	1.7×10^{-11}	1
39.	$H_2CO + OH \longrightarrow r,l\text{-}H_2COHO\cdot \longrightarrow trans{-}HCOHO\cdot + H\cdot \longrightarrow H_2O + CO + H$	F	Y	7.1×10^{-17}		
40.	$H_2CO + OH \longrightarrow H_2CO \cdots HO\cdot \longrightarrow H_2O + HCO$	F	Y	1.1×10^{-12}	$6.1–15\times10^{-12}$	6
41.	$H_2CO + {}^3O \longrightarrow HCO + OH$	F	Y	6.8×10^{-14}	$1.5–1.9\times10^{-13}$	2
*42.	$H_2CO + {}^1O \longrightarrow H_2CO_2\cdot \longrightarrow HCO_2H\cdot \longrightarrow HCO + OH$	F	N	4.6×10^{-10}		
43.	$H_2CO + CH_3 \longrightarrow HCO + CH_4$	F	Y	1.9×10^{-19}	$2.2–4.2\times10^{-18}$	12
44.	$H_2CO + {}^3CH_2 \longrightarrow HCO + CH_3$	F	Y	1.1×10^{-14}	$<1.0\times10^{-14}$	1
45.	$H_2CO + {}^1CH_2 \longrightarrow HCO + CH_3$	F	N	1.5×10^{-12}	2.0×10^{-12}	1
46.	$H_2CO + CH \longrightarrow H_2COCH_a\cdot \longrightarrow H_2COCH_b\cdot \longrightarrow CH_2HCO\cdot \longrightarrow CH_3CO\cdot \longrightarrow CO + CH_3$	F	N	3.1×10^{-11}	3.8×10^{-10}	12
47.	$H_2CO + CH \longrightarrow H_2COCH_c\cdot \longrightarrow HCO + {}^3CH_2$	F	N	1.1×10^{-12}		
48.	$H_2CO + H \longrightarrow HCO + H_2$	F	Y	1.8×10^{-13}	$3.9–6.7\times10^{-14}$	3
*49.	$HCO + H_2CN \longrightarrow H_2CO + HCN$	F	Y	7.0×10^{-15}		
50.	$HCO + HCO \longrightarrow trans{-}C_2H_2O_2\cdot \longrightarrow anti{-}HCOH\cdot + CO\cdot \longrightarrow H_2CO + CO$	F	Y	1.2×10^{-13}	$2.8–750\times10^{-13}$	2
51.	$HCO + HCO \longrightarrow cis{-}C_2H_2O_2\cdot \longrightarrow CO + CO + H_2$	F	N	7.4×10^{-11}	3.6×10^{-11}	2
52.	$HCO + CN \longrightarrow HCOCN\cdot \longrightarrow CO + HCN$	F	N	5.4×10^{-12}		
53.	$HCO + OH \longrightarrow trans{-}HCOHO\cdot \longrightarrow CO + H_2O$	F	N	7.0×10^{-12}	$5–18\times10^{-11}$	7
54.	$HCO + {}^3O \longrightarrow HCO_2\cdot \longrightarrow CO_2 + H$	F	N	2.6×10^{-11}	5.0×10^{-11}	2
55.	$HCO + {}^3O \longrightarrow CO + OH$	F	N	3.4×10^{-11}	5.0×10^{-11}	1
*56.	$HCO + {}^1O \longrightarrow HCO_2\cdot \longrightarrow CO_2 + H$	F	N	1.5×10^{-10}		
*57.	$HCO + NH \longrightarrow H_2CO + {}^4N$	F	Y	3.6×10^{-20}		

*58.	$HCO + NH \longrightarrow CO + NH_2$ and $HCO + NH \longrightarrow HNHCO\cdot \longrightarrow H_2NCO\cdot \longrightarrow CO + NH_2$	F	N	1.4×10^{-11}		
59.	$HCO + {}^4N \longrightarrow {}^3NCOH\cdot \longrightarrow NCO + H$	F	N	2.8×10^{-11}		
60.	$HCO + {}^4N \longrightarrow CO + NH$	F	N	2.2×10^{-11}		
*61.	$HCO + {}^2N \longrightarrow {}^3NCOH\cdot \longrightarrow NCO + H$	F	N	6.6×10^{-11}		
*62.	$HCO + {}^2N \longrightarrow CO + NH$	F	N	4.8×10^{-11}		
63.	$HCO + CH_3 \longrightarrow CO + CH_4$	F	N	1.0×10^{-11}	3.6×10^{-11}–2.0×10^{-10}	4
64.	$HCO + {}^3CH_2 \longrightarrow CH_3 + CO$ and $HCO + {}^3CH_2 \longrightarrow CH_2HCO\cdot \longrightarrow CH_3CO\cdot \longrightarrow CH_3 + CO$	F	N	2.1×10^{-11}	3.0×10^{-11}	1
65.	$HCO + {}^1CH_2 \longrightarrow CH_2HCO\cdot \longrightarrow CH_3CO\cdot \longrightarrow CH_3 + CO$	F	N	1.2×10^{-11}	3.0×10^{-11}	3
66.	$HCO + CH \longrightarrow CO + {}^3CH_2$	F	N	1.5×10^{-11}		
*67.	$HCO + CH \longrightarrow CO + {}^1CH_2$	F	N	4.6×10^{-12}		
68.	$HCO + H \longrightarrow CO + H_2$ and $HCO + H \longrightarrow H_2CO_{(v)}\cdot \longrightarrow CO + H_2$	F	N	6.9×10^{-11}	1.1–5.5×10^{-10}	2
69.	$HCO + H \longrightarrow H_2CO_{(v)}\cdot \longrightarrow CO + H + H$	F	N	2.4×10^{-11}		
70.	$HCO \longrightarrow CO + H$	F	Y	2.2×10^{-2}		
71.	$CO + OH \longrightarrow OH \cdots CO\cdot \longrightarrow$ cis–$HOCO\cdot \longrightarrow CO_2 + H$	F	Y	$^{c}2.9\times10^{-12}$	0.9–9.7×10^{-13}	3
72.	$H_2O + {}^1O \longrightarrow H_2OO\cdot \longrightarrow H_2O_2\cdot \longrightarrow OH + OH$	F	N	4.8×10^{-10}	1.8–3.7×10^{-10}	1
73.	$H_2O + CN \longrightarrow H_2OCN\cdot \longrightarrow OH + HCN$	F	Y	6.6×10^{-15}		
74.	$H_2O + {}^2N \longrightarrow H_2ON\cdot \longrightarrow$ trans–$HNOH\cdot \longrightarrow HNO + H$ and $H_2O + {}^2N \longrightarrow H_2ON\cdot \longrightarrow$ trans–$HNOH\cdot \longrightarrow H_2NO\cdot \longrightarrow HNO + H$	F	N	1.9×10^{-10}		
75.	$H_2O + CH \longrightarrow H_2O \cdots CH\cdot \longrightarrow H_2OCH\cdot \longrightarrow H_2COH\cdot \longrightarrow H_2CO + H$	F	^{d}N	2.0×10^{-10}	1.3–4.5×10^{-11}	4
*76.	$H_2O + CH \longrightarrow OH + {}^3CH_2$	F	Y	3.9×10^{-16}		
77.	$OH + HCN \longrightarrow NCHOH\cdot \longrightarrow HOCN + H$	F	Y	1.2×10^{-15}	0.1–31×10^{-15}	1
78.	$OH + CN \longrightarrow HO \cdots CN\cdot \longrightarrow {}^3HOCN_1\cdot \longrightarrow {}^3HOCN_2\cdot \longrightarrow NCO + H$	F	Y	1.1×10^{-12}		
79.	$OH + CN \longrightarrow HCN + {}^3O$	F	Y	4.5×10^{-13}		
*80.	$OH + CN \longrightarrow HNC + {}^3O$	F	Y	2.3×10^{-17}		
81.	$OH + OH \longrightarrow$ trans–${}^3H_2O_2\cdot \longrightarrow H_2O + {}^3O$	F	N	$^{e}2.5\times10^{-11}$	0.8–2.6×10^{-12}	10
82.	$OH + {}^3O \longrightarrow HO_{2(v)}\cdot \longrightarrow O_2 + H$	F	N	7.4×10^{-11}	2.8–4.2×10^{-11}	2
*83.	$OH + {}^1O \longrightarrow HO_{2(v)}\cdot \longrightarrow O_2 + H$	F	N	1.0×10^{-9}		
84.	$OH + NH \longrightarrow OH \cdots NH\cdot \longrightarrow$ trans–$HNOH\cdot \longrightarrow HNO + H$ and $OH + NH \longrightarrow OH \cdots NH\cdot \longrightarrow$ trans–$HNOH\cdot \longrightarrow H_2NO\cdot \longrightarrow HNO + H$	F	^{f}N	7.0×10^{-12}	3.3×10^{-11}	5
85.	$OH + NH \longrightarrow H_2O + {}^4N$	F	Y	6.8×10^{-13}	3.1×10^{-12}	5
86.	$OH + {}^4N \longrightarrow {}^3OH \cdots N\cdot \longrightarrow {}^3NOH\cdot \longrightarrow NO + H$	F	Y	1.0×10^{-10}	4.2–5.3×10^{-11}	2
*87.	$OH + {}^2N \longrightarrow {}^3OH \cdots N\cdot \longrightarrow {}^3NOH\cdot \longrightarrow NO + H$	F	N	1.5×10^{-10}		
88.	$OH + CH_4 \longrightarrow H_2O + CH_3$	F	Y	1.1×10^{-16}	5.9–11×10^{-15}	54
89.	$OH + CH_3 \longrightarrow {}^3O + CH_4$	F	Y	1.1×10^{-18}	1.8×10^{-17}	16
90.	$OH + CH_3 \longrightarrow H_2O + {}^3CH_2$	F	Y	3.5×10^{-18}		
91.	$OH + {}^3CH_2 \longrightarrow OH \cdots CH_2\cdot \longrightarrow H_2COH\cdot \longrightarrow H_2CO + H$	F	N	4.6×10^{-11}	3.0×10^{-11}	2
92.	$OH + {}^3CH_2 \longrightarrow H_2O + CH$	F	N	7.6×10^{-13}		
93.	$OH + {}^1CH_2 \longrightarrow OH \cdots CH_2\cdot \longrightarrow H_2COH\cdot \longrightarrow H_2CO + H$	F	N	4.6×10^{-11}	5.0×10^{-11}	1
94.	$OH + CH \longrightarrow {}^3OH \cdots CH\cdot \longrightarrow {}^3HCOH\cdot \longrightarrow {}^3H_2CO\cdot \longrightarrow HCO + H$	F	N	3.2×10^{-11}		
95.	$OH + CH \longrightarrow$ anti–$HCOH_{(v)}\cdot \longrightarrow H_2CO_{(v)}\cdot \longrightarrow CO + H_2$	F	N	$^{g}6.3\times10^{-12}$		
96.	$OH + CH \longrightarrow$ anti–$HCOH_{(v)}\cdot \longrightarrow H_2CO_{(v)}\cdot \longrightarrow CO + H + H$	F	N	$^{g}6.3\times10^{-12}$		
97.	$OH + H_2 \longrightarrow H_2O + H$	F	Y	1.5×10^{-15}	5.3–8.5×10^{-15}	4
98.	$OH + H \longrightarrow {}^3O + H_2$	F	Y	6.5×10^{-16}	9.9×10^{-17}–5.6×10^{-16}	1
*99.	${}^3O + H_2CN \longrightarrow CH_2NO\cdot \longrightarrow HCNO + H$	F	Y	4.0×10^{-14}		
*100.	${}^3O + H_2CN \longleftarrow CH_2NO\cdot \longleftarrow HCNO + H$	R	N	9.8×10^{-11}		
101.	${}^3O + H_2CN \longrightarrow CH_2NO\cdot \longrightarrow$	F	Y	8.3×10^{-15}		

	$HCNOH\cdot \longrightarrow OH + HCN$				
102.	$^3O + HCN \longrightarrow {}^3NCOH\cdot \longrightarrow NCO + H$	F	Y	1.5×10^{-18}	
103.	$^3O + HCN \longleftarrow {}^3NCOH\cdot \longleftarrow NCO + H$	R	Y	2.5×10^{-20}	
104.	$^3O + CN \longrightarrow {}^4NCO\cdot \longrightarrow CO + {}^4N$	F	N	1.5×10^{-11}	2.7×10^{-12}–3.7×10^{-11}	1
105.	$^3O + CN \longrightarrow NCO_{(\nu)}\cdot \longrightarrow CO + {}^2N$	F	N	7.1×10^{-12}	9.4×10^{-12}–1.6×10^{-11}	1
106.	$^3O + NH \longrightarrow HNO\cdot \longrightarrow NO + H$	F	N	3.1×10^{-11}	5.0×10^{-11}	2
107.	$^3O + NH \longrightarrow OH + {}^4N$	F	Y	2.2×10^{-14}	$<1.7\times10^{-13}$–5.0×10^{-12}	1
108.	$^3O + CH_4 \longrightarrow OH + CH_3$	F	Y	1.1×10^{-19}	6.6×10^{-19}–6.6×10^{-16}	6
109.	$^3O + CH_3 \longrightarrow CH_3O\cdot \longrightarrow H_2CO + H$	F	N	9.4×10^{-11}	$>3.0\times10^{-11}$–1.9×10^{-10}	1
110.	$^3O + {}^3CH_2 \longrightarrow H_2CO_{(\nu)}\cdot \longrightarrow CO + H + H$	F	N	3.4×10^{-11}	$^h1.0\times10^{-11}$–1.0×10^{-10}	1
111.	$^3O + {}^3CH_2 \longrightarrow H_2CO_{(\nu)}\cdot \longrightarrow CO + H_2$	F	N	3.4×10^{-11}	$^h1.0\times10^{-11}$–1.0×10^{-10}	1
*112.	$^3O + {}^1CH_2 \longrightarrow {}^3H_2CO\cdot \longrightarrow HCO + H$	F	N	2.1×10^{-10}		
113.	$^3O + CH \longrightarrow HCO_{(\nu)}\cdot \longrightarrow CO + H$	F	N	1.1×10^{-10}	6.6×10^{-11}	2
114.	$^3O + CH \longrightarrow {}^4HCO\cdot \longrightarrow {}^4COH\cdot \longrightarrow OH + C$	F	N	2.5×10^{-10}		
115.	$^3O + H_2 \longrightarrow OH + H$	F	Y	7.2×10^{-19}	7.0×10^{-18}–1.1×10^{-17}	10
*116.	$^1O + H_2CN \longrightarrow CH_2NO\cdot \longrightarrow {}^3O + H_2CN$	F	Y	4.5×10^{-10}		
*117.	$^1O + H_2CN \longrightarrow CH_2NO\cdot \longrightarrow HCNO + H$	F	Y	6.0×10^{-13}		
*118.	$^1O + H_2CN \longrightarrow CH_2NO\cdot \longrightarrow HCNOH\cdot \longrightarrow HCN + OH$	F	Y	1.2×10^{-13}		
*119.	$^1O + CN \longrightarrow NCO_{(\nu)}\cdot \longrightarrow CO + {}^2N$	F	N	8.9×10^{-11}		
120.	$^1O + CH_4 \longrightarrow CH_3OH_{(\nu)}\cdot \longrightarrow OH + CH_3$	F	N	5.8×10^{-9}	1.4–4.0×10^{-10}	15
*121.	$^1O + CH_3 \longrightarrow CH_3O\cdot \longrightarrow H_2CO + H$	F	N	4.3×10^{-10}		
*122.	$^1O + {}^3CH_2 \longrightarrow {}^3H_2CO\cdot \longrightarrow HCO + H$	F	N	7.0×10^{-10}		
*123.	$^1O + {}^1CH_2 \longrightarrow H_2CO_{(\nu)}\cdot \longrightarrow CO + H + H$	F	N	1.7×10^{-10}		
*124.	$^1O + {}^1CH_2 \longrightarrow H_2CO_{(\nu)}\cdot \longrightarrow CO + H_2$	F	N	1.7×10^{-10}		
*125.	$^1O + CH \longrightarrow HCO_{(\nu)}\cdot \longrightarrow CO + H$	F	N	9.2×10^{-11}		
126.	$^1O + H_2 \longrightarrow H_2O_{(\nu)}\cdot \longrightarrow OH + H$	F	N	7.1×10^{-10}	1.1–3.0×10^{-10}	2

[a] We introduce a barrier of 17.15 kJ mol^{-1} (half the HF barrier) to this calculation as no barrier is found at the BHandHLYP/aug-cc-pVDZ level of theory (see supplement for more details).

[b] We remove the barrier from this calculation as experiment predicts this reaction to be barrierless below 400 K [446].

[c] We remove the intermediate barriers from this reaction and reduce the barrierless first step by a factor of 3.4 to match the barrier effects at the B3LYP/aug-cc-pVDZ level of theory. Experiments predict this reaction to have little to no barrier [137].

[d] We remove the barrier from the rate limiting third step of this calculation, as experiment predicts this reaction to be barrierless [447].

[e] Simulations did not converge beyond a O-O bond distance of 2.90Å. The rate coefficient is calculated with the variational transition state at this location, which has the highest ΔG.

[f] We remove the barrier from the rate limiting third step of this calculation, as data evaluations suggest little to no barrier for this reaction [448].

[g] This rate coefficient is one half of the calculated rate coefficient for $OH + CH \longrightarrow \text{anti}-HCOH_{(\nu)}\cdot$ as both $CO + H_2$ and $CO + H + H$ are equally probable decay pathways for $\text{anti}-HCOH_{(\nu)}$ [137, 247, 449].

[h] Experimental values are for $^3O + {}^3CH_2 \longrightarrow$ products divided by 2. As both product channels $CO + H + H$ and $CO + H_2$ are suggested to be equally likely [137, 247, 449].

4.3.1.1 Method Limitations

Occasionally computational methods misdiagnose reaction energy barriers. In other words, a method may calculate a barrier when experiments suggest the reaction is barrierless, or a method may calculate no barrier when experiments suggest a small-to-modest-sized barrier (∼1–20 kJ mol^{-1}) exists. We find this to be biggest limitation of applying a consistent computational quantum method to a large number of reactions. This is the main reason for taking a hybrid approach to building CRAHCN-O. Experiments are the most accurate method to calculate rate coefficients, therefore experimental values will always be used when possible. However, for the large number of reactions without experimentally measured rate coefficients, we must use a robust and feasible computational method to calculate and include these reactions in the network.

In four cases (noted in Table 4.3), our chosen computational method (BHandHLYP/aug-cc-pVDZ) predicts barriers at the first step or an intermediate step of reactions that are expected to be barrierless. In one other case, this method predicts a reaction had no barrier, when experiment suggests a barrier of 17.15 kJ mol^{-1} [288]. For these few cases, we artificially remove the barriers from these calculations, or introduce an experimental barrier. Based on the calculations in this paper, we find this method correctly diagnoses barriers ∼92% of the time.

Comparing the barrier diagnosis capabilities of BHandHLYP/aug-cc-pVDZ with two other widely used method in past work [440], we find CCSD/aug-cc-pVTZ and ωB97XD/aug-cc-pVDZ share these limitations. For 11 chosen reactions, BHandHLYP/aug-cc-pVDZ misdiagnosed 4 barriers, CCSD/aug-cc-pVTZ misdiagnosed 5 barriers, and ωB97XD/aug-cc-pVDZ misdiagnosed 2 barriers.

A second limitation of our method is that we do not include a correction factor for quantum mechanical tunneling. This may not be a big concern at 298 K, where our rate coefficient calculations are typically within a factor of two of experimental values, and generally always within an order of magnitude of experimental values. However, tunneling is most relevant at lower temperatures [450].

Given the lack of experimental low temperature ($\lesssim$ 230 K) rate coefficient data for the reactions in this study, we cannot obtain a valid statistical sense of the accuracy of our method for calculating low temperature rate coefficients. However, it is a reasonable assumption that our treatment leads to larger uncertainties at the lower end of our temperature range (50–200 K), where tunneling plays a greater role; possibly up to two orders of magnitude.

4.4 Discussion

4.4.1 Highlighted New Reactions

As we have already noted, we have discovered 45 previously unknown reactions and provide the first calculations of their rate coefficients. In Table 4.4, we highlight 6 of these reactions. These reactions are potentially key pathways for the production and destruction of HCN or H_2CO in planetary atmospheres due to their high rate coefficients

Table 4.4: Highlighted newly discovered reactions in this work, listed with their calculated rate coefficients at 298 K and potential for importance in atmospheres. For simplicity, reaction intermediates are not listed here. See Tables 4.2 and 4.3 for full details of reaction intermediates. Second-order rate coefficients have units cm^{3}s^{-1}. Third-order rate coefficients have units cm^{6}s^{-1}.

Reaction	k(298) calculated	Importance
$^1O + CH_3 \longrightarrow H_2CO + H$	4.3×10^{-10}	H_2CO production in upper atmospheres
$^1O + ^1CH_2 + M \longrightarrow H_2CO + M$	$k_\infty = 3.3\times10^{-10}$ $k_0(N_2) = 6.6\times10^{-27}$ $k_0(CO_2) = 7.7\times10^{-27}$ $k_0(H_2) = 1.2\times10^{-26}$	H_2CO production in lower atmospheres
$^3O + ^3CH_2 + M \longrightarrow H_2CO + M$	$k_\infty = 6.7\times10^{-11}$ $k_0(N_2) = 9.2\times10^{-29}$ $k_0(CO_2) = 1.1\times10^{-28}$ $k_0(H_2) = 1.7\times10^{-28}$	H_2CO production in lower atmospheres
$^1O + H_2CN \longrightarrow HCN + OH$	1.2×10^{-13}	HCN production in upper atmospheres
$H_2CO + ^1O \longrightarrow HCO + OH$	4.6×10^{-10}	H_2CO destruction in upper atmospheres
$^1O + HCN + M \longrightarrow HCNO + M$	$k_\infty = 3.3\times10^{-11}$ $k_0(N_2) = 4.0\times10^{-29}$ $k_0(CO_2) = 4.6\times10^{-29}$ $k_0(H_2) = 8.0\times10^{-29}$	HCN destruction in lower atmospheres

at 298 K, and the reasonably high abundances of their reactants in atmospheres.

Different reactions tend to dominate in different regions of an atmosphere. In the diffuse upper atmosphere (thermosphere), incoming UV radiation breaks apart dominant atmospheric species to produce radicals. In the dense lower atmosphere (troposphere), radicals can be transported from the upper atmosphere via turbulent mixing, or produced by lightning and/or GCRs. In this lower region, there is also sufficient pressure to collisionally deexcite the vibrationally excited intermediates in three-body reactions.

One newly discovered reaction with a great potential to produce substantial amounts H_2CO in upper atmospheres is $^1O + CH_3 \longrightarrow H_2CO + H$. Firstly, there will likely be high concentrations of reactants ^1O and CH_3 in the upper atmospheres of planets containing CO_2 and CH_4, as the former are the direct photodissociation fragments of the latter. Secondly, this reaction has a barrierless rate coefficient of $k(298\text{ K}) =$

4.3×10^{-10} cm^{3}s^{-1}, which is in the 94th percentile for highest two-body reaction rate coefficients in this study. For these reasons, we expect this reaction to be a dominant source of H_2CO in CO_2-rich and CH_4-containing atmospheres such as the early Earth. At the CCSD/aug-cc-pVDZ level of theory, we calculate this rate coefficient to be only 14% lower ($3.7\ \times10^{-10}$ cm^{3}s^{-1}), suggesting this calculation is not very sensitive to the choice of computational method.

In lower planetary atmospheres, we find two new three-body reactions that may be important pathways to H_2CO. These reactions are $^1O + {}^1CH_2 + M \longrightarrow H_2CO + M$ and $^3O + {}^3CH_2 + M \longrightarrow H_2CO + M$. These reactions are most favourable at the high-pressure limit, where their rate coefficients are $k_\infty(298\text{ K}) = 3.3\times10^{-10}$ and 6.7×10^{-11} cm^{3}s^{-1}, respectively. The pressures at which these reaction rate coefficients reach 90% of $k_\infty(298\text{ K})$ in a N_2 bath gas are 0.61 bar and 7.1 bar, respectively. Such pressures would have been present in the evolving early Earth atmosphere ~4.5 billion years ago [47].

For new potentially important routes to HCN, we find $^1O + H_2CN \longrightarrow HCN + OH$, which has a rate coefficient of $k(298\text{ K}) = 1.2\times10^{-13}$ cm^{3}s^{-1}. This reaction has the potential to be an important source of HCN in upper atmospheres with high CO_2 mixing ratios, and low H_2 and CH_4 mixing ratios. The reason for this is that there is a direct competing reaction for HCN production from $H_2CN + H \longrightarrow HCN + H_2$, which has a rate coefficient of $k(298\text{ K}) = 2.2\times10^{-11}$ cm^{3}s^{-1}. Therefore, the ^1O/H ratio in upper atmospheres will determine which of these two reactions dominates. We note also that this reaction has a complex reaction scheme, with two other favourable channels from the $H_2CNO\cdot$ intermediate: $HCNO + H$ and $^3O + H_2CN$. Our calculations of this reaction rate coefficient using two other computational methods (ωB97XD, CCSD) suggests the channel to HCN + OH may be more favourable than our BHandHLYP calculation implies, by up to a factor of ~700 (see theoretical case study 9 in the SI for more details). Given these discrepancies, and the novelty of this reaction, we recommend experimental measurements be performed for the three product channels of $^1O + H_2CN$.

A new reaction with a great potential to destroy H_2CO is $H_2CO + {}^1O \longrightarrow HCO + OH$, which has a barrierless rate coefficient of 4.6×10^{-10} cm^{3}s^{-1} at 298 K. As with the main new production pathway to H_2CO, this rate coefficient is one of the highest two-body rate coefficients in this study, and likely plays a role of attenuating H_2CO in upper atmospheres. At the CCSD/aug-cc-pVDZ level of theory, we calculate this rate coefficient to be only 50% lower (2.3×10^{-10} cm^3s^{-1}) than the value at the BHandHLYP/aug-cc-pVDZ level of theory.

Lastly, we highlight a new HCN destruction pathway in lower atmospheres, $^1O + HCN + M \longrightarrow HCNO + M$. This reaction may be particularly important in attenuating HCN abundances in the troposphere, which is the region where HCN dissolves in rain droplets and makes its way into surface water. This reaction rate coefficient reaches 90% of k_∞(298 K) in a N_2 bath gas at 3 bar.

4.4.2 CRAHCN-O

CRAHCN-O is a chemical reaction network that can be used to simulate the production of HCN and H_2CO in atmospheres ranging from ∼50–400 K dominated by any of the following gases: CO_2, N_2, H_2O, CH_4, and H_2. CRAHCN-O is the amalgamation of the CRAHCN network developed in Pearce et al. [440] and the oxygen extension developed in this work. CRAHCN-O contains experimental rate coefficients (when available), and our consistently calculated theoretical rate coefficients from this work otherwise.

We summarize the oxygen extension in Tables S1 and S2 in the supplementary materials. In addition to the 126 reactions explored in this work, we include one experimental spin-forbidden collisionally induced intersystem crossing reaction ($^1O + M \longrightarrow {}^3O + M$), whose rate coefficient cannot be calculated using our theoretical method.

The original CRAHCN network can be found in the appendices of Pearce et al. [440].

4.5 Conclusions

In this work, we use a novel technique making use of computational quantum chemistry and experimental data to build a consistent reduced atmospheric hybrid chemical network oxygen extension (CRAHCN-O). This network can be used to simulate HCN and H_2CO chemistry in planetary atmospheres dominated by CO_2, N_2, H_2O, CH_4, and H_2.

The oxygen extension contains 127 reactions, and is made up of approximately 30% experimental and 70% consistently calculated theoretical rate coefficients. Below are the main conclusions of this work in bullet point.

- We discover 45 previously unknown reactions, and are the first to calculate their rate coefficients. These new reactions typically involve electronically excited species (e.g., ^{1}O, ^{1}CH$_2$, ^{2}N).
- The majority (∼62%) of our calculated rate coefficients are accurate to within a factor of two of experimental measurements. ∼84% are accurate to within a factor of 6 of experimental values, and the rest are accurate to within about an order of magnitude of experimental values. This level of accuracy is consistent with the uncertainties assigned in large scale experimental data evaluations.
- We identify 6 potentially key new production and destruction pathways for H$_2$CO and HCN from these previously unknown reactions.
- The high, barrierless rate coefficient of $^1\mathrm{O} + \mathrm{CH_3} \longrightarrow \mathrm{H_2CO} + \mathrm{H}$ (k(298 K) = 4.3×10^{-10} cm^{3}s^{-1}) likely makes it a key source of formaldehyde in upper atmospheres where ^{1}O and CH$_3$ are produced from the UV photodissociation of CO$_2$ and CH$_4$, respectively.
- Conversely, the high, barrierless rate coefficient of $\mathrm{H_2CO} + {}^1\mathrm{O} \longrightarrow \mathrm{HCO} + \mathrm{OH}$ (k(298 K) = 4.6 $\times10^{-10}$ cm^{3}s^{-1}) likely makes it a key sink for formaldehyde in upper atmospheres.
- $^1\mathrm{O} + \mathrm{H_2CN} \longrightarrow \mathrm{HCN} + \mathrm{OH}$ is less efficient than the known HCN source, $\mathrm{H_2CN} + \mathrm{H} \longrightarrow \mathrm{HCN} + \mathrm{H_2}$; However the former may dominate HCN production in CO$_2$-rich upper atmospheres with high ^{1}O/H ratios from CO$_2$ photodissociation.
- In lower atmospheres (i.e. high partial pressures), H$_2$CO may form via new reactions between $^1\mathrm{O} + {}^1\mathrm{CH_2}$ and $^3\mathrm{O} + {}^3\mathrm{CH_2}$, which require a collisional third body at the high pressures present in these regions. HCN may be efficiently removed in this region via $^1\mathrm{O} + \mathrm{HCN} + \mathrm{M} \longrightarrow \mathrm{HCNO} + \mathrm{M}$.

Having now filled in the missing chemical data relevant to HCN and H$_2$CO production in CO$_2$- and H$_2$O-rich atmospheres, we intend to couple CRAHCN-O to a 1D chemical kinetic model to simulate the atmosphere of the early Earth.

4.6 Supporting Information

Rate coefficient data, experimental data, Lennard-Jones parameters, theoretical case studies, and quantum chemistry data.

4.7 Acknowledgments

B.K.D.P. is supported by an NSERC Alexander Graham Bell Canada Graduate Scholarship-Doctoral (CGS-D). P.W.A is supported by NSERC, the Canada Research Chairs, and Canarie. R.E.P. is supported by an NSERC Discovery Grant. We acknowledge Compute Canada for allocating the computer time required for this research.

4.8 References

4.9 Supporting Information

4.9.1 CRAHCN-O

In Tables 4.5 and 4.6, we display the Lindemann and the Arrhenius coefficients for the new oxygen reactions in CRAHCN-O. These rate coefficients consist of experimental values when available, and our consistently calculated theoretical values otherwise.

Table 4.5: Lindemann coefficients for the three-body oxygen reactions in the consistent reduced atmospheric hybrid chemical network oxygen extension (CRAHCN-O), valid within the 50–400 K temperature range. Experimental values are used when available, and calculated rate coefficients from this work are used otherwise. k_∞ is the second-order rate coefficient in the high pressure limit with units cm^{3}s^{-1}. k_0 is the third-order rate coefficient in the low pressure limit with units cm^{6}s^{-1}. These values fit into the pressure-dependent rate coefficient equation $k = \frac{k_0[M]/k_\infty}{1+k_0[M]/k_\infty}k_\infty$.

No.	Reaction equation	$k_\infty(298)$	$k_0(298)$	Source(s)
1.	$CO_2 + {}^1O + M \longrightarrow CO_3 + M$	1.6×10^{-10}	(M=N_2) 3.0×10^{-29}	Avg. of exper. vals, This work
			(CO_2) 3.1×10^{-29}	This work
			(H_2) 6.7×10^{-29}	This work
2.	$HCO + {}^2N + M \longrightarrow HCON\cdot + M\cdot \longrightarrow HCNO + M$	2.0×10^{-11}	(N_2) 5.0×10^{-30}	This work
			(CO_2) 5.6×10^{-30}	This work
			(H_2) 9.7×10^{-30}	This work
3.	$HCO + CH_3 + M \longrightarrow CH_3CHO + M$	3.0×10^{-11}	(N_2) 5.3×10^{-27}	Tsang & Hampson [247], This work
			(CO_2) 6.4×10^{-27}	This work
			(H_2) 1.2×10^{-27}	This work

4.	$HCO + H + M \longrightarrow H_2CO + M$	4.9×10^{-11}	(N_2) 7.4×10^{-30}	This work
			(CO_2) 9.5×10^{-30}	This work
			(H_2) 1.4×10^{-29}	This work
5.	$CO + CN + M \longrightarrow NCCO + M$	6.0×10^{-12}	(N_2) 6.2×10^{-31}	This work
			(CO_2) 6.8×10^{-31}	This work
			(H_2) 1.3×10^{-30}	This work
6.	$CO + {}^1O + M \longrightarrow CO_2 + M$	4.6×10^{-11}	(N_2) 2.8×10^{-29}	Avg. of exper. vals, (CO_2) Clerc & Barat [451]
			(CO_2) 2.8×10^{-29}	(CO_2) Clerc & Barat [451]
			(H_2) 2.8×10^{-29}	(CO_2) Clerc & Barat [451]
7.	$CO + {}^1CH_2 + M \longrightarrow CH_2CO + M$	1.3×10^{-11}	(N_2) 1.7×10^{-28}	This work
			(CO_2) 1.9×10^{-28}	This work
			(H_2) 3.3×10^{-28}	This work
8.	$CO + CH + M \longrightarrow HCCO + M$	4.3×10^{-11}	(N_2) 1.2×10^{-29}	This work
			(CO_2) 1.3×10^{-29}	This work
			(H_2) 2.4×10^{-29}	This work
9.	$CO + H + M \longrightarrow HCO + M$	2.7×10^{-12}	(N_2) 1.0×10^{-34}	This work, Avg. of H_2 exper. vals
			(CO_2) 9.9×10^{-35}	(CO) Hochanadel et al. [452]
			(H_2) 1.0×10^{-34}	Avg. of H_2 exper. vals
10.	$OH + H_2CN + M \longrightarrow H_2CNOH + M$	6.0×10^{-12}	(N_2) 6.5×10^{-30}	Nizamov & Dagdigian [453], This work
			(CO_2) 7.4×10^{-30}	This work
			(H_2) 1.3×10^{-29}	This work
11.	$OH + CN + M \longrightarrow HOCN + M$	1.0×10^{-12}	(N_2) 2.7×10^{-30}	This work
			(CO_2) 2.9×10^{-30}	This work
			(H_2) 5.1×10^{-30}	This work
12.	$OH + OH + M \longrightarrow H_2O_2 + M$	1.5×10^{-11}	(N_2) 8.0×10^{-31}	Baulch et al. [137], (N_2) Baulch et al. [137]
			(CO_2) 2.1×10^{-30}	Avg. of CO_2 exper. vals
			(H_2) 4.0×10^{-30}	(H_2O) Baulch et al. [137]
13.	$OH + {}^3O + M \longrightarrow HO_2 + M$	7.4×10^{-11}	(N_2) 8.5×10^{-32}	This work
			(CO_2) 9.4×10^{-32}	This work
			(H_2) 1.8×10^{-31}	This work
14.	$OH + {}^1O + M \longrightarrow HO_2 + M$	1.0×10^{-9}	(N_2) 4.1×10^{-30}	This work
			(CO_2) 4.5×10^{-30}	This work
			(H_2) 8.3×10^{-30}	This work
15.	$OH + NH + M \longrightarrow OH \cdots NH\cdot + M\cdot \longrightarrow$ trans$-HNOH + M$	7.0×10^{-12}	(N_2) 8.5×10^{-31}	This work
			(CO_2) 9.2×10^{-31}	This work
			(H_2) 1.7×10^{-30}	This work
16.	$OH + CH_3 + M \longrightarrow OH \cdots CH_3\cdot + M\cdot \longrightarrow CH_3OH + M$	1.3×10^{-10}	(N_2) 2.1×10^{-27}	This work
			(CO_2) 2.3×10^{-27}	This work
			(H_2) 3.8×10^{-27}	This work
17.	$OH + H + M \longrightarrow H_2O + M$	2.4×10^{-10}	(N_2) 6.9×10^{-31}	This work, (N_2) Baulch et al. [137]
			(CO_2) 9.0×10^{-31}	(CO_2) Zellner et al. [444]
			(H_2) 4.3×10^{-30}	(H_2O) Baulch et al. [137]
18.	${}^3O + CN + M \longrightarrow NCO + M$	7.1×10^{-12}	(N_2) 1.3×10^{-30}	This work
			(CO_2) 1.5×10^{-30}	This work
			(H_2) 2.6×10^{-30}	This work
19.	${}^3O + {}^3O + M \longrightarrow O_2 + M$	1.8×10^{-11}	(N_2) 7.3×10^{-33}	This work, Avg. of N_2 exper. vals
			(CO_2) 7.3×10^{-33}	Avg. of O_2 exper. vals
			(H_2) 7.3×10^{-33}	Avg. of N_2 exper. vals
20.	${}^3O + {}^4N + M \longrightarrow NO + M$	6.6×10^{-11}	(N_2) 8.6×10^{-33}	This work, Avg. of N_2 exper. vals
			(CO_2) 1.8×10^{-32}	(CO_2) Campbell & Thrush [418]
			(H_2) 8.6×10^{-33}	Avg. of N_2 exper. vals
21.	${}^3O + {}^3CH_2 + M \longrightarrow H_2CO + M$	1.9×10^{-11}	(N_2) 9.2×10^{-29}	Tsang & Hampson [247], This work
			(CO_2) 1.1×10^{-28}	This work
			(H_2) 1.7×10^{-28}	This work
22.	${}^3O + CH + M \longrightarrow HCO + M$	6.6×10^{-11}	(N_2) 5.2×10^{-30}	Baulch et al. [137], This work
			(CO_2) 6.2×10^{-30}	This work
			(H_2) 9.9×10^{-30}	This work
23.	${}^3O + H + M \longrightarrow OH + M$	3.5×10^{-10}	(N_2) 2.6×10^{-33}	This work
			(CO_2) 2.9×10^{-33}	This work
			(H_2) 4.6×10^{-33}	This work
24.	${}^1O + HCN + M \longrightarrow HCNO + M$	3.3×10^{-11}	(N_2) 4.0×10^{-29}	This work
			(CO_2) 4.6×10^{-29}	This work
			(H_2) 8.0×10^{-29}	This work
25.	${}^1O + CN + M \longrightarrow NCO + M$	8.9×10^{-11}	(N_2) 1.9×10^{-29}	This work
			(CO_2) 2.1×10^{-29}	This work
			(H_2) 3.6×10^{-29}	This work
26.	${}^1O + {}^1O + M \longrightarrow O_2 + M$	2.3×10^{-10}	(N_2) 8.8×10^{-33}	This work
			(CO_2) 9.6×10^{-33}	This work
			(H_2) 1.8×10^{-32}	This work
27.	${}^1O + CH_4 + M \longrightarrow CH_3OH + M$	2.2×10^{-10}	(N_2) 3.6×10^{-23}	Avg. of exper. vals, This work

			(CO$_2$) 3.9×10^{-23}	This work
			(H$_2$) 6.3×10^{-23}	This work
28.	$^1O + {}^1CH_2 + M \longrightarrow H_2CO + M$	3.3×10^{-10}	(N$_2$) 6.6×10^{-27}	This work
			(CO$_2$) 7.7×10^{-27}	This work
			(H$_2$) 1.2×10^{-26}	This work
29.	$^1O + CH + M \longrightarrow HCO + M$	9.2×10^{-11}	(N$_2$) 4.9×10^{-29}	This work
			(CO$_2$) 5.8×10^{-29}	This work
			(H$_2$) 9.1×10^{-29}	This work
30.	$^1O + H_2 + M \longrightarrow H_2O + M$	2.1×10^{-10}	(N$_2$) 1.2×10^{-29}	Avg. of exper. vals, This work
			(CO$_2$) 1.4×10^{-29}	This work
			(H$_2$) 2.0×10^{-29}	This work
31.	$^1O + H + M \longrightarrow OH + M$	1.1×10^{-9}	(N$_2$) 1.4×10^{-32}	This work
			(CO$_2$) 1.5×10^{-32}	This work
			(H$_2$) 2.3×10^{-32}	This work

Table 4.6: Arrhenius coefficients for the one- and two-body oxygen reactions in the consistent reduced atmospheric hybrid chemical network oxygen extension (CRAHCN-O). Experimental values are used when available, and calculated rate coefficients from this work are used otherwise. For the reactions with barriers from this work, rate coefficients are calculated at 50, 100, 200, 298, and 400 K, and are fit to the modified Arrhenius expression $k(T) = \alpha \left(\frac{T}{300}\right)^{\beta} e^{-\gamma/T}$. Barrierless reaction rate coefficients do not typically vary by more than a factor of 1–3 for temperatures between 50 and 400 K [208, 219–222]. Intermediate molecules are labelled with a bullet, and are included to describe the precise reaction pathway for multi-step reactions. First- and second-order reactions with rate coefficients slower than $k(298\text{ K}) = 10^{-21}$ are not included in this network. First-order rate coefficients have units s^{-1}. Second-order rate coefficients have units cm^{3}s^{-1}.

No.	Reaction equation	Forw./Rev.	α	β	γ	Source
32.	$NCCO \longrightarrow CO + CN$	F	3.4×10^{+7}	14.33	12716	This work
33.	$CO_2 + {}^1O \longrightarrow {}^1CO_3\cdot \longrightarrow {}^3CO_3\cdot \longrightarrow CO_2 + {}^3O$	F	7.4×10^{-11}	0	-133	Dunlea & Ravishankara [454]
34.	$CO_2 + {}^2N \longrightarrow NCO_2\cdot \longrightarrow OCNO\cdot \longrightarrow CO + NO$	F	4.6×10^{-13}	0	0	Avg. of exper. vals
35.	$CO_2 + {}^1CH_2 \longrightarrow {}^1CH_2CO_2\cdot \longrightarrow H_2CO + CO$	F	8.0×10^{-13}	0	0	This work
36.	$CO_2 + CH \longrightarrow CHCO_2\cdot \longrightarrow HCOCO\cdot \longrightarrow HCO + CO$	F	5.7×10^{-12}	0	345	Baulch et al. [137]
37.	$H_2O_2 \longrightarrow OH + OH$	F	2.1×10^{+8}	13.73	11381	This work
38.	$H_2CO + CN \longrightarrow HCN + HCO$	F	1.5×10^{-12}	2.72	-718	Yu et al. [455]
39.	$H_2CO + OH \longrightarrow$ r, l-$H_2COHO\cdot \longrightarrow$ trans$-HCOHO\cdot + H\cdot \longrightarrow H_2O + CO + H$	F	4.8×10^{-13}	0.82	2626	This work
40.	$H_2CO + OH \longrightarrow H_2O + HCO$	F	4.8×10^{-12}	1.18	-225	Baulch et al. [137]
41.	$H_2CO + {}^3O \longrightarrow HCO + OH$	F	1.8×10^{-11}	0.57	1390	Baulch et al. [137]
42.	$H_2CO + {}^1O \longrightarrow H_2CO_2\cdot \longrightarrow HCO_2H\cdot \longrightarrow HCO + OH$	F	4.6×10^{-10}	0	0	This work
43.	$H_2CO + CH_3 \longrightarrow HCO + CH_4$	F	6.8×10^{-12}	0	4450	Baulch et al. [137]
44.	$H_2CO + {}^3CH_2 \longrightarrow HCO + CH_3$	F	3.5×10^{-13}	2.44	1024	This work
45.	$H_2CO + {}^1CH_2 \longrightarrow HCO + CH_3$	F	1.5×10^{-12}	0	0	This work
46.	$H_2CO + CH \longrightarrow H_2COCH_a\cdot \longrightarrow H_2COCH_b\cdot \longrightarrow CH_2HCO\cdot \longrightarrow CH_3CO\cdot \longrightarrow CO + CH_3$	F	1.6×10^{-10}	0	-260	Baulch et al. [137]
47.	$H_2CO + CH \longrightarrow H_2COCH_c\cdot \longrightarrow HCO + {}^3CH_2$	F	1.1×10^{-12}	0	0	This work
48.	$H_2CO + H \longrightarrow HCO + H_2$	F	1.5×10^{-11}	1.05	1650	Baulch et al. [137]
49.	$HCO + H_2CN \longrightarrow H_2CO + HCN$	F	4.6×10^{-14}	2.11	559	This work
50.	$HCO + HCO \longrightarrow$ trans$-C_2H_2O_2\cdot \longrightarrow$ anti$-HCOH\cdot + CO\cdot \longrightarrow H_2CO + CO$	F	4.2×10^{-11}	0	0	Avg. of exper. vals
51.	$HCO + HCO \longrightarrow$ cis$-C_2H_2O_2\cdot \longrightarrow CO + CO + H_2$	F	3.6×10^{-11}	0	0	Yee Quee & Thynne [456]

52.	$HCO + CN \longrightarrow HCOCN\cdot \longrightarrow CO + HCN$	F	5.4×10^{-12}	0	0	This work
53.	$HCO + OH \longrightarrow trans{-}HCOHO\cdot \longrightarrow CO + H_2O$	F	1.7×10^{-10}	0	0	Baulch et al. [137]
54.	$HCO + {}^3O \longrightarrow HCO_2\cdot \longrightarrow CO_2 + H$	F	5.0×10^{-11}	0	0	Baulch et al. [137]
55.	$HCO + {}^3O \longrightarrow CO + OH$	F	5.0×10^{-11}	0	0	Baulch et al. [137]
56.	$HCO + {}^1O \longrightarrow HCO_2\cdot \longrightarrow CO_2 + H$	F	1.5×10^{-10}	0	0	This work
57.	$HCO + NH \longrightarrow H_2CO + {}^4N$	F	2.0×10^{-13}	1.00	4622	This work
58.	$HCO + NH \longrightarrow CO + NH_2$ and $HCO + NH \longrightarrow HNHCO\cdot \longrightarrow H_2NCO\cdot \longrightarrow CO + NH_2$	F	1.4×10^{-11}	0	0	This work
59.	$HCO + {}^4N \longrightarrow {}^3NCOH\cdot \longrightarrow NCO + H$	F	2.8×10^{-11}	0	0	This work
60.	$HCO + {}^4N \longrightarrow CO + NH$	F	2.2×10^{-11}	0	0	This work
61.	$HCO + {}^2N \longrightarrow {}^3NCOH\cdot \longrightarrow NCO + H$	F	6.6×10^{-11}	0	0	This work
62.	$HCO + {}^2N \longrightarrow CO + NH$	F	4.8×10^{-11}	0	0	This work
63.	$HCO + CH_3 \longrightarrow CO + CH_4$	F	2.0×10^{-10}	0	0	Tsang & Hampson [247]
64.	$HCO + {}^3CH_2 \longrightarrow CH_3 + CO$ and $HCO + {}^3CH_2 \longrightarrow CH_2HCO\cdot \longrightarrow CH_3CO\cdot \longrightarrow CH_3 + CO$	F	2.1×10^{-11}	0	0	This work
65.	$HCO + {}^1CH_2 \longrightarrow CH_2HCO\cdot \longrightarrow CH_3CO\cdot \longrightarrow CH_3 + CO$	F	1.2×10^{-11}	0	0	This work
66.	$HCO + CH \longrightarrow CO + {}^3CH_2$	F	1.5×10^{-11}	0	0	This work
67.	$HCO + CH \longrightarrow CO + {}^1CH_2$	F	4.6×10^{-12}	0	0	This work
68.	$HCO + H \longrightarrow CO + H_2$ and $HCO + H \longrightarrow H_2CO_{(v)}\cdot \longrightarrow CO + H_2$	F	1.5×10^{-10}	0	0	Baulch et al. [137]
69.	$HCO + H \longrightarrow H_2CO_{(v)}\cdot \longrightarrow CO + H + H$	F	2.4×10^{-11}	0	0	This work
70.	$HCO \longrightarrow CO + H$	F	$1.7\times10^{+13}$	1.14	10219	This work
71.	$CO + OH \longrightarrow OH\cdots CO\cdot \longrightarrow cis{-}HOCO\cdot \longrightarrow CO_2 + H$	F	5.5×10^{-12}	1.50	-250	Baulch et al. [137]
72.	$H_2O + {}^1O \longrightarrow H_2OO\cdot \longrightarrow H_2O_2\cdot \longrightarrow OH + OH$	F	1.6×10^{-10}	0	-65	Dunlea & Ravishankara [454]
73.	$H_2O + CN \longrightarrow H_2OCN\cdot \longrightarrow OH + HCN$	F	9.4×10^{-13}	1.58	1474	This work
74.	$H_2O + {}^2N \longrightarrow H_2ON\cdot \longrightarrow trans{-}HNOH\cdot \longrightarrow HNO + H$ and $H_2O + {}^2N \longrightarrow H_2ON\cdot \longrightarrow trans{-}HNOH\cdot \longrightarrow H_2NO\cdot \longrightarrow HNO + H$	F	1.9×10^{-10}	0	0	This work
75.	$H_2O + CH \longrightarrow H_2O\cdots CH\cdot \longrightarrow H_2OCH\cdot \longrightarrow H_2COH\cdot \longrightarrow H_2CO + H$	F	1.6×10^{-11}	-1.42	0	Blitz et al. [447]
76.	$H_2O + CH \longrightarrow OH + {}^3CH_2$	F	5.8×10^{-13}	0.38	2178	This work
77.	$OH + HCN \longrightarrow NCHOH\cdot \longrightarrow HOCN + H$	F	5.3×10^{-14}	-1.00	1860	Phillips [457]
78.	$OH + CN \longrightarrow HO\cdots CN\cdot \longrightarrow {}^3HOCN_1\cdot \longrightarrow {}^3HOCN_2\cdot \longrightarrow NCO + H$	F	9.9×10^{-13}	-0.34	-25	This work
79.	$OH + CN \longrightarrow HCN + {}^3O$	F	2.8×10^{-12}	1.07	545	This work
80.	$OH + CN \longrightarrow HNC + {}^3O$	F	4.4×10^{-8}	-6.93	6383	This work
81.	$OH + OH \longrightarrow trans{-}{}^3H_2O_2\cdot \longrightarrow H_2O + {}^3O$	F	1.7×10^{-12}	1.14	50	Baulch et al. [137]
82.	$OH + {}^3O \longrightarrow HO_{2(v)}\cdot \longrightarrow O_2 + H$	F	2.0×10^{-11}	0	-112	Baulch et al. [137]
83.	$OH + {}^1O \longrightarrow HO_{2(v)}\cdot \longrightarrow O_2 + H$	F	1.0×10^{-9}	0	0	This work
84.	$OH + NH \longrightarrow OH\cdots NH\cdot \longrightarrow trans{-}HNOH\cdot \longrightarrow HNO + H$ and $OH + NH \longrightarrow OH\cdots NH\cdot \longrightarrow trans{-}HNOH\cdot \longrightarrow H_2NO\cdot \longrightarrow HNO + H$	F	7.0×10^{-12}	0	0	This work
85.	$OH + NH \longrightarrow H_2O + {}^4N$	F	2.9×10^{-12}	0.69	425	This work
86.	$OH + {}^4N \longrightarrow {}^3OH\cdots N\cdot \longrightarrow {}^3NOH\cdot \longrightarrow NO + H$	F	4.9×10^{-11}	0	0	Avg. of exper. vals
87.	$OH + {}^2N \longrightarrow {}^3OH\cdots N\cdot \longrightarrow {}^3NOH\cdot \longrightarrow NO + H$	F	1.5×10^{-10}	0	0	This work
88.	$OH + CH_4 \longrightarrow H_2O + CH_3$	F	8.8×10^{-13}	1.83	1396	Baulch et al. [137]
89.	$OH + CH_3 \longrightarrow {}^3O + CH_4$	F	9.5×10^{-13}	-0.29	4139	this work
90.	$OH + CH_3 \longrightarrow H_2O + {}^3CH_2$	F	2.2×10^{-12}	1.67	3972	This work
91.	$OH + {}^3CH_2 \longrightarrow OH\cdots CH_2\cdot \longrightarrow H_2COH\cdot \longrightarrow H_2CO + H$	F	4.6×10^{-11}	0	0	This work
92.	$OH + {}^3CH_2 \longrightarrow H_2O + CH$	F	7.6×10^{-13}	0	0	This work
93.	$OH + {}^1CH_2 \longrightarrow OH\cdots CH_2\cdot \longrightarrow H_2COH\cdot \longrightarrow H_2CO + H$	F	4.6×10^{-11}	0	0	This work
94.	$OH + CH \longrightarrow {}^3OH\cdots CH\cdot \longrightarrow {}^3HCOH\cdot \longrightarrow {}^3H_2CO\cdot \longrightarrow HCO + H$	F	3.2×10^{-11}	0	0	This work
95.	$OH + CH \longrightarrow anti{-}HCOH_{(v)}\cdot \longrightarrow H_2CO_{(v)}\cdot \longrightarrow CO + H_2$	F	6.3×10^{-12}	0	0	This work
96.	$OH + CH \longrightarrow anti{-}HCOH_{(v)}\cdot \longrightarrow H_2CO_{(v)}\cdot \longrightarrow CO + H + H$	F	6.3×10^{-12}	0	0	This work
97.	$OH + H_2 \longrightarrow H_2O + H$	F	9.5×10^{-13}	2.00	1490	Baulch et al. [137]

98.	$OH + H \longrightarrow {}^3O + H_2$	F	7.0×10^{-14}	2.80	1950	Baulch et al. [137]
99.	${}^3O + H_2CN \longrightarrow CH_2NO\cdot \longrightarrow HCNOH\cdot \longrightarrow HCNO + H$	F	5.7×10^{-13}	1.72	788	This work
100.	${}^3O + H_2CN \longleftarrow CH_2NO\cdot \longleftarrow HCNO + H$	R	9.8×10^{-11}	0	0	This work
101.	${}^3O + H_2CN \longrightarrow CH_2NO\cdot \longrightarrow HCNOH\cdot \longrightarrow HCN + OH$	F	3.7×10^{-13}	0.86	1127	This work
102.	${}^3O + HCN \longrightarrow {}^3NCOH\cdot \longrightarrow NCO + H$	F	1.3×10^{-11}	0.96	4040	This work
103.	${}^3O + HCN \longleftarrow {}^3NCOH\cdot \longleftarrow NCO + H$	R	1.3×10^{-10}	0.20	5743	This work
104.	${}^3O + CN \longrightarrow {}^4NCO\cdot \longrightarrow CO + {}^4N$	F	7.6×10^{-12}	0	0	Baulch et al. [137]
105.	${}^3O + CN \longrightarrow NCO_{(\nu)}\cdot \longrightarrow CO + {}^2N$	F	9.4×10^{-12}	0	0	Baulch et al. [137]
106.	${}^3O + NH \longrightarrow HNO\cdot \longrightarrow NO + H$	F	3.1×10^{-11}	0	0	This work
107.	${}^3O + NH \longrightarrow OH + {}^4N$	F	4.5×10^{-12}	0.54	1589	This work
108.	${}^3O + CH_4 \longrightarrow OH + CH_3$	F	1.1×10^{-11}	1.56	4270	Baulch et al. [137]
109.	${}^3O + CH_3 \longrightarrow CH_3O\cdot \longrightarrow H_2CO + H$	F	1.4×10^{-10}	0	0	Baulch et al. [137]
110.	${}^3O + {}^3CH_2 \longrightarrow H_2CO_{(\nu)}\cdot \longrightarrow CO + H + H$	F	1.2×10^{-10}	0	0	Baulch et al. [137]
111.	${}^3O + {}^3CH_2 \longrightarrow H_2CO_{(\nu)}\cdot \longrightarrow CO + H_2$	F	8.0×10^{-11}	0	0	Baulch et al. [137]
112.	${}^3O + {}^1CH_2 \longrightarrow {}^3H_2CO\cdot \longrightarrow HCO + H$	F	2.1×10^{-10}	0	0	This work
113.	${}^3O + CH \longrightarrow HCO_{(\nu)}\cdot \longrightarrow CO + H$	F	6.6×10^{-11}	0	0	Baulch et al. [137]
114.	${}^3O + CH \longrightarrow {}^4HCO\cdot \longrightarrow {}^4COH\cdot \longrightarrow OH + C$	F	2.5×10^{-10}	0	0	This work
115.	${}^3O + H_2 \longrightarrow OH + H$	F	3.5×10^{-13}	2.67	3163	Baulch et al. [137]
116.	${}^1O + H_2CN \longrightarrow CH_2NO\cdot \longrightarrow {}^3O + H_2CN$	F	4.5×10^{-10}	0.70	-53	This work
117.	${}^1O + H_2CN \longrightarrow CH_2NO\cdot \longrightarrow HCNO + H$	F				
	(50–200 K)		2.3×10^{-11}	-0.39	1070	This work
	(200–400 K)		1.9×10^{-13}	5.30	-356	
118.	${}^1O + H_2CN \longrightarrow CH_2NO\cdot \longrightarrow HCNOH\cdot \longrightarrow HCN + OH$	F				This work
	(50–200 K)		1.5×10^{-11}	-0.81	1386	This work
	(200–400 K)		1.1×10^{-13}	4.56	-46	
119.	${}^1O + CN \longrightarrow NCO_{(\nu)}\cdot \longrightarrow CO + {}^2N$	F	8.9×10^{-11}	0	0	This work
120.	${}^1O + CH_4 \longrightarrow CH_3OH_{(\nu)}\cdot \longrightarrow OH + CH_3$	F	2.2×10^{-10}	0	0	Avg. of exper. vals
121.	${}^1O + CH_3 \longrightarrow CH_3O\cdot \longrightarrow H_2CO + H$	F	4.3×10^{-10}	0	0	This work
122.	${}^1O + {}^3CH_2 \longrightarrow {}^3H_2CO\cdot \longrightarrow HCO + H$	F	7.0×10^{-10}	0	0	This work
123.	${}^1O + {}^1CH_2 \longrightarrow H_2CO_{(\nu)}\cdot \longrightarrow CO + H + H$	F	1.7×10^{-10}	0	0	This work
124.	${}^1O + {}^1CH_2 \longrightarrow H_2CO_{(\nu)}\cdot \longrightarrow CO + H_2$	F	1.7×10^{-10}	0	0	This work
125.	${}^1O + CH \longrightarrow HCO_{(\nu)}\cdot \longrightarrow CO + H$	F	9.2×10^{-11}	0	0	This work
126.	${}^1O + H_2 \longrightarrow H_2O_{(\nu)}\cdot \longrightarrow OH + H$	F	2.1×10^{-10}	0	0	Avg. of exper. vals
127a.	${}^1O + CO_2 \longrightarrow {}^3O + CO_2$	F	7.4×10^{-11}	0	-133	Dunlea & Ravishankara [458]
127b.	${}^1O + N_2 \longrightarrow {}^3O + N_2$	F	2.1×10^{-11}	0	-115	Dunlea & Ravishankara [458]
127c.	${}^1O + H_2 \longrightarrow {}^3O + H_2$	F	1.4×10^{-10}	0	0	Vranckx et al. [459]

4.9.2 Experimental Data

Experiments and reviews have measured and suggested reaction rate coefficients for several of the reactions in this network at or near ∼298 K. These values are listed in Table 4.7.

Table 4.7: All available experimental or recommended reaction rate coefficients for the reactions in this study. For brevity, only the 10 most recent measurements of $OH + CH_4 \longrightarrow H_2O + CH_3$, $OH + H_2 \longrightarrow H_2O + H$, and ${}^3O + CH_3 \longrightarrow H_2CO + H$ are included; for a complete listing, we refer the reader to the NIST Chemical Kinetics Database [227]. First-order rate coefficients have units s^{-1}. Second-order rate coefficients have units cm^3s^{-1}. Third-order rate coefficients have units cm^6s^{-1}.

k(298K)	Technique	Temp. (K)	Pressure (Torr)	Reference(s)
$CO_2 + {}^1O \longrightarrow$ products				
2.3×10^{-10}	M	300	20	Young et al. [460]

$1.4{\times}10^{-10}$	M	295	25–250	Blitz et al. [461]
$1.0{\times}10^{-10}$	M	297	40	Wine & Ravishankara [462]
$>1.0{\times}10^{-12}$	M			Young & Ung [463]
$CO_2 + {}^1O \longrightarrow {}^3O + CO_2$				
$2.1{\times}10^{-10}$	M	300	15–26	Heidner, III et al. [464]
$1.3{\times}10^{-10}$	M	295	0–0.01	Amimoto et al. [465]
$1.2{\times}10^{-10}$	M	298		Davidson et al. [466]
$1.1{\times}10^{-10}$	M	298	5–50	Dunlea & Ravishankara [454]
$CO_2 + {}^2N \longrightarrow CO + NO$				
$6.8{\times}10^{-13}$	M	300	6	Fell et al. [234]
$6.0{\times}10^{-13}$	M	300	2–5	Black et al. [236]
$5.0{\times}10^{-13}$	M	300	7–15	Lin & Kaufman [467]
$3.5{\times}10^{-13}$	M	300	1–3	Piper et al. [287]
$1.8{\times}10^{-13}$	M	300	26	Husain et al. [288]
$CO_2 + {}^3CH_2 \longrightarrow {}^3H_2CO + CO$				
$3.9{\times}10^{-14}$	M	298	50–700	Laufer & Bass [468]
$3.9{\times}10^{-14}$	S	298		Tsang & Hampson [247]
$CO_2 + CH \longrightarrow HCO + CO$				
$2.1{\times}10^{-12}$	M	298	20	Mehlmann et al. [446]
$1.9{\times}10^{-12}$	M	298	100	Butler et al. [469, 470]
$1.8{\times}10^{-12}$	M	298	100	Berman et al. [471]
$1.8{\times}10^{-12}$	S	298		Baulch et al. [137]
$H_2CO + CN \longrightarrow HCN + HCO$				
$1.7{\times}10^{-11}$	M	298		Yu et al. [455]
$H_2CO + OH \longrightarrow H_2O + HCO$				
$1.5{\times}10^{-11}$	M	298	700	Niki et al. [472]
$1.2{\times}10^{-11}$	M	298	100	Zabarnick et al. [473]
$8.1\text{–}11{\times}10^{-12}$	M	298	20–80	Stief et al. [474]
$9.3{\times}10^{-12}$	M	299	50	Atkinson & Pitts Jr. [475]
$8.4{\times}10^{-12}$	M	299	700	Niki et al. [476]
$8.1{\times}10^{-12}$	M	296	1–4	Temps & Wagner [477]
$7.8{\times}10^{-12}$	M	298	3	Yetter et al. [478]
$6.1{\times}10^{-12}$	M	298	40	Vandooren & Van Tiggelen [479]
$1.0{\times}10^{-11}$	S	300		Baulch et al. [137]
$1.0{\times}10^{-11}$	S	298		Tsang & Hampson [247]
$H_2CO + {}^3O \longrightarrow HCO + OH$				
$1.9{\times}10^{-13}$	M	298	1.6	Chang & Barker [480]
$1.7{\times}10^{-13}$	M	298	50–200	Klemm [481]
$1.7{\times}10^{-13}$	M	298	1.7–4.4	Klemm et al. [482]
$1.5{\times}10^{-13}$	M	300	2	Herron & Penzhorn [483]
$1.5{\times}10^{-13}$	M	300	0.9–1.1	Mack & Thrush [484]
$1.7{\times}10^{-13}$	S	298		Baulch et al. [137]
$1.7{\times}10^{-13}$	S	298		Tsang & Hampson [247]
$H_2CO + CH_3 \longrightarrow CH_4 + HCO$				
$4.2{\times}10^{-18}$	S	298		Tsang & Hampson [247]
$2.2{\times}10^{-18}$	S	298		Baulch et al. [137]
$H_2CO + {}^3CH_2 \longrightarrow CH_3 + HCO$				
$<1.0{\times}10^{-14}$	S	298		Tsang & Hampson [247]
$H_2CO + {}^1CH_2 \longrightarrow CH_3 + HCO$				
$2.0{\times}10^{-12}$	S	298		Tsang & Hampson [247]
$H_2CO + CH \longrightarrow \text{products}$				
$3.8{\times}10^{-10}$	M	298	20–300	Zabarnick et al. [485]
$3.8{\times}10^{-10}$	S	298		Baulch et al. [137]
$H_2CO + H \longrightarrow HCO + H_2$				
$6.7{\times}10^{-14}$	M	298	100–450	Klemm [481]
$5.4{\times}10^{-14}$	M	297	25–116	Ridley et al. [486]
$4.4{\times}10^{-14}$	M	298	1–2	Brennen et al. [487]
$4.2{\times}10^{-14}$	M	298	1–5	Oehlers et al. [488]
$4.1{\times}10^{-14}$	M	298	22.5	Vandooren et al. [489]
$3.9{\times}10^{-14}$	M	298	0.8–2.1	Westenberg & DeHaas [490]
$5.9{\times}10^{-14}$	S	298		Baulch et al. [137]
$5.5{\times}10^{-14}$	S	298		Tsang & Hampson [247]
$HCO + HCO \longrightarrow C_2H_2O_2$				
$5.0{\times}10^{-11}$	M		0.1–10	Stoeckel et al. [491]
$2.8{\times}10^{-13}$	M	298		Yee Quee & Thynne [456]
$HCO + HCO \longrightarrow H_2CO + CO$				
$7.5{\times}10^{-11}$	M	295	10–30	Baggott et al. [492]
$6.3{\times}10^{-11}$	M	298	10	Reilly et al. [493]
$4.5{\times}10^{-11}$	M	298	210–1425	Friedrichs et al. [494]
$3.4{\times}10^{-11}$	M	298	10–20	Veyret et al. [495]

3.0×10^{-11}	M	298		Vedeneev et al. [496]
$HCO + HCO \longrightarrow CO + CO + H_2$				
3.6×10^{-11}	M	298		Yee Quee & Thynne[456]
$HCO + OH \longrightarrow H_2O + CO$				
1.8×10^{-10}	M	296	1–4	Temps & Wagner [477]
1.7×10^{-10}	S	300		Baulch et al. [137]
5.0×10^{-11}	S	300		Tsang & Hampson [247]
$HCO + {}^3O \longrightarrow CO_2 + H$				
5.0×10^{-11}	S	300–2500		Baulch et al. [137]
5.0×10^{-11}	S	298		Tsang & Hampson [247]
$HCO + {}^3O \longrightarrow CO + OH$				
5.0×10^{-11}	S	300–2500		Baulch et al. [137]
5.0×10^{-11}	S	298		Tsang & Hampson [247]
$HCO + CH_3 \longrightarrow CH_3HCO$				
4.4×10^{-11}	M	298	60–76	Mulenko [497]
6.3×10^{-12}	M	298		Yee Quee & Thynne [456]
3.0×10^{-11}	S	298		Tsang & Hampson [247]
$HCO + CH_3 \longrightarrow CO + CH_4$				
3.6×10^{-11}	M	298		Yee Quee & Thynne [456]
2.0×10^{-10}	S	298		Tsang & Hampson [247]
$HCO + {}^3CH_2 \longrightarrow CO + CH_3$				
3.0×10^{-11}	S	298		Tsang & Hampson [247]
$HCO + {}^1CH_2 \longrightarrow CO + CH_3$				
3.0×10^{-11}	S	298		Tsang & Hampson [247]
$HCO + H \longrightarrow CO + H_2$				
5.5×10^{-10}	M	298	251	Reilly et al. [493]
1.8×10^{-10}	M	298	$2–1425\times10^2$	Friedrichs et al. [494]
1.1×10^{-10}	M	298		Ziemer et al. [498]
2.0×10^{-10}	S	298		Tsang & Hampson [247]
1.5×10^{-10}	S	298		Baulch et al. [137]
$CO + OH \longrightarrow CO_2 + H$				
9.7×10^{-13}	M	300	750–112500	Forster et al. [499]
2.3×10^{-13}	M	299	700	Niki et al. [500]
$1.3–1.9\times10^{-13}$	M	296–297	5–10	Frost et al. [501]
1.7×10^{-13}	M	298	150	Bonn & Zetzsch [502]
1.6×10^{-13}	M	298	2	Herron [503]
1.5×10^{-13}	M	300	24	Husain et al. [504]
1.4×10^{-13}	M	300	150	Lissianski et al. [505]
1.4×10^{-13}	M	298	100	Ravishankara & Thompson[506]
1.3×10^{-13}	M	297	5	Frost et al. [507]
8.5×10^{-14}	M	300	1.8	Herron [508]
1.3×10^{-13}	S	298		Baulch et al. [137]
$CO + {}^1O + M \longrightarrow CO_3 + M$				
$k_0(CO_2) = 2.8\times10^{-29}$	M		300	Clerc & Barat [451]
$CO + {}^1O \longrightarrow$ products				
7.3×10^{-11}	M	300	15–26	Heidner, III et al. [464]
5.8×10^{-11}	M	298		Davidson et al. [509]
5.0×10^{-11}	M	300	7–25	Young et al. [460]
$<5.0\times10^{-11}$	M	300	3–17	Noxon [510]
3.3×10^{-12}	M		300	Clerc & Barat [451]
$CO + CH + M \longrightarrow HCCO + M$				
$k_0(Ar) = 4.2\times10^{-30}$	M	298	10–100	Mehlmann et al. [446]
$k_0(Ar) = 4.1\times10^{-30}$	M	298	0.4–4.5	Le Picard et al. [511]
$k_0(Ar) = 4.1\times10^{-30}$	M	298	4–400	Brownsword et al. [512]
$k_0(He) = 4.1\times10^{-30}$	M	298	10–7500	Fulle et al. [513]
$k_0(He) = 3.9\times10^{-30}$	M	298	10–100	Mehlmann et al. [446]
$k_0(He) = 2.4\times10^{-30}$	M	293	12.5–500	Taatjes [514]
$CO + CH \longrightarrow HCCO$				
1.7×10^{-10}	M	298	10–7500	Fulle et al. [513]
5.9×10^{-11}	M	298	high-pressure limit	Mehlmann et al. [446]
3.0×10^{-11}	M	298	0.4–4.5	Le Picard et al. [511]
2.1×10^{-11}	M	298	100	Butler et al. [470]
8.3×10^{-12}	M	298	100	Berman et al. [471]
6.9×10^{-12}	M	298	100	Taatjes [514]
4.8×10^{-12}	M			Bosnali & Perner [271]
$CO + H + M \longrightarrow HCO + M$				
$k_0(H_2) < 3.3\times10^{-34}$	M	298	50–250	Bennett & Blackmore [429]
$k_0(CH_4, H_2O) = 1.6\times10^{-34}$	M	298	760	Hochanadel et al. [452]
$k_0(H_2) = 1.1\times10^{-34}$	M	298		Wang et al. [515]

$k_0(H_2) = 1.1\times10^{-34}$	M	298	800-1220	Hikida et al. [516]
$k_0(H_2) = 1.0\times10^{-34}$	M	298	760	Hochanadel et al. [452]
$k_0(CO) = 9.9\times10^{-35}$	M	298	760	Hochanadel et al. [452]
$k_0(Ar) = 7.2\times10^{-35}$	M	298	800-1220	Hikida et al. [516]
$k_0(H_2) = 8.0\times10^{-35}$	M	298	52–601	Ahumada et al. [517]
$k_0(Kr) = 6.9\times10^{-35}$	M	298	52–601	Ahumada et al. [517]
$k_0(Ar) = 6.2\times10^{-35}$	M	298	52–601	Ahumada et al. [517]
$k_0(He) = 6.0\times10^{-35}$	M	298	52–601	Ahumada et al. [517]
$k_0(Ne) = 4.8\times10^{-35}$	M	298	52–601	Ahumada et al. [517]
$H_2O + {}^1O \longrightarrow OH + OH$				
3.7×10^{-10}	M	300	11	Gauthier & Snelling[518]
3.0×10^{-11}	M	300	15–26	Heidner, III et al. [464]
2.6×10^{-10}	M	300	3–5	Lee & Slanger [519]
2.3×10^{-10}	M	298	10–30	Davidson et al. [520]
2.3×10^{-10}	M	298	1–12	Steit et al. [521]
$1.8–2.3\times10^{-10}$	M	295	20–36	Dunlea & Ravishankara[522]
$1.9–2.2\times10^{-10}$	M	298	7–47	Geriicke & Comes [523]
2.1×10^{-10}	M	298	1–30	Davidson et al. [466]
$H_2O + CH \longrightarrow$ products				
1.3×10^{-11}	M	293	200	Blitz et al. [447]
4.5×10^{-11}	M			Bosnali & Perner [271]
$OH + H_2CN \longrightarrow H_2CNOH$				
6.0×10^{-12}	M	298	120–200	Nizamov & Dagdigian [453]
$OH + HCN \longrightarrow$ products				
3.1×10^{-14}	M	298	75–375	Fritz et al. [524]
1.0×10^{-16}	M	298	10	Phillips [457]
$OH + OH + M \longrightarrow H_2O_2 + M$				
$k_0(H_2O) = 1.8\times10^{-29}$	M	298	100	Caldwell & Back [442]
$k_0(O_2) = 5.1\times10^{-30}$	M	298	100	Caldwell & Back [442]
$k_0(CO_2) = 4.2\times10^{-30}$	M	298	100	Caldwell & Back [442]
$k_0(H_2O) = 4.0\times10^{-30}$	M	298	0.08–105	Zellner et al. [525]
$k_0(N_2) = 3.3\times10^{-30}$	M	298	100	Caldwell & Back [442]
$k_0(Xe) = 1.3\times10^{-30}$	M	298	100	Caldwell & Back [442]
$k_0(Ar) = 9.7\times10^{-31}$	M	298	100	Caldwell & Back [442]
$k_0(He) = 9.2\times10^{-31}$	M	298	750–7500	Sangwan et al. [526]
$k_0(He) = 8.5\times10^{-31}$	M	298	100	Caldwell & Back [442]
$k_0(N_2) = 6.9\times10^{-31}$	M	298	20–825	Zellner et al. [525]
$k_0(H_2O) = 2.8\times10^{-31}$	M	298	200	Black & Porter [443]
$k_0(N_2) = 2.5\times10^{-31}$	M	298	1	Trainor & von Rosenberg Jr. [527]
$k_0(N_2) = 2.5\times10^{-31}$	M	298	1	Trainor & von Rosenberg Jr. [528]
$k_0(O_2) = 7.9\times10^{-32}$	M	298	200	Black & Porter [443]
$k_0(CO_2) = 6.4\times10^{-32}$	M	298	200	Black & Porter [443]
$k_0(N_2) = 5.1\times10^{-32}$	M	298	200	Black & Porter [443]
$k_0(Xe) = 2.0\times10^{-32}$	M	298	200	Black & Porter [443]
$k_0(Ar) = 1.5\times10^{-32}$	M	298	200	Black & Porter [443]
$k_0(He) = 1.3\times10^{-32}$	M	298	200	Black & Porter [443]
$k_0(H_2O) = 4.0\times10^{-30}$	S	300		Baulch et al. [137]
$k_0(N_2) = 8.0\times10^{-31}$	S	300		Baulch et al. [137]
$k_0(N_2) = 6.0\times10^{-31}$	S	298		Tsang & Hampson [247]
$OH + OH \longrightarrow H_2O_2$				
6.5×10^{-11}	M	300	1	Greiner [529]
2.6×10^{-11}	M	298	75000	Fulle et al. [530]
2.4×10^{-11}	M	298	750–7500	Sangwan et al. [526]
2.2×10^{-11}	M	298	750–112500	Forster et al. [499]
1.5×10^{-11}	M	298	20–825	Zellner et al. [525]
1.5×10^{-11}	S	298		Baulch et al. [137]
$OH + OH \longrightarrow H_2O + {}^3O$				
2.6×10^{-12}	M	300	1	Dixon-Lewis et al. [531]
2.3×10^{-12}	M	298	1–4	Westenberg & deHaas [532]
2.1×10^{-12}	M	298	23–78	Trainor & von Rosenberg Jr. [527]
2.1×10^{-12}	M	298	1	Trainor & von Rosenberg Jr. [528]
1.7×10^{-12}	M	298		Farquharson & Smith [533]
$1.3–1.5\times10^{-12}$	M	298	1–2	Clyne & Down [534]
1.4×10^{-12}	M	298	2250–7500	Sangwan & Krasnoperov [535]
1.4×10^{-12}	M	298	1	Bedjanian et al. [536]
1.4×10^{-12}	M	298		Wagner & Zellner [537]
8.4×10^{-13}	M	298	1	Breen & Glass [538]
2.0×10^{-12}	S	298		Tsang & Hampson [247]
1.4×10^{-12}	S	298		Baulch et al. [137]
$OH + {}^3O \longrightarrow O_2 + H$				

4.3×10^{-11}	M	298	1	Breen & Glass [538]
4.2×10^{-11}	M	298	2.5–4	Smith & Stewart [539]
3.9×10^{-11}	M	298	4	Howard & Smith [540]
$2.3–3.8\times10^{-11}$	M	298	0.6-0.9	Westenberg et al. [541]
3.8×10^{-11}	M	298	3.75	Howard & Smith [542]
3.3×10^{-11}	M	298	40	Robertson & Smith [543]
3.2×10^{-11}	M	298	40	Robertson & Smith [544]
3.1×10^{-11}	M	300	1–5	Brune et al. [545]
2.9×10^{-11}	M	298		Lewis & Watson [546]
2.8×10^{-11}	M	300	2–8	Kurzius & Boudart [547]
3.9×10^{-15}	S	298		Tsang & Hampson [247]
2.9×10^{-11}	S	298		Baulch et al. [137]
$OH + NH \longrightarrow HNO + H$				
3.3×10^{-11}	S	298		Cohen & Westberg [448]
$OH + NH \longrightarrow H_2O + {}^4N$				
5.1×10^{-12}	S	298		Cohen & Westberg [448]
$OH + {}^4N \longrightarrow NO + H$				
5.3×10^{-11}	M	298	4	Howard & Smith [540]
5.2×10^{-11}	M	294	2.5–6	Smith & Stewart [539]
5.0×10^{-11}	M	298	3.75	Howard & Smith [542]
4.2×10^{-11}	M	300	1–5	Brune et al. [545]
$OH + CH_4 \longrightarrow H_2O + CH_3$				
1.1×10^{-14}	M	300	1	Wilson & Westenberg [548]
8.5×10^{-15}	M	298	99	Wilson & Westenberg [549]
7.6×10^{-15}	M	298	100	Sharkey & Smith [550]
6.9×10^{-15}	M	298	100	Mellouki et al. [551]
6.6×10^{-15}	M	298	151	Bryukov et al. [552]
6.4×10^{-15}	M	298	100	Bonard et al. [553]
6.4×10^{-15}	M	298	100	Gierczak et al. [554]
$6.2–6.3\times10^{-15}$	M	298	100–300	Vaghjiani & Ravishankara [555]
6.2×10^{-15}	M	298	400–750	Dunlop & Tully [556]
5.9×10^{-15}	M	298	1	Finlayson-Pitts et al. [557]
8.0×10^{-15}	S	298		Baulch et al. [137]
7.9×10^{-15}	S	298		Tsang & Hampson [247]
$OH + CH_3 + M \longrightarrow CH_3OH + M$				
$k_0(SF_6) = 7.2\times10^{-27}$	M	298	64–750	Fagerström et al. [558]
$k_0(He) = 2.6\times10^{-27}$	M	300	0.5–2.5	Humpfer et al. [559]
$k_0(SF_6) = 2.5\times10^{-27}$	M	298	64–750	Fagerström et al. [560]
$k_0(He) = 2.0\times10^{-27}$	M	300	0.2–5	Oser et al. [561]
$k_0(He) = 2.0\times10^{-27}$	M	300	1–7	Oser et al. [562]
$OH + CH_3 \longrightarrow CH_3OH$				
1.7×10^{-10}	M	300	0.5–2.5	Humpfer et al. [559]
1.7×10^{-10}	M	300	1–7	Oser et al. [562]
1.4×10^{-10}	M	298	64–750	Fagerström et al. [560]
1.4×10^{-10}	M	298	64–750	Fagerström et al. [558]
9.4×10^{-11}	M	298	760	Anastasi et al. [563]
9.3×10^{-11}	M	300	0.2–5	Oser et al. [561]
$OH + CH_3 \longrightarrow {}^3O + CH_4$				
1.8×10^{-17}	S	298		Cohen & Westberg [448]
$OH + {}^3CH_2 \longrightarrow H_2CO + H$				
3.0×10^{-11}	S	298		Tsang & Hampson [247]
$OH + {}^1CH_2 \longrightarrow H_2CO + H$				
5.0×10^{-11}	S	298		Tsang & Hampson [247]
$OH + H_2 \longrightarrow H_2O + H$				
8.5×10^{-15}	M	298	760	Sworski et al. [564]
7.2×10^{-15}	M	298	10-20	Smith & Zellner [565]
7.0×10^{-15}	M	298	15	Atkinson et al. [566]
7.0×10^{-15}	M	298	15	Atkinson et al. [567]
6.9×10^{-15}	M	298	50–300	Talukdar et al. [568]
6.7×10^{-15}	M	298	17–100	Orkin et al. [569]
6.2×10^{-15}	M	298	100	Ravishankara et al. [570]
6.1×10^{-15}	M	298	50	Tully & Ravishankara [571]
5.8×10^{-15}	M	298	40–760	Overend et al. [572]
5.3×10^{-15}	M	298	23	Trainor & von Rosenberg Jr. [573]
6.4×10^{-15}	S	298		Tsang & Hampson [247]
6.2×10^{-15}	S	300		Baulch et al. [137]
$OH + H + M \longrightarrow H_2O + M$				
$k_0(CO_2) = 9.0\times10^{-31}$	M	300	3–11	Zellner et al. [444]
$k_0(N_2) = 4.8\times10^{-31}$	M	300	3–11	Zellner et al. [444]
$k_0(Ar) = 2.3\times10^{-31}$	M	300	3–11	Zellner et al. [444]

$k_0(\mathrm{He}) = 1.5\times10^{-31}$	M	300	3–11	Zellner et al. [444]
$k_0(\mathrm{H_2O}) = 4.3\times10^{-30}$	S	300		Baulch et al. [137]
$k_0(\mathrm{N_2}) = 6.8\times10^{-31}$	S	300		Baulch et al. [137]
$k_0(\mathrm{Ar}) = 2.6\times10^{-31}$	S	300		Baulch et al. [137]
$k_0(\mathrm{H_2O}) = 6.8\times10^{-31}$	S	300		Tsang & Hampson [247]
$\mathrm{OH + H \longrightarrow {}^3O + H_2}$				
5.6×10^{-16}	S	300		Kaufman & Del Greco [574]
9.9×10^{-17}	S	298		Cohen & Westberg [433]
1.1×10^{-16}	S	300		Tsang & Hampson [247]
$\mathrm{{}^3O + CN \longrightarrow CO + {}^4N}$				
3.7×10^{-11}	M	298	10–100	Titarchuk & Halpern [575]
2.1×10^{-11}	M	298		Schacke et al. [576]
2.7×10^{-12}	M	298	7	Schmatjko & Wolfrum [577]
1.7×10^{-11}	S	298		Tsang [390]
7.6×10^{-12}	S	298		Baulch et al. [137]
$\mathrm{{}^3O + CN \longrightarrow CO + {}^2N}$				
1.6×10^{-11}	M	298	7	Schmatjko & Wolfrum [577]
9.4×10^{-12}	S	298		Baulch et al. [137]
$\mathrm{{}^3O + {}^3O + M \longrightarrow O_2 + M}$				
$k_0(\mathrm{N_2}) = 7.2\times10^{-33}$–$1.0\times10^{-32}$	M	300	2–5	Morgan et al. [578]
$k_0(\mathrm{O_2}) = 1.0\times10^{-32}$	M	298	1–2	Tchen [579]
$k_0(\mathrm{N_2}) = 4.8\times10^{-33}$	M	298	2–15	Campbell & Gray [580]
$k_0(\mathrm{O_2}) = 4.5\times10^{-33}$	M	300	1–10	Marshall [581]
$k_0(\mathrm{N_2}) = 3.1\times10^{-33}$	M	298	2–10	Campbell & Thrush [582]
$k_0(\mathrm{Ar}) = 2.7\times10^{-33}$	M	300	1	Reeves et al. [583]
$k_0(\mathrm{Ar}) = 1.7\times10^{-33}$	M	298	2–10	Campbell & Thrush [582]
$k_0(\mathrm{He}) = 1.3\times10^{-33}$	M	298	2–10	Campbell & Thrush [582]
$k_0(\mathrm{Ar}) = 3.9\times10^{-34}$	M	300		Kondratiev & Nikitin [584]
$k_0(\mathrm{Ar}) = 1.1\times10^{-33}$	S	298		Tsang & Hampson [247]
$\mathrm{{}^3O + NH \longrightarrow HNO \longrightarrow NO + H}$				
5.0×10^{-11}	S	298		Cohen & Westberg [448]
$\mathrm{{}^3O + NH \longrightarrow OH + {}^4N}$				
5.0×10^{-12}	S	298		Cohen & Westberg [448]
$<1.7\times10^{-13}$	M	298	11–15	Hack et al. [282]
$\mathrm{{}^3O + {}^4N + M \longrightarrow NO + M}$				
$k_0(\mathrm{CO_2}) = 1.8\times10^{-32}$	M	298	2–15	Campbell & Thrush [418]
$k_0(\mathrm{N_2O}) = 1.5\times10^{-32}$	M	298	2–15	Campbell & Thrush [418]
$k_0(\mathrm{N_2}) = 1.1\times10^{-32}$	M	298	2–10	Campbell & Thrush [582]
$k_0(\mathrm{N_2}) = 9.2\times10^{-33}$	M	298	2–15	Campbell & Gray [580]
$k_0(\mathrm{N_2}) = 9.1\times10^{-33}$	M	298	2–9	Kretschmer & Peterson [421]
$k_0(\mathrm{Ar}) = 8.2\times10^{-33}$	M	298	2–10	Campbell & Thrush [582]
$k_0(\mathrm{N_2}) = 5.0\times10^{-33}$	M	298	3–4	Mavroyannis & Winkler [585]
$k_0(\mathrm{He}) = 3.8\times10^{-33}$	M	298	2–10	Campbell & Thrush [582]
$\mathrm{{}^3O + CH_4 \longrightarrow OH + CH_3}$				
6.6×10^{-16}	M	300		Froben [586]
1.2×10^{-17}	M	298	1–2	Westenberg & de Haas [587]
6.6×10^{-19}	M	293	10–150	Falconer et al. [588]
5.0×10^{-18}	S	298		Baulch et al. [137]
4.3×10^{-18}	S	298		Tsang & Hampson [247]
$\mathrm{{}^3O + CH_3 \longrightarrow H_2CO + H}$				
1.9×10^{-10}	M	298		Slagle et al. [589]
1.4×10^{-10}	M	298		Slagle et al. [590]
1.4×10^{-10}	M	298	$<2\times10^{-4}$	Washida [591]
1.2×10^{-10}	M	298	2.8	Washida & Bayes [592]
1.1×10^{-10}	M	298	19	Zellner et al. [593]
1.1×10^{-10}	M	295		Plumb & Ryan [594]
1.0×10^{-10}	M	298		Washida & Bayes [595]
9.4×10^{-11}	M	298	0.1	Seakins & Leone [596]
$>3.0\times10^{-11}$	M	298		Morris, Jr. & Niki [597]
$>3.0\times10^{-11}$	M	300	1–2	Niki et al. [598]
1.4×10^{-10}	S	298		Baulch et al. [137]
1.3×10^{-10}	S	298		Tsang & Hampson [247]
$\mathrm{{}^3O + {}^3CH_2 \longrightarrow products}$				
1.3×10^{-10}	M	296		Böhland et al. [599]
1.3×10^{-10}	M	295		Vinckier & Debruyn [600]
2.0×10^{-10}	S	298		Baulch et al. [137]
1.9×10^{-11}	S	298		Tsang & Hampson [247]
$\mathrm{{}^3O + CH \longrightarrow products}$				
9.5×10^{-11}	M	298	5–15	Messing et al. [274]
9.4×10^{-11}	M	298	5–10	Messing et al. [601]

$^{3}O + CH \longrightarrow CO + H$				
6.6×10^{-11}	S	298		Baulch et al. [137]
$^{3}O + H_2 \longrightarrow OH + H$				
1.1×10^{-17}	M	298	300	Zhu et al. [602]
1.0×10^{-17}	M	297	100–600	Presser & Gordon [603]
9.1×10^{-18}	M	298		Light & Matsumoto [604]
8.5×10^{-18}	S	298		Baulch et al. [137]
7.0×10^{-18}	S	298		Tsang & Hampson [247]
$^{3}O + H + M \longrightarrow OH + M$				
$k_0(M) = 1.0\times10^{-33}$–$8\times10^{-30}$	S	298		Baulch et al. [605]
$k_0(M) = 4.4\times10^{-32}$	S	298		Tsang & Hampson [247]
$^{1}O + CH_4 \longrightarrow OH + CH_3$				
3.8×10^{-10}	M	300	11	Gauthier & Snelling [518]
2.2×10^{-10}	M	300	1–3	Matsumi et al. [606]
1.9×10^{-10}	M	298	10	Vranckx et al. [607]
1.7×10^{-10}	M	298	45	Dillon et al. [608]
1.4×10^{-10}	M	295	25–250	Blitz et al. [461]
4.0×10^{-10}	S	298		Cvetanović [609]
$^{1}O + H_2 \longrightarrow OH + H$				
3.0×10^{-10}	M	300	11	Gauthier & Snelling [518]
2.7×10^{-10}	M	298	0.1	Koppe et al. [610]
2.5×10^{-10}	M	298	7–21	Stief et al. [611]
2.2×10^{-10}	M	298	1	Matsumi et al. [606]
1.2×10^{-10}	M	298		Talukdar & Ravishankara [612]
1.1×10^{-10}	M	298	100	Ogren et al. [613]

M: Monitoring decay of reactants and/or production of products.

S: Suggested value based on experiments and/or evaluations at a range of temperatures.

4.9.3 Lennard-Jones Parameters

Table 4.8: Lennard-Jones force constants used in this study. Values are obtained from viscosity data when possible.

Molecule	σ (Å)	ϵ/k_b (K)	Source
CO_3	$^{a}3.996$	$^{a}190$	Welty et al. [360]
NCCO	$^{b}4.38$	$^{b}339$	Welty et al. [360]
CO_2	3.996	190	Welty et al. [360]
CH_3CHO	3.97	436	Wang et al. [361]
H_2CNOH	$^{e}3.585$	$^{e}507$	Welty et al. [360]
CH_3OH	3.585	507	Welty et al. [360]
CH_2CO	3.97	436	Wang et al. [361]
HCON	$^{c}3.59$	$^{c}498$	Wang et al. [361]
HOCN	$^{c}3.59$	$^{c}498$	Wang et al. [361]
HCNO	$^{c}3.59$	$^{c}498$	Wang et al. [361]
H_2CO	3.59	498	Wang et al. [361]
HCCO	$^{d}4.221$	$^{d}185$	Welty et al. [360]
NCO	$^{g}3.63$	$^{g}569.1$	Reid et al. [359]

H_2O_2	4.196	289.3	Reid et al. [359]
trans−HNOH	[f]3.47	[f]119	Welty et al. [360]
HCO	3.59	498	Wang et al. [361]
HO_2	3.458	107.4	Wang et al. [361]
N_2	3.681	91.5	Welty et al. [360]
H_2O	2.649	356	Welty et al. [360]
O_2	3.433	113	Welty et al. [360]
NO	3.47	119	Welty et al. [360]
OH	2.75	80	Wang et al. [361]
H_2	2.968	33.3	Welty et al. [360]

[a] L-J parameters based on those for CO_2

[b] L-J parameters based on those for NCCN

[c] L-J parameters based on those for H_2CO

[d] L-J parameters based on those for C_2H_2

[e] L-J parameters based on those for CH_3OH

[f] L-J parameters based on those for NO

[g] L-J parameters based on those for HCN

4.9.4 Theoretical Case Studies

The following case studies provide additional details for some of the non-standard reactions in this study. Examples include intersystem crossing reactions, reactions with vibrational intermediates or complex pathways, and reactions where BHandHLYP/aug-cc-pVDZ misdiagnosed the barrier.

4.9.4.1 Case Study 1: $CO_2 + {}^1O \longrightarrow {}^1CO_3\cdot \longrightarrow {}^3CO_3\cdot \longrightarrow CO_2 + {}^3O$

The deexcitation of ${}^1O$ by CO_2 has been studied considerably both experimentally and theoretically [460, 464, 465, 614–622].

Experiments confirm that the dominant quenching pathway leads to ground state oxygen atoms (${}^3O$) [460, 466, 618, 621, 622]. RRKM and statistical models have been used to explore the quenching mechanism [615, 619], the dominant of which is to react ${}^1O$ by CO_2 to form singlet CO_3, which then undergoes intersystem crossing to the triplet CO_3 potential energy surface before decaying into ${}^3O + CO_2$.

An experiment by Sedlacek et al. [617] measures the singlet PES quenching pathway, $CO_2 + {}^1O \longrightarrow {}^1CO_3\cdot \longrightarrow CO + O_2$, to be approximately 1000 times less efficient than the dominant mechanism.

Experimentally measured rate coefficients for the overall quenching of ^1O by CO_2 in the 295–300 K range from 1.0–2.3×10^{-10} cm^3s^{-1} [454, 460–462, 464–466].

In this work, we calculate the rate coefficient for $CO_2 + {}^1O \longrightarrow CO_3$ at the BHandHLYP/aug-cc-pVDZ level of theory to be$k(298\ K) = 3.8\times10^{-11}$ cm^3s^{-1}, and assume this to be the rate-limiting step in the quenching pathway to $CO_2 + {}^3O$. This value is only a factor of 3 lower than the nearest experimental measurement by Wine & Ravishankara [462].

We also include the third-order reaction $CO_2 + {}^1O + M \longrightarrow CO_3 + M$ in our network for M = N_2, CO_2, and H_2.

4.9.4.2 Case Study 2:
$\mathbf{CO_2 + {}^2N \longrightarrow NCO_2\cdot \longrightarrow OCNO\cdot \longrightarrow CO + NO}$

Experimental measurements of the rate coefficient for this reaction at 300 K are between 1.8–6.8×10^{-13} cm^3s^{-1} [234, 236, 287, 288, 467]. Herron [237] reviewed these experiments and suggested a value of 3.6×10^{-13} cm^3s^{-1}.

There have been no theoretical studies performed on this reaction to date.

Husain et al. [288] suggest this reaction has a small energy barrier due to its fairly slow rate coefficient for a reaction of high exothermicity.

We do not find a barrier for this reaction at the BHandHLYP/aug-cc-pVDZ level of theory. We also do not find a barrier at the CCSD/aug-cc-pVDZ level of theory.

On the other hand, at the HF/aug-cc-pVDZ level of theory, we find a barrier of 34.3 kJ mol^{-1} at the transition state for a C-N bond distance of 1.89Å.

In a computational methods comparison study on the reaction of $CH_4 + H \longrightarrow CH_3 + H_2$, we found the variational transition state barrier at the HF/aug-cc-pVDZ level of theory to be approximately twice the size of the barrier calculated at the BHandHLYP/aug-cc-pVDZ level of theory. We insert an artificial barrier of half the HF value (17.15 kJ mol^{-1}) into the calculation for $k(298\ K)$ at the BHandHLYP/aug-cc-pVDZ level of theory, and obtain a rate coefficient of 3.2×10^{-14} cm^3s^{-1}. This value is ∼6 times smaller than the nearest experimental value.

4.9.4.3 Case Study 3: $CO_2 + CH \longrightarrow CHCO_2\cdot \longrightarrow HCOCO\cdot \longrightarrow HCO + CO$

The rate coefficients for this reaction have been measured experimentally at 298 K and range from 1.8–2.1$\times10^{-12}$ cm^{3}s^{-1} [446, 469–471]. Baulch et al. [137] reviewed the earliest of these experimental results and has suggested a k(298 K) value of 1.8$\times10^{-12}$ cm^{3}s^{-1}. Mehlmann et al. [446] predict this reaction to have little of no activation barrier below 400 K.

We find no theoretical studies of this reaction.

We find the first step of this reaction to be the rate-limiting step. At the BHandHLYP/aug-cc-pVDZ level of theory, the first step of this reaction has a barrier; However, at the B3LYP/aug-cc-pVDZ level of theory, this reaction step is barrierless. We remove the barrier from our calculation to match expectation from experiment [446] and obtain an overall rate coefficient of k(298 K) = 3.1$\times10^{-12}$ cm^{3}s^{-1} at the BHandHLYP/aug-cc-pVDZ level of theory. This is within a factor of 1.5 of the nearest experimental value.

4.9.4.4 Case Study 4: $CO_2 + {}^3CH_2 \longrightarrow H_2CO + CO$

Laufer & Bass [468] experimentally measured the rate coefficient for this reaction at 298 K to be 3.9$\times10^{-14}$ cm^{3}s^{-1}. Darwin & Moore [260] performed upper bound experiments on this reaction and found k(298) to be no greater than 1.4$\times10^{-14}$ cm^{3}s^{-1}.

Kovacs & Jackson [623] studied this reaction theoretically, and found the lowest energy path is to form the ${}^3CH_2 \cdots CO_2$ complex, followed the subsequent reaction into ${}^3CH_2CO_2$ over a 19.3 kcal mol^{-1} barrier (at the G2 level of theory). They find that the lowest energy path from the ${}^3CH_2 \cdots CO_2$ complex is to fragment back into ${}^3CH_2$ and CO_2 over a 1.1 kcal mol^{-1} barrier. They also suggest an intersystem crossing reaction from this complex to the singlet surface is unlikely, and that ${}^3CH_2$ would may require collisional reaction to the singlet state in order for this reaction to proceed.

We find similar results to Kovacs & Jackson [623] at the BHandHLYP/aug-cc-pVDZ and CCSD/aug-cc-pVDZ levels of theory. CO_2 + ${}^3CH_2$ proceeds via a barrierless reaction to form the ${}^3CH_2 \cdots CO_2$ complex with a C-C bond distance of 3.25 (3.23) Å at the BHandHLYP/aug-cc-pVDZ (CCSD/aug-cc-pVDZ) level of theory. This reaction efficiently decays back into CO_2 + ${}^3CH_2$, and the barrier to ${}^3CH_2CO_2$ is

15.7 (19.3) kcal mol^{-1} at the BHandHLYP/aug-cc-pVDZ (CCSD/aug-cc-pVDZ) level of theory. We find the rate coefficient for the reaction $CO_2 + {}^3CH_2 \longrightarrow {}^3CH_2 \cdots CO_2 \longrightarrow {}^3CH_2CO_2$ to be k(298 K) = 1.8×10^{-23} (2.3×10^{-25}) cm^{3}s^{-1} at the BHandHLYP/aug-cc-pVDZ (CCSD/aug-cc-pVDZ) level of theory, which is too slow to consider in our network.

Our results and those of Kovacs & Jackson [623] suggest this reaction likely does not occur on the triplet surface. For this reason, we do not include it in our network, and instead only include the singlet surface reaction $CO_2 + {}^1CH_2 \longrightarrow H_2CO + CO$. We find $CO_2 + {}^1CH_2 \longrightarrow H_2CO + CO$ to have a rate coefficient of 8.0×10^{-13} cm^{3}s^{-1} at 298 K, which is only a factor of 2 larger than the experimental value for $CO_2 + {}^3CH_2 \longrightarrow H_2CO + CO$. This adds some evidence to the suggestion that $^3CH_2$ must first collisionally excite to $^1CH_2$ before reacting with CO_2 to produce $H_2CO + CO$.

4.9.4.5 Case Study 5: $HCO + HCO \longrightarrow$ products

Three potential product channels of the self-reaction of HCO have been reported experimentally [456, 492–495, 624].

$$HCO + HCO \longrightarrow cis{-}C_2H_2O_2 \tag{4.19}$$

$$HCO + HCO \longrightarrow H_2CO + CO \tag{4.20}$$

$$HCO + HCO \longrightarrow 2\,CO + H_2 \tag{4.21}$$

Rate coefficients for $HCO + HCO \longrightarrow H_2CO + CO$ have been experimentally measured at 295–298 K and range from 3.0–7.5×10^{-11} cm^{3}s^{-1} [492–496].. The lack of temperature dependence in the range of 298–475 K suggests this reaction is barrierless [495].

Yee Quee & Thynne [456] performed the only experimental measurement of the rate coefficient for $HCO + HCO \longrightarrow 2\,CO + H_2$ at 298 K, which they find to be 3.6 $\times10^{-11}$ cm^{3}s^{-1}.

Rate coefficients for $HCO + HCO \longrightarrow trans{-}C_2H_2O_2$ have been experimentally measured at 298 K to be in the range of 2.8–500×10^{-13} cm^{3}s^{-1} [456, 491].

There are no experimental measurements of the rate coefficient for $HCO+HCO \longrightarrow cis{-}C_2H_2O_2$.

Saheb & Nazari [625] performed theoretical quantum computational simulations, and found the most important product channels to be:

$$\mathrm{HCO + HCO \longrightarrow cis{-}C_2H_2O_2\cdot \longrightarrow 2\,CO + H_2} \tag{4.22}$$

$$\mathrm{HCO + HCO \longrightarrow trans{-}C_2H_2O_2\cdot \longrightarrow anti{-}HCOH + CO} \tag{4.23}$$

We find no direct abstraction reaction for $\mathrm{HCO + HCO \longrightarrow H_2CO + CO}$ on the singlet surface. We do however find an inefficient abstraction reaction for $\mathrm{HCO + HCO \longrightarrow anti{-}HCOH + CO}$, with a k(298 K) rate coefficient of $3.4{\times}10^{-24}$ $\mathrm{cm^3s^{-1}}$ at the BHandHLYP/aug-cc-pVDZ level of theory.

We find the reaction $\mathrm{HCO + HCO \longrightarrow trans{-}C_2H_2O_2}$ to have a barrierless rate coefficient of $4.1{\times}10^{-13}$ $\mathrm{cm^3s^{-1}}$ at 298 K at the BHandHLYP/aug-cc-pVDZ level of theory. At the same level of theory, we calculate the rate coefficient of the subsequent reaction $\mathrm{trans{-}C_2H_2O_2 \longrightarrow anti{-}HCOH + CO}$ (k(298 K) = $7.1{\times}10^{-34}$ $\mathrm{s^{-1}}$) to be slightly smaller than than the decay back into $\mathrm{HCO + HCO}$ (k(298 K) = $1.7{\times}10^{-33}$ $\mathrm{s^{-1}}$). Finally, we find anti−HCOH efficiently isomerizes into $\mathrm{H_2CO}$. We calculate the overall rate coefficient at 298 K for $\mathrm{HCO + HCO \longrightarrow trans{-}C_2H_2O_2 \longrightarrow anti{-}HCOH + CO \longrightarrow H_2CO + CO}$ to be $1.2{\times}10^{-13}$ $\mathrm{s^{-1}}$, which is slightly reduced from the barrierless value due to the slight preference in the decay back to $\mathrm{HCO + HCO}$ over anti−HCOH + CO. This is only a factor of 2 smaller than the nearest experimental value for $\mathrm{HCO + HCO \longrightarrow trans{-}C_2H_2O_2}$ [456].

We calculate the reaction $\mathrm{HCO + HCO \longrightarrow cis{-}C_2H_2O_2\cdot \longrightarrow CO + CO + H_2}$ to have a rate coefficient of k(298 K) = 7.4 $\times10^{-11}$ $\mathrm{cm^3s^{-1}}$ at the BHandHLYP/aug-cc-pVDZ level of theory. This is only a factor of 2 larger than the only experimental value.

4.9.4.6 Case Study 6: $\mathrm{CO + OH \longrightarrow intermediates\cdot \longrightarrow CO_2 + H}$

Experimental measurements of the rate coefficient for this reaction at 296–300 K range from $8.5{\times}10^{-14}$ to $9.7{\times}10^{-13}$ $\mathrm{cm^3s^{-1}}$ [499–508]. Baulch et al. [137] review the kinetic data from experiments and suggest a very slight temperature dependence, suggesting this reaction proceeds with little or no reaction barrier.

There are multiple reaction pathways for this reaction, but the fastest is that which proceeds through the $\mathrm{OH \cdots CO\cdot}$ and cis−HOCO· intermediates [626].

At the BHandHLYP/aug-cc-pVDZ level of theory, we calculate k(298 K) for the barrierless first step, $\mathrm{CO + OH \longrightarrow OH \cdots CO\cdot}$, to be $9.7{\times}10^{-12}$ $\mathrm{cm^3s^{-1}}$. However, we find intermediate barriers at the second and third steps of this calculation at the BHandHLYP/aug-cc-pVDZ level of theory, making the overall rate coefficient for $CO + OH \longrightarrow OH \cdots CO\cdot \longrightarrow \text{cis}-HOCO\cdot \longrightarrow CO_2 + H$, 5.7×10^{-19} cm^{3}s^{-1}. This is several orders of magnitude smaller than the range of experimental values. At the B3LYP/aug-cc-pVDZ level of theory, these barriers are more comparable, resulting in only a factor of 3.4 reduction between the barrierless first step and the overall rate coefficient. *Ab initio* calculations show similar barrier heights to our the B3LYP/aug-cc-pVDZ calculations [626].

We reduce the calculated rate coefficient for the barrierless first step at the BHandHLYP/aug-cc-pVDZ level of theory by a factor of 3.4 to match the barrier effects at the B3LYP/aug-cc-pVDZ level of theory. This gives us a rate coefficient of $k(298) = 2.9\times10^{-12}$ cm^{3}s^{-1}, which is a factor of 3 higher than the nearest experimental value.

4.9.4.7 Case Study 7: $OH + O \longrightarrow HO_{2(\nu)}\cdot \longrightarrow O_2 + H$

Experimental measurements for this reaction at 298–300 K range from 2.3–4.3×10^{-11} cm^{3}s^{-1} [538–547].

This reaction proceeds through HO_2, which, in its ground vibrational state has been noted to be long-lived [627, 628]. Our calculations confirm that the decay of HO_2 into $O_2 + H$ is slow ($< 10^{-47}$ s^{-1}). This suggests this reaction proceeds through an excited vibrational state, as is to be expected when two reactants combine to form a single product [351].

We calculate the rate coefficient of $OH + {}^3O \longrightarrow HO_2$ at 298 K at the BHandHLYP/aug-cc-pVDZ level of theory to be 7.4×10^{-11} cm^{3}s^{-1}, and assume the subsequent vibrational decay into $O_2 + H$. Our calculated rate coefficient is within a factor of 2 of the experimental range.

There are currently no experimental measurements for the rate coefficient of $OH + {}^1O \longrightarrow O_2 + H$, which we find also proceeds through HO_2. We calculate the rate coefficient of $OH + {}^1O \longrightarrow HO_2$ at 298 K at the BHandHLYP/aug-cc-pVDZ level of theory to be 1.0×10^{-9} cm^{3}s^{-1}, and similarly assume the vibrational decay into $O_2 + H$.

4.9.4.8 Case Study 8: $OH + NH \longrightarrow$ products

No experiments have been performed to date on the reaction of $OH + NH$. Cohen & Westberg [448] use analogous reactions to suggest rate coefficients of k(298 K) $= 3.3\times10^{-11}$ cm^3s^{-1} and 5.1×10^{-12} cm^3s^{-1} for $OH + NH \longrightarrow HNO + H$ and $OH + NH \longrightarrow H_2O + {}^4N$, respectively. They suggest little or no barrier exists for either pathway.

Klippenstein et al. [629] performed theoretical transition state theory calculations for this reaction using a range of computational quantum methods. They calculated 298 K reaction rate coefficients of 6.8×10^{-11} cm^3s^{-1} and 1.4×10^{-12} cm^3s^{-1} for $OH + NH \longrightarrow HNO + H$ and $OH + NH \longrightarrow H_2O + {}^4N$, respectively.

We find the $OH + NH \longrightarrow HNO + H$ reaction to proceed through multiple intermediates, including $OH \cdots NH\cdot$, trans$-HNOH\cdot$, and $H_2NO\cdot$. We calculate the barrierless first step of this reaction $OH + NH \longrightarrow OH \cdots NH\cdot$ at 298 K at the BHandHLYP/aug-cc-pVDZ level of theory to be 7.0×10^{-12} cm^3s^{-1}. However, at this level of theory, we find a large forward barrier at the third reaction step (i.e., trans$-HNOH\cdot \longrightarrow HNO + H$), which reduces the overall rate coefficient to 2.6×10^{-14} cm^3s^{-1}. This is over three orders of magnitude smaller than the recommended and theoretical values. Conversely, at the B3LYP/aug-cc-pVDZ level of theory, the third forward reaction step barrier is smaller than the reverse barrier, which makes the barrierless first step the rate limiting step.

We remove the barrier at the third reaction step from our calculation to match the kinetic data and theoretical studies, and obtain an overall rate coefficient for $OH + NH \longrightarrow HNO + H$ of k(298 K) $= 7.0\times10^{-12}$ cm^3s^{-1} at the BHandHLYP/aug-cc-pVDZ level of theory. This value is a factor of 5 smaller than the suggested value [448].

We calculate the rate coefficient for $OH + NH \longrightarrow H_2O + {}^4N$ at 298 K at the BHandHLYP/aug-cc-pVDZ level of theory to be 6.8×10^{-13} cm^3s^{-1}. This is a factor of 5 smaller than the suggested value by Cohen & Westberg [448].

4.9.4.9 Case Study 9: $O + H_2CN \longrightarrow CH_2NO\cdot \longrightarrow$ products

No experiments to date have measured the rate coefficient of ${}^3O + H_2CN \longrightarrow HCN + OH$. Tomeczek & Gradoń [228] suggested a temperature-independent rate of 8.3×10^{-11} cm^3s^{-1} based on calculations using published chemical compositions of the flames of methane, nitrogen and oxygen at >1850 K. They note that this calculation does not include the effects of an energy barrier, and thus this value is not reliable at 298 K. Tomeczek & Gradoń [228] also suggested this same rate coefficient for the reaction $H + H_2CN \longrightarrow HCN + H_2$.

No previous theoretical studies regarding this reaction have been performed.

Unlike $H + H_2CN \longrightarrow HCN + H_2$, which we found in previous work to proceed efficiently through a barrierless abstraction mechanism [335], we find no abstraction pathway for $^3O + H_2CN \longrightarrow HCN + OH$. Instead, we find that ^3O and H_2CN efficiently react to form $CH_2NO\cdot$ with a rate coefficient of $3.1{\times}10^{-11}$ cm^3s^{-1}. This product most commonly decays back into the original reactants; However, there are two other favourable pathways. The mechanistic model for these reactions is shown in Figure 4.1.

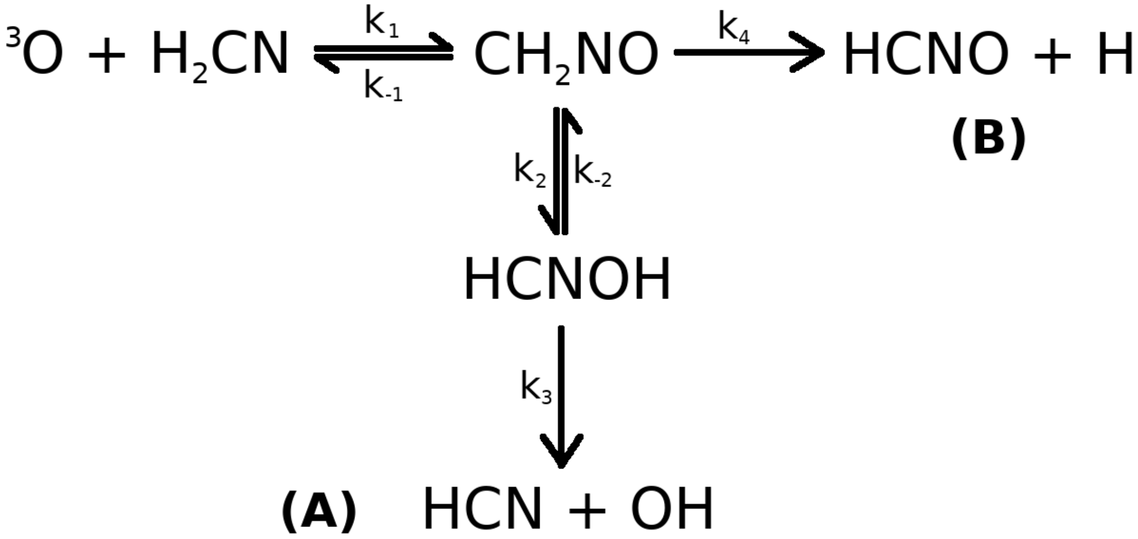

Figure 4.1: Mechanistic model for the reaction of $^3O + H_2CN$. Two efficient product channels on the doublet surface exist: **(A)** $HCN + OH$ and **(B)** $HCNO + H$.

Using the mechanistic model above, we use the steady-state solutions to the kinetic rate equations to calculate the overall rate coefficients for paths A and B. This is done by equating the kinetic rate equations for each species in the mechanistic model to zero (e.g. $d[CH_2NO]/dt = 0 = k_1[^3O + H_2CN] + k_{-2}[HCNOH] - (k_{-1} + k_2)[CH_2NO]$), and substituting these equations into the overall kinetic rate equations for products A and B from the initial reactants. This gives us the following rate coefficients for paths A and B:

$$k_A = \frac{k_1 k_3}{\alpha}, \tag{4.24}$$

$$\alpha = \frac{(k_{-1} + k_2 + k_4)\,(k_{-2} + k_3)}{k_2} - k_{-2}. \tag{4.25}$$

$$k_B = \frac{k_1 k_4}{\beta}, \tag{4.26}$$

$$\beta = k_{-1} + k_2 + k_4 - \frac{k_{-2} k_2}{k_{-2} + k_3}. \tag{4.27}$$

We calculate these rate coefficients at the BHandHLYP/aug-cc-pVDZ level of theory to be $k_A = 4.0\times10^{-14}$ and $k_B = 8.3\times10^{-15}$ cm^3s^{-1} at 298 K, respectively.

We propose that the suggested barrierless rate coefficient for $^3O + H_2CN \longrightarrow HCN + OH$ by Tomeczek & Gradoń [228] is not an accurate estimate for this overall reaction at 298 K. In fact, the large barrier for $CH_2NO\cdot \longrightarrow HCNOH\cdot$ isomerization at 298 K plays a key role in decreasing this overall rate coefficient. We find the isomerization barrier to also have similar heights when using the B3LYP and CCSD computational methods.

We use similar mechanistic modeling to calculate the rate coefficients for the reactions of $^1O + H_2CN \longrightarrow CH_2NO\cdot \longrightarrow$ products; However along with the two decay pathways above, there is an additional decay pathway to $^3O + H_2CN$. We are the first to calculate these three $^1O + H_2CN$ reaction rate coefficients.

At the BHandHLYP/aug-cc-pVDZ level of theory, we calculate the rate coefficients for the reaction of $^1O + H_2CN$ to products (A) $HCN + OH$, (B) $HCNO + H$, and (C) $^3O + H_2CN$, to be 1.2×10^{-13}, 6.0×10^{-13}, and 4.5×10^{-10} cm^3s^{-1}, respectively.

Given the potential importance of $^1O + H_2CN \longrightarrow HCN + OH$ to produce HCN in atmospheres, and the similar barrier heights to the three product channels, we also calculated these rate coefficients at the ωB97XD/aug-cc-pVDZ and CCSD/aug-cc-pVDZ levels of theory.

At the ωB97XD/aug-cc-pVDZ level of theory, we calculate the rate coefficients for the reaction of $^1O + H_2CN$ to products (A), (B), and (C), to be 5.3×10^{-11}, 2.8×10^{-10}, and 6.6×10^{-23} cm^3s^{-1}, respectively.

At the CCSD/aug-cc-pVDZ level of theory, we calculate the rate coefficients for the reaction of $^1O + H_2CN$ to products (A), (B), and (C), to be 8.8×10^{-11}, 1.9×10^{-11}, and 2.2×10^{-10} cm^3s^{-1}.

In the case of BHandHLYP and CCSD, the dominant channel for the reaction of $^1O + H_2CN$ is (C). This is not the case for ωB97XD, where channel (C) is negligible, and the dominant channel is (B). The rate coefficient for the potentially important HCN source, channel (A), varies by a factor of 733 across the three levels of theory. Given these discrepancies, we recommend these reactions be followed up with an experimental study.

4.9.4.10 Case Study 10: $O + CH_2 \longrightarrow$ products

$^3O + ^3CH_2$ combine to form a vibrationally excited H_2CO molecule [449]. In high atmospheric pressures, this molecule can be collisionally deexcited in the reaction

$$^3O + ^3CH_2 + M \longrightarrow H_2CO + M.$$

However, in upper atmospheres, where collisions are less frequent, the vibrationally excited H_2CO will dissociate via 2 equally favourable pathways [137, 247, 449]

$$^3O + ^3CH_2 \longrightarrow H_2CO_{(\nu)} \cdot \longrightarrow CO + H + H$$

$$^3O + ^3CH_2 \longrightarrow H_2CO_{(\nu)} \cdot \longrightarrow CO + H_2$$

Experimental measurements of the rate coefficient of $^3O + ^3CH_2 \longrightarrow$ products at 295–296 K are 1.3×10^{-10} cm^{3}s^{-1} [599, 600]. Reviews of this reaction over a range of temperatures and pressures suggest a wider range of 1.9×10^{-11}–2.0×10^{-10} cm^{3}s^{-1} [137, 247].

We calculate the rate coefficient of $^3O + ^3CH_2 \longrightarrow H_2CO$ at the BHandHLYP/aug-cc-pVDZ level of theory to be $k(298\text{ K}) = 6.7\times10^{-11}$ cm^{3}s^{-1}, which is within the range of suggested values, and only a factor of 2 lower than the two experimental measurements. We allow this reaction to proceed along the two equally favourable dissociation channels, each with a calculated rate coefficient of 3.4×10^{-11} cm^{3}s^{-1}.

Excited oxygen (^1O) and methylene ($^1CH_2$) also react to produce vibrationally excited H_2CO.

We calculate the rate coefficient of $^1O + ^1CH_2 \longrightarrow H_2CO$ at the BHandHLYP/aug-cc-pVDZ level of theory to be $k(298\text{ K}) = 3.3\times10^{-10}$ cm^{3}s^{-1}. We assume that the two dissociation pathways for vibrationally excited H_2CO are also equally favourable for this reaction, and allow this reaction to proceed to form $CO + H + H$ and $CO + H_2$

with equal rate coefficients of 1.7×10^{-10} cm^{3}s^{-1}.

4.9.4.11 Case Study 11: $^1O + CH_4 \longrightarrow CH_3OH_{(\nu)} \longrightarrow OH + CH_3$

^1O and CH_4 mainly react to form vibrationally excited CH_3OH, the dominant subsequent pathway of which is to produce $OH + CH_3$ [461, 518, 606–608, 630, 631].

Experimental measurements of $^1O + CH_4 \longrightarrow OH + CH_3$ from 295–300 K range from 1.4–3.8×10^{-10} [461, 518, 606–609].

We calculate the rate coefficient of $^1O + CH_4 \longrightarrow CH_3OH$ at 298 K with the BHandHLYP/aug-cc-pVDZ level of theory to be 5.8×10^{-9} cm^{3}s^{-1}, and assume the vibrational decay into $OH + CH_3$ as suggested. Our calculated rate coefficient is a factor of 15 larger than the nearest experimental value.

4.9.4.12 Case Study 12: $^1O + H_2 \longrightarrow H_2O_{(\nu)} \longrightarrow OH + H$

Experimental measurements of the rate coefficient for $^1O + H_2 \longrightarrow OH + H$ at 298–300 K are between 1.1 and 3.0×10^{-10} cm^{3}s^{-1} [518, 606, 610–613].

This reaction is known to proceed through vibrationally excited H_2O in its ground electronic state [632, 633].

We calculate the rate coefficient for $^1O + H_2 \longrightarrow H_2O$ at 298 K at the BHandHLYP/aug-cc-pVDZ level of theory to be 7.1×10^{-10} cm^{3}s^{-1}, and assume vibrational decay into $OH + H$, as suggested. This calculated value is a factor of 2 larger than the nearest experimental value.

4.9.5 Quantum Chemistry Data

Quantum Chemistry Data has been moved to Appendix A at the end of this thesis.

Chapter 5

En route to RNA life: From atmospheric HCN to biomolecule production in warm little ponds

> *Within this fireball was all of space, a very special place with information encased.*
>
> — **GZA, *The Spark***

Ben K. D. Pearce, Karan Molaverdikhani, Ralph E. Pudritz, Thomas K. Henning, & Kaitlin E. Cerrillo

N.B. This chapter was submitted to Nature Astronomy on August 31st, 2021.

Abstract

The origin of life on Earth is thought to involve the early appearance of an information molecule such as RNA. The basic building blocks of RNA could either have been delivered by carbonaceous meteorites, or produced by aqueous photochemical processes beginning with the synthesis of hydrogen cyanide (HCN) in the early Earth's atmosphere. Here, we construct a robust, comprehensive physical and non-equilibrium chemical model of the early Earth atmosphere as it is supplied with hydrogen from impact

degassing of meteorites, sourced with water evaporated from the oceans and methane from undersea hydrothermal vents, and in which lightning and external UV-driven chemistry produce HCN. We track the rain-out of HCN into warm little ponds (WLPs) and use a comprehensive sources and sinks numerical model to compute abundances of nucleobases, ribose, and nucleobase precursors such as 2-aminooxazole resulting from aqueous and UV driven chemistry within them. We find that during the early Hadean eon, at 4.4 bya (billion years ago) peak adenine concentrations in ponds can be maintained at $\sim$2.8μM for more than 100 Myr. Meteorite delivery of these molecules to WLPs produce similar peaks in concentration, but are destroyed within months by UV photodissociation, seepage, and hydrolysis. The evolution of the atmosphere due to the decrease of hydrogen by falling impact rates and atmospheric escape, as well as the rise oxygenated species such as CO_2 by volcanic outgassing, drastically reduces these yields. After 4.3 bya, these processes effectively terminate the build up of methane - the critical feed molecule of HCN. Our work points to an origin of RNA on Earth within $\sim$200 Myr of the Moon-forming impact.

Astrophysical, geophysical and fossil evidence suggests that life on Earth emerged in the interval of 4.5–3.7 bya (billion years ago) [44]. A fundamental question on the origin of life is whether a habitable planet is capable of synthesizing biomolecular building blocks that are critical to creating information polymers such as ribonucleic acid (RNA) and proteins [12] which are central to life such as our own. Failing this, the origin of life must depend on the delivery of biomolecules by meteorites [25, 31, 51].

HCN is a key biomolecule precursor because in aqueous solution it reacts to produce several relevant biomolecules for the origin of RNA - widely thought to have been critical for the first life on Earth [76, 78, 79]. The famous Miller-Urey experiments showed that reducing atmospheres rich in H_2 and CH_4 are favorable for HCN production, whereas oxidizing atmospheres rich in CO_2 do not produce as much HCN [14, 85, 175]. This is because unlike oxidized carbon (i.e. CO_2 and CO), reduced carbon (e.g. CH_4, CH_3) efficiently reacts to produce HCN [36, 440, 634]. It is the HCN produced by electrical discharges, once dissolved in the water reservoir in the Miller-Urey apparatus, that produces the plethora of amino acids [17, 34] and nucleobases [18, 635].

However, such experiments do not address the whole planetary and geochemical context of an evolving planet and its atmosphere, nor do they address what conditions actually lead to RNA synthesis sufficient for an RNA world. Given the multiple processes that contribute to the balance of H_2, CH_4, and CO_2 in the early Earth atmosphere, including volcanic outgassing, asteroid impacts, hydrothermal activity in undersea vents, hydrogen escape from the atmosphere, and rain-out, what are the yields of biomolecules in specific environments?

Several invaluable observations are available to constrain early Earth conditions. The analysis of a Zircon mineral inclusion has shown that the early mantle was already oxidized by ∼4.35 billion years ago (bya). This implies that by then, CO_2 was mainly outgassed from volcanoes and dominated H_2 and CH_4 [170]. Before 4.35 bya, isotopic evidence from the Earth's mantle (nitrogen, oxygen, titanium, calcium, chromium, nickel, ruthenium, molybdenum, neodymium, and deuterium) shows that accreting material was most similar to enstatite meteorites [636, 637]. Reduced iron from these impactors would have been oxidized by water, releasing H_2 [129]. Past models predict that the early Earth atmosphere had a slightly reducing composition dominated by species such as N_2, CO_2, CH_4, CO, and H_2 [107, 125, 129].

The ultimate step - actual RNA synthesis - is natural in WLPs on the small land area available on the planet at that time [638]. The crucial point is that in the absence of any biological enzymes, bond formation that leads to RNA polymers involves thermal energy sufficient to remove water between the nucleotide building blocks. Such condensation reactions are well studied experimentally and arise naturally during seasonal or daily wet-dry cycles in WLPs [26–29, 31, 39, 53, 639].

The route to nucleotides remains a big question in prebiotic chemistry. The older approach involved reacting nucleobases, ribose and a phosphorous source with low yields [65]. A newer approach bypasses the need for nucleobases and ribose reactants to obtain nucleotides, but requires other reactants of unknown concentration on early Earth such as glycolaldehyde, cyanamide, glyceraldehyde and cyanoacetylene [42]. The key intermediate in the latter pathway is 2-aminooxazole. Due to the uncertainty in the route to nucleotides, we take an agnostic approach and compute the WLP concentrations of nucleobases, ribose, and 2-aminooxazole.

Non-equilibrium HCN chemistry in the early Earth atmosphere has been modeled in the past for a post-large impact scenario [129], and for a range of initial concentrations of key primordial species such as CH_4 and CO_2 [107, 125].

The holistic non-equilibrium atmosphere-pond coupled chemistry models we develop in this work offer multiple important advancements to these past models, as well as brand-new cutting edge treatments, including: the computation of self-consistent pressure-temperature (P-T) profiles via radiative transfer, the production of HCN and radicals from lightning (i.e. the Miller-Urey scenario), the time-dependent influx of key primordial species from volcanism, ocean geochemistry, impact degassing, and ocean evaporation, and most importantly, the coupling of HCN rain-out to surface WLPs, and the subsequent reaction of HCN into various critical biomolecules in the face of key terrestrial sinks such as hydrolysis, seepage, and UV photodestruction.

Our model also does not require rare, very large impactors (∼400+ km), which would need to vaporize a significant portion of the ocean in order to obtain the slow cooling times favorable for significant atmospheric CH_4 production [129]. The large impact scenario necessarily creates very hot and uninhabitable conditions where methane production is favorable. This world would be devoid of ponds. Instead, we utilize a plentiful source of CH_4 to the Hadean atmosphere from serpentinization and Fischer-Tropsch synthesis. This begins with water-dependent processes in hydrothermal systems wherein Fe- and Mg-rich ultramafic rocks (e.g. olivine) in mid-ocean ridges and forearc systems produces H_2. This H_2 reacts with the aqueous CO_2 in these environments to produce CH_4 [179, 180]. Abiotic methane production has been observed in hydrothermal systems [640, 641]; however, experiments of Fischer-Tropsch synthesis from olivine typically produce very low yields [182]. Therefore, the source and abundance of abiotic methane production in hydrothermal systems is still somewhat uncertain. Models suggest this hydrothermal process can sustain ∼2–2.5 part-per-million (ppm) of CH_4 in the early atmosphere [180]. We note that there is uncertainty with this source of methane as well.

In Figure 5.1, we illustrate our early Earth atmospheric models by focusing on the main sources and sinks for the key molecular species relevant to controlling and determining HCN chemistry. As an overall principle, H_2 and CO_2 are the main species that determine whether the environment is reducing or oxidizing. It is the balance between these two species that determines the concentration of CH_4 - the main precursor to HCN.

In the top left panel, impact degassing produces the H_2. The degassing rate

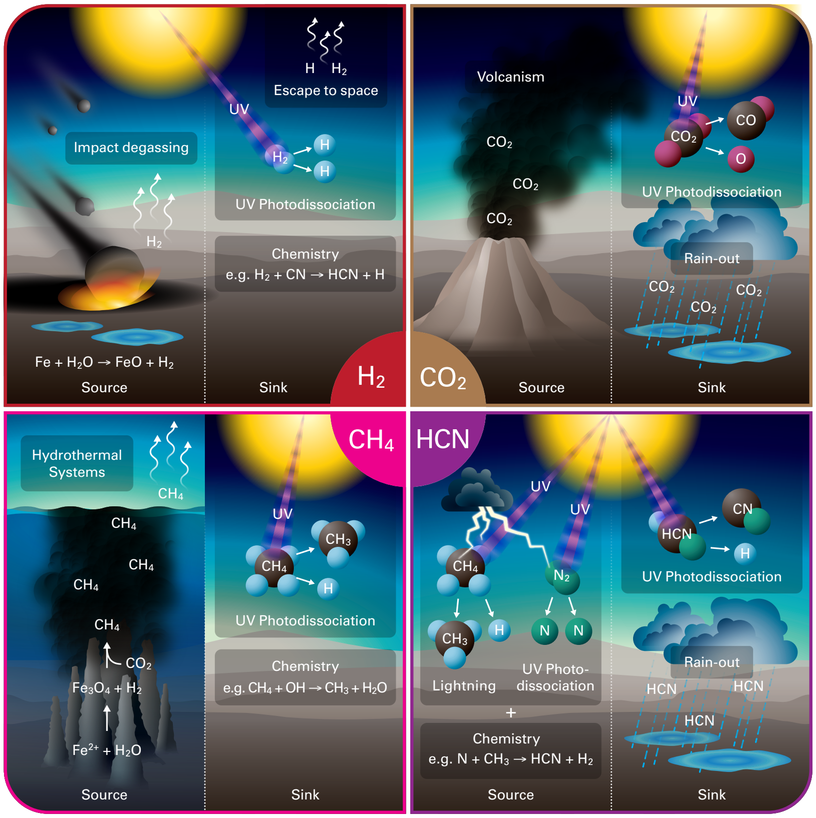

Figure 5.1: An illustration of the sources and sinks of the four key species in our atmospheric model: H_2, CO_2, CH_4, and HCN.

at each epoch is calculated by combining equilibrium H_2 production rates from enstatite chondrite impactors via the reaction $Fe + H_2O \longrightarrow FeO + H_2$ [129] with the bombardment rate on early Earth based on mathematical fits to the observed lunar cratering record [31, 642]. The main sinks for H_2 include UV photodissociation, hydrodynamic escape to space, and disequilibrium chemistry.

In the top right panel, the main source for CO_2 on early Earth is volcanic outgassing [129]. We use a constant Earth-like volcanic CO_2 outgassing rate in all our models [164]. The main sinks for CO_2 are photodissociation in the upper atmosphere, and rain-out in the lower atmosphere.

The main source for CH_4 in our models is production in hydrothermal vent systems [179, 180]. We use a calculated CH_4 outgassing rate from equilibrium models of hydrothermal systems on an Earth-like planet [180]. The main sinks for methane are UV photodissociation and disequilibrium chemistry.

Finally, the main source of HCN is photodissociation or lightning dissociation of species such as N_2 and CH_4 followed by radical chemistry. In the case of lightning, this radical chemistry takes place at high temperature in the lightning channel. The main sinks for HCN are UV photodissociation and rain-out. For further details on the source and sink rates, see Supplementary Information (SI).

We model the early Earth atmosphere during its reducing phase at 4.4 bya for calculated surface temperatures of 78°C (Model A) and 51°C (Model C), as well as its oxidizing phase at 4.0 bya for calculated surface temperatures of 51°C (Model B) and 27°C (Model D). These models differ in atmospheric composition, solar luminosity, UV irradiation intensity, HCN and radical production from lightning and impact bombardment rate. For complete details on these models, see Methods, Table 5.2.

In Figure 5.2A, B, C, and D, we plot the temporal evolution of atmospheric HCN and H_2CO in these four early Earth models. The origin of formaldehyde (H_2CO) is very important to pin down as it is necessary for the formation of ribose, the pyrimidine nucleobases, and 2-aminooxazole.

To give some context for what would be considered high atmospheric HCN abundances, Cassini observed HCN mixing ratios in the heavily reducing atmosphere of Titan to be $\sim10^{-7}$–10^{-6} near the surface (150–300 km), and $\sim10^{-4}$–10^{-2} in the upper atmosphere (700–1050 km) [109–112].

In the early Hadean (reducing) model A, HCN mixing ratios increase at the surface from 10^{-11} to 4.3×10^{-10} from $t = 100$ years to 20 million years. Moving up in altitude

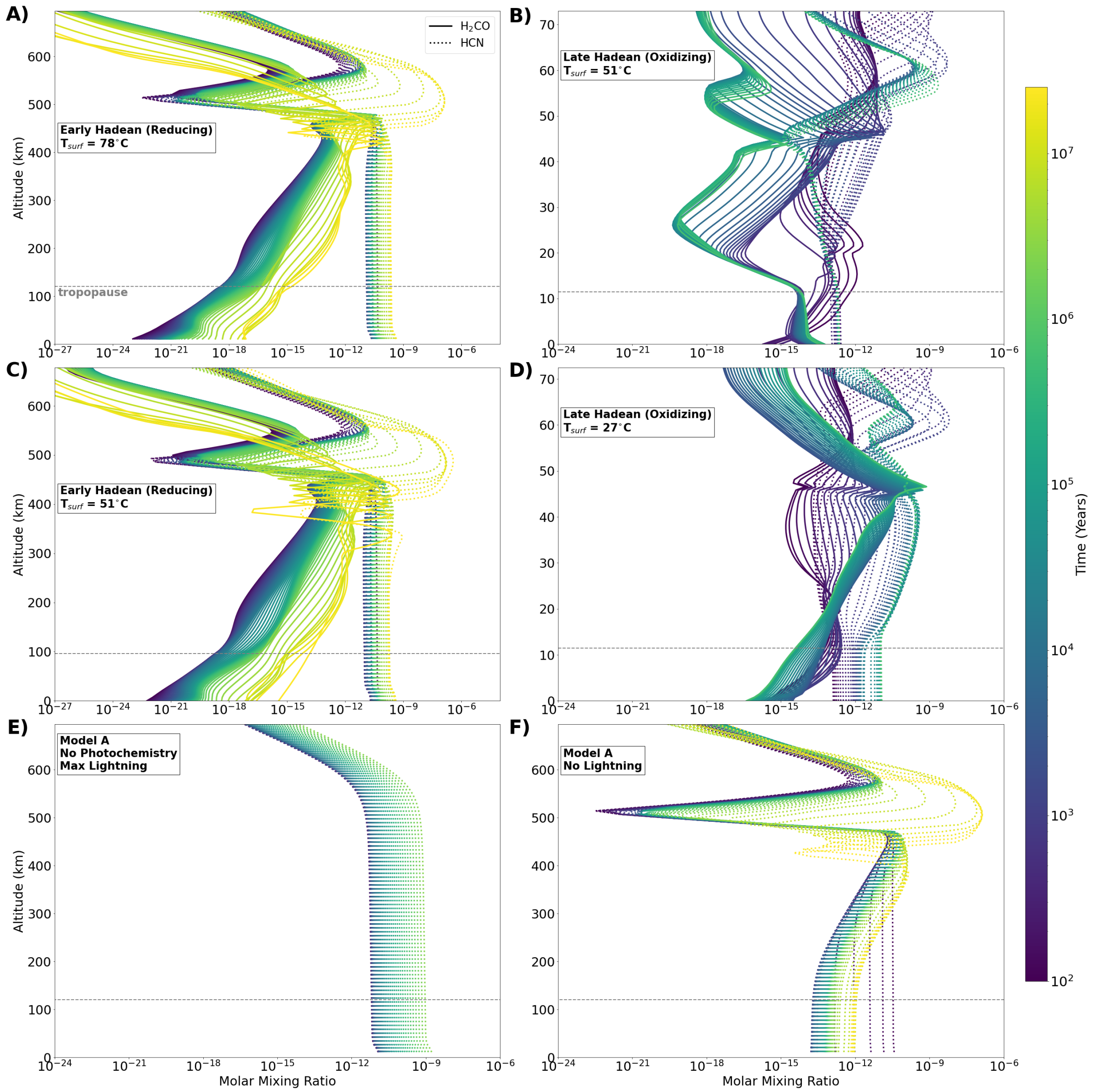

Figure 5.2: **A–D)** H2CO and HCN atmospheric mixing ratios from t = 100 years to 2.5–100 million years for the four early Earth models listed in Table 5.2. Pressures go from P_s=1.13–2 to 10^{-8} bar. Atmospheric scale heights vary primarily due to differences in mean molecular weight. The surface HCN abundances are fairly constant from 20 to 100 million years for the early Hadean (reducing) models. Simulations for the late Hadean (oxidizing) models ran slower than the reducing models, reaching 2.5 million years in the same computation time (1 week). The tropospause is labeled and corresponds to a pressure of ∼0.14 bar. **E)** HCN atmospheric mixing ratio from t = 100 years to 20 million years for model A with photochemistry turned off, and a lightning flash density corresponding to the maximum average value over land on Earth today. **F)** HCN atmospheric mixing ratio from t = 100 years to 50 million years for model A with lightning chemistry turned off.

we see the two regions of HCN production: lightning production of HCN at the surface which turbulently diffuses upwards to ∼500 km, and UV production of HCN at ∼500–600 km, which provides an HCN abundance of $\sim10^{-7}$ at these altitudes after 20 million years. We isolate and display these two regions in Figures 5.2E and F, where we turn off UV photochemistry and lightning chemistry, respectively, for our early Hadean (reducing) model A.

In the late Hadean (oxidizing) model B, HCN production remains fairly steady at the surface around 10^{-13} from $t = 100$ years to ∼1 million years. UV production of HCN produces a peak abundance of $\sim2\times10^{-9}$ at ∼55 km at 1 million years.

It is intriguing that only slight (< factor of 2) differences in HCN mixing ratios exist between the early Hadean (reducing) models C and A, but more substantial differences exist between the late Hadean (oxidizing) models D and B. The HCN abundances at the surface are 2 orders of magnitude higher in model D than in model B; however, neither oxidizing model produces as much HCN as our reducing models. Our calculations reveal that HCN production near the surface is about 2–3 orders of magnitude more favorable in reducing conditions than it is in oxidizing conditions.

In comparison to HCN, H_2CO is much less abundant at the surface in our early Hadean (reducing) models. This suggests the latter would have most likely come from aqueous photolytic production in WLPs rather than the atmosphere. H_2CO builds up from $\sim10^{-23}$ to $\sim10^{-17}$ over 20 million years. The mixing ratio for H_2CO is at its highest value of 10^{-11} in the mid atmosphere of these models at 20 million years. In the late Hadean (oxidizing) model B, H_2CO increases at the surface from $\sim10^{-15}$ to $\sim3\times10^{-14}$ over 1 million years. In the late Hadean (oxidizing) model D, H_2CO decreases at the surface from 10^{-15} to 10^{-17} over 1 million years. We did not explore atmospheric H_2CO production further given its considerably low abundances in all models.

Without lightning chemistry, HCN would be 2–3 orders of magnitude less abundant at the surface during the early Hadean, depending on the average lightning flash density at that time. Lightning, therefore, appears to be crucial for atmospheric HCN production on early Earth, whereas UV is the key driver of aqueous formaldehyde production in WLPs. HCN abundance at the surface is essentially linearly dependent on the lightning flash density, as we see HCN increase by a factor of 24 for a factor of 28.9 increase in lightning flash density (see Figure 5.11). It is therefore worth considering how local volcanic environments may produce large whiffs of HCN during electrical storms, where lightning flash densities are 2–7 greater than the global average on Earth today [163].

The temporal evolution of the dominant atmospheric species at the lowest (surface) layer in the atmosphere is shown in Figure 5.3. The atmospheric rain-out rates for HCN and H_2CO from this layer provides the influx rates into the WLPs.

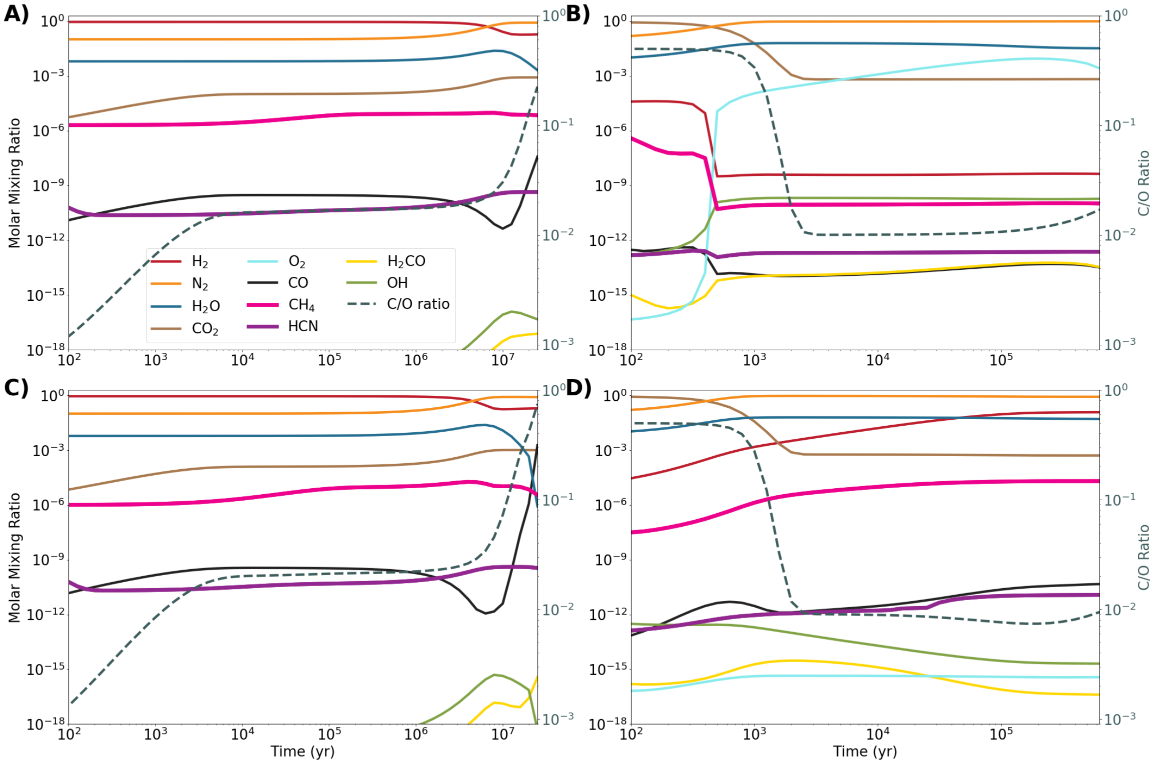

Figure 5.3: Abundances of key species in the lowest atmospheric layer as a function of time in our four early Earth models. The evolving C/O ratio at the surface layer is the dotted line with values labeled on the right side of the y-axis. Model details are in Table 5.2.

HCN mixing ratios in the lowest atmospheric layer are correlated with CH_4 mixing ratios in all our models. The HCN and CH_4 curves are bolded in Figure 5.3 to emphasize this point. In Figure 5.10, we plot the molar ratio of HCN to CH_4 over time and find an average value of $\sim 10^{-5}$ for the early Hadean (reducing) models and 10^{-6}–10^{-3} for the late Hadean (oxidizing) models.

HCN surface abundances also generally follow the trend of the H_2 surface abundances in the late Hadean (oxidizing) models B and D. This may be due to the fact that hydrogen is required for many of the dominant pathways to HCN.

There is an anti-correlation between OH and CH_4 in our oxidizing models. This can be explained by the reaction $OH + CH_4 \longrightarrow H_2O + CH_3$, which depletes the methane abundance. The lack of correlation in the CH_4 and HCN abundances from t = 100–500 in model B may be explained by the fact that this reaction leaves behind CH_3: a key precursor to HCN [440].

These correlations and anti-correlations are consistent with the atmospheric observations we see for Titan and present-day Earth, respectively. Titan's atmosphere is abundant in HCN (10^{-7}–10^{-2}) [109–112] due to the high abundances of reducing gases such as CH_4 (∼5.7%), and H_2 (∼0.1%) and low concentrations of oxidizing gases such as CO_2 (10–20 ppb) and H_2O (0.5–8 ppb) [108, 336]. On the other hand, HCN on Earth today is present in low abundances $\sim10^{-10}$ [643] because of the high abundance of oxidizing gases in our atmosphere such as O_2 (21%), H_2O (0–3%) and CO_2 (∼400 ppm) and modest ∼1 ppm levels of CH_4.

We tested the hypothesis presented in several exo-atmosphere studies that the C/O ratio controls their chemical composition [124, 340, 644–648]. In our early Hadean (reducing) models, the C/O ratio at the lowest atmospheric layer increases from 10^{-3} to 10^{-2} in the first few thousand years, and then to 0.1–1 after 20 million years. In the late Hadean (oxidizing), the C/O ratio decreases from 0.5 to $\sim10^{-2}$ in the first few thousand years, and remains near this value until the simulation ends. Evidently the C/O ratios in our models are set mainly by the increase and decrease of CO_2 and CO at the surface, and in the late Hadean (oxidizing) models, also by the fluctuation of O_2. The key biomolecule precursor species CH_4 and HCN it seems, are not dependent on the C/O ratio.

In Figure 5.4A, we display the concentrations of adenine in our model warm little pond from aqueous production for different HCN rain-out (influx) rates from our early Hadean (reducing) and late Hadean (oxidizing) atmospheric models (see Figure 5.9 for rainout rates). Adenine concentrations are displayed as shaded regions to cover the range of experimental yields of adenine production from HCN. We also display the peak adenine concentrations using the HCN rain-out rate from an early Hadean atmospheric model with lightning flash densities matching the maximum average value on Earth today (see Figure 5.11). Lastly, we display for comparison the concentrations of adenine from meteoritic and interplanetary dust particle (IDP) delivery calculated using the same source/sink pond models in Pearce et al. [31].

Adenine concentrations from aqueous production peak at 0.11 μM (15 ppb) and

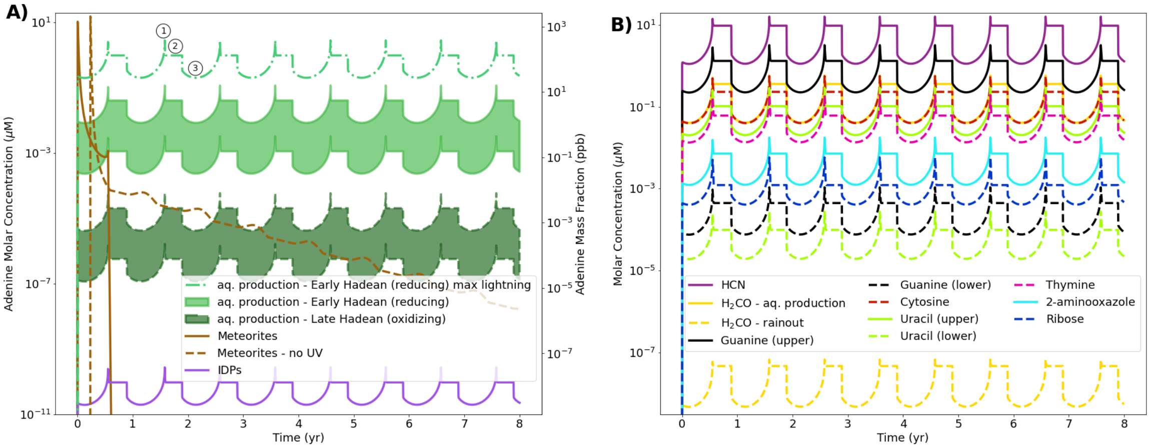

Figure 5.4: **A)** Comparative histories of adenine concentrations in warm little ponds from aqueous production (this work), versus delivery from meteorites and interplanetary dust particles (IDPs) [31]. Concentrations are calculated using the sources and sinks pond model developed in Pearce et al. [31] that cycles between ∼6 months of wet and ∼6 months of dry conditions; the one exception is the "Meteorites - no UV" model which is calculated for a pond that never dries up and for which UV is never turned on. Aqueous production of adenine is sourced from atmospheric rain-out of HCN multiplied by the range of experimental yields (see Table 5.8). Sinks include UV photodissociation in the dry phase, and hydrolysis and seepage in the wet phase. At location (1), the pond has dried down to 1 mm creating the maximum concentration. At location (2), UV irradiation is turned on and the concentration reduces until production from HCN influx and destruction from UV dissociation equilibrate. Finally, at location (3), precipitation has filled the pond up to its highest point, resulting in the concentration minimum. This cycle repeats annually. Hydrolysis has no affect on these curves, as the other two sinks are more efficient and occur on shorter timescales. The meteorite and IDP curves are taken directly from Pearce et al. [31]. **B)** Calculations of pond concentrations of various biomolecules as a result of atmospheric rain-out of HCN or H_2CO (yellow dotted line) for our early Hadean (reducing) model with a lightning flash density corresponding to the maximum average value on Earth today. See Table 5.8 for the experimental yields and sink rates used in the model calculations.

3.4×10^{-4} μM (0.05 pptr) for our early Hadean (reducing) and late Hadean (oxidizing) models, respectively. Increasing the lightning flash density of our early Hadean (reducing) model to the maximum average on Earth today leads to a peak adenine concentration of 2.8 μM (378 ppb). This is only a factor of $\sim$4 smaller than the peak adenine concentration from meteoritic delivery of 10.6 μM (1.43 ppm); however, the adenine concentration from aqueous production is sustained for more than 100 million years rather than days.

Adenine concentrations from delivery by IDPs are the most dilute in our WLP models. They are about 4 orders of magnitude lower in concentration than aqueous production during the late Hadean (oxidizing) phase.

In Figure 5.4B, we plot the pond concentrations of HCN and H_2CO from atmospheric rain-out, as well as the concentrations of nucleobases, ribose, H_2CO and 2-aminooxazole from aqueous HCN-based production. All values are for the early Hadean (reducing) phase for the maximum lighting flash density (28.9 flashes km^{-2} yr^{-1}). HCN concentrations peak at 16 μM and reduce to approximately 1.1 μM when the water level in the pond is highest.

Formaldehyde in WLPs likely did not come directly from the atmosphere during the early Hadean. H_2CO concentrations from aqueous photolytic production peak at 0.58 μM in max lightning conditions, which is approximately 7 orders of magnitude higher than the maximum H_2CO concentration from atmospheric rain-out. On the other hand, for our late Hadean (oxidizing) model B, the H_2CO rain-out rate is similar than the HCN rain-out rate (see Figure 5.9). Therefore, in oxidizing conditions H_2CO in WLPs may have come directly from the atmosphere.

For maximum lightning conditions during the early Hadean, guanine, cytosine, uracil and thymine concentrations peak at 3.2, 0.56, 0.29 and 0.19 μM, respectively, and 2-aminooxazole and ribose concentrations peak at 0.018, and 0.006 μM, respectively. Our model solves another main limitation of meteorites as a source of prebiotic nucleobases, in that cytosine and thymine are not present in meteorites [88, 89, 97].

In Table 5.1, we summarize the peak concentrations of key biomolecules and biomolecule precursors in our model WLP for the maximum lightning conditions in our early Hadean (reducing) atmosphere.

Of critical importance is how high pond concentrations of biomolecules such as nucleobases, ribose, and 2-aminooxazole would need to be in order for polymerization processes and protocells to emerge. Laboratory experiments that react nucleobases

Table 5.1: Summary of the peak concentrations of biomolecules and biomolecule precursors in WLPs from our max lightning early Hadean (reducing) model.

Molecule	Early Hadean (max lightning) (μM)
HCN	16
H_2CO (aq. production)	0.58
H_2CO (rain-out)	$\sim 10^{-8}$
Adenine	2.8
Guanine	3.2
Cytosine	0.56
Uracil	0.29
Thymine	0.19
2-aminooxazole	0.018
Ribose	0.006

to produce low yields of nucleosides and nucleotides typically use 100μM–100mM concentrations of nucleobases [64, 65, 649]. The lowest end of this experimental concentration range is two orders of magnitude higher than the maximum adenine concentration from our early Hadean (4.4 bya) model; however, there are various mechanisms that we did not model which could increase nucleobase concentrations in WLPs. For example, adsorption to mineral surfaces, sequestration into amphiphilic multilamellar matrices, and mineral gels provide potential opportunities for further concentration beyond the wet-dry cycles we model here [51, 650]. Furthermore, local bursts of HCN production due to electrical storms in volcanoes may provide nearby WLPs with several orders of magnitude higher HCN rain-out rates than we model here.

Concentrations of ribose and 2-aminooxazole in our models are the most dilute of the RNA building blocks, in the nM range; however, laboratory experiments use much higher concentrations than this for nucleotide synthesis, typically in the mM to M range [42, 64, 65, 649]. Our results present a challenge to experimental work to determine the levels that are sufficient for nucleotide synthesis in realistic prebiotic conditions.

We conclude that the initial rate of H_2 impact degassing soon after the moon forming impact with the Earth is sufficiently high to keep its atmosphere in a chemically reducing state. Lightning-dominated HCN formation from methane in the lower atmosphere rains out into WLPs steadily over a hundred million years. There, aqueous chemistry continuously drives nucleobase and perhaps nucleotide percusor synthesis to levels that polymerization by condensation reactions can occur. Overall, this steady input totally dominates that which is possible from more isolated meteoritic infall events. With a declining bombardment throughout the Hadean eon [31, 642], the transition from reducing to oxidizing atmospheric conditions would be somewhat linear from 4.4 to 4.0 bya. After 4.3 bya, the reducing conditions for new biomolecular formation and the emergence of life, disappear. The planetary and atmospheric processes modeled here are quite general and may occur on other newly formed earth-like planets in habitable zones. This could be tested by measuring HCN and methane concentrations in their atmospheres.

Methods

Non-Equilibrium Atmospheric Chemistry

ChemKM is a 1D chemical kinetic model for disequilibrium atmospheric chemistry calculations that makes use of the Double precision Livermore Solver for Ordinary Differential Equations (DLSODE) from the ODEPACK collection [651]. The error for this solver is controlled by the relative error tolerance and the absolute error tolerence, which are set to 10^{-5} and 10^{-99} respectively to insure numerical stability. ChemKM has been benchmarked with several other chemical kinetic codes[1], and has been used in the past to simulate the atmospheres of Titan [440], as well as cold, hot and ultra-hot gaseous exoplanets [340, 375]. Atmospheric rain-out was newly developed in ChemKM for this work. Simulations were run on the cluster for approximately 1 week. In this time, our models reached 1–100 million years of simulated time.

CRAHCN-O is a consistent reduced atmospheric hybrid chemical network now containing 259 two- and three-body reactions for the production of HCN and H_2CO in atmospheres dominated by any of H_2, CO_2, N_2, CH_4, and H_2O. We introduce 28 new reactions to CRAHCN-O in this work, in order to avoid the atmospheric build up of species that previously had no reaction sinks (see Tables 5.3 and 5.4 for details). We have tested an oxygenless version of this network (CRAHCN) by modeling HCN production in Titan's atmosphere, and our computed HCN profile agreed very well with the Cassini observations [440].

---

[1] https://www.issibern.ch/teams/1dchemkinetics/

Atmospheric Pressure-Temperature Profiles

petitRADTRANS is a 1D radiative transfer code based on the correlated-k method for gas absorption and the Guillot temperature model [652]. It is typically used to model exoplanet atmospheres to obtain transmission and thermal spectra, e.g., Molaverdikhani et al. [340]; Mollière et al. [653]; Wang et al. [654]. We build upon its existing functionality to calculate P-T profiles self-consistently with tropospheric water vapor in sequence with the Arden Buck equation [655].

P-T structure calculations are performed using petitRADTRANS [656], and atmospheric chemistry is calculated using ChemKM [340, 375] coupled with an updated version of the CRAHCN-O chemical network [440, 634]. We are the first to calculate composition-dependent P-T profiles for modeling HCN chemistry in the early Earth atmosphere. Past models have used a general habitable P-T profile, or estimated the surface temperature using an analytic equation for a moist adiabat [107, 125, 129].

For complete details on our atmospheric models, see the SI.

Lightning Production of Molecules

We follow the thermodynamic treatment from Chameides & Walker [161] for the lightning production of HCN and other species on early Earth. Based on our initial atmospheric compositions, we calculate the equilibrium abundances of HCN, H_2, N_2, H_2O, CO_2, CH_4, O_2, NO, OH, H, ^4N, CO, ^3O, and CH_3, in a 1 cm^2 lightning channel extending through the lowest layer in our atmospheres at a freeze out temperature $T_F = 2000$ K. We use thermochemical data from the JANAF tables [657], and the ChemApp Software library for Gibbs free energy minimization (distributed by GTT Technologies, http://gtt.mch.rwth-aachen.de/gtt-web/).

We then use the resultant mixing ratios to calculate the influx of each of these species into the lowest layer of our atmospheres. These species were chosen as they are dominant equilibrium products in the early Earth lightning models by Chameides & Walker [161]. The freeze out temperature (T_F) was chosen to most accurately model the HCN produced in a lightning strike, as this is the key species of interest in this paper. Although freeze out temperatures typically range from 1000–5000 K across species, one freeze out temperature must be chosen to conserve the elemental abundances in the lightning strike. A non-equilibrium approach was also considered; however, an extensive high-temperature (up to 30000 K) chemical kinetic network would be required and is perhaps unnecessary given the $< \mu$s equilibrium timescale above 10000 K compared to the $\sim 10\mu$s timescale of eddy diffusion, and the $\sim$100 ms cooling time of a lightning channel [162].

Table 5.2: Summary of the four early Earth atmospheric models in this work. Initial compositions for each model are chosen to A) align with typical assumptions for reducing (H_2-dominant) or oxidizing (CO_2-dominant) conditions at the chosen epoch, and B) yield calculated P-T profiles with habitable surface conditions (i.e. 0 °C $\leq$ T_s $\leq$ 100 °C) (see Figure 5.6 for P-T profiles).

Model	Description	Date (bya)	P_s (bar)	T_s (°C)	Molar Composition	Surface flux ($\frac{1}{cm^2 s}$)	Lightning ($\frac{1}{cm^2 s}$)
A	Early Hadean (Reducing)	4.4	1.5	78	H_2: 90% N_2: 10% CH_4: 2 ppm H_2O: Figure 5.5	H_2: 2.3×10^{11} CO_2: 3.0×10^{11} CH_4: 6.8×10^{8} H_2O: 2.0×10^{9}	H: 5.4×10^{7} ^{4}N: 1.1×10^{7} OH: 2.3×10^{5} NO: 4.8×10^{4} ^{3}O: 3.1×10^{4} O_2: 1.3×10^{2} CH_3: 7.3×10^{1} HCN: 2.1×10^{1}
B	Late Hadean (Oxidizing)	4.0	2	51	CO_2: 90% N_2: 10% CH_4: 10 ppm H_2O: Figure 5.5	H_2: 2.3×10^{10} CO_2: 3.0×10^{11} CH_4: 6.8×10^{8} H_2O: 2.0×10^{9}	CO: 6.5×10^{6} ^{3}O: 3.4×10^{6} O_2: 1.4×10^{6} ^{4}N: 1.2×10^{6} NO: 5.0×10^{5} H: 1.2×10^{5} OH: 5.0×10^{4} HCN: 3.4×10^{4} CH_3: 5.0×10^{1}
C	Early Hadean (Reducing)	4.4	1.13	51	H_2: 90% N_2: 10% CH_4: 1 ppm H_2O: Figure 5.5	H_2: 2.3×10^{11} CO_2: 3.0×10^{11} CH_4: 6.8×10^{8} H_2O: 2.0×10^{9}	H: 4.4×10^{7} ^{4}N: 8.6×10^{6} OH: 3.0×10^{5} NO: 6.0×10^{4} ^{3}O: 2.3×10^{4} O_2: 9.8×10^{1} CH_3: 2.8×10^{1} HCN: 9.0×10^{0}
D	Late Hadean (Oxidizing)	4.0	2	27	CO_2: 90% N_2: 10% CH_4: 1.5 ppm H_2O: Figure 5.5	H_2: 2.3×10^{10} CO_2: 3.0×10^{11} CH_4: 6.8×10^{8} H_2O: 2.0×10^{9}	CO: 6.5×10^{6} ^{3}O: 3.4×10^{6} O_2: 1.4×10^{6} ^{4}N: 1.2×10^{8} NO: 5.0×10^{5} H: 1.2×10^{5} OH: 5.0×10^{4} HCN: 3.4×10^{4} CH_3: 4.9×10^{1}

P_s: Surface Pressure
T_s: Surface Temperature

Complete Impact-Atmosphere-Ocean Coupling Models

The main assumption of our models is that the surface of the Earth maintained habitability (i.e. 0°C < T < 100°C), which is key for the presence of WLPs and the origin of life. We begin with assumed reducing and oxidizing atmospheric compositions for the early and late Hadean, respectfully, and calculate the initial P-T profiles and tropospheric water vapor based on these compositions. We adjust both initial methane concentration and surface pressure to obtain calculated temperature profiles that fall within the habitable range. We smooth the initial water profiles from our calculations to 1% at the surface, and include ocean-atmosphere coupling by imposing an ocean evaporation rate of 2×10^9 cm^{-2} s^{-1} to maintain a water mixing ration of ∼0.1–1% at the surface.

In Table 5.2, we summarize the four early Earth atmospheric models in our study. We model two epochs which vary in atmospheric composition, solar luminosity, UV irradiation intensity, and asteroid bombardment rate. These models correspond to the early Hadean, at 4.4 bya (billion years ago) and the late Hadean, at 4.0 bya. We compute two habitable P-T profiles for each model by slightly adjusting the methane content and/or surface pressure. The luminosity, UV intensity, and asteroid bombardment rate at each epoch are based on stellar evolution models [658, 659], observations of solar analogs [660], and the lunar cratering record [642], respectively.

Biomolecule Chemistry in Warm Little Ponds: Sources and Sinks

Our atmospheric models are coupled (via rain-out) with the sources and sinks warm little pond model (WLP) we first developed in Pearce et al. [31]. Biomolecule abundances are described by first-order linear differential equations and are solved numerically. The evolving concentrations of nucleobases, ribose, formaldehyde, and 2-aminooxazole in our WLP models are driven by the rate of incoming HCN from rain-out, and biomolecule losses due to UV dissociation, seepage, and hydrolysis. Given experimental reaction rates are fast ($\lesssim$ days), we apply experimental reaction yields to our HCN pond concentrations in order to estimate the pond concentrations of formaldehyde, nucleobases, ribose, and 2-aminooxazole.

We utilize the experimental result that ultraviolet (UV) irradiation of liquid water produces solvated electrons, enabling a chemical pathway from HCN to formaldehyde (H_2CO) [39] in ponds. H_2CO can also enter ponds directly from the atmosphere [43]. Aqueous solutions containing HCN and H_2CO can produce nucleobases (i.e., adenine, guanine, cytosine, uracil, thymine) [38, 106, 183], which are the base-pairing components of RNA and DNA, as well was ribose [9, 40], which binds with phosphate to make up the RNA backbone.

Furthermore, irradiated and wet-dry cycled or flowing solutions of HCN in the presence of phosphorous and dissolved salts enable the production of 2-aminooxazole: a key intermediate in the Powner–Sutherland pathway for producing the pyrimidine building blocks of RNA (cytidine and uridine monophosphate) [39, 41, 42]. Finally, Becker et al. [635] recently presented a pathway to RNA nucleosides that involves the wet-dry cycling of solutions containing HCN and other atmospheric precursors. Such prebiotic chemistry experiments and models are based on the assumption that species such as HCN and H_2CO would be present and concentrated in WLPs on early Earth.

In Table 5.8 we summarize the sources and sinks of our pond models. See Section 5 and Pearce et al. [31] for complete details regarding these models.

Warm-Wet Cycling in WLPs

We have found that ponds that are roughly 1 meter in radius and depth and are cylindrical in shape are an optimal fiducial estimate for subsequent RNA polymer synthesis by wet-dry cycles [31]. We use the "intermediate" hot early Earth environment from Pearce et al. [31], which is based on the seasonal sinusoidal precipitation rates in Indonesia [661, 662]. Precipitation coupled with evaporation and seepage produces a natural wet-dry cycle within the pond that has a ∼6-month wet phase followed by a ∼6-month dry phase. Various pond environments were explored in Pearce et al. [31], and were found to produce similar results in terms of peak nucleobase concentrations.

Comparison with other Methods and Experiments

We have developed multiple new methods that have greatly enhanced the capabilities of non-equilibrium calculations of atmospheric HCN on early Earth. These include the calculation of composition-dependent pressure-temperature (P-T) profiles using a radiative transfer code, the inclusion of lightning chemistry and the time-dependent influx of H_2, CO_2, and CH_4 from impact degassing, volcanism, and oceanic geochemistry, respectively.

Past non-equilibrium atmospheric models for the Archean (∼3.8–2.5 bya) have computed HCN production for a range of CH_4, H_2, and CO_2 abundances using a commonly suggested input P-T profile for early Earth [107, 125]. These models imposed CH_4 abundances in the 10–1000 ppm range, either did not fix H_2 or imposed H_2 abundances in the 0.01–1% range, and imposed CO_2 abundances in the 0.04–3% range. Our strategy is different, as we begin with initial reducing (4.4 bya) or oxidizing (4.0 bya) conditions that are thought to represent each epoch, and calculate the composition-dependent input P-T profiles using a radiative transfer code. Then, we allow the concentrations of all species to evolve over time based on their source and sink rates at each epoch.

For example, CO_2 reaches a steady surface abundance of ∼0.04–0.08% in our models based on the source rates from volcanic outgassing and association chemistry balanced with the sink rates from atmospheric rain-out and photodissociation. Similarly, our end-of-simulation H_2 abundances (19% and 4 ppb for reducing and oxidizing models, respectively) are balanced by the source rate from epoch-dependent impact bombardment, and the sink rates from hydrodynamic escape, photodissociation, and chemistry. CH_4 abundances are based on source rates from oceanic sources balanced with sink rates from photodissociation and chemistry. Surface CH_4 abundances reach end-of-simulation values that are 1 to 4 orders of magnitude lower than the range of CH_4 concentrations imposed in the past Archean models. Given the correlation between HCN production and CH_4 abundance, our calculated surface HCN concentrations tend to be lower than those calculated in these Archean models. The Archean models compute HCN mixing ratios near the surface to be $\sim 10^{-12}$–10^{-7}, which is similar in range to the surface HCN abundances in our reducing 4.4 bya models after 20 Myr ($\sim 10^{-8}$–10^{-9}), and up to an order of magnitude higher than the HCN surface abundances in our 4.0 bya oxidizing models of 10^{-13}–10^{-11} after ∼1 Myr.

Zahnle et al. [129] modeled non-equilibrium chemistry from a post-large body impact with input P-T profiles based on a simple analytic equation for a moist adiabat. These models began with concentrations of H_2, CO, CO_2, CH_4, and NH_3 that result from various impactors equilibrating with different mineral redox buffers. They found that impactors at least Vesta in size (525 km) are required to sustain the high temperatures required for rapid methane production (e.g. 0.1–10 bars). These models produced post-impact atmospheric CH_4 abundances of ∼3%, which resulted in similarly high (∼ a few %) HCN abundances for a few million years after impact.

The analytic equation Zahnle et al. [129] used for obtaining a habitable surface and P-T profile for their non-equilibrium chemistry models does not consider the strength of various opacity sources such as H_2-H_2 collisional induced absorption (CIA). We are unable to obtain habitable surfaces when modeling H_2 atmospheres >2 bars using the equations of radiative transfer. In our radiative transfer models, we find H_2-H_2 CIA produces a strong greenhouse effect above ∼1.13 bar of H_2. The surface temperature of our early Hadean (reducing) model A, which has 1.5 bars of H_2, 2 ppm CH_4, and ppm-range H_2O, is reaching the upper bounds of habitability at 78°C. This suggests that the resultant high atmospheric pressures of H_2 and CH_4 from the large-body impacts modeled by Zahnle et al. [129] would produce atmospheric temperatures too hot for WLPs to exist. More research needs to be done to understand whether a post-large body impact could provide high HCN rain-out rates to WLPs once the atmosphere cools to habitable temperatures.

Atmospheric models of nitrogen-rich rocky exoplanets that use C/O ratio as an adjustable parameter produce HCN mixing ratios of 10^{-8}–10^{-7} for atmospheric C/O ratios near 0.5, and HCN mixing ratios of $\sim10^{-3}$ for C/O ratios > 1.5 [124]. We do not use C/O as an adjustable parameter, as we find that the balance of outgassing and losses of species such as CO_2, H_2O, and CH_4 in our models lead to surface C/O ratios that vary from ∼0.001–0.8 over the course of the simulations. These C/O ratios are generally lower than those explored by Rimmer & Rugheimer [124].

Miller-Urey experiments have shown that reducing conditions are more favorable than oxidizing conditions for biomolecule production [13, 14]. For example, Schlesinger & Miller [14] found a ∼3–4 order of magnitude difference in amino acid yields when switching from reducing (H_2-dominant) to oxidizing (CO_2-dominant) experimental conditions. This is consistent with our results, where we have shown that the early reducing phase of the Hadean eon at 4.4 bya produces atmospheric HCN and RNA building blocks 2–3 orders of magnitude higher in concentration than during the late oxidizing phase at 4.0 bya. Some Miller-Urey experiments have shown reasonable success of amino acid production in CO_2/N_2 conditions when buffering the solution with calcium carbonate [13]; however, this is likely demonstrating catalytic effects that increase amino acid production yields from low HCN concentrations.

Acknowledgments

We thank David Catling for his critical analysis of an early draft of this paper. We thank Steve Benner, Jeffrey Bada, David Deamer, Bruce Damer, Oliver Trapp, Paul Higgs, Greg Slater and Paul Rimmer for interesting discussions regarding this work. This research is part of a collaboration between the Origins Institute at McMaster University and the Heidelberg Initiative for the Origins of Life. The research of BKDP was supported by an NSERC Alexander Graham Bell Canada Graduate Scholarship-Doctoral (CGS-D) and Ontario Graduate Scholarship. REP is supported by an NSERC

Discovery Grant. T.H. acknowledges support from the European Research Council under the Horizon 2020 Framework Program via the ERC Advanced Grant Origins 83 24 28. We acknowledge Compute Canada for allocating the computer time required for this research. We thank Steve Janzen at McMaster Media Resources for his superb work in rendering Figure 1.

Author Contributions

B.K.D.P., K.M., R.E.P., and T.H. designed research; B.K.D.P. performed research; K.M. performed atmospheric chemistry simulations; B.K.D.P. performed numerical pond simulations; K.E.C. and B.K.D.P. performed P-T profile simulations; B.K.D.P. and R.E.P. analyzed data; and B.K.D.P., R.E.P., and T.H. wrote the paper.

Competing Interests

No competing financial interests exist.

Supplementary Information

Supplementary Methods

Atmospheric Simulations

Self-consistent disequilibrium atmospheric simulations are carried out iteratively using the consistent reduced atmospheric hybrid chemical network oxygen extension (CRAHCN-O) [440, 634] coupled with a 1D chemical kinetic model (ChemKM) [340, 375], with input pressure-temperature (P-T) structures calculated using petitRADTRANS [656].

CRAHCN-O now contains 259 one-, two-, and three-body reactions, whose rate coefficients are gathered from experiments when available (∼40%), and are otherwise calculated using accurate, consistent, theoretical quantum methods (∼60%). Approximately 93 of the reactions in CRAHCN-O were missing from the literature prior to their discovery in Pearce et al. [335, 440, 634]. This network can be used to calculate HCN and H_2CO chemistry in atmospheres characterized by any of N_2, CO_2, CH_4, H_2O, and H_2. We added 28 new reactions to CRAHCN-O after our preliminary simulations showed the artificial build up of species that previously had no reaction sinks. We list the new two-body and three-body reactions in Tables 5.3 and 5.4, respectively.

All values are experimental, except for the low- and high-pressure limit rate coefficients for $C_2H + H + M \longrightarrow C_2H_2 + M$ and the high-pressure limit rate coefficient for $C + H_2 + M \longrightarrow {}^3CH_2 + M$, as there were no experimental values available. For these reactions, we calculate the rate coefficients using the same validated theoretical and computational quantum methods developed in Pearce et al. [440, 634] for the other three-body reactions in CRAHCN-O.

Table 5.3: New two-body reactions added to CRAHCN-O for our early Earth atmospheric models, and their experimental Arrhenius coefficients. These are the most efficient sink reactions for species that would otherwise erroneously build up over ten-to-hundred million year timescales. The Arrhenius expression is $k(T) = \alpha \left(\frac{T}{300}\right)^{\beta} e^{-\gamma/T}$.

Reaction Equation	α	β	γ	Source(s)
$HCCO + NO \longrightarrow HCNO + CO$	$1.4{\times}10^{-11}$	0	-320	Carl et al. [663]
$HCCO + NO \longrightarrow HCN + CO_2$	$6.1{\times}10^{-12}$	-0.72	-200	Carl et al. [663]
$HCCO + {}^3O \longrightarrow CO + CO + H$	$1.6{\times}10^{-10}$	0	0	Baulch et al. [137]
$HCCO + H \longrightarrow CO + 3\,CH_2$	$2.1{\times}10^{-10}$	0	0	Glass et al. [664], Frank et al. [665]
$NCO + O_2 \longrightarrow CO_2 + NO$	$1.3{\times}10^{-12}$	0	0	Schacke et al. [666]
$NCO + NO \longrightarrow N_2 + CO_2$	$1.6{\times}10^{-11}$	0	0	Cooper et al. [667], Cooper & Hershberger [668]
$NCO + {}^3O \longrightarrow NO + CO$	$6.4{\times}10^{-11}$	-1.14	0	Becker et al. [669]
$NCO + H \longrightarrow NH + CO$	$2.2{\times}10^{-11}$	0	0	Becker et al. [669]
$HO_2 + {}^3O \longrightarrow O_2 + OH$	$5.4{\times}10^{-11}$	0	0	Baulch et al. [137]
$HO_2 + OH \longrightarrow H_2O + O_2$	$4.8{\times}10^{-11}$	0	-250	Baulch et al. [137]
$HO_2 + H \longrightarrow H_2O + {}^3O$	$5.0{\times}10^{-11}$	0	866	Baulch et al. [137]
$HO_2 + H \longrightarrow O_2 + H_2$	$7.1{\times}10^{-11}$	0	710	Baulch et al. [137]
$HO_2 + H \longrightarrow OH + OH$	$2.8{\times}10^{-10}$	0	440	Baulch et al. [137]
$O_2 + HCO \longrightarrow CO + HO_2$	$8.5{\times}10^{-11}$	0	850	Tsang & Hampson [247]
$O_2 + C_2H \longrightarrow HCCO + {}^3O$	$1.0{\times}10^{-12}$	0	0	Tsang & Hampson [247]
$O_2 + C_2H \longrightarrow HCO + CO$	$4.0{\times}10^{-12}$	0	0	Tsang & Hampson [247]
$O_2 + CN \longrightarrow NCO + {}^3O$	$1.1{\times}10^{-11}$	0	-205	Baulch et al. [137]
$O_2 + {}^4N \longrightarrow NO + {}^3O$	$4.5{\times}10^{-12}$	1.0	3720	Baulch et al. [670]
$O_2 + CH \longrightarrow OH + CO$	$5.0{\times}10^{-11}$	0	0	Lichtin et al. [671, 672]
$O_2 + C \longrightarrow CO + {}^3O$	$3.0{\times}10^{-11}$	0	0	Duncanson Jr. & Guillory [673], Messing et al. [674] Geppert et al. [675], Dorthe et al. [676] Becker et al. [677], Husain & Young [678] Husain & Kirsch [679], Braun et al. [680] Martinotti et al. [681]
$NO + {}^4N \longrightarrow N_2 + {}^3O$	$3.1{\times}10^{-11}$	0	0	Atkinson et al. [682]
$NO + {}^2N \longrightarrow N_2 + {}^3O$	$6.0{\times}10^{-11}$	0	0	Herron [237]
$NO + C \longrightarrow CN + {}^3O$	$2.5{\times}10^{-11}$	0	0	Baulch et al. [670]
$C_2H + CH_4 \longrightarrow C_2H_2 + CH_3$	$3.0{\times}10^{-12}$	0	250	Tsang & Hampson [247]
$C_2H + {}^3O \longrightarrow OH + CO$	$1.7{\times}10^{-11}$	0	0	Baulch et al. [137]

Table 5.4: New three-body reactions added to CRAHCN-O for our early Earth atmospheric models, and their calculated or experimental Lindemann coefficients. These are the most efficient high-pressure sink reactions for species that would otherwise erroneously build up over ten-to-hundred million year timescales. Experimental rate coefficients are listed when available, otherwise we calculate them using canonical variational transition state theory and Rice–Ramsperger–Kassel–Marcus/ master equation theory at the BHandHLYP/aug-cc-pVDZ level of theory (see Pearce et al. [440, 634] for details on how these calculations are performed. k_∞ is the second-order rate coefficient in the high pressure limit with units cm^3s^{-1}. k_0 is the third-order rate coefficient in the low pressure limit with units cm^6s^{-1}. These values fit into the pressure-dependent rate coefficient equation $k = \frac{k_0[M]/k_\infty}{1+k_0[M]/k_\infty}k_\infty$.

Reaction equation	$k_\infty(298)$	$k_0(298)$	Source(s)
$O_2 + H + M \longrightarrow HO_2 + M$	7.5×10^{-11}	$(M=N_2)\ 3.9\times10^{-30}\ T^{-0.8}$ $(CO_2)\ 5.8\times10^{-30}\ T^{-0.8}$ $(H_2)\ 4.3\times10^{-30}\ T^{-0.8}$	(N_2) Baulch et al. [137] (H_2O) Baulch et al. [137] (H_2) Baulch et al. [137]
$C_2H + H + M \longrightarrow C_2H_2 + M$	2.3×10^{-11}	$(M=N_2)\ 5.8\times10^{-28}$ $(CO_2)\ 7.1\times10^{-28}$ $(H_2)\ 4.2\times10^{-28}$	This work
$C + H_2 + M \longrightarrow {}^3CH_2 + M$	1.6×10^{-9}	$(M=N_2)\ 7.0\times10^{-32}$ $(CO_2)\ 7.0\times10^{-32}$ $(H_2)\ 7.0\times10^{-32}$	This work, Husain & Young [678], Husain & Kirsch [679]

The ChemKM code takes as input: A) a chemical network, B) an atmospheric pressure-temperature (P-T) structure, C) an eddy diffusion profile to characterize turbulent mixing, D) the solar radiation spectrum at the top-of-atmosphere (TOA), E) wavelength-dependent photochemical reactions, and F) incoming and outgoing molecular fluxes from the surface and TOA (i.e. impact degassing, volcanic outgassing, rain-out, hydrogen escape, and chemical production from lightning). ChemKM uses the plane-parallel two-stream approximation to calculate radiative transfer, and includes both photoabsorption and Rayleigh scattering. The pressure profiles remain static throughout the simulations; therefore we must assume that pressure has reached equilibrium with the influx and outflux of atmospheric gases. This assumption is valid for our models, as our H_2 impact degassing rates never exceed the H_2 escape rates.

P-T structures for Early Earth models are calculated using the petitRADTRANS software package [656]. petitRADTRANS is a 1D radiative transfer code that uses the Guillot analytic temperature model [652] and correlated-k opacity tables to solve for atmospheric temperatures of planets with no surface boundary condition. Visible opacities are calculated using the Planck mean, and infrared opacities are calculated using the Rosseland mean [683]. Our models are all 100 layers, from surface pressures of ∼1–2 bar to TOA pressures of 1×10^{-8} bar. We implement cloudless and hazeless models given the large uncertainties of these parameters for the early atmosphere. We note that the lack of biogenic CCN would have led to a shorter lifetime for optically thick convective clouds during the Hadean [684], reducing their contribution to both the greenhouse and albedo when compared with those of modern Earth [685].

In Figure 5.5 we display the initial water vapor profiles in the troposphere of our four early Earth models. We make an incremental improvement over the standard Manabe & Wetherald [686] water vapor profile for Earth's atmosphere by calculating tropospheric water abundances in two steps. In the first step, we iterate the Arden Buck equation [655], which is dependent on temperature, and the P-T calculations from petitRADTRANS, which are dependent on water composition. To avoid a runaway greenhouse due to water vapor feedback, we parameterize the strength of water vapor feedback by decreasing the relative humidity (RH) by $\beta = 6\%$ for every °C of warming [687]. In step two, we smooth out these profiles to avoid numerical instabilities in ChemKM. We use the calculated water vapor at the tropopause and linearly increase the mixing ratio moving downwards in altitude to reach a typical water vapor abundance of 1% for wet rocky planets [164]. The tropopause is chosen to be 0.14 bar, similar to the present day Earth [688].

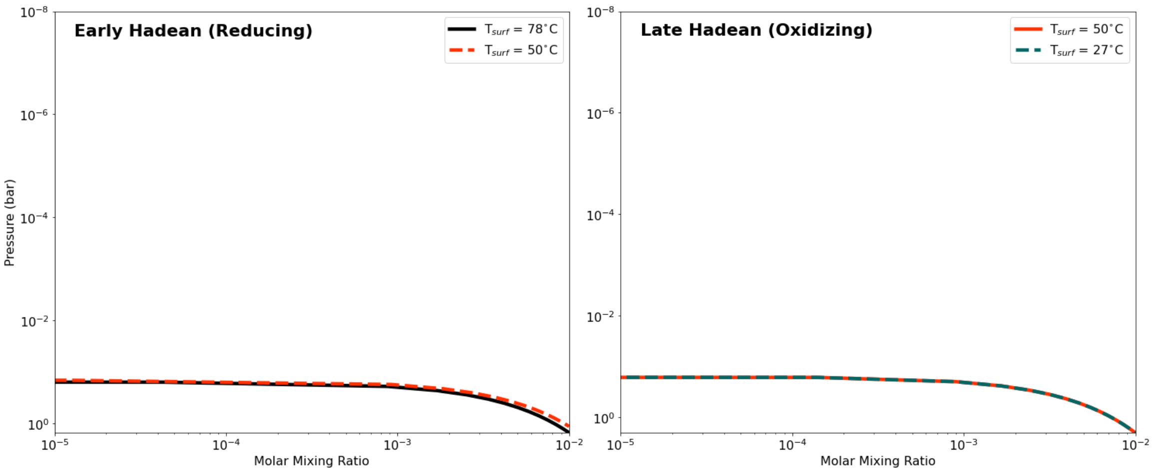

Figure 5.5: Initial tropospheric water vapor profiles for our 4 early Earth models.

The three main inputs for our P-T structure calculations are A) input composition, B) equilibrium temperature (T_{eq}), and C) internal temperature (T_{int}). Initial guesses for input compositions were selected to represent reducing (H_2/N_2-dominant) or oxidizing (CO_2/N_2-dominant) phases of the early (4.4 bya) and late (4.0 bya) Hadean eon. Surface pressure and methane abundance are adjusted from 1–2 bar and 1–10 ppm, respectively, to maintain habitable surface temperatures (i.e. $0\ °C \leq T_s \leq 100$

°C) (see Table 5.2). Equilibrium temperatures are calculated using the equation below.

$$T_{\text{eq}} = \left(\frac{(1-A)L_{\odot}}{16\pi\sigma a^2} \right)^{1/4}, \tag{5.1}$$

where T_{eq} is equilibrium temperature, A is albedo, $L_{\odot}$ is solar luminosity, σ is the Stefan-Boltzmann constant, and a is the semi-major axis of the planet.

Luminosities for the Sun at 4.4 bya ($0.705L_{\odot}$) and 4.0 bya ($0.728L_{\odot}$) are obtained from a pre-computed stellar evolution model of a Sun-like star [658, 659]. The Hadean Earth would have been mostly covered in water; therefore, albedo is taken to be 0.06, which is consistent with a cloudless water world [689].

Internal heat flow is taken to be three times the present value, which is compatible with thermal modeling of the Hadean [176]. Using the Stefan-Boltzmann law, this results in internal temperatures of $T_{\text{int}} = 43.3$ K.

In Figure 5.6, we display the P-T profiles for our four Hadean models.

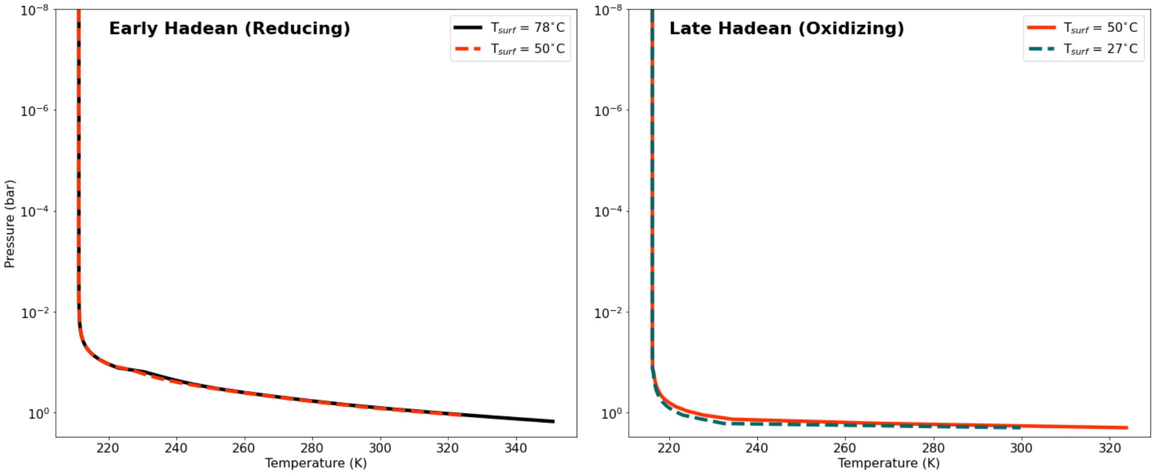

Figure 5.6: Pressure-Temperature profiles for our 4 early Earth models, calculated with petitRADTRANS using the input compositions displayed in Table 5.2.

In Figure 5.7, we display the eddy diffusion profile used for all our early Earth modes. This is the standard profile for early Earth and analogous exoplanets [107, 125, 690, 691].

The TOA radiation for our models is based on the solar mean [376] with a solar zenith angle of 50°; however, we increase the UV flux to simulate the increased activity of the young Sun. In Table 5.5, we display the multiplicative factors used in our

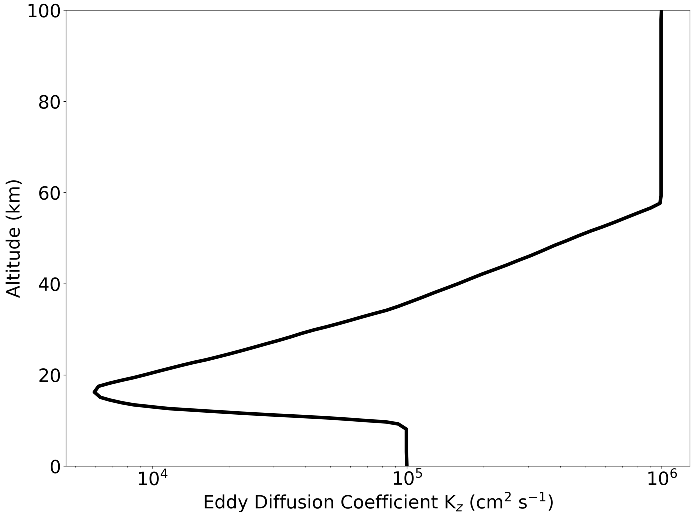

Figure 5.7: Eddy diffusion profile for all early Earth models, characterizing turbulent mixing in the atmosphere. This is the standard K_z profile used for atmospheric simulations of early Earth and analogous exoplanets [107, 125, 690, 691].

models for each UV wavelength interval. Values are based on observations of young solar analogs (ages ∼0.1–7 Gyr) [660].

Table 5.5: Multiplicative increase in UV irradiation from present day values based on observations of young solar analogs [660].

Model	1–20 Å	20–360 Å	360–920 Å	920–1200 Å
4.0 bya	60	10	9	7
4.4 bya	500	60	30	20

Our 33 photochemical reactions mostly match those from the Titan models by Hébrard et al. [133]; however, we update the H_2O absorption cross-sections with the recent near-UV experimental measurements from Ranjan et al. [690], we remove erroneous CO_2 absorption below 202 nm [690], and we add photochemistry for O_2 and HO_2 following treatments in Hu et al. [164] and CH_3OH using experimental cross-sections from Lange et al. [692] and Burton et al. [693].

We couple planetary surface processes to our atmospheric models by adding influxes of species to the lowest layer of our atmospheres. These include: H_2 impact degassing, CO_2 outgassing from volcanoes, CH_4 outgassing from hydrothermal systems, H_2O evaporation from the ocean, and chemical production (e.g. HCN, CO, ^3O, H) due to lightning.

Equilibrium chemistry calculations performed by Zahnle et al. [129] for enstatite chondrite impactors suggest that H_2 degassing via the reaction $Fe + H_2O \longrightarrow FeO + H_2$ scales linearly with impactor mass, at a rate of $\sim 10^{-21}$ mol H_2 cm^{-2} g^{-1} impactor. Mathematical fits to the lunar cratering record provide us with an estimate of the rate of impactors on early Earth at a given epoch. In Figure 5.8, we display our model bombardments rates, which lie between the minimum and maximum bombardment fits [31, 642]. These bombardment rates are 1.2×10^{25} g Gyr^{-1} and 1.2×10^{24} g Gyr^{-1} at 4.4 bya and 4.0 bya, respectively. Multiplying the H_2 degassing abundance per unit mass by the mass delivery rates at 4.4 bya and 4.0 bya gives us H_2 impact degassing rates of 2.3×10^{11} cm^{-2} s^{-1} and 2.3×10^{10} cm^{-2} s^{-1} for the early and late Hadean models, respectively.

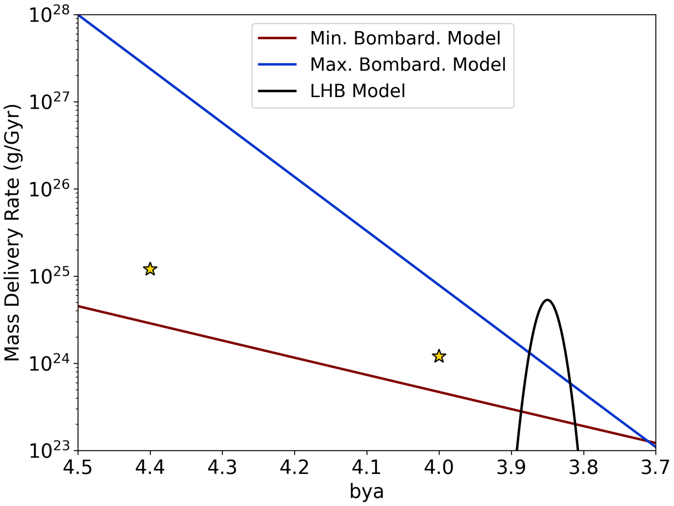

Figure 5.8: Three early Earth bombardment models from Pearce et al. [31] based on fits to the lunar cratering record. The gold stars represent the bombardment rates we used to calculate H_2 impact degassing for our 4.4 and 4.0 bya atmospheric models.

We model H and H_2 escape using the approximation developed by Zahnle et al. [129, 165] which blends energy-limited and diffusion-limited escape. The equation is

$$\left(\frac{dN_{H_2}}{dt}\right)_{esc} = -\frac{AS}{\sqrt{1+B^2S^2}}\frac{N_{H_2}}{\Sigma_j N_j}(cm^{-2}s^{-1}) \tag{5.2}$$

where A = 2×10^{12} cm^{-2} s^{-1}, $B^2 = 0.006$, S is the XUV and FUV irradiation relative to modern Sun (i.e. 30 and 9 for 4.4 and 4.0 bya, respectively), N_{H_2} is the number of

H_2 molecules, and N_j is the number of molecules of species j.

The limits of H_2 degassing to assume a static pressure profile in equilibrium with H_2 escape would be ~2.3×10^{13} and 1.4×10^{13} cm^{-2} s^{-1} at 4.4 and 4.0 bya, respectively.

We use a constant CO_2 outgassing rate of 3.0×10^{11} cm^{-2} s^{-1} in all our models, which is consistent with Earth-like volcanic outgassing used in other atmospheric models [164].

Guzmán-Marmolejo et al. [180] modeled the production of CH_4 in hydrothermal systems for an Earth-like planet, and calculated a production rate of 6.8×10^{8} cm^{-2} s^{-1}. Guzmán-Marmolejo et al. [180] also modeled H_2 production in hydrothermal systems; however, the rates of H_2 produced in hydrothermal environments are orders of magnitude lower than the rates of H_2 production from impact degassing.

We do not include loss of CH_4 due to haze production, as our CH_4/CO_2 ratio never exceeds 0.1 (which is a common identifier for haze production) [694].

Lightning chemistry in the context of the origin of life was first developed experimentally in the 1950's [12]. The fundamental Miller-Urey experiment involves sending an electric discharge through a combination of reduced gases to trigger dissociation. The radicals produced in this process then react to form biomolecule precursors such as HCN and H_2CO [34, 695]. These precursors condense into a reservoir, where aqueous chemistry produces biomolecules such as amino acids [12, 17] and nucleobases [18].

Present-day Earth has an average global lightning flash density of ~2 flashes km^{-2} yr^{-1} [163]. However, above just the oceans, this average density drops to 0.3–0.6 flashes km^{-2} yr^{-1}. Given the smaller coverage of continental crust above sea water during the Hadean, we set the global lightning flash density for our models to 1 flash km^{-2} yr^{-1}; however, we also explore the maximum lightning flash density measured over land on Earth today (28.9 flashes km^{-2} yr^{-1}).

We considered both non-equilibrium and equilibrium approaches for modeling lightning chemistry. For our non-equilibrium approach, we integrated the production of key radicals for the first ~40μs of a lightning strike using the pressure and temperature evolution from Ardaseva et al. [159]. However, this approach had accuracy issues as a complete high-temperature reaction network is required to accurately calculate the chemical evolution within a cooling lightning channel. This approach also led to some insensible results such as HCN production that is independent of lightning flash density.

Therefore, we use an equilibrium approach for modeling the lightning production

Table 5.6: Equilibrium abundances (molar mixing ratios) from lightning chemistry occurring in our four early Earth models. Thermodynamic simulations are based on initial concentrations in Table 5.2 for a freeze out temperature of T_F = 2000 K.

Species	Model A	Model B	Model C	Model D
HCN	1.9×10^{-7}	2.1×10^{-3}	1.1×10^{-7}	2.1×10^{-3}
H_2	3.8×10^{-1}	1.1×10^{-4}	3.3×10^{-1}	1.1×10^{-4}
H	5.0×10^{-1}	7.4×10^{-3}	5.4×10^{-1}	7.4×10^{-3}
N_2	1.7×10^{-2}	1.1×10^{-2}	1.3×10^{-2}	1.1×10^{-2}
^4N	1.0×10^{-1}	7.3×10^{-2}	1.1×10^{-1}	7.3×10^{-2}
H_2O	1.6×10^{-3}	4.6×10^{-5}	2.3×10^{-3}	4.6×10^{-5}
^3O	2.8×10^{-3}	2.1×10^{-1}	2.8×10^{-3}	2.1×10^{-1}
OH	2.1×10^{-3}	3.1×10^{-3}	3.7×10^{-3}	3.1×10^{-3}
NO	4.4×10^{-4}	3.1×10^{-2}	7.3×10^{-4}	3.1×10^{-2}
O_2	1.2×10^{-5}	8.7×10^{-2}	1.2×10^{-5}	8.7×10^{-2}
CH_4	5.1×10^{-7}	4.6×10^{-8}	2.1×10^{-7}	4.6×10^{-8}
CH_3	6.7×10^{-7}	3.1×10^{-6}	3.4×10^{-7}	3.1×10^{-6}
CO	6.8×10^{-9}	4.1×10^{-1}	1.0×10^{-8}	4.1×10^{-1}
CO_2	2.9×10^{-11}	1.7×10^{-1}	6.9×10^{-11}	1.7×10^{-1}

of HCN and other species based on the lightning chemistry models for HCN and NO production by Chameides & Walker [161]. Lightning channels heat up to a point (~30000 K) [158] where the equilibrium timescale is less than 1μs [162]. This is fast compared to the hundred millisecond cooling timescale of a lightning channel, as well as the 10μs eddy diffusion timescale in the lowest layer in our atmospheres.

Chemical abundances rapidly reach equilibrium while the lightning channel is above the freeze out temperature (T_F). The freeze out temperature is the temperature at which the concentration of a species can still be described by its equilibrium value. Beyond this point, there is not enough time at a given temperature for equilibrium to be reached, and thus the concentrations are frozen into the gas for the remainder of the cooling of the lightning channel. Reaction rate coefficients that break down a species are used to roughly determine the freeze out temperature, e.g., HCN + M → CN + H + M. Typical freeze out temperatures range from 1000–5000 K. The freeze out temperature for HCN is ~2000–2500 K for lightning strikes similar in energy to Earth today (10^5 J m^{-1}) [161]. Other species such as NO have higher freeze out temperatures near 3000–3500 K for similar lightning discharge energies, but can also be ∼2000 K for the highest discharge energies (10^15 J m^{-1}). We adopt $T_F = 2000$ K for our equilibrium calculations to estimate the mixing ratios for HCN and 13 other dominant equilibrium products in the early Earth lightning models by Chameides & Walker [161].

Equilibrium calculations are performed using the thermochemical data from the JANAF tables [657], and the ChemApp Software library (distributed by GTT Technologies, http://gtt.mch.rwth-aachen.de/gtt-web/).

In Table 5.6, we display the equilibrium mixing ratios based on the initial abundances in our four early Earth models for a freeze out temperature of $T_F = 2000$ K.

For our fiducial models, we introduce HCN and other species to the bottom layer of the atmosphere at a rate that corresponds to 1 flash km^{-2} yr^{-1}. The species influx rates from lightning chemistry are calculated along a lightning channel extending through the first layer of the atmosphere using the following equation:

$$\frac{d[M]}{dAdt} = \frac{n_M P \Delta H \dot{f} \sigma_l}{k_B T \gamma} \left(\frac{1}{100}\right)^3 \left(\frac{1}{10000}\right)^2, \tag{5.3}$$

where $\frac{d[M]}{dAdt}$ is the molar concentration of species M produced per cm^2 per second, n_M is the molar mixing ratio of species M produced in the lightning strike (cm^{-3}), ΔH is the height of the lowest atmospheric layer (cm), $\dot{f}$ is the lightning flash density in flashes km^{-2} yr^{-1}, σ_l is the cross section of the lightning channel (∼1 cm^2), $\gamma = 3{,}600 \cdot 24 \cdot 365.25$ s yr^{-1}, and the remainder is unit conversion.

In Table 5.7, we list the deposition velocities for the species that are rained out of the lowest layer in our atmospheric models.

We apply a CO_2 deposition velocity of 1.0×10^{-4} cm s^{-1}, which is estimated in Hu et al. [164] to produce a CO_2 lifetime consistent with the lifetime of silicate weathering on Earth. We use a CO deposition velocity of 1×10^{-8} cm s^{-1}, calculated from a 2-box model [698]. We also use a deposition velocity of 1×10^{-8} cm s^{-1} for O_2, given its similar solubility and diffusivity to CO [701]. We use the standard HCN deposition velocity of 7.0×10^{-3} cm s^{-1} that is used in other early Earth models [107, 125]. Additional deposition velocities are chosen to be consistent with other rocky exoplanet atmospheric models [164, 690]. Major species not listed in this table (e.g. H_2 and CH_4) are not very soluble in water, therefore we do not include rain-out for these species [168].

Table 5.7: Deposition velocities for the chemical species in our early Earth models.

Species	Deposition (cm s^{-1})	Source
CO_2	1×10^{-4}	Archer [696]
CH_3OH	0.1	Wohlfahrt et al. [697]
O_2	1×10^{-8}	this work
CO	1×10^{-8}	Kharecha et al. [698]
H_2O_2	0.5	Hauglustaine et al. [699]
C_2H_6	1×10^{-5}	Hu et al. [164]
HO_2	1	Ranjan et al. [690]
H_2CO	0.1	Wagner et al. [700]
HCO	0.1	Ranjan et al. [690]
HCN	7×10^{-3}	Tian et al. [107]
OH	1	Ranjan et al. [690]
^3O	1	Ranjan et al. [690]
H	1	Ranjan et al. [690]

Warm little pond models

In Table 5.8, we display the sources and sinks for nucleobases, ribose and 2-aminooxazole in our warm little pond models. All biomolecule reaction yields are based on HCN. For cytosine, uracil, thymine, ribose, and 2-aminooxazole, which require formaldehyde as a reactant, we use a formaldehyde yield from HCN of 3.6%, which is three times the glyceronitrile yield from radiolytic aqueous HCN experiments performed by Yi et al. [39].

Table 5.8: Sources and sinks for the five nucleobases, ribose, and 2-aminooxazole in our warm little pond model. HCN enters our ponds from rain-out calculated in our antecedent atmospheric model, and is multiplied by experimental and theoretical yields to simulate the *in situ* production of key RNA biomolecules. H_2CO, which is a key reactant for cytosine, uracil, and ribose synthesis is produced in our ponds directly from HCN [39]. HCN reactions are fast (experiments last < days) in comparison to the duration of our models.

Biomolecule	Yield from HCN	Yield reference	Sinks	Sink rate	Sink reference
Adenine	$0.005–0.18^a$	Oró & Kimball [37], Hill & Orgel [703], Wakamatsu et al. [704]	Photodestruction	1.0×10^{-4} $photon^{-1}$	Poch et al. [702]
			Seepage	2.6 mm solution d^{-1}	Boyd [705], Pearce et al. [31]
			Hydrolysis	5.0×10^{-10} s^{-1}	Levy & Miller [706]
Guanine	$6.7\times10^{-5}–0.2^b$	Miyakawa et al. [707], Larowe & Regnier [38]	Photodestruction	1.0×10^{-4} $photon^{-1}$ ^{c}	Poch et al. [702]
			Seepage	2.6 mm solution d^{-1}	Boyd [705], Pearce et al. [31]

			Hydrolysis	4.8×10^{-10} s^{-1}	Levy & Miller [706]
Cytosine	0.036^{d}	Yi et al. [39], Larowe & Regnier [38]	Photodestruction	1.0×10^{-4} photon^{-1} ^{c}	Poch et al. [702]
			Seepage	2.6 mm solution d^{-1}	Boyd [705], Pearce et al. [31]
			Hydrolysis	1.2×10^{-8} s^{-1}	Levy & Miller [706]
Uracil	1.7×10^{-5}–0.018^{bd}	Miyakawa et al. [707], Yi et al. [39], Larowe & Regnier [38]	Photodestruction	1.0×10^{-4} photon^{-1} ^{c}	Poch et al. [702]
			Seepage	2.6 mm solution d^{-1}	Boyd [705], Pearce et al. [31]
			Hydrolysis	1.4×10^{-11} s^{-1}	Levy & Miller[706]
Thymine	0.012^{d}	Yi et al. [39], Larowe & Regnier [38]	Photodestruction	1.0×10^{-4} photon^{-1} ^{c}	Poch et al. [702]
			Seepage	2.6 mm solution d^{-1}	Boyd [705], Pearce et al. [31]
			Hydrolysis	2.8×10^{-12} s^{-1}	Levy & Miller [706]
2-Amino-oxazole	0.0011	Yi et al. [39],	Photodestruction	1.0×10^{-4} photon^{-1} ^{c}	Poch et al. [702]
			Seepage	2.6 mm solution d^{-1}	Boyd [705], Pearce et al. [31]
			Hydrolysis	none^{e}	
Ribose	3.6×10^{-4} ^{f}	Yi et al. [39], Shapiro [708]	Photodestruction	1.0×10^{-4} photon^{-1} ^{c}	Poch et al. [702]
			Seepage	2.6 mm solution d^{-1}	Boyd [705], Pearce et al. [31]
			Hydrolysis	none^{g}	

[a] Yield range is based on experiments with and without catalysts, e.g., ammonium formate.

[b] Lower yield value is from experiment. Upper value is the theoretical yield.

[c] Photodestruction rate assumed to be similar to that of adenine.

[d] Yield is based on radiolytic experiments for the Kiliani–Fischer synthesis of glyceronitrile [39], for which H_2CO is initially produced from irradiated solutions of HCN and water. We multiply the glyceronitrile yield by 3, given 3 times fewer HCN molecules are required for antecedent H_2CO synthesis. H_2CO is then assumed to be the limiting reagent in the theoretical reaction from Larowe & Regnier [38], for which we assume the 100% theoretical yield.

[e] There are no known hydrolysis experiments for 2-aminooxazole; however, it is known to be fairly stable [709]. We assume the other two sinks dominate the loss of this species.

[f] Ribose yields from lab experiments of the formose reaction are uncertain; however, 1% has been suggested.

[g] We assume sufficient borate is present in our ponds to stabilize ribose from hydrolysis [710].

We consider two yields for adenine production from HCN in our pond solutions based on experiments: a lower yield of 0.5% based on aqueous reactions of HCN [37], and an upper yield of 18% based on HCN reactions with more ideal conditions for forming adenine (e.g., solutions containing NH_3, ammonium formate [703, 704].

For guanine and uracil we consider lower yields of 0.0067% and 0.0017%, respectively, based on experiments of frozen ammonium cyanide solutions [707]. We use theoretical yields for the upper bounds. Guanine has a theoretical yield of 20% based on the theoretical HCN-based reaction equation $5\,\mathrm{HCN} + \mathrm{H_2O} \longrightarrow \mathrm{guanine} + \mathrm{H_2}$ [38]. Uracil has a theoretical yield of 50%; however, it is based on H_2CO as a limiting reagent ($2\,\mathrm{HCN} + 2\,\mathrm{H_2CO} \longrightarrow \mathrm{uracil} + \mathrm{H_2}$ [38]. Experiments of the Kiliani–Fischer synthesis of glyceronitrile produce H_2CO as an intermediate from aqueous solutions of HCN [39]. Yields of glyceronitirile production are 1.2%; however, theory suggests 3 intermediate HCN molecules are involved in this reaction. Considering this, we apply a yield of 3.6% for H_2CO production from HCN. For uracil, this results in an upper yield of 50% × 3.6% = 1.8%.

Given the lack of experiments producing cytosine and thymine from aqueous HCN, we only consider the theoretical upper yields for these species base on the reaction equations $3\,\mathrm{HCN} + \mathrm{H_2CO} \longrightarrow \mathrm{cytosine}$ and $2\,\mathrm{HCN} + 3\,\mathrm{H_2CO} \longrightarrow \mathrm{thymine} + \mathrm{H_2O}$ [38]. Again, since H_2CO is the limiting reagent for these theoretical reactions, we apply the yield of 3.6% for H_2CO production from HCN, resulting in yields of 3.6% and 1.2% for cytosine and thymine production from HCN, respectively.

For 2-aminooxazole, we consider a yield of 0.11% based on radiolytic experiments of aqueous solutions of HCN [39].

Finally, experiments of ribose synthesis from H_2CO have identified ribose as a product, but yields remain uncertain. Shapiro [708] suggests 1% as an upper bound, therefore we consider this yield and also apply the yield of 3.6% for H_2CO production from HCN to obtain an overall yield of 0.036%.

Supplementary Results

Biomolecule Concentrations

In Table 5.9, we display the peak concentrations of HCN, H_2CO, and various RNA building blocks from our fiducial coupled atmosphere and warm little pond models. Concentrations of biomolecules from the early Hadean (reducing) model are approximately 3 orders of magnitude higher than concentrations from the late Hadean (oxidizing) model. The exception is H_2CO from rain-out, which is 3 orders of magnitude higher in the oxidizing atmospheric conditions of the late Hadean compared with the reducing conditions of the early Hadean.

Rain-out Rates

In Figure 5.9, we display the rain-out rates for HCN, H_2CO, and CO_2 as a function of time. These water-soluble species, and a few others, are removed from the lowest layer of our atmospheric models at each time step. The HCN rain-out rate for the early Hadean (reducing) model A is 2.0×10^{-6} kg m^{-2} yr^{-1} at 20 million years. This is about 3 orders of magnitude higher than the HCN rain-out rate for the late Hadean (oxidizing) model B of 1.9×10^{-9} kg m^{-2} yr^{-1}, but only 1.5 orders of magnitude higher than the HCN rain-out rate for the late Hadean (oxidizing) model D. The HCN rain-out rate for model C is approximately a factor of 2 lower than model A at 20 million years. Model D differs from model B by a factor of 48 at 700,000 years. We use the 20 million year and 700,000 million year HCN rain-out rates from models A

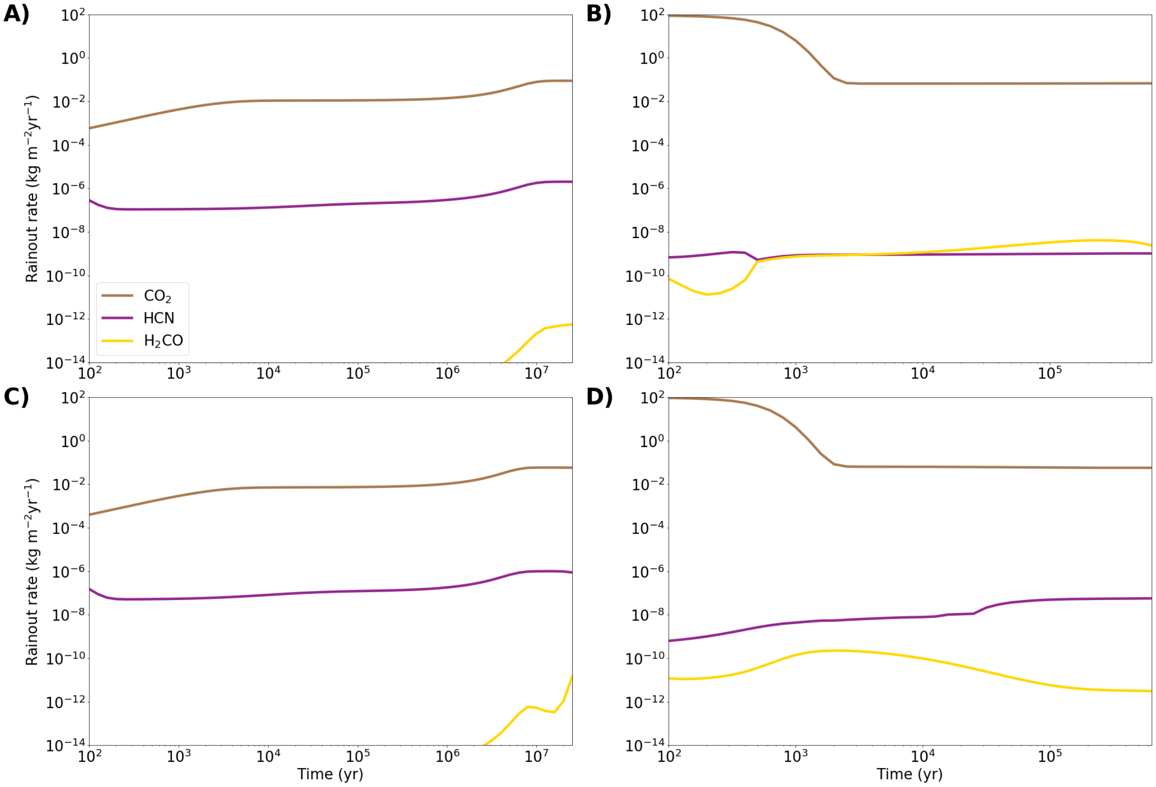

Figure 5.9: Rain-out rates of HCN, CO_2, and H_2CO from the lowest atmospheric layer as a function of time in our four early Earth models. Models parameters are listed in Table 5.2.

Table 5.9: Summary of the peak concentrations of biomolecules and biomolecule precursors for our fiducial atmosphere and WLP models. Lightning rates of 1 flash km^{-2} yr^{-1} were used for these calculations.

Molecule	Early Hadean (reducing) (μM)	Late Hadean (oxidizing) (μM)
HCN	0.66	3.4×10^{-4}
H_2CO (aq. production)	0.024	$\sim10^{-5}$
H_2CO (rain-out)	$\sim10^{-7}$	7.1×10^{-4}
Adenine	0.11	$\sim10^{-5}$
Guanine	0.13	$\sim10^{-5}$
Cytosine	0.023	$\sim10^{-5}$
Uracil	0.012	$\sim10^{-6}$
Thymine	0.008	$\sim10^{-6}$
2-aminooxazole	7.3×10^{-4}	$\sim10^{-7}$
Ribose	2.4×10^{-3}	$\sim10^{-7}$

and B, respectively, for influx into our subsequent warm little pond models.

The H_2CO rain-out rate for the early Hadean (reducing) A is 5.6×10^{-13} at 20 million years. This is about 4 orders of magnitude lower than the H_2CO rain-out rate for the late Hadean (oxidizing) model B of 4.1×10^{-9} kg m^{-2} yr^{-1} at 700,000 years. For the late Hadean (oxidizing) model B, rain-out of HCN is more abundant than rain-out of H_2CO for the first ∼500 years, but on long timescales H_2CO rain-out dominates HCN rain-out.

HCN to CH4 Ratio

In Figure 5.10, we display the molar abundance ratio of HCN/CH_4 in the lowest atmospheric layer. For the early Hadean (reducing) models A and C, the average HCN/CH_4 ratio is $\sim2\times10^{-5}$. For the late Hadean (oxidizing) models B and D, the average HCN/CH_4 ratios are 10^{-3} and 10^{-6}, respectively. The HCN/CH_4 ratios are fairly tight for models A, C, and D, varying by about 1 order of magnitude over the simulation timescales. Conversely, the HCN/CH_4 ratio for model B varies by over 3 orders of magnitude from $t = 100$ to 1000 years before stabilizing for the remainder of the simulation time.

Maximum Lightning Flash Density

In Figure 5.11, we plot the molar HCN mixing ratio as a function of altitude for our early Hadean (reducing) model A using an increased lightning flash density 28.9

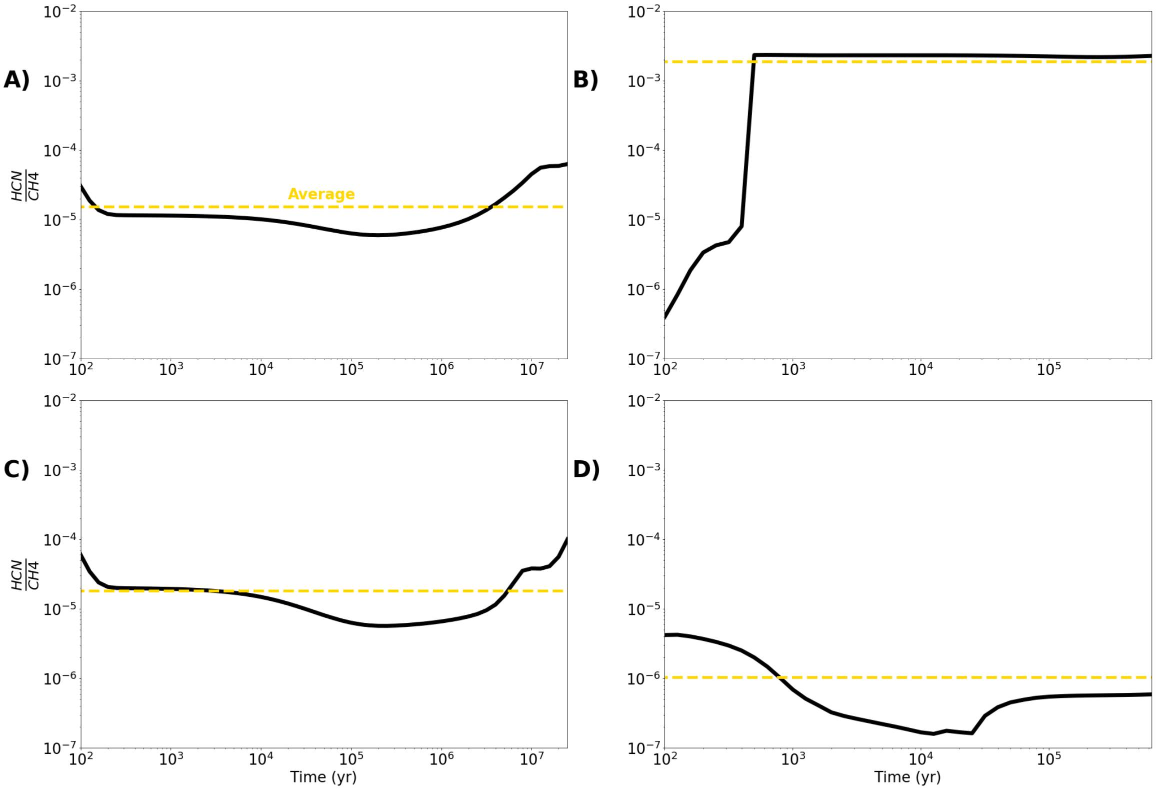

Figure 5.10: The molar abundance ratio of HCN to CH4 in the lowest atmospheric layer for our four early Earth models. Models parameters are listed in Table 5.2.

times greater than our fiducial rate. This lightning flash density is the highest average value measured over land on Earth today [163].

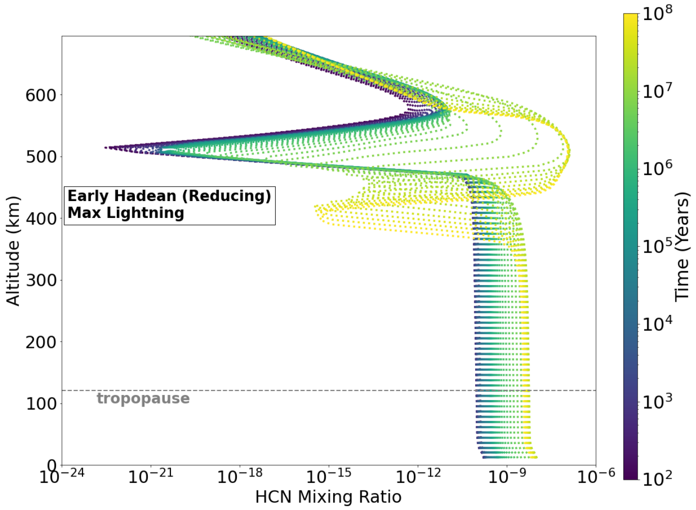

Figure 5.11: The molar abundance of HCN from $t = 100$ years to 100 million years for model A with an increased lightning flash density of 28.9 flashes km^{-2} yr^{-1}. This flash density is the maximum average value measured over land on Earth today [163]. Models parameters are listed in Table 5.2.

From 100 to 100 million years, the HCN mixing ratio increases at the surface from $\sim 10^{-10}$–10^{-8}. The HCN mixing ratio at the surface is a factor of 24 higher than the HCN mixing ratio produced after 20 million years using a lower flash density of 1 flash km^{-2} yr^{-1}. This shows that HCN production by lightning is approximately linearly dependent with lightning flash density.

Chapter 6

Conclusions & Future Work

> ” *I'm leaving home for the coastline*
> *Some place under the sun*
> *I feel my heart for the first time*
> *Cause now I'm moving on yeah, I'm moving on*
>
> — **Hollow Coves, *Coastline***

The aim of this thesis is to determine if and when early Earth was biogenic, i.e., capable of producing key biomolecules for the origin of life rather than requiring they be delivered by meteorites. We focus on the hypothesis that first life emerged in warm little ponds (WLPs) as self-replicating RNA. In this scenario, we find a route to RNA on a biogenic early Earth at 4.4 bya, initiated by lightning- and UV-driven HCN production in the reducing atmosphere, followed by HCN rain-out and subsequent aqueous chemistry in WLPs cycling between wet and dry conditions. This biogenic phase lasted for at least 100 million years, but was over by 4.0 bya due to the transition into oxidizing atmospheric conditions that are unfavourable for HCN production. This result advances present knowledge of how WLPs obtained RNA building blocks for life, and places a time constraint on the emergence of life from a biogenic atmosphere based on the early declining rate of impact bombardment inferred from the lunar cratering record.

Looking back at the the time interval or the origin of life in Figure 1.1, the earliest point after the Moon-forming impact at which Earth's magma ocean could have cooled and solidified, and water condensed out to for the first oceans, was 4.5 bya. Models based on Hf–W, Rb–Sr, and U–Pb dating of lunar mantle material brought back from the Apollo missions estimate the Moon-forming impact to be an average of ∼69 Myr after the formation of the Solar System, 4.568 bya [711–715]. The largest uncertainty in early Earth's habitability boundary is the cooling and solidification time of the post-impact magma mantle, for which models suggest occurred as rapidly as 20,000 years [45], ocurred at a slower pace of 1.5 million years [46], or was very sluggish and took 100 million years to complete [47]. For the fast and mid-range estimates, early Earth could have cooled to below the boiling point of water as early as ∼4.5 bya, after which the first WLPs could form on any rising volcanic land masses [51, 638].

In this thesis, we find that early Earth was biogenic at least up until 4.3 bya, which would provide an approximate 200 million year window of opportunity for an RNA world to emerge in WLPs from a steady source of building blocks. After this, ponds could still obtain some RNA building blocks from meteorites, such as 3 of the 4 nucleobases in RNA [88, 89], and ribose [92]; however, given meteoritic depositions are not a steady source, they can only offer boosts in concentration of these building blocks to ppm levels for about a week after deposition. After about a week, concentrations from meteoritic sources drop to ppb levels due to UV photodissociation and seepage, and sub-ppb levels after about 6 months up to a few years depending on meteorite fragment size [31]. Our past models of meteoritic deposition probability for a linearly declining bombardment and a linear increase in pond growth from 4.5–3.7 bya suggest that a few thousand carbon-rich meteorite depositions occurred in WLPs during this period. However, no single pond was likely to get more than a single deposition [31].

Our models suggest, between 4.3 and 4.0 bya, that the bombardment rate decreased to a point at which oxygen species such as H_2O and CO_2 dominated over H_2, and HCN was no longer favourably produced. This is because CH_4, which is the main precursor to HCN, is prone to oxidation. It may be the case that the RNA world had to rely on metabolic pathways for building block production to continue to evolve beyond this point. For example, if RNA evolution driven by wet-dry cycles led to the emergence of a primitive ribosome, protein catalysts could be produced to assist in RNA building block synthesis. At this point, RNA could transition from being the information and catalyst of life, to being the middle person to transcribe and translate DNA information into protein catalysts.

Considering the timescales of evolution, 200 million years might seem like a long enough time for first life to emerge on Earth. For example, it took approximately

65.9 million years for *Homo sapiens* to evolve from plesiadapiforms (the first primates, somewhat similar in bone structure to lemurs) [716]. Both the biological evolutionary path from one living thing to another and the chemical evolution from replicating RNA strands (i.e. RNA replicases) to life as we know it are processses of Darwinian evolution. All that is required for Darwinian evolution, are mechanisms for replication, selection, and generation of diversity in the population [717]. In a WLP, each new dry phase generates a diverse population of RNA, as polymerization occurs in dehydrated conditions when phosphodiester bond formation is thermodynamically favourable [27, 51, 53]. Hydrolysis in the wet-phase applies a selection pressure to the RNA population, where emergent RNA replicases have higher fitnesses to survive by making copies faster than hydrolysis destroys them [639]. These RNA strands were also likely encapsulated by fatty acid vesicles (spherical prebiotic compartments) in WLPs, which reduces the volume for RNA interactions, and offers additional selection effects, e.g. where RNA strands that strengthen the vesicle membrane allow an entire protocell to survive until the dry phase [51, 52].

What is unclear, is how many non-functional RNA sequences were polymerized in the dry phase before the event occurred that established a stable small group of replicators. In other words, what is the size of RNA replicase sequence space in comparison to non-functional RNA sequence space? The process of a replicating ribozyme emerging in a WLP may require a long “searching and waiting” period [44].

When considering the emergence of life in a WLP as described above, it would seem like a meteoritic origin of RNA building blocks would be a much more chance scenario. Without a constant source of RNA building blocks, UV dissociation, seepage and hydrolysis are constantly depleting the finite supply of meteoritic RNA building blocks, and thus the timer for the search period through RNA sequence space is possibly only on the order of weeks. On the other hand, our results suggest that the timer for the search through RNA sequences during the biogenic phase of early Earth is potentially $\sim$200 million years.

But how long would it take to search through RNA sequence space to find a replicating ribozyme? Is 200 million years a lot or a little? Ribose or 2-aminooxazle would seem to be the limiting reactants in producing RNA building blocks in our ponds, for the early and more modern approaches to forming nucleotides, respectively. These species peak at 6 nM and 18 nM in our ponds for maximum lightning conditions at 4.4 bya. Conversely, nucleobases are all present in the μM range. For example, if we consider the entire amount of ribose in the bottom 1 mm of pond solution right before the dry phase, our 1 meter-radius ponds could produce up to 1×10^{-8} moles of nucleotides. If we guess that the first self-replicating ribozyme had a sequence length of 65 nt, which is on the lower end of the ribozymes used in the lab to demonstrate replicative activity [59–62], then we can multiply this nucleotide abundance by Avogadro's number and divide by 65 to get the maximum number of RNA sequences of length 65 that could be produced per wet-dry cycle. This works out to approximately 92 trillion.

We don't know exactly how many sequences of length 65 are replicators, but we do have some hints from *in vitro* evolution experiments performed by Bartel & Szostak [718]. In these experiments, they began with a random pool of 10^{15} RNA strands and performed repeated cycles of *in vitro* selection to isolate ribozymes that could ligate two RNA strands aligned on a template. After 10 rounds of cycling, they detected 65 RNA strands that were capable of carrying out the particular ligation reaction out of the pool of 10^{15}. This experiment suggests that potentially 1 in 15 trillion RNA strands could exhibit replicative behaviors such as ligation. Given our estimate that 92 trillion RNA strands of length 65 could be produced per wet-dry cycle, it could be that the "searching and waiting" period is only a handful of wet-dry cycles.

Once the first RNA replicases emerge, with the continuing selection pressure from wet-dry cycles, chemical evolution can proceed rather efficiently. In the experiments by Bartel & Szostak [718], 10 rounds of *in vitro* selection led to the emergence of ribozymes with reaction rates 7 million times faster than the uncatalyzed reaction rate. Ribozyme replication only takes $\sim$ 10 milliseconds to 2 hours to occur in the laboratory [60]. In comparison to the reproductive life cycles of our primate ancestors (several years), chemical evolution has a bit of an edge in efficiency over primate biological evolution.

If the RNA replicase occurrence rate is approximately 1 in 15 trillion, we might expect that RNA worlds would be fairly regular on Earth-like planets that have early biogenic phases such as ours. Unfortunately, we cannot yet say anything quantitative about the probability of life elsewhere in the Galaxy. After all, we are a sample size of $n = 1$ and there is a strong selection bias in estimating the probability of life beyond Earth.

In any case, the origin of RNA on biogenic worlds, as laid out in this thesis, is expected to be a universal process in stellar systems with habitable Earth-like worlds.

To date, 60 potentially habitable exoplanets have been discovered [719], and Bayesian analyses of the Kepler exoplanet data suggest that one in two stars is likely to host a habitable rocky planet [720]. Impact bombardment rates on such planets would be the highest as planetesimals slowly cleared out of the protoplanetary disk during the formation of these worlds. Any WLPs formed on the rising continental crusts of these planets would then be fed by HCN produced in a reducing atmosphere driven by the high rates of H_2 impact degassing. It would be expected too, that due to H_2 escape and the decreasing bombardment rate moving forward in time that these worlds would transition towards oxidizing conditions, and out of biogenicity.

Super-Earth's (2–10 $M_\oplus$) are massive enough to hold onto their reducing H_2 atmospheres, thus it is tempting to consider the sustained biogenicity of these worlds. However, H_2-H_2 collisional induced absorption due to the high surface pressures (hundreds to thousands of bars [721]) on such worlds may provide too thick of a thermal blanket for clement surface temperatures to exist [177]. Indeed, it may be the case that biogenicity is just an early phase of habitable terrestrial planets, and perhaps the slow oxidation of the atmosphere provides the necessary environmental selection pressure for the RNA world to evolve into a self-sustaining chemical system.

We now briefly summarize the work carried out in each chapter of this thesis, and state our main conclusions.

6.1 Conclusions

In Chapter 2, we develop an accurate and feasible method for calculating theoretical reaction rate coefficients in the gas phase, and apply this method to reactions related to HCN chemistry in reducing planetary atmospheres. This method is based on canonical variational transition state theory (CVT) paired with computational quantum chemistry simulations with the Becke–Half-and-Half–Lee–Yang–Parr (BHandHLYP) density functional and the augmented correlation-consistent polarized valence double-ζ (aug-cc-pVDZ) basis set. We perform calculations on 27 reactions with experimentally measured rate coefficients, and 15 reactions with missing/unknown values.

In Chapter 3, we expanded and improved upon this method, and explored the entire field of reactions for a list of primary species in planetary atmospheres dominated by N_2, H_2, and CH_4. We introduce calculations of three-body reactions based on Rice–Ramsperger–Kassel–Marcus/master equation (RRKM/ME) theory. We calculated a total of 102 reaction rate coefficients in this chapter, including 33 reactions that were previously undiscovered in the literature. From here, we built a consistent reduced atmospheric hybrid chemical network (CRAHCN) containing experimental rate coefficients when available (32%) and our calculated rate coefficients otherwise (68%). In an effort to validate our approach, we then couple CRAHCN to a 1D atmospheric chemical kinetics code (ChemKM) to model HCN production in the atmosphere of Titan: a world with a diverse set of HCN observations performed by the Cassini spacecraft.

Below we summarize the main conclusions from Chapters 2 and 3.

- Overall, we find computational quantum chemistry simulations at the BHandHLYP/aug-cc-pVDZ level of theory paired with CVT and/or RRKM/ME to be a feasible and accurate method for calculating rate coefficients for a large set of gas phase reactions for a range of temperatures and pressures. Our rate coefficient calculations are most commonly within a factor of two of experimental values, and generally always within an order of magnitude of these values. This level of accuracy is consistent with the uncertainties assigned in large-scale experimental data evaluations (e.g. Baulch et al. [137]).

- The HCN profile from our fiducial model of Titan's atmosphere agrees very well with the Cassini observations and is in line with the three most recent Titan models in the literature. These agreements suggest that our chemistry is accurate for modeling HCN in reducing environments.

- Using sensitivity analyses, we find that only 19 reactions are responsible for the production and destruction of HCN in Titan's atmosphere. This result demonstrates the power of using reduced (e.g. 100–300 reaction) chemical networks to better understand the chemistry of a given species. Sensitivity analyses such as the ones we performed in this chapter would not be computationally feasible on 1000+ reaction chemical networks.

- Through analysis of the 19 dominant reactions, we are able to understand the complete story of how HCN is produced in Titan's atmosphere. First, UV radiation in the upper atmosphere, and GCRs in the lower atmosphere, break apart CH_4, N_2, and H_2 into their reactive radicals (e.g. $^1CH_2$, ^2N, H). Second, some of these radicals get processed via chemical reactions to form direct HCN precursors (e.g., CH_3). Next, HCN production occurs through three main channels

- $^2N + CH_4 + H \longrightarrow H_2CN + H_2 + H \longrightarrow HCN + 2\,H_2$ (∼32–38%),
- $^4N + CH_3 \longrightarrow H_2CN + H \longrightarrow HCN + H_2$ (∼20–25%),
- $^2N + CH_3 \longrightarrow H_2CN + H \longrightarrow HCN + H_2$ (∼2%),

where percentages refer to the final contribution of each reaction to overall HCN production on Titan. Finally, UV radiation breaks down HCN into CN and H, and CN is recycled back into HCN via the dominant source of HCN in Titan's atmosphere,

- $CN + CH_4 \longrightarrow HCN + CH_3$ (∼36–46%).

- The first and fourth reactions mostly occur in the lower atmosphere, and the first, second and third reactions occur in the upper atmosphere. In the upper atmosphere, where reactant densities are low, the rate coefficient part of rate equation tends to dictate the dominant reactions. In the lower atmosphere, where CH_4 densities are high, the reactant density part of the rate equation dictates the dominant reactions.

- The third reaction above is first discovered and calculated in this thesis (Chapter 2). This discovery provides validation for our approach of exploring relevant missing reactions with quantum chemistry methods and including these reactions in disequilibrium atmospheric models.

- $HCN + {}^2N \longrightarrow N_2 + CH$ is the main sink for HCN. In contrast, UV photodissociation is not an effective sink for HCN, because it produces a CN molecule that reacts with CH_4 to reform HCN.

- GCRs triple the total production of HCN in Titan's atmosphere; however, they do not affect which reactions dominate HCN production and destruction.

In Chapter 4, we expand on our calculations in the previous two chapters, and explore unknown chemistry related to HCN and H_2CO production in atmospheres dominated by N_2, CO_2, H_2, CH_4, and H_2O. We calculate the rate coefficients for 126 new reactions, including 45 reactions that were previously undiscovered prior to this work. We then develop an oxygen extension to CRAHCN called CRAHCN-O, which contains experimental rate coefficients when available, and our consistently calculated values otherwise.

Finally, in Chapter 5, we we make a major new step in understanding the origin of RNA on a biogenic early Earth with the development of two new powerful computational treatments that couple terrestrial geochemistry, radiative transfer, atmospheric photochemistry, lightning chemistry and aqueous pond chemistry. In the first, we use CRAHCN-O network and two specially developed atmosphere codes to model HCN and H_2CO production in early Earth's atmosphere. Then, we couple the rain-out of HCN from our atmospheric models to a comprehensive warm little pond model to compute the *in situ* production of RNA building blocks. We then compare the nucleobase concentrations from *in situ* production at two epochs (4.4 and 4.0 bya) with those from meteoritic delivery.

The major conclusions of this thesis are as follows:

- During the early reducing phase of the Hadean (4.4 bya), atmospheric HCN rained into ponds and produced adenine concentrations of up to $\sim$2.8μM for maximum lightning conditions. These peak concentrations are a factor of 4 lower than the peak concentrations from meteoritic delivery ($\sim$10μM); however, peak concentrations from meteorites deplete after $\sim$a week, whereas aqueous production remains steady for at least 100 million years due to the persistent source of precursor HCN entering ponds. These calculations show that the early Earth is likely to have been biogenic at 4.4 bya, and that this phase lasted for at least 100 million years.

- Peak adenine concentrations from aqueous production are 2–3 orders of magnitude lower during the late oxidizing phase of the Hadean (4.0 bya) than during the early reducing phase (4.4 bya). These calculations show that by 4.0 bya, early Earth was no longer biogenic due to oxidation of the atmosphere. In an oxidizing atmosphere, the main limiting HCN precursor, CH_4, is oxidized into CO_2. In reducing conditions, CH_4 is maintained at nearly constant ppm-level abundances, and is readily converted into HCN.

- These two main results provide a firm theoretical foundation for an origin of life within about 200 million years after the Moon-forming impact and cooling of the magma ocean, when the *in situ* production of RNA building blocks was at its peak.

- During the early Hadean (4.4 bya), peak concentrations for guanine, cytosine, uracil and thymine are in the μM range and peak concentrations for 2-aminooxazole and ribose are in the nM range. We note that meteoritic analyses have looked for cytosine and thymine in meteorites and have not measured detectable levels (e.g. [88]). This suggests the biogenic phase of the Hadean may one of the only plausible origins of these RNA and DNA building blocks.
- The dominant source of formaldehyde (H_2CO) to WLPs during the early Hadean (4.4 bya) is aqueous photolytic production from HCN. However, when conditions became more oxidizing at 4.0 bya, H_2CO production in the atmosphere increases, and the dominant source of H_2CO to WLPs becomes direct rain-out from the atmosphere.
- The high atmospheric abundance of HCN near the surface of our early Hadean (reducing) model is largely driven by lightning chemistry. Although both lightning and UV light produce the same reactive radical species (e.g. CH_3, ^4N), HCN is more rapidly produced when these radicals are formed at high density, where lightning occurs. The rate law for chemical reactions is based on reactant density; therefore, in the diffuse upper regions of the atmosphere, where photochemistry occurs, HCN reactions proceed more slowly. Thus, our models favour a lightning-based Miller-Urey scenario for the origin of RNA building blocks.
- HCN production is linearly dependent on lightning flash density; therefore, environments with immense surges of lightning such as electrical storms in volcanoes may produce bursts of HCN that would rain out into ponds at rates that are potentially orders of magnitude higher than the rates in our models. These concentrating local effects may provide a solution for the issue that the peak biomolecule concentrations produced in our pond models are at least 2 orders of magnitude lower than the starting concentrations typically used for prebiotic chemistry experiments in the lab.

While meteoritic delivery provided a burst of biomolecular input into ponds at slightly higher concentrations as we find, the peak pond concentrations from delivery are not sustained for more than a week. On the other hand, the steady synthesis of biomolecules in these biogenic processes during the early Hadean offer significant support for wet-dry cycling WLPs to produce RNA polymers. We have shown that these results are robust for different temperature regimes, and occur as a consequence of the natural degassing of volatiles from a newly formed Earth, or any terrestrial planet of similar composition.

It is remarkable how this rich combination of astrophysical, geochemical and atmospherical processes leads quite naturally to such an early appearance of biomolecules critical to the RNA world, on Earth.

6.2 Future Work

Moving forward with our new understanding of the early biogenic phase of the prebiotic planet, there are some experimental and theoretical studies that we intend to do to better understand the process of RNA building block production on biogenic worlds. Firstly, more experimental work needs to be done to demonstrate that plausible early Earth atmospheres can lead to the production of A) nucleobases, and B) ribose. Stanley Miller began this work in the 1950's, using atmospheric gases such as NH_3, H_2, CH_4 and H_2O to produce the building blocks of proteins [12]. Since then, a couple groups have demonstrated nucleobase synthesis from Miller-Urey experiments with atmospheres composed of NH_3 and CO, and H_2O [18, 19].

It is unlikely, given it's reactivity, that NH_3 will dominate the nitrogen component of planetary atmospheres in comparison to inert N_2. We have found that N_2 takes over as the dominant atmospheric component in all of our early Earth models on long timescales. With this knowledge in hand, we intend to perform Miller-Urey experiments with atmospheric compositions matcing our early Hadean models (i.e. N_2, H_2, CH_4, and H_2O), with the intent on demonstrating the process of nucleobase and ribose production on biogenic worlds.

These experiments may also help fill a gap in our understanding of how nucleotides form in aqueous solution. For example, 2-aminooxazole is a key intermediate in the Powner-Sutherland approach to nucleotide synthesis [42]. The results from this thesis suggest that 2-aminooxazole would be slightly more favourably produced than ribose during the early Hadean. However, no experimental study has compared the simultaneous yields of these two products from photolytic HCN-based aqueous chemistry. We intend to measure the abundances of both of theses species in Miller-Urey experiments in order to verify which of these molecules is a more likely intermediate to nucleotide synthesis.

On the theoretical side, one of the biggest improvements that can be made to our 1D atmospheric chemical kinetics models is to consistently calculate temperature profiles at each simulation time step. Our simulated pressure-temperature profiles for the early and late Hadean atmospheres suggest atmospheric composition and surface temperature are strongly dependent on one another. For example, factor of 2–8 changes to methane composition affect the surface temperature by ∼25°C. Moreover, our preliminary models suggest that H_2-H_2 collision-induced absorption provides the majority of the warming effects in our reducing atmospheric models. Tracking how the atmospheric temperature changes as a function of H_2 degassing from impacts would be a major advancement to chemical kinetics modeling, and could further improve the accuracy of the chemical results.

Bibliography

[1] Aristotle. *Book I 983b.* Perseus Project (cit. on p. 1).

[2] M. Morange. “What history tells us XIII. Fifty years of the Central Dogma”. In: *J. Biosci.* 33 (2008), pp. 171–175 (cit. on p. 1).

[3] D. Deamer. “Darwin’s prescient guess”. In: *Proc. Nat. Acad. Sci. U.S.A.* 114 (2017), pp. 11264–11265 (cit. on p. 2).

[4] C. Darwin. *To J. D. Hooker 1 February [1871].* Darwin Correspondence Project, 1871 (cit. on p. 2).

[5] A. I. Oparin. *The origin of life.* Moscow: Izd. Moskovshii Rabochii, 1924 (cit. on p. 2).

[6] J. B. S. Haldane. “The origin of life”. In: *Rationalist Annual.* 148 (1929), pp. 3–10 (cit. on p. 2).

[7] R. Shapiro. “The Oparin-Haldane Hypothesis”. In: *Origins: A Skeptic’s Guide to the Creation of Life on Earth.* Toronto: Bantam Books, 1987, pp. 109–111 (cit. on p. 2).

[8] A. Strecker. “Ueber einen neuen aus Aldehyd-Ammoniak und Blausäure entstehenden Körper”. In: *Liebigs Ann. Chem.* 91 (1854), pp. 349–351 (cit. on pp. 2, 142).

[9] A. Butlerow. “Bildung einer zuckerartigen Substanz durch Synthese”. In: *Ann. Chem. Pharm.* 120 (1861), pp. 295–298 (cit. on pp. 2, 4, 15, 142, 203).

[10] W. Löb. “Über das Verhalten des Formamids unter der Wirkung der stillen Entlandung. Ein Beitrag zur Frage der Stickstoff-Assimilation”. In: *Ber. Dtsch. Chem. Ges.* 46 (1913), pp. 684–697 (cit. on p. 2).

[11] H. J. Cleaves. “Prebiotic Chemistry: What We Know, What We Don’t”. In: *Evo. Edu. Outreach* 5 (2013), pp. 342–360 (cit. on p. 2).

[12] S. L. Miller. “A Production of Amino Acids Under Possible Primitive Earth Conditions”. In: *Science* 117 (1953), pp. 528–529 (cit. on pp. 2, 29, 188, 214, 234).

[13] H. J. Cleaves, J. H. Chalmers, A. Lazcano, S. L. Miller, and J. L. Bada. “A reassessment of prebiotic organic synthesis in neutral planetary atmospheres”. In: *Orig. Life Evol. Biosph.* 38 (2008), pp. 105–115 (cit. on pp. 2, 206).

[14] AG Schlesinger and S. L. Miller. “Prebiotic synthesis in atmospheres containing CH_4, CO, and CO_2”. In: *J. Mol. Evol.* 19 (1983), pp. 376–382 (cit. on pp. 2, 29, 188, 206).

[15] D. Ring, Y. Wolman, N. Friedman, and S. L. Miller. “Prebiotic synthesis of hydrophobic and protein amino acids”. In: *Proc. Nat. Acad. Sci. U.S.A.* 69 (1972), pp. 765–768 (cit. on p. 2).

[16] Y. Wolman, W. J. Haverland, and S. L. Miller. “Nonprotein amino acids from spark discharges and their comparison with the murchison meteorite amino acids”. In: *Proc. Nat. Acad. Sci. U.S.A.* 69 (1972), pp. 809–811 (cit. on p. 2).

[17] J. L. Bada. “New insights into prebiotic chemistry from Stanley Miller’s spark discharge experiments”. In: *Chem. Soc. Rev.* 42 (2013), pp. 2186–2196 (cit. on pp. 2, 4, 12, 34, 36, 189, 214).

[18] M. Ferus, F. Pietrucci, A. M. Saitta, A. Knížek, P. Kubelík, O. Ivanek, V. Shestivska, and S. Civiš. “Formation of nucleobases in a Miller–Urey reducing atmosphere”. In: *Proc. Nat. Acad. Sci. U.S.A.* 114 (2017), pp. 4306–4311 (cit. on pp. 2, 4, 36, 189, 214, 234).

[19] S. Miyakawa, H. Yamanashi, K. Kobayashi, H. J. Cleaves, and S. L. Miller. “Prebiotic synthesis from CO atmospheres: Implications for the origins of life”. In: *Proc. Nat. Acad. Sci. U.S.A.* 99 (2002), pp. 14628–14631 (cit. on pp. 2, 234).

[20] R. Hayatsu. “Orgueil Meteorite: Organic Nitrogen Contents”. In: *Science* 146 (1964-12), pp. 1291–1293 (cit. on p. 2).

[21] J. Raia. Thesis. University of Houston. 1966 (cit. on p. 2).

[22] K. Kvenvolden, J. Lawless, K. Pering, E. Peterson, J. Flores, C. Ponnamperuma, I. R. Kaplan, and C. B. Moore. “Evidence for Extraterrestrial Amino-acids and Hydrocarbons in the Murchison Meteorite”. In: *Nature* 228 (1970), pp. 923–926 (cit. on p. 2).

[23] E. Anders. “Pre-biotic organic matter from comets and asteroids”. In: *Nature* 342.6247 (1989-11), pp. 255–257 (cit. on p. 3).

[24] L. Mukhin, M. Gerasimov, and E. Safonova. “Origin of precursors of organic molecules during evaporation of meteorites and mafic terrestrial rocks”. In: *Nature* 340 (1989), pp. 46–48 (cit. on p. 3).

[25] C. Chyba and C. Sagan. “Endogenous production, exogenous delivery and impact-shock synthesis of organic molecules: an inventory for the origins of life”. In: *Nature* 355 (1992-01), pp. 125–132 (cit. on pp. 3, 11, 14, 188).

[26] S. Dagar, S. Sarkar, and S. Rajamani. “Geochemical influences on nonenzymatic oligomerization of prebiotically relevant cyclic nucleotides”. In: *RNA* 26 (2020), pp. 756–769 (cit. on pp. 3, 8, 189).

[27] L. Da Silva, M.-C. Maurel, and D. Deamer. “Salt-Promoted Synthesis of RNA-like Molecules in Simulated Hydrothermal Conditions”. In: *J. Mol. Evol.* 80 (2015), pp. 86–97 (cit. on pp. 3, 7, 8, 189, 227).

[28] V. DeGuzman, W. Vercoutere, H. Shenasa, and D. Deamer. “Generation of Oligonucleotides Under Hydrothermal Conditions by Non-enzymatic Polymerization”. In: *J. Mol. Evol.* 78 (2014), pp. 251–262 (cit. on pp. 3, 8, 189).

[29] S. Rajamani, A. Vlassov, S. Benner, A. Coombs, F. Olasagasti, and D. Deamer. “Lipid-assisted Synthesis of RNA-like Polymers from Mononucleotides”. In: *Orig. Life Evol. Biosph.* 38 (2008-02), pp. 57–74 (cit. on pp. 3, 8, 189).

[30] B. K. D. Pearce. MSc Thesis. McMaster University. 2017 (cit. on p. 3).

[31] B. K. D. Pearce, R. E. Pudritz, D. A. Semenov, and Th. Henning. “Origin of the RNA World: The Fate of Nucleobases in Warm Little Ponds”. In: *Proc. Nat. Acad. Sci. U.S.A.* 114 (2017), pp. 11327–11332 (cit. on pp. 3, 13, 14, 188, 189, 192, 196, 197, 200, 203, 204, 213, 217, 218, 226).

[32] E Pierazzo and C. F. Chyba. “Cometary Delivery of Biogenic Elements to Europa”. In: *Icarus* 157.1 (2002), pp. 120–127 (cit. on p. 3).

[33] R. Fall. “Chapter 2 - Biogenic Emissions of Volatile Organic Compounds from Higher Plants”. In: *Reactive Hydrocarbons in the Atmosphere.* Ed. by C. N. Hewitt. San Diego: Academic Press, 1999, pp. 41–96 (cit. on p. 3).

[34] S. L. Miller. “The Mechanism of Synthesis of Amino Acids by Electric Discharges”. In: *Biochim. Biophys. Acta.* 23 (1957), pp. 480–489 (cit. on pp. 4, 90, 189, 214).

[35] Clifford N. Matthews. “The HCN World”. In: *Origins: Genesis, Evolution and Diversity of Life.* Ed. by Joseph Seckbach. Dordrecht: Springer Netherlands, 2004, pp. 121–135 (cit. on p. 4).

[36] D. Catling and J. F. Kasting. “Planetary atmospheres and life”. In: *Planets and life - the emerging science of astrobiology.* Ed. by W. T. Sullivan, III and J. A. Baross. Cambridge: Cambridge University Press, 2007, pp. 91–116 (cit. on pp. 4, 12, 16, 24, 34, 36, 37, 54, 75, 90, 91, 143, 188).

[37] J. Oró and A. P. Kimball. “Synthesis of Purines under Possible Primitive Earth Conditions I. Adenine from Hydrogen Cyanide”. In: *Arch Biochem Biophys* 94 (1961), pp. 217–227 (cit. on pp. 4, 15, 217, 218).

[38] D. E. Larowe and P. Regnier. “Thermodynamic Potential for the Abiotic Synthesis of Adenine, Cytosine, Guanine, Thymine, Uracil, Ribose, and Deoxyribose in Hydrothermal Systems”. In: *Orig. Life Evol. Biosph.* 38 (2008-10), pp. 383–397 (cit. on pp. 4, 15, 34, 142, 203, 217–219).

[39] R. Yi, Q. P. Tran, S. Ali, I. Yoda, Z. R. Adam, H. J. Cleaves, and A. C. Fahrenbach. “A continuous reaction network that produces RNA precursors”. In: *Proc. Natl. Acad. Sci. U.S.A.* 117 (2020), pp. 13267–13274 (cit. on pp. 4, 8, 15, 189, 203, 204, 217–219).

[40] R. Breslow. “On the mechanism of the formose reaction”. In: *Tetrahedron Letts.* 1 (1959), pp. 22–26 (cit. on pp. 4, 15, 142, 203).

[41] D. J. Ritson, C. Battilocchio, S. V. Ley, and J. D. Sutherland. “Mimicking the surface and prebiotic chemistry of early Earth using flow chemistry”. In: *Nat. Commun.* 9 (2018), p. 1821 (cit. on pp. 4, 204).

[42] M. W. Powner, B. Gerland, and J. D. Sutherland. “Synthesis of activated pyrimidine ribonucleotides in prebiotically plausible conditions”. In: *Nature* 459 (2009-05), pp. 239–242 (cit. on pp. 4, 8, 15, 31, 189, 199, 204, 234).

[43] J. P. Pinto, G. R. Gladstone, and Y. L. Yung. "Photochemical Production of Formaldehyde in Earth's Primitive Atmosphere". In: *Science* 210 (1980), pp. 183–185 (cit. on pp. 4, 143, 203).

[44] B. K. D. Pearce, A. S. Tupper, R. E. Pudritz, and P. G. Higgs. "Constraining the Time Interval for the Origin of Life on Earth". In: *Astrobiology* 18 (2018-03), pp. 343–364 (cit. on pp. 5, 6, 188, 227).

[45] J. Monteux, D. Andrault, and H. Samuel. "On the cooling of a deep terrestrial magma ocean". In: *Earth Planet. Sci. Lett.* 448 (2016-08), pp. 140–149 (cit. on pp. 5, 226).

[46] T. Lebrun, H. Massol, E. ChassefièRe, A. Davaille, E. Marcq, P. Sarda, F. Leblanc, and G. Brandeis. "Thermal evolution of an early magma ocean in interaction with the atmosphere". In: *J. Geophys. Res. Planets* 118 (2013-06), pp. 1155–1176 (cit. on pp. 5, 226).

[47] K. Zahnle, N. Arndt, C. Cockell, A. Halliday, E. Nisbet, F. Selsis, and N. H. Sleep. "Emergence of a Habitable Planet". In: *Space Sci Rev* 129 (2007-03), pp. 35–78 (cit. on pp. 5, 161, 226).

[48] A. P. Nutman, V. C. Bennett, C. R. L. Friend, M. J. Van Kranendonk, and A. R. Chivas. "Rapid emergence of life shown by discovery of 3,700-million-year-old microbial structures". In: *Nature* 537 (2016-09), pp. 535–538 (cit. on p. 5).

[49] M. T. Rosing. "13C-Depleted Carbon Microparticles in >3700-Ma Sea-Floor Sedimentary Rocks from West Greenland". In: *Science* 283 (1999-01), p. 674 (cit. on p. 5).

[50] Y. Ohtomo, T. Kakegawa, A. Ishida, T. Nagase, and M. T. Rosing. "Evidence for biogenic graphite in early Archaean Isua metasedimentary rocks". In: *Nature Geosci* 7 (2014), pp. 25–28 (cit. on p. 5).

[51] B. Damer and D. W. Deamer. "The Hot Spring Hypothesis for an Origin of Life". In: *Astrobiology* 20 (2020), pp. 429–452 (cit. on pp. 6, 7, 9, 188, 199, 226, 227).

[52] B. Damer and D. W. Deamer. "Coupled Phases and Combinatorial Selection in Fluctuating Hydrothermal Pools: A Scenario to Guide Experimental Approaches to the Origin of Cellular Life". In: *Life* 5 (2015-03), pp. 872–887 (cit. on pp. 6, 34, 227).

[53] D. S. Ross and D. Deamer. “Dry/Wet Cycling and the Thermodynamics and Kinetics of Prebiotic Polymer Synthesis”. In: *Life* 6 (2016), p. 28 (cit. on pp. 7, 189, 227).

[54] W. Martin and M. J. Russell. “On the origin of biochemistry at an alkaline hydrothermal vent”. In: *Phil. Trans. R. Soc. Lond. B* 362 (2007), pp. 1887–1926 (cit. on p. 7).

[55] E. Smith and H. J. Morowitz. “Universality in intermediary metabolism”. In: *Proc. Nat. Acad. Sci. U.S.A.* 101 (2004), pp. 13168–13173 (cit. on pp. 7, 9).

[56] W. Martin and M. J. Russell. “On the origins of cells: a hypothesis for the evolutionary transitions from abiotic geochemistry to chemoautotrophic prokaryotes, and from prokaryotes to nucleated cells”. In: *Phil. Trans. R. Soc. Lond. B* 358 (2003), pp. 59–85 (cit. on pp. 7, 9).

[57] G. Wächtershäuser. “Before Enzymes and Templates: Theory of Surface Metabolism”. In: *Microbiol. Rev.* 4 (1988), pp. 452–484 (cit. on pp. 7, 9).

[58] W. Martin, J. Baross, D. Kelley, and M. J. Russell. “Hydrothermal vents and the origin of life”. In: *Nat Rev Microbiol* 6 (2008), pp. 805–814 (cit. on p. 7).

[59] K. F. Tjhung, M. N. Shokhirev, D. P. Horning, and G. F. Joyce. “An RNA polymerase ribozyme that synthesizes its own ancestor”. In: *Proc. Nat. Acad. Sci. U.S.A.* 117 (2020), pp. 2906–2913 (cit. on pp. 8, 9, 228).

[60] T. A. Lincoln and G. F. Joyce. “Self-Sustained Replication of an RNA Enzyme”. In: *Science* 323 (2009), pp. 1229–1232 (cit. on pp. 8, 9, 228).

[61] J. Attwater, A. Wochner, and P. Holliger. “In-ice evolution of RNA polymerase ribozyme activity”. In: *Nat Chem* 5 (2013), pp. 1011–1018 (cit. on pp. 8, 9, 228).

[62] J. Rogers and G. F. Joyce. “A ribozyme that lacks cytidine”. In: *Nature* 402 (1999), pp. 323–325 (cit. on pp. 8, 9, 228).

[63] I. Nam, J. K. Lee, H. G. Nam, and R. N. Zare. “Abiotic production of sugar phosphates and uridine ribonucleoside in aqueous microdroplets”. In: *Proc. Nat. Acad. Sci. U.S.A.* 114 (2017), pp. 12396–12400 (cit. on p. 8).

[64] I. Nam, H. G. Nam, and R. N. Zare. “Abiotic synthesis of purine and pyrimidine ribonucleosides in aqueous microdroplets”. In: *Proc. Nat. Acad. Sci. U.S.A.* 115 (2018), pp. 36–40 (cit. on pp. 8, 199).

[65] C. Ponnamperuma, C. Sagan, and R. Mariner. “Synthesis of Adenosine Triphosphate Under Possible Primitive Earth Conditions”. In: *Nature* 199 (1963-07), pp. 222–226 (cit. on pp. 8, 189, 199).

[66] S. Becker, J. Feldmann, S. Wiedemann, H. Okamura, C. Schneider, K. Iwan, A. Crisp, M. Rossa, T. Amatov, and T. Carell. “Unified prebiotically plausible synthesis of pyrimidine and purine RNA ribonucleotides”. In: *Science* 366 (2019), pp. 76–82 (cit. on p. 8).

[67] J. S. Teichert, F. M. Kruse, and O. Trapp. “Direct Prebiotic Pathway to DNA Nucleosides”. In: *Angew. Chem. Int. Ed. Engl.* 58 (2019), pp. 9944–9947 (cit. on p. 8).

[68] N. Lane. “Proton gradients at the origin of life”. In: *Bioessays* 39 (2017), p. 1600217 (cit. on p. 9).

[69] Rogier Braakman. “Mapping metabolism onto the prebiotic organic chemistry of hydrothermal vents”. In: *Proc. Nat. Acad. Sci. U.S.A.* 110.33 (2013), pp. 13236–13237 (cit. on p. 9).

[70] K. R. Popper. *Conjectures and Refutations: The Growth of Scientific Knowledge.* London, U.K.: Routledge, 1963 (cit. on p. 9).

[71] D. Deamer. “Conjecture and hypothesis: The importance of reality checks”. In: *Beilstein J. Org. Chem.* 13 (2017), pp. 620–624 (cit. on p. 9).

[72] J. P. Ferris. “Montmorillonite-catalysed formation of RNA oligomers: the possible role of catalysis in the origins of life”. In: *Philos. Trans. R. Soc. Lond. B Biol. Sci.* 361 (2006), pp. 1777–1786 (cit. on p. 9).

[73] H. Ogasawara, A. Yoshida, E. Imai, H. Honda, K. Hatori, and K. Matsuno. “Synthesizing oligomers from monomeric nucleotides in simulated hydrothermal environments”. In: *Orig. Life Evol. Biosph.* 30 (2000), pp. 519–526 (cit. on p. 9).

[74] B. T. Burcar, L. M. Barge, D. Trail, E. B. Watson, M. J. Russell, and L. B. McGown. “RNA Oligomerization in Laboratory Analogues of Alkaline Hydrothermal Vent Systems”. In: *Astrobiology* 15 (2015-07), pp. 509–522. DOI: `10.1089/ast.2014.1280` (cit. on p. 9).

[75] A. Rich. "On the problems of evolution and biochemical information transfer". In: *Horizons In Biochemistry.* Ed. by M. Kasha and B. Pullman. New York: Academic Press, 1962, pp. 103–126 (cit. on p. 9).

[76] W. Gilbert. "Origin of life: The RNA world". In: *Nature* 319 (1986-02), p. 618 (cit. on pp. 9, 188).

[77] C. Woese. "The genetic code". In: New York: Harper and Row, 1967, p. 179 (cit. on p. 9).

[78] F. H. C. Crick. "The Origin of the Genetic Code". In: *J. Mol. Biol.* 38 (1968), p. 367 (cit. on pp. 9, 188).

[79] F. H. C. Orgel. "Evolution of the genetic apparatus". In: *J. Mol. Biol.* 38 (1968), p. 381 (cit. on pp. 9, 188).

[80] J. P. Dworkin, A. Lazcano, and S. L. Miller. "The roads to and from the RNA world". In: *J. Theor. Biol.* 222 (2003), pp. 127–134 (cit. on p. 9).

[81] S. Fisher. "Are RNA Viruses Vestiges of an RNA World?" In: *J. Gen. Philos. Sci.* 41 (2010), pp. 121–141 (cit. on p. 10).

[82] Lumen Learning. *Structure and Function of RNA.* 2020-05. URL: `https://courses.lumenlearning.com/microbiology/chapter/structure-and-function-of-rna/` (cit. on p. 11).

[83] E. I. Jiménez, C. Gibard, and R. Krishnamurthy. "Prebiotic Phosphorylation and Concomitant Oligomerization of Deoxynucleosides to form DNA". In: *Angew. Chem. Int. Ed. Engl.* 60 (2020), pp. 10775–10783 (cit. on p. 10).

[84] Oró J. and E. Stephen-Sherwood. "The Prebiotic Synthesis of Oligonucleotides". In: *Cosmochemical Evolution and the Origins of Life.* Ed. by J. Oró, S. L. Miller, C. Ponnamperuma, and R. S. Young. Dordrecht: Springer, 1974 (cit. on p. 10).

[85] S. L. Miller. "The Formation of Organic Compounds on the Primitive Earth". In: *Ann. N. Y. Acad. Sci.* 69 (1957), pp. 260–275 (cit. on pp. 12, 15, 34, 188).

[86] L. M. V. Martel. *Better Know a Meteorite Collection: Natural History Museum, London, United Kingdom.* 2009-07. URL: `http://www.psrd.hawaii.edu/July09/Meteorites.London.Museum.html` (cit. on p. 12).

[87] M. Richmond. *The Interstellar Medium: Dust.* 2017-06. URL: `http://www.star.ucl.ac.uk/~msw/teaching/PHAS2521/ism_dust_files/ism_dust.html` (cit. on p. 12).

[88] M. P. Callahan, K. E. Smith, H. J. Cleaves, J. Ruzicka, J. C. Stern, D. P. Glavin, C. H. House, and J. P. Dworkin. “Carbonaceous meteorites contain a wide range of extraterrestrial nucleobases”. In: *Proc. Natl. Acad. Sci. U.S.A.* 108 (2011-08), pp. 13995–13998 (cit. on pp. 12, 198, 226, 233).

[89] B. K. D. Pearce and R. E. Pudritz. “Seeding the Pregenetic Earth: Meteoritic Abundances of Nucleobases and Potential Reaction Pathways”. In: *Astrophys. J.* 807 (2015-07), p. 85 (cit. on pp. 12, 34, 36, 198, 226).

[90] D. P. Glavin, J. P. Dworkin, A. Aubrey, O. Botta, J. H. Doty, Z. Martins, and J. L. Bada. “Amino acid analyses of Antarctic CM2 meteorites using liquid chromatography-time of flight-mass spectrometry”. In: *Meteorit Planet Sci* 41 (2006-06), pp. 889–902 (cit. on p. 12).

[91] A. K. Cobb and R. E. Pudritz. “Nature’s Starships. I. Observed Abundances and Relative Frequencies of Amino Acids in Meteorites”. In: *Astrophys. J.* 783, 140 (2014-03), p. 140 (cit. on pp. 12, 34).

[92] Yoshihiro Furukawa, Yoshito Chikaraishi, Naohiko Ohkouchi, Nanako O. Ogawa, Daniel P. Glavin, Jason P. Dworkin, Chiaki Abe, and Tomoki Nakamura. “Extraterrestrial ribose and other sugars in primitive meteorites”. In: *Proc. Nat. Acad. Sci. U.S.A.* 116.49 (2019), pp. 24440–24445 (cit. on pp. 12, 226).

[93] G. Cooper, N. Kimmich, W. Belisle, J. Sarinana, K. Brabham, and L. Garrel. “Carbonaceous meteorites as a source of sugar-related organic compounds for the early Earth”. In: *Nature* 414 (2001-12), pp. 879–883 (cit. on p. 12).

[94] R. W. Hilts, C. D. K. Herd, D. N. Simkus, and G. F. Slater. “Soluble organic compounds in the Tagish Lake meteorite”. In: *Meteorit Planet Sci* 49 (2014-04), pp. 526–549 (cit. on p. 12).

[95] James C.-Y. Lai, Ben K. D. Pearce, Ralph E. Pudritz, and Drake Lee. “Meteoritic abundances of fatty acids and potential reaction pathways in planetesimals”. In: *Icarus* 319 (2019), pp. 685–700 (cit. on p. 12).

[96] B. K. D. Pearce. Undergraduate Thesis. University of British Columbia. 2015 (cit. on p. 13).

[97] B. K. D. Pearce and R. E. Pudritz. “Meteorites and the RNA World: A Thermodynamic Model of Nucleobase Synthesis within Planetesimals”. In: *Astrobiology* 16 (2016-11), pp. 853–872 (cit. on pp. 13, 198).

[98] Thomas Stephan, Elmar K. Jessberger, Wolfgang Klöck, Harald Rulle, and Joachim Zehnpfenning. “TOF-SIMS analysis of interplanetary dust”. In: *Earth Planet. Sci. Lett.* 128.3 (1994), pp. 453–467 (cit. on p. 13).

[99] M. Nuevo, C. K. Materese, and S. A. Sandford. “The Photochemistry of Pyrimidine in Realistic Astrophysical Ices and the Production of Nucleobases”. In: *Astrophys. J.* 793, 125 (2014-10), p. 125 (cit. on p. 13).

[100] C. K. Materese, M. Nuevo, and S. A. Sandford. “The Formation of Nucleobases from the Ultraviolet Photoirradiation of Purine in Simple Astrophysical Ice Analogues”. In: *Astrobiology* 17 (2017), pp. 761–770 (cit. on p. 13).

[101] C. Meinert, I. Myrgorodska, P. de Marcellus, T. Buhse, L. Nahon, S. V. Hoffmann, L. L. S. d’Hendecourt, and U. J. Meierhenrich. “Ribose and related sugars from ultraviolet irradiation of interstellar ice analogs”. In: *Science* 352 (2016-04), pp. 208–212 (cit. on p. 13).

[102] G. G. Managadze, W. B. Brinckerhoff, and A. E. Chumikov. “Molecular synthesis in hypervelocity impact plasmas on the primitive Earth and in interstellar clouds”. In: *Geophys. Res. Lett.* 30 (2003), p. 1247 (cit. on p. 14).

[103] A. Bar-Nun, N. Bar-Nun, S. H. Bauer, and C. Sagan. “Shock Synthesis of Amino Acids in Simulated Primitive Environments”. In: *Science* 168 (1970), pp. 470–473 (cit. on p. 14).

[104] Z. Martins, M. C. Price, N. Goldman, M. A. Sephton, and M. J. Burchell. “Shock synthesis of amino acids from impacting cometary and icy planet surface analogues”. In: *Nat. Geosci.* 6 (2013-12), pp. 1045–1049 (cit. on pp. 14, 36).

[105] M. Ferus, R. Michalčíková, V. Shestivská, J. Sponer, J. E. Sponer, and S. Civiš. “High-Energy Chemistry of Formamide: A Simpler Way for Nucleobase Formation”. In: *J. Phys. Chem. A* 118 (2014), pp. 719–736 (cit. on p. 14).

[106] M. Ferus, F. Pietrucci, A. M. Saitta, O. Ivanek, A. Knizek, P. Kubelík, M. Krus, L. Juha, R. Dudzak, J. Dostál, A. Pastorek, L. Petera, J. Hrncirova, H. Saeidfirozeh, V. Shestivská, J. Sponer, J. E. Sponer, P. Rimmer, S. Civiš, and G. Cassone. “Prebiotic synthesis initiated in formaldehyde by laser plasma

simulating high-velocity impacts". In: *Astron. Astrophys.* 626 (2019-06), A52 (cit. on pp. 14, 142, 203).

[107] F. Tian, J. F. Kasting, and K. Zahnle. "Revisiting HCN formation in Earth's early atmosphere". In: *Earth Planet. Sci. Lett.* 308 (2011-08), pp. 417–423 (cit. on pp. 15, 16, 27, 34, 45, 143, 189, 190, 201, 204, 211, 212, 216, 217).

[108] S. M. Hörst. "Titan's atmosphere and climate". In: *J. Geophys. Res. Planets* 122 (2017-03), pp. 432–482 (cit. on pp. 15, 45, 90, 91, 196).

[109] B. A. Magee, J. H. Waite, K. E. Mandt, J. Westlake, J. Bell, and D. A. Gell. "INMS-derived composition of Titan's upper atmosphere: Analysis methods and model comparison". In: *Planet. Space Sci.* 57 (2009-12), pp. 1895–1916 (cit. on pp. 15, 91, 192, 196).

[110] S. Vinatier, B. Bézard, C. A. Nixon, A. Mamoutkine, R. C. Carlson, D. E. Jennings, E. A. Guandique, N. A. Teanby, G. L. Bjoraker, F. Michael Flasar, and et al. "Analysis of Cassini/CIRS limb spectra of Titan acquired during the nominal mission. I. Hydrocarbons, nitriles and CO_2 vertical mixing ratio profiles". In: *Icarus* 205 (2010-02), pp. 559–570 (cit. on pp. 15, 34, 91, 109, 192, 196).

[111] A. Adriani, B. M. Dinelli, M. López-Puertas, M. García-Comas, M. L. Moriconi, E. D'Aversa, B. Funke, and A. Coradini. "Distribution of HCN in Titan's upper atmosphere from Cassini/VIMS observations at 3 μm". In: *Icarus* 214 (2011-08), pp. 584–595 (cit. on pp. 15, 34, 91, 192, 196).

[112] T. T. Koskinen, R. V. Yelle, D. S. Snowden, P. Lavvas, B. R. Sandel, F. J. Capalbo, Y. Benilan, and R. A. West. "The mesosphere and lower thermosphere of Titan revealed by Cassini/UVIS stellar occultations". In: *Icarus* 216 (2011-12), pp. 507–534 (cit. on pp. 15, 91, 192, 196).

[113] S. A. Stern et al. "The Pluto system: Initial results from its exploration by New Horizons". In: *Science* 350.6258 (2015) (cit. on p. 15).

[114] E. Lellouch, M. Gurwell, B. Butler, T. Fouchet, P. Lavvas, D. F. Strobel, B. Sicardy, A. Moullet, R. Moreno, D. Bockelée-Morvan, N. Biver, L. Young, D. Lis, J. Stansberry, A. Stern, H. Weaver, E. Young, X. Zhu, and J. Boissier. "Detection of CO and HCN in Pluto's atmosphere with ALMA". In: *Icarus* 286 (2017-04), pp. 289–307 (cit. on pp. 15, 91).

[115] Kevin H. Baines and W.M.Hayden Smith. “The atmospheric structure and dynamical properties of Neptune derived from ground-based and IUE spectrophotometry”. In: *Icarus* 85.1 (1990), pp. 65–108 (cit. on p. 15).

[116] Erich Karkoschka and Martin Tomasko. “The haze and methane distributions on Uranus from HST-STIS spectroscopy”. In: *Icarus* 202.1 (2009), pp. 287–309 (cit. on p. 15).

[117] A. Marten, D. Gautier, T. Owen, D. B. Sanders, H. E. Matthews, S. K. Atreya, R. P. J. Tilanus, and J. R. Deane. “First Observations of CO and HCN on Neptune and Uranus at Millimeter Wavelengths and Their Implications for Atmospheric Chemistry”. In: *Astrophys. J.* 406 (1993-03), p. 285 (cit. on pp. 16, 91).

[118] C. R. Webster, P. R. Mahaffy, S. K. Atreya, J. E. Moores, G. J. Flesch, C. Malespin, C. P. McKay, G. Martinez, C. L. Smith, J. Martin-Torres, J. Gomez-Elvira, M.-P. Zorzano, M. H. Wong, M. G. Trainer, A. Steele, D. Archer, B. Sutter, P. J. Coll, C. Freissinet, P.-Y. Meslin, R. V. Gough, C. H. House, A. Pavlov, J. L. Eigenbrode, D. P. Glavin, J. C. Pearson, D. Keymeulen, L. E. Christensen, S. P. Schwenzer, R. Navarro-Gonzalez, J. Pla-García, S. C. R. Rafkin, Á. Vicente-Retortillo, H. Kahanpää, D. Viudez-Moreiras, M. D. Smith, A.-M. Harri, M. Genzer, D. M. Hassler, M. Lemmon, J. Crisp, S. P. Sander, R. W. Zurek, and A. R. Vasavada. “Background levels of methane in Mars’ atmosphere show strong seasonal variations”. In: *Science* 360.6393 (2018), pp. 1093–1096 (cit. on p. 16).

[119] E. Gillen, P. B. Rimmer, and D. C. Catling. “Statistical analysis of Curiosity data shows no evidence for a strong seasonal cycle of martian methane”. In: *Icarus* 336, 113407 (2020-01), p. 113407 (cit. on p. 16).

[120] O. Korablev, A. C. Vandaele, F. Montmessin, A. A. Fedorova, A. Trokhimovskiy, F. Forget, F. Lefèvre, F. Daerden, I. R. Thomas, L. Trompet, J. T. Erwin, S. Aoki, S. Robert, L. Neary, S. Viscardy, A. V. Grigoriev, N. I. Ignatiev, A. Shakun, A. Patrakeev, D. A. Belyaev, J.-L. Bertaux, K. S. Olsen, L. Baggio, J. Alday, Y. S. Ivanov, B. Ristic, J. Mason, Y. Willame, C. Depiesse, L. Hetey, S. Berkenbosch, R. Clairquin, C. Queirolo, B. Beeckman, E. Neefs, M. R. Patel, G. Bellucci, J.-J. López-Moreno, C. F. Wilson, G. Etiope, L. Zelenyi, H. Svedhem, J. L. Vago, Acs, and NOMAD Science Teams. “No detection of methane on

Mars from early ExoMars Trace Gas Orbiter observations". In: *Nature* 568 (2019), pp. 517–520 (cit. on p. 16).

[121] J. C. Stern, B. Sutter, C. Freissinet, R. Navarro-González, C. P. McKay, P. D. Archer, A. Buch, A. E. Brunner, P. Coll, J. L. Eigenbrode, A. G. Fairen, H. B. Franz, D. P. Glavin, S. Kashyap, A. C. McAdam, D. W. Ming, A. Steele, C. Szopa, J. J. Wray, F. J. Martín-Torres, M.-P. Zorzano, P. G. Conrad, P. R. Mahaffy, and et al. "Evidence for indigenous nitrogen in sedimentary and aeolian deposits from the Curiosity rover investigations at Gale crater, Mars". In: *Proc. Nat. Acad. Sci. U.S.A.* 112.14 (2015), pp. 4245–4250 (cit. on p. 16).

[122] A. Tsiaras, M. Rocchetto, I. P. Waldmann, O. Venot, R. Varley, G. Morello, M. Damiano, G. Tinetti, E. J. Barton, S. N. Yurchenko, and J. Tennyson. "Detection of an Atmosphere Around the Super-Earth 55 Cancri e". In: *Astrophys. J.* 820, 99 (2016-04), p. 99 (cit. on pp. 16, 91).

[123] R. J. MacDonald and N. Madhusudhan. "Signatures of Nitrogen Chemistry in Hot Jupiter Atmospheres". In: *Astrophys. J.* 850.1 (2017-11), p. L15 (cit. on pp. 16, 91).

[124] P. B. Rimmer and S. Rugheimer. "Hydrogen cyanide in nitrogen-rich atmospheres of rocky exoplanets". In: *Icarus* 329 (2019-09), pp. 124–131 (cit. on pp. 16, 91, 196, 206).

[125] K. J. Zahnle. "Photochemistry of Methane and the Formation of Hydrocyanic Acid (HCN) in the Earth's Early Atmosphere". In: *J. Geophys. Res.* 91 (1986), pp. 2819–2834 (cit. on pp. 16, 34, 143, 189, 190, 201, 204, 211, 212, 216).

[126] J. C. Loison, E. Hébrard, M. Dobrijevic, K. M. Hickson, F. Caralp, V. Hue, G. Gronoff, O. Venot, and Y. Bénilan. "The neutral photochemistry of nitriles, amines and imines in the atmosphere of Titan". In: *Icarus* 247 (2015-02), pp. 218–247 (cit. on pp. 16, 34, 91, 94, 101, 108, 109, 111, 112).

[127] Venot, O., Hébrard, E., Agúndez, M., Dobrijevic, M., Selsis, F., Hersant, F., Iro, N., and Bounaceur, R. "A chemical model for the atmosphere of hot Jupiters". In: *Astron. Astrophys.* 546 (2012), A43 (cit. on pp. 16, 101).

[128] Ellis R. Lippincott, Richard V. Eck, Margaret O. Dayhoff, and Carl Sagan. "Thermodynamic Equilibria in Planetary Atmospheres". In: *Astrophys. J.* 147 (1967-02), p. 753 (cit. on p. 16).

[129] K. J. Zahnle, R. Lupu, D. C. Catling, and N. Wogan. “Creation and Evolution of Impact-generated Reduced Atmospheres of Early Earth”. In: *Planet. Sci. J.* 1 (2020), p. 11 (cit. on pp. 16, 26–28, 189, 190, 192, 201, 205, 206, 213).

[130] V. Vuitton, R. V. Yelle, S. J. Klippenstein, S. M. Hörst, and P. Lavvas. “Simulating the density of organic species in the atmosphere of Titan with a coupled ion-neutral photochemical model”. In: *Icarus* 324 (2019-05), pp. 120–197 (cit. on pp. 16, 26, 91, 92, 94, 101, 108, 109, 111, 112).

[131] K. Willacy, M. Allen, and Y. Yung. “A New Astrobiological Model of the Atmosphere of Titan”. In: *Astrophys. J.* 829.2 (2016-10), p. 79 (cit. on pp. 16, 91, 94, 101, 108–112).

[132] Cheng Li, Xi Zhang, Joshua A. Kammer, Mao-Chang Liang, Run-Lie Shia, and Yuk L. Yung. “A non-monotonic eddy diffusivity profile of Titan’s atmosphere revealed by Cassini observations”. In: *Planet. Space Sci.* 104 (2014-12), pp. 48–58 (cit. on pp. 16, 91, 109, 110).

[133] E. Hébrard, M. Dobrijevic, J. C. Loison, A. Bergeat, and K. M. Hickson. “Neutral production of hydrogen isocyanide (HNC) and hydrogen cyanide (HCN) in Titan’s upper atmosphere”. In: *Astron. Astrophys.* 541, A21 (2012-05), A21 (cit. on pp. 16, 25, 27, 34, 91, 101, 212).

[134] D. K. Maity, W. T. Duncan, and T. N. Truong. “Direct ab Initio Dynamics Studies of the Hydrogen Abstraction Reactions of Hydrogen Atom with Fluoromethanes”. In: *J. Phys. Chem. A* 103 (1999), pp. 2152–2159 (cit. on pp. 17, 41, 58, 60).

[135] M. Akbar Ali and J. R. Barker. “Comparison of Three Isoelectronic Multiple-Well Reaction Systems: $OH + CH_2O$, $OH + CH_2CH_2$, and $OH + CH_2NH$”. In: *J. Phys. Chem. A* 119 (2015), pp. 7578–7592 (cit. on pp. 17, 99, 152).

[136] T. N. Truong. “A direct ab initio dynamics approach for calculating thermal rate constants using variational transition state theory and multidimensional semiclassical tunneling methods. An application to the $CH_4 + H \longleftrightarrow CH_3 + H_2$ reaction”. In: *J. Chem. Phys.* 100 (1994), pp. 8014–8025 (cit. on pp. 17, 58–60).

[137] D. L. Baulch, C. J. Cobos, R. A. Cox, C. Esser, P. Frank, Th. Just, J. A. Kerr, M. J. Pilling, J. Troe, R. W. Walker, and et al. "Evaluated kinetic data for combustion modelling". In: *J. Phys. Chem. Ref. Data* 21 (1992), pp. 411–429 (cit. on pp. 17, 46, 56, 57, 60, 62, 72, 74, 78, 95, 103, 127–133, 135, 148, 153, 155, 158, 165–174, 177, 179, 184, 208, 209, 230).

[138] Yserentant H. "The Electronic Schrödinger Equation". In: *Regularity and Approximability of Electronic Wave Functions. Lecture Notes in Mathematics, vol 2000.* Berlin, Heidelberg: Springer, 2010 (cit. on p. 18).

[139] P. Hohenberg and W. Kohn. "Inhomogeneous Electron Gas". In: *Phys. Rev.* 136 (3B 1964-11), B864–B871 (cit. on p. 19).

[140] W. Kohn and L. J. Sham. "Self-Consistent Equations Including Exchange and Correlation Effects". In: *Phys. Rev.* 140 (4A 1965-11), A1133–A1138 (cit. on p. 19).

[141] A. D. Becke. "Perspective: Fifty years of density-functional theory in chemical physics". In: *J. Chem. Phys.* 140 (2014), 18A301 (cit. on p. 19).

[142] K. Capelle. "A Bird's-Eye View of Density-Functional Theory". In: *Braz. J. Phys.* 36 (2006), pp. 1318–1343 (cit. on p. 19).

[143] L. Noodleman, T. Lovell, W.-G. Han, T. Liu, R.A. Torres, and F. Himo. "2.39 - Density Functional Theory". In: *Comprehensive Coordination Chemistry II.* Ed. by Jon A. McCleverty and Thomas J. Meyer. Oxford: Pergamon, 2003, pp. 491–510 (cit. on p. 19).

[144] I. Y. Zhang and A. Grüneis. "Coupled Cluster Theory in Materials Science". In: *Front. Mater.* 6 (2019), p. 123 (cit. on pp. 19, 96).

[145] Z. Ul-Haq. *Introduction to Geometry Optimization.* 2016-05. URL: `https://th.fhi-berlin.mpg.de/sitesub/meetings/DFT-workshop-2016/uploads/Meeting/May_6_Qasmi.pdf` (cit. on p. 20).

[146] D. G. Truhlar. "Generalized Transition State Theory". In: *Theory of Chemical Reaction Dynamics.* Ed. by M. Baer. Boca Raton, FL: CRC Press, 1985, pp. 65–137 (cit. on pp. 20, 41, 42, 96, 97, 149, 150).

[147] D. G. Truhlar and B. C. Garrett. "Variational Transition-State Theory". In: *Acc. Chem. Res.* 13 (1980), pp. 440–448 (cit. on pp. 20, 42, 97, 150).

[148] Avogadro: an open-source molecular builder and visualization tool. Version 1.2.0. http://avogadro.cc/ (cit. on pp. 21, 148).

[149] H. Eyring. “The Activated Complex in Chemical Reactions”. In: *J. Chem. Phys.* 3 (1935), p. 107 (cit. on pp. 20, 41, 97, 150).

[150] M. G. Evans and M. Polanyi. “Some applications of the transition state method to the calculation of reaction velocities, especially in solution”. In: *Trans. Faraday Soc.* 31 (1935), pp. 875–894 (cit. on p. 20).

[151] W. Forst. *Unimolecular Reactions: A Concise Introduction.* Cambridge, U.K.: Cambridge University Press, 2003 (cit. on pp. 22, 92, 96, 144).

[152] Raymond T. Pierrehumbert. *Principles of Planetary Climate.* Cambridge, U.K.: Cambridge University Press, 2010 (cit. on pp. 22, 23).

[153] H. Keller-Rudek, G. K. Moortgat, R. Sander, and R. Sörensen. “The MPI-Mainz UV/VIS spectral atlas of gaseous molecules of atmospheric interest”. In: *Earth Syst. Sci. Data* 5 (2013), pp. 365–373 (cit. on p. 24).

[154] H. Sato. “Photodissociation of Simple Molecules in the Gas Phase”. In: *Chem. Rev.* 101 (2014), pp. 2687–2726 (cit. on p. 24).

[155] S. L. Guberman. “The vibrational dependence of dissociativerecombination: Rate constants for N_2^+”. In: *J. Chem. Phys.* 141 (2014), p. 204307 (cit. on p. 24).

[156] G. Gronoff, J. Lilensten, L. Desorgher, and E. Flückiger. “Ionization processes in the atmosphere of Titan. I. Ionization in the whole atmosphere”. In: *Astron. Astrophys.* 506.2 (2009-11), pp. 955–964 (cit. on pp. 24, 25, 91, 102).

[157] G. Gronoff, C. Mertens, J. Lilensten, L. Desorgher, E. Flückiger, and P. Velinov. “Ionization processes in the atmosphere of Titan. III. Ionization by high-Z nuclei cosmic rays”. In: *Astron. Astrophys.* 529, A143 (2011-05), A143 (cit. on pp. 24, 25, 91, 102).

[158] R. E Orville. “A High-Speed Time-Resolved Spectroscopic Study of the Lightning Return Stroke: Part II. A Quantitative Analysis”. In: *J. Atmos. Sci.* 25 (1968), pp. 839–851 (cit. on pp. 25, 215).

[159] A. Ardaseva, P. B. Rimmer, I. Waldmann, M. Rocchetto, S. N. Yurchenko, C. Helling, and J. Tennyson. “Lightning chemistry on Earth-like exoplanets”. In: *Mon. Not. R. Astron. Soc.* 470 (2017), pp. 187–196 (cit. on pp. 25, 214).

[160] W. H. Brune, P. J. McFarland, E. Bruning, S. Waugh, D. MacGorman, D. O. Miller, J. M. Jenkins, X. Ren, J. Mao, and J. Peischl. "Extreme oxidant amounts produced by lightning in storm clouds". In: *Science* 372.6543 (2021), pp. 711–715 (cit. on p. 25).

[161] W. L. Chameides and J. C. G. Walker. "Rates of fixation by lightning of carbon and nitrogen in possible primitive atmospheres". In: *Orig. Life* 11.4 (1981), pp. 291–302 (cit. on pp. 25, 201, 215, 216).

[162] R. D. Hill, R. G. Rinker, and H. D. Wilson. "Atmospheric Nitrogen Fixation by Lightning". In: *J. Atmos. Sci.* 37 (1980), pp. 179–192 (cit. on pp. 25, 202, 215).

[163] G. Hodosán, Ch. Helling, R. Asensio-Torres, I. Vorgul, and P. B. Rimmer. "Lightning climatology of exoplanets and brown dwarfs guidedby Solar system data". In: *Mon. Not. R. Astron. Soc.* 461 (2016), pp. 3927–3947 (cit. on pp. 25, 195, 214, 223).

[164] R. Hu, S. Seager, and W. Bains. "Photochemistry in Terrestrial Exoplanet Atmospheres I: Photochemistry Model and Benchmark Cases". In: *Astrophys. J.* 761 (2012), p. 2 (cit. on pp. 25, 27, 192, 210, 212, 214, 216, 217).

[165] K. J. Zahnle, M. Gacesa, and D. C. Catling. "Strange messenger: A new history of hydrogen on Earth, as told by Xenon". In: *Geochim. Cosmochim. Acta* 244 (2019), pp. 56–85 (cit. on pp. 26, 27, 213).

[166] D. C. Catling and K. J. Zahnle. "The Planetary Air Leak". In: *Sci. Am.* 300 (2009), pp. 36–43 (cit. on p. 26).

[167] C. E. Harman, E. W. Schwieterman, J. C. Schottelkotte, and J. F. Kasting. "Abiotic O_2 Levels on Planets around F, G, K, and M Stars: Possible False Positives for Life?" In: *Astrophys. J.* 812.2, 137 (2015-10), p. 137 (cit. on p. 27).

[168] R. Sander. *Henry's Law Constants.* Ed. by P. J. Linstrom and W. G. Mallard. Gaithersburg MD, 20899: National Institute of Standards and Technology, 2020. URL: `https://doi.org/10.18434/T4D303` (cit. on pp. 27, 216).

[169] Lyassine Allou, Lahcen El Maimouni, and Stéphane Le Calvé. "Henry's law constant measurements for formaldehyde and benzaldehyde as a function of temperature and water composition". In: *Atmos. Environ.* 45.17 (2011), pp. 2991–2998 (cit. on p. 27).

[170] D. Trail, E. B. Watson, and N. D. Tailby. “The oxidation state of Hadean magmas and implications for early Earth’s atmosphere”. In: *Nature* 480 (2011), pp. 79–82 (cit. on pp. 28, 143, 189).

[171] S. Aulbach and V. Stagno. “Evidence for a reducing Archean ambient mantle and its effects on the carbon cycle”. In: *Geology* 44.9 (2016-09), pp. 751–754 (cit. on p. 28).

[172] R. W. Nicklas, I. S. Puchtel, R. D. Ash, P. M. Piccoli, E. Hanski, E. G. Nisbet, P. Waterton, D. G. Pearson, and A. D. Anbar. “Secular mantle oxidation across the Archean-Proterozoic boundary: Evidence from V partitioning in komatiites and picrites”. In: *Geochim. Cosmochim. Acta* 250 (2019-04), pp. 49–75 (cit. on p. 28).

[173] C. -L. Chou. “Fractionation of Siderophile Elements in the Earth’s Upper Mantle”. In: *Lunar and Planetary Science Conference.* Vol. 1. Lunar and Planetary Science Conference. 1978-01, pp. 219–230 (cit. on p. 28).

[174] H. Genda, R. Brasser, and S. J. Mojzsis. “The terrestrial late veneer from core disruption of a lunar-sized impactor”. In: *Earth Planet. Sci. Lett.* 480 (2017), pp. 25–32 (cit. on p. 28).

[175] Steven A. Benner, Elizabeth A. Bell, Elisa Biondi, Ramon Brasser, Thomas Carell, Hyo-Joong Kim, Stephen J. Mojzsis, Arthur Omran, Matthew A. Pasek, and Dustin Trail. “When did Life Likely Emerge on Earth in an RNA-First Process?” In: *ChemSystemsChem* 2 (2020), e1900035 (cit. on pp. 28, 188).

[176] N. H. Sleep. “The Hadean-Archaean environment”. In: *Cold Spring Harbor Perspect. Biol.* 2 (2010-05), a002527 (cit. on pp. 28, 211).

[177] R. Wordsworth and R. Pierrehumbert. “Hydrogen-nitrogen greenhouse warming in Earth’s early atmosphere”. In: *Science* 339 (2013), pp. 64–67 (cit. on pp. 28, 229).

[178] James F. Kasting. “How Was Early Earth Kept Warm?” In: *Science* 339.6115 (2013), pp. 44–45 (cit. on p. 28).

[179] N. G. Holm, C. Oze, O. Mousis, J. H. Waite, and A. Guilbert-Lepoutre. “Serpentinization and the Formation of H2 and CH4 on Celestial Bodies (Planets, Moons, Comets)”. In: *Astrobiology* 15 (2015), pp. 587–600 (cit. on pp. 29, 190, 192).

[180] A. Guzmán-Marmolejo, A. Segura, and E. Escobar-Briones. "Abiotic Production of Methane in Terrestrial Planets". In: *Astrobiology* 13 (2013), pp. 550–559 (cit. on pp. 29, 190, 192, 214).

[181] A. S. Bradley. "The sluggish speed of making abiotic methane". In: *Proc. Natl. Acad. Sci. U.S.A.* 113 (2016), pp. 13944–13946 (cit. on p. 29).

[182] J. Krissansen-Totton, S. Olson, and D. C. Catling. "Disequilibrium biosignatures over Earth history and implications for detecting exoplanet life". In: *Sci. Adv.* 4.1 (2018-01), eaao5747 (cit. on pp. 29, 190).

[183] J. Oró. "Mechanism of Synthesis of Adenine from Hydrogen Cyanide under Possible Primitive Earth Conditions". In: *Nature* 191 (1961-09), pp. 1193–1194 (cit. on pp. 34, 90, 142, 203).

[184] J. P. Joshi Ferris, P. C. Edelson, E. H., and J. G. Lawless. "HCN: A Plausible Source of Purines, Pyrimidines and Amino Acids on the Primitive Earth". In: *J. Mol. Evol.* 11 (1978), pp. 293–311 (cit. on p. 34).

[185] P. P. Lavvas, A. Coustenis, and I. M. Vardavas. "Coupling photochemistry with haze formation in Titan's atmosphere, Part I: Model description". In: *Planet. Space Sci.* 56 (2008-01), pp. 27–66 (cit. on p. 34).

[186] P. P. Lavvas, A. Coustenis, and I. M. Vardavas. "Coupling photochemistry with haze formation in Titan's atmosphere, Part II: Results and validation with Cassini/Huygens data". In: *Planet. Space Sci.* 56 (2008-01), pp. 67–99 (cit. on pp. 34, 91).

[187] V. A. Krasnopolsky. "A photochemical model of Titan's atmosphere and ionosphere". In: *Icarus* 201 (2009-05), pp. 226–256 (cit. on pp. 34, 91).

[188] J. A. Pople. "Nobel Lecture: Quantum chemical models". In: *Rev. Mod. Phys.* 71 (1999), pp. 1267–1274 (cit. on p. 35).

[189] J. A. Pople. "Theoretical Models for Chemistry". In: *Proceedings of the Summer Research Conference on Theoretical Chemistry, Energy Structure and Reactivity.* Ed. by D. W. Smith. New York: John Wiley & Sons, 1973, pp. 51–61 (cit. on p. 35).

[190] A. K. Cobb, R. E. Pudritz, and B. K. D. Pearce. "Nature's Starships II. Simulating the Synthesis of Amino Acids in Meteorite Parent Bodies". In: *Astrophys. J.* 809 (2015-08), p. 6 (cit. on p. 36).

[191] E. Lellouch, P. N. Romani, and J. Rosenqvist. “The Vertical Distribution and Origin of HCN in Neptune’s Atmosphere”. In: *Icarus* 108 (1994), pp. 112–136 (cit. on p. 36).

[192] H. J. Cleaves, C. Neish, M. P. Callahan, E. Parker, F. M. Fernández, and J. P. Dworkin. “Amino acids generated from hydrated Titan tholins: Comparison with Miller-Urey electric discharge products”. In: *Icarus* 237 (2014-07), pp. 182–189 (cit. on p. 36).

[193] X. Shi, Q.-Z. Yin, H. Gao, Y.-C. Chang, W. M. Jackson, R. C. Wiens, and C.-Y. Ng. “Branching Ratios in Vacuum Ultraviolet Photodissociation of CO and N_2: Implications for Oxygen and Nitrogen Isotopic Compositions of the Solar Nebula”. In: *Astrophys. J.* 850 (2017-11), p. 48 (cit. on pp. 37, 90, 143).

[194] B. Gans, S. Boyé-Péronne, M. Broquier, M. Delsaut, S. Douin, C. E. Fellows, P. Halvick, J.-C. Loison, R. R. Lucchese, and D. Gauyacq. “Photolysis of methane revisited at 121.6 nm and at 118.2 nm: quantum yields of the primary products, measured by mass spectrometry”. In: *Phys. Chem. Chem. Phys.* 13 (2011), pp. 8140–8152 (cit. on pp. 37, 90, 143).

[195] G. Marston, F. L. Nesbitt, and L. J. Stief. “Branching ratios in the $N+CH_3$ reaction: Formation of the methylene amidogen (H_2CN) radical”. In: *J. Chem. Phys.* 91 (1989), pp. 3483–3491 (cit. on pp. 37, 48, 54, 56, 66, 67, 70, 71, 105, 106, 129, 131).

[196] K. Devriendt, M. Van Poppel, W. Boullart, and J. Peeters. “Kinetic Investigation of the $CH_2(X^3B_1) + H \longrightarrow CH(X^2\Pi) + H_2$ Reaction in the Temperature Range 400 K < T < 1000 K”. In: *J. Phys. Chem.* 99 (1995), pp. 16953–16959 (cit. on pp. 39, 57, 72, 73, 132, 138).

[197] W. Boullart and J. Peeters. “Product distributions of the C_2H_2 + O and HCCO + H reactions. Rate constant of methylene(X^3B_1) + H”. In: *J. Phys. Chem.* 96 (1992), pp. 9810–9816 (cit. on pp. 39, 57, 72, 73, 132).

[198] T. Böhland, F. Temps, and H. Gg. Wagner. “A Direct Study of the Reactions of $CH_2(X^3B_1)$ Radicals with H and D Atoms”. In: *J. Phys. Chem.* 91 (1987), pp. 1205–1209 (cit. on pp. 39, 57, 72, 73, 132).

[199] S. Zabarnick, J. W. Fleming, and M. C. Lin. “Kinetic study of the reaction $CH(X^2\Pi) + H_2 \longleftrightarrow CH_2(X^3B_1) + H$ in the temperature range 372 to 675 K”. In: *J. Phys. Chem.* 85 (1986), pp. 4373–4376 (cit. on pp. 39, 57, 72–74, 132, 133).

[200] T. Böhland and F. Temps. “Direct Determination of the Rate Constant for the Reaction $CH_2 + H \longrightarrow CH + H_2$”. In: *Ber. Bunsenges. Phys. Chem.* 88 (1984), p. 459 (cit. on pp. 39, 57, 72, 73, 132).

[201] J. Grebe and K. H. Homann. “Kinetics of the Species $OH(A^2\Sigma^+)$, $OH(X_2\Pi)$ and $CH(X^2\Pi)$ in the System $C_2H_2/O/H$”. In: *Ber. Bunsenges. Phys. Chem.* 86 (1982), p. 581 (cit. on pp. 39, 57, 72, 73, 132).

[202] K. H. Becker, R. Kurtenbach, and P. Wiesen. “Temperature and pressure dependence of the reaction CH + H_2”. In: *J. Chem. Phys.* 95 (1991), pp. 2390–2394 (cit. on pp. 39, 57, 74, 127, 133).

[203] W. Braun, A. M. Bass, and M. Pilling. “Flash Photolysis of Ketene and Diazomethane: The Production and Reaction Kinetics of Triplet and Singlet Methylene”. In: *J. Chem. Phys.* 52 (1970), pp. 5131–5143 (cit. on pp. 39, 56, 57, 74, 76, 80, 81, 131–133, 139).

[204] A. O. Langford, H. Petek, and C. B. Moore. “Collisional removal of $CH_2(^1A_1)$: Absolute rate constants for atomic and molecular collisional partners at 295 K”. In: *J. Chem. Phys.* 78 (1983), pp. 6650–6659 (cit. on pp. 39, 56, 57, 74, 80, 131, 132, 137, 139).

[205] M. N. R. Ashfold, M. A. Fullstone, G. Hancock, and G. W. Ketley. “Singlet Methylene Kinetics: Direct Measurements of Removal Rates of $\tilde{a}^1A_1$ and b^1B_1 CH_2 and CD_2”. In: *Chem. Phys.* 55 (1981), pp. 245–257 (cit. on pp. 39, 56, 57, 74, 80, 131, 132, 137).

[206] H. Umemoto, T. Nakae, H. Hashimoto, K. Kongo, and M. Kawasaki. “Reactions of $N(2^2D)$ with methane and deuterated methanes”. In: *J. Chem. Phys.* 109 (1998), pp. 5844–5848 (cit. on pp. 39, 56, 58, 64–66, 131).

[207] D. G. Truhlar and B. C. Garrett. “Variational Transition State Theory”. In: *Annu. Rev. Phys. Chem.* 35 (1984), pp. 159–189 (cit. on pp. 41, 92, 96, 144, 149).

[208] H. Li, B.-Z. Chen, and M.-B. Huang. "CASPT2 investigation of ethane dissociation and methyl recombination using canonical variational transition state theory". In: *Int. J. Chem. Kinet.* 40 (2008), pp. 161–173 (cit. on pp. 41, 46, 50, 59, 98, 128, 152, 166).

[209] J. I. Steinfeld, J. S. Fransisco, and W. L. Hase. *Chemical Kinetics and Dynamics.* New Jersey: Prentice-Hall, 1989 (cit. on p. 41).

[210] P. Hänggi, P. Talkner, and M. Borkovec. "Reaction-rate theory: fifty years after Kramers". In: *Rev. Mod. Phys.* 62 (1990), pp. 251–341 (cit. on p. 41).

[211] X. You, H. Wang, E. Goos, C.-J. Sung, and S. J Klippenstein. "Reaction Kinetics of CO + HO_2 to Products: Ab Initio Transition State Theory Study with Master Equation Modeling". In: *J. Phys. Chem. A* 111 (2007), pp. 4031–4042 (cit. on p. 41).

[212] A. Fernández-Ramos, B. A. Ellingson, R. Meana-Pañeda, J. M. C. Marques, and D. G. Truhlar. "Symmetry numbers and chemical reaction rates". In: *Theor. Chem. Account* 118 (2007), pp. 813–826 (cit. on pp. 41, 44).

[213] S. H. Robertson, A. F. Wagner, and D. M. Wardlaw. "Canonical flexible transition state theory revisited". In: *J. Chem. Phys.* 103 (1995), pp. 2917–2928 (cit. on p. 41).

[214] M. J. Frisch, G. W. Trucks, H. B. Schlegel, G. E. Scuseria, M. A. Robb, J. R. Cheeseman, G. Scalmani, V. Barone, G. A. Petersson, H. Nakatsuji, and et al. *Gaussian 09*, Revision E.01; Gaussian, Inc.: Wallingford, CT, 2009 (cit. on pp. 42, 45, 97, 148).

[215] J. W. Ochterski. *Thermochemistry in Gaussian.* Wallingford, CT: Gaussian Inc., 2000, pp. 1–19 (cit. on pp. 43, 44).

[216] A. D. Becke. "A new mixing of Hartree-Fock and local density-functional theories". In: *J. Chem. Phys.* 98 (1993), pp. 1372–1377 (cit. on pp. 45, 95, 147).

[217] C. Lee, W. Yang, and R. G. Parr. "Development of the Colle-Salvetti correlation-energy formula into a functional of the electron density". In: *Phys. Rev. B* 37 (1988), pp. 785–789 (cit. on pp. 45, 95, 147).

[218] C. S. Cockell. *Astrobiology: Understanding Life in the Universe.* New Jersey: Wiley-Blackwell, 2015 (cit. on p. 45).

[219] D. C. Clary. "Fast Chemical Reactions: Theory Challenges Experiment". In: *Annu. Rev. Phys. Chem.* 41 (1990), pp. 61–90 (cit. on pp. 46, 50, 98, 128, 152, 166).

[220] W. L. Hase, S. L. Mondro, R. J. Duchovic, and D. M. Hirst. "Thermal Rate Constant for $H + CH3 \longrightarrow CH4$ Recombination. 3. Comparison of Experiment and Canonical Variational Transition State Theory". In: *J. Am. Chem. Soc.* 109 (1987), pp. 2916–2922 (cit. on pp. 46, 50, 59, 98, 128, 152, 166).

[221] A. W. Jasper, S. J. Klippenstein, and L. B. Harding. "Secondary Kinetics of Methanol Decomposition: Theoretical Rate Coefficients for $^3CH_2$ + OH, $^3CH_2$ + $^3CH_2$, and $^3CH_2$ + CH_3". In: *J. Phys. Chem. A* 111 (2007), pp. 8699–8707 (cit. on pp. 46, 50, 59, 76, 98, 128, 152, 166).

[222] J. Daranlot, X. Hu, C. Xie, J.-C. Loison, P. Caubet, M. Costes, V. Wakelam, D. Xie, H. Guo, and K. Hickson. "Low temperature rate constants for the $N(^4S)$ + $CH(X^2\Pi_r)$ reaction. Implications for N_2 formation cycles in dense interstellar clouds". In: *Phys. Chem. Chem. Phys.* 15 (2013), pp. 13888–13896 (cit. on pp. 46, 50, 57, 59, 81, 98, 128, 131, 152, 166).

[223] D. Semenov, F. Hersant, V. Wakelam, A. Dutrey, E. Chapillon, S. Guilloteau, T. Henning, R. Launhardt, V. Piétu, and K. Schreyer. "Chemistry in disks. IV. Benchmarking gas-grain chemical models with surface reactions". In: *Astron. Astrophys.* 522, A42 (2010-11), A42 (cit. on p. 46).

[224] L. J. Stief, G. Marston, D. F. Nava, W. A. Payne, and F. L. Nesbitt. "Rate constant for the reaction of $N(^4S)$ with CH_3 AT 298 K". In: *Chem. Phys. Lett.* 147 (1988), pp. 570–574 (cit. on pp. 48, 56, 66, 68, 70, 71, 129, 131).

[225] A. Cimas and A. Largo. "The Reaction of Nitrogen Atoms with Methyl Radicals: Are Spin-Forbidden Channels Important?" In: *J. Phys. Chem. A* 110 (2006), pp. 10912–10920 (cit. on pp. 49, 54, 59, 67, 68).

[226] T. Yanai, D. P. Tew, and N. C. Handy. "A new hybrid exchange–correlation functional using the Coulomb-attenuating method (CAM-B3LYP)". In: *Chem. Phys. Lett.* 393 (2004), pp. 51–57 (cit. on p. 49).

[227] J. A. Manion, R. E. Huie, R. D. Levin, D. R. Burgess Jr., V. L. Orkin, W. Tsang, W. S. McGivern, J. W. Hudgens, V. D. Knyazev, D. B. Atkinson, and et al. *NIST Chemical Kinetics Database*; NIST Standard Reference

Database Number 17, Version 7.0 (Web Version), Release 1.6.8, Data version 2015.09, National Institute of Standards and Technology: Gaithersburg, MD, http://kinetics.nist.gov/, (retrieved May 10, 2018) (cit. on pp. 55, 130, 168).

[228] J. Tomeczek and B. Gradoń. "The role of N_2O and NNH in the formation of NO via HCN in hydrocarbon flames". In: *Combust. Flame* 133 (2003), pp. 311–322 (cit. on pp. 55, 62, 130, 181–183).

[229] F. L. Nesbitt, G. Marston, and L. J. Stief. "Kinetic Studies of the Reactions of H_2CN and D_2CN Radicals with N and H". In: *J. Phys. Chem.* 94 (1990), pp. 4946–4951 (cit. on pp. 55, 105, 106, 124, 128, 130, 134, 135).

[230] D. G. Horne and R. G. W. Norrish. "The Photolysis of Acyclic Azines and the Electronic Spectra of R_1R_2CN Radicals". In: *Proc. R. Soc. Lond. A Math. Phys. Sci.* 315 (1970), pp. 301–322 (cit. on pp. 55, 63).

[231] R. H. Lawrence, Jr. and R .F. Firestone. "Kinetics of thermal deuterium atom reactions with methane and ethane". In: *J. Am. Chem. Soc.* 88 (1966), pp. 4564–4570 (cit. on pp. 56, 60, 62, 132).

[232] W. E. Jones and J .L. Ma. "An electron spin resonance study of the reactions of hydrogen atoms with halocarbons". In: *Can. J. Chem.* 64 (1986), pp. 2192–2195 (cit. on pp. 56, 60, 62, 132).

[233] T. Takayanagi, Y. Kurosaki, K. Sato, K. Misawa, Y. Kobayashi, and S. Tsunashima. "Kinetic Studies on the N(^{2}D, ^{2}P) + CH_4 and CD_4 Reactions: The Role of Nonadiabatic Transitions on Thermal Rate Constants". In: *J. Chem. Phys. A* 103 (1999), pp. 250–255 (cit. on pp. 56, 59, 64, 105, 106, 108, 125, 131).

[234] B. Fell, I. V. Rivas, and D. L. McFadden. "Kinetic Study of Electronically Metastable Nitrogen Atoms, N(2^2D_J), by Electron Spin Resonance Absorption". In: *J. Phys. Chem.* 85 (1981), pp. 224–228 (cit. on pp. 56, 58, 64, 83, 131, 169, 176).

[235] H. Umemoto, N. Hachiya, E. Matsunaga, A. Suda, and M. Kawasaki. "Rate constants for the deactivation of N ^{2}D by simple hydride and deuteride molecules". In: *Chem. Phys. Lett.* 296 (1998), pp. 203–207 (cit. on pp. 56, 64, 131).

[236] G. Black, T. G. Slanger, G. A. St. John, and R. A. Young. “Vacuum-Ultraviolet Photolysis of N_2O. IV. Deactivation of $N(^2D)$”. In: *J. Chem. Phys.* 51 (1969), pp. 116–121 (cit. on pp. 56, 58, 64, 83, 131, 169, 176).

[237] J. T. Herron. “Evaluated Chemical Kinetics Data for Reactions of $N(^2D)$, $N(^2P)$ and $N_2(A^3\Sigma_u^+)$ in the Gas Phase”. In: *J. Phys. Chem. Ref. Data* 28 (1999), pp. 1453–1483 (cit. on pp. 56, 58, 64, 83, 129, 131, 176, 208).

[238] M. Brouard, M. T. Macpherson, and M. J. Pilling. “Experimental and RRKM Modeling Study of the CH_3 + H and CH_3 + D Reactions”. In: *J. Phys. Chem.* 93 (1989), pp. 4047–4059 (cit. on pp. 56, 105, 106, 132).

[239] J.-T. Cheng and C.-T. Yeh. “Pressure Dependence of the Rate Constant of the Reaction $H + CH3 \longrightarrow CH4$”. In: *J. Phys. Chem.* 81 (1977), pp. 1982–1984 (cit. on pp. 56, 132).

[240] J.-T. Cheng, Y.-S. Lee, and C.-T. Yeh. “The Triplet Mercury Photosensitized Decomposition of Ethane at High Intensity”. In: *J. Phys. Chem.* 81 (1977), pp. 687–690 (cit. on pp. 56, 132).

[241] T. J. Sworski, C. J. Hochanadel, and P. J. Ogren. “Flash Photolysis of H_2O Vapor in CH_4. H and OH Yields and Rate Constants for CH_3 Reactions with H and OH”. In: *J. Phys. Chem.* 84 (1980), pp. 129–134 (cit. on pp. 56, 132).

[242] R. Patrick, M. J. Pilling, and G. J. Rogers. “A high pressure rate constant for $CH3 + H$ and an analysis of the kinetics of the $CH3 + H \longrightarrow CH4$ reaction”. In: *Chem. Phys.* 53 (1980), pp. 279–291 (cit. on pp. 56, 132).

[243] J. V. Michael, D. T. Osborne, and G. N. Suess. “Reaction H + C_2H_4: Investigation into the effects of pressure, stoichiometry, and the nature of the third body species”. In: *J. Chem. Phys.* 58 (1973), pp. 2800–2806 (cit. on pp. 56, 132).

[244] C. J. Cobos and J. Troe. “The Dissociation-Recombination System $CH4 + M \longleftrightarrow CH3 + H + M$: Reevaluated Experiments from 300 to 3000 K”. In: *Z. Phys. Chem. N. F.* 167 (1990), pp. 129–149 (cit. on pp. 56, 132).

[245] W. Tsang. “Rate Constants for the Decomposition and Formation of Simple Alkanes Over Extended Temperature and Pressure Ranges”. In: *Combust. Flame* 78 (1989), pp. 71–86 (cit. on pp. 56, 132).

[246] P. C. Kobrinsky and P. D. Pacey. “The Reaction of Methyl Radicals with Molecular Hydrogen”. In: *Can. J. Chem.* 52 (1974), pp. 3665–3670 (cit. on pp. 56, 132).

[247] W. Tsang and R. F. Hampson. “Chemical Kinetic Data Base for Combustion Chemistry. Part I. Methane and Related Compounds”. In: *J. Phys. Chem. Ref. Data* 15 (1986), pp. 1087–1279 (cit. on pp. 56, 57, 72–74, 77, 78, 80, 81, 95, 103, 127, 129, 131–133, 137, 148, 155, 158, 164, 165, 167, 169–174, 184, 208).

[248] J. A. Miller and C. T. Bowman. “Mechanism and Modeling of Nitrogen Chemistry in Combustion”. In: *Prog. Energy Combust. Sci.* 15 (1989), pp. 287–338 (cit. on pp. 56, 67, 70, 105, 106, 131).

[249] D. Walter, H.-H. Grotheer, J. W. Davies, M. J. Pilling, and A. F. Wagner. “Experimental and theoretical study of the recombination reaction $CH_3 + CH_3 \longrightarrow C_2H_6$”. In: *Twenty-Third Symposium (International) on Combustion.* Vol. 23. Seattle: The Combustion Institute, 1991, pp. 107–114 (cit. on pp. 56, 132).

[250] M. T. Macpherson, M. J. Pilling, and M. J. C. Smith. “Determination of the absorption cross section for methyl at 216.36 nm and the absolute rate constant for methyl radical recombination over the temperature range 296-577 K”. In: *J. Phys. Chem.* 89 (1985), pp. 2268–2274 (cit. on pp. 56, 132).

[251] H. Du, J. P. Hessler, and P. J. Ogren. “Recombination of Methyl Radicals. 1. New Data between 1175 and 1750 K in the Falloff Region”. In: *J. Phys. Chem.* 100 (1996), pp. 974–983 (cit. on pp. 56, 132).

[252] D. Slagle I. R. Gutman, J. W. Davies, and M. J. Pilling. “Study of the recombination reaction $CH_3 + CH_3 \longrightarrow C_2H_6$. 1. Experiment”. In: *J. Phys. Chem.* 92 (1988), pp. 2455–2462 (cit. on pp. 56, 132).

[253] M. Sangwan, C. Yan, E. N. Chesnokov, and L. N. Krasnoperov. “Reaction $CH_3 + CH_3 \longrightarrow C_2H_6$ Studied over the 292-714 K Temperature and 1-100 bar Pressure Ranges”. In: *J. Phys. Chem. A* 119 (2015), pp. 7847–7857 (cit. on pp. 56, 132).

[254] J. Pagsberg P. Munk, A. Sillesen, and C. Anastasi. “UV spectrum and kinetics of hydroxymethyl radicals”. In: *Chem. Phys. Lett.* 146 (1988), pp. 375–381 (cit. on pp. 56, 132).

[255] H. Hippler, K. Luther, A. R. Ravishankara, and J. Troe. “High-Pressure Effects in the Recombination Reaction $CH_3 + CH_3 \longrightarrow C_2H_6$”. In: *Z. Phys. Chem. N. F.* 142 (1984), pp. 1–12 (cit. on pp. 56, 132).

[256] A. Fahr, A. Laufer, R. Klein, and W Braun. “Reaction Rate Determinations of Vinyl Radical Reactions with Vinyl, Methyl, and Hydrogen Atoms”. In: *J. Phys. Chem.* 95 (1991), pp. 3218–3224 (cit. on pp. 56, 132).

[257] B. Wang and C. Fockenberg. “Direct Measurement of the Rate Constant for the $CH_2(X^3B_1)$ + CH_3 Reaction at 300 K”. In: *J. Phys. Chem. A* 105 (2001), pp. 8449–8455 (cit. on pp. 56, 57, 78, 80, 132).

[258] N. L. Arthur. “Methyl-radical absorption cross-section at 216.4 nm and rate constant for methyl-radical recombination”. In: *J. Chem. Soc., Faraday Trans. 2* 82 (1986), pp. 331–336 (cit. on pp. 56, 132).

[259] C. Anastasi and N. L. Arthur. “Rate constants for the reactions of CH_3 radicals with C_2H_5, i-C_3H_7 and t-C_4H_9 radicals”. In: *J. Chem. Soc., Faraday Trans. 2* 83 (1987), pp. 277–287 (cit. on pp. 56, 132).

[260] D. C. Darwin and C. B. Moore. “Reaction Rate Constants (295 K) for $^3CH_2$ with H_2S, SO_2, and NO_2: Upper Bounds for Rate Constants with Less Reactive Partners”. In: *J. Phys. Chem.* 99 (1995), pp. 13467–13470 (cit. on pp. 57, 132, 177).

[261] M. J. Pilling and J. A. Robertson. “Flash photolysis of ketene. Photolysis mechanism and rate constants for singlet and triplet methylene”. In: *J. Chem. Soc., Faraday Trans. 1* 73 (1977), pp. 968–984 (cit. on pp. 57, 132).

[262] R. Deters, M. Otting, H. Gg. Wagner, F. Temps, and S. Dobe. “Rate constant for the reaction CH_3+$CH_2(X^3B_1)$ at 298 K”. In: *Ber. Bunsenges. Phys. Chem.* 102 (1998), pp. 978–981 (cit. on pp. 57, 78, 132).

[263] A. H. Laufer and A. M. Bass. “Mechanism and rate constant of the reaction between methylene and methyl radicals”. In: *J. Phys. Chem.* 79 (1975), pp. 1635–1638 (cit. on pp. 57, 78, 80, 132).

[264] M. J. Pilling and J. A. Robertson. “A rate constant for $CH_2(^3B_1)$ + CH_3”. In: *Chem. Phys. Lett.* 33 (1975), pp. 336–339 (cit. on pp. 57, 78, 80, 132).

[265] T. Böhland, S. Dobe, F. Temps, and H. Gg. Wagner. "Kinetics of the Reactions between $CH_2(X^3B_1)$-Radicals and Saturated Hydrocarbons in the Temperature Range 296 K $\leq$ T $\leq$ 707 K". In: *Ber. Bunsenges. Phys. Chem.* 89 (1985), pp. 1110–1116 (cit. on pp. 57, 80, 81, 131).

[266] R. A. Brownsword, A. Canosa, B. R. Rowe, I. R. Sims, I. W. M. Smith, D. W. A. Stewart, A. C. Symonds, and D. Travers. " Kinetics over a wide range of temperature (13-744 K): Rate constants for the reactions of CH(ν=0) with H_2 and D_2 and for the removal of CH(ν=1) by H_2 and D_2". In: *J. Chem. Phys.* 106 (1997), pp. 7662–7677 (cit. on pp. 57, 74, 129, 133).

[267] D. Fulle and H. Hippler. "The temperature and pressure dependence of the reaction $CH + H \longleftrightarrow CH3 \longleftrightarrow CH2 + H$". In: *J. Chem. Phys.* 106 (1997), pp. 8691–8698 (cit. on pp. 57, 74, 133, 138).

[268] M. R. Berman and M. C. Lin. "Kinetics and mechanisms of the reactions of CH and CD with H_2 and D_2". In: *J. Chem. Phys.* 81 (1984), pp. 5743–5752 (cit. on pp. 57, 74, 133).

[269] A. McIlroy and F. P. Tully. "CH+H_2 reaction kinetics: Temperature and pressure dependence and Rice-Ramsperger-Kassel-Marcus-master-equation calculation". In: *J. Chem. Phys.* 99 (1993), pp. 3597–3603 (cit. on pp. 57, 59, 133).

[270] J. E. Butler, L. P. Goss, M. C. Lin, and J. W. Hudgens. "Production, detection and reactions of the CH radical". In: *Chem. Phys. Lett.* 63 (1979), pp. 104–107 (cit. on pp. 57, 74, 82, 131, 133, 137).

[271] M. W. Bosnali and D. Perner. "Notizen: Reaktionen von pulsradiolytisch erzeugtem CH($^2\Pi$) mit Methan und anderen Substanzen". In: *Z. Naturforsch.* 26 (1971), pp. 1768–1769 (cit. on pp. 57, 74, 82, 131, 133, 137, 170, 171).

[272] W. Braun, J. R. McNesby, and A. M. Bass. "Flash Photolysis of Methane in the Vacuum Ultraviolet. II. Absolute Rate Constants for Reactions of CH with Methane, Hydrogen, and Nitrogen". In: *J. Chem. Phys.* 46 (1967), pp. 2071–2080 (cit. on pp. 57, 74, 82, 127, 131, 133, 137).

[273] R. A. Brownsword, S. D. Gatenby, L. B. Herbert, I. W. M. Smith, D. W. A. Stewart, and A. C. Symonds. "Kinetics of reactions between neutral free radicals. Rate constants for the reaction of CH radicals with N atoms between

216 and 584 K". In: *J. Chem. Soc. Faraday Trans.* 92 (1996), pp. 723–727 (cit. on pp. 57, 81, 131).

[274] I. Messing, S. V. Filseth, C. M. Sadowski, and D. Carrington. "Absolute rate constants for the reactions of CH with O and N atoms". In: *J. Chem. Phys.* 74 (1981), pp. 3874–3881 (cit. on pp. 57, 81, 131, 173).

[275] W. Braun, K. H. Welge, and J. R. McNesby. "Flash Photolysis of Methane in the Vacuum Ultraviolet. I. End-Product Analysis". In: *J. Chem. Phys.* 45 (1966), pp. 2650–2656 (cit. on pp. 57, 82, 127, 131, 133, 137).

[276] J. E. Butler, J. E. Fleming, L. P. Goss, and M. C. Lin. "Kinetics of CH Radical Reactions with Selected Molecules at Room Temperature". In: *J. Chem. Phys.* 56 (1981), pp. 355–365 (cit. on pp. 57, 82, 131, 137).

[277] M. R. Berman and M. C. Lin. "Kinetics and mechanisms of the reactions of CH with CH_4, C_2H_6 and n-C_4H_10". In: *J. Chem. Phys.* 82 (1983), pp. 435–442 (cit. on pp. 57, 82, 105, 106, 108, 125, 131, 137).

[278] M. A. Blitz, D. G. Johnson, M. Pesa, M. J. Pilling, S. H. Robertson, and P. W. Seakins. "Reaction of CH radicals with methane isotopomers". In: *J. Chem. Soc. Faraday Trans.* 93 (1997), pp. 1473–1479 (cit. on pp. 57, 82, 105, 108, 125, 131, 137).

[279] A. Canosa, I. R. Sims, D. Travers, I. W. M. Smith, and B. R. Rowe. "Reactions of the methylidine radical with CH_4, C_2H_2, C_2H_4, C_2H_6, and but-1-ene studied between 23 and 295K with a CRESU apparatus." In: *Astron. Astrophys.* 323 (1997-07), pp. 644–651 (cit. on pp. 57, 82, 131, 137).

[280] H. Thiesemann, J. MacNamara, and C. A. Taatjes. "Deuterium Kinetic Isotope Effect and Temperature Dependence in the Reactions of CH[$^2\Pi$] with Methane and Acetylene". In: *J. Phys. Chem. A* 101 (1997), pp. 1881–1886 (cit. on pp. 57, 82, 105, 108, 125, 131, 137).

[281] L. Adam, W. Hack, H. Zhu, Z.-W. Qu, and R. Schinke. "Experimental and theoretical investigation of the reaction $NH(X^3\Sigma^-) + H(^2S) \text{->} N(^4S) + H2(X^1\Sigma_g^+)$". In: *J. Chem. Phys.* 122 (2005), p. 114301 (cit. on pp. 57, 59, 83, 129, 131).

[282] W. Hack, H. Gg. Wagner, and A. Zasypkin. "Elementary reactions of NH ($a^1\Delta$) and $NH(X^3\Sigma)$ with N, O and NO". In: *Ber. Bunsenges. Phys. Chem.* 98 (1994), pp. 156–164 (cit. on pp. 58, 84, 128, 130, 173).

[283] A. A. Konnov and J. De Ruyck. “Kinetic Modeling of the Decomposition and Flames of Hydrazine”. In: *Combust. Flame* 124 (2001), pp. 106–126 (cit. on pp. 58, 84, 130).

[284] G. Black, R. L. Sharpless, T. G. Slanger, and D. C. Lorents. “Quantum yields for the production of O(^{1}S), N(^{2}D), and $N_2(A^3\Sigma_u^+)$ from the vacuum uv photolysis of N_2O”. In: *J. Chem. Phys.* 62 (1975), pp. 4266–4273 (cit. on pp. 58, 83, 131).

[285] T. Suzuki, Y. Shihira, T. Sato, H. Umemoto, and S. Tsunashima. “Reactions of N(2^2D) and N(2^2P) with H_2 and D_2”. In: *J. Chem. Soc. Faraday Trans.* 89 (1993), pp. 995–999 (cit. on pp. 58, 59, 83, 84, 93, 125, 128, 131).

[286] H. Umemoto, N. Hachiya, E. Matsunaga, A. Suda, and M. Kawasaki. “Rate constants for the deactivation of N(2^2D) by simple hydride and deuteride molecules”. In: *Chem. Phys. Lett.* 296 (1998), pp. 203–207 (cit. on pp. 58, 83, 131).

[287] L. G. Piper, M. E. Donahue, and W. T. Rawlins. “Rate Coefficients for N(^{2}D) Reactions”. In: *J. Phys. Chem.* 91 (1987), pp. 3883–3888 (cit. on pp. 58, 83, 131, 169, 176).

[288] D. Husain, S. K. Mitra, and A. N. Young. “Kinetic Study of Electronically Excited Nitrogen Atoms, N(2^2D_J,2^2P_J), by Attenuation of Atomic Resonance Radiation in the Vacuum Ultra-violet”. In: *J. Chem. Soc., Faraday Trans. 2* 70 (1974), pp. 1721–1731 (cit. on pp. 58, 83, 131, 159, 169, 176).

[289] P. D. Whitefield and F. E. Hovis. “Rate Constants for the Reactions of N(^{2}D) atoms with with O_2, H_2 and HF”. In: *Chem. Phys. Lett.* 135 (1987), pp. 454–458 (cit. on pp. 58, 83, 131).

[290] D. Husain, L. J. Kirsch, and J. R. Wiesenfeld. “Collisional quenching of electronically excited nitrogen atoms, N(2^2D_J, 2^2P_J) by time-resolved atomic absorption spectroscopy”. In: *Faraday Discuss. Chem. Soc.* 53 (1972), pp. 201–210 (cit. on pp. 58, 83, 131).

[291] J. R. Barker, D. G. Keil, J. V. Michael, and D. T. Osborne. “Reaction $H+C_2H_4$: Comparison of Three Experimental Techniques”. In: *J. Chem. Phys.* 52 (1970), pp. 2079–2088 (cit. on p. 58).

[292] B. Kerkeni and D. C. Clary. “Kinetic Isotope Effects in the Reactions of D Atoms with CH_4, C_2H_6, and CH_3OH: Quantum Dynamics Calculations”. In: *J. Phys. Chem. A* 108 (2004), pp. 8966–8972 (cit. on p. 58).

[293] T. N. Truong and W. Duncan. “A new direct ab initio dynamics method for calculating thermal rate constants from density functional theory”. In: *J. Chem. Phys.* 101 (1994), pp. 7408–7414 (cit. on pp. 58, 60).

[294] J. Espinosa-García and J. C. Corchado. “Recalibration of Two Earlier Potential Energy Surfaces for the $\mathrm{CH4} + \mathrm{H} \longrightarrow \mathrm{CH3} + \mathrm{H2}$ Reaction. Application of Variational Transition-State Theory and Analysis of the Kinetic Isotope Effects Using Rectilinear and Curvilinear Coordinates”. In: *J. Phys. Chem.* 100 (1996), pp. 16561–16567 (cit. on pp. 58, 60).

[295] M. J. T. Jordan and R. G. Gilbert. “Classical trajectory studies of the reaction $\mathrm{CH4} + \mathrm{H} \longrightarrow \mathrm{CH3} + \mathrm{H2}$”. In: *J. Chem. Phys.* 102 (1995), pp. 5669–5682 (cit. on pp. 58, 60).

[296] T. Joseph, R. Steckler, and D. G. Truhlar. “A new potential energy surface for the $\mathrm{CH3} + \mathrm{H2} \longleftrightarrow \mathrm{CH4} + \mathrm{H}$ reaction: Calibration and calculations of rate constants and kinetic isotope effects by variational transition state theory and semiclassical tunneling calculations”. In: *J. Chem. Phys.* 87 (1987), pp. 7036–7049 (cit. on pp. 58, 60).

[297] B. Kerkeni and D. C. Clary. “Ab initio rate constants from hyperspherical quantum scattering: Application to $\mathrm{H} + \mathrm{CH4} \longrightarrow \mathrm{H2} + \mathrm{CH3}$”. In: *J. Chem. Phys.* 120 (2004), pp. 2308–2318 (cit. on pp. 58, 60).

[298] T. C. Clark and J. E. Dove. “Examination of Possible Non-Arrhenius Behavior in the reactions”. In: *Can. J. Chem.* 51 (1973), pp. 2147–2154 (cit. on pp. 58, 60).

[299] J. Pu and D .G. Truhlar. “Parametrized direct dynamics study of rate constants of H with CH_4 from 250 to 2400 K”. In: *J. Chem. Phys.* 116 (2002), pp. 1468–1478 (cit. on pp. 58, 60).

[300] R. J. Berry, C. J. Ehlers, D. R. Burgess, Jr., M. R. Zachariah, and P. Marshall. “A computational study of the reactions of atomic hydrogen with fluoromethanes: kinetics and product channels”. In: *Chem. Phys. Lett.* 269 (1997), pp. 107–116 (cit. on pp. 58, 60).

[301] M. G. Bryukov, I. R. Slagle, and V. D. Knyazev. "Kinetics of Reactions of H Atoms With Methane and Chlorinated Methanes". In: *J. Phys. Chem. A* 105 (2001), pp. 3107–3122 (cit. on pp. 58, 59).

[302] C. Gonzalez, J. J. W. McDouall, and H. B. Schlegel. "Ab Initio Study of the Reactions between Methane and OH, H, and ^{3}O". In: *J. Phys. Chem.* 94 (1990), pp. 7467–7471 (cit. on pp. 58, 60).

[303] T. V. Alves, A. G. S. de Oliveira Filho, and F. R. Ornellas. "The reaction of methyl radical with nitrogen atom on the triplet potential energy surface: A CCSD(T)/CBS characterization". In: *Chem. Phys. Lett.* 457 (2008), pp. 36–41 (cit. on pp. 59, 67, 68).

[304] W. L. Hase and R. J. Duchovic. "Thermal rate constant for $\mathrm{H + CH3 \longrightarrow CH4}$ recombination. Comparison of quasiclassical trajectory and variational transition state theory". In: *J. Chem. Phys.* 83 (1985), pp. 3448–3453 (cit. on p. 59).

[305] M. J. Pilling. "Association reactions of atoms and radicals". In: *Int. J. Chem. Kinet.* 21 (1989), pp. 267–291 (cit. on p. 59).

[306] W. Forst. "Microcanonical Variational Theory of Radical Recombination by Inversion of Interpolated Partition Function, with Examples: CH_3 + H, CH_3 + CH_3". In: *J. Phys. Chem.* 95 (1991), pp. 13612–3620 (cit. on p. 59).

[307] J. Troe and V. G. Ushakov. "The dissociation/recombination reaction $\mathrm{CH4\,(^{+}M) \longleftrightarrow CH3 + H\,(^{+}M)}$: A case study for unimolecular rate theory". In: *J. Chem. Phys.* 136 (2012), p. 214309 (cit. on p. 59).

[308] L. B. Harding, Y. Georgievskii, and S. J. Klippenstein. "Predictive Theory for Hydrogen Atom-Hydrocarbon Radical Association Kinetics". In: *J. Phys. Chem. A* 109 (2005), pp. 4646–4656 (cit. on p. 59).

[309] J. Takahashi, T. Momose, and T. Shida. "Thermal rate constants for $\mathrm{SiH4 \longleftrightarrow SiH3 + H}$ and $\mathrm{CH4 \longleftrightarrow CH3 + H}$ by Canonical Variational Transition State Theory". In: *Bull. Chem. Soc. Jpn.* 67 (1994), pp. 74–85 (cit. on p. 59).

[310] D. M. Wardlaw and R. A. Marcus. "Unimolecular reaction rate theory for transition states of any looseness. 3. Application to methyl radical recombination". In: *J. Phys. Chem.* 90 (1986), pp. 5383–5393 (cit. on p. 59).

[311] K. V. Darvesh, R. J. Boyd, and P. D. Pacey. “Recombination of Methyl Radicals: Ab Initio Potential and Transition-State Theory Calculations”. In: *J. Phys. Chem.* 93 (1989), pp. 4772–4779 (cit. on p. 59).

[312] M. Pesa, M. Pilling, S. H. Robertson, and D. M. Wardlaw. “Application of the Canonical Flexible Transition State Theory to CH_3, CF_3, and CCl_3 Recombination Reactions”. In: *J. Phys. Chem. A* 102 (1998), pp. 8526–8536 (cit. on p. 59).

[313] S. J. Klippenstein and L. B. Harding. “A Direct Transition State Theory Based Study of Methyl Radical Recombination Kinetics”. In: *J. Phys. Chem. A* 103 (1999), pp. 9388–9398 (cit. on p. 59).

[314] S. J. Klippenstein, Y. Georgievskii, and L. B. Harding. “Predictive theory for the combination kinetics of two alkyl radicals”. In: *Phys. Chem. Chem. Phys.* 8 (2006), pp. 1133–1147 (cit. on p. 59).

[315] A. F. Wagner and D. M. Wardlaw. “Study of the recombination reaction $CH_3 + CH_3 \longrightarrow C_2H_6$. 2. Theory”. In: *J. Phys. Chem.* 92 (1988), pp. 2462–2471 (cit. on p. 59).

[316] B. Wang, H. Hou, L. M. Yoder, J. T. Muckerman, and C. Fockenberg. “Experimental and Theoretical Investigations on the Methyl-Methyl Recombination Reaction”. In: *J. Phys. Chem. A* 107 (2003), pp. 11414–11426 (cit. on p. 59).

[317] F. Lorant, F. Behar, W. Goddard, III, and Y. Tang. “Ab Initio Investigation of Ethane Dissociation Using Generalized Transition State Theory”. In: *J. Phys. Chem. A* 105 (2001), pp. 7896–7904 (cit. on p. 59).

[318] K.-W. Lu, H. Matsui, C.-L. Huang, P. Raghunath, N.-S. Wang, and M. C. Lin. “Shock Tube Study on the Thermal Decomposition of CH_3OH”. In: *J. Phys. Chem.* 114 (2010), pp. 5493–5502 (cit. on pp. 59, 75).

[319] E. Herbst, R. Terzieva, and D. Talbi. “Calculations on the rates, mechanisms, and interstellar importance of the reactions between C and NH_2 and between N and CH_2”. In: *Mon. Not. R. Astron. Soc.* 311 (2000), pp. 869–876 (cit. on pp. 59, 75, 76).

[320] J. Mayneris, A. Saracibar, E. M. Goldfield, M. González, E. García, and S. K. Gray. “Theoretical Study of the Complex-Forming $CH + H_2 \longrightarrow CH_2 + H$ Reaction”. In: *J. Phys. Chem. A* 110 (2006), pp. 5542–5548 (cit. on pp. 59, 74).

[321] P. J. S. B. Caridade, S. P. J. Rodrigues, F. Sousa, and A. J. C. Varandas. “Unimolecular and Bimolecular Calculations for HN_2”. In: *J. Phys. Chem. A* 109 (2005), pp. 2356–2363 (cit. on pp. 59, 84).

[322] Z.-F. Xu, D.-C. Fang, and X.-Y. Fu. “Ab Initio Studies on the Dynamical Properties of the Reaction $NH(X^3\Sigma^-) + H \longrightarrow N(^4S) + H_2$”. In: *J. Phys. Chem. A* 101 (1997), pp. 4432–4436 (cit. on pp. 59, 83).

[323] R. Z. Pascual, G. C. Schatz, G. Lendvay, and D. Troya. “Quasiclassical Trajectory and Transition State Theory Studies of the $N(^4S) + H_2 \longleftrightarrow NH(X^3\Sigma^-) + H$ Reaction”. In: *J. Chem. Phys.* 106 (2002), pp. 4125–4136 (cit. on pp. 59, 83).

[324] T. Takayanagi, H. Kobayashi, and S. Tsunashima. “Reaction dynamics for the $N(^2D)$ + H_2 reaction”. In: *J. Chem. Soc. Faraday Trans.* 92 (1996), pp. 1311–1314 (cit. on pp. 59, 83).

[325] H. Kobayashi, T. Takayanagi, K. Yokoyama, T. Sato, and S. Tsunashima. “Quasiclassical Trajectory Studies of $N(^2D)$ + H_2 Reaction on a Fitted ab initio Potential-energy Surface ”. In: *J. Chem. Soc. Faraday Trans.* 91 (1995), pp. 3771–3777 (cit. on pp. 59, 83, 84).

[326] L. A. Pederson, G. C. Schatz, T.-S. Ho, T. Hollebeek, H. Rabitz, L. B. Harding, and G. Lendvay. “Potential energy surface and quasiclassical trajectory studies of the $N(^2D)$ + H_2 reaction”. In: *J. Chem. Phys.* 110 (1999), pp. 9091–9100 (cit. on pp. 59, 83, 84).

[327] C.-M. Ouk, N. Zvereva-Loëte, Y. Scribano, and B. Bussery-Honvault. “Transition State Theory Thermal Rate Constants and RRKM-Based Branching Ratios for the $N(^2D)$ + CH_4 Reaction Based on Multi-State and Multi-Reference Ab Initio Calculations of Interest for the Titan’s Chemistry”. In: *J. Comput. Chem.* 33 (2012), pp. 2211–2224 (cit. on pp. 64, 65).

[328] N. Balucani, A. Bergeat, L. Cartechini, G. G. Volpi, D. Skouteris, and M. Rosi. “Combined Crossed Molecular Beam and Theoretical Studies of the N(^{2}D) + CH_4 Reaction and Implications for Atmospheric Models of Titan”. In: *J. Phys. Chem. A* 113 (2009), pp. 11138–11152 (cit. on pp. 64, 65, 106).

[329] C.-M. Ouk, N. Zvereva-Loëte, and B. Bussery-Honvault. “Towards a converged barrier height for the entrance channel transition state of the N(^{2}D) + CH_4 reaction and its implication for the chemistry in Titan’s atmosphere”. In: *Chem. Phys. Lett.* 515 (2011), pp. 13–18 (cit. on p. 65).

[330] S. Chiba and F. Yoshida. “Theoretical study of N (^{4}S, ^{2}D) + CH_3 ($^2A_2''$) reaction mechanisms revisited: The importance of spin-forbidden and roaming dynamics processes”. In: *Chem. Phys. Lett.* 595-596 (2014), pp. 103–108 (cit. on p. 67).

[331] R. Becerra, C. E. Canosa-Mas, H. M. Frey, and R. Walsh. “Studies of Methylene Chemistry by Pulsed Laser-induced Decomposition of Ketene”. In: *J. Chem. Soc., Faraday Trans. 2* 83 (1987), pp. 435–448 (cit. on p. 76).

[332] A. Yu, C. Chen, and M. Huang. “An ab initio study on the reaction of CH($X^2\pi$) with CH_4”. In: *Can. J. Chem.* 71 (1993), pp. 512–519 (cit. on p. 82).

[333] Z.-X. Wang, C. Chen, and M. Huang. “Theoretical study on the insertion reaction of CH($X^2\pi$) with CH_4”. In: *Can. J. Chem.* 75 (1997), pp. 996–1001 (cit. on pp. 82, 106, 137).

[334] R. J. Donovan and D. Husain. “Recent Advances in the Chemistry of Electronically Excited Atoms”. In: *Chem. Rev.* 70 (1970), pp. 489–516 (cit. on p. 83).

[335] B. K. D. Pearce, P. W. Ayers, and R. E. Pudritz. “A Consistent Reduced Network for HCN Chemistry in Early Earth and Titan Atmospheres: Quantum Calculations of Reaction Rate Coefficients”. In: *J. Phys. Chem. A* 123 (2019-02), pp. 1861–1873 (cit. on pp. 90, 92, 93, 96, 98, 102, 104, 115, 123, 124, 128, 129, 137–139, 144, 146, 148, 182, 207).

[336] D. C. Catling. “Planetary Atmospheres”. In: *Physics of Terrestrial Planets and Moons.* Ed. by G. Schubert. Treatise on Geophysics, 2nd Ed. Oxford: Elsevier, 2015, pp. 429–472 (cit. on pp. 91, 196).

[337] E. Hébrard, M. Dobrijevic, Y. Bénilan, and F. Raulin. “Photochemical kinetics uncertainties in modeling Titan’s atmosphere: First consequences”. In: *Planet. Space Sci.* 55.10 (2007-07), pp. 1470–1489 (cit. on p. 91).

[338] O. Venot, R. Bounaceur, M. Dobrijevic, E. Hébrard, T. Cavalié, P. Tremblin, B. Drummond, and B. Charnay. “Reduced chemical scheme for modelling warm to hot hydrogen-dominated atmospheres”. In: *Astron. Astrophys.* 624 (2019), A58 (cit. on p. 92).

[339] S. Lebonnois, J. Burgalat, P. Rannou, and B. Charnay. “Titan global climate model: A new 3-dimensional version of the IPSL Titan GCM”. In: *Icarus* 218 (2012), pp. 707–722 (cit. on p. 92).

[340] K. Molaverdikhani, T. Henning, and P. Mollière. “From Cold to Hot Irradiated Gaseous Exoplanets: Fingerprints of Chemical Disequilibrium in Atmospheric Spectra”. In: *Astrophys. J.* 883.2 (2019-10), p. 194 (cit. on pp. 92, 101, 196, 200, 201, 207).

[341] K. Douglas, M. A. Blitz, W. Feng, D. E. Heard, J. M. C. Plane, E. Slater, K. Willacy, and P. W. Seakins. “Low temperature studies of the removal reactions of $^1CH_2$ with particular relevance to the atmosphere of Titan”. In: *Icarus* 303 (2018), pp. 10–21 (cit. on pp. 93, 128).

[342] T. H. Dunning, Jr. “Gaussian basis sets for use in correlated molecular calculations. I. The atoms boron through neon and hydrogen”. In: *J. Chem. Phys.* 90 (1989), pp. 1007–1023 (cit. on pp. 95, 147).

[343] R. A. Kendall and T. H. Dunning, Jr. “Electron affinities of the first-row atoms revisited. Systematic basis sets and wave functions”. In: *J. Chem. Phys.* 96 (1992), pp. 6796–6806 (cit. on pp. 95, 147).

[344] D. E. Woon and T. H. Dunning, Jr. “Gaussian-basis sets for use in correlated molecular calculations. 3. The atoms aluminum through argon”. In: *J. Chem. Phys.* 98 (1993), pp. 1357–1371 (cit. on pp. 95, 147).

[345] J. Chai and M. Head-Gordon. “Long-range corrected hybrid density functionals with damped atom-atom dispersion corrections”. In: *Phys. Chem. Chem. Phys.* 10 (2008), pp. 6615–6620 (cit. on p. 96).

[346] R. J. Bartlett. “Coupled-cluster approach to molecular structure and spectra: a step toward predictive quantum chemistry”. In: *J. Phys. Chem.* 93 (1989), pp. 1697–1708 (cit. on p. 96).

[347] A. J. Cohen, P. Mori-Sánchez, and W. Yang. “Challenges for Density Functional Theory”. In: *Chem. Rev.* 112 (2012), pp. 289–320 (cit. on p. 96).

[348] R. O. Ramabhadran and K. Raghavachari. “Extrapolation to the Gold-Standard in Quantum Chemistry: Computationally Efficient and Accurate CCSD(T) Energies for Large Molecules Using an Automated Thermochemical Hierarchy”. In: *J. Chem. Theory Comput.* 9 (2013), pp. 3986–3994 (cit. on p. 96).

[349] N. Mardirossian and M. Head-Gordon. “Thirty years of density functional theory in computational chemistry: an overview and extensive assessment of 200 density functionals”. In: *Mol. Phys.* 115 (2017), pp. 2315–2372 (cit. on p. 96).

[350] R. J. Bartlett and M. Musiał. “Coupled-cluster theory in quantum chemistry”. In: *Rev. Mod. Phys.* 79 (2007), pp. 291–352 (cit. on p. 96).

[351] C. Vallance. *An Introduction to Chemical Kinetics.* 2053-2571. San Rafael, CA: Morgan & Claypool Publishers, 2017 (cit. on pp. 98, 136, 138, 139, 151, 180).

[352] H.-H. Carstensen and A. M. Dean. “Chapter 4 The Kinetics of Pressure-Dependent Reactions”. In: *Comprehensive Chemical Kinetics.* Ed. by R. Carr. Vol. 42. Amsterdam: Elsevier, 2007, pp. 101–184 (cit. on pp. 99, 151).

[353] J. R. Barker, T. L. Nguyen, J. F. Stanton, C. Aieta, M. Ceotto, F. Gabas, T. J. D. Kumar, C. G. L. Li, L. L. Lohr, A. Maranzana, N. F. Ortiz, J. M. Preses, J. M. Simmie, J. A. Sonk, and P. J. Stimac. *MultiWell-2019 Software Suite.* University of Michigan Ann Arbor, Michigan, USA, 2020. URL: `http://clasp-research.engin.umich.edu/multiwell/` (cit. on pp. 99, 151).

[354] J. R. Barker. “Multiple-Well, multiple-path unimolecular reaction systems. I. MultiWell computer program suite”. In: *Int. J. Chem. Kinet.* 33 (2001), pp. 232–245 (cit. on pp. 99, 151, 152).

[355] J. R. Barker. “Energy transfer in master equation simulations: A new approach”. In: *Int. J. Chem. Kinet.* 41 (2009), pp. 748–763 (cit. on pp. 99, 151).

[356] M. J. Pilling and S. H. Robertson. “Master Equation Models for Chemical Reactions of Importance in Combustion”. In: *Annu. Rev. Phys. Chem.* 54 (2003), pp. 245–275 (cit. on pp. 99, 151).

[357] C.-M. Gong, H.-B. Ning, Z.-R. Li, and X.-Y. Li. “Theoretical and kinetic study of reaction $C_2H + C_3H_6$ on the C_5H_7 potential energy surface”. In: *Theor. Chem. Acc.* 134 (2015), p. 1599 (cit. on pp. 100, 152).

[358] L. Zhao, L. Ye, F. Zhang, and L. Zhang. “Thermal Decomposition of 1-Pentanol and Its Isomers: A Theoretical Study”. In: *J. Phys. Chem. A.* 116 (2012), pp. 9238–9244 (cit. on pp. 100, 152).

[359] R. C. Reid, J. M. Prausnitz, and T. K. Sherwood. *The Properties of Gases and Liquids, Third Edition.* New York: McGraw-Hill, Inc, 1977, p. 683 (cit. on pp. 100, 134, 152, 174, 175).

[360] J. R. Welty, C. E. Wicks, R. E. Wilson, and G. L. Rorrer. *Fundamentals of Momentum, Heat, and Mass Transfer, 5th Edition.* Hoboken, NJ: John Wiley & Sons, Inc., 2008, p. 711 (cit. on pp. 100, 133, 134, 152, 174, 175).

[361] H. Wang, E. Dames, B. Sirjean, D. A. Sheen, R. Tango, A. Violi, J. Y. W. Lai, F. N. Egolfopoulos, D. F. Davidson, R. K. Hanson, C. T. Bowman, C. K. Law, W. Tsang, N. P. Cernansky, D. L. Miller, and R. P. Lindstedt. A high-temperature chemical kinetic model of n-alkane (up to n-dodecane), cyclohexane, and methyl-, ethyl-, n-propyl and n-butyl-cyclohexane oxidation at high temperatures, JetSurF version 2.0, September 19, 2010 (http://web.stanford.edu/group/haiwanglab/JetSurF/JetSurF2.0/index.html). (cit. on pp. 100, 134, 152, 174, 175).

[362] Agúndez, M., Venot, O., Iro, N., Selsis, F., Hersant, F., Hébrard, E., and Dobrijevic, M. “The impact of atmospheric circulation on the chemistry of the hot Jupiter HD 209458b”. In: *Astron. Astrophys.* 548 (2012), A73 (cit. on p. 101).

[363] Agúndez, M., Parmentier, V., Venot, O., Hersant, F., and Selsis, F. “Pseudo 2D chemical model of hot-Jupiter atmospheres: application to HD 209458b and HD 189733b”. In: *Astron. Astrophys.* 564 (2014), A73 (cit. on p. 101).

[364] P. B. Rimmer and Ch. Helling. "A Chemical Kinetics Network for Lightning and Life in Planetary Atmospehres". In: *Astrophys. J. Suppl. Ser.* 224.1 (2016), p. 9 (cit. on p. 101).

[365] P. Tremblin, D. S. Amundsen, P. Mourier, I. Baraffe, G. Chabrier, B. Drummond, D. Homeier, and O. Venot. "Fingering Convection and Cloudless Models for Cool Brown Dwarf Atmospheres". In: *Astrophys. J.* 804.1 (2015), p. L17 (cit. on p. 101).

[366] Drummond, B., Tremblin, P., Baraffe, I., Amundsen, D. S., Mayne, N. J., Venot, O., and Goyal, J. "The effects of consistent chemical kinetics calculations on the pressure-temperature profiles and emission spectra of hot Jupiters". In: *Astron. Astrophys.* 594 (2016), A69 (cit. on p. 101).

[367] P. Tremblin, G. Chabrier, N. J. Mayne, D. S. Amundsen, I. Baraffe, F. Debras, B. Drummond, J. Manners, and S. Fromang. "Advection of Potential Temperature in the Atmosphere of Irradiated Exoplanets: A Robust Mechanism to Explain Radius Inflation". In: *Astrophys. J.* 841.1 (2017), p. 30 (cit. on p. 101).

[368] R. Kopparapu, J. F. Kasting, and K. J. Zahnle. "A Photochemical Model for the Carbon-Rich Planet WASP-12b". In: *Astrophys. J.* 745.1 (2011), p. 77 (cit. on p. 101).

[369] Y. Miguel and L. Kaltenegger. "Exploring Atmospheres of Hot Mini-Neptunes and Extrasolar Giant Planets Orbiting Different Stars with Application to HD 97658b, WASP-12b, CoRoT-2b, XO-1b, and H 189733b". In: *Astrophys. J.* 780.2 (2013), p. 166 (cit. on p. 101).

[370] Julianne I. Moses, C. Visscher, J. J. Fortney, A. P. Showman, N. K. Lewis, C. A. Griffith, S. J. Klippenstein, M. Shabram, A. J. Friedson, M. S. Marley, and R. S. Freedman. "Disequilibrium Carbon, Oxygen, and Nitrogen Chemistry in the Atmospheres of HD 189733b and HD 209458b". In: *Astrophys. J.* 737.1 (2011), p. 15 (cit. on p. 101).

[371] J. I. Moses, M. R. Line, C. Visscher, M. R. Richardson, N. Nettelmann, J. J. Fortney, T. S. Barman, K. B. Stevenson, and N. Madhusudhan. "Compositional Diversity in the Atmospheres of Hot Neptunes, with Application to GJ 436b". In: *Astrophys. J.* 777.1 (2013), p. 34 (cit. on p. 101).

[372] J. I. Moses, M. S. Marley, K. Zahnle, M. R. Line, J. J. Fortney, T. S. Barman, C. Visscher, N. K. Lewis, and M. J. Wolff. “On the Composition of Young, Directly Imaged Giant Planets”. In: *Astrophys. J.* 829.2 (2016), p. 66 (cit. on p. 101).

[373] Venot, O., Hébrard, E., Agúndez, M., Decin, L., and Bounaceur, R. “New chemical scheme for studying carbon-rich exoplanet atmospheres”. In: *Astron. Astrophys.* 577 (2015), A33 (cit. on p. 101).

[374] S.-M. Tsai, J. R. Lyons, L. Grosheintz, P. B. Rimmer, D. Kitzmann, and K. Heng. “VULCAN: An Open-source, Validated Chemical Kinetics Python Code for Exoplanetary Atmospheres”. In: *ApJS* 228.2 (2017), p. 20 (cit. on p. 101).

[375] K. Molaverdikhani, Helling, Ch., Lew, B. W. P., MacDonald, R. J., Samra, D., Iro, N., Woitke, P., and Parmentier, V. “Understanding the atmospheric properties and chemical composition of the ultra-hot Jupiter HAT-P-7b - II. Mapping the effects of gas kinetics”. In: *Astron. Astrophys.* 635 (2020), A31 (cit. on pp. 101, 200, 201, 207).

[376] G. Thuillier, L. Floyd, T. N. Woods, R. Cebula, E. Hilsenrath, M. Hersé, and D. Labs. “Solar irradiance reference spectra for two solar active levels”. In: *Adv. Space Res.* 34.2 (2004-01), pp. 256–261 (cit. on pp. 101, 211).

[377] S. M. Hörst, V. Vuitton, and R. V. Yelle. “Origin of oxygen species in Titan’s atmosphere”. In: *J. Geophys. Res. Planets* 113.E10, E10006 (2008-10), E10006 (cit. on pp. 101, 109, 110).

[378] G. M. Provencher and D. J. McKenney. “CN Emission in Active Nitrogen. II. The Role of Energy Transfer and Atom Transfer Reactions in CN($X^2\Sigma^+$) Excitation”. In: *Can. J. Chem.* 50 (1972), pp. 2527–2536 (cit. on pp. 103, 127, 130).

[379] G. E. Bullock and R. Cooper. “Reactions of cyanogen radicals. Part 3.- Arrhenius parameters for reactions with alkanes ”. In: *Phys. Chem. Chem. Phys.* 68 (1972), pp. 2185–2190 (cit. on pp. 105, 106, 108, 126, 136).

[380] J. M. Ribeiro and A. M. Mebel. “Reaction mechanism and rate constants of the $CH + CH_4$ reaction: a theoretical study”. In: *Mol. Phys.* 113 (2015), pp. 1865–1872 (cit. on pp. 106, 137).

[381] M.-A. ter Horst, G. C. Schatz, and L. B. Harding. “Potential energy surface and quasiclassical trajectory studies of the CN+H_2 reaction”. In: *J. Chem. Phys.* 105 (1996), pp. 558–571 (cit. on pp. 126, 136).

[382] S. Zabarnick, J. W. Fleming, and M. C. Lin. “Direct measurement of rate constants for the reactions of CH and CD with HCN and DCN”. In: *Chem. Phys.* 150 (1991), pp. 109–115 (cit. on pp. 127, 130).

[383] N. Basco, J. E. Nicholas, R. G. W. Norrish, and W. H. J. Vickers. “Vibrationally excited cyanogen radicals produced in the flash photolysis of cyanogen and cyanogen halides”. In: *Proc. R. Soc. Lond. A Math. Phys. Eng. Sci.* 272 (1963), pp. 147–163 (cit. on pp. 127, 130).

[384] B. Atakan, D. Kocis, J. Wolfrum, and P. Nelson. “Direct investigations of the kinetics of the reactions of CN radicals with N atoms and $^3CH_2$ radicals with NO”. In: *Twenty-Fourth Symposium (International) on Combustion.* Vol. 24. Seattle: The Combustion Institute, 1992, pp. 691–699 (cit. on pp. 127, 130, 135).

[385] A. R. Whyte and L. F. Phillips. “Rate of reaction of N with CN ($\nu = 0{,}1$)”. In: *Chem. Phys. Lett.* 98 (1983), pp. 590–593 (cit. on pp. 127, 130, 135).

[386] R. L. Brown. “A measurement of the rate of the reaction $N + H + M \longrightarrow NH + M$”. In: *Int. J. Chem. Kinet.* 5 (1973), pp. 663–668 (cit. on pp. 127, 131).

[387] I. R. Slagle, D. Gutman, J. W. Davies, and M. J. Pilling. “Study of the recombination reaction $CH3 + CH3 \longrightarrow C2H6$. 1. Experiment”. In: *J. Phys. Chem.* 92 (1988), pp. 2455–2462 (cit. on pp. 127, 132).

[388] M. T. MacPherson, M. J. Pilling, and M. J. C. Smith. “The pressure and temperature dependence of the rate constant for methyl radical recombination over the temperature range 296-577 K”. In: *Chem. Phys. Lett.* 94 (1983), pp. 430–433 (cit. on pp. 127, 132).

[389] K. H. Becker, B. Engelhardt, P. Wiesen, and K. D. Bayes. “Rate constants for $CH(X^2\Pi)$ reactions at low total pressures”. In: *Chem. Phys. Lett.* 154 (1989), pp. 342–348 (cit. on pp. 127, 133).

[390] W. Tsang. “Chemical Kinetic Data Base for Propellant Combustion. II. Reactions Involving CN, NCO, and HNCO”. In: *J. Phys. Chem. Ref. Data* 21 (1992), pp. 753–791 (cit. on pp. 128, 130, 173).

[391] J. E. Nicholas, A. I. Spiers, and N. A. Martin. “Kinetics and mechanism in the decomposition of NH_3 in a radio-frequency pulse discharge”. In: *Plasma Chem. Plasma Process.* 6 (1986), pp. 39–51 (cit. on pp. 128, 130).

[392] M. González, A. Saracibar, and E. Garcia. “Capture and dissociation in the complex-forming $CH + H_2 \longrightarrow CH_2 + H$, $CH + H_2$ reactions”. In: *Phys. Chem. Chem. Phys.* 13 (2011), pp. 3421–3428 (cit. on pp. 129, 138).

[393] S. Zabarnick and M. C. Lin. “Kinetics of $CN(X^2\Sigma^+)$ radical reactions with HCN, BrCN and CH_3CN”. In: *Chem. Phys.* 134 (1989), pp. 185–191 (cit. on p. 130).

[394] D. L. Yang, T. Yu, and M. C. Lin. “CN radical reactions with hydrogen cyanide and cyanogen: Comparison of theory and experiment”. In: *J. Chem. Phys.* 97 (1992), pp. 222–226 (cit. on p. 130).

[395] X. Li, N. Sayah, and W. M. Jackson. “Laser measurements of the effects of vibrational energy on the reactions of CN”. In: *J. Chem. Phys.* 81 (1984), pp. 833–840 (cit. on p. 130).

[396] C. Anastasi and D. U. Hancock. “Reaction of CN radicals with CH_4 and O_2”. In: *Phys. Chem. Chem. Phys.* 84 (1988), pp. 9–15 (cit. on pp. 130, 136).

[397] D. A. Lichtin and M. C. Lin. “Kinetics of CN radical reactions with selected molecules at room temperature”. In: *Chem. Phys.* 96 (1985), pp. 473–482 (cit. on pp. 130, 136).

[398] B. Atakan and J. Wolfrum. “Kinetic studies of the reactions of CN radicals with alkanes in the temperature range between 294 and 1260 K”. In: *Chem. Phys. Lett.* 186 (1991), pp. 547–552 (cit. on pp. 130, 136).

[399] R. J. Balla and L. Pasternack. “Kinetics of gas-phase CN by diode laser absorption”. In: *J. Phys. Chem.* 91 (1987), pp. 73–78 (cit. on pp. 130, 136).

[400] L. R. Copeland, F. Mohammad, M. Zahedi, D. H. Volman, and W. M. Jackson. “Rate constants for CN reactions with hydrocarbons and the product HCN vibrational populations: Examples of heavy-light-heavy abstraction reactions”. In: *J. Chem. Phys.* 96 (1992), pp. 5817–5826 (cit. on pp. 130, 136).

[401] I. R. Sims, J.-L. Queffleс, D. Travers, B. R. Rowe, L. B. Herbert, J. Karthäuser, and I. W. M. Smith. "Rate constants for the reactions of CN with hydrocarbons at low and ultra-low temperatures". In: *Chem. Phys. Lett.* 211 (1993), pp. 461–468 (cit. on pp. 130, 136).

[402] L. B. Herbert, I. W. M. Smith, and R. D. Spencer-Smith. "Rate constants for the elementary reactions between CN radicals and CH_4, C_2H_6, C_2H_4, C_3H_6, and C_2H_2 in the range: $295 \leq T/K \leq 700$". In: *Int. J. Chem. Kinet.* 24 (1992), pp. 791–802 (cit. on pp. 130, 136).

[403] D. L. Yang, T. Yu, M. C. Lin, and C. F. Melius. "The reaction of CN with CH_4 and CD_4: an experimental and theoretical study". In: *Chem. Phys.* 177 (1993), pp. 271–280 (cit. on pp. 130, 136).

[404] N. Sayah, X. Li, and W. M. Jackson. "Laser induced fluorescence studies of CN reactions with alkanes, alkenes and substituted aliphatic species". In: *J Photochem. Photobiol. A Chem.* 45 (1988), pp. 177–194 (cit. on pp. 130, 136).

[405] N. Choi, M. A. Blitz, K. McKee, M. J. Pilling, and P. W. Seakins. "H atom branching ratios from the reactions of CN radicals with C_2H_2 and C_2H_4". In: *Chem. Phys. Lett.* 384 (2004), pp. 68–72 (cit. on pp. 130, 136).

[406] G. He, I. Tokue, and R. G. MacDonald. "Thermal Rate Constant for CN + $H_2/D_2 \rightarrow$ HCN/DCN + H/D Reaction from T = 293 to 380 K". In: *J. Phys. Chem A* 102 (1998), pp. 4585–4591 (cit. on pp. 130, 136).

[407] Q. Sun, D. L. Yang, N. S. Wang, J. M. Bowman, and M. C. Lin. "Experimental and reduced dimensionality quantum rate coefficients for $\mathrm{H2(D2) + CN \longrightarrow H(D)CN + H(D)}$". In: *J. Chem. Phys.* 93 (1990), pp. 4730–4739 (cit. on pp. 130, 136).

[408] I. R. Sims and I. W. M. Smith. "Rate constants for the reactions $\mathrm{CN(v{=}0), CN(v{=}1) + H2, D2 \longrightarrow HCN, DCN + H, D}$ between 295 and 768 K, and comparisons with transition state theory calculations". In: *Chem. Phys. Lett.* 149 (1988), pp. 565–571 (cit. on pp. 130, 136).

[409] J. De Juan, I. W. M. Smith, and B. Veyret. "Pulsed photolysis-laser-induced fluorescence measurements of the rate constants for reactions of the cyanogen radical with hydrogen, oxygen, ammonia, hydrogen chloride, hydrogen bromide,

and hydrogen iodide". In: *J. Phys. Chem.* 91 (1987), pp. 69–72 (cit. on pp. 130, 136).

[410] B. Atakan, A. Jacobs, M. Wahl, R. Weller, and J. Wolfrum. "Kinetic studies of the gas-phase reactions of CN with O_2 and H_2 from 294 to 1000 K". In: *Chem. Phys. Lett.* 154 (1989), pp. 449–453 (cit. on pp. 130, 136).

[411] A. Jacobs, M. Wahl, R. Weller, and J. Wolfrum. "Measurements of absolute rate coefficients for the reactions of CN radicals with H_2O, H_2, and CO_2 in the temperature range 295 $K \leq T \leq 1027$ K". In: *Twenty-Second Symposium (International) on Combustion.* Vol. 22. Seattle: The Combustion Institute, 1989, pp. 1093–1100 (cit. on pp. 130, 136).

[412] V. A. Emelkin and V. V. Marusin. "ESR investigation of the interaction of atomic nitrogen with chlorine". In: *Kinet. Catal.* 19 (1978), p. 1123 (cit. on p. 131).

[413] W. Brennen and E. C. Shane. "Nitrogen afterglow and the rate of recombination of nitrogen atoms in the presence of nitrogen, argon, and helium". In: *J. Phys. Chem.* 75 (1971), pp. 1552–1564 (cit. on p. 131).

[414] V. A. Emelkin and V. V. Marusin. "ESR study of the recombination of nitrogen atoms in the afterglow". In: *Kinet. Catal.* 19 (1978), p. 1118 (cit. on p. 131).

[415] K. M. Evenson and D. S. Burch. "Atomic-Nitrogen Recombination". In: *J. Chem. Phys.* 45 (1966), pp. 2450–2460 (cit. on p. 131).

[416] P. Harteck, R. R. Reeves, and G. Mannella. "Rate of Recombination of Nitrogen Atoms". In: *J. Chem. Phys.* 29 (1958), pp. 608–610 (cit. on p. 131).

[417] M. A. A. Clyne and D. H. Stedman. "Rate of recombination of nitrogen atoms". In: *J. Phys. Chem.* 71 (1967), pp. 3071–3073 (cit. on p. 131).

[418] I. M. Campbell and B. A. Thrush. "Behaviour of carbon dioxide and nitrous oxide in active nitrogen". In: *Trans. Faraday Soc.* 62 (1966), pp. 3366–3374 (cit. on pp. 131, 165, 173).

[419] I. M. Campbell and B. A. Thrush. "The recombination of nitrogen atoms and the nitrogen afterglow". In: *Proc. R. Soc. Lond. A Math. Phys. Eng. Sci.* 296 (1967), pp. 201–221 (cit. on p. 131).

[420] R. M. Lambert, M. I. Christie, R. C. Golesworthy, and J. W. Linnett. "Mass spectrometric study of the reaction of nitrogen atoms with acetaldehyde". In: *Proc. R. Soc. Lond. A Math. Phys. Eng. Sci.* 302 (1968), pp. 167–183 (cit. on p. 131).

[421] C. B. Kretschmer and H. L. Petersen. "Kinetics of Three-Body Atom Recombination". In: *J. Chem. Phys.* 39 (1963), pp. 1772–1778 (cit. on pp. 131, 173).

[422] C. Mavroyannis and C. A. Winkler. "The reaction of nitrogen atoms with hydrogen atoms". In: *Can. J. Chem.* 40 (1962), pp. 240–245 (cit. on p. 131).

[423] G. L. Pratt and I. Veltman. "Addition of ethyl radicals to nitric oxide". In: *Phys. Chem. Chem. Phys.* 70 (1974), pp. 1840–1850 (cit. on p. 132).

[424] G. L. Pratt and S. W. Wood. "Kinetics of the reaction of methyl radicals with oxygen". In: *Phys. Chem. Chem. Phys.* 80 (1984), pp. 3419–3427 (cit. on p. 132).

[425] J. Grebe and K. H. Homann. "Blue-green Chemiluminescence in the System $C_2H_2/O/H$. Formation of the Emitters $CH(A^2\Delta)$, $C2(d^3\Pi_g)$ and C_2H^*". In: *BBGPC* 86 (1982), pp. 587–597 (cit. on p. 133).

[426] H. Eberius, K. Hoyermann, and H. Gg. Wagner. "Zur Reaktion $H + H + H_2O \longrightarrow H_2 + H_2O$". In: *BBGPC* 73 (1969), pp. 962–966 (cit. on p. 133).

[427] L. P. Walkauskas and F. Kaufman. "Gas phase hydrogen atom recombination". In: *Fifteenth Symposium (International) on Combustion.* Vol. 15. Seattle: The Combustion Institute, 1975, pp. 691–699 (cit. on p. 133).

[428] K. P. Lynch, T. C. Schwab, and J. V. Michael. "Lyman-α absorption photometry at high pressure and atom density kinetic results for H recombination". In: *Int. J. Chem. Kinet.* 8 (1976), pp. 651–671 (cit. on p. 133).

[429] J. E. Bennett and D. R. Blackmore. "Rates of gas-phase hydrogen-atom recombination at room temperature in the presence of added gases". In: *Thirteenth Symposium (International) on Combustion.* Vol. 13. Seattle: The Combustion Institute, 1971, pp. 51–59 (cit. on pp. 133, 170).

[430] D. W. Trainor, D. O. Ham, and F. Kaufman. "Gas phase recombination of hydrogenand deuterium atoms". In: *J. Chem. Phys.* 58 (1973), pp. 4599–4609 (cit. on p. 133).

[431] D. N. Mitchell and D. J. LeRoy. "An experimental test of the orbiting resonance theory of hydrogen atom recombination at room temperature". In: *J. Chem. Phys.* 67 (1977), pp. 1042–1050 (cit. on p. 133).

[432] L. Teng and C. A. Winkler. "The Rate of Recombination of H Atoms in the Presence of NH_3". In: *Can. J. Chem.* 51 (1973), pp. 3771–3773 (cit. on p. 133).

[433] N. Cohen and K. R. Westberg. "Chemical Kinetic Data Sheets for High-Temperature Chemical Reactions". In: *J. Phys. Chem. Ref. Data* 12 (1983), pp. 531–590 (cit. on pp. 133, 173).

[434] D.-C. Che and K. Liu. "A crossed-beam study of the reaction of CN + D_2. Is CN really a spectator bond?" In: *Chem. Phys. Lett.* 243 (1995), pp. 290–296 (cit. on p. 136).

[435] L. B. Harding, R. Guadagnini, and G. C. Schatz. "Theoretical Studies of the Reactions $H + CH \longrightarrow C + H_2$ and $C + H_2 \longrightarrow CH_2$ Using an ab Initio Global Ground-State Potential Surface for CH_2". In: *J. Phys. Chem.* 97 (1993), pp. 5472–5481 (cit. on p. 139).

[436] S. L. Miller and J. E. Van Trump. "The Strecker synthesis in the primitive ocean". In: *Origin of Life.* Ed. by Y. Wolman. Dordrecht, The Netherlands: Reidel, 1981, pp. 135–141 (cit. on p. 142).

[437] J. A. Schmidt, M. S. Johnson, and R. Schinke. "Carbon dioxide photolysis from 150 to 210 nm: Singlet and triplet channel dynamics, UV-spectrum, andisotope effects". In: *Proc. Nat. Acad. Sci. U.S.A.* 110 (2013), pp. 17691–17696 (cit. on p. 143).

[438] V. Engel, V. Staemmler, R. L. Vander Wal, F. F. Crim, R. J. Sension, B. Hudson, P. Andreson, S. Hennig, K. Weide, and R. Schinke. "Photodissociation of water in the first absorption band: a prototype for dissociation on a repulsive potential energy surface". In: *J. Phys. Chem.* 96 (1992), pp. 3201–3213 (cit. on p. 143).

[439] T. P. Stecher and D. A. Williams. "Photodestruction of Hydrogen Molecules in H I Regions". In: *Astrophys. J. Lett.* 149 (1967-07), p. L29. DOI: `10.1086/180047` (cit. on p. 143).

[440] B. K. D. Pearce, K. Molaverdikhani, R. E. Pudritz, Th. Henning, and E. Hébrard. "HCN production in Titan's Atmosphere: Coupling quantum chemistry and disequilibrium atmospheric modeling". In: *Astrophys. J* 901 (2020), p. 110 (cit. on pp. 144–148, 159, 162, 188, 196, 200, 201, 207–209, 313).

[441] M. D. Hanwell, D. E. Curtis, D. C. Lonie, T. Vandermeersch, E. Zurek, and G. R. Hutchison. "Avogadro: An advanced semantic chemical editor, visualization, and analysis platform". In: *J. Cheminform.* 4 (2012), p. 17 (cit. on p. 148).

[442] J. Caldwell and R. A. Back. "Combination reactions of hydroxyl radicals in the flash photolysis of water vapour". In: *Trans. Faraday Soc.* 61 (1965), pp. 1939–1945 (cit. on pp. 153, 171).

[443] G. Black and G. Porter. "Vacuum ultra-violet flash photolysis of water vapour". In: *Proc. R. Soc. Lond. A Math. Phys. Sci.* 266 (1962), pp. 185–197 (cit. on pp. 153, 171).

[444] *Kinetics of the recombination reaction* $OH + H + M \rightarrow H_2O + M$ *at low temperatures.* Vol. 16. Seattle: The Combustion Institute, 1977, pp. 939–948 (cit. on pp. 153, 165, 172, 173).

[445] G. Bravo-Pérez, J. R. Alvarez-Idaboy, A. G. Jiménez, and A. Cruz-Torres. "Quantum chemical and conventional TST calculations of rate constants for the OH + alkane reaction". In: *Chem. Phys.* 310 (2005), pp. 213–223 (cit. on p. 156).

[446] C. Mehlmann, M. J. Frost, D. E. Heard, B. J. Orr, and P. F. Nelson. "Rate constants for removal of CH(D) ($\nu = 0$ and 1) by collisions with N_2, CO, O_2, NO and NO_2 at 298 K and with CO_2 at $296 \leq T/K \leq 873$". In: *J. Chem. Soc., Faraday Trans.* 92 (1996), pp. 2335–2341 (cit. on pp. 158, 169, 170, 177).

[447] M. A. Blitz, M. Pesa, M. J. Pilling, and P. W. Seakins. "Reaction of CH with H_2O: Temperature Dependence and Isotope Effect". In: *J. Phys. Chem. A* 103 (1999), pp. 5699–5704 (cit. on pp. 158, 167, 171).

[448] N. Cohen and K. R. Westberg. "Chemical Kinetic Data Sheets for High-Temperature Reactions. Part II". In: *J. Phys. Chem. Ref. Data* 20 (1991), pp. 1211–1311 (cit. on pp. 158, 172, 173, 181).

[449] *Dynamics and mechanisms of CO production from the reactions of CH_2 radicals with $O(^3P)$ and O_2.* Vol. 18. Seattle: The Combustion Institute, 1981, pp. 811–818 (cit. on pp. 158, 184).

[450] J. Meisner and J. Kästner. "Atom Tunneling in Chemistry". In: *Angew Chem Int Ed Engl* 55 (2016), pp. 5400–5413 (cit. on p. 159).

[451] M. Clerc and F. Barat. "Kinetics of CO Formation Studied by Far-uv Flash Photolysis of CO_2". In: *J. Chem. Phys.* 46 (1967), pp. 107–110 (cit. on pp. 165, 170).

[452] C. J. Hochanadel, T. J. Sworski, and P. J. Ogren. "Ultraviolet spectrum and reaction kinetics of the formyl radical". In: *J. Phys. Chem.* 84 (1980), pp. 231–235 (cit. on pp. 165, 170, 171).

[453] B. Nizamov and P. J. Dagdigian. "Spectroscopic and Kinetic Investigation of Methylene Amidogen by Cavity Ring-Down Spectroscopy". In: *J. Phys. Chem. A* 107 (2003), pp. 2256–2263 (cit. on pp. 165, 171).

[454] E. J. Dunlea and A. R. Ravishankara. "Kinetic studies of the reactions of $O(^1D)$ with several atmospheric molecules". In: *Phys. Chem. Chem. Phys.* 6 (2004), pp. 2152–2161 (cit. on pp. 166, 167, 169, 176).

[455] T. Yu, D. L. Yang, and M. C. Lin. "Kinetics of CN radical reactions with formaldehyde and 1,3,5-trioxane". In: *Int. J. Chem. Kinet.* 25 (1993), pp. 1053–1064 (cit. on pp. 166, 169).

[456] M. J. Yee Quee and J. C. J. Thynne. "The Photolysis of Organic Esters". In: *Ber. Bunsenges. Phys. Chem.* 72 (1968), pp. 211–217 (cit. on pp. 166, 169, 170, 178, 179).

[457] L. F. Phillips. "Rate of Reaction of OH with HCN Between 298 and 563 K". In: *Aust. J. Chem.* 32 (1979), pp. 2571–2577 (cit. on pp. 167, 171).

[458] E.-J. Dunlea and A. R. Ravishankara. "Kinetic studies of the reactions of $O(^1D)$ with several atmospheric molecules". In: *Phys. Chem. Chem. Phys.* 6 (2004), pp. 2152–2161 (cit. on p. 168).

[459] S. Vranckx, J. Peeters, and S. Carl. "Kinetics of $O(^1D) + H_2O$ and $O(^1D) + H_2$: absolute rate coefficients and $O(^3P)$ yields between 227 and 453 K". In: *Phys. Chem. Chem. Phys.* 12 (2010), pp. 9213–9221 (cit. on p. 168).

[460] R. A. Young, G. Black, and T. G. Slanger. "Reaction and Deactivation of $O(^1D)^*$". In: *J. Chem. Phys.* 49 (1968), pp. 4758–4768 (cit. on pp. 168, 170, 175, 176).

[461] M. A. Blitz, T. J. Dillon, D. E. Heard, M. J. Pilling, and I. D. Trought. "Laser induced fluorescence studies of the reactions of $O(^1D_2)$ with N_2, O_2, N_2O, CH_4, H_2, CO_2, Ar, Kr and n-C_4H_10". In: *Phys. Chem. Chem. Phys.* 6 (2004), pp. 2162–2171 (cit. on pp. 169, 174, 176, 185).

[462] P. H. Wine and A. R. Ravishankara. "Kinetics of $O(^1D)$ interactions with the atmospheric gases N_2, N_2O, H_2O, H_2, CO_2, and O_3". In: *Chem. Phys. Lett.* 77 (1981), pp. 103–109 (cit. on pp. 169, 176).

[463] R. A. Young and A. Y.-M. Ung. "Optical Studies of the Photolysis of CO_2 at 1470 Å". In: *J. Chem. Phys.* 44 (1966), pp. 3038–3040 (cit. on p. 169).

[464] R. F. Heidner, III, D. Husain, and J. R. Wiesenfeld. "Kinetic Investigation of Electronically Excited Oxygen Atoms, $O(2^1D_2)$, by Time-resolved Attenuation of Atomic Resonance Radiation in the Vacuum Ultra-violet ". In: *J. Chem. Soc., Faraday Trans. 2* 69 (1973), pp. 927–938 (cit. on pp. 169–171, 175, 176).

[465] S. T Amimoto, A. P. Force, R. G. Gulotty, Jr., and J .R. Wiesenfeld. "Collisional deactivation of $O(2^1D_2)$ by the atmospheric gases". In: *J. Chem.Phys.* 71 (1979), pp. 3640–3647 (cit. on pp. 169, 175, 176).

[466] J. A Davidson, C. M. Sadowski, H. I. Schiff, G .E. Streit, C. J. Howard, and A. L. Jennings D. A. Schmeltekopf. "Absolute rate constant determinations for the deactivation of $O(^1D)$ by time resolved decay of $O(^1D) \longrightarrow O(^3P)$ emission". In: *J. Chem.Phys.* 64 (1976), pp. 57–62 (cit. on pp. 169, 171, 175, 176).

[467] C.-L. Lin and F. Kaufman. "Reactions of Metastable Nitrogen Atoms". In: *J. Chem.Phys.* 55 (1971), pp. 3760–3770 (cit. on pp. 169, 176).

[468] A. H. Laufer and A. M. Bass. "Reaction between triplet methylene and CO_2: rate constant determination". In: *Chem. Phys. Lett.* 46 (1977), pp. 151–155 (cit. on pp. 169, 177).

[469] D. R. Crosley, ed. *Kinetics of CH Radical Reactions Important to Hydrocarbon Combustion Systems.* Vol. 134. ACS Symposium Series. 1980, pp. 397–401 (cit. on pp. 169, 177).

[470] J. E. Butler, J. W. Fleming, L. P. Goss, and M. C. Lin. “Kinetics of CH radical reactions with selected molecules at room temperature”. In: *Chem. Phys.* 56 (1981), pp. 355–365 (cit. on pp. 169, 170, 177).

[471] *Temperature dependence of CH radical reactions with O_2, NO, CO and CO_2*. Vol. 19. 1982, pp. 73–79 (cit. on pp. 169, 170, 177).

[472] H. Niki, P. D. Maker, C. M. Savage, and L. P. Breitenbach. “Relative rate constants for the reaction of hydroxyl radical with aldehydes”. In: *J. Phys. Chem.* 82 (1978), pp. 132–134 (cit. on p. 169).

[473] S. Zabarnick, J. W. Fleming, and M. C. Lin. “Kinetics of hydroxyl radical reactions with formaldehyde and 1,3,5-trioxane between 290 and 600 K”. In: *Int. J. Chem. Kinet.* 20 (1988), pp. 117–129 (cit. on p. 169).

[474] L. J. Stief, D. F. Nava, W. A. Payne, and J. V. Michael. “Rate constant for the reaction of hydroxyl radical with formaldehyde over the temperature range 228-362 K”. In: *J. Phys. Chem.* 73 (1980), pp. 2254–2258 (cit. on p. 169).

[475] R. Atkinson and J. N. Pitts Jr. “Kinetics of the reactions of the OH radical with HCHO and CH_3CHO over the temperature range 299-426K”. In: *J. Chem. Phys.* 68 (1978), pp. 3581–3584 (cit. on p. 169).

[476] H. Niki, P. D. Maker, C. M. Savage, and L. P. Breitenbach. “An Fourier transform infrared study of the kinetics and mechanism for the reaction of hydroxyl radical with formaldehyde”. In: *J. Phys. Chem.* 88 (1984), pp. 5342–5344 (cit. on p. 169).

[477] F. Temps and H. Gg. Wagner. “Rate Constants for the Reactions of OH-Radicals with CH_2O and HCO”. In: *Ber. Bunsenges. Phys. Chem.* 88 (1984), pp. 415–418 (cit. on pp. 169, 170).

[478] R. A. Yetter, H. Rabitz, and F. L. Dryer. “Evaluation of the rate constant for the reaction $OH + H_2CO$: Application of modeling and sensitivity analysis techniques for determination of the product branching ratio”. In: *J. Chem. Phys.* 91 (1989), pp. 4088–4097 (cit. on p. 169).

[479] *Reaction mechanisms of combustion in low pressure acetylene-oxygen flames*. Vol. 16. 1977, pp. 1133–1144 (cit. on p. 169).

[480] J. S. Chang and J. R. Barker. "Reaction rate and products for the reaction oxygen(^{3}P) + H_2CO". In: *J. Phys. Chem.* 83 (1979), pp. 3059–3064 (cit. on p. 169).

[481] R. B. Klemm. "Absolute rate parameters for the reactions of formaldehyde with O atoms and H atoms over the temperature range 250–500 K". In: *J. Chem. Phs.* 71 (1979), pp. 1987–1993 (cit. on p. 169).

[482] R. B. Klemm, E. G. Skolnik, and J. V. Michael. "Absolute rate parameters for the reaction of O(^{3}P) with H_2CO over the temperature range 250 to 750 K". In: *J. Chem. Phys.* 72 (1980), pp. 1256–1264 (cit. on p. 169).

[483] J. T. Herron and R. D. Penzhorn. "Mass spectrometric study of the reactions of atomic oxygen with ethylene and formaldehyde". In: *J. Phys. Chem.* 73 (1969), pp. 191–196 (cit. on p. 169).

[484] G. P. R. Mack and B. A. Thrush. "Reaction of oxygen atoms with carbonyl compounds. Part 1.–Formaldehyde". In: *J. Chem. Soc., Faraday Trans. 1* 69 (1973), pp. 208–215 (cit. on p. 169).

[485] *Temperature dependence of CH radical reactions with H_2O and CH_2O.* Vol. 21. 1988, pp. 713–719 (cit. on p. 169).

[486] B. A. Ridley, J. A. Davenport, L. J. Stief, and K. H. Welge. "Absolute Rate Constant for the Reaction $H+H_2CO$". In: *J. Chem. Phys.* 57 (1972), pp. 520–523 (cit. on p. 169).

[487] W. R. Brennen, I. D. Gay, G. P. Glass, and H. Niki. "Reaction of atomic hydrogen with formaldehyde". In: *J. Chem. Phys.* 43 (1965), pp. 2569–2570 (cit. on p. 169).

[488] C. Oehlers, H. Gg. Wagner, H. Ziemer, and S. Dóbé. "An Investigation of the D/H Addition-Elimination and H Atom Abstraction Channels in the Reaction $D + H_2CO$ in the Temperature Range 296 K $\leq$ T $\leq$ 780 K". In: *J. Phys. Chem. A* 104 (2000), pp. 10500–10510 (cit. on p. 169).

[489] J. Vandooren, L. Oldenhove de Guertechin, and P. J. Van Tiggelen. "Kinetics in a lean formaldehyde flame". In: *Combust. Flame* 64 (1986), pp. 127–139 (cit. on p. 169).

[490] A. A. Westenberg and N. DeHaas. "Measurement of the rate constant for $H + H_2CO \longrightarrow H_2 + HCO$ at 297-652K". In: *J. Phys. Chem.* 76 (1972), pp. 2213–2214 (cit. on p. 169).

[491] F. Stoeckel, M. D. Schuh, N. Goldstein, and G. H. Atkinson. "Time-resolved intracavity laser spectroscopy: 266 nm photodissociation of acetaldehyde vapor to form HCO". In: *Chem. Phys.* 95 (1985), pp. 135–144 (cit. on pp. 169, 178).

[492] J. E. Baggott, H. M. Frey, P. D. Lightfoot, and R. Walsh. "The absorption cross section of the HCO radical at 614.59 nm and the rate constant for HCO+HCO -> H_2CO+CO". In: *Chem. Phys. Lett.* 132 (1986), pp. 225–230 (cit. on pp. 169, 178).

[493] J. P. Reilly, J. H. Clark, J. B. Moore, and G. C. Pimentel. "HCO production, vibrational relaxation, chemical kinetics, and spectroscopy following laser photolysis of formaldehyde". In: *J. Chem. Phys.* 69 (1978), pp. 4381–4394 (cit. on pp. 169, 170, 178).

[494] G. Friedrichs, J. T. Herbon, D. F. Davidson, and R. K. Hanson. "Quantitative detection of HCO behind shock waves: The thermal decomposition of HCO". In: *Phys. Chem. Chem. Phys.* 4 (2002), pp. 5778–5788 (cit. on pp. 169, 170, 178).

[495] B. Veyret, P. Roussel, and R. Lesclaux. "Absolute rate constant for the disproportionation reaction of formyl radicals from 295 to 475 K". In: *Chem. Phys. Lett.* 103 (1984), pp. 389–392 (cit. on pp. 169, 178).

[496] V. Vedeneev, E. Sviridenkov, V. Nadtocenko, S. Ceskis, and O. Sarkisov. "Spectroscopic study of elementary reactions involving HCO, NH_2 and HNO". In: *J. Chem. Phys.* 4 (1984), pp. 111–120 (cit. on pp. 170, 178).

[497] S. A. Mulenko. "Investigation of the recombination of the hco radical in an atmosphere of argon and helium by the method of internal resonator laser spectroscopy". In: *J. Appl. Spectrosc.* 33 (1980), pp. 688–694 (cit. on p. 170).

[498] H. Ziemer, S. Dobé, H. Gg. Wagner, M. Olzman, B. Viskolcz, and F. Temps. "Kinetics of the reactions of HCO with H and D atoms". In: *Ber. Bunsenges. Phys. Chem.* 102 (1998), pp. 897–905 (cit. on p. 170).

[499] R. Forster, M. Frost, D. Fulle, H. F. Hamann, H. Hippler, A. Schlepegrell, and J. Troe. "High pressure range of the addition of HO to HO, NO, NO_2, and CO. I. Saturated laser induced fluorescence measurements at 298 K". In: *J. Chem. Phys.* 103 (1995), pp. 2949–2958 (cit. on pp. 170, 171, 179).

[500] H. Niki, P. D. Maker, C. M. Savage, and L. P. Breitenbach. "Fourier transform infrared spectroscopic study of the kinetics for the OH radical reaction of $^{13}C^{16}O$ and $^{12}C^{18}O$". In: *J. Phys. Chem.* 88 (1984), pp. 2116–2119 (cit. on pp. 170, 179).

[501] M. J. Frost, P. Sharkey, and I. W. M. Smith. "Reaction between OH (OD) radicals and CO at temperatures down to 80 K: experiment and theory". In: *J. Phys. Chem.* 97 (1993), pp. 12254–12259 (cit. on pp. 170, 179).

[502] B. Bohn and C. Zetzsch. "Formation of HO_2 from OH and C_2H_2 in the presence of O_2". In: *J. Chem. Soc., Faraday Trans.* 94 (1998), pp. 1203–1210 (cit. on pp. 170, 179).

[503] J. T. Herron. "Reaction kinetics involving ground $X^2\Pi$ and excited $A^2\Sigma^+$ hydroxyl radicals. Part 1.-Quenching kinetics of OH $A^2\Sigma^+$ and rate constants for reactions of OH $X^2\Pi$ with CH_3CCl_3 and CO". In: *J. Chem. Soc., Faraday Trans. 2* 75 (1979), pp. 569–581 (cit. on pp. 170, 179).

[504] D. Husain, J. M. C. Plane, and N. K. H. Slater. "Kinetic investigation of the reactions of $OH(X^2\Pi)$ with the hydrogen halides, HCl, DCl, HBr and DBr by time-resolved resonance fluorescence ($A^2\Sigma^+$-$X^2\Pi$) ". In: *J. Chem. Soc., Faraday Trans. 2* 77 (1981), pp. 1949–1962 (cit. on pp. 170, 179).

[505] V. Lissianski, H. Yang, Z. Qin, M. R. Mueller, K. S. Shin, and W. C. Gardiner Jr. "High-temperature measurements of the rate coefficient of the $H + CO_2 \rightarrow CO + OH$ reaction". In: *Chem. Phys. Lett.* 240 (1995), pp. 57–62 (cit. on pp. 170, 179).

[506] A. R. Ravishankara and R. L. Thompson. "Kinetic study of the reaction of OH with CO from 250 to 1040 K". In: *Chem. Phys. Lett.* 99 (1983), pp. 377–381 (cit. on pp. 170, 179).

[507] M. J. Frost, P. Sharkey, and I. W. M. Smith. "Energy and structure of the transition states in the reaction $OH + CO \rightarrow H + CO_2$". In: *Faraday Discuss. Chem. Soc.* 91 (1991), pp. 305–317 (cit. on pp. 170, 179).

[508] J. T. Herron. “Mass-Spectrometric Study of the Rate of the Reaction CO + OH”. In: *J. Chem. Phys.* 45 (1966), pp. 1854–1855 (cit. on pp. 170, 179).

[509] J. A. Davidson, H. I. Schiff, T. J. Brown, and C. J. Howard. “Temperature dependence of the deactivation of O(^{1}D) by CO from 113-333 K”. In: *J. Chem. Phys.* 69 (1978), pp. 1216–1217 (cit. on p. 170).

[510] J. F. Noxon. “Optical Emission from O(^{1}D)and $O_2(b^1\Sigma_g)$ in Ultraviolet Photolysis of O_2 and CO_2”. In: *J. Chem. Phys.* 52 (1970), pp. 1852–1873 (cit. on p. 170).

[511] S. D. Le Picard, A. Canosa, B. R. Rowe, R. A. Brownsword, and I. W. M. Smith. “Determination of the limiting low pressure rate constants of the reactions of CH with N2 and CO: a CRESU measurement at 53 K”. In: *J. Chem. Soc., Faraday Trans.* 94 (1998), pp. 2889–2893 (cit. on p. 170).

[512] R. A. Brownsword, L. B. Herbert, I. W. M. Smith, and D. W. A. Stewart. “Pressure and temperature dependence of the rate constants for the association reactions of CH radicals with CO and N_2 between 202 and 584 K”. In: *J. Chem. Soc., Faraday Trans.* 92 (1996), pp. 1087–1094 (cit. on p. 170).

[513] D. Fulle, H. Hippler, and F. Striebel. “The high-pressure range of the reaction CH($^2\Pi$) + CO + M $\longrightarrow$ HCCO + M”. In: *J. Chem. Phys.* 108 (1998), pp. 6709–6716 (cit. on p. 170).

[514] C. A. Taatjes. “Association and isotopic exchange reactions of CH(CD)[$X^2\Pi$]+CO ”. In: *J. Chem. Phys.* 106 (1997), pp. 1786–1795 (cit. on p. 170).

[515] H. Y. Wang, J. A. Eyre, and L. M. Dorfman. “Activation energy for the gas phase reaction of hydrogen atoms with carbon monoxide”. In: *J. Chem. Phys.* 59 (1973), pp. 5199–5200 (cit. on p. 170).

[516] T. Hikida, J. A. Eyre, and L. M. Dorfman. “Pulse Radiolysis Studies. XX. Kinetics of Some Addition Reactions of Gaseous Hydrogen Atoms by Fast Lyman-α Absorption Spectrophotometry ”. In: *J. Chem. Phys.* 54 (1971), pp. 3422–3428 (cit. on p. 171).

[517] J. J. Ahumada, J. V. Michael, and D. T. Osborne. “Pressure Dependence and Third Body Effects on the Rate Constants for H+O_2,H+NO, and H+CO”. In: *J. Chem. Phys.* 57 (1972), pp. 3736–3745 (cit. on p. 171).

[518] M. J. E. Gauthier and D. R. Snelling. “La photolyse de l′ozone a 253.7 nm: Desactivation de $O(^1D)$ et de $O_2(^1\Sigma)$ par les gaz de l′atmosphere”. In: *J. Photochem.* 4 (1975), pp. 27–50 (cit. on pp. 171, 174, 185).

[519] L. C. Lee and T. G. Slanger. “Atmospheric OH production-The $O(^1D) + H_2O$ reaction rate”. In: *Geophys. Res. Lett.* 6 (1979), pp. 165–166 (cit. on p. 171).

[520] J. A. Davidson, H. I. Schiff, G. E. Streit, J. R. McAfee, A. L. Schmeltekopf, and C. J. Howard. “Temperature dependence of $O(^1D)$ rate constants for reactions with N_2O, H_2, CH_4, HCl, and NH_3”. In: *J. Chem. Phys.* 67 (1977), pp. 5021–5025 (cit. on p. 171).

[521] G. E. Streit, C. J. Howard, A. L. Schmeltekopf, J. A. Davidson, and H. I. Schiff. “Temperature dependence of $O(^1D)$ rate constants for reactions with O_2, N_2, CO_2, O_3, and H_2O”. In: *J. Chem. Phys.* 65 (1976), pp. 4761–4764 (cit. on p. 171).

[522] E.-J. Dunlea and A. R. Ravishankara. “Measurement of the rate coefficient for the reaction of $O(^1D)$ with H_2O and re-evaluation of the atmospheric OH production rate”. In: *Phys. Chem. Chem. Phys.* 6 (2004), pp. 3333–3340 (cit. on p. 171).

[523] K.-H. Geriicke and F. J. Comes. “Energy partitioning in the reaction $O(^1D) + H_2O \longrightarrow OH + OH$.: The influence of $O(^1D)$ translational energy on the reaction rate constant”. In: *Chem. Phys. Lett.* 81 (1981), pp. 218–222 (cit. on p. 171).

[524] B. Versino and H. Ott, eds. *Laboratory Kinetic Investigations of the Tropospheric Oxidation of Selected Industrial Emissions.* Dordrecht: D. Reidel Publishing Company, 1982 (cit. on p. 171).

[525] R. Zellner, F. Ewig, R. Paschke, and G. Wagner. “Pressure and temperature dependence of the gas-phase recombination of hydroxyl radicals”. In: *J. Phys. Chem.* 92 (1988), pp. 4184–4190 (cit. on p. 171).

[526] M. Sangwan, E. N. Chesnokov, and L. N. Krasnoperov. “Reaction OH + OH Studied over the 298-834 K Temperature and 1 - 100 bar Pressure Ranges”. In: *J. Phys. Chem. A* 116 (2012), pp. 6282–6294 (cit. on p. 171).

[527] *Energy partitioning in the products of elementary reactions involving OH-radicals.* Vol. 15. 1975, pp. 755–764 (cit. on p. 171).

[528] D. W. Trainor and C. W. von Rosenberg Jr. "Flash photolysis study of the gas phase recombination of hydroxyl radicals". In: *J. Chem. Phys.* 61 (1974), pp. 1010–1015 (cit. on p. 171).

[529] N. R. Greiner. "Hydroxyl radical kinetics by kinetic spectroscopy. III. Reactions with hydrogen peroxide in the range 300-458 K". In: *J. Phys. Chem.* 72 (1968), pp. 406–410 (cit. on p. 171).

[530] D. Fulle, H. F. Hamann, H. Hippler, and J. Troe. "High-pressure range of the addition of HO to HO. III. Saturated laser-induced fluorescence measurements between 200 and 700 K". In: *J. Chem. Phys.* 105 (1996), pp. 1001–1006 (cit. on p. 171).

[531] G. Dixon-Lewis, W. E. Wilson, and A. A. Westenberg. "Studies of Hydroxyl Radical Kinetics by Quantitative ESR". In: *J. Chem Phys.* 44 (1966), pp. 2877–2884 (cit. on p. 171).

[532] A. A. Westenberg and N. deHaas. "Rate of the Reaction OH + OH → H_2O + O". In: *J. Chem Phys.* 58 (1973), pp. 4066–4071 (cit. on p. 171).

[533] G. K. Farquharson and R. H. Smith. "Rate constants for the gaseous reactions OH + C_2H_4 and OH + OH". In: *Aust. J. Chem.* 33 (1980), pp. 1425–1435 (cit. on p. 171).

[534] M. A. A. Clyne and S. Down. "Kinetic behaviour of OH $X^2\Pi$ and $A^2\sigma^+$ using molecular resonance fluorescence spectrometry". In: *J. Chem Soc., Faraday Trans. 2* 70 (1974), pp. 253–266 (cit. on p. 171).

[535] M. Sangwan and L. N. Krasnoperov. "Disproportionation Channel of Self-Reaction of Hydroxyl Radical, OH + OH → H_2O + O, Studied by Time-Resolved Oxygen Atom Trapping". In: *J. Phys. Chem. A* 116 (2012), pp. 11817–11822 (cit. on p. 171).

[536] Y. Bedjanian, G. Le Bras, and G. Poulet. "Kinetic Study of OH + OH and OD + OD Reactions". In: *J. Phys. Chem. A* 103 (1999), pp. 7017–7025 (cit. on p. 171).

[537] G. Wagner and R. Zellner. "Temperature Dependence of the Reaction OH + OH → H2O + O". In: *Ber. Bunsenges. Phys. Chem.* 85 (1981), pp. 1122–1128 (cit. on p. 171).

[538] J. E. Breen and G. P. Glass. “Rate of Some Hydroxyl Radical Reactions”. In: *Combust. Flame* 52 (1970), pp. 1082–1086 (cit. on pp. 171, 172, 180).

[539] I. W. M. Smith and D. W. A. Stewart. “Low-temperature kinetics of reactions between neutral free radicals. Rate constants for the reactions of OH radicals with N atoms ($103 \leq T/K \leq 294$) and with O atoms ($158 \leq T/K \leq 294$)”. In: *J. Chem. Soc., Faraday Trans.* 90 (1994), pp. 3221–3227 (cit. on pp. 172, 180).

[540] M. J. Howard and I. W. M. Smith. “Direct Rate Measurements on the Reactions $N + OH \rightarrow NO + H$ and $O + OH \rightarrow O_2 + H$ from 250 to 515 K”. In: *J. Chem. Soc., Faraday Trans. 2* 77 (1981), pp. 997–1008 (cit. on pp. 172, 180).

[541] A. A. Westenberg, N. De Haas, and J. M. Roscoe. “Radical reactions in an electron spin resonance cavity homogeneous reactor”. In: *J. Phys. Chem.* 74 (1970), pp. 3431–3438 (cit. on pp. 172, 180).

[542] M. J. Howard and I. W. M. Smith. “Direct rate measurements on the reactions $N + OH \rightarrow NO + H$ And $O + OH \rightarrow O_2 + H$”. In: *Chem. Phys. Lett.* 69 (1980), pp. 40–44 (cit. on pp. 172, 180).

[543] R. Robertson and G. P. Smith. “Temperature Dependence of O + OH at 136-377 K Using Ozone Photolysis”. In: *J. Phys. Chem. A* 110 (2006), pp. 6673–6679 (cit. on pp. 172, 180).

[544] R. Robertson and G. P. Smith. “Photolytic measurement of the O + OH rate constant at 295 K”. In: *Chem. Phys. Lett.* 358 (2002), pp. 157–162 (cit. on pp. 172, 180).

[545] W. H. Brune, J. J. Schwab, and J. G. Anderson. “Laser magnetic resonance, resonance fluorescence, and resonance absorption studies of the reaction kinetics of $O + OH \rightarrow H + O_2$, $O + HO_2 \rightarrow OH + O_2$, $N + OH \rightarrow H + NO$, and $N + HO_2 \rightarrow$ products at 300 K between 1 and 5 torr”. In: *J. Phys. Chem.* 87 (1983), pp. 4503–4514 (cit. on pp. 172, 180).

[546] R. S. Lewis and R. T. Watson. “Temperature dependence of the reaction $O(^3P) + OH(^2\Pi) \rightarrow O_2 + H$”. In: *J. Phys. Chem.* 84 (1980), pp. 3495–3503 (cit. on pp. 172, 180).

[547] S. C. Kurzius and M. Boudart. “Kinetics of the branching step in the hydrogen-oxygen reaction”. In: *Combust. Flame* 12 (1968), pp. 477–491 (cit. on pp. 172, 180).

[548] *Study of the reaction of hydroxyl radical with methane by quantitative ESR.* Vol. 11. 1967, pp. 1143–1150 (cit. on p. 172).

[549] *Direct measurements of the rate coefficient for the reaction OH + $CH_4 \rightarrow CH_3$ + H_2O over 300-1500 K.* Vol. 20. 1984, pp. 703–713 (cit. on p. 172).

[550] P. Sharkey and I. W. M. Smith. "Kinetics of elementary reactions at low temperatures: rate constants for the reactions of OH with HCl ($298 \geq T/K \geq 138$), CH_4($298 \geq T/K \geq 178$) and C_2H_6($298 \geq T/K \geq 138$)". In: *J. Chem. Soc., Faraday Trans.* 89 (1993), pp. 631–637 (cit. on p. 172).

[551] A. Mellouki, S. Téton, G. Laverdet, A. Quilgars, and G. Le Bras. "Kinetic studies of OH reactions with H_2O_2, C_3H_8 and CH_4 using the pulsed laser photolysis - laser induced fluorescence method". In: *J. Chim. Phys.* 91 (1994), pp. 473–487 (cit. on p. 172).

[552] M. G. Bryukov, V. D. Knyazev, S. M. Lomnicki, C. A. McFerrin, and B. Dellinger. "Temperature-Dependent Kinetics of the Gas-Phase Reactions of OH with Cl_2, CH_4, and C_3H_8". In: *J. Phys. Chem. A* 108 (2004), pp. 10464–10472 (cit. on p. 172).

[553] A. Bonard, V. Daële, J.-L. Delfau, and C. Vovelle. "Kinetics of OH Radical Reactions with Methane in the Temperature Range 295-660 K and with Dimethyl Ether and Methyl-tert-butyl Ether in the Temperature Range 295-618 K". In: *J. Phys. Chem. A* 106 (2002), pp. 4384–4389 (cit. on p. 172).

[554] T. Gierczak, R. K. Talukdar, S. C. Herndon, G. L. Vaghjiani, and A. R Ravishankara. "Rate Coefficients for the Reactions of Hydroxyl Radicals with Methane and Deuterated Methanes". In: *J. Phys. Chem. A* 101 (1997), pp. 3125–3134 (cit. on p. 172).

[555] G. L. Vaghjiani and A. R. Ravishankara. "New measurement of the rate coefficient for the reaction of OH with methane". In: *Nature* 350 (1992), pp. 406–409 (cit. on p. 172).

[556] J. R. Dunlop and F. P. Tully. "A kinetic study of OH radical reactions with methane and perdeuterated methane". In: *J. Phys. Chem.* 97 (1993), pp. 11148–11150 (cit. on p. 172).

[557] B. J. Finlayson-Pitts, M. J. Ezell, T. M. Jayaweera, H. N. Berko, and C. C. Lai. "Kinetics of the reactions of OH with methyl chloroform and methane: Implications for global tropospheric OH and the methane budget". In: *Geophys. Res. Lett.* 19 (1992), pp. 1371–1374 (cit. on p. 172).

[558] K. Fagerström, A. Lund, G. Mahmoud, J. T. Jodkowski, and E. Ratajczak. "Kinetics of the cross reaction between methyl and hydroxyl radicals". In: *Chem. Phys. Lett.* 204 (1993), pp. 226–234 (cit. on p. 172).

[559] *The reaction system CH_3+OH at intermediate temperatures. Appearance of a new product channel.* Vol. 25. 1994, pp. 721–731 (cit. on p. 172).

[560] K. Fagerström, A. Lund, G. Mahmoud, J. T. Jodkowski, and E. Ratajczak. "Pressure and temperature dependence of the gas-phase reaction between methyl and hydroxyl radicals". In: *Chem. Phys. Lett.* 224 (1994), pp. 43–50 (cit. on p. 172).

[561] H. Oser, N. D. Stothard, R. Humpfer, and H.-H. Grotheer. "Direct measurement of the reaction CH_3 + OH at ambient temperature in the pressure range 0.3–6.2 mbar". In: *J. Phys. Chem.* 96 (1992), pp. 5359–5363 (cit. on p. 172).

[562] *Direct measurement of the reaction CH_3+OH and its pathways between 300 and 480 K.* Vol. 24. 1992, pp. 597–604 (cit. on p. 172).

[563] C. Anastasi, S. Beverton, T. Ellermann, and P. Pagsberg. "Reaction of CH, Radicals with OH at Room Temperature and Pressure". In: *J. Chem. Soc., Faraday Trans.* 87 (1991), pp. 2325–2329 (cit. on p. 172).

[564] T. J. Sworski, C. J. Hochanadel, and P. J. Ogren. "Flash photolysis of H_2O in CH_4. H and OH yields and rate constants for CH_3 reactions with H and OH". In: *J. Phys. Chem.* 84 (1980), pp. 192–134 (cit. on p. 172).

[565] I. W. M. Smith and R. Zellner. "Rate measurements of reactions of OH by resonance absorption. Part 3.-Reactions of OH with H_2, D_2 and hydrogen and deuterium halides". In: *J. Chem. Soc., Faraday Trans. 2* 70 (1974), pp. 1045–1056 (cit. on p. 172).

[566] R. Atkinson, D. A. Hansen, and J. N. Pitts Jr. "Rate constants for the reaction of the OH radical with H_2 and NO (M=Ar and N_2)". In: *J. Chem. Phys.* 62 (1975), pp. 3284–3288 (cit. on p. 172).

[567] R. Atkinson, D. A. Hansen, and J. N. Pitts Jr. “Rate constants for the reaction of OH radicals with CHF_2Cl, CF_2Cl_2, $CFCl_3$, and H_2 over the temperature range 297-434 °K”. In: *J. Chem. Phys.* 63 (1975), pp. 1703–1706 (cit. on p. 172).

[568] R. K. Talukdar, T. Gierczak, L. Goldfarb, Y. Rudich, B. S. Madhava Rao, and A. R. Ravishankara. “Kinetics of Hydroxyl Radical Reactions with Isotopically Labeled Hydrogen”. In: *J. Phys. Chem.* 100 (1996), pp. 3037–3043 (cit. on p. 172).

[569] V. L. Orkin, S. N. Kozlov, G. A. Poskrebyshev, and M. J. Kurylo. “Rate Constant for the Reaction of OH with H_2 between 200 and 480 K”. In: *J. Phys. Chem. A* 110 (2006), pp. 6978–6985 (cit. on p. 172).

[570] A. R. Ravishankara, J. M. Nicovich, R. L. Thompson, and F. P. Tully. “Kinetic study of the reaction of hydroxyl with hydrogen and deuterium from 250 to 1050 K”. In: *J. Phys. Chem.* 85 (1981), pp. 2498–2503 (cit. on p. 172).

[571] F. P. Tully and A. R. Ravishankara. “Flash photolysis-resonance fluorescence kinetic study of the reactions $OH + H_2 \rightarrow H_2O + H$ and $OH + CH_4 \rightarrow H_2O + CH_3$ from 298 to 1020 K”. In: *J. Phys. Chem.* 84 (1980), pp. 3126–3130 (cit. on p. 172).

[572] R. P. Overend, G. Paraskevopoulos, and R. J. Cvetanović. “Rates of OH Radical Reactions. I. Reactions with H_2, CH_4, C_2H_6, and C_3H_8 at 295K”. In: *Can. J. Chem.* 53 (1975), pp. 3374–3382 (cit. on p. 172).

[573] *Energy partitioning in the products of elementary reactions involving OH-radicals.* Vol. 15. Seattle: The Combustion Institute, 1975, pp. 755–764 (cit. on p. 172).

[574] *Fast reactions of OH radicals.* Vol. 9. Seattle: The Combustion Institute, 1963, pp. 659–668 (cit. on p. 173).

[575] T. A. Titarchuk and J. B. Halpern. “Kinetics of CN reactions with $O(^3P)$ and SO_2”. In: *Chem. Phys. Lett.* 232 (1995), pp. 192–196 (cit. on p. 173).

[576] H. Schacke, K. J. Schmatjko, and J. Wolfrum. “Reaktionen von Molekülen in definierten Schwingungszuständen (I) Die Reaktionen CN(v") + O und CN(v") + O_2”. In: *Ber. Bunsenges. Phys. Chem.* 77 (1973), pp. 248–253 (cit. on p. 173).

[577] K. J. Schmatjko and J. Wolfrum. “Direct determination of the product energy distribution in the reaction of O-atoms with CN radicals”. In: *Sixteenth Symposium (International) on Combustion.* Vol. 16. Seattle: The Combustion Institute, 1977, pp. 819–827 (cit. on p. 173).

[578] J. E. Morgan, L. Elias, and H. I. Schiff. “Recombination of Oxygen Atoms in the Absence of O_2”. In: *J. Chem. Phys.* 33 (1960), pp. 930–931 (cit. on p. 173).

[579] H. Tchen. “Étude cinétique par R. P. E. des atomes d′oxygène 3p dans la post-décharge”. In: *Rev. Phys. Appl.* 7 (1972), pp. 205–212 (cit. on p. 173).

[580] I. M. Campbell and C. N. Gray. “Rate constants for $O(^3P)$ recombination and association with $N(^4S)$”. In: *Chem. Phys. Lett.* 18 (1973), pp. 607–609 (cit. on p. 173).

[581] T. C. Marshall. “Studies of Atomic Recombination of Nitrogen, Hydrogen, and Oxygen by Paramagnetic Resonance”. In: *Phys. Fluids* 5 (1962), pp. 743–753 (cit. on p. 173).

[582] I. M. Campbell and B. A. Thrush. “The association of oxygen atoms and their combination with nitrogen atoms”. In: *Proc. R. Soc. Lond. A Math. Phys. Sci.* 296 (1967), pp. 222–232 (cit. on p. 173).

[583] R. R. Reeves, G. Mannella, and P. Harteck. “Rate of Recombination of Oxygen Atoms”. In: *J. Chem. Phys.* 32 (1960), pp. 632–633 (cit. on p. 173).

[584] V. N. Kondratiev and E. E. Nikitin. “Rate Constants for the Process $O_2 + Ar \longleftrightarrow O + O + Ar$”. In: *J. Chem. Phys.* 45 (1966), pp. 1078–1079 (cit. on p. 173).

[585] C. Mavroyannis and C. A. Winkler. “The reaction of nitrogen atoms with oxygen atoms in the absence of oxygen molecules”. In: *Can. J. Chem.* 39 (1961), pp. 1601–1607 (cit. on p. 173).

[586] F. W. Froben. “Die Reaktion von O-Atomen mit Methan, Chloroform und Tetrachlorkohlenstoff”. In: *Ber. Bunsenges. Phys. Chem.* 72 (1968), pp. 996–998 (cit. on p. 173).

[587] A. A. Westenberg and N. de Haas. “Atom—Molecule Kinetics at High Temperature Using ESR Detection. Technique and Results for $O + H_2$, $O + CH_4$, and $O + C_2H_6$”. In: *J. Chem. Phys.* 46 (1967), pp. 490–501 (cit. on p. 173).

[588] J. W. Falconer, D. E. Hoare, and R. Overend. “Photolysis of carbon dioxide and methane mixtures at 873 and 293 K with 163.3 nm light”. In: *J. Chem. Soc., Faraday Trans. 1* 69 (1973), pp. 1541–1546 (cit. on p. 173).

[589] I. R. Slagle, F. J. Pruss, Jr., and D. Gutman. “Kinetics into the steady state. I. study of the reaction of oxygen atoms with methyl radicals”. In: *Int. J. Chem. Kinet.* 6 (1974), pp. 111–123 (cit. on p. 173).

[590] I. R. Slagle, D. Sarzyński, and D. Gutman. “Kinetics of the reaction between methyl radicals and oxygen atoms between 294 and 900 K”. In: *J. Phys. Chem.* 91 (1987), pp. 4375–4379 (cit. on p. 173).

[591] N. Washida. “Reaction of methyl radicals with O(^{3}P), O_2 and NO”. In: *J. Chem. Phys.* 73 (1980), pp. 1665–1672 (cit. on p. 173).

[592] N. Washida and K. D. Bayes. “The rate of reaction of methyl radicals with atomic oxygen”. In: *Chem. Phys. Lett.* 23 (1973), pp. 373–375 (cit. on p. 173).

[593] R. Zellner, D. Hartmann, J. Karthäuser, D. Rhäsa, and G. Weibring. “A laser photolysis/LIF study of the reactions of O(^{3}P) atoms with CH_3 and CH_3O_2 radicals”. In: *J. Chem. Soc., Faraday Trans. 2* 84 (1988), pp. 549–568 (cit. on p. 173).

[594] I. C. Plumb and K. R. Ryan. “Kinetics of the reactions of CH3 with O(^{3}P) and O_2 at 295 K”. In: *Int. J. Chem. Kinet.* 14 (1982), pp. 861–874 (cit. on p. 173).

[595] N. Washida and K. D. Bayes. “The reactions of methyl radicals with atomic and molecular oxygen”. In: *Int. J. Chem. Kinet.* 8 (1976), pp. 777–794 (cit. on p. 173).

[596] P. W. Seakins and S. R. Leone. “A laser flash photolysis/time-resolved FTIR emission study of a new channel in the reaction of methyl + oxygen atom: production of carbon monoxide(v)”. In: *J. Phys. Chem.* 96 (1992), pp. 4478–4485 (cit. on p. 173).

[597] E. D. Morris, Jr. and H. Niki. “Reaction of methyl radicals with atomic oxygen”. In: *Chem. Phys. Lett.* 5 (1973), pp. 47–53 (cit. on p. 173).

[598] *Mass spectrometric study of the kinetics and mechanism of the ethylene-atomic oxygen reaction by the discharge-flow technique at 300 K.* Vol. 12. Seattle: The Combustion Institute, 1969, pp. 277–288 (cit. on p. 173).

[599] T. Böhland, F. Temps, and H. Gg. Wagner. “Direct Investigation of the Reaction $CH_2(X^3B_1) + O(^3P)$ with the LMR”. In: *Ber. Bunsenges. Phys. Chem.* 88 (1984), pp. 1222–1228 (cit. on pp. 173, 184).

[600] *Reactions of methylene in the oxidation process of acetylene with oxygen atoms at 295 K.* Vol. 17. Seattle: The Combustion Institute, 1979, pp. 623–631 (cit. on pp. 173, 184).

[601] I. Messing, D. Carrington, S. V. Filseth, and C. M. Sadowski. “Absolute rate constant for the CH + O reaction”. In: *Chem. Phys. Lett.* 74 (1980), pp. 56–57 (cit. on p. 173).

[602] Y.-F. Zhu, S. Arepalli, and R. J. Gordon. “The rate constant for the reaction $O(^3P)+D_2$ at low temperatures”. In: *J. Chem. Phys.* 90 (1989), pp. 183–188 (cit. on p. 174).

[603] N. Presser and R. J. Gordon. “The kinetic isotope effect in the reaction of $O(^3P)$ with H_2, D_2, and HD”. In: *J. Chem. Phys.* 82 (1985), pp. 1291–1297 (cit. on p. 174).

[604] G. C. Light and J. H. Matsumoto. “Experimental measurement of the rate of the reaction $O(^3P) + H_2(v{=}0) \longrightarrow OH(v{=}0) + H$ at T = 298 K”. In: *Int. J. Chem. Kinet.* 12 (1980), pp. 451–468 (cit. on p. 174).

[605] D. L. Baulch, D. D. Drysdale, D. G. Horne, and A. C. Lloyd. *Evaluated Kinetic Data for High Temperature Reactions, Vol. 1: Homogeneous Gas Phase Reactions of the H_2-O_2 Systems.* London: Butterworths, 1972 (cit. on p. 174).

[606] Y. Matsumi, K. Tonokura, Y. Inagaki, and M. Kawasaki. “Isotopic branching ratios and translational energy release of hydrogen and deuterium atoms in reaction of oxygen (^1D) atoms with alkanes and alkyl chlorides”. In: *J. Phys. Chem.* 97 (1993), pp. 6816–6821 (cit. on pp. 174, 185).

[607] S. Vranckx, J. Peeters, and S. Carl. “A temperature dependence kinetic study of $O(^1D) + CH_4$: overall rate coefficient and product yields”. In: *Phys. Chem. Chem. Phys.* 10 (2008), pp. 5714–5722 (cit. on pp. 174, 185).

[608] T. J. Dillon, A. Horowitz, and J. N. Crowley. “Absolute rate coefficients for the reactions of $O(^1D)$ with a series of n-alkanes”. In: *Chem. Phys. Lett.* 443 (2007), pp. 12–16 (cit. on pp. 174, 185).

[609] R. J. Cvetanović. “Excited State Chemistry in the Stratosphere”. In: *Can. J. Chem.* 52 (1974), pp. 1452–1464 (cit. on pp. 174, 185).

[610] S. Koppe, T. Laurent, P. D. Naik, H.-R. Volpp, J. Wolfrum, T. Arusi-Parpar, and S. Rosenwaks. “Absolute rate constants and reactive cross sections for the reactions of $O(^1D)$ with molecular hydrogen and deuterium”. In: *Chem. Phys. Lett.* 214 (1993), pp. 546–552 (cit. on pp. 174, 185).

[611] L. J. Stief, W. A. Payne, and R. B. Klemm. “A flash photolysis-resonance fluorescence study of the formation of $O(^1D)$ in the photolysis of water and the reaction of $O(^1D)$ with H_2, Ar, and He”. In: *J. Chem. Phys.* 62 (1975), pp. 4000–4008 (cit. on pp. 174, 185).

[612] R. K. Talukdar and A. R. Ravishankara. “Rate coefficients for $O(^1D) + H_2$ D_2, HD reactions and H atom yield in $O(^1D)$ + HD reaction”. In: *Chem. Phys. Lett.* 253 (1996), pp. 177–183 (cit. on pp. 174, 185).

[613] P. J. Ogren, T. J. Sworski, C. J. Hochanadel, and J.-M. Cassel. “Flash Photolysis of O_3 in O_2 and $O_2 + H_2$ Mixtures. Kinetics of $O_2(^1\Sigma_g^+) + O_3$ and $O(^1D) + H_2$ Reactions”. In: *J. Phys. Chem.* 86 (1982), pp. 238–242 (cit. on pp. 174, 185).

[614] D. Nuñez-Reyes and K. M. Hickson. “Kinetics of the Gas-Phase $O(^1D) + CO_2$ and $C(^1D) + CO_2$ Reactions over the 50-296 K Range”. In: *J. Phys. Chem. A* 112 (2018), pp. 4002–4008 (cit. on p. 175).

[615] A. M. Mebel, M. Hayashi, V. V. Kislov, and S. H. Lin. “Theoretical Study of Oxygen Isotope Exchange and Quenching in the $O(^1D) + CO_2$ Reaction”. In: *J. Phys. Chem. A* 108 (2004), pp. 7983–7994 (cit. on p. 175).

[616] L. Zhu, T. G. Kreutz, S. A. Hewitt, and G. W. Flynn. “Diode laser probing of vibrational, rotational,and translational excitation of CO_2 following collisions with $O(^1D)$. I. Inelastic scattering”. In: *J. Chem. Phys.* 93 (1990), pp. 3277–3288 (cit. on p. 175).

[617] A. J. Sedlacek, D. R. Harding, R. E. Weston, T. G. Kreutz, and G. W. Flynn. “Probing the $O(^1D)+CO_2$ reaction withsecond-derivative modulated diode laserspectroscopy”. In: *J. Chem. Phys.* 91 (1989), pp. 7550–7556 (cit. on pp. 175, 176).

[618] R. G. Shortridge and M. C. Lin. “CO vibrational population distributions in the reactions of COS with O(^{3}P$_J$) and O(^{1}D$_2$) atoms”. In: *Chem. Phys. Lett.* 35 (1975), pp. 146–150 (cit. on p. 175).

[619] J. C. Tully. “Reactions of O(^{1}D) with atmospheric molecules”. In: *J. Chem. Phys.* 62 (1975), pp. 1893–1898 (cit. on p. 175).

[620] I. D. Clark and J. F. Noxon. “Optical Emission from O(^{1}D) and $O_2(b^1\Sigma_g)$ in Ultraviolet Photolysis of O_2 and CO_2. II”. In: *J. Chem.Phys.* 57 (1972), pp. 1033–1038 (cit. on p. 175).

[621] E. C. Zipf. “The collisional deactivation of metastable atoms and molecules in the upper atmosphere”. In: *Can. J. Chem.* 47 (1969), pp. 1863–1870 (cit. on p. 175).

[622] G. Paraskevopoulos and R. Cvetanovic. “Competitive Reactions of the Excited Oxygen Atoms, O(^{1}D)*”. In: *J. Am. Chem. Soc.* 91 (1969), pp. 7572–7577 (cit. on p. 175).

[623] D. Kovacs and J. E. Jackson. “$CH_2 + CO_2 \longrightarrow CH_2O + CO$, One-Step Oxygen Atom Abstraction or Addition/Fragmentation via α-Lactone?” In: *J. Phys. Chem. A* 105 (2001), pp. 7579–7587 (cit. on pp. 177, 178).

[624] L. N. Krasnoperov, E. N. Chesnokov, H. Stark, and A. R. Ravishankara. “Elementary reactions of formyl (HCO) radical studied by laser photolysis—transient absorption spectroscopy”. In: *Proc. Combust. Inst.* 30 (2005), pp. 935–943 (cit. on p. 178).

[625] V. Saheb and A. Nazari. “Products of the Self-Reaction of HCO Radicals: Theoretical Kinetics Studies”. In: *Phys. Chem. Res.* 7 (2019), pp. 81–94 (cit. on p. 178).

[626] J. Li, Y. Wang, B. Jiang, J. Ma, R. Dawes, D. Xie, J. M. Bowman, and H. Guo. “Communication: A chemically accurateglobal potential energy surface for the $HO + CO \to H + CO_2$ reaction”. In: *J. Chem. Phys.* 136 (2012), p. 041103 (cit. on pp. 179, 180).

[627] D. E. Skinner, T. C. Germann, and W. H. Miller. “Quantum Mechanical Rate Constants for $O + OH = H + O_2$ for Total Angular Momentum $J > 0$”. In: *J. Phys. Chem. A* 102 (1998), pp. 3828–3834 (cit. on p. 180).

[628] F. Lique, M. Jorfi, P. Honvault, P. Halvick, S. Y. Lin, H. Guo, D. Q. Xie, P. J. Dagdigian, J. Kłos, and M. H. Alexander. "O + OH → O_2 + H: A key reaction for interstellar chemistry. New theoreticalresults and comparison with experiment". In: *J. Chem. Phys.* 131 (2009), p. 221104 (cit. on p. 180).

[629] S. J. Klippenstein, L. B. Harding, B. Ruscic, R. Sivaramakrishnan, N. K. Srinivasan, M.-C. Su, and J. V. Michael. "Thermal Decomposition of NH2OH and Subsequent Reactions: Ab Initio Transition State Theory and Reflected Shock Tube Experiments". In: *J. Phys. Chem. A* 113 (2009), pp. 10241–10259 (cit. on p. 181).

[630] H.-G. Yu and J. T. Muckerman. "MRCI Calculations of the Lowest Potential Energy Surface for CH_3OH and Direct ab Initio Dynamics Simulations of the $O(^1D)$ + CH_4 Reaction". In: *J. Phys. Chem. A* 108 (2004), pp. 8615–8623 (cit. on p. 185).

[631] A. H. H. Chang and S. H. Lin. "A theoretical study of the $O(^1D)$ + CH_4 reaction II". In: *Chem. Phys. Lett.* 384 (2004), pp. 229–235 (cit. on p. 185).

[632] F. J. Aoiz, L. Bañares, and V. J. Herrero. "Dynamics of Insertion Reactions of H_2 Molecules with Excited Atoms". In: *J. Phys. Chem. A* 110 (2006), pp. 12546–12565 (cit. on p. 185).

[633] S. Y. Lin and H. Guo. "Adiabatic and Nonadiabatic State-to-State Quantum Dynamics for $O(^1D)$ + $H_2(X^1\Sigma_g^+$, ν_i = j_i = 0) -> $OH(X^2\Pi$, ν_f, j_f) + $H(^2S)$ Reaction". In: *J. Phys. Chem. A* 113 (2009), pp. 4285–4293 (cit. on p. 185).

[634] B. K. D. Pearce, P. W. Ayers, and R. E. Pudritz. "CRAHCN-O: A consistent reduced atmospheric hybrid chemical network oxygen extension for hydrogen cyanide and formaldehyde chemistry in CO2-, N2-, H2O-, CH4-, and H2-dominated atmospheres". In: *J. Phys. Chem. A.* 124 (2020), pp. 8594–8606 (cit. on pp. 188, 201, 207–209, 313).

[635] S. Becker, C. Schneider, H. Okamura, A. Crisp, T. Amatov, D. Dejmek, and T. Carell. "Wet-dry cycles enable the parallel origin of canonical and non-canonical nucleosides by continuous synthesis". In: *Nat. Commun.* 9 (2018), p. 163 (cit. on pp. 189, 204).

[636] N. Dauphas. "The isotopic nature of the Earth's accreting material through time". In: *Nature* 541 (2017), pp. 521–524 (cit. on p. 189).

[637] L. Piani, Y. Marrocchi, T. Rigaudier, L. G. Vacher, D. Thomassin, and B. Marty. "Earth's water may have been inherited from material similar to enstatite chondrite meteorites". In: *Science* 369 (2020), pp. 1110–1113 (cit. on p. 189).

[638] M. T. McCulloch and V. C. Bennett. "Evolution of the early Earth: Constraints from ^{143}Nd-^{142}Nd isotopic systematics". In: *Lithos* 30 (1993), pp. 237–255 (cit. on pp. 189, 226).

[639] P. Higgs. "Phosphorylation with inorganic phosphates at moderate temperatures". In: *Life* 6 (2016), p. 24 (cit. on pp. 189, 227).

[640] J. Fiebig, A. B. Woodland, J. Spangenberg, and W. Oschmann. "Natural evidence for rapid abiogenic hydrothermal generation of CH_4". In: *Geochim. Cosmochim. Acta* 71.12 (2007), pp. 3028–3039 (cit. on p. 190).

[641] A. S. Bradley and R. E. Summons. "Multiple origins of methane at the Lost City Hydrothermal Field". In: *Earth Planet. Sci. Lett.* 297.1 (2010), pp. 34–41 (cit. on p. 190).

[642] C. F. Chyba. "Impact delivery and erosion of planetary oceans in the early inner solar system". In: *Nature* 343 (1990-01), pp. 129–133 (cit. on pp. 192, 200, 203, 213).

[643] R. J. Cicerone and R. Zellner. "The atmospheric chemistry of hydrogen cyanide (HCN)". In: *J. Geophys. Res. Oceans* 88 (1983), pp. 10689–10696 (cit. on p. 196).

[644] K. I. Oberg, .R. Murray-Clay, and E. A. Bergin. "The Effects of Snowlines on C/O in Planetary Atmospheres". In: *Astrophys. J. Lett.* 743.1 (2011-12), p. L16 (cit. on p. 196).

[645] N. Madhusudhan. "C/O Ratio as a Dimension for Characterizing Exoplanetary Atmospheres". In: *Astrophys. J.* 758.1 (2012-10), p. 36 (cit. on p. 196).

[646] P. Mollière, R. van Boekel, C. Dullemond, T. Henning, and C. Mordasini. "Model Atmospheres of Irradiated Exoplanets: The Influence of Stellar Parameters, Metallicity, and the C/O Ratio". In: *Astrophys. J.* 813, 47 (2015-11), p. 47. DOI: `10.1088/0004-637X/813/1/47` (cit. on p. 196).

[647] K. Molaverdikhani, T. Henning, and P. Mollière. “From Cold to Hot Irradiated Gaseous Exoplanets: Toward an Observation-based Classification Scheme”. In: *Astrophys. J.* 873.1, 32 (2019-03), p. 32 (cit. on p. 196).

[648] K. Molaverdikhani, T. Henning, and P. Mollière. “The Role of Clouds on the Depletion of Methane and Water Dominance in the Transmission Spectra of Irradiated Exoplanets”. In: *Astrophys. J.* 899.1, 53 (2020-08), p. 53 (cit. on p. 196).

[649] W. D. Fuller, R. A. Sanchez, and L. E. Orgel. “Studies in Prebiotic Synthesis VI. Synthesis of Purine Nucleosides”. In: *J. Mol. Biol.* 67 (1972), pp. 25–33 (cit. on p. 199).

[650] D. W. Deamer. “The Role of Lipid Membranes in Life’s Origin”. In: *Life* 7 (2017), p. 5 (cit. on p. 199).

[651] et al. Stepleman R. S., ed. *ODEPACK, A Systematized Collection of ODE Solvers.* Vol. 1. IMACS Transactions of Scientific Computation. North-Holland, Amsterdam, 1983, pp. 55–64 (cit. on p. 200).

[652] T. Guillot. “On the radiative equilibrium of irradiated planetary atmospheres”. In: *Astron. Astrophys.* 520 (2010-09), A27 (cit. on pp. 201, 209).

[653] P. Mollière, T. Stolker, S. Lacour, G. P. P. L. Otten, J. Shangguan, B. Charnay, T. Molyarova, M. Nowak, Th. Henning, G. -D. Marleau, D. A. Semenov, E. van Dishoeck, F. Eisenhauer, P. Garcia, R. Garcia Lopez, J. H. Girard, A. Z. Greenbaum, S. Hinkley, P. Kervella, L. Kreidberg, A. -L. Maire, E. Nasedkin, L. Pueyo, I. A. G. Snellen, A. Vigan, J. Wang, P. T. de Zeeuw, and A. Zurlo. “Retrieving scattering clouds and disequilibrium chemistry in the atmosphere of HR 8799e”. In: *Astron. Astrophys.* 640 (2020-08), A131 (cit. on p. 201).

[654] J. Wang, J. J. Wang, B. Ma, J. Chilcote, S. Ertel, O. Guyon, I. Ilyin, N. Jovanovic, P. Kalas, J. Lozi, B. Macintosh, K. G. Strassmeier, and J. Stone. “On the Chemical Abundance of HR 8799 and the Planet c”. In: *Astrophys. J.* 160.3 (2020-09), p. 150 (cit. on p. 201).

[655] A. L. Buck. “New Equations for Computing Vapor Pressure and Enhancement Factor”. In: *J. Appl. Meteor.* 20 (1981), pp. 1527–1532 (cit. on pp. 201, 210).

[656] P. Mollière, J. P. Wardenier, R. van Boekel, Th. Henning, K. Molaverdikhani, and I. A. G. Snellen. "petitRADTRANS. A Python radiative transfer package for exoplanet characterization and retrieval". In: *Astron. Astrophys.* 627 (2019-07), A67 (cit. on pp. 201, 207, 209).

[657] D. R. Stull and H. Prophet. Washington, DC: U.S. Govt. Printing Office, 1971 (cit. on pp. 201, 216).

[658] R. Heller, J.-P. Dude, M. Winkler, J. Reitner, and L. Gizon. "Habitability of the early Earth: Liquid water under a faint young Sun facilitated by strong tidal heating due to a nearby Moon". In: *ArXiv e-prints* (2020). arXiv: `2007.03423 [astro-ph.EP]` (cit. on pp. 203, 211).

[659] I. Baraffe, D. Homeier, F. Allard, and G. Chabrier. "New evolutionary models for pre-main sequence and main sequence low-mass stars down to the hydrogen-burning limit". In: *Astron. Astrophys.* 577 (2015-05), A42 (cit. on pp. 203, 211).

[660] I. Ribas, E. F. Guinan, M. Güdel, and M. Audard. "Evolution of the Solar Activity Over Time and Effects on Planetary Atmospheres: I. High-Energy Irradiances (1-1700 A)". In: *Astrophys. J.* 622 (2005), pp. 680–694 (cit. on pp. 203, 212).

[661] W. R. Berghuijs and R. A. Woods. "A simple framework to quantitatively describe monthly precipitation and temperature climatology". In: *Int. J. Climatol.* 36 (2016), pp. 3161–3174 (cit. on p. 204).

[662] R. H. Reichle, R. D. Koster, G. J. M. De Lannoy, B. A. Forman, Q. Liu, S. P. P. Mahanama, and A. Touré. "Assessment and Enhancement of MERRA Land Surface Hydrology Estimates". In: *J. Clim.* 24 (2011), pp. 6322–6338 (cit. on p. 204).

[663] S. Carl, S. Qian, L. Vereecken, and J. Peeters. "Absolute rate coefficient of the HCCO plus NO reaction over the range T=297-802 K". In: *J. Phys. Chem. A* 106 (2000), pp. 12242–12247 (cit. on p. 208).

[664] G. P. Glass, S. S. Kumaran, and J. V. Michael. "Photolysis of Ketene at 193 nm and the Rate Constant for H + HCCO at 297 K". In: *J. Phys. Chem. A* 104 (2000), pp. 8360–8367 (cit. on p. 208).

[665] *Acetylene oxidation: The reaction C_2H_2 + O at high temperatures.* Vol. 21. 1988, pp. 885–893 (cit. on p. 208).

[666] H. Schacke, K. Schmatjko, and J. Wolfrum. "Reaktionen von CN-Radikalen im H-C-N-O-System". In: *Arch. Proces. Spalania* 5 (1974), p. 363 (cit. on p. 208).

[667] W. F. Cooper, J. Park, and J. F. Hershberger. "Product channel dynamics of the NCO + NO reaction". In: *J. Phys. Chem.* 97 (1993), pp. 3283–3290 (cit. on p. 208).

[668] W. F. Cooper and J. F. Hershberger. "Measurement of product branching ratios of the NCO + NO reaction". In: *J. Phys. Chem.* 96 (1992), pp. 771–775 (cit. on p. 208).

[669] K. H. Becker, R. Kurtenabch, F. Schmidt, and P. Wiesen. "Kinetics of the NCO radical reacting with atoms and selected molecules". In: *Combust. Flame* 120 (2000), pp. 570–577 (cit. on p. 208).

[670] D. L. Baulch, C. J. Cobos, R. A. Cox, P. Frank, G. Hayman, Th. Just, J. A. Kerr, T. Murrells, M. J. Pilling, J. Troe, R. W. Walker, and J. Warnatz. "Evaluated kinetic data for combusion modelling. Supplement I". In: *J. Phys. Chem. Ref. Data* 23 (1994), pp. 847–1033 (cit. on p. 208).

[671] D. A. Lichtin, M. R. Berman, and M. C. Lin. "NH($A^3\Pi \longrightarrow X^3\Sigma^-$) Chemiluminescence from the CH($X^2\Pi$) + NO reaction". In: *Chem. Phys. Lett.* 108 (1984), pp. 18–24 (cit. on p. 208).

[672] D. A. Lichtin, M. R. Berman, and M. C. Lin. "Kinetic studies of initiated reactions of CH and CN radicals". In: *Bull. Soc. Chim. Belg.* 92 (1983), p. 656 (cit. on p. 208).

[673] J. A. Duncanson Jr. and W. A. Guillory. "The state-selective reactions of vibrationally excited CH($X^2\Pi$) with oxygen and nitrogen". In: *J. Chem. Phys.* 78 (1983), p. 4958 (cit. on p. 208).

[674] I. Messing, C. M. Sadowski, and S. V. Filseth. "Absolute rate constant for the reaction of CH with O_2". In: *Chem. Phys. Lett.* 66 (1979), pp. 95–99 (cit. on p. 208).

[675] W. D. Geppert, D. Reignier, T. Stoecklin, C. Naulin, M. Costes, D. Chastaing, S. D. Le Picard, I. R. Sims, and I. W. M. Smith. "Comparison of the cross-sections and thermal rate constants for the reactions of C(^{3}P$_J$) atoms with O_2 and NO". In: *Chem. Phys. Lett.* 2 (2000), pp. 2873–2881 (cit. on p. 208).

[676] G. Dorthe, P. Caubet, T. Vias, B. Barrere, and J. Marchais. "Fast flow studies of atomic carbon kinetics at room temperature". In: *J. Phys. Chem.* 95 (1991), pp. 5109–5116 (cit. on p. 208).

[677] K. H. Becker, K. J. Brockmann, and P. Wiesen. "Spectroscopic identification of C(^{3}P) atoms in halogenomethane + H flame systems and measurements of C(^{3}P) reaction rate constants by two-photon laser-induced fluorescence". In: *J. Chem. Soc., Faraday Trans. 2* 84 (1988), pp. 455–461 (cit. on p. 208).

[678] D. Husain and A. N. Young. "Kinetic investigation of ground state carbon atoms, C(2^{3}P$_J$) ". In: *J. Chem. Soc., Faraday Trans. 2* 71 (1975), pp. 525–531 (cit. on pp. 208, 209).

[679] D. Husain and L. J. Kirsch. "Reactions of atomic carbon C(2^{3}P$_J$) by kinetic absorption spectroscopy in the vacuum ultra-violet". In: *Trans. Faraday Soc.* 67 (1971), pp. 2025–2035 (cit. on pp. 208, 209).

[680] W. Braun, A. M. Bass, D. D. Davis, and J. D. Simmons. "Flash photolysis of carbon suboxide: absolute rate constants for reactions of C(^{3}P) and C(^{1}D) with H_2, N_2, CO, NO, O_2 and CH_4". In: *Proc. R. Soc. Lond. A Math Phys. Sci.* 312 (1969), pp. 417–434 (cit. on p. 208).

[681] F. F. Martinotti, M. J. Welch, and A. P. Wolf. "The reactivity of thermal carbon atoms in the gas phase". In: *Chem. Commun.* (1969), pp. 115–116 (cit. on p. 208).

[682] R. Atkinson, D. L. Baulch, R. A. Cox, R. F. Hampson Jr., J. A. Kerr, and J. Troe. "Evaluated Kinetic and Photochemical Data for Atmospheric Chemistry: Supplement III". In: *J. Phys. Chem. Ref. Data* 18 (1989), pp. 881–1097 (cit. on p. 208).

[683] Vivien Parmentier and Tristan Guillot. "A non-grey analytical model for irradiated atmospheres. I. Derivation". In: *Astron. Astrophys.* 562 (2014-02), A133 (cit. on p. 209).

[684] M. T. Rosing, D. K. Bird, N. H. Sleep, and C. J. Bjerrum. “No climate paradox under the faint early Sun”. In: *Nature* 464.7289 (2010), pp. 744–749 (cit. on p. 210).

[685] B. Charnay, E. T. Wolf, B. Marty, and F. Forget. “Is the Faint Young Sun Problem for Earth Solved?” In: *Space Sci. Rev.* 216 (2020), p. 90 (cit. on p. 210).

[686] S. Manabe and Wetherald. R. T. “Thermal Equilibrium of the Atmosphere with a Given Distribution of Relative Humidity”. In: *J. Atmos. Sci.* 24.3 (1967), pp. 241–259 (cit. on p. 210).

[687] I. M. Held and B. J. Soden. “Water Vapor Feedback and Global Warming”. In: *Annu. Rev. Energy Environ.* 25 (2000), pp. 441–475 (cit. on p. 210).

[688] T. D. Robinson and D. C. Catling. “Common 0.1 bar tropopause in thick atmospheres set by pressure-dependent infrared transparency”. In: *Nat. Geosci.* 7 (2014), pp. 12–15 (cit. on p. 210).

[689] A. Roesch, M. Wild, R. Pinker, and A. Ohmura. “Comparison of spectral surface albedos and their impact on the general circulation model simulated surface climate”. In: *J. Geophys. Res. Atmos.* 107.D14 (2002), p. 4221 (cit. on p. 211).

[690] Sukrit Ranjan, Edward W. Schwieterman, Chester Harman, Alexander Fateev, Clara Sousa-Silva, Sara Seager, and Renyu Hu. “Photochemistry of Anoxic Abiotic Habitable Planet Atmospheres: Impact of New H2O Cross Sections”. In: *Astorphys. J.* 896.2 (2020-06), p. 148 (cit. on pp. 211, 212, 216, 217).

[691] G. Arney, S. D. Domagal-Goldman, V. S. Meadows, E. T. Wolf, E. Schwieterman, B. Charnay, M. Claire, E. Hébrard, and M. G. Trainer. “The Pale Orange Dot: The Spectrum and Habitability of Hazy Archean Earth”. In: *Astrobiology* 16 (2016-11), pp. 873–899 (cit. on pp. 211, 212).

[692] E. Lange, A. I. Lozano, N. C. Jones, S. V. Hoffman, S. Kumar, M. A. Smiałek, Duflot D., M. J. Brunger, and P. Limao-Vieira. “Absolute Photoabsorption Cross-Sections of Methanol for Terrestrial and Astrophysical Relevance”. In: *J. Phys. Chem. A* 124 (2020), pp. 8496–8508 (cit. on p. 212).

[693] G. R. Burton, W. F. Chan, G. Cooper, and C. E. Biron. “Absolute oscillator strengths for photoabsorption (6–360 eV) and ionic photofragmentation (10–80 eV) of methanol”. In: *Chem. Phys.* 167 (1992), pp. 349–367 (cit. on p. 212).

[694] M. G. Trainer, A. A. Pavlov, H. L. DeWitt, J. L. Jimenez, C. P. McKay, O. B. Toon, and M. A. Tolbert. “Organic haze on Titan and the early Earth”. In: *Proc. Natl. Acad. Sci. U.S.A.* 103 (2006), pp. 18035–18042 (cit. on p. 214).

[695] J. L. Bada. “One of the foremost experiments of the twentieth century: Stanley Miller and the origin of prebiotic chemistry”. In: *Metode Sci. Stud. J.* 6 (2016), pp. 183–189 (cit. on p. 214).

[696] D. Archer. Princeton, NJ: Princeton Univ. Press, 2010 (cit. on p. 217).

[697] G. Wohlfahrt, C. Amelynck, C. Ammann, A. Arneth, I. Bamberger, A. H. Goldstein, L. Gu, A. Guenther, A. Hansel, B. Heinesch, T. Holst, L. Hörtnag, T. Karl, Q. Laffineur, A. Neftel, K. McKinney, J. W. Munger, S. G. Pallardy, G. W. Schade, R. Seco, and N. Schoon. “An ecosystem-scale perspective of the net land methanol flux: synthesis of micrometeorological flux measurements”. In: *Atmos. Chem. Phys.* 15 (2015), pp. 7413–7427 (cit. on p. 217).

[698] P. Kharecha, J. Kasting, and J. Sieffert. “A coupled atmosphere-ecosystem model of the early Archean Earth”. In: *Geobiology* 3 (2005), pp. 53–76 (cit. on pp. 216, 217).

[699] D. A. Hauglustaine, C. Granier, G. P. Brasseur, and G. Mégie. “The importance of atmospheric chemistry in the calculation of radiative forcing on the climate system”. In: *J. Geophys. Res. Atmos.* 99 (1994), pp. 1173–1186 (cit. on p. 217).

[700] V. Wagner, R. von Glasow, H. Fischer, and P. J. Crutzen. “Are CH_2O measurements in the marine boundary layer suitable for testing the current understanding of CH_4 photooxidation?: A model study”. In: *J. Geophys. Res. Atmos.* 107 (1994), p. 4029 (cit. on p. 217).

[701] C. E. Harman, E. W. Schwieterman, J. C. Schottelkotte, and J. F. Kasting. “Abiotic O_2 Levels on Planets around F, G, K, and M Stars: Possible False Positives for Life?” In: *Astrophys. J.* 812.2, 137 (2015-10), p. 137 (cit. on p. 216).

[702] O. Poch, M. Jaber, F. Stalport, S. Nowak, T. Georgelin, J.-F. Lambert, C. Szopa, and P. Coll. “Effect of Nontronite Smectite Clay on the Chemical Evolution of Several Organic Molecules under Simulated Martian Surface Ultraviolet Radiation Conditions”. In: *Astrobiology* 15 (2015-03), pp. 221–237 (cit. on pp. 217, 218).

[703] A. Hill and L. E. Orgel. “Synthesis of Adenine from HCN Tetramer and Ammonium Formate”. In: *Orig. Life Evol. Biosph.* 32 (2002-04), pp. 99–102 (cit. on pp. 217, 218).

[704] H. Wakamatsu, Y. Yamada, T. Saito, I. Kumashiro, and T. Takenishi. “Synthesis of Adenine by Oligomerization of Hydrogen Cyanide”. In: *J. Org. Chem.* 31 (1966-06), pp. 2035–2036 (cit. on pp. 217, 218).

[705] C. E. Boyd. “Hydrology of Small Experimental Fish Ponds at Auburn, Alabama”. In: *Trans. Am. Fish. Soc.* 111 (1982), pp. 638–644 (cit. on pp. 217, 218).

[706] M. Levy and S. L. Miller. “The stability of the RNA bases: Implications for the origin of life”. In: *Proc. Natl. Acad. Sci. U.S.A.* 93 (1998-07), pp. 7933–7938 (cit. on pp. 217, 218).

[707] S. Miyakawa, H. J. Cleaves, and S. L. Miller. “The Cold Origin of Life: B. Implications Based on Pyrimidines and Purines Produced From Frozen Ammonium Cyanide Solutions”. In: *Orig. Life Evol. Biosph.* 32 (2002-06), pp. 209–218 (cit. on pp. 217, 218).

[708] R. Shapiro. “Prebiotic ribose synthesis: A critical analysis”. In: *Orig. Life Evol. Biosph.* 18 (1988), pp. 71–85 (cit. on pp. 218, 219).

[709] R. Szabla, J. E. Sponer, J. Sponer, and R. W. Góra. “Theoretical studies of the mechanism of 2-aminooxazole formation under prebiotically plausible conditions”. In: *Phys. Chem. Chem. Phys.* 15 (2013), pp. 7812–7818 (cit. on p. 218).

[710] A. Ricardo, M. A. Carrigan, A. N. Olcott, and S. A. Benner. “Borate Minerals Stabilize Ribose”. In: *Science* 9 (2004-01), p. 196 (cit. on p. 218).

[711] M. Touboul, T. Kleine, B. Bourdon, H. Palme, and R. Wieler. “Late formation and prolonged differentiation of the Moon inferred from W isotopes in lunar metals”. In: *Nature* 450 (2007-12), pp. 1206–1209 (cit. on p. 226).

[712] M. Touboul, T. Kleine, B. Bourdon, H. Palme, and R. Wieler. “Tungsten isotopes in ferroan anorthosites: Implications for the age of the Moon and lifetime of its magma ocean”. In: *Icarus* 199 (2009-02), pp. 245–249 (cit. on p. 226).

[713] A. N. Halliday. “A young Moon-forming giant impact at 70-110 million years accompanied by late-stage mixing, core formation and degassing of the Earth”. In: *Philos. Trans. R. Soc. Lond. A* 366 (2008), pp. 4163–4181 (cit. on p. 226).

[714] M. Barboni, P. Boehnke, B. Keller, I. E. Kohl, B. Schoene, E. D. Young, and K. D. McKeegan. “Early formation of the Moon 4.51 billion years ago”. In: *Sci. Adv.* 3 (2017), e1602365 (cit. on p. 226).

[715] A. Bouvier and M. Wadhwa. “The age of the Solar System redefined by the oldest Pb-Pb age of a meteoritic inclusion”. In: *Nature Geosci.* 3 (2010-09), pp. 637–641 (cit. on p. 226).

[716] G. P. W. Mantilla, S. G. B. Chester, W. A. Clemens, J. R. Moore, C. J. Sprain, B. T. Hovatter, W. S. Mitchell, W. W. Mans, R. Mundil, and P. R. Renne. “Earliest Palaeocene purgatoriids and the initial radiation of stem primates”. In: *R. Soc. open sci.* 8 (2021), p. 210050 (cit. on p. 227).

[717] P. G. Higgs. “Chemical Evolution and the Evolutionary Definition of Life”. In: *J. Mol. Evol.* 84 (2017), pp. 225–235 (cit. on p. 227).

[718] D. P. Bartel and J. W. Szostak. “Isolation of New Ribozymes from a Large Pool of Random Sequences”. In: *Science* 261 (1993), pp. 1411–1418 (cit. on p. 228).

[719] Planetary Habitability Laboratory. *Habitable Exoplanets Catalog.* 2017-04. URL: `http://phl.upr.edu/projects/habitable-exoplanets-catalog` (cit. on p. 229).

[720] S. Bryson, M. Kunimoto, R. K. Kopparapu, J. L. Coughlin, W. J. Borucki, D. Koch, V. S. Aguirre, C. Allen, G. Barentsen, N. M. Batalha, T. Berger, A. Boss, L. A. Buchhave, C. J. Burke, D. A. Caldwell, J. R. Campbell, J. Catanzarite, H. Chandrasekaran, W. J. Chaplin, J. L. Christiansen, J. Christensen-Dalsgaard, D. R. Ciardi, B. D. Clarke, W. D. Cochran, J. L. Dotson, L. R. Doyle, E. S. Duarte, E. W. Dunham, A. K. Dupree, M. Endl, J. L. Fanson, E. B. Ford, M. Fujieh, III Gautier T. N., J. C. Geary, R. L. Gilliland, F. R. Girouard,

A. Gould, M. R. Haas, C. E. Henze, M. J. Holman, A. W. Howard, S. B. Howell, D. Huber, R. C. Hunter, J. M. Jenkins, H. Kjeldsen, J. Kolodziejczak, K. Larson, D. W. Latham, J. Li, S. Mathur, S. Meibom, C. Middour, R. L. Morris, T. D. Morton, F. Mullally, S. E. Mullally, D. Pletcher, A. Prsa, S. N. Quinn, E. V. Quintana, D. Ragozzine, S. V. Ramirez, D. T. Sanderfer, D. Sasselov, S. E. Seader, M. Shabram, A. Shporer, J. C. Smith, J. H. Steffen, M. Still, G. Torres, J. Troeltzsch, J. D. Twicken, A. K. Uddin, J. E. Van Cleve, J. Voss, L. M. Weiss, W. F. Welsh, B. Wohler, and K. A. Zamudio. “The Occurrence of Rocky Habitable-zone Planets around Solar-like Stars from Kepler Data”. In: *Astrophys. J.* 161.1 (2021-01), p. 36 (cit. on p. 229).

[721] Eric D. Lopez and Jonathan J. Fortney. “Understanding the Mass-Radius Relation for Sub-neptunes: Radius as a Proxy for Composition”. In: *Astrophys. J.* 792.1 (2014-09), p. 1 (cit. on p. 229).

Appendix A

Quantum Chemistry Data

In Tables A.1, A.2, A.3, and A.4, we display the quantum chemistry data calculated for the reactions in Chapter 3. These tables correspond with Tables B1–B4 published in Appendix B of Pearce et al. [440]. In Table A.5, we display the quantum chemistry data calculated for the reactions in Chapter 4. This table corresponds with Table S5 published in the Supporting Information of Pearce et al. [634].

Table A.1: Quantum Chemistry Data at the BHandHLYP/aug-cc-pVDZ level of theory. Cartesian coordinates are in angstroms. Energies are in kJ mol^{-1}. E_e is the electronic energy, ZPE is the zero point energy, and q_x are the partition functions.

Reac.	Species	Geometry (Atom, X, Y, Z)	E_e + ZPE	E_e + Gibbs	$q_t/V(m^{-3})$	q_e	q_v	q_r
1	HCN	N, 0.00000, 0.00000, 0.64811 C, 0.00000, 0.00000, -0.49567 H, 0.00000, 0.00000, -1.56273	-245122.398339	-245173.207015	1.36E+32	1	1.05E+00	1.38E+02
	CH	C, 0.00000, 0.00000, 0.16040 H, 0.00000, 0.00000, -0.96239	-100985.100094	-101029.197992	4.54E+31	2	1.00E+00	1.44E+01
	TS	N, -0.76358, 0.08731, -0.00001 C, -1.89773, -0.05651, 0.00000 H, -2.95631, -0.19091, 0.00001 C, 2.94136, -0.10639, 0.00000 H, 2.03961, 0.55715, 0.00001	-346112.801943	-346186.778031	2.45E+32	2	4.55E+01	1.36E+04
	$HCNCH_a$	N, 0.00148, 0.00058, -0.00133 C, 1.20814, 0.11819, -0.07762 H, 2.02209, -0.40519, 0.40294 C, -1.23930, -0.16654, -0.03274 H, -1.84556, 0.69126, 0.26850	-346294.121599	-346357.474914	2.45E+32	2	1.61E+00	6.51E+03
2	CN	N, 0.00000, 0.00000, 0.53434 C, 0.00000, 0.00000, -0.62339	-243282.319290	-243333.949747	1.28E+32	2	1.00E+00	1.06E+02
	TS	N, 0.00000, 0.00000, 2.70742 C, 0.00000, 0.00000, 1.55000 C, 0.00000, 0.00000, -1.55000 N, 0.00000, 0.00000, -2.70742	-486566.187624	-486639.801393	3.63E+32	1	3.31E+02	1.62E+03
	NCCN	N, 0.00000, 0.00000, 1.83954 N, 0.00000, 0.00000, -1.83954 C, 0.00000, 0.00000, 0.69244 C, 0.00000, 0.00000, -0.69244	-487158.907377	-487217.912864	3.63E+32	1	2.26E+00	6.53E+02
3	CN	N, 0.00000, 0.00000, 0.53434 C, 0.00000, 0.00000, -0.62339	-243282.319290	-243333.949747	1.28E+32	2	1.00E+00	1.06E+02
	TS	N, 0.00000, 0.00000, 1.70471	-486570.094368	-486647.097658	3.63E+32	1	6.14E+02	3.42E+03

		C, 0.00000, 0.00000, 2.86117 C, 0.00000, 0.00000, -1.61529 N, 0.00000, 0.00000, -2.77261						
	CNCN	N, -0.69198, 0.00006, 0.00136 C, -1.86610, -0.00005, 0.00367 C, 0.61572, 0.00003, -0.00121 N, 1.76373, -0.00003, -0.00347	-487073.896312	-487118.521936	3.63E+32	1	1.87E+00	2.38E+00
4	CN	N, 0.00000, 0.00000, 0.53434 C, 0.00000, 0.00000, -0.62339	-243282.319290	-243333.949747	1.28E+32	2	1.00E+00	1.06E+02
	NH	N, 0.00000, 0.00000, -0.00325 H, 0.00000, 0.00000, 1.03180	-144933.050538	-144978.308907	5.63E+31	3	1.00E+00	1.24E+01
	TS	N, 0.58197, -1.89103, 0.00000 C, 0.00000, -0.89073, 0.00000 N, -0.61583, 2.24945, 0.00000 H , 0.23703, 2.83539, 0.00000	-388221.594888	-388295.536845	2.54E+32	2	3.07E+01	1.42E+04
	HNCN	N, -1.29395, 0.02090, -0.00000 C, -0.11079, 0.00123, 0.00000 N, 1.15517, -0.13112, -0.00000 H, 1.63619, 0.76421, -0.00000	-388694.203267	-388756.367230	2.54E+32	2	1.23E+00	3.07E+03
5/52	CN	N, 0.00000, 0.00000, 0.53434 C, 0.00000, 0.00000, -0.62339	-243282.319290	-243333.949747	1.28E+32	2	1.00E+00	1.06E+02
	^{4}N	N, 0.00000, 0.00000, 0.00000	-143303.088167	-143303.088167	5.07E+31	4	1.00E+00	1.00E+00
	TS	N, 0.00000, 0.00000, -1.93885 C, 0.00000, 0.00000, -0.78139 N, 0.00000, 0.00000, 2.60861	-386587.890641	-386657.474267	2.45E+32	3	2.72E+01	1.91E+03
	CN$_2$	N, 0.00000, 0.00000, 1.22410 C, 0.00000, 0.00000, 0.00000 N, 0.00000, 0.00000, -1.22410	-387063.565603	-387120.620344	2.45E+32	3	1.29E+00	2.58E+02
6/53	CN	N, 0.00000, 0.00000, 0.53434 C, 0.00000, 0.00000, -0.62339	-243282.319290	-243333.949747	1.28E+32	2	1.00E+00	1.06E+02
	^{2}N	N, 0.00000, 0.00000, 0.00000	-143024.189856	-143024.189856	5.07E+31	2	1.00E+00	1.00E+00
	TS	N, 0.00000, 0.00000, -2.06487 C, 0.00000, 0.00000, -0.90738 N, 0.00000, 0.00000, 2.84262	-386310.656219	-386381.794142	2.45E+32	3	4.33E+01	2.25E+03
	CN$_2$	N, 0.00000, 0.00000, 1.22410 C, 0.00000, 0.00000, 0.00000 N, 0.00000, 0.00000, -1.22410	-387063.565603	-387120.620344	2.45E+32	3	1.29E+00	2.58E+02
7	CN	N, 0.00000, 0.00000, 0.53434 C, 0.00000, 0.00000, -0.62339	-243282.319290	-243333.949747	1.28E+32	2	1.00E+00	1.06E+02
	CH$_3$	C, 0.00000, -0.00018, 0.00042 H, -0.93570, -0.53955, -0.00085 H, 0.93580, -0.53939, -0.00085 H, -0.00010, 1.08002, -0.00085	-104455.380974	-104507.305488	5.63E+31	2	1.08E+00	2.53E+02
	TS	N, -2.45144, 0.00112, -0.16220 C, -1.29638, 0.00061, -0.08579 C, 2.76473, -0.00127, 0.18294 H, 2.85301, 0.23880, -0.86645 H, 2.76179, -1.03319, 0.50199 H, 2.73516, 0.79055, 0.91698	-347740.911250	-347818.279484	2.54E+32	1	1.10E+02	3.16E+04
	CH$_3$CN	N, -1.42840, 0.00000, -0.00000 C, -0.28170, -0.00000, 0.00000 C, 1.17541, 0.00000, -0.00000 H, 1.54550, 0.89417, -0.50003 H, 1.54550, -0.88012, -0.52436 H, 1.54550, -0.01404, 1.02439	-348246.291120	-348309.282116	2.54E+32	1	1.42E+00	7.40E+03
8	CN	N, 0.00000, 0.00000, 0.53434 C, 0.00000, 0.00000, -0.62339	-243282.319290	-243333.949747	1.28E+32	2	1.00E+00	1.06E+02
	^{3}CH$_2$	C, 0.00000, 0.00000, 0.10395 H, 0.00000, -0.99689, -0.31186 H, 0.00000, 0.99689, -0.31186	-102701.224038	-102749.428218	5.08E+31	3	1.01E+00	8.96E+01
	TS	N, 0.16423, 2.27874, 0.00000 C, 0.00000, 1.13295, 0.00000 C, -0.24132, -2.80967, 0.00000 H, 0.14913, -2.94544, 0.99804 H, 0.14913, -2.94544, -0.99804	-345986.730684	-346064.133050	2.45E+32	2	7.76E+01	2.35E+04
	CH$_2$CN	N, 1.35314, 0.00000, 0.00000 C, 0.19060, -0.00001, 0.00000 C, -1.19240, 0.00000, 0.00000 H, -1.73057, 0.93601, 0.00000 H, -1.73058, -0.93600, 0.00000	-346564.991808	-346628.628677	2.45E+32	2	1.40E+00	5.05E+03

9	CN	N, 0.00000, 0.00000, 0.53434 C, 0.00000, 0.00000, -0.62339	-243282.319290	-243333.949747	1.28E+32	2	1.00E+00	1.06E+02
	$^{1}CH_2$	C, 0.00000, 0.17399, 0.00000 H, 0.86403, -0.52196, 0.00000 H, -0.86403, -0.52196, 0.00000	-102649.483309	-102697.613975	5.08E+31	1	1.00E+00	1.31E+02
	TS	N, -2.46797, -0.00002, -0.00001 C, -1.31059, 0.00003, 0.00002 C, 2.96941, -0.00001, -0.00001 H, 3.66148, -0.86593, 0.00001 H, 3.66141, 0.86596, 0.00001	-345935.788108	-346015.033574	2.45E+32	2	1.72E+02	2.24E+04
	CH_2CN	N, 1.35314, 0.00000, 0.00000 C, 0.19060, -0.00001, 0.00000 C, -1.19240, 0.00000, 0.00000 H, -1.73057, 0.93601, 0.00000 H, -1.73058, -0.93600, 0.00000	-346564.991808	-346628.628677	2.45E+32	2	1.40E+00	5.05E+03
10	CN	N, 0.00000, 0.00000, 0.53434 C, 0.00000, 0.00000, -0.62339	-243282.319290	-243333.949747	1.28E+32	2	1.00E+00	1.06E+02
	CH	C, 0.00000, 0.00000, 0.16040 H, 0.00000, 0.00000, -0.96239	-100985.100094	-101029.197992	4.54E+31	2	1.00E+00	1.44E+01
	TS	N, 1.88160, 0.04989, -0.00002 C, 0.72976, -0.05904, 0.00004 C, -2.36024, -0.06187, -0.00002 H, -3.38833, 0.37626, 0.00004	-344283.545205	-344354.543975	2.36E+32	3	1.87E+01	5.12E+03
	$^{3}HCCN$	N, -1.28160, 0.01171, 0.00000 C, -0.08625, 0.01570, -0.00000 C, 1.21490, -0.08477, 0.00000 H, 2.19935, 0.33243, 0.00000	-344845.446838	-344907.174969	2.36E+32	3	1.50E+00	1.51E+03
11	CN	N, 0.00000, 0.00000, 0.53434 C, 0.00000, 0.00000, -0.62339	-243282.319290	-243333.949747	1.28E+32	2	1.00E+00	1.06E+02
	CH	C, 0.00000, 0.00000, 0.16040 H, 0.00000, 0.00000, -0.96239	-100985.100094	-101029.197992	4.54E+31	2	1.00E+00	1.44E+01
	TS	N, 2.07842, 0.11628, -0.00002 C, 0.95421, -0.15892, 0.00002 C, -2.83567, -0.12840, -0.00001 H, -3.26013, 0.90992, 0.00003	-344272.746523	-344346.063611	2.36E+32	1	4.43E+01	1.65E+04
	$^{1}HCCN$	N, -1.26348, 0.01994, 0.00000 C, -0.09808, 0.00643, -0.00000 C, 1.27584, -0.16493, 0.00000 H, 1.77782, 0.81150, 0.00000	-344766.495428	-344827.396526	2.36E+32	1	1.45E+00	3.36E+03
12	CN	N, 0.00000, 0.00000, 0.53434 C, 0.00000, 0.00000, -0.62339	-243282.319290	-243333.949747	1.28E+32	2	1.00E+00	1.06E+02
	H	H, 0.00000, 0.00000, 0.00000	-1307.704984	-1307.704984	9.79E+29	2	1.00E+00	1.00E+00
	TS	N, 0.00000, 0.00000, -0.81946 C, 0.00000, 0.00000, 0.33803 H, 0.00000, 0.00000, 3.70803	-244592.147108	-244650.346567	1.36E+32	1	9.60E+00	2.97E+02
	HCN	N, 0.00000, 0.00000, 0.64811 C, 0.00000, 0.00000, -0.49567 H, 0.00000, 0.00000, -1.56273	-245122.398339	-245173.207015	1.36E+32	1	1.05E+00	1.38E+02
13/70	^{4}N	N, 0.00000, 0.00000, 0.00000	-143303.088167	-143303.088167	5.07E+31	4	1.00E+00	1.00E+00
	$^{3}CH_2$	C, 0.00000, 0.00000, 0.10395 H, 0.00000, -0.99689, -0.31186 H, 0.00000, 0.99689, -0.31186	-102701.224038	-102749.428218	5.08E+31	3	1.01E+00	8.96E+01
	TS	C, 1.57889, 0.00000, -0.09079 N, -1.86978, 0.00000, 0.00484 H, 1.80756, -0.99713, 0.25544 H, 1.80757, 0.99713, 0.25544	-246006.522337	-246074.837847	1.43E+32	2	8.15E+00	9.79E+03
	H_2CN	C, -0.50346, 0.00000, 0.00005 N, 0.73653, 0.00000, -0.00006 H, -1.06749, 0.93849, 0.00008 H, -1.06748, -0.93850, 0.00008	-246571.579821	-246629.894802	1.43E+32	2	1.02E+00	1.39E+03
14	^{4}N	N, 0.00000, 0.00000, 0.00000	-143303.088167	-143303.088167	5.07E+31	4	1.00E+00	1.00E+00
	TS	N, 0.00000, 0.00000, 1.92000 N, 0.00000, 0.00000, -1.92000	-286606.695105	-286661.308131	1.43E+32	1	1.00E+00	6.35E+02
	N_2	N, 0.00000, 0.00000, 0.54524 N, 0.00000, 0.00000, -0.54524	-287431.443420	-287479.813007	1.43E+32	1	1.00E+00	5.12E+01
15	^{4}N	N, 0.00000, 0.00000, 0.00000	-143303.088167	-143303.088167	5.07E+31	4	1.00E+00	1.00E+00
	H	H, 0.00000, 0.00000, 0.00000	-1307.704984	-1307.704984	9.79E+29	2	1.00E+00	1.00E+00
	TS	N, 0.00000, 0.00000, 0.46625 H, 0.00000, 0.00000, -3.26375	-144611.321768	-144662.936473	5.63E+31	3	1.00E+00	1.61E+02
	NH	N, 0.00000, 0.00000, -0.00325	-144933.050538	-144978.308907	5.63E+31	3	1.00E+00	1.24E+01

		H, 0.00000, 0.00000, 1.03180						
16/75	^{2}N	N, 0.00000, 0.00000, 0.00000	-143024.189856	-143024.189856	5.07E+31	2	1.00E+00	1.00E+00
	^{3}CH$_2$	C, 0.00000, 0.00000, 0.10395 H, 0.00000, -0.99689, -0.31186 H, 0.00000, 0.99689, -0.31186	-102701.224038	-102749.428218	5.08E+31	3	1.01E+00	8.96E+01
	TS	C, 1.62503, -0.00000, -0.09502 N, -1.91358, 0.00001, 0.00430 H, 1.82238, -0.99717, 0.26999 H, 1.82250, 0.99714, 0.27000	-245898.876837	-245967.284239	1.43E+32	2	8.02E+00	1.03E+04
	H$_2$CN	C, -0.50346, 0.00000, 0.00005 N, 0.73653, 0.00000, -0.00006 H, -1.06749, 0.93849, 0.00008 H, -1.06748, -0.93850, 0.00008	-246571.579821	-246629.894802	1.43E+32	2	1.02E+00	1.39E+03
17/77	^{2}N	N, 0.00000, 0.00000, 0.00000	-143024.189856	-143024.189856	5.07E+31	2	1.00E+00	1.00E+00
	^{1}CH$_2$	C, 0.00000, 0.17399, 0.00000 H, 0.86403, -0.52196, 0.00000 H, -0.86403, -0.52196, 0.00000	-102649.483309	-102697.613975	5.08E+31	1	1.00E+00	1.31E+02
	TS	C, 1.58160, 0.00000, -0.12834 N, -1.90566, 0.00000, 0.00986 H, 1.92501, -0.92282, 0.35051 H, 1.92501, 0.92282, 0.35051	-245876.60472	-245943.520839	1.43E+32	2	4.58E+00	9.89E+03
	H$_2$CN	C, -0.50346, 0.00000, 0.00005 N, 0.73653, 0.00000, -0.00006 H, -1.06749, 0.93849, 0.00008 H, -1.06748, -0.93850, 0.00008	-246571.579821	-246629.894802	1.43E+32	2	1.02E+00	1.39E+03
18	^{2}N	N, 0.00000, 0.00000, 0.00000	-143024.189856	-143024.189856	5.07E+31	2	1.00E+00	1.00E+00
	TS	N, 0.00000, 0.00000, 1.95000 N, 0.00000, 0.00000, -1.95000	-286391.952835	-286446.642000	1.43E+32	1	1.00E+00	6.55E+02
	N$_2$	N, 0.00000, 0.00000, 0.54524 N, 0.00000, 0.00000, -0.54524	-287431.443420	-287479.813007	1.43E+32	1	1.00E+00	5.12E+01
19	^{2}N	N, 0.00000, 0.00000, 0.00000	-143024.189856	-143024.189856	5.07E+31	2	1.00E+00	1.00E+00
	H	H, 0.00000, 0.00000, 0.00000	-1307.704984	-1307.704984	9.79E+29	2	1.00E+00	1.00E+00
	TS	N, 0.00000, 0.00000, 0.44250 H, 0.00000, 0.00000, -3.0975f0	-144332.302007	-144383.656787	5.63E+31	3	1.00E+00	1.45E+02
	NH	N, 0.00000, 0.00000, -0.00325 H, 0.00000, 0.00000, 1.03180	-144933.050538	-144978.308907	5.63E+31	3	1.00E+00	1.24E+01
20/82	CH$_4$	C, 0.00006, -0.00000, -0.00001 H, -1.07741, 0.05086, 0.15637 H, 0.23679, -0.86565, -0.61803 H, 0.33754, 0.90709, -0.50065 H, 0.50273, -0.09229, 0.96235	-106174.920693	-106226.540649	6.21E+31	1	1.01E+00	4.36E+02
	^{1}CH$_2$	C, 0.00000, 0.17399, 0.00000 H, 0.86403, -0.52196, 0.00000 H, -0.86403, -0.52196, 0.00000	-102649.483309	-102697.613975	5.08E+31	1	1.00E+00	1.31E+02
	TS	C, -0.00806, 0.00802, 0.00701 H, 0.07029, -0.02310, 1.11147 H, 1.05259, 0.00169, -0.31133 C, 0.32334, 2.72536, 0.35891 H, 0.20227, 3.51229, -0.38377 H, -0.17412, 2.99764, 1.28722 H, 1.37962, 2.53981, 0.53629 H, -0.18449, 1.82949, -0.06140	-208827.940551	-208896.563244	1.59E+32	1	1.48E+01	1.10E+04
	C$_2$H$_6$	C, -0.76053, 0.00001, -0.00000 C, 0.76053, -0.00001, 0.00000 H, -1.15654, 0.65419, 0.77923 H, -1.15654, 0.34777, -0.95614 H, -1.15657, -1.00190, 0.17691 H, 1.15654, -0.34777, 0.95614 H, 1.15657, 1.00190, -0.17691 H, 1.15654, -0.65419, -0.77923	-209247.484949	-209308.094616	1.59E+32	1	1.34E+00	4.80E+03
21	CH$_3$	C, 0.00000, -0.00018, 0.00042 H, -0.93570, -0.53955, -0.00085 H, 0.93580, -0.53939, -0.00085 H, -0.00010, 1.08002, -0.00085	-104455.380974	-104507.305488	5.63E+31	2	1.08E+00	2.53E+02
	TS	C, 1.62000, 0.00063, -0.00005 C, -1.62000, -0.00063, 0.00005 H, 1.65102, -0.73297, 0.79158 H, 1.65081, -0.31812, -1.03119 H, 1.65031, 1.05301, 0.23946 H, -1.65081, 0.31794, 1.03124	-208914.219732	-208987.229636	1.59E+32	1	5.67E+01	1.68E+04

		H, -1.65031, -1.05297, -0.23966 H, -1.65102, 0.73311, -0.79144						
	C_2H_6	C, -0.76053, 0.00001, -0.00000 C, 0.76053, -0.00001, 0.00000 H, -1.15654, 0.65419, 0.77923 H, -1.15654, 0.34777, -0.95614 H, -1.15657, -1.00190, 0.17691 H, 1.15654, -0.34777, 0.95614 H, 1.15657, 1.00190, -0.17691 H, 1.15654, -0.65419, -0.77923	-209247.484949	-209308.094616	1.59E+32	1	1.34E+00	4.80E+03
22	CH_3	C, 0.00000, -0.00018, 0.00042 H, -0.93570, -0.53955, -0.00085 H, 0.93580, -0.53939, -0.00085 H, -0.00010, 1.08002, -0.00085	-104455.380974	-104507.305488	5.63E+31	2	1.08E+00	2.53E+02
	H	H, 0.00000, 0.00000, 0.00000	-1307.704984	-1307.704984	9.79E+29	2	1.00E+00	1.00E+00
	TS	C, -0.33871, -0.00000, 0.00000 H, -0.34637, 1.04082, 0.28812 H, 3.07129, 0.00002, 0.00000 H, -0.34630, -0.76993, 0.75732 H, -0.34632, -0.27089, -1.04544	-105765.011880	-105824.642236	6.21E+31	1	6.06E+00	1.83E+03
	CH_4	C, 0.00006, -0.00000, -0.00001 H, -1.07741, 0.05086, 0.15637 H, 0.23679, -0.86565, -0.61803 H, 0.33754, 0.90709, -0.50065 H, 0.50273, -0.09229, 0.96235	-106174.920693	-106226.540649	6.21E+31	1	1.01E+00	4.36E+02
23/92	$^3CH_2$	C, 0.00000, 0.00000, 0.10395 H, 0.00000, -0.99689, -0.31186 H, 0.00000, 0.99689, -0.31186	-102701.224038	-102749.428218	5.08E+31	3	1.01E+00	8.96E+01
	TS	C, 1.67392, 0.00000, 0.06012 C, -1.67392, 0.00000, -0.06012 H, 2.03581, -0.99563, -0.14828 H, 2.03581, 0.99563, -0.14829 H, -2.03580, 0.99563, 0.14831 H, -2.03580, -0.99563, 0.14829	-205407.969502	-205484.135257	1.44E+32	1	2.82E+02	1.34E+04
	C_2H_4	C, 0.66260, 0.00000, -0.00001 C, -0.66260, 0.00000, -0.00004 H, 1.23042, -0.92259, 0.00004 H, 1.23042, 0.92259, 0.00004 H, -1.23042, 0.92259, 0.00010 H, -1.23042, -0.92259, 0.00010	-206070.742845	-206128.939678	1.44E+32	1	1.04E+00	2.59E+03
24/96	$^3CH_2$	C, 0.00000, 0.00000, 0.10395 H, 0.00000, -0.99689, -0.31186 H, 0.00000, 0.99689, -0.31186	-102701.224038	-102749.428218	5.08E+31	3	1.01E+00	8.96E+01
	H	H, 0.00000, 0.00000, 0.00000	-1307.704984	-1307.704984	9.79E+29	2	1.00E+00	1.00E+00
	TS	C, 0.00000, 0.34834, 0.00000 H, -0.81124, -2.96376, 0.00000 H, 0.40562, 0.43686, -0.99709 H, 0.40562, 0.43686, 0.99709	-104010.854944	-104071.422603	5.63E+31	2	6.37E+00	1.40E+03
	CH_3	C, 0.00000, -0.00018, 0.00042 H, -0.93570, -0.53955, -0.00085 H, 0.93580, -0.53939, -0.00085 H, -0.00010, 1.08002, -0.00085	-104455.380974	-104507.305488	5.63E+31	2	1.08E+00	2.53E+02
25/97	$^1CH_2$	C, 0.00000, 0.17399, 0.00000 H, 0.86403, -0.52196, 0.00000 H, -0.86403, -0.52196, 0.00000	-102649.483309	-102697.613975	5.08E+31	1	1.00E+00	1.31E+02
	TS	C, -1.78750, 0.00000, 0.03805 C, 1.99685, -0.00000, -0.16889 H, -2.46075, 0.86666, -0.11561 H, -2.46074, -0.86666, -0.11562 H, 1.83269, -0.86243, 0.50817 H, 1.83269, 0.86244, 0.50814	-205303.566494	-205376.203577	1.44E+32	1	5.68E+01	1.60E+04
	C_2H_4	C, 0.66260, 0.00000, -0.00001 C, -0.66260, 0.00000, -0.00004 H, 1.23042, -0.92259, 0.00004 H, 1.23042, 0.92259, 0.00004 H, -1.23042, 0.92259, 0.00010 H, -1.23042, -0.92259, 0.00010	-206070.742845	-206128.939678	1.44E+32	1	1.04E+00	2.59E+03
26/99	$^1CH_2$	C, 0.00000, 0.17399, 0.00000 H, 0.86403, -0.52196, 0.00000 H, -0.86403, -0.52196, 0.00000	-102649.483309	-102697.613975	5.08E+31	1	1.00E+00	1.31E+02

	H_2	H, 0.00000, 0.00000, 0.37683 H, 0.00000, 0.00000, -0.37683	-3031.139750	-3061.369757	2.77E+30	1	1.00E+00	3.52E+00
	TS	C, -0.00943, 0.04730, -0.00739 H, -0.00350, -0.06982, 1.09563 H, 1.06280, -0.06982, -0.26629 H, -0.19002, -2.61283, -0.14879 H, 0.38560, -2.41667, 0.30191	-105680.780589	-105738.279039	6.21E+31	1	3.00E+00	1.57E+03
	CH_4	C, 0.00006, -0.00000, -0.00001 H, -1.07741, 0.05086, 0.15637 H, 0.23679, -0.86565, -0.61803 H, 0.33754, 0.90709, -0.50065 H, 0.50273, -0.09229, 0.96235	-106174.920693	-106226.540649	6.21E+31	1	1.01E+00	4.36E+02
27/ 100/ 101	$^1CH_2$	C, 0.00000, 0.17399, 0.00000 H, 0.86403, -0.52196, 0.00000 H, -0.86403, -0.52196, 0.00000	-102649.483309	-102697.613975	5.08E+31	1	1.00E+00	1.31E+02
	H	H, 0.00000, 0.00000, 0.00000	-1307.704984	-1307.704984	9.79E+29	2	1.00E+00	1.00E+00
	TS	C, 0.28767, 0.00000, -0.17522 H, -2.36569, -0.00001, 0.01259 H, 0.31985, -0.86451, 0.51937 H, 0.31981, 0.86451, 0.51937	-103959.594682	-104016.688805	5.63E+31	2	2.41E+00	9.13E+02
	CH_3	C, 0.00000, -0.00018, 0.00042 H, -0.93570, -0.53955, -0.00085 H, 0.93580, -0.53939, -0.00085 H, -0.00010, 1.08002, -0.00085	-104455.380974	-104507.305488	5.63E+31	2	1.08E+00	2.53E+02
28	CH	C, 0.00000, 0.00000, 0.16040 H, 0.00000, 0.00000, -0.96239	-100985.100094	-101029.197992	4.54E+31	2	1.00E+00	1.44E+01
	TS	C, -2.55027, 0.00002, -0.00002 C, 2.22973, -0.00003, 0.00002 H, -1.42820, -0.00008, -0.00003 H, 3.35142, 0.00016, 0.00003	-201971.024595	-202018.204830	1.28E+32	1	1.46E+01	1.86E+03
	C_2H_2	C, 0.00000, 0.00000, 0.59918 C, 0.00000, 0.00000, -0.59918 H, 0.00000, 0.00000, 1.66311 H, 0.00000, 0.00000, -1.66311	-202839.521617	-202889.287969	1.28E+32	1	1.15E+00	1.74E+02
29/ 103	CH	C, 0.00000, 0.00000, 0.16040 H, 0.00000, 0.00000, -0.96239	-100985.100094	-101029.197992	4.54E+31	2	1.00E+00	1.44E+01
	H_2	H, 0.00000, 0.00000, 0.37683 H, 0.00000, 0.00000, -0.37683	-3031.139750	-3061.369757	2.77E+30	1	1.00E+00	3.52E+00
	TS	H, 0.26436, 2.18183, 0.00000 H, 0.80634, 1.65234, 0.00000 C, 0.00000, -0.59561, 0.00000 H, -1.07069, -0.26050, 0.00000	-104017.536841	-104075.229578	5.63E+31	2	2.55E+00	1.09E+03
	CH_3	C, 0.00000, -0.00018, 0.00042 H, -0.93570, -0.53955, -0.00085 H, 0.93580, -0.53939, -0.00085 H, -0.00010, 1.08002, -0.00085	-104455.380974	-104507.305488	5.63E+31	2	1.08E+00	2.53E+02
30/ 104	CH	C, 0.00000, 0.00000, 0.16040 H, 0.00000, 0.00000, -0.96239	-100985.100094	-101029.197992	4.54E+31	2	1.00E+00	1.44E+01
	H	H, 0.00000, 0.00000, 0.00000	-1307.704984	-1307.704984	9.79E+29	2	1.00E+00	1.00E+00
	TS	C, 0.00000, 0.36913, 0.00000 H, 1.11986, 0.42442, 0.00000 H, -1.11986, -2.63919, 0.00000	-102294.045744	-102351.525816	5.08E+31	3	2.43E+00	7.78E+02
	$^3CH_2$	C, 0.00000, 0.00000, 0.10395 H, 0.00000, -0.99689, -0.31186 H, 0.00000, 0.99689, -0.31186	-102701.224038	-102749.428218	5.08E+31	3	1.01E+00	8.96E+01
31	CH	C, 0.00000, 0.00000, 0.16040 H, 0.00000, 0.00000, -0.96239	-100985.100094	-101029.197992	4.54E+31	2	1.00E+00	1.44E+01
	H	H, 0.00000, 0.00000, 0.00000	-1307.704984	-1307.704984	9.79E+29	2	1.00E+00	1.00E+00
	TS	C, 0.00000, 0.38237, 0.00000 H, 1.11054, 0.22839, 0.00000 H, -1.11054, -2.52259, 0.00000	-102294.106131	-102348.593133	5.08E+31	1	2.19E+00	7.78E+02
	$^1CH_2$	C, 0.00000, 0.17399, 0.00000 H, 0.86403, -0.52196, 0.00000 H, -0.86403, -0.52196, 0.00000	-102649.483309	-102697.613975	5.08E+31	1	1.00E+00	1.31E+02
32	H	H, 0.00000, 0.00000, 0.00000	-1307.704984	-1307.704984	9.79E+29	2	1.00E+00	1.00E+00
	TS	H, 0.00000, 0.00000, 1.85000 H, 0.00000, 0.00000, -1.85000	-2615.974686	-2654.096946	2.77E+30	1	1.00E+00	4.24E+01
	H_2	H, 0.00000, 0.00000, 0.37683 H, 0.00000, 0.00000, -0.37683	-3031.139750	-3061.369757	2.77E+30	1	1.00E+00	3.52E+00
35	H_2CN	C, -0.50346, 0.00000, 0.00005	-246571.579821	-246629.894802	1.43E+32	2	1.02E+00	1.39E+03

		N, 0.73653, 0.00000, -0.00006 H, -1.06749, 0.93849, 0.00008 H, -1.06748, -0.93850, 0.00008						
	NH	N, 0.00000, 0.00000, -0.00325 H, 0.00000, 0.00000, 1.03180	-144933.050538	-144978.308907	5.63E+31	3	1.00E+00	1.24E+01
	TS	C, 0.73737, 0.44137, 0.00000 N, 1.53028, -0.48839, 0.00000 H, 1.01092, 1.50049, 0.00000 H, -0.40710, 0.25487, 0.00000 N, -1.97746, 0.00575, -0.00000 H, -1.89782, -1.02503, 0.00001	-391498.426303	-391570.816589	2.73E+32	2	9.19E+00	2.36E+04
36	H_2CN	C, -0.50346, 0.00000, 0.00005 N, 0.73653, 0.00000, -0.00006 H, -1.06749, 0.93849, 0.00008 H, -1.06748, -0.93850, 0.00008	-246571.579821	-246629.894802	1.43E+32	2	1.02E+00	1.39E+03
	^4N	N, 0.00000, 0.00000, 0.00000	-143303.088167	-143303.088167	5.07E+31	4	1.00E+00	1.00E+00
	TS	C, 1.11018, 0.34835, 0.00000 N, 0.40694, -0.67793, 0.00000 H, 0.68665, 1.35455, 0.00000 H, 2.19962, 0.24787, 0.00000 N, -1.77085, 0.15042, 0.00000	-389877.025148	-389945.857882	2.64E+32	3	2.08E+00	1.72E+04
37	H_2CN	C, -0.50346, 0.00000, 0.00005 N, 0.73653, 0.00000, -0.00006 H, -1.06749, 0.93849, 0.00008 H, -1.06748, -0.93850, 0.00008	-246571.579821	-246629.894802	1.43E+32	2	1.02E+00	1.39E+03
	^4N	N, 0.00000, 0.00000, 0.00000	-143303.088167	-143303.088167	5.07E+31	4	1.00E+00	1.00E+00
	TS	C, -0.61856, 0.42372, 0.00000 N, -1.44713, -0.45229, 0.00000 H, -0.73203, 1.50778, 0.00000 H, 0.56977, 0.09565, 0.00000 N, 2.00050, -0.13995, 0.00000	-389859.274143	-389928.353673	2.64E+32	3	1.99E+00	1.98E+04
38	H_2CN	C, -0.50346, 0.00000, 0.00005 N, 0.73653, 0.00000, -0.00006 H, -1.06749, 0.93849, 0.00008 H, -1.06748, -0.93850, 0.00008	-246571.579821	-246629.894802	1.43E+32	2	1.02E+00	1.39E+03
	^2N	N, 0.00000, 0.00000, 0.00000	-143024.189856	-143024.189856	5.07E+31	2	1.00E+00	1.00E+00
	TS	C, 1.25249, 0.37783, 0.00000 N, 0.61439, -0.68665, 0.00000 H, 0.74820, 1.34797, 0.00000 H, 2.34722, 0.36706, 0.00000 N, -2.13015, 0.11779, 0.00000	-389770.217183	-389842.310787	2.64E+32	3	5.48E+00	2.43E+04
39	H_2CN	C, -0.50346, 0.00000, 0.00005 N, 0.73653, 0.00000, -0.00006 H, -1.06749, 0.93849, 0.00008 H, -1.06748, -0.93850, 0.00008	-246571.579821	-246629.894802	1.43E+32	2	1.02E+00	1.39E+03
	^2N	N, 0.00000, 0.00000, 0.00000	-143024.189856	-143024.189856	5.07E+31	2	1.00E+00	1.00E+00
	TS	C, -1.19854, 0.36771, 0.00000 N, -0.53772, -0.68350, 0.00000 H, -0.71929, 1.34994, 0.00000 H, -2.29249, 0.32844, 0.00000 N, 1.99529, 0.12855, 0.00000	-389770.983829	-389839.118179	2.64E+32	1	3.77E+00	2.14E+04
40/42	H_2CN	C, -0.50346, 0.00000, 0.00005 N, 0.73653, 0.00000, -0.00006 H, -1.06749, 0.93849, 0.00008 H, -1.06748, -0.93850, 0.00008	-246571.579821	-246629.894802	1.43E+32	2	1.02E+00	1.39E+03
	CH	C, 0.00000, 0.00000, 0.16040 H, 0.00000, 0.00000, -0.96239	-100985.100094	-101029.197992	4.54E+31	2	1.00E+00	1.44E+01
	TS($^1H_2CNCH$)	C, 1.62012, -0.17355, 0.00173 N, 0.49776, 0.35177, -0.00095 H, 1.73068, -1.26022, 0.07476 H, 2.52757, 0.43434, -0.06889 C, -2.50370, -0.24358, -0.02051 H, -2.44110, 0.86624, 0.11346	-347566.780214	-347646.204214	2.54E+32	1	3.53E+02	2.26E+04
	$^1H_2CNCH$	C, 1.16896, 0.00000, 0.01860 N, -0.09646, 0.00000, 0.00311 H, 1.70259, -0.94062, 0.02575 H, 1.70260, 0.94062, 0.02575 C, -1.30535, 0.00000, -0.15653 H, -1.91163, 0.00000, 0.75431	-348011.303619	-348073.756387	2.54E+32	1	1.44E+00	5.89E+03
	TS(H_2CNC_a+H)	N, 0.10662, -0.11917, 0.00000	-347782.680330	-347849.620078	2.54E+32	1	4.99E+00	1.03E+04

		C, 1.26337, -0.35599, 0.00000 H, 2.32639, 1.86247, 0.00000 C, -1.20365, 0.11552, 0.00000 H, -1.71552, 0.20726, 0.94564 H, -1.71552, 0.20726, -0.94564						
	TS(HCN+^{1}CH$_2$)	C, 2.49373, -0.00000, -0.18807 N, -0.75428, 0.00000, 0.09126 H, 2.29824, 0.86180, 0.48121 H, 2.29823, -0.86179, 0.48123 C, -1.88857, -0.00000, -0.04875 H, -2.94745, -0.00001, -0.18034	-347778.272115	-347851.295147	2.54E+32	1	3.41E+01	1.76E+04
41	H$_2$CN	C, -0.50346, 0.00000, 0.00005 N, 0.73653, 0.00000, -0.00006 H, -1.06749, 0.93849, 0.00008 H, -1.06748, -0.93850, 0.00008	-246571.579821	-246629.894802	1.43E+32	2	1.02E+00	1.39E+03
	CH	C, 0.00000, 0.00000, 0.16040 H, 0.00000, 0.00000, -0.96239	-100985.100094	-101029.197992	4.54E+31	2	1.00E+00	1.44E+01
	TS	C, 1.44461, 0.29188, 0.00000 N, 0.56154, -0.57774, -0.00000 H, 1.18242, 1.35434, 0.00000 H, 2.50423, 0.01776, 0.00001 C, -2.29014, 0.28729, -0.00000 H, -2.54428, -0.80292, 0.00002	-347567.541609	-347645.022739	2.54E+32	3	4.74E+01	2.55E+04
43	H$_2$CN	C, -0.50346, 0.00000, 0.00005 N, 0.73653, 0.00000, -0.00006 H, -1.06749, 0.93849, 0.00008 H, -1.06748, -0.93850, 0.00008	-246571.579821	-246629.894802	1.43E+32	2	1.02E+00	1.39E+03
	H	H, 0.00000, 0.00000, 0.00000	-1307.704984	-1307.704984	9.79E+29	2	1.00E+00	1.00E+00
	TS	C, -0.24004, 0.30788, 0.00000 N, 0.82681, -0.31274, 0.00000 H, -1.21126, -0.23198, -0.00000 H, -2.85683, -0.82746, 0.00000 H, -0.27931, 1.40138, 0.00000	-247881.510034	-247942.915228	1.51E+32	1	2.50E+00	3.73E+03
44	H$_2$CN	C, -0.50346, 0.00000, 0.00005 N, 0.73653, 0.00000, -0.00006 H, -1.06749, 0.93849, 0.00008 H, -1.06748, -0.93850, 0.00008	-246571.579821	-246629.894802	1.43E+32	2	1.02E+00	1.39E+03
	TS	C, -0.16571, -0.00012, 0.13198 N, 0.18272, 0.00008, 1.23364 H, 1.40834, -0.00002, -0.89602 H, -0.75247, -0.00036, -0.76206	-246412.093824	-246471.474757	1.43E+32	2	1.15E+00	1.89E+03
45	HCN	N, 0.00000, 0.00000, 0.64811 C, 0.00000, 0.00000, -0.49567 H, 0.00000, 0.00000, -1.56273	-245122.398339	-245173.207015	1.36E+32	1	1.05E+00	1.38E+02
	CN	N, 0.00000, 0.00000, 0.53434 C, 0.00000, 0.00000, -0.62339	-243282.319290	-243333.949747	1.28E+32	2	1.00E+00	1.06E+02
	TS	N, -0.69373, 1.67036, 0.00000 C, 0.39976, 1.28833, 0.00000 H, 1.46398, 1.16961, 0.00000 C, 0.00000, -0.96651, 0.00000 N, 0.14194, -2.11329, 0.00000	-488406.854785	-488481.681535	3.73E+32	2	1.26E+01	3.35E+04
46	HCN	N, 0.00000, 0.00000, 0.64811 C, 0.00000, 0.00000, -0.49567 H, 0.00000, 0.00000, -1.56273	-245122.398339	-245173.207015	1.36E+32	1	1.05E+00	1.38E+02
	^{2}N	N, 0.00000, 0.00000, 0.00000	-143024.189856	-143024.189856	5.07E+31	2	1.00E+00	1.00E+00
	TS	N, 0.00000, 0.00000, 0.79665 C, 0.00000, 0.00000, 1.94046 H, 0.00000, 0.00000, 3.00752 N, 0.00000, 0.00000, -2.88955	-388150.409707	-388218.578189	2.54E+32	2	1.92E+01	2.21E+03
47	HCN	N, 0.00000, 0.00000, 0.64811 C, 0.00000, 0.00000, -0.49567 H, 0.00000, 0.00000, -1.56273	-245122.398339	-245173.207015	1.36E+32	1	1.05E+00	1.38E+02
	^{1}CH$_2$	C, 0.00000, 0.17399, 0.00000 H, 0.86403, -0.52196, 0.00000 H, -0.86403, -0.52196, 0.00000	-102649.483309	-102697.613975	5.08E+31	1	1.00E+00	1.31E+02
	TS	N, 0.75428, 0.00001, 0.09125 C, 1.88857, -0.00000, -0.04874 H, 2.94745, -0.00002, -0.18031 C, -2.49373, -0.00001, -0.18807 H, -2.29824, 0.86180, 0.48121	-347778.272115	-347851.295147	2.54E+32	1	3.41E+01	1.76E+04

		H, -2.29821, -0.86179, 0.48124						
48/49	HCN	N, 0.00000, 0.00000, 0.64811 C, 0.00000, 0.00000, -0.49567 H, 0.00000, 0.00000, -1.56273	-245122.398339	-245173.207015	1.36E+32	1	1.05E+00	1.38E+02
	H	H, 0.00000, 0.00000, 0.00000	-1307.704984	-1307.704984	9.79E+29	2	1.00E+00	1.00E+00
	TS(HCNH)	N, 0.04557, 0.00005, 0.03268 H, -0.18267, 0.00002, 1.58600 C, 1.12876, -0.00012, -0.38119 H, 2.17966, -0.00030, -0.57483	-246399.433663	-246458.061077	1.43E+32	2	1.15E+00	1.39E+03
	HCNH	N, 0.11148, 0.58631, 0.00000 H, -0.77382, 1.09266, 0.00000 C, 0.11148, -0.63322, 0.00000 H, -0.67543, -1.39750, 0.00000	-246509.347595	-246567.284503	1.43E+32	2	1.03E+00	1.17E+03
	TS(HNC + H)	N, 0.28317, 0.00001, 0.20866 H, -0.35446, 0.00004, 0.97119 C, 1.08224, -0.00005, -0.63973 H, 3.00889, -0.00063, -0.18318	-246374.698827	-246434.883163	1.43E+32	2	1.70E+00	1.76E+03
	HNC	C, 0.00000, 0.00000, 0.73583 N, 0.00000, 0.00000, -0.42762 H, 0.00000, 0.00000, -1.42168	-245073.122955	-245124.317580	1.36E+32	1	1.24E+00	1.35E+02
	H	H, 0.00000, 0.00000, 0.00000	-1307.704984	-1307.704984	9.79E+29	2	1.00E+00	1.00E+00
50	CN	N, 0.00000, 0.00000, 0.53434 C, 0.00000, 0.00000, -0.62339	-243282.319290	-243333.949747	1.28E+32	2	1.00E+00	1.06E+02
	NH	N, 0.00000, 0.00000, -0.00325 H, 0.00000, 0.00000, 1.03180	-144933.050538	-144978.308907	5.63E+31	3	1.00E+00	1.24E+01
	TS	N, -1.92509, -0.00172, 0.00000 C, -0.76797, 0.00267, 0.00000 H, 1.33920, 0.00133, 0.00000 N, 2.39203, -0.00076, 0.00000	-388211.993435	-388271.552902	2.54E+32	4	5.24E+00	1.26E+02
51	CN	N, 0.00000, 0.00000, 0.53434 C, 0.00000, 0.00000, -0.62339	-243282.319290	-243333.949747	1.28E+32	2	1.00E+00	1.06E+02
	NH	N, 0.00000, 0.00000, -0.00325 H, 0.00000, 0.00000, 1.03180	-144933.050538	-144978.308907	5.63E+31	3	1.00E+00	1.24E+01
	TS	N, 1.80919, -0.20050, 0.00000 N, -0.62679, 0.26469, 0.00000 H, 1.84969, 0.83173, -0.00001 C, -1.68775, -0.21351, -0.00000	-388212.232355	-388283.044716	2.54E+32	2	1.08E+01	1.14E+04
54	CN	N, 0.00000, 0.00000, 0.53434 C, 0.00000, 0.00000, -0.62339	-243282.319290	-243333.949747	1.28E+32	2	1.00E+00	1.06E+02
	CH_4	C, 0.00006, -0.00000, -0.00001 H, -1.07741, 0.05086, 0.15637 H, 0.23679, -0.86565, -0.61803 H, 0.33754, 0.90709, -0.50065 H, 0.50273, -0.09229, 0.96235	-106174.920693	-106226.540649	6.21E+31	1	1.01E+00	4.36E+02
	TS	N, -0.00600, 0.01583, -0.18485 C, -0.00345, 0.00994, 0.97100 C, 0.00299, -0.00529, 3.94989 H, 0.94069, -0.45114, 4.27433 H, 0.00063, 0.00046, 2.83097 H, -0.08016, 1.02657, 4.28407 H, -0.84949, -0.59637, 4.27736	-349461.950130	-349538.570096	2.64E+32	2	6.42E+01	1.93E+04
55	CN	N, 0.00000, 0.00000, 0.53434 C, 0.00000, 0.00000, -0.62339	-243282.319290	-243333.949747	1.28E+32	2	1.00E+00	1.06E+02
	CH_3	C, 0.00000, -0.00018, 0.00042 H, -0.93570, -0.53955, -0.00085 H, 0.93580, -0.53939, -0.00085 H, -0.00010, 1.08002, -0.00085	-104455.380974	-104507.305488	5.63E+31	2	1.08E+00	2.53E+02
	TS	N, -0.00032, -0.00008, 0.03799 C, 0.00010, 0.00001, 1.19345 C, 0.00117, 0.00023, 4.08597 H, -0.95019, 0.00027, 4.59569 H, 0.00076, 0.00015, 2.97345 H, 0.95292, 0.00027, 4.59497	-347737.484973	-347812.198826	2.54E+32	3	2.99E+01	1.33E+04
56	CN	N, 0.00000, 0.00000, 0.53434 C, 0.00000, 0.00000, -0.62339	-243282.319290	-243333.949747	1.28E+32	2	1.00E+00	1.06E+02
	CH	C, 0.00000, 0.00000, 0.16040 H, 0.00000, 0.00000, -0.96239	-100985.100094	-101029.197992	4.54E+31	2	1.00E+00	1.44E+01
	TS	N, 0.00572, -0.00001, 0.00211 C, -0.01046, 0.00001, 1.15963 H, 0.29200, 0.00000, 3.68156	-344267.815834	-344339.237311	2.36E+32	3	3.92E+01	2.89E+03

		C, 0.23351, 0.00007, 4.80927						
57	CN	N, 0.00000, 0.00000, 0.53434 C, 0.00000, 0.00000, -0.62339	-243282.319290	-243333.949747	1.28E+32	2	1.00E+00	1.06E+02
	CH	C, 0.00000, 0.00000, 0.16040 H, 0.00000, 0.00000, -0.96239	-100985.100094	-101029.197992	4.54E+31	2	1.00E+00	1.44E+01
	TS	C, -1.72171, -0.02308, 0.00000 N, -0.55194, 0.02741, -0.00002 H, 0.89797, 0.01069, 0.00024 C, 2.21598, -0.01069, -0.00002	-344297.536494	-344360.913439	2.36E+32	3	4.28E+00	1.03E+03
58	CN	N, 0.00000, 0.00000, 0.53434 C, 0.00000, 0.00000, -0.62339	-243282.319290	-243333.949747	1.28E+32	2	1.00E+00	1.06E+02
	H_2	H, 0.00000, 0.00000, 0.37683 H, 0.00000, 0.00000, -0.37683	-3031.139750	-3061.369757	2.77E+30	1	1.00E+00	3.52E+00
	TS	N, -0.00096, 0.00000, 0.01749 C, 0.00120, 0.00000, 1.17136 H, 0.00867, 0.00000, 2.78134 H, 0.01468, 0.00000, 3.59742	-246318.639151	-246366.583407	1.43E+32	2	2.06E+00	1.04E+01
59	NH	N, 0.00000, 0.00000, -0.00325 H, 0.00000, 0.00000, 1.03180	-144933.050538	-144978.308907	5.63E+31	3	1.00E+00	1.24E+01
	TS	N, 0.00000, 1.48000, -0.00001 H, 1.01877, 1.30347, 0.00003 N, 0.00000, -1.48000, -0.00001 H, -1.01877, -1.30347, 0.00003	-289872.872241	-289936.031269	1.59E+32	1	5.07E+00	3.54E+03
60	NH	N, 0.00000, 0.00000, -0.00325 H, 0.00000, 0.00000, 1.03180	-144933.050538	-144978.308907	5.63E+31	3	1.00E+00	1.24E+01
	TS	N, 1.17657, -0.12837, 0.00000 H, -0.13327, -0.10756, 0.00000 H, 1.36132, 0.88573, 0.00000 N, -1.35200, 0.01721, 0.00000	-289832.730971	-289896.296952	1.59E+32	5	1.18E+00	3.59E+03
61	NH	N, 0.00000, 0.00000, -0.00325 H, 0.00000, 0.00000, 1.03180	-144933.050538	-144978.308907	5.63E+31	3	1.00E+00	1.24E+01
	^4N	N, 0.00000, 0.00000, 0.00000	-143303.088167	-143303.088167	5.07E+31	4	1.00E+00	1.00E+00
	TS	N, 0.06792, -1.51015, 0.00000 N, 0.06792, 1.69985, 0.00000 H, -0.95083, -1.32792, 0.00000	-288237.960263	-288301.780917	1.51E+32	2	2.19E+00	5.65E+03
62	NH	N, 0.00000, 0.00000, -0.00325 H, 0.00000, 0.00000, 1.03180	-144933.050538	-144978.308907	5.63E+31	3	1.00E+00	1.24E+01
	^2N	N, 0.00000, 0.00000, 0.00000	-143024.189856	-143024.189856	5.07E+31	2	1.00E+00	1.00E+00
	TS	N, 0.00000, 0.00000, -1.67637 N, 0.00000, 0.00000, 2.06363 H, 0.00000, 0.00000, -2.71077	-287959.567996	-288022.858299	1.51E+32	2	7.64E+00	1.30E+03
63	NH	N, 0.00000, 0.00000, -0.00325 H, 0.00000, 0.00000, 1.03180	-144933.050538	-144978.308907	5.63E+31	3	1.00E+00	1.24E+01
	CH_3	C, 0.00000, -0.00018, 0.00042 H, -0.93570, -0.53955, -0.00085 H, 0.93580, -0.53939, -0.00085 H, -0.00010, 1.08002, -0.00085	-104455.380974	-104507.305488	5.63E+31	2	1.08E+00	2.53E+02
	TS	C, 1.52138, 0.01677, 0.00000 H, 1.64444, -0.50939, 0.93538 H, 1.33617, 1.08031, -0.00011 H, 1.64447, -0.50958, -0.93527 N, -1.74740, 0.10590, 0.00000 H, -1.52156, -0.90330, 0.00000	-249391.521726	-249465.319280	1.59E+32	2	4.99E+01	1.32E+04
64	NH	N, 0.00000, 0.00000, -0.00325 H, 0.00000, 0.00000, 1.03180	-144933.050538	-144978.308907	5.63E+31	3	1.00E+00	1.24E+01
	$^3CH_2$	C, 0.00000, 0.00000, 0.10395 H, 0.00000, -0.99689, -0.31186 H, 0.00000, 0.99689, -0.31186	-102701.224038	-102749.428218	5.08E+31	3	1.01E+00	8.96E+01
	TS	C, 1.52801, 0.00871, -0.08755 N, -1.60694, -0.10144, 0.05236 H, 1.59932, -1.05868, 0.05643 H, -1.42283, 0.84043, -0.33262 H, 1.90405, 0.87604, 0.43497	-247639.478316	-247709.429513	1.51E+32	1	2.93E+01	9.99E+03
65	NH	N, 0.00000, 0.00000, -0.00325 H, 0.00000, 0.00000, 1.03180	-144933.050538	-144978.308907	5.63E+31	3	1.00E+00	1.24E+01
	$^1CH_2$	C, 0.00000, 0.17399, 0.00000 H, 0.86403, -0.52196, 0.00000 H, -0.86403, -0.52196, 0.00000	-102649.483309	-102697.613975	5.08E+31	1	1.00E+00	1.31E+02
	TS	C, 1.74213, 0.00000, -0.16933 N, -1.57191, -0.00000, 0.02953	-247586.138659	-247656.439047	1.51E+32	3	1.15E+01	9.79E+03

		H, 1.56518, -0.86259, 0.50456						
		H, -2.57979, 0.00001, -0.19981						
		H, 1.56517, 0.86258, 0.50457						
66/67	NH	N, 0.00000, 0.00000, -0.00325	-144933.050538	-144978.308907	5.63E+31	3	1.00E+00	1.24E+01
		H, 0.00000, 0.00000, 1.03180						
	CH	C, 0.00000, 0.00000, 0.16040	-100985.100094	-101029.197992	4.54E+31	2	1.00E+00	1.44E+01
		H, 0.00000, 0.00000, -0.96239						
	TS(HNCH)	N, -1.60713, 0.10784, 0.00485	-245923.393756	-245991.346947	1.43E+32	2	8.64E+00	7.97E+03
		H, -1.08487, -0.78310, -0.04454						
		C, 1.71301, -0.14820, 0.00755						
		H, 2.05673, 0.91741, -0.03469						
	HNCH	N, 0.11148, 0.58631, 0.00000	-246509.347595	-246567.284503	1.43E+32	2	1.03E+00	1.17E+03
		H, -0.77382, 1.09266, 0.00000						
		C, 0.11148, -0.63322, 0.00000						
		H, -0.67543, -1.39750, 0.00000						
	TS(HCN + H)	N, 0.04557, 0.00005, 0.03268	-246399.433663	-246458.061078	1.43E+32	2	1.15E+00	1.39E+03
		H, -0.18267, 0.00002, 1.58600						
		C, 1.12876, -0.00012, -0.38119						
		H, 2.17966, -0.00030, -0.57483						
	TS(HNC + H)	N, 0.28317, 0.00001, 0.20866	-246374.698827	-246434.883164	1.43E+32	2	1.70E+00	1.76E+03
		H, -0.35446, 0.00004, 0.97119						
		C, 1.08224, -0.00005, -0.63973						
		H, 3.00889, -0.00063, -0.18318						
68	NH	N, 0.00000, 0.00000, -0.00325	-144933.050538	-144978.308907	5.63E+31	3	1.00E+00	1.24E+01
		H, 0.00000, 0.00000, 1.03180						
	H	H, 0.00000, 0.00000, 0.00000	-1307.704984	-1307.704984	9.79E+29	2	1.00E+00	1.00E+00
	TS	N, 0.00000, 0.38654, 0.00000	-146239.402195	-146288.023829	6.20E+31	4	1.08E+00	3.02E+01
		H, 0.04830, -0.67963, 0.00000						
		H, -0.04830, -2.02617, 0.00000						
69	^{4}N	N, 0.00000, 0.00000, 0.00000	-143303.088167	-143303.088167	5.07E+31	4	1.00E+00	1.00E+00
	CH_3	C, 0.00000, -0.00018, 0.00042	-104455.380974	-104507.305488	5.63E+31	2	1.08E+00	2.53E+02
		H, -0.93570, -0.53955, -0.00085						
		H, 0.93580, -0.53939, -0.00085						
		H, -0.00010, 1.08002, -0.00085						
	TS	C, -1.46781, -0.00001, 0.00000	-247760.994333	-247830.052860	1.51E+32	3	5.67E+00	1.20E+04
		N, 1.89219, 0.00001, -0.00000						
		H, -1.47960, 0.53361, -0.93883						
		H, -1.47934, -1.07988, 0.00729						
		H, -1.47954, 0.54624, 0.93155						
71	^{4}N	N, 0.00000, 0.00000, 0.00000	-143303.088167	-143303.088167	5.07E+31	4	1.00E+00	1.00E+00
	$^1CH_2$	C, 0.00000, 0.17399, 0.00000	-102649.483309	-102697.613975	5.08E+31	1	1.00E+00	1.31E+02
		H, 0.86403, -0.52196, 0.00000						
		H, -0.86403, -0.52196, 0.00000						
	TS	C, -0.00811, -0.01553, -0.01855	-245983.906280	-246051.959240	1.43E+32	4	3.95E+00	9.09E+03
		N, 0.00309, 0.00565, 3.32137						
		H, 1.03789, 0.00441, -0.34143						
		H, -0.60563, 0.84353, -0.34065						
72	^{4}N	N, 0.00000, 0.00000, 0.00000	-143303.088167	-143303.088167	5.07E+31	4	1.00E+00	1.00E+00
	CH	C, 0.00000, 0.00000, 0.16040	-100985.100094	-101029.197992	4.54E+31	2	1.00E+00	1.44E+01
		H, 0.00000, 0.00000, -0.96239						
	TS	C, 0.07893, 1.74410, 0.00000	-244290.028198	-244355.179980	1.36E+32	3	2.38E+00	6.59E+03
		H, -1.02612, 1.54676, 0.00000						
		N, 0.07893, -1.71590, 0.00000						
73	^{2}N	N, 0.00000, 0.00000, 0.00000	-143024.189856	-143024.189856	5.07E+31	2	1.00E+00	1.00E+00
	CH_4	C, 0.00006, -0.00000, -0.00001	-106174.920693	-106226.540649	6.21E+31	1	1.01E+00	4.36E+02
		H, -1.07741, 0.05086, 0.15637						
		H, 0.23679, -0.86565, -0.61803						
		H, 0.33754, 0.90709, -0.50065						
		H, 0.50273, -0.09229, 0.96235						
	TS	C, 1.14429, -0.00636, -0.00000	-249220.457273	-249286.105275	1.59E+32	2	2.96E+00	8.26E+03
		H, 1.71615, 0.91947, -0.00022						
		H, 1.33095, -0.59070, -0.89664						
		H, 1.33107, -0.59035, 0.89684						
		H, 0.06604, 0.31038, 0.00002						
		N, -1.61571, -0.00152, 0.00000						
74	^{2}N	N, 0.00000, 0.00000, 0.00000	-143024.189856	-143024.189856	5.07E+31	2	1.00E+00	1.00E+00
	CH_3	C, 0.00000, -0.00018, 0.00042	-104455.380974	-104507.305488	5.63E+31	2	1.08E+00	2.53E+02
		H, -0.93570, -0.53955, -0.00085						
		H, 0.93580, -0.53939, -0.00085						
		H, -0.00010, 1.08002, -0.00085						

	TS	C, -1.54714, 0.00001, 0.00000 N, 1.99286, -0.00001, -0.00000 H, -1.55590, -1.04208, 0.28340 H, -1.55559, 0.76648, 0.76078 H, -1.55575, 0.27563, -1.04417	-247653.309451	-247723.213388	1.51E+32	3	7.19E+00	1.33E+04
76	^2N	N, 0.00000, 0.00000, 0.00000	-143024.189856	-143024.189856	5.07E+31	2	1.00E+00	1.00E+00
	$^3CH_2$	C, 0.00000, 0.00000, 0.10395 H, 0.00000, -0.99689, -0.31186 H, 0.00000, 0.99689, -0.31186	-102701.224038	-102749.428218	5.08E+31	3	1.01E+00	8.96E+01
	TS	C, 1.61238, 0.00000, -0.09634 N, -1.89618, 0.00000, 0.00418 H, 1.79951, -0.99701, 0.27439 H, 1.79950, 0.99701, 0.27439	-245899.134136	-245968.780774	1.43E+32	4	6.71E+00	1.02E+04
78	^2N	N, 0.00000, 0.00000, 0.00000	-143024.189856	-143024.189856	5.07E+31	2	1.00E+00	1.00E+00
	CH	C, 0.00000, 0.00000, 0.16040 H, 0.00000, 0.00000, -0.96239	-100985.100094	-101029.197992	4.54E+31	2	1.00E+00	1.44E+01
	TS	C, 0.07870, 1.80034, 0.00000 H, -1.02309, 1.58561, 0.00000 N, 0.07870, -1.76966, 0.00000	-244182.737140	-244248.251242	1.36E+32	3	2.59E+00	6.99E+03
79	^2N	N, 0.00000, 0.00000, 0.00000	-143024.189856	-143024.189856	5.07E+31	2	1.00E+00	1.00E+00
	H_2	H, 0.00000, 0.00000, 0.37683 H, 0.00000, 0.00000, -0.37683	-3031.139750	-3061.369757	2.77E+30	1	1.00E+00	3.52E+00
	TS	N, 0.00000, 0.00000, 0.70391 H, 0.00000, 0.37736, -2.46369 H, 0.00000, -0.37736, -2.46369	-146056.549247	-146111.395942	6.20E+31	2	2.21E+00	3.65E+02
80/81	CH_4	C, 0.00006, -0.00000, -0.00001 H, -1.07741, 0.05086, 0.15637 H, 0.23679, -0.86565, -0.61803 H, 0.33754, 0.90709, -0.50065 H, 0.50273, -0.09229, 0.96235	-106174.920693	-106226.540649	6.21E+31	1	1.01E+00	4.36E+02
	$^3CH_2$	C, 0.00000, 0.00000, 0.10395 H, 0.00000, -0.99689, -0.31186 H, 0.00000, 0.99689, -0.31186	-102701.224038	-102749.428218	5.08E+31	3	1.01E+00	8.96E+01
	TS	C, -1.39525, -0.00000, -0.00045 H, -1.90508, -0.95551, 0.00152 H, -1.90536, 0.95536, 0.00152 C, 1.26201, -0.00001, 0.00031 H, -0.03525, 0.00010, -0.00152 H, 1.54808, 0.92030, -0.50162 H, 1.54820, -0.89399, -0.54706 H , 1.54883, -0.02617, 1.04796	-208835.110791	-208909.055373	1.59E+32	3	4.49E+01	1.03E+04
	CH_3	C, 0.00000, -0.00018, 0.00042 H, -0.93570, -0.53955, -0.00085 H, 0.93580, -0.53939, -0.00085 H, -0.00010, 1.08002, -0.00085	-104455.380974	-104507.305488	5.63E+31	2	1.08E+00	2.53E+02
83	CH_4	C, 0.00006, -0.00000, -0.00001 H, -1.07741, 0.05086, 0.15637 H, 0.23679, -0.86565, -0.61803 H, 0.33754, 0.90709, -0.50065 H, 0.50273, -0.09229, 0.96235	-106174.920693	-106226.540649	6.21E+31	1	1.01E+00	4.36E+02
	CH	C, 0.00000, 0.00000, 0.16040 H, 0.00000, 0.00000, -0.96239	-100985.100094	-101029.197992	4.54E+31	2	1.00E+00	1.44E+01
	TS	C, 1.81516, -0.14846, 0.00000 H, 1.61965, 0.95566, 0.00000 C, -1.25136, -0.00240, 0.00000 H, -1.27232, 0.62160, 0.89187 H, -0.34695, -0.62257, -0.00001 H, -1.27232, 0.62162, -0.89186 H, -2.11089, -0.67118, -0.00001	-207162.118562	-207233.700194	1.51E+32	2	2.51E+01	1.13E+04
84/85	CH_4	C, 0.00006, -0.00000, -0.00001 H, -1.07741, 0.05086, 0.15637 H, 0.23679, -0.86565, -0.61803 H, 0.33754, 0.90709, -0.50065 H, 0.50273, -0.09229, 0.96235	-106174.920693	-106226.540649	6.21E+31	1	1.01E+00	4.36E+02
	H	H, 0.00000, 0.00000, 0.00000	-1307.704984	-1307.704984	9.79E+29	2	1.00E+00	1.00E+00
	TS	C, 0.00001, 0.00005, -0.00795 H, -0.00002, 0.00039, 1.43205 H, 1.05971, 0.00002, -0.23722 H, -0.52983, -0.91775, -0.23699 H, -0.52987, 0.91772, -0.23740	-107436.827886	-107493.404785	6.80E+31	2	1.19E+00	1.24E+03

		H, -0.00003, 0.00060, 2.30674						
	CH_3	C, 0.00000, -0.00018, 0.00042 H, -0.93570, -0.53955, -0.00085 H, 0.93580, -0.53939, -0.00085 H, -0.00010, 1.08002, -0.00085	-104455.380974	-104507.305488	5.63E+31	2	1.08E+00	2.53E+02
	H_2	H, 0.00000, 0.00000, 0.37683 H, 0.00000, 0.00000, -0.37683	-3031.139750	-3061.369757	2.77E+30	1	1.00E+00	3.52E+00
86	CH_3	C, 0.00000, -0.00018, 0.00042 H, -0.93570, -0.53955, -0.00085 H, 0.93580, -0.53939, -0.00085 H, -0.00010, 1.08002, -0.00085	-104455.380974	-104507.305488	5.63E+31	2	1.08E+00	2.53E+02
	$^3CH_2$	C, 0.00000, 0.00000, 0.10395 H, 0.00000, -0.99689, -0.31186 H, 0.00000, 0.99689, -0.31186	-102701.224038	-102749.428218	5.08E+31	3	1.01E+00	8.96E+01
	TS	C, 0.00350, 0.00625, -0.00618 C, -0.01035, -0.01727, 3.28371 H, 1.05266, -0.00454, 3.54575 H, -0.55110, 0.89815, 3.54524 H, -1.07591, -0.00955, 0.00033 H, 0.55415, -0.92229, 0.00019 H, 0.52969, 0.94596, -0.09010	-207138.171376	-207213.139903	1.51E+32	2	7.26E+01	1.52E+04
87	CH_3	C, 0.00000, -0.00018, 0.00042 H, -0.93570, -0.53955, -0.00085 H, 0.93580, -0.53939, -0.00085 H, -0.00010, 1.08002, -0.00085	-104455.380974	-104507.305488	5.63E+31	2	1.08E+00	2.53E+02
	$^1CH_2$	C, 0.00000, 0.17399, 0.00000 H, 0.86403, -0.52196, 0.00000 H, -0.86403, -0.52196, 0.00000	-102649.483309	-102697.613975	5.08E+31	1	1.00E+00	1.31E+02
	TS	C, 1.61336, 0.00000, -0.02267 C, -1.82444, 0.00000, -0.14565 H, -1.80710, -0.86362, 0.55004 H, -1.80710, 0.86362, 0.55004 H, 1.08601, 0.00000, -0.96631 H, 1.89731, -0.93483, 0.43808 H, 1.89731, 0.93483, 0.43808	-207107.145843	-207182.277151	1.51E+32	2	7.49E+01	1.58E+04
88	CH_3	C, 0.00000, -0.00018, 0.00042 H, -0.93570, -0.53955, -0.00085 H, 0.93580, -0.53939, -0.00085 H, -0.00010, 1.08002, -0.00085	-104455.380974	-104507.305488	5.63E+31	2	1.08E+00	2.53E+02
	CH	C, 0.00000, 0.00000, 0.16040 H, 0.00000, 0.00000, -0.96239	-100985.100094	-101029.197992	4.54E+31	2	1.00E+00	1.44E+01
	TS	C, -1.45731, 0.01166, 0.00000 H, -1.53611, -0.52414, 0.93461 H, -1.36355, 1.08695, 0.00051 H, -1.53612, -0.52326, -0.93511 C, 1.91016, 0.14225, -0.00000 H, 1.71868, -0.96306, -0.00001	-205441.667794	-205512.362007	1.44E+32	1	3.13E+01	1.33E+04
89	CH_3	C, 0.00000, -0.00018, 0.00042 H, -0.93570, -0.53955, -0.00085 H, 0.93580, -0.53939, -0.00085 H, -0.00010, 1.08002, -0.00085	-104455.380974	-104507.305488	5.63E+31	2	1.08E+00	2.53E+02
	CH	C, 0.00000, 0.00000, 0.16040 H, 0.00000, 0.00000, -0.96239	-100985.100094	-101029.197992	4.54E+31	2	1.00E+00	1.44E+01
	TS	C, -1.57040, 0.01311, 0.00000 H, -1.73272, -0.50245, -0.93528 H, -1.73272, -0.50240, 0.93531 H, -1.29159, 1.05660, -0.00003 C, 2.02731, 0.14158, 0.00000 H, 2.01556, -0.97988, 0.00000	-205442.820389	-205519.902443	1.44E+32	1	1.21E+02	1.51E+04
90/91	CH_3	C, 0.00000, -0.00018, 0.00042 H, -0.93570, -0.53955, -0.00085 H, 0.93580, -0.53939, -0.00085 H, -0.00010, 1.08002, -0.00085	-104455.380974	-104507.305488	5.63E+31	2	1.08E+00	2.53E+02
	H	H, 0.00000, 0.00000, 0.00000	-1307.704984	-1307.704984	9.79E+29	2	1.00E+00	1.00E+00
	TS	C, -0.29794, 0.00000, -0.00000 H, -0.76224, -0.97668, 0.00000 H, -0.76221, 0.97670, 0.00000 H, 1.24206, -0.00001, -0.00000 H, 2.07002, -0.00001, 0.00000	-105706.192804	-105763.239668	6.21E+31	3	1.40E+00	9.35E+02
	$^3CH_2$	C, 0.00000, 0.00000, 0.10395	-102701.224038	-102749.428218	5.08E+31	3	1.01E+00	8.96E+01

		H, 0.00000, -0.99689, -0.31186 H, 0.00000, 0.99689, -0.31186						
	H_2	H, 0.00000, 0.00000, 0.37683 H, 0.00000, 0.00000, -0.37683	-3031.139750	-3061.369757	2.77E+30	1	1.00E+00	3.52E+00
93	$^3CH_2$	C, 0.00000, 0.00000, 0.10395 H, 0.00000, -0.99689, -0.31186 H, 0.00000, 0.99689, -0.31186	-102701.224038	-102749.428218	5.08E+31	3	1.01E+00	8.96E+01
	$^1CH_2$	C, 0.00000, 0.17399, 0.00000 H, 0.86403, -0.52196, 0.00000 H, -0.86403, -0.52196, 0.00000	-102649.483309	-102697.613975	5.08E+31	1	1.00E+00	1.31E+02
	TS	C, 0.00867, 0.03565, 0.00649 C, -0.00827, -0.03474, 3.52574 H, 1.07099, 0.01842, -0.25941 H, -0.52864, -0.88948, -0.22749 H, -0.89196, 0.56774, 3.37789 H, 1.02821, 0.17657, 3.74430	-205381.966550	-205458.996094	1.44E+32	3	1.22E+02	1.47E+04
94	$^3CH_2$	C, 0.00000, 0.00000, 0.10395 H, 0.00000, -0.99689, -0.31186 H, 0.00000, 0.99689, -0.31186	-102701.224038	-102749.428218	5.08E+31	3	1.01E+00	8.96E+01
	CH	C, 0.00000, 0.00000, 0.16040 H, 0.00000, 0.00000, -0.96239	-100985.100094	-101029.197992	4.54E+31	2	1.00E+00	1.44E+01
	TS	C, 1.88315, -0.13675, 0.00771 H, 1.63700, 0.95598, -0.04343 C, -1.51417, -0.00238, -0.00581 H, -1.78611, -1.04696, -0.00916 H, -2.06481, 0.92572, 0.04122	-203690.485549	-203762.235213	1.36E+32	2	3.08E+01	1.09E+04
95	$^3CH_2$	C, 0.00000, 0.00000, 0.10395 H, 0.00000, -0.99689, -0.31186 H, 0.00000, 0.99689, -0.31186	-102701.224038	-102749.428218	5.08E+31	3	1.01E+00	8.96E+01
	CH	C, 0.00000, 0.00000, 0.16040 H, 0.00000, 0.00000, -0.96239	-100985.100094	-101029.197992	4.54E+31	2	1.00E+00	1.44E+01
	TS	C, -1.75776, -0.00000, 0.16620 H, -1.90010, 0.00001, -0.94536 C, 1.54076, 0.00000, -0.10920 H, 1.60103, -0.99725, 0.30169 H, 1.60103, 0.99724, 0.30170	-203690.910880	-203763.907657	1.36E+32	4	2.57E+01	1.08E+04
98	$^1CH_2$	C, 0.00000, 0.17399, 0.00000 H, 0.86403, -0.52196, 0.00000 H, -0.86403, -0.52196, 0.00000	-102649.483309	-102697.613975	5.08E+31	1	1.00E+00	1.31E+02
	CH	C, 0.00000, 0.00000, 0.16040 H, 0.00000, 0.00000, -0.96239	-100985.100094	-101029.197992	4.54E+31	2	1.00E+00	1.44E+01
	TS	C, 1.90269, 0.00071, -0.15554 H, 1.70188, -0.00445, 0.94656 C, -1.47200, -0.00014, 0.03382 H, -2.14324, -0.86876, -0.11101 H, -2.14277, 0.86978, -0.10524	-203645.565870	-203717.864263	1.36E+32	2	4.05E+01	1.04E+04
102	CH	C, 0.00000, 0.00000, 0.16040 H, 0.00000, 0.00000, -0.96239	-100985.100094	-101029.197992	4.54E+31	2	1.00E+00	1.44E+01
	TS	C, -1.85115, 0.01891, 0.00000 C, 2.11689, -0.10583, 0.00000 H, 1.35696, 0.71798, -0.00000 H, -2.95140, -0.19649, -0.00000	-201973.243143	-202042.842522	1.28E+32	3	1.51E+01	6.59E+03

Table A.2: Quantum Chemistry Data at the ωB97XD/aug-cc-pVDZ level of theory. Cartesian coordinates are in angstroms. Energies are in kJ mol^{-1}.

Reac.	Species	Geometry (Atom, X, Y, Z)	E_e + ZPE	E_e + Gibbs	q_t/V (m^{-3})	q_e	q_v	q_r
22	CH_3	C, 0.00000, -0.00000, 0.00000 H, -0.88473, -0.63289, 0.00000 H, -0.10575, 1.08262, 0.00000 H, 0.99047, -0.44973, 0.00000	-104483.836143	-104535.821043	5.63E+31	2	1.08E+00	2.58E+02
	H	H, 0.00000, 0.00000, 0.00000	-1318.707191	-1318.707191	9.79E+29	2	1.00E+00	1.00E+00
	TS	C, -0.31271, 0.00005, -0.00001 H, -0.32638, 0.84037, 0.69066 H, 2.85729, -0.00052, 0.00013 H, -0.32805, -1.01825, 0.38233	-105801.789884	-105859.858068	6.21E+31	1	3.62E+00	1.63E+03

		H, -0.32660, 0.17809, -1.07307						
	CH_4	C, 0.00000, -0.00000, -0.00000 H, -0.01988, 0.27551, 1.06089 H, -0.31766, -1.04317, -0.11265 H, -0.68099, 0.65183, -0.55962 H, 1.01851, 0.11585, -0.38860	-106226.692928	-106278.357517	6.21E+31	1	1.01E+00	4.43E+02
32	H	H, 0.00000, 0.00000, 0.00000	-1318.707191	-1318.707191	9.79E+29	2	1.00E+00	1.00E+00
	TS	H, 0.00000, 0.00000, 1.60500 H, 0.00000, 0.00000, -1.60500	-2634.082760	-2673.667423	2.77E+30	1	2.40E+00	3.19E+01
	H_2	H, 0.00000, 0.00000, 0.37904 H, 0.00000, 0.00000, -0.37904	-3050.376789	-3080.635676	2.77E+30	1	1.00E+00	1.78E+00
37	H_2CN	C, -0.50550, 0.00000, 0.00004 N, 0.74091, 0.00000, -0.00006 H, -1.07671, 0.94468, 0.00009 H, -1.07669, -0.94470, 0.00009	-246620.091185	-246678.461301	1.43E+32	2	1.02E+00	1.41E+03
	^4N	N, 0.00000, 0.00000, 0.00000	-143290.704826	-143290.704826	5.07E+31	4	1.00E+00	1.00E+00
	TS	C, -0.64933, 0.42046, 0.00000 N, -1.50824, -0.45980, 0.00000 H, -0.85287, 1.50344, 0.00000 H, 0.47125, 0.13507, 0.00000 N, 2.11933, -0.13466, 0.00000	-389908.932850	-389979.128218	2.64E+32	3	2.82E+00	2.19E+04
52	CN	N, 0.00000, 0.00000, 0.54016 C, 0.00000, 0.00000, -0.63018	-243328.585851	-243380.271444	1.28E+32	2	1.00E+00	1.09E+02
	^4N	N, 0.00000, 0.00000, 0.00000	-143290.704826	-143290.704826	5.07E+31	4	1.00E+00	1.00E+00
	TS	N, 0.00000, 0.00000, -2.01713 C, 0.00000, 0.00000, -0.84693 N, 0.00000, 0.00000, 2.74307	-386621.297503	-386690.873253	2.45E+32	3	2.46E+01	2.10E+03
54	CN	N, 0.00000, 0.00000, 0.54016 C, 0.00000, 0.00000, -0.63018	-243328.585851	-243380.271444	1.28E+32	2	1.00E+00	1.09E+02
	CH_4	C, 0.00000, -0.00000, -0.00000 H, -0.01988, 0.27551, 1.06089 H, -0.31766, -1.04317, -0.11265 H, -0.68099, 0.65183, -0.55962 H, 1.01851, 0.11585, -0.38860	-106226.692928	-106278.357517	6.21E+31	1	1.01E+00	4.43E+02
	TS	N, 2.14215, 0.00029, -0.00086 C, 0.97393, -0.00047, 0.00138 C, -2.09537, 0.00010, -0.00029 H, -2.43300, -0.99002, 0.32279 H, -0.97607, -0.00162, 0.00479 H, -2.43201, 0.77702, 0.69381 H, -2.42529, 0.21481, -1.02194	-349564.625558	-349642.621287	2.64E+32	2	1.06E+02	2.04E+04
61	NH	N, 0.00000, 0.00000, 0.13067 H, 0.00000, 0.00000, -0.91471	-144934.956651	-144980.264905	5.63E+31	3	1.00E+00	1.26E+01
	^4N	N, 0.00000, 0.00000, 0.00000	-143290.704826	-143290.704826	5.07E+31	4	1.00E+00	1.00E+00
	TS	N, 0.06765,-1.67340, 0.00000 N, 0.06765, 1.87660, 0.00000 H, -0.94709, -1.42245, 0.00000	-288226.371306	-288290.302231	1.51E+32	2	1.88E+00	6.87E+03
69	^4N	N, 0.00000, 0.00000, 0.00000	-143290.704826	-143290.704826	5.07E+31	4	1.00E+00	1.00E+00
	CH_3	C, 0.00000, -0.00000, 0.00000 H, -0.88473, -0.63289, 0.00000 H, -0.10575, 1.08262, 0.00000 H, 0.99047, -0.44973, 0.00000	-104483.836143	-104535.821043	5.63E+31	2	1.08E+00	2.58E+02
	TS	C, -1.61826, -0.00003, -0.00001 N, 2.08174, 0.00003, 0.00001 H, -1.62082, 0.36668, -1.02414 H, -1.62041, -1.07030, 0.19448 H, -1.62135, 0.70356, 0.82962	-247776.303624	-247846.294203	1.51E+032	3	6.79E+00	1.46E+04
73	^2N	N, 0.00000, 0.00000, 0.00000	-143005.449147	-143005.449147	5.07E+31	2	1.00E+00	1.00E+00
	CH_4	C, 0.00000, -0.00000, -0.00000 H, -0.01988, 0.27551, 1.06089 H, -0.31766, -1.04317, -0.11265 H, -0.68099, 0.65183, -0.55962 H, 1.01851, 0.11585, -0.38860	-106226.692928	-106278.357517	6.21E+31	1	1.01E+00	4.43E+02
	TS	C, 1.08852, -0.01027, 0.00000 H, 1.56418, 0.97496, -0.00003 H, 1.27316, -0.58308, -0.91072 H, 1.27318, -0.58302, 0.91075 H, -0.06139, 0.28190, 0.00000 N, -1.51147, -0.00416, 0.00000	-249283.290739	-249347.150776	1.59E+32	2	1.59E+00	7.48E+03

82	CH_4	C, 0.00000, -0.00000, -0.00000	-106226.692928	-106278.357517	6.21E+31	1	1.01E+00	4.43E+02
		H, -0.01988, 0.27551, 1.06089						
		H, -0.31766, -1.04317, -0.11265						
		H, -0.68099, 0.65183, -0.55962						
		H, 1.01851, 0.11585, -0.38860						
	$^1CH_2$	C, 0.00000, 0.17714, 0.00000	-102670.419046	-102718.628477	5.08E+31	1	1.00E+00	1.35E+02
		H, 0.86764, -0.53143, 0.00000						
		H, -0.86764, -0.53142, 0.00000						
	TS	C, -1.66483, 0.00133, -0.17126	-208905.440060	-208976.556978	1.59E+32	1	3.47E+01	1.28E+04
		H, -1.57125, 0.86815, 0.53125						
		H, -1.60543, -0.86699, 0.53291						
		C, 1.32010, -0.00047, 0.00279						
		H, 2.05688, -0.40874, -0.69746						
		H, 1.56709, 1.03615, 0.25428						
		H, 1.28430, -0.61253, 0.91001						
		H, 0.33674, -0.02125, -0.52016						
83	CH_4	C, 0.00000, -0.00000, -0.00000	-106226.692928	-106278.357517	6.21E+31	1	1.01E+00	4.43E+02
		H, -0.01988, 0.27551, 1.06089						
		H, -0.31766, -1.04317, -0.11265						
		H, -0.68099, 0.65183, -0.55962						
		H, 1.01851, 0.11585, -0.38860						
	CH	C, 0.00000, 0.00000, 0.16209	-100984.504106	-101028.651888	4.54E+31	2	1.00E+00	1.47E+01
		H, 0.00000, 0.00000, -0.97256						
	TS	C,-1.25221, -0.13624, 0.01306	-207229.735689	-207294.068315	1.51E+32	2	2.50E+00	6.07E+03
		H, -1.19737, 0.97470, -0.05598						
		C, 0.88157, 0.02666, 0.00504						
		H, 1.54551, -0.84752, -0.00036						
		H, 1.07437, 0.68338, -0.84468						
		H, 0.92124, 0.53760, 0.96776						
		H, -0.11991, -0.69068, -0.17533						
96	$^3CH_2$	C, 0.00000, 0.00000, 0.10496	-102716.893022	-102765.165465	5.08E+31	3	1.01E+00	4.60E+01
		H, 0.00000, -1.00530, -0.31487						
		H, 0.00000, 1.00530, -0.31487						
	H	H, 0.00000, 0.00000, 0.00000	-1318.707191	-1318.707191	9.79E+29	2	1.00E+00	1.00E+00
	TS	C, 0.00000, 0.26757, 0.00000	-104035.195954	-104096.349100	5.63E+31	2	8.99E+00	1.26E+03
		H, 0.14497, -2.96918, 0.00000						
		H, -0.07248, 0.68188, 1.00490						
		H, -0.07248, 0.68188, -1.00490						

Table A.3: Quantum Chemistry Data at the CCSD/aug-cc-pVTZ level of theory. Cartesian coordinates are in angstroms. Energies are in kJ mol^{-1}.

Reac.	Species	Geometry (Atom, X, Y, Z)	E_e + ZPE	E_e + Gibbs	q_t/V (m^{-3})	q_e	q_v	q_r
22	CH_3	C, 0.00000, 0.00000, 0.00000	-104308.024787	-104359.991308	5.63E+31	2	1.10E+00	2.52E+02
		H, -0.90220, 0.59027, 0.00000						
		H, 0.96228, 0.48619, 0.00000						
		H, -0.06009, -1.07646, 0.00000						
	H	H, 0.00000, 0.00000, 0.00000	-1312.280561	-1312.280561	9.79E+29	2	1.00E+00	1.00E+00
	TS	C, -0.39600, 0.00000, 0.00000	-105558.117229	-105619.286128	6.21E+31	1	8.38E+00	2.46E+03
		H, -0.42269, -0.52471, -0.94049						
		H, 3.64400, -0.00002, 0.00001						
		H, -0.42262, 1.07685, 0.01583						
		H, -0.42271, -0.55213, 0.92466						
	CH_4	C, 0.00000, 0.00000, -0.00000	-106042.088772	-106093.698225	6.21E+31	1	1.01E+00	4.34E+02
		H, 0.02570, -0.06702, 1.08609						
		H, 0.82927, -0.56756, -0.41826						
		H, -0.94024, -0.40787, -0.36653						
		H, 0.08527, 1.04245, -0.30130						
32	H	H, 0.00000, 0.00000, 0.00000	-1312.280561	-1312.280561	9.79E+29	2	1.00E+00	1.00E+00
	TS	H, 0.00000, 0.00000, 1.84500	-2625.069418	-2663.175925	2.77E+30	1	1.00E+00	4.22E+01
		H, 0.00000, 0.00000, -1.84500						
	H_2	H, 0.00000, 0.00000, 0.37149	-3052.429930	-3082.591674	2.77E+30	1	1.00E+00	1.71E+00
		H, 0.00000, 0.00000, -0.37149						
37	H_2CN	C, -0.50667, -0.00000, 0.00006	-246242.260731	-246300.599341	1.43E+32	2	1.02E+00	1.40E+03
		N, 0.74043, -0.00000, -0.00009						
		H, -1.07150, 0.93594, 0.00012						
		H, -1.07152, -0.93592, 0.00013						

	^{4}N	N, 0.00000, 0.00000, 0.00000	-143127.472659	-143127.472659	5.07E+31	4	1.00E+00	1.00E+00
	TS	C, 0.61985, 0.42511, 0.00001 N, 1.45723, -0.45248, -0.00000 H, 0.72822, 1.50790, -0.00002 H, -0.55289, 0.09713, 0.00000 N,-2.01358, -0.14119, -0.00000	-389346.779168	-389416.058237	2.64E+32	3	2.13E+00	2.01E+04
52	CN	N, 0.00000, 0.00000, 0.53871 C, 0.00000, 0.00000, -0.62849	-242982.169504	-243033.839344	1.28E+32	2	1.00E+00	1.08E+02
	^{4}N	N, 0.00000, 0.00000, 0.00000	-143127.472659	-143127.472659	5.07E+31	4	1.00E+00	1.00E+00
	TS	N, 0.00000, 0.00000, -1.82602 C, 0.00000, 0.00000, -0.65907 N, 0.00000, 0.00000, 2.39093	-386113.573062	-386181.925329	2.45E+32	3	1.95E+01	1.62E+03
54	CN	N, 0.00000, 0.00000, 0.53871 C, 0.00000, 0.00000, -0.62849	-242982.169504	-243033.839344	1.28E+32	2	1.00E+00	1.08E+02
	CH$_4$	C, 0.00000, 0.00000, -0.00000 H, 0.02570, -0.06702, 1.08609 H, 0.82927, -0.56756, -0.41826 H, -0.94024, -0.40787, -0.36653 H, 0.08527, 1.04245, -0.30130	-106042.088772	-106093.698225	6.21E+31	1	1.01E+00	4.34E+02
	TS	N, 2.01206, -0.00001, 0.00000 C, 0.84801, 0.00002, -0.00000 C, -1.93747, -0.00001, 0.00000 H, -2.25189, -1.00852, 0.25504 H, -0.79199, 0.00001, -0.00000 H, -2.25190, 0.72512, 0.74587 H, -2.25189, 0.28338, -1.00091	-349017.589506	-349091.313546	2.64E+32	2	2.20E+01	1.75E+04
61	NH	N, 0.00000, 0.00000, 0.12966 H, 0.00000, 0.00000, -0.90761	-144752.762704	-144798.034201	5.63E+31	3	1.00E+00	1.24E+01
	^{4}N	N, 0.00000, 0.00000, 0.00000	-143127.472659	-143127.472659	5.07E+31	4	1.00E+00	1.00E+00
	TS	N, 0.06867, -1.31490, 0.00000 N, 0.06867, 1.48510, 0.00000 H, -0.96130, -1.19134, 0.00000	-287882.646097	-287944.744423	1.51E+32	2	1.41E+00	4.36E+03
69	^{4}N	N, 0.00000, 0.00000, 0.00000	-143127.472659	-143127.472659	5.07E+31	4	1.00E+00	1.00E+00
	CH$_3$	C, 0.00000, 0.00000, 0.00000 H, -0.90220, 0.59027, 0.00000 H, 0.96228, 0.48619, 0.00000 H, -0.06009, -1.07646, 0.00000	-104308.024787	-104359.991308	5.63E+31	2	1.10E+00	2.52E+02
	TS	C, 1.13028, 0.00000, 0.00000 N, -1.48972, 0.00000, 0.00000 H, 1.21543, -0.64819, 0.85777 H, 1.21544, -0.41876, -0.99023 H, 1.21543, 1.06695, 0.13246	-247418.437472	-247483.51574	1.51E+32	3	1.83E+00	7.45E+03
73	^{2}N	N, 0.00000, 0.00000, 0.00000	-142851.180004	-142851.180004	5.07E+31	2	1.00E+00	1.00E+00
	CH$_4$	C, 0.00000, 0.00000, -0.00000 H, 0.02570, -0.06702, 1.08609 H, 0.82927, -0.56756, -0.41826 H, -0.94024, -0.40787, -0.36653 H, 0.08527, 1.04245, -0.30130	-106042.088772	-106093.698225	6.21E+31	1	1.01E+00	4.34E+02
	TS	N, -1.61616, -0.00057, 0.00000 C, 1.13384, -0.00564, 0.00000 H, 0.21628, 0.60447, 0.00002 H, 1.97187, 0.68933, -0.00002 H, 1.16093, -0.62797, -0.89080 H, 1.16097, -0.62797, 0.89080	-248898.699623	-248965.712885	1.59E+32	2	5.18E+00	8.20E+03
82	CH$_4$	C, 0.00000, 0.00000, -0.00000 H, 0.02570, -0.06702, 1.08609 H, 0.82927, -0.56756, -0.41826 H, -0.94024, -0.40787, -0.36653 H, 0.08527, 1.04245, -0.30130	-106042.088772	-106093.698225	6.21E+31	1	1.01E+00	4.34E+02
	^{1}CH$_2$	C, 0.00000, 0.17470, 0.00000 H, 0.86117, -0.52409, 0.00000 H, -0.86117, -0.52409, 0.00000	-102506.779508	-102554.912799	5.08E+31	1	1.00E+00	1.31E+02
	TS	C, -1.43389, 0.00000, -0.16650 H, -1.37683, 0.86404, 0.52337 H, -1.37687, -0.86403, 0.52337 C, 1.14027, -0.00000, 0.00690 H, 1.67885, -0.89603, -0.29272 H, 1.67886, 0.89599, -0.29281 H, 0.97417, 0.00005, 1.07944 H, 0.18355, -0.00002, -0.58307	-208550.721882	-208618.121093	1.59E+32	1	1.02E+01	9.70E+03

83	CH_4	C, 0.00000, 0.00000, -0.00000 H, 0.02570, -0.06702, 1.08609 H, 0.82927, -0.56756, -0.41826 H, -0.94024, -0.40787, -0.36653 H, 0.08527, 1.04245, -0.30130	-106042.088772	-106093.698225	6.21E+31	1	1.01E+00	4.34E+02
	CH	C, 0.00000, 0.00000, 0.16003 H, 0.00000, 0.00000, -0.96019	-100826.548775	-100870.633545	4.54E+31	2	1.00E+00	1.43E+01
	TS	C, 2.66373, 0.00006, -0.00020 H, 3.78376, -0.00030, 0.00097 C, -1.97627, -0.00002, 0.00004 H, -2.34183, 0.30009, -0.98056 H, -0.88755, 0.00124, -0.00121 H, -2.33888, -1.00030, 0.23070 H, -2.34029, 0.69901, 0.75110	-206868.561407	-206947.208259	1.51E+32	2	2.17E+02	2.25E+04
96	$^3CH_2$	C, 0.00000, 0.10622, 0.00000 H, 0.99043, -0.31866, 0.00000 H, -0.99043, -0.31866, 0.00000	-102549.727437	-102599.680200	5.08E+31	3	1.00E+00	9.07E+01
	H	H, 0.00000, 0.00000, 0.00000	-1312.280561	-1312.280561	9.79E+29	2	1.00E+00	1.00E+00
	TS	C, 0.00000, 0.31994, 0.00000 H, -0.83836, -2.69569, 0.00000 H, 0.41918, 0.38802, -0.99054 H, 0.41918, 0.38802, 0.99054	-103864.317912	-103923.964021	5.63E+31	2	5.14E+00	1.20E+03

Table A.4: Quantum Chemistry Data at the BHandHLYP/aug-cc-pVTZ level of theory. Cartesian coordinates are in angstroms. Energies are in kJ mol^{-1}.

Reac.	Species	Geometry (Atom, X, Y, Z)	E_e + ZPE	E_e + Gibbs	q_t/V (m^{-3})	q_e	q_v	q_r
22	CH_3	C, 0.00000, 0.00000, 0.00001 H, -0.81893, -0.68980, -0.00001 H, -0.18792, 1.05411, -0.00001 H, 1.00685, -0.36432, -0.00001	-104491.954189	-104543.826193	5.63E+31	2	1.08E+00	2.46E+02
	H	H, 0.00000, 0.00000, 0.00000	-1309.084906	-1309.084906	9.79E+29	2	1.00E+00	1.00E+00
	TS	C, -0.10146, -0.14251, -0.28723 H, -0.97597, 0.47519, -0.29533 H, 0.92130, 1.29402, 2.60801 H, -0.12812, -1.10176, 0.18765 H, 0.79158, 0.18763, -0.77697	-105803.026495	-105862.572835	6.21E+31	1	5.99E+00	1.79E+03
	CH_4	C, -0.00000, 0.00000, 0.00000 H, -1.04973, -0.22330, 0.13147 H, 0.55571, -0.36530, 0.85253 H, 0.36102, -0.48101, -0.89853 H, 0.13299, 1.06961, -0.08546	-106217.466921	-106269.026490	6.21E+31	1	1.00E+00	4.25E+02
32	H	H, 0.00000, 0.00000, 0.00000	-1309.084906	-1309.084906	9.79E+29	2	1.00E+00	1.00E+00
	TS	H, 0.00000, 0.00000, 1.84500 H, 0.00000, 0.00000, -1.84500	-2618.744589	-2656.853721	2.77E+30	1	1.00E+00	4.22E+01
	H_2	H, 0.00000, 0.00000, 0.36852 H, 0.00000, 0.00000, -0.36852	-3045.136291	-3075.258652	2.77E+30	1	1.00E+00	1.68E+00
37	H_2CN	C, -0.49924, 0.00000, 0.00004 N, 0.73117, 0.00000, -0.00006 H, -1.06139, 0.93012, 0.00008 H, -1.06139, -0.93012, 0.00008	-246632.323389	-246690.575358	1.43E+32	2	1.02E+00	1.36E+03
	^4N	N, 0.00000, 0.00000, 0.00000	-143324.598878	-143324.598878	5.07E+31	4	1.00E+00	1.00E+00
	TS	C, -0.61857, 0.41903, 0.00000 N, -1.44321, -0.44846, 0.00000 H, -0.73336, 1.49492, 0.00000 H, 0.55767, 0.09757, 0.00000 N, 1.99851, -0.13821, 0.00000	-389940.528117	-390009.615524	2.64E+32	3	2.02E+00	1.95E+04
52	CN	N, 0.00000, 0.00000, 0.52910 C, 0.00000, 0.00000, -0.61728	-243337.071467	-243388.652040	1.28E+32	2	1.00E+00	1.04E+02
	^4N	N, 0.00000, 0.00000, 0.00000	-143324.598878	-143324.598878	5.07E+31	4	1.00E+00	1.00E+00
	TS	N, 0.00000, 0.00000, -1.91401 C, 0.00000, 0.00000, -0.76784 N, 0.00000, 0.00000, 2.57216	-386664.316320	-386733.726664	2.45E+32	3	2.61E+01	1.86E+03
54	CN	N, 0.00000, 0.00000, 0.52910 C, 0.00000, 0.00000, -0.61728	-243337.071467	-243388.652040	1.28E+32	2	1.00E+00	1.04E+02
	CH_4	C, -0.00000, 0.00000, 0.00000 H, -1.04973, -0.22330, 0.13147	-106217.466921	-106269.026490	6.21E+31	1	1.00E+00	4.25E+02

		H, 0.55571, -0.36530, 0.85253 H, 0.36102, -0.48101, -0.89853 H, 0.13299, 1.06961, -0.08546						
	TS	N, -2.07017, -0.00000, -0.00000 C, -0.92556, 0.00000, 0.00000 C, 2.01836, 0.00000, 0.00000 H, 2.34335, 0.68550, -0.76808 H, 0.90443, 0.00001, 0.00001 H, 2.34335, 0.32242, 0.97769 H, 2.34334, -1.00792, -0.20963	-349557.678485	-349633.411033	2.64E+32	2	4.62E+01	1.87E+04
61	NH	N, 0.00000, 0.00000, 0.12847 H, 0.00000, 0.00000, -0.89930	-144963.020621	-145008.244858	5.63E+31	3	1.00E+00	1.22E+01
	^4N	N, 0.00000, 0.00000, 0.00000	-143324.598878	-143324.598878	5.07E+31	4	1.00E+00	1.00E+00
	TS	N, 0.06765, -1.50415, 0.00000 N, 0.06765, 1.69585, 0.00000 H, -0.94715, -1.34197, 0.00000	-288289.336047	-288352.986044	1.51E+32	2	2.06E+00	5.60E+03
69	^4N	N, 0.00000, 0.00000, 0.00000	-143324.598878	-143324.598878	5.07E+31	4	1.00E+00	1.00E+00
	CH_3	C, 0.00000, 0.00000, 0.00001 H, -0.81893, -0.68980, -0.00001 H, -0.18792, 1.05411, -0.00001 H, 1.00685, -0.36432, -0.00001	-104491.954189	-104543.826193	5.63E+31	2	1.08E+00	2.46E+02
	TS	C, -1.45890, -0.00000, -0.00001 N, 1.88110, 0.00000, 0.00001 H, -1.47142, 1.02753, -0.30062 H, -1.47131, -0.77411, -0.73957 H, -1.47158, -0.25343, 1.04017	-247818.986377	-247888.016023	1.51E+032	3	5.72E+00	1.18E+04
73	^2N	N, 0.00000, 0.00000, 0.00000	-143049.628589	-143049.628589	5.07E+31	2	1.00E+00	1.00E+00
	CH_4	C, -0.00000, 0.00000, 0.00000 H, -1.04973, -0.22330, 0.13147 H, 0.55571, -0.36530, 0.85253 H, 0.36102, -0.48101, -0.89853 H, 0.13299, 1.06961, -0.08546	-106217.466921	-106269.026490	6.21E+31	1	1.00E+00	4.25E+02
	TS	C, 1.13172, -0.00650, 0.00000 H, 1.71292, 0.90391, 0.00003 H, 1.30981, -0.58891, -0.88952 H, 1.30980, -0.58896, 0.88950 H, 0.06514, 0.32394, -0.00000 N, -1.59828, -0.00156, 0.00000	-249288.898807	-249356.190372	1.59E+32	2	5.92E+00	8.03E+03
82	CH_4	C, -0.00000, 0.00000, 0.00000 H, -1.04973, -0.22330, 0.13147 H, 0.55571, -0.36530, 0.85253 H, 0.36102, -0.48101, -0.89853 H, 0.13299, 1.06961, -0.08546	-106217.466921	-106269.026490	6.21E+31	1	1.00E+00	4.25E+02
	$^1CH_2$	C, 0.00000, 0.00000, 0.17124 H, 0.00000, 0.85853, -0.51372 H, 0.00000, -0.85853, -0.51372	-102677.641797	-102723.976621	5.08E+31	1	1.00E+00	6.35E+01
	TS	C, -1.44245, 0.00000, -0.16418 H, -1.40679, 0.86112, 0.51234 H, -1.40679, -0.86112, 0.51234 C, 1.15186, 0.00000, 0.00780 H, 1.67906, -0.88998, -0.30274 H, 1.67905, 0.89000, -0.30271 H, 1.01109, -0.00002, 1.07597 H, 0.18790, 0.00000, -0.55688	-208897.836612	-208964.889256	1.59E+32	1	8.83E+00	9.77E+03
83	CH_4	C, -0.00000, 0.00000, 0.00000 H, -1.04973, -0.22330, 0.13147 H, 0.55571, -0.36530, 0.85253 H, 0.36102, -0.48101, -0.89853 H, 0.13299, 1.06961, -0.08546	-106217.466921	-106269.026490	6.21E+31	1	1.00E+00	4.25E+02
	CH	C, 0.00000, 0.00000, 0.15856 H, 0.00000, 0.00000, -0.95139	-101005.214050	-101049.254187	4.54E+31	2	1.00E+00	1.41E+01
	TS	C, -1.84378, -0.14809, -0.00100 H, -1.66479, 0.94632, 0.00490 C, 1.27284, -0.00286, -0.00027 H, 2.05489, -0.68549, -0.30162 H, 1.04706, 0.66729, -0.81788 H, 1.59341, 0.56559, 0.86110 H, 0.39510, -0.58801, 0.26113	-207224.017350	-207297.512971	1.51E+32	2	5.30E+01	1.15E+04
96	$^3CH_2$	C, 0.00000, 0.10344, 0.00000 H, 0.98672, -0.31032, 0.00000	-102730.073032	-102779.933902	5.08E+31	3	1.00E+00	8.74E+01

	H, -0.98672, -0.31032, 0.00000						
H	H, 0.00000, 0.00000, 0.00000	-1309.084906	-1309.084906	9.79E+29	2	1.00E+00	1.00E+00
TS	C, 0.00000, 0.34749, 0.00000	-104041.111206	-104101.558092	5.63E+31	2	6.17E+00	1.38E+03
	H, 0.80805, -2.95509, 0.00000						
	H, -0.40402, 0.43507, 0.98676						
	H, -0.40402, 0.43507, -0.98676						

Table A.5: Quantum Chemistry Simulation Data at the BHandHLYP/aug-cc-pVDZ level of theory. Cartesian coordinates are in angstroms. Energies are in kJ mol^{-1}. E_e is the electronic energy, ZPE is the zero point energy, and q_x are the partition functions (t: translational, e: electronic, v:vibrational, r:rotational).

Reac.	Species	Geometry (Atom, X, Y, Z)	E_e + ZPE	q_t/V (m^{-3})	q_e	q_v	q_r
1/33	CO_2	O, 0.00000, 0.00000, 1.15274	-494917.399028	2.82E+32	1	1.07E+00	5.23E+02
		O, 0.00000, 0.00000, -1.15274					
		C, 0.00000, 0.00000, 0.00000					
	^1O	O, 0.00000, 0.00000, 0.00000	-196788.921964	6.19E+31	1	1.00E+00	1.00E+00
	TS	O, 1.15275, 1.18505, 0.00000	-691707.204162	4.49E+32	1	1.07E+00	1.26E+05
		O, -1.15275, 1.18630, 0.00000					
		C, 0.00000, 1.18425, 0.00000					
		O, -0.00000, -3.25954, 0.00000					
	CO_3	O, 0.77156, -0.80876, 0.00000	-691904.373961	4.49E+32	1	1.14E+00	2.10E+04
		O, -0.00000, 1.42285, 0.00000					
		C, 0.00000, 0.25955, 0.00000					
		O, -0.77156, -0.80876, 0.00000					
2	HCO	C, 0.06118, 0.57927, 0.00000	-298768.200141	1.51E+32	2	1.00E+00	7.26E+02
		O, 0.06118, -0.58725, 0.00000					
		H, -0.85649, 1.22238, 0.00000					
	^2N	N, 0.00000, 0.00000, 0.00000	-143024.189856	5.07E+31	2	1.00E+00	1.00E+00
	TS	C, 0.76711, 0.41879, -0.00000	-441966.317654	2.73E+32	1	8.98E+00	3.02E+04
		O, 1.58153, -0.41503, 0.00000					
		H, 0.96548, 1.52043, 0.00001					
		N, -2.60291, -0.10184, 0.00000					
	HCON	N, -0.86610, 0.41919, 0.00000	-442240.538001	2.73E+32	1	1.13E+00	6.70E+03
		C, -0.11780, -0.57337, 0.00000					
		H, -0.15944, -1.65573, -0.00000					
		O, 0.86612, 0.27020, 0.00000					
3	HCO	C, 0.06118, 0.57927, 0.00000	-298768.200141	1.51E+32	2	1.00E+00	7.26E+02
		O, 0.06118, -0.58725, 0.00000					
		H, -0.85649, 1.22238, 0.00000					
	CH_3	C, 0.00000, -0.00018, 0.00042	-104455.380974	5.63E+31	2	1.08E+00	2.53E+02
		H, -0.93570, -0.53955, -0.00085					
		H, 0.93580, -0.53939, -0.00085					
		H, -0.00010, 1.08002, -0.00085					
	TS	C, 0.88372, 0.43321, -0.00001	-403228.049716	2.83E+32	1	1.10E+02	3.37E+04
		O, 1.69253, -0.40737, 0.00000					
		H, 1.09010, 1.53196, 0.00003					
		C, -2.20157, -0.09394, 0.00000					
		H, -1.99765, -1.15406, -0.00023					
		H, -2.36283, 0.42288, -0.93450					
		H, -2.36272, 0.42250, 0.93473					
	CH_3HCO	C, 0.23234, 0.39590, 0.00000	-403547.142484	2.83E+32	1	2.04E+00	1.18E+04
		O, 1.22430, -0.27597, 0.00000					
		H, 0.31342, 1.50005, 0.00000					
		C, -1.16060, -0.14740, -0.00000					
		H, -1.14984, -1.23540, -0.00002					
		H, -1.69424, 0.22607, -0.87809					
		H, -1.69423, 0.22604, 0.87812					
4	HCO	C, 0.06118, 0.57927, 0.00000	-298768.200141	1.51E+32	2	1.00E+00	7.26E+02
		O, 0.06118, -0.58725, 0.00000					
		H, -0.85649, 1.22238, 0.00000					
	H	H, 0.00000, 0.00000, 0.00000	-1307.704984	9.79E+29	2	1.00E+00	1.00E+00
	TS	C, -0.28186, 0.33762, 0.00000	-300077.773286	1.59E+32	1	5.26E+00	4.04E+03
		O, 0.67158, -0.33299, -0.00000					
		H, -0.28760, 1.45702, -0.00001					
		H, -3.39393, -0.81883, -0.00000					

	H_2CO	C, 0.00000, -0.52451, 0.00000 H, 0.00000, -1.10548, -0.93804 H, 0.00000, -1.10548, 0.93804 O, 0.00000, 0.66975, 0.00000	-300426.644475	1.59E+32	1	1.00E+00	1.39E+03
5/32	CO	C, 0.00000, 0.00000, -0.64038 O, 0.00000, 0.00000, 0.48029	-297385.023729	1.43E+32	1	1.00E+00	1.06E+02
	CN	N, 0.00000, 0.00000, 0.53434 C, 0.00000, 0.00000, -0.62339	-243282.319290	1.28E+32	2	1.00E+00	1.06E+02
	TS	C, 1.13871, 0.41518, 0.00000 O, 2.04295, -0.24325, 0.00000 C, -1.16088, -0.01782, 0.00000 N, -2.31580, -0.06260, 0.00000	-540672.179190	3.84E+32	2	2.24E+01	2.35E+04
	NCCO	C, 0.37853, 0.66420, 0.00000 O, -0.21702, 1.66650, 0.00000 C, 0.00000, -0.71311, 0.00000 N, -0.07643, -1.86265, 0.00000	-540810.648060	3.84E+32	2	2.11E+00	1.29E+04
6	CO	C, 0.00000, 0.00000, -0.64038 O, 0.00000, 0.00000, 0.48029	-297385.023729	1.43E+32	1	1.00E+00	1.06E+02
	^1O	O, 0.00000, 0.00000, 0.00000	-196788.921964	6.19E+31	1	1.00E+00	1.00E+00
	TS	C, 0.00000, 0.99997, 0.00000 O, 0.02096, 2.12000, 0.00000 O, -0.02096, -2.86997, 0.00000	-494175.802924	2.82E+32	1	5.76E+00	5.40E+02
	CO_2	O, 0.00000, 0.00000, 1.15274 O, 0.00000, 0.00000, -1.15274 C, 0.00000, 0.00000, 0.00000	-494917.399028	2.82E+32	1	1.07E+00	5.23E+02
7	CO	C, 0.00000, 0.00000, -0.64038 O, 0.00000, 0.00000, 0.48029	-297385.023729	1.43E+32	1	1.00E+00	1.06E+02
	$^1CH_2$	C, 0.00000, 0.17399, 0.00000 H, 0.86403, -0.52196, 0.00000 H, -0.86403, -0.52196, 0.00000	-102649.483309	5.08E+31	1	1.00E+00	1.31E+02
	TS	C, 2.47339, -0.00000, -0.19261 H, 2.41166, 0.86347, 0.50078 H, 2.41166, -0.86347, 0.50078 C, -0.77250, 0.00000, 0.11035 O, -1.87858, 0.00000, -0.06351	-400037.72065	2.63E+32	1	2.15E+01	1.84E+04
	CH_2CO	C, 0.00000, 1.20512, 0.00000 H, 0.00000, 1.73207, -0.94080 H, 0.00000, 1.73207, 0.94080 C, 0.00000, -0.10497, 0.00000 O, 0.00000, -1.25813, 0.00000	-400388.686988	2.63E+32	1	2.15E+01	1.84E+04
8	CO	C, 0.00000, 0.00000, -0.64038 O, 0.00000, 0.00000, 0.48029	-297385.023729	1.43E+32	1	1.00E+00	1.06E+02
	CH	C, 0.00000, 0.00000, 0.16040 H, 0.00000, 0.00000, -0.96239	-100985.100094	4.54E+31	2	1.00E+00	1.44E+01
	TS	O, 1.82058, -0.05901, 0.00001 C, 0.71145, 0.09535, -0.00002 C, -2.71813, -0.17214, 0.00000 H, -2.52455, 0.93281, 0.00002	-398372.996120	2.54E+32	2	2.18E+01	1.37E+04
	HCCO	O, 1.18704, 0.00714, 0.00000 C, 0.02509, 0.03870, 0.00000 C, -1.25522, -0.13284, 0.00000 H, -2.11561, 0.50772, 0.00000	-398657.883874	2.54E+32	2	1.30E+00	2.38E+03
9/70	CO	C, 0.00000, 0.00000, -0.64038 O, 0.00000, 0.00000, 0.48029	-297385.023729	1.43E+32	1	1.00E+00	1.06E+02
	H	H, 0.00000, 0.00000, 0.00000	-1307.704984	9.79E+29	2	1.00E+00	1.00E+00
	TS	C, 0.11420, 0.54220, 0.00000 O, 0.11420, -0.58284, 0.00000 H, -1.59873, 1.40955, 0.00000	-298683.580276	1.51E+32	2	1.20E+00	1.41E+03
	HCO	C, 0.06118, 0.57927, 0.00000 O, 0.06118, -0.58725, 0.00000 H, -0.85649, 1.22238, 0.00000	-298768.200141	1.51E+32	2	1.00E+00	7.26E+02
10	OH	O, 0.00000, 0.00000, 0.10734 H, 0.00000, 0.00000, -0.85876	-198772.724511	6.78E+31	2	1.00E+00	1.09E+01
	H_2CN	C, -0.50346, 0.00000, 0.00005 N, 0.73653, 0.00000, -0.00006 H, -1.06749, 0.93849, 0.00008 H, -1.06748, -0.93850, 0.00008	-246571.579821	1.43E+32	2	1.02E+00	1.39E+03
	TS	C, -2.37784, 0.00002, 0.00000 N, -1.13825, -0.00003, -0.00000 H, -2.94152, 0.93860, 0.00000	-445348.754555	2.92E+32	1	8.34E+01	2.81E+04

		H, -2.94161, -0.93850, 0.00000 O, 3.23175, 0.00002, -0.00000 H, 2.26392, -0.00008, 0.00002					
	H_2CNOH	C, 1.12891, 0.03186, 0.00000 N, 0.00000, -0.52723, 0.00000 H, 1.99406, -0.61679, 0.00000 H, 1.24226, 1.11291, 0.00000 O, -1.02428, 0.39277, 0.00000 H, -1.81556, -0.13885, 0.00000	-445534.784357	2.92E+32	1	1.26E+00	9.21E+03
11	OH	O, 0.00000, 0.00000, 0.10734 H, 0.00000, 0.00000, -0.85876	-198772.724511	6.78E+31	2	1.00E+00	1.09E+01
	CN	N, 0.00000, 0.00000, 0.53434 C, 0.00000, 0.00000, -0.62339	-243282.319290	1.28E+32	2	1.00E+00	1.06E+02
	TS	O, 2.02443, -0.06749, 0.00004 H, 2.25767, 0.87068, -0.00016 C, -0.83094, -0.23012, -0.00008 N, -1.92392, 0.14999, 0.00005	-442062.400452	2.73E+32	1	1.94E+01	1.33E+04
	HOCN	O, -1.10707, -0.10788, 0.00000 H, -1.51638, 0.75904, 0.00000 C, 0.17972, -0.00835, 0.00000 N, 1.32780, 0.02201, 0.00000	-442526.105760	2.73E+32	1	1.20E+00	3.09E+03
12/37	OH	O, 0.00000, 0.00000, 0.10734 H, 0.00000, 0.00000, -0.85876	-198772.724511	6.78E+31	2	1.00E+00	1.09E+01
	TS	H, 2.54691, 0.64509, 0.00001 O, 1.92094, -0.09102, -0.00000 O, -2.09755, 0.01948, -0.00001 H, -1.13405, -0.07280, 0.00008	-397549.192985	1.92E+32	1	5.74E+00	7.66E+03
	H_2O_2	H, -0.77756, 0.90318, 0.46392 O, 0.00000, 0.70715, -0.05799 O, 0.00000, -0.70715, -0.05799 H, 0.77756, -0.90318, 0.46392	-397675.0332	1.92E+32	1	1.18E+00	1.80E+03
13/82	OH	O, 0.00000, 0.00000, 0.10734 H, 0.00000, 0.00000, -0.85876	-198772.724511	6.78E+31	2	1.00E+00	1.09E+01
	^{3}O	O, 0.00000, 0.00000, 0.00000	-197065.919094	6.19E+31	3	1.00E+00	1.00E+00
	TS	O, 0.05549, -1.30535, 0.00000 H, -0.88787, -1.51445, 0.00000 O, 0.05549, 1.49465, 0.00000	-395840.349553	1.83E+32	2	1.99E+00	4.59E+03
	HO_2	O, 0.05455, -0.59846, 0.00000 H, -0.87278, -0.86200, 0.00000 O , 0.05455, 0.70621, 0.00000	-396037.107149	1.83E+32	2	1.00E+00	1.01E+03
14/83	OH	O, 0.00000, 0.00000, 0.10734 H, 0.00000, 0.00000, -0.85876	-198772.724511	6.78E+31	2	1.00E+00	1.09E+01
	^{1}O	O, 0.00000, 0.00000, 0.00000	-196788.921964	6.19E+31	1	1.00E+00	1.00E+00
	TS	O, 0.05201, -1.95355, 0.00000 H, -0.83215, -2.34312, 0.00000 O, 0.05201, 2.24645, 0.00000	-395562.986482	1.83E+32	2	3.93E+00	9.64E+03
	HO_2	O, 0.05455, -0.59846, 0.00000 H, -0.87278, -0.86200, 0.00000 O , 0.05455, 0.70621, 0.00000	-396037.107149	1.83E+32	2	1.00E+00	1.01E+03
15/84	OH	O, 0.00000, 0.00000, 0.10734 H, 0.00000, 0.00000, -0.85876	-198772.724511	6.78E+31	2	1.00E+00	1.09E+01
	NH	N, 0.00000, 0.00000, -0.00325 H, 0.00000, 0.00000, 1.03180	-144933.050538	5.63E+31	3	1.00E+00	1.24E+01
	TS	O, -2.17408, 0.00399, 0.00000 H, -1.20704, -0.02598, 0.00000 N, 2.19591, -0.00793, 0.00000 H, 3.22830, 0.04955, 0.00000	-343708.426804	1.75E+32	2	5.54E+00	1.91E+03
	trans−HNOH	O, 0.61481, 0.14770, 0.00000 H, 1.08132, -0.68683, -0.00002 N, -0.69487, -0.17685, 0.00000 H, -1.13566, 0.74315, -0.00002	-343946.299730	1.75E+32	2	1.03E+00	1.59E+03
16	OH	O, 0.00000, 0.00000, 0.10734 H, 0.00000, 0.00000, -0.85876	-198772.724511	6.78E+31	2	1.00E+00	1.09E+01
	CH_3	C, 0.00000, -0.00018, 0.00042 H, -0.93570, -0.53955, -0.00085 H, 0.93580, -0.53939, -0.00085 H, -0.00010, 1.08002, -0.00085	-104455.380974	5.63E+31	2	1.08E+00	2.53E+02
	TS	O, 2.09354, 0.00024, -0.00019 C, -1.97646, -0.00054, 0.00045 H, -2.00791, 0.82878, 0.69215	-303228.966649	1.75E+32	1	2.25E+01	1.89E+04

		H, -1.99100, -1.01453, 0.37303 H, -2.01663, 0.18355, -1.06337 H, 1.12603, 0.00353, -0.00297					
	CH_3OH	C, -0.66089, 0.02058, -0.00000 H, -1.08060, -0.98379, 0.00002 H, -1.01884, 0.54531, 0.89096 H, 1.14827, 0.73955, -0.00000 H, -1.01889, 0.54529, -0.89094 O, 0.74192, -0.12123, -0.00000	-303559.118023	1.75E+32	1	2.25E+01	1.89E+04
17	OH	O, 0.00000, 0.00000, 0.10734 H, 0.00000, 0.00000, -0.85876	-198772.724511	6.78E+31	2	1.00E+00	1.09E+01
	H	H, 0.00000, 0.00000, 0.00000	-1307.704984	9.79E+29	2	1.00E+00	1.00E+00
	TS	O, 0.00000, 0.34111, 0.00000 H, 0.86325, -0.09257, 0.00000 H, -0.86325, -2.63628, 0.00000	-200081.985222	7.40E+31	1	2.35E+00	6.75E+02
	H_2O	O, 0.00000, 0.00000, 0.11552 H, 0.00000, 0.75819, -0.46207 H, 0.00000, -0.75819, -0.46207	-200534.424509	7.40E+31	1	1.00E+00	8.42E+01
18/105	^3O	O, 0.00000, 0.00000, 0.00000	-197065.919094	6.19E+31	3	1.00E+00	1.00E+00
	CN	N, 0.00000, 0.00000, 0.53434 C, 0.00000, 0.00000, -0.62339	-243282.319290	1.28E+32	2	1.00E+00	1.06E+02
	TS	N, 0.00798, 2.00597, 0.00000 C, 0.00000, 0.84844, 0.00000 O, -0.00698, -2.39155, 0.00000	-440349.175060	2.63E+32	2	5.74E+00	1.92E+03
	NCO	N, 0.00000, 0.00000, -1.25802 C, 0.00000, 0.00000, -0.03723 O, 0.00000, 0.00000, 1.12869	-440893.44121	2.63E+32	2	1.14E+00	5.23E+02
19	^3O	O, 0.00000, 0.00000, 0.00000	-197065.919094	6.19E+31	3	1.00E+00	1.00E+00
	TS	O, 0.00000, 0.00000, 1.68500 O, 0.00000, 0.00000, -1.68500	-394132.721728	1.75E+32	1	1.00E+00	5.58E+02
	O_2	O, 0.00000, 0.00000, 0.59090 O, 0.00000, 0.00000,-0.59090	-394357.104834	1.75E+32	1	1.00E+00	6.87E+01
20	^3O	O, 0.00000, 0.00000, 0.00000	-197065.919094	6.19E+31	3	1.00E+00	1.00E+00
	^4N	N, 0.00000, 0.00000, 0.00000	-143303.088167	5.07E+31	4	1.00E+00	1.00E+00
	TS	O, 0.00000, 0.00000, 1.73133 N, 0.00000, 0.00000, -1.97867	-340369.447179	1.59E+32	2	1.00E+00	1.26E+03
	NO	N, 0.00000, 0.00000, -0.60608 O, 0.00000, 0.00000, 0.53032	-340897.750289	1.59E+32	2	1.00E+00	1.19E+02
21/110/ 111	^3O	O, 0.00000, 0.00000, 0.00000	-197065.919094	6.19E+31	3	1.00E+00	1.00E+00
	$^3CH_2$	C, 0.00000, 0.00000, 0.10395 H, 0.00000, -0.99689, -0.31186 H, 0.00000, 0.99689, -0.31186	-102701.224038	5.08E+31	3	1.01E+00	8.96E+01
	TS	C, -1.75812, 0.00000, -0.10105 H, -1.88717, -0.99758, 0.29252 H, -1.88706, 0.99760, 0.29251 O, 1.79037, -0.00000, 0.00266	-299769.148387	1.59E+32	1	7.92E+00	1.11E+04
	H_2CO	C, 0.00000, -0.52451, 0.00000 H, 0.00000, -1.10548, -0.93804 H, 0.00000, -1.10548, 0.93804 O, 0.00000, 0.66975, 0.00000	-300426.644475	1.59E+32	1	1.00E+00	1.39E+03
22/113	^3O	O, 0.00000, 0.00000, 0.00000	-197065.919094	6.19E+31	3	1.00E+00	1.00E+00
	CH	C, 0.00000, 0.00000, 0.16040 H, 0.00000, 0.00000, -0.96239	-100985.100094	4.54E+31	2	1.00E+00	1.44E+01
	TS	C, -0.07140, 1.87828, 0.00000 H, 0.99963, 1.54414, 0.00000 O, -0.07140, -1.60172, 0.00000	-298053.759583	1.59E+32	2	2.19E+00	6.85E+03
	HCO	C, 0.06118, 0.57927, 0.00000 O, 0.06118, -0.58725, 0.00000 H, -0.85649, 1.22238, 0.00000	-298768.200141	1.51E+32	2	1.00E+00	7.26E+02
23	^3O	O, 0.00000, 0.00000, 0.00000	-197065.919094	6.19E+31	3	1.00E+00	1.00E+00
	H	H, 0.00000, 0.00000, 0.00000	-1307.704984	9.79E+29	2	1.00E+00	1.00E+00
	TS	O, 0.00000, 0.00000, 0.40000 H, 0.00000, 0.00000, -3.20000	-198374.076468	6.78E+31	2	1.00E+00	1.51E+02
	OH	O, 0.00000, 0.00000, 0.10734 H, 0.00000, 0.00000, -0.85876	-198772.724511	6.78E+31	2	1.00E+00	1.09E+01
24	^1O	O, 0.00000, 0.00000, 0.00000	-196788.921964	6.19E+31	1	1.00E+00	1.00E+00
	HCN	N, 0.00000, 0.00000, 0.64811 C, 0.00000, 0.00000, -0.49567 H, 0.00000, 0.00000, -1.56273	-245122.398339	1.36E+32	1	1.05E+00	1.38E+02
	TS	N, 0.00000, -1.06045, 0.00000	-441914.02557	2.73E+32	1	8.34E+00	8.25E+02

		C, 0.02645, -2.20367, 0.00000 H, 0.05117, -3.27048, 0.00000 O, -0.02623, 2.98946, 0.00000					
	HCNO	N, 0.02185, -0.00027, 0.00000 C, 1.16967, -0.00244, 0.00000 H, 2.23036, 0.01076, 0.00000 O, -1.17517, 0.00072, 0.00000	-442327.940896	2.73E+32	1	1.36E+00	4.47E+01
25/119	^{1}O	O, 0.00000, 0.00000, 0.00000	-196788.921964	6.19E+31	1	1.00E+00	1.00E+00
	CN	N, 0.00000, 0.00000, 0.53434 C, 0.00000, 0.00000, -0.62339	-243282.319290	1.28E+32	2	1.00E+00	1.06E+02
	TS	N, 0.00966, 2.10501, 0.00000 C, 0.00000, 0.94749, 0.00000 O, -0.00846, -2.55250, 0.00000	-440073.39254	2.63E+32	2	2.09E+01	2.19E+03
	NCO	N, 0.00000, 0.00000, -1.25802 C, 0.00000, 0.00000, -0.03723 O, 0.00000, 0.00000, 1.12869	-440893.44121	2.63E+32	2	1.14E+00	5.23E+02
26	^{1}O	O, 0.00000, 0.00000, 0.00000	-196788.921964	6.19E+31	1	1.00E+00	1.00E+00
	TS	O, 0.00000, 0.00000, 2.04500 O, 0.00000, 0.00000, -2.04500	-393578.707096	1.75E+32	1	1.00E+00	8.22E+02
	O$_2$	O, 0.00000, 0.00000, 0.59090 O, 0.00000, 0.00000,-0.59090	-394357.104834	1.75E+32	1	1.00E+00	6.87E+01
27/120	^{1}O	O, 0.00000, 0.00000, 0.00000	-196788.921964	6.19E+31	1	1.00E+00	1.00E+00
	CH$_4$	C, 0.00006, -0.00000, -0.00001 H, -1.07741, 0.05086, 0.15637 H, 0.23679, -0.86565, -0.61803 H, 0.33754, 0.90709, -0.50065 H, 0.50273, -0.09229, 0.96235	-106174.920693	6.21E+31	1	1.01E+00	4.36E+02
	TS	O, -0.00883, -0.00036, 0.00001 C, 0.00176, 0.00007, 4.10000 H, 1.08254, -0.00454, 4.23687 H, -0.46157, -0.63868, 4.85102 H, -0.37408, 1.01698, 4.20726 H, -0.24178, -0.37626, 3.10643	-302964.255863	1.75E+32	1	3.99E+01	1.88E+04
	CH$_3$OH	C, -0.66089, 0.02058, -0.00000 H, -1.08060, -0.98379, 0.00002 H, -1.01884, 0.54531, 0.89096 H, 1.14827, 0.73955, -0.00000 H, -1.01889, 0.54529, -0.89094 O, 0.74192, -0.12123, -0.00000	-303559.118023	1.75E+32	1	2.25E+01	1.89E+04
28/123/124	^{1}O	O, 0.00000, 0.00000, 0.00000	-196788.921964	6.19E+31	1	1.00E+00	1.00E+00
	^{1}CH$_2$	C, 0.00000, 0.17399, 0.00000 H, 0.86403, -0.52196, 0.00000 H, -0.86403, -0.52196, 0.00000	-102649.483309	5.08E+31	1	1.00E+00	1.31E+02
	TS	C, -0.00000, -2.12831, 0.00000 H, 0.00001, -2.82181, -0.86541 H, 0.00001, -2.82181, 0.86541 O, -0.00000, 2.30169, 0.00000	-299440.687835	1.59E+32	1	9.50E+00	1.45E+04
	H$_2$CO	C, 0.00000, -0.52451, 0.00000 H, 0.00000, -1.10548, -0.93804 H, 0.00000, -1.10548, 0.93804 O, 0.00000, 0.66975, 0.00000	-300426.644475	1.59E+32	1	1.00E+00	1.39E+03
29/125	^{1}O	O, 0.00000, 0.00000, 0.00000	-196788.921964	6.19E+31	1	1.00E+00	1.00E+00
	CH	C, 0.00000, 0.00000, 0.16040 H, 0.00000, 0.00000, -0.96239	-100985.100094	4.54E+31	2	1.00E+00	1.44E+01
	TS	C, 0.00040, 2.16520, 0.00000 H, -0.00558, 3.28715, 0.00000 O, 0.00040, -2.03480, 0.00000	-297776.097205	1.59E+32	2	2.48E+00	1.64E+03
	HCO	C, 0.06118, 0.57927, 0.00000 O, 0.06118, -0.58725, 0.00000 H, -0.85649, 1.22238, 0.00000	-298768.200141	1.51E+32	2	1.00E+00	7.26E+02
30/126	^{1}O	O, 0.00000, 0.00000, 0.00000	-196788.921964	6.19E+31	1	1.00E+00	1.00E+00
	H$_2$	H, 0.00000, 0.00000, 0.37683 H, 0.00000, 0.00000, -0.37683	-3031.139750	2.77E+30	1	1.00E+00	3.52E+00
	TS	O, -0.03050, 0.00000, -0.04133 H, -0.07372, 0.00000, 3.22838 H, 0.42785, 0.00000, 2.66290	-199821.299327	7.40E+31	1	1.69E+00	3.05E+02
	H$_2$O	O, 0.00000, 0.00000, 0.11552 H, 0.00000, 0.75819, -0.46207 H, 0.00000, -0.75819, -0.46207	-200534.424509	7.40E+31	1	1.00E+00	8.42E+01
31	^{1}O	O, 0.00000, 0.00000, 0.00000	-196788.921964	6.19E+31	1	1.00E+00	1.00E+00

	H	H, 0.00000, 0.00000, 0.00000	-1307.704984	9.79E+29	2	1.00E+00	1.00E+00
	TS	O, 0.00000, 0.00000, 0.40111	-198097.052086	6.78E+31	2	1.00E+00	1.52E+02
		H, 0.00000, 0.00000, -3.208897					
	OH	O, 0.00000, 0.00000, 0.10734	-198772.724511	6.78E+31	2	1.00E+00	1.09E+01
		H, 0.00000, 0.00000, -0.85876					
34	CO_2	O, 0.00000, 0.00000, 1.15274	-494917.399028	2.82E+32	1	1.07E+00	5.23E+02
		O, 0.00000, 0.00000, -1.15274					
		C, 0.00000, 0.00000, 0.00000					
	^2N	N, 0.00000, 0.00000, 0.00000	-143024.189856	5.07E+31	2	1.00E+00	1.00E+00
	TS	O, -0.86912, -0.18695, 0.00000	-637970.617821	4.27E+32	2	1.55E+00	3.16E+04
		O, 0.82054, 1.38960, 0.00000					
		C, 0.00000, 0.59496, 0.00000					
		N, 0.05552, -1.88442, 0.00000					
35	CO_2	O, 0.00000, 0.00000, 1.15274	-494917.399028	2.82E+32	1	1.07E+00	5.23E+02
		O, 0.00000, 0.00000, -1.15274					
		C, 0.00000, 0.00000, 0.00000					
	$^1CH_2$	C, 0.00000, 0.17399, 0.00000	-102649.483309	5.08E+31	1	1.00E+00	1.31E+02
		H, 0.86403, -0.52196, 0.00000					
		H, -0.86403, -0.52196, 0.00000					
	TS	O, -0.18028, 0.00179, 0.13798	-597572.747704	4.27E+32	1	2.26E+00	3.51E+04
		O, 0.00273, -0.00097, 2.44510					
		C, 1.87376, -0.00106, 0.08413					
		H, 1.89316, 0.87643, -0.57756					
		H, 1.89070, -0.87713, -0.57949					
		C, 0.01552, 0.00025, 1.29877					
36	CO_2	O, 0.00000, 0.00000, 1.15274	-494917.399028	2.82E+32	1	1.07E+00	5.23E+02
		O, 0.00000, 0.00000, -1.15274					
		C, 0.00000, 0.00000, 0.00000					
	CH	C, 0.00000, 0.00000, 0.16040	-100985.100094	4.54E+31	2	1.00E+00	1.44E+01
		H, 0.00000, 0.00000, -0.96239					
	TS	O, 0.08464, 0.17353, -0.00075	-595888.681116	4.16E+32	2	2.21E+00	2.83E+04
		O, 0.14479, -0.08889, 2.30201					
		C, 0.30010, 0.02434, 1.16779					
		C, 1.97451, -0.06352, 0.21201					
		H, 2.20906, 0.46573, -0.72551					
38	H_2CO	C, 0.00000, -0.52451, 0.00000	-300426.644475	1.59E+32	1	1.00E+00	1.39E+03
		H, 0.00000, -1.10548, -0.93804					
		H, 0.00000, -1.10548, 0.93804					
		O, 0.00000, 0.66975, 0.00000					
	CN	N, 0.00000, 0.00000, 0.53434	-243282.319290	1.28E+32	2	1.00E+00	1.06E+02
		C, 0.00000, 0.00000, -0.62339					
	TS	C, -1.59264, 0.42271, 0.00000	-543711.303085	4.06E+32	2	1.64E+02	6.13E+04
		O, -2.43063, -0.41920, 0.00000					
		H, -1.82790, 1.50034, 0.00000					
		H, -0.50772, 0.16496, 0.00000					
		C, 1.79717, -0.17616, 0.00000					
		N, 2.93621, 0.02986, 0.00000					
39	H_2CO	C, 0.00000, -0.52451, 0.00000	-300426.644475	1.59E+32	1	1.00E+00	1.39E+03
		H, 0.00000, -1.10548, -0.93804					
		H, 0.00000, -1.10548, 0.93804					
		O, 0.00000, 0.66975, 0.00000					
	OH	O, 0.00000, 0.00000, 0.10734	-198772.724511	6.78E+31	2	1.00E+00	1.09E+01
		H, 0.00000, 0.00000, -0.85876					
	TS	C, -0.47128, 0.58564, 0.03055	-499174.684035	3.12E+32	2	2.07E+00	1.53E+04
		H, -0.39530, 1.10409, 0.99025					
		H, -0.37939, 1.19869, -0.87035					
		O, -0.98079, -0.54821, -0.03120					
		O, 1.28145, -0.06128, -0.04899					
		H, 1.19707, -0.94064, 0.33831					
40	H_2CO	C, 0.00000, -0.52451, 0.00000	-300426.644475	1.59E+32	1	1.00E+00	1.39E+03
		H, 0.00000, -1.10548, -0.93804					
		H, 0.00000, -1.10548, 0.93804					
		O, 0.00000, 0.66975, 0.00000					
	OH	O, 0.00000, 0.00000, 0.10734	-198772.724511	6.78E+31	2	1.00E+00	1.09E+01
		H, 0.00000, 0.00000, -0.85876					
	TS($H_2CO \cdots HO$)	C, 2.18732, 0.23648, 0.00000	-499203.669555	3.12E+32	2	1.58E+02	4.45E+04
		H, 2.20924, 1.33906, -0.00001					
		H, 3.16350, -0.27616, 0.00002					
		O, 1.15885, -0.37226, -0.00001					
		H, -2.25487, -0.16518, 0.00001					

		O, -3.18908, 0.08268, 0.00000					
	$H_2CO \cdots HO$	C, 1.50833, 0.32662, 0.00000 H, 1.23510, 1.39327, -0.00004 H, 2.58204, 0.08647, 0.00006 O, 0.67771, -0.53625, -0.00001 O, -2.13399, 0.13053, 0.00000 H, -1.21695, -0.19369, 0.00002	-499213.793483	3.12E+32	2	1.98E+01	2.63E+04
	$TS(H_2O + HCO)$	C, 0.72110, 0.45885, 0.00000 H, 1.03115, 1.52036, 0.00000 H, -0.42319, 0.30139, -0.00001 O, 1.48873, -0.44329, 0.00000 O, -1.88081, -0.00753, 0.00000 H, -1.79788, -0.96824, 0.00000	-499195.617147	3.12E+32	2	8.89E+00	2.45E+04
41	H_2CO	C, 0.00000, -0.52451, 0.00000 H, 0.00000, -1.10548, -0.93804 H, 0.00000, -1.10548, 0.93804 O, 0.00000, 0.66975, 0.00000	-300426.644475	1.59E+32	1	1.00E+00	1.39E+03
	^3O	O, 0.00000, 0.00000, 0.00000	-197065.919094	6.19E+31	3	1.00E+00	1.00E+00
	TS	C, -0.59392, 0.42546, 0.00000 H, -0.77716, 1.51734, 0.00000 H, 0.60545, 0.13501, 0.00000 O, -1.43123, -0.39780, 0.00000 O, 1.89813, -0.12784, 0.00000	-497479.543088	3.02E+32	3	2.33E+00	2.04E+04
42	H_2CO	C, 0.00000, -0.52451, 0.00000 H, 0.00000, -1.10548, -0.93804 H, 0.00000, -1.10548, 0.93804 O, 0.00000, 0.66975, 0.00000	-300426.644475	1.59E+32	1	1.00E+00	1.39E+03
	^1O	O, 0.00000, 0.00000, 0.00000	-196788.921964	6.19E+31	1	1.00E+00	1.00E+00
	TS	C, -1.77953, 0.34320, 0.00000 H, -1.48268, 1.40545, 0.00000 H, -2.86259, 0.13442, -0.00000 O, -0.97089, -0.53624, 0.00000 O, 2.84870, 0.08636, 0.00000	-497218.371475	3.02E+32	1	3.92E+01	4.27E+04
43	H_2CO	C, 0.00000, -0.52451, 0.00000 H, 0.00000, -1.10548, -0.93804 H, 0.00000, -1.10548, 0.93804 O, 0.00000, 0.66975, 0.00000	-300426.644475	1.59E+32	1	1.00E+00	1.39E+03
	CH_3	C, 0.00000, -0.00018, 0.00042 H, -0.93570, -0.53955, -0.00085 H, 0.93580, -0.53939, -0.00085 H, -0.00010, 1.08002, -0.00085	-104455.380974	5.63E+31	2	1.08E+00	2.53E+02
	TS	C, 0.78646, 0.45348, 0.00000 H, 1.07291, 1.52901, 0.00000 H, -0.51355, 0.21771, 0.00000 O, 1.57243, -0.42799, 0.00000 C, -1.89866, -0.09510, 0.00000 H, -1.90272, -1.18086, -0.00001 H, -2.28144, 0.35391, 0.91205 H, -2.28144, 0.35392, -0.91204	-404839.859919	2.92E+32	2	2.61E+01	2.82E+04
44	H_2CO	C, 0.00000, -0.52451, 0.00000 H, 0.00000, -1.10548, -0.93804 H, 0.00000, -1.10548, 0.93804 O, 0.00000, 0.66975, 0.00000	-300426.644475	1.59E+32	1	1.00E+00	1.39E+03
	$^3CH_2$	C, 0.00000, 0.00000, 0.10395 H, 0.00000, -0.99689, -0.31186 H, 0.00000, 0.99689, -0.31186	-102701.224038	5.08E+31	3	1.01E+00	8.96E+01
	TS	C, 0.14050, 0.09150, 0.05065 O, 0.06828, -0.07800, 1.21819 H, 0.89195, -0.40846, -0.59523 C, -1.56816, 1.76660, -1.21646 H, -0.63273, 0.85440, -0.54742 H, -2.29851, 2.25059, -0.58010 H, -1.47869, 1.90289, -2.28736	-403114.922172	2.83E+32	3	1.19E+01	2.48E+04
45	H_2CO	C, 0.00000, -0.52451, 0.00000 H, 0.00000, -1.10548, -0.93804 H, 0.00000, -1.10548, 0.93804 O, 0.00000, 0.66975, 0.00000	-300426.644475	1.59E+32	1	1.00E+00	1.39E+03
	$^1CH_2$	C, 0.00000, 0.17399, 0.00000 H, 0.86403, -0.52196, 0.00000 H, -0.86403, -0.52196, 0.00000	-102649.483309	5.08E+31	1	1.00E+00	1.31E+02

	TS	C, -0.68910, 0.48572, -0.08639 O, -1.38273, -0.46949, 0.05703 H, -0.94950, 1.48003, 0.31230 C, 2.03635, -0.06055, -0.09460 H, 0.26632, 0.44354, -0.67581 H, 1.72584, -1.10952, 0.07940 H, 1.93572, 0.39090, 0.91387	-403080.446732	2.83E+32	1	1.22E+01	2.60E+04
46	H_2CO	C, 0.00000, -0.52451, 0.00000 H, 0.00000, -1.10548, -0.93804 H, 0.00000, -1.10548, 0.93804 O, 0.00000, 0.66975, 0.00000	-300426.644475	1.59E+32	1	1.00E+00	1.39E+03
	CH	C, 0.00000, 0.00000, 0.16040 H, 0.00000, 0.00000, -0.96239	-100985.100094	4.54E+31	2	1.00E+00	1.44E+01
	TS	C, 1.06314, 0.52104, 0.00000 H, 1.80273, 1.34082, 0.00000 H, 0.00007, 0.80950, 0.00000 O, 1.40579, -0.62540, -0.00000 C, -2.65560, 0.06709, -0.00001 H, -3.49440, -0.67583, 0.00003	-401415.141966	2.73E+32	2	3.29E+01	4.06E+04
47	H_2CO	C, 0.00000, -0.52451, 0.00000 H, 0.00000, -1.10548, -0.93804 H, 0.00000, -1.10548, 0.93804 O, 0.00000, 0.66975, 0.00000	-300426.644475	1.59E+32	1	1.00E+00	1.39E+03
	CH	C, 0.00000, 0.00000, 0.16040 H, 0.00000, 0.00000, -0.96239	-100985.100094	4.54E+31	2	1.00E+00	1.44E+01
	TS	C, 1.08832, 0.24164, 0.00000 H, 2.10074, -0.17241, 0.00000 H, 0.95325, 1.32808, 0.00000 O, 0.13808, -0.50703, 0.00000 C, -1.57241, 0.05352, 0.00000 H, -1.25410, 1.12959, -0.00000	-401442.155736	2.73E+32	2	3.98E+00	1.17E+04
48	H_2CO	C, 0.00000, -0.52451, 0.00000 H, 0.00000, -1.10548, -0.93804 H, 0.00000, -1.10548, 0.93804 O, 0.00000, 0.66975, 0.00000	-300426.644475	1.59E+32	1	1.00E+00	1.39E+03
	H	H, 0.00000, 0.00000, 0.00000	-1307.704984	9.79E+29	2	1.00E+00	1.00E+00
	TS	C, 0.30393, 0.29916, 0.00000 H, 0.44476, 1.39878, 0.00000 H, 1.38940, -0.36012, 0.00000 O, -0.74353, -0.23991, 0.00000 H, 2.29052, -0.91436, 0.00000	-301720.745549	1.67E+32	2	1.41E+00	3.18E+03
49	HCO	C, 0.06118, 0.57927, 0.00000 O, 0.06118, -0.58725, 0.00000 H, -0.85649, 1.22238, 0.00000	-298768.200141	1.51E+32	2	1.00E+00	7.26E+02
	H_2CN	C, -0.50346, 0.00000, 0.00005 N, 0.73653, 0.00000, -0.00006 H, -1.06749, 0.93849, 0.00008 H, -1.06748, -0.93850, 0.00008	-246571.579821	1.43E+32	2	1.02E+00	1.39E+03
	TS	C, -1.44215, -0.44322, 0.00000 N, -2.34396, 0.37970, -0.00000 H, -1.57250, -1.52975, 0.00000 H, -0.32410, -0.09039, 0.00000 C, 1.30754, 0.42132, 0.00000 H, 1.35232, 1.53659, 0.00000 O, 2.21995, -0.30537, -0.00000	-545332.454817	4.17E+32	1	4.02E+01	5.76E+04
50	HCO	C, 0.06118, 0.57927, 0.00000 O, 0.06118, -0.58725, 0.00000 H, -0.85649, 1.22238, 0.00000	-298768.200141	1.51E+32	2	1.00E+00	7.26E+02
	TS(trans$-C_2H_2O_2$)	C, 1.44538, -0.41941, -0.00002 O, 2.35078, 0.31649, 0.00001 H, 1.50835, -1.53463, 0.00001 C, -1.44538, 0.41941, 0.00001 O, -2.35078, -0.31649, 0.00000 H, -1.50835, 1.53463, -0.00003	-597543.869830	4.27E+32	1	1.20E+02	6.31E+04
	trans$-C_2H_2O_2$	O, 1.70599, 0.17033, -0.00001 O, -1.70599, -0.17032, -0.00001 C, 0.65011, -0.38894, 0.00001 C, -0.65011, 0.38894, 0.00001 H, 0.54322, -1.48641, 0.00003 H, -0.54322, 1.48641, 0.00003	-597808.108026	4.27E+32	1	2.77E+00	2.48E+04

	TS(anti−HCOH + CO)	O, -1.89257, 0.11748, 0.00000 O, 1.47449, -0.48359, 0.00000 C, -0.81507, -0.24983, 0.00000 C, 1.01515, 0.66227, 0.00000 H, 0.36217, -0.99882, 0.00000 H, 1.78192, 1.45305, 0.00000	-597543.515387	4.27E+32	1	2.64E+00	3.37E+04
51	HCO	C, 0.06118, 0.57927, 0.00000 O, 0.06118, -0.58725, 0.00000 H, -0.85649, 1.22238, 0.00000	-298768.200141	1.51E+32	2	1.00E+00	7.26E+02
	TS	C, -3.21999, 0.45642, 0.00056 O, -3.82943, -0.53056, -0.00062 H, -3.64889, 1.50598, 0.00221 C, 3.22001, 0.45642, -0.00056 O, 3.82941, -0.53056, 0.00061 H, 3.64892, 1.50597, -0.00222	-597252.486589	4.27E+32	1	5.45E+03	2.47E+05
52	HCO	C, 0.06118, 0.57927, 0.00000 O, 0.06118, -0.58725, 0.00000 H, -0.85649, 1.22238, 0.00000	-298768.200141	1.51E+32	2	1.00E+00	7.26E+02
	CN	N, 0.00000, 0.00000, 0.53434 C, 0.00000, 0.00000, -0.62339	-243282.319290	1.28E+32	2	1.00E+00	1.06E+02
	TS	C, 1.92935, 0.44928, -0.00000 O, 2.65542, -0.45810, 0.00000 H, 2.21156, 1.53080, 0.00000 C, -2.07362, -0.09641, -0.00000 N, -3.22704, 0.00240, 0.00000	-542054.462932	3.95E+32	1	1.67E+02	7.95E+04
53	HCO	C, 0.06118, 0.57927, 0.00000 O, 0.06118, -0.58725, 0.00000 H, -0.85649, 1.22238, 0.00000	-298768.200141	1.51E+32	2	1.00E+00	7.26E+02
	OH	O, 0.00000, 0.00000, 0.10734 H, 0.00000, 0.00000, -0.85876	-198772.724511	6.78E+31	2	1.00E+00	1.09E+01
	TS	C, -0.92930, 0.41679, -0.00001 O, -1.76441, -0.39597, 0.00000 H, -1.08742, 1.52276, 0.00000 O, 2.36403, -0.00313, 0.00000 H, 1.86621, -0.83067, -0.00003	-497546.364688	3.02E+32	1	3.64E+01	3.32E+04
54	HCO	C, 0.06118, 0.57927, 0.00000 O, 0.06118, -0.58725, 0.00000 H, -0.85649, 1.22238, 0.00000	-298768.200141	1.51E+32	2	1.00E+00	7.26E+02
	^{3}O	O, 0.00000, 0.00000, 0.00000	-197065.919094	6.19E+31	3	1.00E+00	1.00E+00
	TS	C, -0.91822, 0.43888, 0.00063 O, -1.68693, -0.43685, -0.00021 H, -1.17411, 1.52862, -0.00159 O, 2.52236, -0.08339, -0.00006	-495836.418546	2.92E+32	2	8.51E+00	3.46E+04
55	HCO	C, 0.06118, 0.57927, 0.00000 O, 0.06118, -0.58725, 0.00000 H, -0.85649, 1.22238, 0.00000	-298768.200141	1.51E+32	2	1.00E+00	7.26E+02
	^{3}O	O, 0.00000, 0.00000, 0.00000	-197065.919094	6.19E+31	3	1.00E+00	1.00E+00
	TS	C, 1.11161, 0.61321, -0.00001 O, 1.49004, -0.48723, 0.00000 H, 0.03627, 0.94174, 0.00005 O, -2.32828, -0.09040, -0.00000	-495837.193069	2.92E+32	2	1.17E+01	3.30E+04
56	HCO	C, 0.06118, 0.57927, 0.00000 O, 0.06118, -0.58725, 0.00000 H, -0.85649, 1.22238, 0.00000	-298768.200141	1.51E+32	2	1.00E+00	7.26E+02
	^{1}O	O, 0.00000, 0.00000, 0.00000	-196788.921964	6.19E+31	1	1.00E+00	1.00E+00
	TS	C, -1.12673, 0.41429, -0.00003 O, -1.93331, -0.42516, 0.00001 H, -1.32485, 1.51568, 0.00006 O, 2.94396, -0.07502, 0.00000	-495559.276017	2.92E+32	2	1.22E+01	4.52E+04
57	HCO	C, 0.06118, 0.57927, 0.00000 O, 0.06118, -0.58725, 0.00000 H, -0.85649, 1.22238, 0.00000	-298768.200141	1.51E+32	2	1.00E+00	7.26E+02
	NH	N, 0.00000, 0.00000, -0.00325 H, 0.00000, 0.00000, 1.03180	-144933.050538	5.63E+31	3	1.00E+00	1.24E+01
	TS	C, -0.54840, 0.43585, 0.00000 O, -1.36093, -0.41218, 0.00000 H, -0.77366, 1.52479, 0.00000 N, 2.02120, -0.14040, 0.00000 H, 0.80313, 0.14032, 0.00000	-443659.565616	2.83E+32	4	2.37E+00	2.00E+04
58	HCO	C, 0.06118, 0.57927, 0.00000	-298768.200141	1.51E+32	2	1.00E+00	7.26E+02

		O, 0.06118, -0.58725, 0.00000					
		H, -0.85649, 1.22238, 0.00000					
	NH	N, 0.00000, 0.00000, -0.00325	-144933.050538	5.63E+31	3	1.00E+00	1.24E+01
		H, 0.00000, 0.00000, 1.03180					
	$TS(CO + NH_2)$	C, 1.00716, -0.60363, 0.00000	-443708.520689	2.83E+32	2	2.37E+01	3.02E+04
		O, 1.51647, 0.44434, 0.00000					
		H, -0.10268, -0.79887, -0.00000					
		N, -2.27732, -0.01975, 0.00000					
		H, -2.13079, 1.00422, 0.00000					
	TS(HNHCO)	C, 0.79683, 0.38808, -0.00001	-443705.666770	2.83E+32	2	3.91E+01	2.95E+04
		O, 1.68245, -0.37024, 0.00001					
		H, 0.88661, 1.50171, 0.00001					
		N, -2.43159, 0.01415, 0.00001					
		H, -2.10606, -0.96738, -0.00005					
59	HCO	C, 0.06118, 0.57927, 0.00000	-298768.200141	1.51E+32	2	1.00E+00	7.26E+02
		O, 0.06118, -0.58725, 0.00000					
		H, -0.85649, 1.22238, 0.00000					
	^4N	N, 0.00000, 0.00000, 0.00000	-143303.088167	5.07E+31	4	1.00E+00	1.00E+00
	TS	C, -0.72905, 0.41600, 0.00000	-442073.879138	2.73E+32	3	8.67E+00	2.84E+04
		O, -1.55200, -0.40943, -0.00000					
		H, -0.91590, 1.51955, -0.00001					
		N, 2.52945, -0.10573, 0.00000					
60	HCO	C, 0.06118, 0.57927, 0.00000	-298768.200141	1.51E+32	2	1.00E+00	7.26E+02
		O, 0.06118, -0.58725, 0.00000					
		H, -0.85649, 1.22238, 0.00000					
	^4N	N, 0.00000, 0.00000, 0.00000	-143303.088167	5.07E+31	4	1.00E+00	1.00E+00
	TS	C, -0.96022, 0.53343, -0.00000	-442073.275273	2.73E+32	3	6.16E+00	3.08E+04
		O, -1.70117, -0.36597, 0.00000					
		H, 0.16249, 0.44888, 0.00001					
		N, 2.74403, -0.10310, -0.00000					
61	HCO	C, 0.06118, 0.57927, 0.00000	-298768.200141	1.51E+32	2	1.00E+00	7.26E+02
		O, 0.06118, -0.58725, 0.00000					
		H, -0.85649, 1.22238, 0.00000					
	^2N	N, 0.00000, 0.00000, 0.00000	-143024.189856	5.07E+31	2	1.00E+00	1.00E+00
	TS	C, -0.78848, 0.42135, 0.00001	-441966.299275	2.73E+32	3	9.33E+00	3.12E+04
		O, -1.59612, -0.41902, -0.00000					
		H, -0.99546, 1.52140, -0.00001					
		N, 2.64219, -0.09962, -0.00000					
62	HCO	C, 0.06118, 0.57927, 0.00000	-298768.200141	1.51E+32	2	1.00E+00	7.26E+02
		O, 0.06118, -0.58725, 0.00000					
		H, -0.85649, 1.22238, 0.00000					
	^2N	N, 0.00000, 0.00000, 0.00000	-143024.189856	5.07E+31	2	1.00E+00	1.00E+00
	TS	C, -1.02091, 0.53057, 0.00000	-441965.902825	2.73E+32	3	6.31E+00	3.35E+04
		O, -1.76359, -0.36744, 0.00000					
		H, 0.10155, 0.44424, 0.00000					
		N, 2.87609, -0.09831, 0.00000					
63	HCO	C, 0.06118, 0.57927, 0.00000	-298768.200141	1.51E+32	2	1.00E+00	7.26E+02
		O, 0.06118, -0.58725, 0.00000					
		H, -0.85649, 1.22238, 0.00000					
	CH_3	C, 0.00000, -0.00018, 0.00042	-104455.380974	5.63E+31	2	1.08E+00	2.53E+02
		H, -0.93570, -0.53955, -0.00085					
		H, 0.93580, -0.53939, -0.00085					
		H, -0.00010, 1.08002, -0.00085					
	TS	C, -1.18076, 0.58286, 0.00000	-403229.239068	2.83E+32	1	1.63E+02	3.94E+04
		O, -1.80285, -0.40268, 0.00000					
		H, -0.05231, 0.63844, 0.00000					
		C, 2.37921, -0.09594, 0.00000					
		H, 2.60699, 0.39621, -0.93455					
		H, 2.07031, -1.13118, 0.00011					
		H, 2.60705, 0.39639, 0.93444					
64	HCO	C, 0.06118, 0.57927, 0.00000	-298768.200141	1.51E+32	2	1.00E+00	7.26E+02
		O, 0.06118, -0.58725, 0.00000					
		H, -0.85649, 1.22238, 0.00000					
	$^3CH_2$	C, 0.00000, 0.00000, 0.10395	-102701.224038	5.08E+31	3	1.01E+00	8.96E+01
		H, 0.00000, -0.99689, -0.31186					
		H, 0.00000, 0.99689, -0.31186					
	$TS(CH_3 + CO)$	C, 1.18089, -0.58830, 0.00001	-401475.384064	2.73E+32	2	1.46E+02	3.90E+04
		O, 1.76377, 0.42079, -0.00000					
		H, 0.06058, -0.69428, -0.00001					
		C, -2.55962, 0.07216, 0.00000					

		H, -3.28708, -0.72572, -0.00001 H, -2.61129, 1.15053, 0.00001					
	TS(CH_2HCO)	C, 0.88495, 0.42556, -0.00000 O, 1.70057, -0.40713, 0.00000 H, 1.07614, 1.52704, -0.00000 C, -2.39692, -0.07616, 0.00000 H, -2.55118, -1.14473, -0.00000 H, -3.05762, 0.77835, 0.00001	-401473.748377	2.73E+32	2	1.12E+02	3.36E+04
65	HCO	C, 0.06118, 0.57927, 0.00000 O, 0.06118, -0.58725, 0.00000 H, -0.85649, 1.22238, 0.00000	-298768.200141	1.51E+32	2	1.00E+00	7.26E+02
	$^1CH_2$	C, 0.00000, 0.17399, 0.00000 H, 0.86403, -0.52196, 0.00000 H, -0.86403, -0.52196, 0.00000	-102649.483309	5.08E+31	1	1.00E+00	1.31E+02
	TS	C, -0.82757, 0.32128, 0.00001 O, -1.79760, -0.32405, 0.00001 H, -0.77593, 1.43708, -0.00008 C, 2.51354, 0.07736, -0.00003 H, 2.52039, -0.61837, -0.86354 H, 2.52045, -0.61811, 0.86370	-401422.503868	2.73E+32	2	8.57E+01	3.13E+04
66	HCO	C, 0.06118, 0.57927, 0.00000 O, 0.06118, -0.58725, 0.00000 H, -0.85649, 1.22238, 0.00000	-298768.200141	1.51E+32	2	1.00E+00	7.26E+02
	CH	C, 0.00000, 0.00000, 0.16040 H, 0.00000, 0.00000, -0.96239	-100985.100094	4.54E+31	2	1.00E+00	1.44E+01
	TS	C, -1.00243, 0.52281, 0.00000 O, -1.75206, -0.37324, 0.00000 H, 0.11410, 0.43659, -0.00002 C, 2.70696, -0.00384, -0.00000 H, 3.67526, -0.56446, 0.00001	-399758.934558	2.63E+32	3	2.76E+01	3.09E+04
67	HCO	C, 0.06118, 0.57927, 0.00000 O, 0.06118, -0.58725, 0.00000 H, -0.85649, 1.22238, 0.00000	-298768.200141	1.51E+32	2	1.00E+00	7.26E+02
	CH	C, 0.00000, 0.00000, 0.16040 H, 0.00000, 0.00000, -0.96239	-100985.100094	4.54E+31	2	1.00E+00	1.44E+01
	TS	C, 0.95316, -0.57236, -0.06467 O, 1.55803, 0.41893, 0.04383 H, -0.17127, -0.65680, -0.06725 C, -2.54630, -0.03468, 0.08692 H, -2.73409, 0.94753, -0.41695	-399761.111098	2.63E+32	1	2.66E+01	3.08E+04
68/69	HCO	C, 0.06118, 0.57927, 0.00000 O, 0.06118, -0.58725, 0.00000 H, -0.85649, 1.22238, 0.00000	-298768.200141	1.51E+32	2	1.00E+00	7.26E+02
	H	H, 0.00000, 0.00000, 0.00000	-1307.704984	9.79E+29	2	1.00E+00	1.00E+00
	TS($CO + H_2$)	C, 0.10339, -0.52516, -0.00001 O, -0.66721, 0.34873, 0.00000 H, 1.22122, -0.40653, 0.00005 H, 3.49608, 0.76762, -0.00001	-300077.962322	1.59E+32	1	4.64E+00	4.25E+03
	TS(H_2CO)	C, -0.28186, 0.33762, 0.00000 O, 0.67158, -0.33299, -0.00000 H, -0.28760, 1.45702, -0.00001 H, -3.39393, -0.81883, -0.00000	-300077.773286	1.59E+32	1	5.26E+00	4.04E+03
71	CO	C, 0.00000, 0.00000, -0.64038 O, 0.00000, 0.00000, 0.48029	-297385.023729	1.43E+32	1	1.00E+00	1.06E+02
	OH	O, 0.00000, 0.00000, 0.10734 H, 0.00000, 0.00000, -0.85876	-198772.724511	6.78E+31	2	1.00E+00	1.09E+01
	TS	O, 0.00000, 0.00000, 2.70789 H, 0.00000, 0.00000, 1.73998 C, 0.00000, 0.00000,-1.03211 O, 0.00000, 0.00000, -2.15130	-496160.381617	2.92E+32	2	2.35E+01	2.55E+03
72	H_2O	O, 0.00000, 0.00000, 0.11552 H, 0.00000, 0.75819, -0.46207 H, 0.00000, -0.75819, -0.46207	-200534.424509	7.40E+31	1	1.00E+00	8.42E+01
	^1O	O, 0.00000, 0.00000, 0.00000	-196788.921964	6.19E+31	1	1.00E+00	1.00E+00
	TS	H, -1.88062, 0.75858, 0.39238 O, -1.58903, -0.00000, -0.10594 H, -1.88068, -0.75855, 0.39240 O, 2.05919, -0.00000, 0.00784	-397326.729119	1.92E+32	1	6.89E+00	1.12E+04
73	H_2O	O, 0.00000, 0.00000, 0.11552 H, 0.00000, 0.75819, -0.46207	-200534.424509	7.40E+31	1	1.00E+00	8.42E+01

		H, 0.00000, -0.75819, -0.46207					
	CN	N, 0.00000, 0.00000, 0.53434 C, 0.00000, 0.00000, -0.62339	-243282.319290	1.28E+32	2	1.00E+00	1.06E+02
	TS(H_2OCN)	O, 2.08577, 0.00000, -0.06154 H, 2.49878, -0.75915, 0.34133 H, 2.49878, 0.75915, 0.34133 C, -1.06261, 0.00000, -0.16237 N, -2.18687, 0.00000, 0.11198	-443824.893350	2.83E+32	2	9.43E+01	1.73E+04
	H_2OCN	O, 1.54613, 0.01966, 0.06013 H, 1.66854, 0.07098, -0.88769 H, 1.48124, -0.91327, 0.26476 C, -0.65504, 0.35401, 0.09666 N, -1.65551, -0.20558, -0.06257	-443834.360904	2.83E+32	2	2.57E+01	1.35E+04
	TS(OH + HCN)	N, 1.75725, 0.08450, -0.04306 C, 0.62537, -0.11926, 0.05446 H, -0.82101, -0.40068, 0.33516 O, -1.68801, -0.04415, -0.06984 H, -1.72792, 0.87798, 0.19825	-443802.027871	2.83E+32	2	6.63E+00	9.16E+03
74	H_2O	O, 0.00000, 0.00000, 0.11552 H, 0.00000, 0.75819, -0.46207 H, 0.00000, -0.75819, -0.46207	-200534.424509	7.40E+31	1	1.00E+00	8.42E+01
	^{2}N	N, 0.00000, 0.00000, 0.00000	-143024.189856	5.07E+31	2	1.00E+00	1.00E+00
	TS	O, 1.09981, 0.00000, -0.11558 H, 1.26171, 0.76121, 0.43633 H, 1.26170, -0.76122, 0.43633 N, -1.61741, 0.00000, 0.00743	-343579.105176	1.75E+32	2	4.61E+00	6.00E+03
75	H_2O	O, 0.00000, 0.00000, 0.11552 H, 0.00000, 0.75819, -0.46207 H, 0.00000, -0.75819, -0.46207	-200534.424509	7.40E+31	1	1.00E+00	8.42E+01
	CH	C, 0.00000, 0.00000, 0.16040 H, 0.00000, 0.00000, -0.96239	-100985.100094	4.54E+31	2	1.00E+00	1.44E+01
	TS	O, -0.00000, -1.50496, 0.00000 H, -0.00001, -2.08192, -0.75874 H, -0.00001, -2.08192, 0.75874 C, -0.00000, 2.47505, 0.00000 H, 0.00006, 1.35321, 0.00000	-301522.701458	1.67E+32	2	3.93E+01	9.93E+03
76/92	H_2O	O, 0.00000, 0.00000, 0.11552 H, 0.00000, 0.75819, -0.46207 H, 0.00000, -0.75819, -0.46207	-200534.424509	7.40E+31	1	1.00E+00	8.42E+01
	CH	C, 0.00000, 0.00000, 0.16040 H, 0.00000, 0.00000, -0.96239	-100985.100094	4.54E+31	2	1.00E+00	1.44E+01
	TS	O, -0.71798, 0.12903, -0.06268 H, -0.02388, -0.65891, -0.55561 H, -1.11251, -0.35890, 0.66244 C, 0.92714, -0.14736, 0.06666 H, 1.31739, 0.86979, -0.00541	-301498.502225	1.67E+32	2	1.32E+00	2.82E+03
	OH	O, 0.00000, 0.00000, 0.10734 H, 0.00000, 0.00000, -0.85876	-198772.724511	6.78E+31	2	1.00E+00	1.09E+01
	$^3CH_2$	C, 0.00000, 0.00000, 0.10395 H, 0.00000, -0.99689, -0.31186 H, 0.00000, 0.99689, -0.31186	-102701.224038	5.08E+31	3	1.01E+00	8.96E+01
77	OH	O, 0.00000, 0.00000, 0.10734 H, 0.00000, 0.00000, -0.85876	-198772.724511	6.78E+31	2	1.00E+00	1.09E+01
	HCN	N, 0.00000, 0.00000, 0.64811 C, 0.00000, 0.00000, -0.49567 H, 0.00000, 0.00000, -1.56273	-245122.398339	1.36E+32	1	1.05E+00	1.38E+02
	TS	N, 1.18289, -0.45813, 0.00000 C, 0.53038, 0.50741, 0.00000 H, 0.29374, 1.55076, 0.00000 O, -1.31803, -0.04783, 0.00000 H, -1.21204, -1.00567, -0.00000	-443875.717780	2.83E+32	2	1.87E+00	1.34E+04
78	OH	O, 0.00000, 0.00000, 0.10734 H, 0.00000, 0.00000, -0.85876	-198772.724511	6.78E+31	2	1.00E+00	1.09E+01
	CN	N, 0.00000, 0.00000, 0.53434 C, 0.00000, 0.00000, -0.62339	-243282.319290	1.28E+32	2	1.00E+00	1.06E+02
	TS(HO $\cdots$ CN)	C, -2.32702, -0.06687, 0.00000 N, -2.73556, 0.80898, -0.00001 O, 1.05860, -0.23905, -0.00000 H, 2.14288, 0.16576, 0.00000	-442060.005996	2.73E+32	3	5.33E+01	1.75E+04
	HO $\cdots$ CN	C, -0.57866, -0.37506, 0.00000	-442071.736730	2.73E+32	3	1.19E+01	1.16E+04

		N, -1.57329, 0.21644, 0.00000 O, 1.62266, -0.02542, 0.00000 H, 1.50373, 0.93862, 0.00000					
	TS(^{3}HOCN$_{1}$)	O, 1.31726, -0.06057, -0.11557 H, 1.41697, -0.47382, 0.75883 C, -0.47337, 0.51436, 0.07208 N, -1.30212, -0.30396, -0.03811	-442065.795223	-4.42E+05	3	1.87E+00	1.06E+04
	^{3}HOCN$_{1}$	O, 1.00788, -0.18867, -0.07300 H, 1.59896, 0.17125, 0.59267 C, -0.15259, 0.44358, -0.05620 N, -1.24949, -0.18905, 0.04693	-442201.236892	2.73E+32	3	1.38E+00	6.50E+03
	TS(^{3}HOCN$_{2}$)	O, 1.07076, -0.23701, 0.00000 H, 1.04987, 0.95445, -0.00000 C, -0.10294, 0.31551, 0.00000 N, -1.28547, -0.13592, 0.00000	-442054.894147	2.73E+32	3	1.47E+00	6.08E+03
79	OH	O, 0.00000, 0.00000, 0.10734 H, 0.00000, 0.00000, -0.85876	-198772.724511	6.78E+31	2	1.00E+00	1.09E+01
	CN	N, 0.00000, 0.00000, 0.53434 C, 0.00000, 0.00000, -0.62339	-243282.319290	1.28E+32	2	1.00E+00	1.06E+02
	TS	O, 1.77507, -0.07477, 0.00000 H, 0.93798, 0.53268, 0.00000 C, -0.54988, 0.09824, 0.00000 N, -1.69132, -0.07485, 0.00000	-442050.029096	2.73E+32	3	4.92E+00	5.45E+03
80	OH	O, 0.00000, 0.00000, 0.10734 H, 0.00000, 0.00000, -0.85876	-198772.724511	6.78E+31	2	1.00E+00	1.09E+01
	CN	N, 0.00000, 0.00000, 0.53434 C, 0.00000, 0.00000, -0.62339	-243282.319290	1.28E+32	2	1.00E+00	1.06E+02
	TS	O, -1.47228, -0.16710, 0.00000 H, -0.76057, 0.60968, 0.00000 N, 0.63490, 0.49714, 0.00000 C, 1.34908, -0.45881, 0.00000	-442023.178107	2.73E+32	3	5.20E+00	1.32E+04
81	OH	O, 0.00000, 0.00000, 0.10734 H, 0.00000, 0.00000, -0.85876	-198772.724511	6.78E+31	2	1.00E+00	1.09E+01
	TS	H, 1.14564, -0.83725, -0.00002 O, 1.44781, 0.08292, 0.00000 O, -1.44744, -0.08304, 0.00000 H, -1.14860, 0.83818, -0.00002	-397324.930652	1.92E+32	3	2.29E+00	6.78E+03
85	OH	O, 0.00000, 0.00000, 0.10734 H, 0.00000, 0.00000, -0.85876	-198772.724511	6.78E+31	2	1.00E+00	1.09E+01
	NH	N, 0.00000, 0.00000, -0.00325 H, 0.00000, 0.00000, 1.03180	-144933.050538	5.63E+31	3	1.00E+00	1.24E+01
	TS	O, 0.05070, -1.15122, 0.00000 H, -0.90707, -1.27429, 0.00000 N, 0.05070, 1.44403, 0.00000 H, 0.14658, 0.37578, 0.00000	-343699.917559	1.75E+32	4	1.36E+00	3.77E+03
86	OH	O, 0.00000, 0.00000, 0.10734 H, 0.00000, 0.00000, -0.85876	-198772.724511	6.78E+31	2	1.00E+00	1.09E+01
	^{4}N	N, 0.00000, 0.00000, 0.00000	-143303.088167	5.07E+31	4	1.00E+00	1.00E+00
	TS	N, 0.00000, 0.00000, 2.12773 O, 0.00000, 0.00000, -1.76227 H, 0.00000, 0.00000, -0.79594	-342075.455071	1.67E+32	3	7.93E+00	1.40E+03
87	OH	O, 0.00000, 0.00000, 0.10734 H, 0.00000, 0.00000, -0.85876	-198772.724511	6.78E+31	2	1.00E+00	1.09E+01
	^{2}N	N, 0.00000, 0.00000, 0.00000	-143024.189856	5.07E+31	2	1.00E+00	1.00E+00
	TS	N, 0.00000, 0.00000, 2.47080 O, 0.00000, 0.00000, -2.02920 H, 0.00000, 0.00000, -1.06200	-341799.071312	1.67E+32	3	3.84E+00	1.87E+03
88	OH	O, 0.00000, 0.00000, 0.10734 H, 0.00000, 0.00000, -0.85876	-198772.724511	6.78E+31	2	1.00E+00	1.09E+01
	CH$_{4}$	C, 0.00006, -0.00000, -0.00001 H, -1.07741, 0.05086, 0.15637 H, 0.23679, -0.86565, -0.61803 H, 0.33754, 0.90709, -0.50065 H, 0.50273, -0.09229, 0.96235	-106174.920693	6.21E+31	1	1.01E+00	4.36E+02
	TS	C, -1.21215, -0.01020, 0.00000 H, -1.46698, -0.54700, 0.90908 H, -1.46698, -0.54699, -0.90909 H, -1.55136, 1.02213, 0.00001 H, 0.02596, 0.10426, 0.00000 O, 1.28596, 0.10848, 0.00000	-304916.333491	1.84E+32	2	5.67E+00	8.57E+03

		H, 1.44458, -0.83906, 0.00000					
89/108	OH	O, 0.00000, 0.00000, 0.10734 H, 0.00000, 0.00000, -0.85876	-198772.724511	6.78E+31	2	1.00E+00	1.09E+01
	CH_3	C, 0.00000, -0.00018, 0.00042 H, -0.93570, -0.53955, -0.00085 H, 0.93580, -0.53939, -0.00085 H, -0.00010, 1.08002, -0.00085	-104455.380974	5.63E+31	2	1.08E+00	2.53E+02
	TS	O, -0.00007, -0.00013, -0.00044 C, -0.00002, -0.00004, 2.50190 H, 1.05722, -0.00003, 2.74763 H, -0.53051, -0.90983, 2.76246 H, -0.52076, 0.92007, 2.74764 H, -0.00299, -0.00512, 1.18955	-303192.942164	1.75E+32	3	1.47E+00	7.34E+03
	^3O	O, 0.00000, 0.00000, 0.00000	-197065.919094	6.19E+31	3	1.00E+00	1.00E+00
	CH_4	C, 0.00006, -0.00000, -0.00001 H, -1.07741, 0.05086, 0.15637 H, 0.23679, -0.86565, -0.61803 H, 0.33754, 0.90709, -0.50065 H, 0.50273, -0.09229, 0.96235	-106174.920693	6.21E+31	1	1.01E+00	4.36E+02
90	OH	O, 0.00000, 0.00000, 0.10734 H, 0.00000, 0.00000, -0.85876	-198772.724511	6.78E+31	2	1.00E+00	1.09E+01
	CH_3	C, 0.00000, -0.00018, 0.00042 H, -0.93570, -0.53955, -0.00085 H, 0.93580, -0.53939, -0.00085 H, -0.00010, 1.08002, -0.00085	-104455.380974	5.63E+31	2	1.08E+00	2.53E+02
	TS	O, 1.20499, 0.00000, -0.10296 H, 1.34393, -0.00000, 0.84773 H, -0.00448, 0.00000, -0.13864 C, -1.25104, 0.00000, 0.01772 H, -1.73656, 0.96513, 0.00413 H, -1.73656, -0.96513, 0.00413	-303191.306477	1.75E+32	3	3.53E+00	6.49E+03
91	OH	O, 0.00000, 0.00000, 0.10734 H, 0.00000, 0.00000, -0.85876	-198772.724511	6.78E+31	2	1.00E+00	1.09E+01
	$^3CH_2$	C, 0.00000, 0.00000, 0.10395 H, 0.00000, -0.99689, -0.31186 H, 0.00000, 0.99689, -0.31186	-102701.224038	5.08E+31	3	1.01E+00	8.96E+01
	TS	C, -1.96653, -0.00000, -0.07282 H, -2.26898, 0.99852, 0.20670 H, -2.26889, -0.99855, 0.20669 O, 1.92265, -0.00000, 0.00728 H, 0.95586, 0.00006, -0.03469	-301475.536976	1.67E+32	2	1.71E+01	1.32E+04
93	OH	O, 0.00000, 0.00000, 0.10734 H, 0.00000, 0.00000, -0.85876	-198772.724511	6.78E+31	2	1.00E+00	1.09E+01
	$^1CH_2$	C, 0.00000, 0.17399, 0.00000 H, 0.86403, -0.52196, 0.00000 H, -0.86403, -0.52196, 0.00000	-102649.483309	5.08E+31	1	1.00E+00	1.31E+02
	TS	C, -2.44506, 0.00000, 0.00000 H, -3.13818, -0.86525, -0.00001 H, -3.13818, 0.86525, -0.00001 O, 2.43494, 0.00000, -0.00000 H, 1.46726, -0.00000, 0.00001	-301424.906834	1.67E+32	2	1.24E+01	1.77E+04
94	OH	O, 0.00000, 0.00000, 0.10734 H, 0.00000, 0.00000, -0.85876	-198772.724511	6.78E+31	2	1.00E+00	1.09E+01
	CH	C, 0.00000, 0.00000, 0.16040 H, 0.00000, 0.00000, -0.96239	-100985.100094	4.54E+31	2	1.00E+00	1.44E+01
	TS	C, 0.00000, 0.00000, 2.37260 H, 0.00000, 0.00000, 3.49322 O, 0.00000, 0.00000, -2.07740 H, 0.00000, 0.00000, -1.10959	-299760.379217	1.59E+32	3	1.14E+01	1.84E+03
95/96	OH	O, 0.00000, 0.00000, 0.10734 H, 0.00000, 0.00000, -0.85876	-198772.724511	6.78E+31	2	1.00E+00	1.09E+01
	CH	C, 0.00000, 0.00000, 0.16040 H, 0.00000, 0.00000, -0.96239	-100985.100094	4.54E+31	2	1.00E+00	1.44E+01
	TS	O, 1.29353, 0.10161, -0.00059 H, 1.07320, -0.83833, 0.00525 C, -1.61513, -0.15543, -0.00081 H, -1.73068, 0.95803, 0.00430	-299772.178214	1.59E+32	1	3.59E+00	6.81E+03
97	OH	O, 0.00000, 0.00000, 0.10734 H, 0.00000, 0.00000, -0.85876	-198772.724511	6.78E+31	2	1.00E+00	1.09E+01
	H_2	H, 0.00000, 0.00000, 0.37683	-3031.139750	2.77E+30	1	1.00E+00	3.52E+00

		H, 0.00000, 0.00000, -0.37683					
	TS	O, 0.30315, -0.10744, 0.00000 H, 0.44412, 0.84567, 0.00000 H, -1.03684, -0.11258, 0.00000 H, -1.83251, 0.12645, 0.00000	-201777.115667	8.02E+31	2	1.16E+00	4.52E+02
98/115	OH	O, 0.00000, 0.00000, 0.10734 H, 0.00000, 0.00000, -0.85876	-198772.724511	6.78E+31	2	1.00E+00	1.09E+01
	H	H, 0.00000, 0.00000, 0.00000	-1307.704984	9.79E+29	2	1.00E+00	1.00E+00
	TS	O, -0.00007, 0.00000, 0.00695 H, 0.00016, 0.00000, 1.21695 H, 0.00032, 0.00000, 2.11574	-200053.453913	7.40E+31	3	1.10E+00	6.56E+01
	^{3}O	O, 0.00000, 0.00000, 0.00000	-197065.919094	6.19E+31	3	1.00E+00	1.00E+00
	H_2	H, 0.00000, 0.00000, 0.37683 H, 0.00000, 0.00000, -0.37683	-3031.139750	2.77E+30	1	1.00E+00	3.52E+00
99/100/ 101	^{3}O	O, 0.00000, 0.00000, 0.00000	-197065.919094	6.19E+31	3	1.00E+00	1.00E+00
	H_2CN	C, -0.50346, 0.00000, 0.00005 N, 0.73653, 0.00000, -0.00006 H, -1.06749, 0.93849, 0.00008 H, -1.06748, -0.93850, 0.00008	-246571.579821	1.43E+32	2	1.02E+00	1.39E+03
	TS(CH_2NO)	C, -1.17076, 0.51441, 0.00000 N, -1.43659, -0.69718, 0.00000 H, -1.96887, 1.26430, -0.00004 H, -0.13238, 0.86080, 0.00004 O, 2.39774, -0.04141, -0.00000	-443639.120847	2.83E+32	2	8.34E+00	3.93E+04
	CH_2NO	C, -1.10868, 0.12008, 0.00000 N, 0.06743, -0.35642, 0.00000 H, -1.92868, -0.58030, 0.00000 H, -1.27043, 1.19243, 0.00000 O, 1.17239, 0.14529, 0.00000	-443897.716844	2.83E+32	2	1.18E+00	6.75E+03
	TS(HCNO + H)	C, -1.01152, 0.43493, 0.00000 N, 0.00000, -0.12833, 0.00000 H, -2.06888, 0.55214, 0.00000 H, -0.60205, 2.58631, 0.00000 O, 1.09251, -0.60621, 0.00000	-443628.579465	2.83E+32	2	1.99E+00	7.86E+03
	HCNO	N, 0.02185, -0.00027, 0.00000 C, 1.16967, -0.00244, 0.00000 H, 2.23036, 0.01076, 0.00000 O, -1.17517, 0.00072, 0.00000	-442327.940896	2.73E+32	1	1.36E+00	4.47E+01
	H	H, 0.00000, 0.00000, 0.00000	-1307.704984	9.79E+29	2	1.00E+00	1.00E+00
	TS(HCNOH)	C, 0.01434, -0.00045, 0.00190 N, 0.00003, 0.00007, 1.24192 H, 1.35095, 0.00005, 0.03246 H, -0.76839, -0.00108, -0.74539 O, 1.46065, 0.00063, 1.28767	-443625.880451	2.83E+32	2	1.16E+00	8.32E+03
	HCNOH	C, 1.13711, 0.29236, 0.00000 N, 0.15491, -0.44299, 0.00000 H, 2.17692, -0.01488, 0.00000 H, -1.07487, 1.00421, -0.00000 O, -1.12614, 0.04468, 0.00000	-443791.239692	2.83E+32	2	1.32E+00	7.41E+03
	TS(HCN + OH)	C, 0.03328, 0.00008, 0.03546 N, 0.00597, 0.00012, 1.22817 H, 0.70873, -0.00010, -0.80034 O, -1.48608, 0.00048, 1.88445 H, -2.05048, 0.00059, 1.10631	-443764.756273	2.83E+32	2	1.82E+00	9.57E+03
102/103	^{3}O	O, 0.00000, 0.00000, 0.00000	-197065.919094	6.19E+31	3	1.00E+00	1.00E+00
	HCN	N, 0.00000, 0.00000, 0.64811 C, 0.00000, 0.00000, -0.49567 H, 0.00000, 0.00000, -1.56273	-245122.398339	1.36E+32	1	1.05E+00	1.38E+02
	TS(^{3}NCOH)	N, -1.13197, 0.37849, 0.00000 C, 0.00000, 0.67094, 0.00000 H, 0.85045, 1.32090, 0.00000 O, 0.88417, -0.99949, 0.00000	-442153.408158	2.73E+32	3	1.36E+00	1.17E+04
	^{3}NCOH	N, -1.20011, -0.25305, 0.00000 C, 0.00408, 0.38112, 0.00000 H, -0.02616, 1.48060, 0.00000 O, 1.05030, -0.24950, 0.00000	-442333.955917	2.73E+32	3	1.10E+00	7.47E+03
	TS(NCO + H)	N, -1.26179, -0.12562, 0.00000 C, -0.05403, 0.06003, -0.00000 H, 0.18851, 1.79314, 0.00000 O, 1.12103, -0.15925, 0.00000	-442173.054775	2.73E+32	3	1.15E+00	6.63E+03

	NCO	N, 0.00000, 0.00000, -1.25802	-440893.44121	2.63E+32	2	1.14E+00	5.23E+02
		C, 0.00000, 0.00000, -0.03723					
		O, 0.00000, 0.00000, 1.12869					
	H	H, 0.00000, 0.00000, 0.00000	-1307.704984	9.79E+29	2	1.00E+00	1.00E+00
104	^{3}O	O, 0.00000, 0.00000, 0.00000	-197065.919094	6.19E+31	3	1.00E+00	1.00E+00
	CN	N, 0.00000, 0.00000, 0.53434	-243282.319290	1.28E+32	2	1.00E+00	1.06E+02
		C, 0.00000, 0.00000, -0.62339					
	TS	C, 0.00000, 0.63892, 0.00000	-440356.875652	2.63E+32	4	1.25E+00	9.58E+03
		O, -1.01780, -1.05945, 0.00000					
		N, 1.16321, 0.66316, 0.00000					
106	^{3}O	O, 0.00000, 0.00000, 0.00000	-197065.919094	6.19E+31	3	1.00E+00	1.00E+00
	NH	N, 0.00000, 0.00000, -0.00325	-144933.050538	5.63E+31	3	1.00E+00	1.24E+01
		H, 0.00000, 0.00000, 1.03180					
	TS	N, 0.06397, 1.48451, 0.00000	-342002.972893	1.67E+32	1	2.29E+00	5.13E+03
		H, -0.95957, 1.33241, 0.00000					
		O, 0.06397, -1.46549, 0.00000					
107	^{3}O	O, 0.00000, 0.00000, 0.00000	-197065.919094	6.19E+31	3	1.00E+00	1.00E+00
	NH	N, 0.00000, 0.00000, -0.00325	-144933.050538	5.63E+31	3	1.00E+00	1.24E+01
		H, 0.00000, 0.00000, 1.03180					
	TS	N, -0.00010, 0.00000, 0.00292	-341984.221572	1.67E+32	5	1.12E+00	5.64E+02
		H, 0.00018, 0.00000, 1.13190					
		O, 0.00052, 0.00000, 2.48190					
109	^{3}O	O, 0.00000, 0.00000, 0.00000	-197065.919094	6.19E+31	3	1.00E+00	1.00E+00
	CH_3	C, 0.00000, -0.00018, 0.00042	-104455.380974	5.63E+31	2	1.08E+00	2.53E+02
		H, -0.93570, -0.53955, -0.00085					
		H, 0.93580, -0.53939, -0.00085					
		H, -0.00010, 1.08002, -0.00085					
	TS	C, -1.66894, -0.00071, 0.00146	-301523.504861	1.67E+32	2	9.00E+00	1.43E+04
		H, -1.70398, -0.20404, -1.05871					
		O, 1.88105, 0.00081, -0.00165					
		H, -1.64859, -0.81774, 0.70751					
		H, -1.68219, 1.01954, 0.35561					
112	^{3}O	O, 0.00000, 0.00000, 0.00000	-197065.919094	6.19E+31	3	1.00E+00	1.00E+00
	$^{1}CH_2$	C, 0.00000, 0.17399, 0.00000	-102649.483309	5.08E+31	1	1.00E+00	1.31E+02
		H, 0.86403, -0.52196, 0.00000					
		H, -0.86403, -0.52196, 0.00000					
	TS	C, 1.72138, 0.00000, -0.16790	-299717.767352	1.59E+32	3	4.38E+00	1.02E+04
		H, 1.61465, 0.86374, 0.51996					
		H, 1.61465, -0.86374, 0.51996					
		O, -1.69470, 0.00000, -0.00406					
114	^{3}O	O, 0.00000, 0.00000, 0.00000	-197065.919094	6.19E+31	3	1.00E+00	1.00E+00
	CH	C, 0.00000, 0.00000, 0.16040	-100985.100094	4.54E+31	2	1.00E+00	1.44E+01
		H, 0.00000, 0.00000, -0.96239					
	TS	C, 0.03805, 0.00000, 0.00739	-298053.609930	1.59E+32	4	2.20E+00	6.90E+03
		H, -0.08343, 0.00000, 1.12287					
		O, 3.25815, 0.00000, 1.32701					
116/117/	^{1}O	O, 0.00000, 0.00000, 0.00000	-196788.921964	6.19E+31	1	1.00E+00	1.00E+00
118	H_2CN	C, -0.50346, 0.00000, 0.00005	-246571.579821	1.43E+32	2	1.02E+00	1.39E+03
		N, 0.73653, 0.00000, -0.00006					
		H, -1.06749, 0.93849, 0.00008					
		H, -1.06748, -0.93850, 0.00008					
	TS(CH_2NO)	C, -0.00026, -2.06042, 0.00000	-443364.228372	2.83E+32	2	7.58E+01	2.15E+04
		N, 0.00000, -0.82063, 0.00000					
		H, -0.00039, -2.62401, -0.93865					
		H, -0.00039, -2.62401, 0.93865					
		O, 0.00030, 2.91937, 0.00000					
	CH_2NO	C, -1.10868, 0.12008, 0.00000	-443897.716844	2.83E+32	2	1.18E+00	6.75E+03
		N, 0.06743, -0.35642, 0.00000					
		H, -1.92868, -0.58030, 0.00000					
		H, -1.27043, 1.19243, 0.00000					
		O, 1.17239, 0.14529, 0.00000					
	TS($^{3}O + H_2CN$)	C, -1.17076, 0.51441, 0.00000	-443639.120847	2.83E+32	2	8.34E+00	3.93E+04
		N, -1.43659, -0.69718, 0.00000					
		H, -1.96887, 1.26430, -0.00004					
		H, -0.13238, 0.86080, 0.00004					
		O, 2.39774, -0.04141, -0.00000					
	TS(HCNO + H)	C, -1.01152, 0.43493, 0.00000	-443628.579465	2.83E+32	2	1.99E+00	7.86E+03
		N, 0.00000, -0.12833, 0.00000					
		H, -2.06888, 0.55214, 0.00000					
		H, -0.60205, 2.58631, 0.00000					

		O, 1.09251, -0.60621, 0.00000					
	TS(HCNOH)	C, 0.01434, -0.00045, 0.00190	-443625.880451	2.83E+32	2	1.16E+00	8.32E+03
		N, 0.00003, 0.00007, 1.24192					
		H, 1.35095, 0.00005, 0.03246					
		H, -0.76839, -0.00108, -0.74539					
		O, 1.46065, 0.00063, 1.28767					
	HCNOH	C, 1.13711, 0.29236, 0.00000	-443791.239692	2.83E+32	2	1.32E+00	7.41E+03
		N, 0.15491, -0.44299, 0.00000					
		H, 2.17692, -0.01488, 0.00000					
		H, -1.07487, 1.00421, -0.00000					
		O, -1.12614, 0.04468, 0.00000					
	TS(HCN + OH)	C, 0.03328, 0.00008, 0.03546	-443764.756273	2.83E+32	2	1.82E+00	9.57E+03
		N, 0.00597, 0.00012, 1.22817					
		H, 0.70873, -0.00010, -0.80034					
		O, -1.48608, 0.00048, 1.88445					
		H, -2.05048, 0.00059, 1.10631					
121	^{1}O	O, 0.00000, 0.00000, 0.00000	-196788.921964	6.19E+31	1	1.00E+00	1.00E+00
	CH$_3$	C, 0.00000, -0.00018, 0.00042	-104455.380974	5.63E+31	2	1.08E+00	2.53E+02
		H, -0.93570, -0.53955, -0.00085					
		H, 0.93580, -0.53939, -0.00085					
		H, -0.00010, 1.08002, -0.00085					
	TS	C, -1.93246, -0.00001, 0.00003	-301245.952754	1.67E+32	2	1.03E+01	1.90E+04
		H, -1.94189, -0.95530, -0.50390					
		O, 2.17754, 0.00002, -0.00003					
		H, -1.94115, 0.04121, 1.07930					
		H, -1.94251, 0.91405, -0.57530					
122	^{1}O	O, 0.00000, 0.00000, 0.00000	-196788.921964	6.19E+31	1	1.00E+00	1.00E+00
	^{3}CH$_2$	C, 0.00000, 0.00000, 0.10395	-102701.224038	5.08E+31	3	1.01E+00	8.96E+01
		H, 0.00000, -0.99689, -0.31186					
		H, 0.00000, 0.99689, -0.31186					
	TS	C, -2.00426, -0.00000, -0.10318	-299491.422997	1.59E+32	3	7.05E+00	1.42E+04
		H, -2.08479, 0.99757, 0.30347					
		H, -2.08468, -0.99758, 0.30347					
		O, 2.02438, 0.00000, 0.00152					